


2021

# Maternal Engineered Nanomaterial Inhalation Exposure: Cardiac Molecular Reprogramming in Progeny through Epigenetic and Epitranscriptomic Mechanisms

Amina Kunovac  
*West Virginia University School of Medicine*

Follow this and additional works at: <https://researchrepository.wvu.edu/etd>

 Part of the [Cardiovascular Diseases Commons](#), [Disorders of Environmental Origin Commons](#), [Genomics Commons](#), and the [Toxicology Commons](#)

---

## Recommended Citation

Kunovac, Amina, "Maternal Engineered Nanomaterial Inhalation Exposure: Cardiac Molecular Reprogramming in Progeny through Epigenetic and Epitranscriptomic Mechanisms" (2021). *Graduate Theses, Dissertations, and Problem Reports*. 10255.  
<https://researchrepository.wvu.edu/etd/10255>

This Dissertation is protected by copyright and/or related rights. It has been brought to you by the The Research Repository @ WVU with permission from the rights-holder(s). You are free to use this Dissertation in any way that is permitted by the copyright and related rights legislation that applies to your use. For other uses you must obtain permission from the rights-holder(s) directly, unless additional rights are indicated by a Creative Commons license in the record and/ or on the work itself. This Dissertation has been accepted for inclusion in WVU Graduate Theses, Dissertations, and Problem Reports collection by an authorized administrator of The Research Repository @ WVU. For more information, please contact [researchrepository@mail.wvu.edu](mailto:researchrepository@mail.wvu.edu).

# **Maternal Engineered Nanomaterial Inhalation Exposure: Cardiac Molecular Reprogramming in Progeny through Epigenetic and Epitranscriptomic Mechanisms**

Amina Kunovac

Dissertation submitted to the School of Medicine at West Virginia University in partial fulfillment of the requirements for the degree of:

Doctor of Philosophy in Exercise Physiology

John M. Hollander, Ph.D, Chair  
Paul D. Chantler, Ph.D.  
Roberta Leonardi, Ph.D.  
Timothy R. Nurkiewicz, Ph.D.

I. Mark Olfert, Ph.D.

Department of Human Performance, Division of Exercise Physiology, West Virginia  
University, Morgantown, WV, USA – 2021

Keywords: Mitochondria, Epitranscriptome, Cardiac, ENM, Fetal, Gestation, m6A. Proteome

Copyright 2021 Amina Kunovac

## Abstract

### **Maternal Engineered Nanomaterial Inhalation Exposure: Cardiac Molecular Reprogramming in Progeny through Epigenetic and Epitranscriptomic Mechanisms**

Amina Kunovac

**Introduction:** Nano-titanium dioxide (TiO<sub>2</sub>), a prominently utilized engineered nanomaterial (ENM), is being employed for its physiochemical properties in several fields including the food industry, manufacturing, and biomedicine. As the prevalence of this ENM, and other particulate matter grows, so does the concern for antagonistic consequences on long-term heart function in vulnerable populations, which until now have not been investigated. Due to the reliance of the heart on the ATP generating capacity of mitochondria for contraction, understanding the role of mitochondrial bioenergetics and structure is pivotal in understanding the repercussions of particulate matter exposure during gestation. As the mass population in cities, where particulate matter exposure is highest, do not have many options for mitigating their exposure, it is of utmost importance that strategies are developed that limit the detriments associated with xenobiotic exposure. Understanding the mechanisms, both epigenetic and epitranscriptomic, that regulate mitochondrial and cardiac function under these circumstances will allow for a better understanding of potential therapeutic or preventative strategies and mitigate the disease burden related to particulate matter exposure each year. The purpose of this compilation of work is to identify the mechanisms contributing to the acute and chronic pathological effects of ENM inhalation exposure during gestation as a prerequisite to developing strategies to reduce risks to public health.

**Methods and Results:** Using an inhalation exposure paradigm that mimics the lung burden seen in an occupational setting, we first examined the effects of maternal nano-TiO<sub>2</sub> inhalation exposure during gestation on the cardiac function of wild type offspring at the fetal (acute) and adult (chronic) stage using both conventional and speckle tracking stress-strain echocardiographic assessments. Cardiac contractile function was decreased in both the fetal (gestational day 15 (GD 15)) and the adult (11 weeks) offspring. Assessment of mitochondrial bioenergetic and electron transport chain (ETC) complex activities revealed a decreased oxygen consumption rate in offspring and decreased ETC Complex IV at both the fetal and adult stage following maternal ENM inhalation exposure during gestation. Furthermore ELISA-based assessment of 5-methylcytosine (5mC methylation) and Dnmt expression pointed to the involvement of epigenetic mechanisms in altered mitochondrial and cardiac function. Implementation of a novel breeding strategy, using a transgenic mouse model that overexpresses mitochondrial phospholipid hydroperoxide glutathione peroxidase (mPHGPx), an antioxidant enzyme, determined that enhanced antioxidant expression in the maternal environment can mitigate the effects of gestational nano-TiO<sub>2</sub> inhalation exposure on fetal and adult offspring cardiac and mitochondrial function. N<sup>6</sup>-methyladenosine (m<sup>6</sup>A) was implicated as a modulator of altered mPHGPx activity following maternal ENM exposure in adult offspring, suggesting that epitranscriptomics also has a regulatory role in the adverse effects of particulate matter exposure.

Conclusions: The work presented in this presentation demonstrates the ability for ENM inhalation exposure during gestation to alter cardiac function through a mechanism that involves altering mitochondrial function and elevating ROS levels. These studies also provide evidence that there is likely overlap and interplay between epitranscriptomic and epigenetic mechanisms that contribute to changes in the mitochondrial proteome that reduces the ability of the mitochondrion to regulate stress in the form of ROS and leads to dysfunction. Limiting ROS levels through mitochondrially-targeted antioxidant defense enhancement provides a potential preventative route that may allow for the evasion of the adverse cardiac outcomes in offspring that are gestationally exposed to xenobiotics.

## **Dedication**

To My Parents: Šemsa and Esad Kunovac

Without your hard work and perseverance, this would have never been possible. Thank you for your unconditional love and support throughout this whole process and for always taking an interest in my research even when it made no sense at all. We did it.

Additionally, I would like to thank the following people for their constant support and encouragement: Kemal, Sarah, Teta, Kenan, Strina, Adjo, Alma, Lamija, Belmin, and my husband, Quincy.

## LIST OF ABBREVIATIONS AND DEFINITIONS

5-mC	5-Methylcytosine
7-KCh	7-ketocholesterol
ACE	Angiotensin I-converting enzyme
Acta1	Actin alpha 1 (ACTA1)
AMPK $\alpha$ 2 <sup>-/-</sup>	AMP-activated protein kinase $\alpha$ 2 knockout
Ang II	Angiotensin II (ANG)
ANP	Atrial natriuretic peptide (NPPA)
AT III	Antithrombin III (SERPINC1)
AT <sub>1</sub> R	Angiotensin II type I receptor (ATGR1)
Bax	Bcl-2-associated X protein
BC	Black carbon
Bcl-2	B-cell lymphoma 2
BNP	Brain natriuretic peptide (NPPB)
$\beta$ -MHC	$\beta$ -myosin heavy chain
C3	Complement factor 3
Ca <sup>2+</sup>	Calcium
CAP	Concentrated ambient particles
CaV1.2	Calcium channel, voltage-dependent, L type, alpha 1C subunit
CK	Creatine kinase
CO	Carbon monoxide
Colla1	Collagen type I alpha 1

Col3a1	Collagen type III alpha 1
COX-2	Cyclooxygenase-2 (PTGS2)
CPT1A	Carnitine palmitoyltransferase
CREB	cAMP response element binding protein
CRP	C-reactive protein
CsA	Cyclosporin A
cTnI	Cardiac troponin I
cTnT	Cardiac troponin T
CVD	Cardiovascular disease
CXCL1	C-X-C motif chemokine ligand 1
D2D	D-dimer
DNMT	DNA methyltransferase
DRP1	Dynamin-related protein 1
EC	Elemental carbon
EGFR	Epidermal growth factor receptor
ENM	Engineered nanomaterials
eNOS	Endothelial nitric oxide synthase
EPC	Endothelial progenitor cells
ER	Endoplasmic reticulum
ET-1	Endothelin-1(EDN1)
F3	Tissue factor III
FBA/B/G	Fibrinogen genes
FIS1	Fission 1

GADD153	Growth arrest and DNA damage 153
GATA	GATA sequence binding protein
GRP78	Glucose regulated protein 78
GSH-Px	Glutathione peroxidase
GSK3 $\beta$	Glycogen synthase kinase 3 beta
GST	Glutathione S-transferase
GST-P	Glutathione s-transferase P
GTSM1	Glutathione s-transferase mu 1
H3K27me3	Histone 3 lysine 27 trimethylation
H3K4me3	Histone 3 lysine 4 trimethylation
HDL	High-density lipoprotein
HDM	House dust mite
HIF	Hypoxia inducible factor
HO-1	Heme oxygenase-1(HMOX)
HOI	HDL oxidative index
HOMA-IR	Homeostatic Model Assessment of Insulin Resistance
HRV	Heart rate variability
HSP70	Heat-shock protein 70 kD
ICAM-1	Intercellular adhesion molecule 1
IFN- $\gamma$	Interferon gamma (IFNG)
IKK	Inhibitor of I $\kappa$ B kinase-2
IL	Interleukin
CXCL8	Interleukin 8



iNOS	Inducible nitric oxide (NOS2)
IP-10	IFN $\gamma$ -induced protein 10
IPA	Ingenuity Pathway Analysis
Isop	F2-isoprostane
JNK	C-Jun NH <sub>2</sub> -terminal kinase
LDH	Lactate dehydrogenase (LDHB)
LDL-C	Low-density lipoprotein cholesterol
LINE-1	Long interspersed nuclear element-1
MAPK	Mitogen activated protein kinase
MCP-1	Monocyte chemoattractant protein 1
MDA	Malondialdehyde
Mef2c	Myocyte enhancer factor
MeHg	Methylmercury
METTL	Methyltransferase like protein
Mfn1	Mitofusin 1
MIP-1	Macrophage inflammatory protein
MMP9	Matrix metalloproteinase
mPHGPx	Mitochondrial phospholipid hydroperoxide glutathione peroxidase
MPO	Myeloperoxidase
mPTP	Mitochondrial permeability transition pore
MT-RNR1	Mitochondrial 12s RNA
MT-TF	Mitochondrially encoded tRNA phenylalanine
M <sup>6</sup> A	N <sup>6</sup> -methyladenosine

NCX	Na <sup>+</sup> /Ca <sup>2+</sup> exchanger
NF-κB	Nuclear factor-kappa beta (NFκB1)
NO <sub>2</sub>	Nitrogen dioxide
NOX-4	NADPH oxidase 4
NRF2	Nuclear factor erythroid-derived 2-like 2
OC	Organic carbon
OGG1	8-oxoguanine DNA glycosylase
OPA1	Mitochondrial dynamin like GTPase
PAH	Polycyclic aromatic hydrocarbons
PAI-1	Plasminogen activator inhibitor-1
PAMR1	Peptidase domain containing associated with muscle regeneration 1
Pb	Lead Acetate
PDH	Pyruvate dehydrogenase
PF-4	Platelet factor 4
PIGF	Placental growth factor
PM	Particulate Matter
p-PLN	Phosphorylated phospholamban
PRDX5	Peroxiredoxin 5
PRNP	Prion protein
PTPRF	Protein tyrosine phosphatase receptor type F
ROS	Reactive oxygen species
RYR2	Ryanodine receptor 2
SAA	Serum amyloid A

SELP	P-selectin
SERCA2	Sarco/endoplasmic reticulum Ca <sup>2+</sup> -ATPase (ATP2A2)
SHR	Spontaneously hypertensive rats
SiNP	Silica nanoparticles
SIRT	Sirtuin
SO <sub>2</sub>	Sulfur dioxide
SO <sub>4</sub>	Sulfate
SOD	Superoxide dismutase
SOS1	SOS Ras/Rac Guanine Nucleotide Exchange Factor 1
STAT	Signal transducer and activator of transcription
TFPI	Tissue factor pathway inhibitor
TGFβ-1	Transforming growth factor beta 1
TIMP3	Tissue inhibitor of metalloproteinase 3
TiO <sub>2</sub>	Titanium dioxide
TLR2	Toll-like receptor 2
TLR4	Toll-like receptor 4
TNFR2	Tumor necrosis factor receptor 2 (LTBR)
TNF-α	Tumor necrosis factor alpha
t-PA	Tissue-type plasminogen activator (PLAT)
TRPA1	Transient receptor potential cation channel A1
UCP2	Uncoupling protein 2
UFCP	Ultrafine carbon particles
UFP	Ultrafine particles

VCAM-1	Vascular Cell Adhesion Protein 1
VEGF	Vascular endothelial growth factor (VEGFA)
vWF	Von Willebrand factor
WT	Wild type

# TABLE OF CONTENTS

<b>Abstract</b> .....	ii
<b>Dedication</b> .....	iv
<b>List of Abbreviations and Definitions</b> .....	v
<b>Table of Contents</b> .....	xii
<b>Specific Aims</b> .....	xv
<b>Chapter 1: Literature Review</b> .....	1
Abstract .....	3
• Introduction .....	4
• Summarized Recent Findings Table 1.1 .....	9
• Cardiac Remodeling .....	12
• Cardiac Hemodynamics .....	16
• Coagulation .....	21
• Vascular Dysfunction .....	23
• Cellular Stress and Death .....	26
• Mitochondrial Bioenergetics and Ultrastructure .....	27
• Gestational Exposure.....	30
○ Oxidative Stress and Inflammation .....	31
○ Cellular Function .....	32
○ Epigenetics and Transcriptional Regulation .....	33
• Future Directions.....	35
• Overview .....	38
• Funding .....	39
• References .....	40
<b>Chapter 2: Specific Aim 1</b>	
<b>ROS Promote Epigenetic Remodeling and Cardiac Dysfunction in Offspring Following Maternal Engineered Nanomaterial (ENM) Exposure</b> .....	54
• Abstract .....	55
• Background .....	57

- Methods .....59
- Results .....69
- Discussion .....73
- Conclusions .....77
- Acknowledgements .....78
- References .....80
- Tables and Table Legends .....85
- Figures and Figure Legends .....87
- Supplemental Tables and Table Legends .....107
- Supplemental Figures and Figure Legends .....117

**Chapter 3: Specific Aim 2 – Enhanced Antioxidant Capacity Prevents Epitranscriptomic and Cardiac Alterations in Adult Offspring Gestationally-Exposed to ENM .....124**

- Abstract .....125
- Introduction .....126
- Materials and Methods .....128
- Results .....138
- Discussion .....142
- Acknowledgements .....146
- References .....147
- Tables and Table Legends .....153
- Figures and Figure Legends .....157
- Supplemental Tables and Table Legends .....176

**Chapter 4: Specific Aim 3 – Increased N<sup>6</sup>-Methyladenosine in Fetal Offspring following Gestational Nano-TiO<sub>2</sub> Inhalation Exposure Decreases Mitochondrial Transcript and Protein Expression .....190**

- Abstract .....191
- Introduction .....192
- Material & Methods .....194
- Results .....203
- Discussion .....206
- Acknowledgements .....209
- References .....211

- Tables and Table Legends .....215
- Figures and Figure Legends .....217
- Supplemental Figures and Figure Legends .....237
  
- Chapter 5: General Discussion .....250**
  - Limitations .....259
  - Future Directions .....260
  - Conclusions .....262
  - References .....264
  
- Chapter 6: Supplemental Material: Left Ventricular Segmental Stress-Strain Identifies  
Unique Myocardial Deformation Patterns Following Intrinsic and Extrinsic Stressors in  
Mice .....267**
  - Abstract .....268
  - Introduction .....269
  - Methods .....270
  - Results .....273
  - Discussion .....277
  - Conclusions .....280
  - Declarations .....281
  - Acknowledgements .....282
  - References .....284
  - Tables and Table Legends .....286
  - Figures and Figure Legends .....290
  - Supplemental Tables and Table Legends .....305
  - Supplemental Figures and Figure Legends .....309
  
- Curriculum Vitae .....322**

## Specific Aims:

Xenobiotic exposure is a causative agent of cardiovascular dysfunction, ensuing as a result of mitochondrial bioenergetic dysregulation. The implementation of engineered nanomaterials (ENMs) in consumer products, manufacturing processes, and clinical applications is expanding rapidly despite our limited understanding of their impacts on human health. Exposure to ENMs are of particular concern for vulnerable populations such as the developing fetus, which is prone to deleterious effects that can alter the epigenomic profile and result in sustained dysfunction or susceptibility to other metabolic disturbances into adulthood. Our laboratory was the first to evaluate the consequences of maternal ENM inhalation exposure during gestation. The findings of this study indicated that gestational nano-TiO<sub>2</sub> exposure has a detrimental impact on cardiac contractile function, mitochondrial respiration and bioenergetics that are sustained into adulthood. The functional deficits seen following ENM inhalation exposure have been attributed to increased production of reactive oxygen species (ROS), that was ameliorated by overexpression of mitochondria phospholipid hydroperoxide glutathione peroxidase (mPHGPx), an antioxidant enzyme that protects cells from oxidative stress. ROS insult has the capacity to induce mRNA epigenetic modifications, such as 5-methylcytosine or epitranscriptomic changes, such as N<sup>6</sup>-methyladenosine (m<sup>6</sup>A), which is predicted to occur in a critical region of the 3' UTR of mPHGPx and can thus alter mRNA stability. However, there is a paucity of information regarding the effects of the altered epigenetic/epitranscriptomic mechanisms and whether they are connected to changes in the mitochondrial proteome in progeny. The studies outlined in this dissertation address these critical *gaps in knowledge* and are designed to determine if enhanced antioxidant protection can provide a protective role to offspring following maternal ENM inhalation exposure and elucidate the epigenomic remodeling mechanisms that impact development. The *long-term goal* of these studies is to identify mechanisms contributing to the pathological effects of xenobiotic exposure as a prerequisite to developing strategies for reducing risks to public health.

The *objectives of this dissertation* are to: (1) determine whether maternal engineered nanomaterial (ENM) inhalation exposure influences progeny cardiac function and epigenomic remodeling (2) elucidate the impact of mPHGPx overexpression in various contexts on contractile function and mitochondrial bioenergetics in offspring following maternal ENM inhalation exposure; and (3)



determine whether disruption of mitochondrial bioenergetics and cardiovascular dysfunction elicited by maternal exposure can be attributed to epitranscriptomic remodeling that is associated with an altered mitochondrial proteome that is incapable of managing high levels of ROS. My *central hypothesis* is that changes in the m<sup>6</sup>A methylome, concomitant with an altered mitochondrial proteome at the fetal stage, precipitate cardiac contractile dysfunction that is sustained into adulthood following maternal ENM inhalation exposure. Sustained dysfunction may be averted through limiting ROS via overexpression of mPHGPx. Preliminary data from our lab indicate that ENM exposure results in altered mitochondrial and cardiac contractile function as a result of elevated ROS levels and diminished antioxidant capacity. Additionally, our laboratory has shown that following exposure, fetal offspring presented with an altered transcriptome and changes in DNA histone modifications. We have chosen nano-TiO<sub>2</sub> as a representative ENM because it is widely tested in academic, industrial, and biomedical research. To test our central hypothesis, we propose three *Specific Aims*:

**Specific Aim 1:** *Elucidate the effects of maternal nano-TiO<sub>2</sub> inhalation exposure on cardiac contractile function and mitochondrial function in fetal offspring and whether these detriments persist into adulthood.* We will test our working hypothesis that maternal nano-TiO<sub>2</sub> inhalation exposure during gestation may evoke an ROS response resulting in mitochondrial bioenergetic disruption and cardiac contractile dysfunction in offspring that persists into adulthood.

- 1.1** Evaluate cardiac contractile function using conventional and speckle tracking stress-strain parameters in fetal (gestational day (GD) 15) and adult (11 weeks) offspring following maternal nano-TiO<sub>2</sub> inhalation exposure during gestation.
- 1.2** Examine the effects of inhalation nano-TiO<sub>2</sub> during gestation on fetal and adult offspring cardiac mitochondrial bioenergetics and ultrastructure.
- 1.3** Determine the role of epigenetic modifications and their mediators in modulating mitochondrial function in offspring maternal nano-TiO<sub>2</sub> inhalation exposure during gestation.

The *expected outcomes* of Specific Aim 1 are that cardiac function is negatively altered following gestational ENM inhalation exposure along with mitochondrial dysregulation in fetal and adult offspring, likely as a result of reprogramming that causes changes in ROS levels.

**Specific Aim 2:** *Determine whether enhanced mPHGPx expression preserves cardiac contractile function and bioenergetics in adult offspring following maternal ENM inhalation exposure, and whether m<sup>6</sup>A methylation contributes to altered antioxidant capacity.* We will test our working hypothesis that enhanced antioxidant defense at the level of the dam and fetus will provide the most impactful protection by lessening cardiac contractile dysfunction and bioenergetic disruption in adult offspring following gestational ENM exposure. The enhanced antioxidant defense will mitigate the contractile and mitochondrial dysfunction by evading changes to the m<sup>6</sup>A methylome.

- 2.1 Determine whether increasing ROS scavenging through mPHGPx expression in maternal, fetal, or both provides the most protective profile.
- 2.2 Elucidate whether enhanced antioxidant protection has the ability to mitigate ROS levels such that cardiac function and mitochondrial activity are restored.
- 2.3 Ascertain whether m<sup>6</sup>A plays a role in diminished mitochondrial bioenergetics and ROS scavenging ability at the adult stage following maternal ENM inhalation exposure during gestation and whether mPHGPx overexpression ameliorates these consequences.

The *expected outcomes* of Specific Aim 2 are that overexpression of mPHGPx in the fetus combined with the overexpression of mPHGPx in the pregnant dam will provide the most protective profile, thereby lowering mitochondrial ROS levels, ameliorating mitochondrial dysregulation, and preserving proper cardiac function following maternal ENM inhalation exposure.

**Specific Aim 3:** *Evaluate the epitranscriptomic changes and the mechanism associated with increased ROS following maternal ENM inhalation exposure that contribute to mitochondrial and cardiac dysfunction at the fetal stage.* We will test our working hypothesis that nuclear and changes to the epitranscriptome of mitochondrial genes following maternal ENM inhalation exposure contribute to cardiac dysfunction at the fetal stage that persists into adulthood as a result of altered regulator expression.

- 3.1** Explicate the repercussions of maternal nano-TiO<sub>2</sub> inhalation exposure during gestation on the overall m<sup>6</sup>A methylome in wild type fetal offspring to determine the role of epitranscriptomics in diminished cardiac function.
- 3.2** Elucidate how maternal nano-TiO<sub>2</sub> inhalation exposure during gestation alters the mitochondrial proteome in wild type fetal offspring and whether these changes are associated with epitranscriptomic reprogramming.

The *expected outcomes* of Specific Aim 3 are that changes in m<sup>6</sup>A of crucial nuclear-encoded mitochondrial mRNA will correlate with a deficient mitochondrial proteome that can account for diminished mitochondrial bioenergetics that occurs in fetal offspring following gestational ENM exposure and contributes to the long-term cardiac effects that also persist into adulthood.

With respect to the overall expected outcomes, successful completion of these studies will provide fundamental information concerning the relationship between epigenetic/epitranscriptomic regulation during the critical window of fetal development and the subsequent long-term cardiovascular effects. The information will aid in the design of protective antioxidant strategies and assessment of consumer risks to ensure safer development of nanotechnologies.

## **RESEARCH STRATEGY**

**SIGNIFICANCE.** While nanotechnology has provided important advancements in biomedical engineering, the increased interactions of nanomaterials and biological tissue warrants assessments of associated toxicological effects (2, 4, 16). Engineered nanomaterials (ENMs) pose occupational and public risks due their abundance in consumer products (17, 20) and the primary route of exposure, inhalation, allows particles to enter the bloodstream and systemically impact the body (20). Nano titanium dioxide (TiO<sub>2</sub>), one of the most utilized ENMs, is incorporated into versatile industrial, environmental, and consumer products (17), with application in consumer products escalating by 300% from 2011 to 2013 (22). Maternal ENM exposure during gestation interferes with fetal development and has long-term consequences for offspring that persist into adulthood (2, 4, 11, 21). Over the last decade, the developmental origins of health and diseases (DOHaD) hypothesis has increased emphasis on understanding how parental exposure to environmental stressors can alter the susceptibility of offspring to various diseases including obesity (24). Currently, 40% of all adults (over the age of 20) in the United States are obese (8), which is one of the top risk factors for heart disease. Cardiovascular disease is the leading cause of death, accounting for every 1 in 4 deaths in the US (1). Understanding the risk factors that increase the propensity for developing cardiovascular disease and how they can be prevented is critical in lowering the associated death toll.

Previous studies, in conjunction with preliminary data presented in this application, provide the **scientific premise** for the proposed experimentation. Our laboratory was the first to report sustained (into adulthood) cardiac contractile dysfunction following maternal nano-TiO<sub>2</sub> inhalation exposure during gestation (10, 19). These effects were associated with disruption to the fetal cardiac epigenome, dysregulated mitochondrial bioenergetics, and decreased mPHGPx expression levels in offspring. Increased reactive oxygen species (ROS) generation indicated oxidative stress following acute ENM inhalation exposure (15), which could be linked to cardiac contractile dysfunction through epigenomic changes such as DNA methylation and post-translation histone modifications (12). These data support the proposition that targeted interventions lessening ROS during gestation may provide relief from the damaging effects of ENMs. Elevated ROS has also been associated with altered levels of N<sup>6</sup>-methyladenosine (m<sup>6</sup>A), the most prevalent mRNA modification in higher eukaryotes, which regulates transcription and

translation (13, 23, 26). Investigation of m<sup>6</sup>A sites in crucial coding regions of nuclear genome-encoded mitochondrial mRNA that are pivotal in antioxidant defense is therefore pertinent as it will provide insight into the mechanism by which ROS may be controlling mPHGPx protein expression. Further, understanding the repercussions of early-life exposure in terms of susceptibility to obesity and other metabolic diseases, such as diabetes, mellitus is critical, as epigenomic adaptations may alter the ability of an organism to cope with a secondary insult (7). Maternal exposure to particulate matter, as it relates to the susceptibility of offspring to develop obesity, have previously been investigated in several epidemiological studies (3, 5, 6, 14, 24). All in all, the previous studies suggest a critical need for understanding the epigenetic mechanisms involved in developmental reprogramming that causes such detriments. Our laboratory has shown that in mice, following a single ENM inhalation exposure, fatty acid metabolism has been impacted (9, 10). Additionally, diminished m<sup>6</sup>A methylation has been demonstrated in diabetic patients, concomitant with elevated fat mass and obesity-associated (FTO) protein expression, a well characterized m<sup>6</sup>A demethylase (18, 25).

The contribution of this work is **significant** because it will identify epitranscriptomic mechanisms contributing to the cardiovascular deficits elicited by ENM exposure as a prerequisite for assessing consumer and occupational risks. Additionally, this work will determine the benefit of enhanced antioxidant defense in attenuating cardiac dysfunction associated with ENM exposure. This information will be critical as we consider public health risks of nanotechnology, while aiding in the development of biomarkers and prophylactic strategies to lessen cardiovascular complications associated with ENM inhalation exposure. The proposed research is **conceptually** and **mechanistically innovative** because it is the first study to propose m<sup>6</sup>A modifications as a contributing cause of cardiac dysfunction elicited by ENM inhalation exposure. The proposed research is **technically innovative** in its application of echocardiographic imaging of offspring *in utero* and application of a transgenic mouse model that overexpresses mPHGPx as an antioxidant protective strategy to prevent mitochondrial and cardiac deficits in progeny following maternal ENM inhalation exposure. Understanding the epitranscriptomic changes that occur and establishing a therapeutic approach that may attenuate elevated ROS and its associated detriments, enhances the **impact** of the studies.

## References

1. **Benjamin EJ, Muntner P, Alonso A, Bittencourt MS, Callaway CW, Carson AP, Chamberlain AM, Chang AR, Cheng S, Das SR, Delling FN, Djousse L, Elkind MSV, Ferguson JF, Fornage M, Jordan LC, Khan SS, Kissela BM, Knutson KL, Kwan TW, Lackland DT, Lewis TT, Lichtman JH, Longenecker CT, Loop MS, Lutsey PL, Martin SS, Matsushita K, Moran AE, Mussolino ME, O'Flaherty M, Pandey A, Perak AM, Rosamond WD, Roth GA, Sampson UKA, Satou GM, Schroeder EB, Shah SH, Spartano NL, Stokes A, Tirschwell DL, Tsao CW, Turakhia MP, VanWagner LB, Wilkins JT, Wong SS, Virani SS, American Heart Association Council on E, Prevention Statistics C, and Stroke Statistics S.** Heart Disease and Stroke Statistics-2019 Update: A Report From the American Heart Association. *Circulation* 139: e56-e528, 2019.
2. **Bommarito PA, Martin E, and Fry RC.** Effects of prenatal exposure to endocrine disruptors and toxic metals on the fetal epigenome. *Epigenomics* 9: 333-350, 2017.
3. **Chiu YM, Hsu HL, Wilson A, Coull BA, Pendo MP, Baccarelli A, Kloog I, Schwartz J, Wright RO, Taveras EM, and Wright RJ.** Prenatal particulate air pollution exposure and body composition in urban preschool children: Examining sensitive windows and sex-specific associations. *Environ Res* 158: 798-805, 2017.
4. **Crispi F, Miranda J, and Gratacos E.** Long-term cardiovascular consequences of fetal growth restriction: biology, clinical implications, and opportunities for prevention of adult disease. *Am J Obstet Gynecol* 218: S869-S879, 2018.
5. **Fleisch AF, Luttmann-Gibson H, Perng W, Rifas-Shiman SL, Coull BA, Kloog I, Koutrakis P, Schwartz JD, Zanobetti A, Mantzoros CS, Gillman MW, Gold DR, and Oken E.** Prenatal and early life exposure to traffic pollution and cardiometabolic health in childhood. *Pediatr Obes* 12: 48-57, 2017.
6. **Fleisch AF, Rifas-Shiman SL, Koutrakis P, Schwartz JD, Kloog I, Melly S, Coull BA, Zanobetti A, Gillman MW, Gold DR, and Oken E.** Prenatal exposure to traffic pollution: associations with reduced fetal growth and rapid infant weight gain. *Epidemiology* 26: 43-50, 2015.
7. **Foulds CE, Trevino LS, York B, and Walker CL.** Endocrine-disrupting chemicals and fatty liver disease. *Nat Rev Endocrinol* 13: 445-457, 2017.
8. **Hales CM, Fryar CD, Carroll MD, Freedman DS, and Ogden CL.** Trends in Obesity and Severe Obesity Prevalence in US Youth and Adults by Sex and Age, 2007-2008 to 2015-2016. *JAMA* 319: 1723-1725, 2018.
9. **Hathaway QA, Durr AJ, Shepherd DL, Pinti MV, Brandebura AN, Nichols CE, Kunovac A, Goldsmith WT, Friend SA, Abukabda AB, Fink GK, Nurkiewicz TR, and Hollander JM.** miRNA-378a as a key regulator of cardiovascular health following engineered nanomaterial inhalation exposure. *Nanotoxicology* 1-20, 2019.
10. **Hathaway QA, Nichols CE, Shepherd DL, Stapleton PA, McLaughlin SL, Stricker JC, Rellick SL, Pinti MV, Abukabda AB, McBride CR, Yi J, Stine SM, Nurkiewicz TR, and Hollander JM.** Maternal-engineered nanomaterial exposure disrupts progeny cardiac function and bioenergetics. *Am J Physiol Heart Circ Physiol* 312: H446-H458, 2017.
11. **Hougaard KS, Campagnolo L, Chavatte-Palmer P, Tarrade A, Rousseau-Ralliard D, Valentino S, Park MV, de Jong WH, Wolterink G, Piersma AH, Ross BL, Hutchison GR, Hansen JS, Vogel U, Jackson P, Slama R, Pietroiusti A, and Cassee FR.** A perspective on the developmental toxicity of inhaled nanoparticles. *Reprod Toxicol* 56: 118-140, 2015.

12. **Kietzmann T, Petry A, Shvetsova A, Gerhold JM, and Gorlach A.** The epigenetic landscape related to reactive oxygen species formation in the cardiovascular system. *Br J Pharmacol* 174: 1533-1554, 2017.
13. **Kmietczyk V, Riechert E, Kalinski L, Boileau E, Malovrh E, Malone B, Gorska A, Hofmann C, Varma E, Jurgensen L, Kamuf-Schenk V, Altmuller J, Tappu R, Busch M, Most P, Katus HA, Dieterich C, and Volkers M.** m(6)A-mRNA methylation regulates cardiac gene expression and cellular growth. *Life Sci Alliance* 2: 2019.
14. **Mao G, Nachman RM, Sun Q, Zhang X, Koehler K, Chen Z, Hong X, Wang G, Caruso D, Zong G, Pearson C, Ji H, Biswal S, Zuckerman B, Wills-Karp M, and Wang X.** Individual and Joint Effects of Early-Life Ambient Exposure and Maternal Prepregnancy Obesity on Childhood Overweight or Obesity. *Environ Health Perspect* 125: 067005, 2017.
15. **Nichols CE, Shepherd DL, Hathaway QA, Durr AJ, Thapa D, Abukabda A, Yi J, Nurkiewicz TR, and Hollander JM.** Reactive oxygen species damage drives cardiac and mitochondrial dysfunction following acute nano-titanium dioxide inhalation exposure. *Nanotoxicology* 12: 32-48, 2018.
16. **Pietrojusti A, Stockmann-Juvala H, Lucaroni F, and Savolainen K.** Nanomaterial exposure, toxicity, and impact on human health. *Wiley Interdiscip Rev Nanomed Nanobiotechnol* 2018.
17. **Robichaud CO, Uyar AE, Darby MR, Zucker LG, and Wiesner MR.** Estimates of upper bounds and trends in nano-TiO<sub>2</sub> production as a basis for exposure assessment. *Environ Sci Technol* 43: 4227-4233, 2009.
18. **Shen F, Huang W, Huang JT, Xiong J, Yang Y, Wu K, Jia GF, Chen J, Feng YQ, Yuan BF, and Liu SM.** Decreased N(6)-methyladenosine in peripheral blood RNA from diabetic patients is associated with FTO expression rather than ALKBH5. *J Clin Endocrinol Metab* 100: E148-154, 2015.
19. **Stapleton PA, Hathaway QA, Nichols CE, Abukabda AB, Pinti MV, Shepherd DL, McBride CR, Yi J, Castranova VC, Hollander JM, and Nurkiewicz TR.** Maternal engineered nanomaterial inhalation during gestation alters the fetal transcriptome. *Part Fibre Toxicol* 15: 3, 2018.
20. **Stebounova LV, Morgan H, Grassian VH, and Brenner S.** Health and safety implications of occupational exposure to engineered nanomaterials. *Wiley Interdiscip Rev Nanomed Nanobiotechnol* 4: 310-321, 2012.
21. **Sun J, Zhang Q, Wang Z, and Yan B.** Effects of nanotoxicity on female reproductivity and fetal development in animal models. *Int J Mol Sci* 14: 9319-9337, 2013.
22. **Vance ME, Kuiken T, Vejerano EP, McGinnis SP, Hochella MF, Jr., Rejeski D, and Hull MS.** Nanotechnology in the real world: Redeveloping the nanomaterial consumer products inventory. *Beilstein J Nanotechnol* 6: 1769-1780, 2015.
23. **Wang SR, Wang JQ, Zhang XE, Fu BS, Song YY, Ma P, Gu K, Zhou X, Zhang XL, Tian T, and Zhou X.** N-6-Methyladenine hinders RNA- and DNA-directed DNA synthesis: application in human rRNA methylation analysis of clinical specimens. *Chem Sci* 7: 1440-1446, 2016.
24. **Xu YY, Wang WJ, Chen MJ, Zhou J, Huang XK, Tao SM, Pan B, Li ZZ, Xie XY, Li WH, Kan HD, and Ying ZK.** Developmental programming of obesity by maternal exposure to concentrated ambient PM<sub>2.5</sub> is maternally transmitted into the third generation in a mouse model. *Particle and Fibre Toxicology* 16: 2019.

25. **Yang Y, Shen F, Huang W, Qin S, Huang JT, Sergi C, Yuan BF, and Liu SM.** Glucose Is Involved in the Dynamic Regulation of m6A in Patients With Type 2 Diabetes. *J Clin Endocrinol Metab* 104: 665-673, 2019.
26. **Zhong X, Yu J, Frazier K, Weng X, Li Y, Cham CM, Dolan K, Zhu X, Hubert N, Tao Y, Lin F, Martinez-Guryn K, Huang Y, Wang T, Liu J, He C, Chang EB, and Leone V.** Circadian Clock Regulation of Hepatic Lipid Metabolism by Modulation of m(6)A mRNA Methylation. *Cell Rep* 25: 1816-1828 e1814, 2018.



# **Chapter 1:**

# **Literature Review**

# **Cardiovascular Adaptations to Particle Inhalation Exposure: Molecular Mechanisms of the Toxicology**

Amina Kunovac<sup>1,2,3</sup>, Quincy A. Hathaway<sup>1,2,3</sup>, Mark V. Pinti<sup>2,4</sup>, Andrew D. Taylor<sup>1,2</sup>, and John  
M. Hollander<sup>1,2,3\*</sup>

Modified from the following publication: American Journal of Physiology Heart and Circulation  
Physiology. 2020 June 12; 1;319(2):H282-H305. doi: 10.1152/ajpheart.00026.2020.

<sup>1</sup>Division of Exercise Physiology, West Virginia University School of Medicine, Morgantown, WV, USA.  
<sup>2</sup>Mitochondria, Metabolism & Bioenergetics Working Group, West Virginia University School of Medicine,  
Morgantown, WV, USA. <sup>3</sup>Center for Inhalation Toxicology (iTOX), West Virginia University School of Medicine,  
Morgantown, WV, USA. <sup>4</sup>West Virginia University School of Pharmacy, Morgantown, WV, USA.

***Running Title: Cardiovascular Molecular Pathways following Exposure***

**Keywords:** Heart, Mitochondria, Gestation, Genomics, Particulate Matter, Engineered  
Nanomaterial, UFP, PM<sub>2.5</sub>

**Abstract:**

Ambient air, occupational settings, and the use and distribution of consumer products all serve as conduits for toxicant exposure through inhalation. While the pulmonary system remains a primary target following inhalation exposure, cardiovascular implications are exceptionally culpable for increased morbidity and mortality. The epidemiological evidence for cardiovascular dysfunction resulting from acute or chronic inhalation exposure to particulate matter has been well documented, but the mechanisms driving the resulting disturbances remain elusive. In the current review, we aim to summarize the cellular and molecular mechanisms that are directly linked to cardiovascular health following exposure to a variety of inhaled toxicants. The purpose of this review is to provide a comprehensive overview of the biochemical changes in the cardiovascular system following particle inhalation exposure and to highlight potential biomarkers that exist across multiple exposure paradigms. We attempt to integrate these molecular signatures in an effort to provide direction for future investigations. This review also characterizes how molecular responses are modified in at-risk populations, specifically the impact of environmental exposure during critical windows of development. Maternal exposure to particulate matter during gestation can lead to fetal epigenetic reprogramming, resulting in long-term deficits to the cardiovascular system. In both direct and indirect (gestational) exposures, connecting the biochemical mechanisms with functional deficits outlines pathways that can be targeted for future therapeutic intervention. Ultimately, future investigations integrating “omics” based approaches will better elucidate the mechanisms that are altered by xenobiotic inhalation exposure, identify biomarkers, and guide in clinical decision making.

## Introduction

Irrespective of diet, physical fitness, or other controllable risk factors, the quality and contents of the air we breathe are often unavoidable. In industrial cities and large metropolitan areas, the most pervasive mode of exposure to aerosolized toxicants is through the ambient air. Long term exposure to ambient air pollution contributes to 7.6% of global mortality, with 91% of the world's population residing in places where air quality exceeds the guideline limits put forth by the World Health Organization (WHO) (31, 171, 172). The number of annual premature deaths as a result of outdoor air pollution are staggering, with projections indicating 6-9 million deaths in 2060 (18, 121). Subsequently, the predicted economic costs are increasing substantially as a repercussion of the illnesses resulting from exposure (121). The importance of lowering ambient fine particulate matter exposure is highlighted specifically by the notion that if all countries met the WHO Air Quality Guidelines, life expectancy could increase by over 7 months (2). This becomes a daunting task with increasing urbanization (171) and implementation of nanoparticles for their advantageous physical, chemical, and biological properties in industrial, commercial and medical sectors (136).

There are numerous factors that contribute to the diminishing air quality including industrial sources, energy power plants, traffic, agriculture, and fires (37, 80, 142). Particulate matter (PM) is the sum of all organic and inorganic compounds dispersed in the solid and liquid phases that can be carried by air (22, 81). PM components are typically categorized by particle size including coarse ( $PM_{10}$ ;  $\leq 10 \mu\text{m}$  in diameter), fine ( $PM_{2.5}$ ;  $\leq 2.5 \mu\text{m}$  in diameter), and ultrafine (UFP,  $PM_{0.1}$ ;  $\leq 0.1 \mu\text{m}$  in diameter) particles. However, the surface area, chemical composition, number, solubility and reactivity are some of the other characteristics that must be considered (16, 22, 106, 148). Decreasing the size of particulates from  $PM_{10}$  to  $PM_{2.5}$  increases the capacity for the material to travel further into the bronchoalveolar airways and allows for a broader interaction area (53, 175). Similar to  $PM_{2.5}$ , UFP, also have the capacity to penetrate deeply into the alveoli of the tracheobronchial airways (117, 150), but UFP exhibit an increased capacity for interstitialization and can transport systemically throughout the body due to their high surface-to-volume ratios (22, 40, 106, 117, 148). Because the bulk of cardiovascular effects originate from fine PM and nanoparticles (53, 144), this review will focus on  $PM_{2.5}$ , UFP, and engineered nanomaterials (ENM).

ENM (at least one dimension  $\leq 100$  nm in diameter), which are similar in size to UFP, are anthropogenic materials that pose additional risk to public cardiovascular health (82, 125, 136, 146). Nanomaterials represent an ever-increasing vehicle for inhalation toxicology (85). Whether during the manufacturing of nanomaterials (85) or in consumer use (113), production and rate of application continue to rise (7, 68). While inhalation studies examining ENMs and UFP typically differ in the number and standardization of compounds found within the mixtures, both share commonality in the nanometer scale that permits similar dispersion within the lungs during inhalation (148). Nanomaterials, similar to UFP, exist exclusively at a biological scale that alters the dynamics of interactions with organic matter (112, 157), potentially altering toxicities compared to their micrometer-sized equivalents (22, 53, 144, 148). One example of ENM, is nano-titanium dioxide ( $\text{TiO}_2$ ), which is predominantly used for its photocatalytic properties, like its ability to refract light and enhance colors. Nano- $\text{TiO}_2$  is therefore implemented in products such as paint pigments, sunscreen, paper, pharmaceuticals, tattoo ink, and water purification systems. There are specific physicochemical properties of inhaled particles that determine its applications. The size, composition, pore size, and surface charge and chemistry are some of the main properties that govern the applicability of inhaled particles (60). In the attempt to understand the biological effects of inhaled particles, particularly on the cardiovascular system, these varying properties have posed a challenge such that any attempt to understand an individual particle or co-exposure would require each particle within the exposure to be purified and characterized based on the many relevant particle properties. Our laboratory has specifically focused on understanding the mechanisms associated with nano- $\text{TiO}_2$  inhalation exposure. Although the properties of nano- $\text{TiO}_2$  may differ from other inhaled particles by size, solubility, porosity, crystallinity, shape, etc., we utilize this particle as a surrogate to focus on the mechanism that is elicited by almost all inhaled particle exposures, increased reactive oxygen species (ROS) (61). It is outside the scope of most studies to identify the unique spectrum of molecular changes that each ENM may produce (14). Using a surrogate particle is beneficial in that it eliminates the variability introduced when a mixture of particles is present that contain particulate matter of varying physicochemical properties.

There are three prevailing theories on the mechanism by which inhaled pollutants result in deleterious effects on the cardiovascular system (106, 107, 115, 117). The first of these theories involves inflammation, whereby particles that reach the lungs initiate an inflammatory response

that leads to the release of cytokines and other mediators that can then be introduced into the circulation, causing downstream effects (107). The other possibility is that, based on the size of the particles, they may not only enter the systemic circulation but also translocate across the alveolar wall and impact the cardiovascular system directly (typically only applies to ultrafine particles), such as by influencing the vascular endothelium. Lastly, the particles may affect autonomic regulation and alter the parasympathetic: sympathetic balance through sensory receptors on the alveolar surface. This can result in changes in heart rate variability and other parameters of cardiac function. It would be naive to state that one of these specific pathways is solely responsible for the cardiovascular effects induced by inhaled particle exposure. A more likely scenario is that all three pathways work in concert, and likely contribute and exacerbate the effects of each one. For example, an initial inflammatory response may result in tissue damage that increases permeability and makes it easier for particles to translocate and incite further damage. Regardless of the initial response within the lungs, understanding the cardiovascular molecular pathways that exposure mediates is essential for identifying appropriate prophylactic and/or therapeutic strategies. A potential starting point in developing prophylactic and/or therapeutic strategies for limiting particle-induced cardiovascular effects would be limiting reactive oxygen species (ROS) production and dissipation (107). This is instrumental as oxidative stress has the potential to contribute to all three prevailing theories that explain how inhaled particles could cause cardiovascular effects and furthermore likely promotes interactions between the three pathways. Depending on the physicochemical properties of the inhaled particle, the surface chemicals of the particulate matter (such as special coatings that are utilized for its specific effects) or other pollutants in the air may interact and result in redox reactions that produce free radicals. As mentioned previously, inhaled particles can also activate inflammatory cells, which causes a release of cytokines and oxidative mediators. Lastly, oxidative stress can be a response from the particle interaction with tissue enzymes like the stimulation of xanthine oxidase or depletion of antioxidant defenses (107). Due to the high likelihood that ROS is involved in the cardiovascular effects of inhaled particles, increasing antioxidant protection is a promising therapeutic strategy that requires further explication.

According to the WHO, over four million people die every year from outdoor air pollution, with cardiovascular disease accounting for about 40% of those deaths (2, 91, 172). While the pulmonary system is considered the primary site of interaction with these particles, secondary

target organs, such as the heart and circulatory system, may be subject to the most detrimental long-term effects. The overt epidemiological risk of cardiovascular injury following chronic and acute inhalation exposure to PM<sub>2.5</sub>, UFP, and ENM has been well documented and includes increased propensity for ischemic heart disease, heart failure, out-of-hospital cardiac arrests, arrhythmias, atherosclerosis, and other cardiovascular complications (16, 28, 58, 128-130, 134, 152, 156, 187). The effects of PM inhalation exposure on the heart function of individuals who are susceptible to cardiovascular disease (CVD) have also gained recent interest. One of the main points of concern emanates from the increasing rate of patients with diet-induced obesity and type 2 diabetes (24). These populations with metabolic disorders can have further modifications to insulin-signaling pathways that arise from inhalation exposure, ultimately increasing susceptibility and aggravating underlying pathophysiology (5, 15, 26, 74, 122, 124, 130).

Among those whom are most vulnerable to the repercussions of inhaled particulates, are those exposed at a critical point in development, such as during gestation. While the main focus has been on the effects of toxicant inhalation exposure directly to an individual, recent studies have highlighted the importance of understanding how exposure during gestation impacts future progeny (12, 13, 52, 87, 100, 104, 108). Maternal inhalation exposure to particles can affect offspring through both direct and indirect mechanisms or a combination of the two (41). Direct effects can ensue if the particle size enables the particulate matter to enter the maternal blood, cross the placental barrier, and directly damage fetal tissue via inflammatory and oxidative stress pathways. Indirect mechanisms can occur if the particle inhalation results in deep instillation of the particle in the lower airways that result in oxidative stress and inflammatory responses. Subsequently, this response may trigger the release of inflammatory mediators that can reach the placenta and fetus resulting in short and long-term repercussions. Lastly, it is possible that a similar response occurs if the particles inhaled reach the placental tissue (even if they are unable to cross the barrier) and incite an oxidative stress and inflammatory response that compromises the placental function and thereby causes oxidative stress, inflammation, growth restriction, preterm birth, as well as cardiovascular and behavioral impairments. It is important to recognize that maternal inflammation may not directly indicate that fetal inflammation is occurring, but the placenta may act as a sensor of maternal inflammation and thereby initiate an adaptive response that causes changes to the fetal environment and potentially reprogramming (41). As per the developmental origins of health and diseases (DOHaD) hypothesis, a baleful gestational

environment results in epigenetic alterations and has a notable influence on the health of the offspring (11, 49). Currently, there are limited studies defining the longitudinal cardiovascular effects of offspring exposed to inhaled particles during gestation and whether exposure increases susceptibility to metabolic diseases at a later point in life due to alterations in overlapping pathways (17, 72). Delineating the long-term effects of inhaled particle exposure on cardiovascular function, particularly in progeny, along with the molecular mechanisms governing predisposition to CVD is critical for limiting premature mortality rates. One potential way that is being investigated is increasing antioxidant protection to evade the cardiovascular defects that are associated with inhaled particulate matter exposure as the balance of oxidants and antioxidants are critical for physiological homeostasis. Under normal pregnancy conditions, the maternal environment can maintain this balance (41). However, because inhaled particles result in excessive amounts of ROS production through direct and indirect pathways, the intrinsic antioxidant system may not be able to manage these levels and can thereby result in diminished antioxidant capacity and elevated oxidative stress. One of the studies that will be discussed in this dissertation, therefore implements antioxidant protection in different contexts to determine which context will provide the most protective profile for long-term offspring cardiovascular health.

The compilation of the works presented herein serves to examine the molecular pathways that are implicated in cardiovascular adaptations to various inhaled particles and attempts to provide a cohesive framework of how each of these molecular pathways has been evaluated across multiple models. Summarized findings of these molecular mechanisms for various exposures and exposure models are presented in **Table 1.1**. Furthermore, there are limited studies examining the cardiovascular consequences of gestational PM exposure on progeny. Therefore, this review will also focus on the effects of PM exposure during gestation on the cardiovascular system in progeny and highlight the molecular pathways that PM exposure alters during this critical window of fetal development. The studies discussed also highlight the necessity for unbiased omics approaches in understanding the indirect mechanisms that play a role in long-term cardiovascular health defects following inhaled particle exposure (41). The following sections are divided into categories, with each section interweaving similar molecular pathways/responses to PM inhalation exposure.



Study	Findings	Model	Exposure
<b>PM<sub>2.5</sub></b>			
(6)	Fine PM <sub>2.5</sub> and coarse PM decreased Alu and TLR4 methylation, respectively	15 local participants	PM <sub>2.5</sub> collected in downtown Toronto. Administered 250 and 200 µg/m <sup>3</sup> per session
(17)	No changes seen in inflammatory markers related to PM <sub>2.5</sub> exposure (monocytes, TNF-α, IL-10, IL-6, IL-8, IL-1β)	25 healthy male and female participants 18-50 years old	PM <sub>2.5</sub> data obtained from Dearborn, Tecumesh, and Dexter, MI. 3 sub-acute integrated 5-day-long exposure periods in Dearborn, MI (mean concentration of 11.5 ± 4.8 µg/m <sup>3</sup> )
(19)	PM <sub>2.5</sub> exposure was associated with mtDNA D-Loop methylation in peripheral blood leukocytes	48 male participants	PM <sub>2.5</sub> collected January 2007 to June 2012 in Boilermaker Union Local 29, Quincy, MA
(30)	Elemental carbon (48 genes), PM <sub>2.5</sub> (49 genes), and organic carbon (260 genes) differentially effected the transcriptome	63 pick-up and delivery drivers and dock workers	PM <sub>2.5</sub> collected February 2009 and October 2010 from 10 trucking terminals in the northeastern US (CT, MA, MD, NJ, NY, and PA).
(33)	PM <sub>2.5</sub> increased STAT3, which promoted microRNA-21 expression, leading to decreased TIMP3 and increased MMP9	Male Sprague Dawley rats, 6 wks old	PM <sub>2.5</sub> collected in Beijing, China. Trachea drip, 4 mg/kg b.w. every 3 days for 36 days
(38)	PM <sub>2.5</sub> reduced intracellular Ca <sup>2+</sup> via decreased RYR2 and increased SERCA2a	Male Balb/c mice, 6–8 wks old	PM <sub>2.5</sub> collected Hebei, China. Intratracheal instillation of 0.5 mg at Day 0 and Day 2
(39)	PM <sub>2.5</sub> exposure with vitamin E and omega-3 polyunsaturated fatty acid administration decreased inflammation (TNF-α, IL-1β, IL-6)	Sprague Dawley rats, 6–8 wks old	PM <sub>2.5</sub> collected May–September 2015 in Shanghai, China. Intratracheal instillation every other day, for 6 days at 10 mg/kg b.w. or 1.5 mL/kg b.w.
(44)	Increased LINE-1 methylation with increasing dose of PM <sub>2.5</sub>	66 male participants	PM <sub>2.5</sub> collected (pre and post-welding shift) January 2010–June 2012 in Boilermaker Union Local 29, Quincy, MA
(51)	PM <sub>2.5</sub> increasing concentration was associated with decreasing levels of ET-1 (negatively) and PF-4 (positively).	15 young, healthy, non-smoking subjects	PM <sub>2.5</sub> ambient air concentrations in Utah Valley from 2 monitoring sites (Lindon, North Provo) measured daily (January–March 2009). Blood collections done during high (PM <sub>2.5</sub> >40 µg/m <sup>3</sup> ), moderate (PM <sub>2.5</sub> ~ 20–40 µg/m <sup>3</sup> ), and low (PM <sub>2.5</sub> <10 µg/m <sup>3</sup> ) concentrations.
(56)	Exercise during DE (PM <sub>2.5</sub> ) exposure decreased ET-1 and increased NOx, but was not modified by exercise intensity	18 male participants	PM <sub>2.5</sub> collected a 5.5-kW diesel engine under a constant 2.5 kW load. Exposure of 300 µg/m <sup>3</sup> over 6/30-minute low and high intensity cycling periods
(59)	PM <sub>2.5</sub> increased expression of ICAM-1, VCAM, and CRP in sedentary mice, and increased VCAM in exercised mice	Male ob/ob mice, 12 wks old	PM <sub>2.5</sub> collected Columbus, OH. Average 32 µg/m <sup>3</sup> for 6 hrs/day, 5 days/week for 9 months through a whole-body inhalation system
(62)	PM <sub>2.5</sub> decreased VEGF-induced Akt/eNOS phosphorylation and circulating levels of Flk-1 <sup>+</sup> /Sca-1 <sup>+</sup> cells (EPCs)	C57BL/6J male mice, 8–12 wks old	PM <sub>2.5</sub> collected June 2009 and December 2010 in Louisville, KY. Whole-body exposure, 6 hr/day for 4-30 days at 30-100 µg/m <sup>3</sup>
(63)	PM <sub>2.5</sub> reduced insulin stimulated Akt phosphorylation and circulating levels of Flk-1 <sup>+</sup> /Sca-1 <sup>+</sup> cells (EPCs), elevated oxidative stress (SOD2,GST-P), caused inflammasome activation (IL-1β, pro-IL-18 cleavage, activation of Casp-1)	C57BL/6J male mice, 8 wks old (control/high-fat diet), C57BL/6J male mice, 12 wks old (control diet, pre-treated with Metformin/Rosiglitazone)	PM <sub>2.5</sub> collected June 2009 and December 2010 in Louisville, KY. Whole-body exposure, 6 hr/day for 9 or 30 days at 30-120 µg/m <sup>3</sup>
(64)	PM <sub>2.5</sub> decreased insulin-stimulated Akt/eNOS phosphorylation and IκBα, antioxidant treatment attenuated vascular insulin resistance and inflammation	C57BL/6J male mice, 12 wks old (control/high-fat diet), pre-treated with TEMPOL	PM <sub>2.5</sub> collected June 2009 and December 2010 in Louisville, KY. Whole-body exposure, 6 hr/day for 9 or 30 days at 30-120 µg/m <sup>3</sup>
(79)	PM <sub>2.5</sub> increased phospho-EGFR (Tyr1068), phospho-Akt (Thr308), NLRP3, NF-κB-p52/p100, and NF-κB-p65 in heart, as well as CXCL1, IL-6, IL-18, and NLRP12 mRNA	BALB/c mice, 6–8 wks old	PM <sub>2.5</sub> collected November 2014 in a major city of central China. Intratracheal instillation of 4.0 mg/kg b.w. for 5 consecutive days.
(93)	PM <sub>2.5</sub> decreased SOS1, CREB, GSK3b, and GRB2 expression, fucoidan treatment rescued all but CREB levels.	C57BL/6J mice, 8 wks old	PM <sub>2.5</sub> collected November–December 2016 in Taipei, Taiwan. 100µg/m <sup>3</sup> , 28 days, 6 hrs/day
(95)	PM <sub>2.5</sub> caused mitochondrial size/cristae deformation (increased FIS1, MFN1, MFN2, DRP1, OPA1), inflammation (increased TNF-α, IL-6, IL-1β), decreased SOD, increased MDA and iNOS	Sprague Dawley rats	PM <sub>2.5</sub> collected January 2013 in Taiyuan, China. Intratracheal instillation of 0.375, 1.5, 6.0, and 24.0 mg/kg b.w. performed 5 times
(98)	PM <sub>2.5</sub> increased Caspase-3, Bax, Bcl-2 in heart, and NF-κB in cardiac myocytes	Male C57/BL6 mice, 8 wks old	PM <sub>2.5</sub> was collected in, Nanjing, China. 10µg PM <sub>2.5</sub> (10µl) twice a week/intranasal instillation.
(99)	Acute PM <sub>2.5</sub> exposure decreased 5-mC methylation and DNMT1 mRNA expression in heart and blood. Chronic PM <sub>2.5</sub> exposure decreased these factors only in blood	C57BL/6J male mice, 7 wks old	PM <sub>2.5</sub> (collection location not stated), whole-body acute exposure (24 hrs -PM <sub>2.5</sub> dose of 271.8 ± 86.8 µg/m <sup>3</sup> ) and chronic exposure (140 days-PM <sub>2.5</sub> dose of 271.8 ± 86.8 µg/m <sup>3</sup> )
(103)	PM <sub>2.5</sub> increased inflammation, high intensity exercise stimulates reduced inflammation (eHSP70)	Male B6.129SF2/J mice, 30 days old	PM <sub>2.5</sub> collected in São Paulo, Brazil, 5 µg nasotropic instillation daily before exercise 12 wks
(114)	DEP (PM <sub>2.5</sub> ) increased PAI-1, fibrinogen, lipid peroxidation, IL-6. Nootkatone pretreatment alleviated all and reduced thrombosis with increased Nrf2 and HO-1 activation.	BALB/C mice, 8 wks old	Diesel exhaust particles (DEP) with a geometric mean aerodynamic diameter of 215 nm from the National Institute of Standards and Technology, MD, USA. Intratracheal instillation of 30 µg/mouse
(123)	PM <sub>2.5</sub> exposure in atherosclerosis model increased MDA and NOX-4 subunits (p22 <sup>phox</sup> , p47 <sup>phox</sup> ) in cardiac tissue	Male ApoE <sup>-/-</sup> Tg mice, 8 wks old	PM <sub>2.5</sub> collected June–October 2013 in Shanghai, China. Intratracheal installation at 0–30 mg/kg b.w
(127)	PM <sub>2.5</sub> exposure was associated with elevated levels of CD14 <sup>+</sup> , CD16 <sup>+</sup> , CD4 <sup>+</sup> , CD8 <sup>+</sup> , endothelial microparticles (annexin V <sup>+</sup> /CD41 <sup>+</sup> /CD31 <sup>+</sup> ), anti-angiogenic (TNFα, IP-10) and pro-inflammatory cytokines (MCP-1, MIP-1α/β, IL-6, IL-1β), and sICAM-1, sVCAM-1 as well as decreased pro-angiogenic growth factors (EGF, sCD40L, PDGF, RANTES, GROα, and VEGF).	72 young, healthy, non-smoking subjects (24 individuals per 3 winter/ spring time periods (2013, 2014, and 2015))	PM <sub>2.5</sub> ambient air concentrations in Utah Valley from 3 monitoring sites (Lindon, North Provo, and Spanish Fork) measured daily. At Lindon and North Provo sites, hourly PM <sub>2.5</sub> concentrations were used to estimate the average concentration for the ~24-h period before each blood draw
(131)	PM <sub>2.5</sub> increased fibrosis (Col1a1, Col3a1), oxidative stress (NOX-4), transcription factor binding (TGFB1, SMAD3)	Female C57BL/6, 10 months and 4 wks old	PM <sub>2.5</sub> collected 2012 and 2013 from Taiyuan, Northern China. 3 mg/kg, b.w. PM <sub>2.5</sub> oropharyngeal aspiration every other day for 4 wks

(133)	CAPs exposure increased 7-KCh in plasma and aortic plaques, and increased CD36 expression in plaque-macrophages and CD36 uptake of oxidized lipids	ApoE <sup>-/-</sup> Tg and LDLR <sup>-/-</sup> Tg mice, 8 wks old	Concentrated ambient PM <sub>2.5</sub> collected in Columbus, OH. Mice xposed for 6 months to 9.1±7.3 μg/m <sup>3</sup>
(135)	12.4% decrease in RHI for every 10μg/m <sup>3</sup> increase in PM <sub>2.5</sub> . IsoP, angiopoietin 1, VEGF, PlGF, MMP-9, ICAM-1 positively associated with 10μg/m <sup>3</sup> increases in PM <sub>2.5</sub> , decreased VCAM-1.	100 male and female participants (44% had type 2 diabetes, 52% had diagnosis of hypertension)	PM <sub>2.5</sub> levels obtained from 5 monitoring stations in Jefferson County, KY (June 2011–May 2013) with average concentration of 11.45μg/m <sup>3</sup> .
(140)	PM <sub>2.5</sub> increased Hsp-70, HO-1, MPO in heart as well as laminin, collagen, and calcium signaling proteins (181 upregulated, 178 downregulated genes)	Male BALB/c mice, 7–8 wks old	PM <sub>2.5</sub> with high PAH, nitrite, and organic carbon levels collected winter 2008 in an urban site (Milano, Italy). Intratracheal instillation on days 0, 3 and 6, at 0.3 mg/mouse
(157)	TRPA1 activation increases negative cardiovascular responses to CAPs exposure through myocardial dyssynchrony.	Trpa1 <sup>tm1Kyk/J</sup> (Trpa1 <sup>-/-</sup> ) Tg female mice	PM <sub>2.5</sub> collected November–December of 2014 in Triangle Park, NC. 3 hrs/day, 2 days/week, 8 total whole-body exposures
(161)	PM <sub>2.5</sub> exposure increased oxidative stress (PRNP) and endoplasmic reticulum stress (GRP78). Nanoparticles found in myocardial ER and in abnormal mitochondria	30 children and young adults ~20 years old	PM <sub>2.5</sub> data obtained in Mexico City Metropolitan Area 1997-2012
(165)	PM <sub>2.5</sub> increased fibrosis and collagen genes, and oxidative stress (8-OHdg and 4-HNE), reduced antioxidant genes (PRDX5)	Male AMPK α2 <sup>-/-</sup> Tg mice, 6–8 wks old	PM <sub>2.5</sub> collected April–October 2016 in Beijing, China. Intratracheal instillation for 6 months at 10 mg/kg (64μg/m <sup>3</sup> ).
(167)	PM <sub>2.5</sub> exposure in hyperlipidemic rats increased CRP, JNK and P53 phosphorylation, and increased Bax and Caspase-3 in the heart, decreased SOD	Male Wistar rats, 8 wks old, on high-fat diet	PM <sub>2.5</sub> collected October–December 2012 in Beijing, China. Endotracheal instillation of suspension at 0, 4, 40 mg/kg
(170)	Higher PM <sub>2.5</sub> resulted in myosin heavy chain isoform switch (increased β-MHC) and decreased SERCA2a	C57BL/6 male mice, 8 wks old	Concentrated PM <sub>2.5</sub> in Columbus, OH. Mean daily concentration of PM <sub>2.5</sub> in the exposure chamber was 85.3 μg/m <sup>3</sup> . Mice were exposed for 6 h/d, 5 d/wk, for 9 months.
(173)	PM <sub>2.5</sub> increased MDA, iNOS activity, TNF-α, IL-1β, along with NOX4 and NOX subunits as p67 <sup>phox</sup> , p47 <sup>phox</sup> and p22 <sup>phox</sup> in the heart and reduced SOD activity	C57BL/6 mice, 6–8 wks old	PM <sub>2.5</sub> collected September 2013 in Zhengzhou, Taiwan. Instilled with 1.5, 3.0, 6.0 mg/kg BW 5 days/wk for 2 wks
(181)	PM <sub>2.5</sub> decreased GSH-Px, increased MDA and sICAM-1. SeY treatment reduced inflammation markers (TNF-α, IL-1β, sICM-1)	Male Sprague Dawley rats, 7 wks old	PM <sub>2.5</sub> collected September–November 2015 in Shanghai, China. Intratracheal instillation at 40 mg/kg
(185)	PM <sub>2.5</sub> exposure in diabetic model induced NF-κB, COX-2, MAPK in heart, IκB inhibitor restored function through NF-κB reduction	KKay Tg mice, 7 wks old	PM <sub>2.5</sub> collected Polaris in Columbus, Ohio. Intratracheal instillation for 6 hr/day, 5 day/week, 8 weeks at dose of 1.6 mg/kg
(186)	PM <sub>2.5</sub> increased DNA damage (increased OGG1 and GADD153, decreased MTH1 and XRCC1) in the heart and decreased SOD	Male Wistar rats	PM <sub>2.5</sub> containing PAHs collected Taiyuan, China. Intratracheal instillation of 1.5 mg/kg b.w. PM <sub>2.5</sub> , 1.6 × 10 <sup>-4</sup> mg/kg b.w. 1-NP, 1.2 × 10 <sup>-4</sup> mg/kg b.w. 9-NA
(188)	Higher PM <sub>2.5</sub> correlated with increased blood TLR2 methylation, flavonoid intake decreased TLR2 methylation	Normative Aging Study, 573 participants	PM <sub>2.5</sub> data collected from Harvard School of Public Health
<i>Gestational</i>			
(27)	PM <sub>2.5</sub> exposure increased GATA4, NKX2-5 and inflammatory markers (TNF-α and IL-1β) homocysteine exacerbates these effects	Female Sprague Dawley rats, 10 wks old, neonatal progeny	PM <sub>2.5</sub> collected Fujian, China. Exposed during gestation and lactation (~42 days) to 36.5 μg/m <sup>3</sup> through a whole-body inhalation system.
(57)	DE PM <sub>2.5</sub> caused promoter methylation of microRNA-133a-2 in progeny and cardiovascular stress decreased microRNA 133a-2 expression	Female C57BL/6 12–14 wks old, 12 wk-old progeny	PM <sub>2.5</sub> collected a single cylinder Yanmar diesel engine, operating at 82% load ~300 μg/m <sup>3</sup> for 6 hrs/day for a total of 5 days during pregnancy
(153)	PM <sub>2.5</sub> preconception exposure increased inflammatory markers (IL-6, IL-15, NfκB, CRP, CD26E, CD26P, VCAM-1, MCP-1), fibrosis (Col3a1), Ca <sup>2+</sup> regulation (SERCA2a, p-PLN), and altered epigenetics (DNMT1↓, SIRT1↑, SIRT2↑)	Paternal and maternal FVB mice exposure – male 12 wk-old progeny	PM <sub>2.5</sub> collected Columbus, OH. Average 38.58 μg/m <sup>3</sup> for 6 hrs/day, 5 days/week for 3 months through a whole-body inhalation system preconception
(154)	PM <sub>2.5</sub> induced changes in calcium dynamics by decreasing NCX and Cav1.2	Female FVB mice, 12 wks old 14-day old progeny	PM <sub>2.5</sub> collected Columbus, Ohio. Exposed 6 hr/day, 5 days/week, average 91.78 μg/m <sup>3</sup> through a whole-body inhalation system during pregnancy
(155)	PM <sub>2.5</sub> decreased SIRT1, SIRT2, increased DNMT1, DNMT3a, DNMT3b, decreased Ca <sup>2+</sup> markers (NCX, p-PLN, SERCA2a) and increased IL-1β, IL-6, Col-1, MMP9, MMP13A	Female FVB mice, 12 wks old 12 wk-old progeny	PM <sub>2.5</sub> collected Columbus, OH. 6 hr/day, 7 days/week throughout pregnancy, average 73.61 μg/m <sup>3</sup> through a whole-body inhalation system
(164)	PM <sub>2.5</sub> caused a dose-dependent increase of OPA1, MFN1, DRP1, and FIS1 in progeny.	Female Wistar rats, 10–12 wks old, 1-day old progeny	PM <sub>2.5</sub> collected September 2014 to March 2016 in Harbin, China. Administered dropwise, 3 doses (0.375 mg/kg, 1.5 mg/kg, and 6.0 mg/kg) during pregnancy
(174)	PM <sub>2.5</sub> increased histone acetyltransferase (H3K9ac), GATA4, and MEF2c. Exposure also increased histone acetylation of GATA4/MEF2c promoters	Female C57BL/6 mice, 12 wks old, 1 day and 16 wk-old progeny	PM <sub>2.5</sub> collected Chongqing, China. Gestational exposure by ultrasonic nebulization, 2 hours a day during pregnancy, at ~300 μg/m <sup>3</sup>
<b>UFP</b>			
(4)	UFP exposure increased AT <sub>1</sub> R protein along with Act1 and Col3a1 in the heart, with decreased HO-1 expression	Male Sprague-Dawley rats	UFP collected north of Mexico City (May–July 2009). Acute (3 days, 5 hr/day) and sub-chronic (8 weeks, 4 days/week, 5 hr/day) exposure to varying concentrations.
(36)	UCAPs exposure decreased blood plasminogen and thrombomodulin, increased CRP and SAA. GSTM1 null participants had worse outcomes	34 participants with metabolic syndrome, ~48 years old	UCAPs collected at US EPA facility Chapel Hill, NC. Whole-body exposure for 2-hrs at average particle concentration of 189,000 particles/cm <sup>3</sup> .

(70)	UFP exposure cause mitochondrial mPTP deficits, Cyclosporin A resulted in attenuation	Male Sprague-Dawley rats	UFP collected US EPA facility Chapel Hill, NC. 100 µg UFP laryngopharynx instillation
(90)	TAA-PNC of UFP was positively associated with CRP and TNFR2 in white non-Hispanic participants	408 individuals aged 40-91 years old	UFP (near-highway, long-term exposure) Dorchester, South Boston, Chinatown (Boston)
(147)	Elemental carbon UFP exposure increased platelet CD40L and vWF, and decreased circulating CD40L	19 type 2 diabetics, 30-60 years old, never smoked	UFP particles were generated at 32nm. Elemental carbon UFP through mouth piece for 2 hr at 50 µg/m <sup>3</sup>
(159)	UFCP exposure increased CRP and fibrinogen in systemic circulation	Male spontaneously hypertensive rats (SHRs), 12-13 months old	UFCP exposure at 180µg/m <sup>3</sup> in a 24-hour time frame
(183)	Increasing UFCP concentrations prevented the beneficial effects of captopril in reducing AngII.	Spontaneously hypertensive rats (SHRs), 10 wks old	UFP collected Beijing, China. Intratracheal instillation of UFCP (0.15 mg/kg, 0.45 mg/kg and 1.35 mg/kg) and captopril administration.
<i>Gestational</i>			
(109)	UFP exposure induced placental HSD11B2 DNA methylation, elevated IL-1β, IL-6 and MCP-1, and caused increased activation of AT1R and ACE	Female C57BL/6J <i>p<sup>um</sup>/p<sup>um</sup></i> mice, 6 wks old. Gestational Day 17.5 progeny	UFP collected in northern Mexico City (April-June 2016). Intratracheal instillation of 12 µg or 400 µg/kg during pregnancy
(139)	UFP exposure caused higher serum levels of IL-10 in C67BL/6 progeny	Female C57BL/6 and BALB/C mice. Progeny 0-4 wks old	UFP generated with average mass concentration of 101.94 µg/m <sup>3</sup> . 24-h daily mean dose of 25 µg/m <sup>3</sup> during pregnancy
<b>Engineered Nanomaterials and Advanced Materials</b>			
(54)	Carbon nanoparticle-inhalation, compared to intra-arterial injection, was more detrimental to cardiac tissue with perturbation of inflammatory and endothelial/epithelial pathways	Female BALB/cJ mice, 10-12 wks old	Carbon nanoparticles with primary particle diameter of 10 ± 2 nm. Administered through intra-arterial infusion (30mm <sup>2</sup> per animal) and inhalation (lung deposited dose 10,000mm <sup>2</sup> ). Whole body exposure for 4 or 24 hours
(65)	Nano-TiO <sub>2</sub> -exposed microRNA-378a Tg mice had higher MFN1 levels (fusion), and preserved metabolic profiles and ultrastructure in the heart	FVB and miRNA-378a knockout Tg mice aged 14-18 wks old	Nano-TiO <sub>2</sub> , particle size (21 nm)/surface area (48.08 m <sup>2</sup> /g). Whole-body inhalation exposure at a dose of 11.09 mg/m <sup>3</sup> for 4 hrs
(71)	Nano-TiO <sub>2</sub> exposure increased inflammatory markers (NF-κB, TNF-α, IL-4, IL-6, TGF-β, CK, CRP, IFN-γ) and transcriptional regulators (STAT1, STAT3, STAT6, GATA3, GATA4)	CD-1 (ICR) male mice, 4 wks old	Nano-TiO <sub>2</sub> prepared through hydrolysis of Ti(OBu) <sub>4</sub> . Administered via nasal instillation of mice every other day for 6 months. Treatment of 1.25 - 5 mg/kg TiO <sub>2</sub> NPs
(77)	Nano-TiO <sub>2</sub> exposure caused blood specific activation of C3, and heart-specific activation of the complement cascade	Female C57BL/6 mice, 8 wks old	Nano-TiO <sub>2</sub> , UV-Titan L181. 6.0 mg Ti/m <sup>3</sup> -10 mg TiO <sub>2</sub> /m <sup>3</sup> administered through intratracheal instillation
(116)	Nano-TiO <sub>2</sub> -exposed mPHGPx Tg mice had reduced ROS and preserved electron transport chain complex constituents in the heart	Male FVB and male mPHGPx Tg mice 10-12 wks	Nano-TiO <sub>2</sub> , particle size (21 nm)/surface area (48.08 m <sup>2</sup> /g). 11.58 ± 0.27 µg lung deposition, whole-body inhalation exposure for 6 hrs
<i>Gestational</i>			
(66)	Nano-TiO <sub>2</sub> exposure increased cardiac mitochondrial proton leak (UCP2), and fatty acid metabolism (increased CPT1A and PDH phosphorylation)	Female Sprague Dawley rats 10-12 wks, 12 wk-old progeny	Nano-TiO <sub>2</sub> , particle size (21 nm)/surface area (48.08 m <sup>2</sup> /g). 7.79 ± 0.26 days, 5 hr/day, 10.35 ± 0.13 mg/m <sup>3</sup> through a whole-body inhalation system during pregnancy
(87)	Nano-TiO <sub>2</sub> exposure increased ROS (H <sub>2</sub> O <sub>2</sub> ), global 5-mC methylation, DNMT1 protein expression, and HIF-1α activity and downregulated mPHGPx in the heart	Female FVB 12 wks old, Gestational day 15 fetal progeny, 11 wk-old adult progeny	Nano-TiO <sub>2</sub> , particle size (21 nm)/surface area (48.08 m <sup>2</sup> /g). Whole-body inhalation exposure at a dose of 12.09 ± 0.26 mg/m <sup>3</sup> for 6 days (over 8-day period), 6hr/day, starting from gestational day 5
(143)	Nano-TiO <sub>2</sub> exposure resulted in cardiac mitochondrial epigenomic remodeling (increased H3K4Me3) and decreased transcriptomic immune response	Female Sprague Dawley rats 10-12 wks old, Gestational day 20 fetal progeny	Nano-TiO <sub>2</sub> , particle size (21 nm)/surface area (48.08 m <sup>2</sup> /g). Whole-body inhalation exposure at a dose of 10.35 ± 0.13 mg/m <sup>3</sup> for 7.79 ± 0.26 days during gestation
(145)	Nano-TiO <sub>2</sub> exposure decreased State 3 and State 4 mitochondrial respiration	Female Sprague Dawley rats, female 11-16 wk old progeny	Nano-TiO <sub>2</sub> , particle size (21 nm)/surface area (48.08 m <sup>2</sup> /g). Whole-body inhalation exposure at a dose of 10.6 ± 0.3 mg/m <sup>3</sup> for 6.8 ± 0.5 days during gestation
<b>Multi-component Exposure</b>			
(9)	Higher PM <sub>2.5</sub> BC, and mass PM <sub>2.5</sub> exacerbated hypomethylation of IFN-γ and ICAM-1	Normative Aging Study, 777 elderly men	PM <sub>2.5</sub> mass concentration and PM <sub>2.5</sub> BC concentration measured hourly at the Harvard supersite Boston, MA
(10)	Higher black carbon concentration associated with 12% reduction in F3 methylation	Normative Aging Study, 777 elderly men	PM <sub>2.5</sub> , BC, SO <sub>4</sub> , and ozone concentrations of ambient air collected from Boston, MA were measured hourly
(32)	Increases in PM <sub>2.5</sub> , BC, and UFP concentrations were positively associated with inflammation (CRP and fibrinogen) and coagulation, but not endothelial dysfunction, Delta-C increasing concentrations associated positively with fibrinogen and negatively with MPO	135 patients undergoing cardiac catheterization	Ambient air pollution, Delta-C (wood-smoke), PM <sub>2.5</sub> , BC, UFP collected from New York State Department of Environmental Conservation (DEC) site in Rochester, NY
(43)	PM <sub>2.5</sub> levels, but not UFP, were positively associated with hsa-miR-197-3p and hsa-miR-99a-5p	59 volunteers (20 were healthy, 20 had COPD, 19 had ischemic heart disease)	Ambient air pollution exposure (personal exposure level measurements of PM <sub>10</sub> and PM <sub>2.5</sub> , UFP, nitrogen oxides, BC, CO) during 2-hour walk. Oxford Street or Hyde Park, London, England
(48)	SiNP and Pb co-exposure elevated markers of heart failure (ANP and BNP), inflammation (CRP, IL-6, TNF-α) in heart and increased ANGII and ET-1 in serum. T-PA, TFPI, AT III decreased while fibrinogen and D2D increased with co-exposure	Sprague Dawley rats, 6 wks old	Stöber technique was used to synthesize SiNPs. Intratracheal instillation of 2 mg/kg body SiNPs and/ or 0.25 mg/kg of lead acetate (Pb) for 30 days.

(84)	54 circulating miRNAs were correlated with dose of exposure and pollution type	24 non-smoking adults	PM <sub>2.5</sub> , NO <sub>2</sub> , UFP, BC, PM <sub>10</sub> collected on Oxford Street in London, 2-hour exposure
(86)	UFP, CO, SO <sub>2</sub> exposure was associated with increased inflammatory markers (IL-6, IL-8, ET-1) in blood	52 men and women 18-34 years old	UFP, CO, SO <sub>2</sub> concentrations collected in Sault Ste. Marie, Ontario, Canada (Summer of 2010). Occupational air pollution
(96)	PM <sub>2.5</sub> and SO <sub>4</sub> increases associated with CRP levels, NO <sub>x</sub> positively associated with IL-6, BC, sulfate, ozone positively associated with TNFR2	3,996 non-smoking participants Framingham Offspring cohort cycle 7 and 8 and Third Generation cohort 1	PM <sub>2.5</sub> , BC, SO <sub>4</sub> <sup>2-</sup> , nitrogen oxides, and ozone collected at the Boston Harvard Supersite and assessed as 7-day moving average
(97)	Higher PM <sub>2.5</sub> and BC concentrations were associated with lower P-selectin levels	3,820 non-smoking participants Framingham Offspring cohort cycle 7 and 8 and Third Generation cohort 1	PM <sub>2.5</sub> , BC, SO <sub>4</sub> <sup>2-</sup> , nitrogen oxides, and ozone collected at the Boston Harvard Supersite and assessed as 7-day moving average
(101)	Nickel, barium, and silver levels were positively correlated with VEGF, UCHL1, and cortisol	53 healthy participants, 18–60 years old	Particulate matter collected in downtown Toronto, Canada. 130-min exposure to PM <sub>10</sub> (213 µg/m <sup>3</sup> ), PM <sub>2.5</sub> (238 µg/m <sup>3</sup> ), and/or concentrated UFP (213µg/m <sup>3</sup> )
(102)	Higher BC is associated with decreased methylation of Alu and both increased SO <sub>4</sub> and BC resulted in decreased methylation of LINE-1	Normative Aging Study, 706 individuals	PM <sub>2.5</sub> , BC, SO <sub>4</sub> data collected from Harvard School of Public Health during January 1995 to November 2007
(110)	PM <sub>2.5</sub> concentration was positively associated with 69 differentially methylated regions, 13 CpG sites, including altered methylation of KNDC1 and FAM50B. UFP was also associated with 15 differentially methylated regions	157 non-smoking adults	PM <sub>2.5</sub> and UFP levels collected in personal and ambient air pollution, measured in 24-hour intervals, part of EXPOSOMICS project conducted in 4 European countries (December 2013–February 2015)
(118)	BC was associated with sVCAM-1, sICAM-1, and vWF. PM <sub>2.5</sub> was associated with sVCAM-1 and sICAM-1 in patients not taking statins. In smokers, PM <sub>2.5</sub> and BC were positively associated with sVCAM-1	60 male and 37 female participants with type 2 diabetes (smokers and non-smokers)	PM <sub>2.5</sub> (1998–2002) and BC (1999–2002) measured hourly and SO <sub>4</sub> <sup>2-</sup> measured daily (1999–2002) at the Harvard School of Public Health (Boston, MA)
(132)	PM <sub>2.5</sub> mass concentration showed positive trend with HDL-oxidant index (HOI). Changes not seen with ozone co-exposure.	30 participants, 19–37 years old	PM <sub>2.5</sub> (149 µg/m <sup>3</sup> ), ozone (221 µg/m <sup>3</sup> ), and PM <sub>2.5</sub> and ozone data collected from Toronto, Canada as part of Clean Air Research Center Project.
(158)	PM <sub>2.5</sub> and quasi-ultrafine particles <0.50 µm dysregulated parasympathetic response and increased IFN-γ methylation in blood	12 healthy participants	Particulate matter collected Milan, Italy. Inhalation to mixture (PM <sub>10</sub> , PM <sub>2.5</sub> , PM <sub>1.0</sub> and PM <sub>0.5</sub> µm) over 2 sessions
(160)	PM <sub>2.5</sub> exposure was associated with higher inflammation (CRP) and coagulation (platelet count in blood)	3275 participants	Ambient air pollution PM <sub>10</sub> and PM <sub>2.5</sub> levels from the German Heinz Nixdorf Recall Study, three adjacent cities (Essen, Mülheim, Bochum)
(163)	Co-exposure potentiated increases in CRP, IL-6, CK, LDH, and MDA, and decreased SOD	Male Wistar rats (age not defined)	PM <sub>2.5</sub> (varying doses), ozone (0.81 ppm), PM <sub>2.5</sub> and ozone collected June–October 2011 in Shanghai, China. Administered as whole-body inhalation exposure (ozone) and intratracheal instillation (PM <sub>2.5</sub> )
(169)	BC, CO, NO <sub>x</sub> , and PAHs positively associated with IL-6 and TNF-α, quasi-ultrafine particles <0.25 µm were also associated with IL-6. Associations were stronger for haplotype H than haplotype U	36 participants, ~84 years old	Particulate matter (PM-varying sizes), nitrogen oxides (NO <sub>x</sub> ), carbon monoxide (CO), organic and elemental carbon (OC and EC), collected from four retirement communities in the Los Angeles air basin
(176)	SiNP and MeHg co-exposure caused cardiac injury through changes in serum biomarker activity including increased SERCA2, cTnT, ANP, and BNP	Sprague Dawley rats, 6 wks old	Silica nanoparticles (SiNPs) and methylmercury (MeHg) administered through intratracheal instillation 10 times over 30 days at doses of 0.25 mg/kg (MeHg) and 2 mg/kg (SiNPs)
(184)	Co-exposure (PM <sub>2.5</sub> , SO <sub>2</sub> , and NO <sub>2</sub> ) causes endothelial dysfunction (increased ET-1 and decreased eNOS) and inflammation (increased COX-2, iNOS, TNF-α, IL-6)	Male C57BL/6 mice, 6–8 wks	PM <sub>2.5</sub> , SO <sub>2</sub> , and NO <sub>2</sub> , collected Taiyuan, China. Intranasal instillation every other day for 6 hrs/28 days, 0.5/3.5 mg/m <sup>3</sup> SO <sub>2</sub> , 0.2/2 mg/m <sup>3</sup> NO <sub>2</sub> , 1/10 mg/kg PM <sub>2.5</sub>

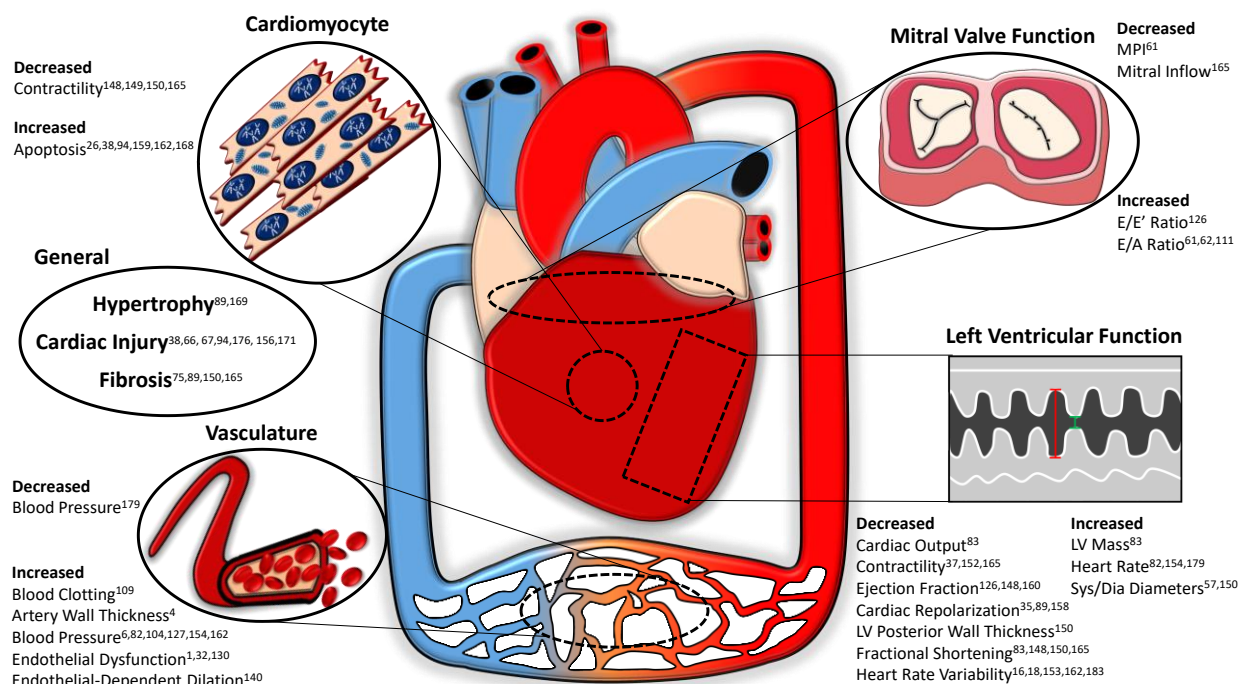
**Table 1.1: Summarized Recent Findings.** Summarized findings of the molecular mechanisms contributing to cardiovascular complications following particle inhalation exposure. Studies are organized by exposure (PM<sub>2.5</sub>, UFP, ENM, and Multi-component), including subsections for gestational and preconception exposures. All abbreviations are defined in the Glossary of Abbreviations provided.

### *Cardiac Remodeling*

While inhalation exposure directly impacts the lungs, the subsequent downstream adaptations of the heart can lead to sustained cardiac remodeling. This remodeling can be presented

in the form of fibrosis, hypertrophy, and other structural changes to both the cardiomyocyte and the surrounding connective tissue of the heart. In understanding how this process occurs, examining the biochemical signature linked to cardiac remodeling changes associated with toxicant inhalation exposure can provide insight for future investigations into prevention and treatment. The reported cardiovascular adaptations that occur as a result of toxicant inhalation exposure are depicted in **Figure 1.1**.

**Figure 1.1: Cardiovascular Changes following Exposure.**



**Figure 1.1:** Summary of the cardiovascular changes following particulate inhalation exposures and the associated studies detailing these findings. Sys = systolic, Dia = diastolic, LV = left ventricular, MPI = myocardial performance index.

Cardiac fibrosis involves the imbalance of extracellular matrix production and degradation, which results in accumulation of scar tissue. Cardiac fibrosis, which occurs as a result of PM

exposure, therefore decreases compliance, impairing the ability of the heart to contract and relax properly. PM<sub>2.5</sub> exposure results in elevation of several genes linked to collagen deposition (collagen type I alpha 1 (Col1a1) and collagen type III alpha 1 (Col3a1)) and the fibrogenic growth factor, transforming growth factor beta 1 (TGFβ-1) (131). Simultaneously, NADPH oxidase (NOX-4) is increased, matching the resultant cardiac dysfunction and prooxidative environment found in the heart following PM exposure. Of note, Qin et al. also further demonstrated that the effects of PM<sub>2.5</sub> are worse in older mice, making them more susceptible to prolonged cardiac systolic dysfunction marked by decreased ejection fraction and increased E/E' ratio when compared to juveniles (131). PM<sub>2.5</sub>-induced fibrosis is also related to cardiac inflammation in the hearts of mice, which show elevated expression of inflammatory genes including interleukin (IL)-6, IL-18, and C-X-C motif chemokine ligand 1 (CXCL1) (79). Inflammation and fibrosis in the heart may be attributed to increased phosphorylation and therefore activation of epidermal growth factor receptor (EGFR)/Akt signaling and increased expression of nuclear factor-kappa beta (NF-κB) following inhalation exposure. NF-κB expression in the heart is likewise increased as a result of PM<sub>2.5</sub> exposure in diabetic mice, along with cyclooxygenase-2 (COX-2) and mitogen activated protein kinase (MAPK), indicating high oxidative stress and inflammation (185). Intracerebroventricular injection of an inhibitor of IκB kinase-2 (IKK) analog (IMD-0354), which regulates the nuclear translocation of NF-κB, can remediate the inflammatory response that occurs following PM exposure. While NF-κB plays an important role in the cardiovascular effects of PM inhalation exposure, other inflammatory markers contribute to cardiac remodeling. Cardiac injury and inflammation that occurred following PM<sub>2.5</sub> exposure were attenuated with supplementation of vitamin E and omega-3 polyunsaturated fatty acids prior to the exposure in rats by decreasing expression of tumor necrosis factor-α (TNF-α), IL-1β, and IL-6 (39). In addition to TNF-α and IL-1β, PM<sub>2.5</sub> exposure also induces soluble intercellular adhesion molecule 1 (ICAM-1) (181). Together, these inflammatory markers can form a positive feedback loop with NF-κB, amplifying PM-induced cardiac fibrosis and remodeling. Selenium yeast (SeY) supplementation can similarly serve as a pretreatment protective strategy, as reported in Sprague Dawley rats that were subsequently exposed to PM<sub>2.5</sub> (181). PM-exposed rats who were administered SeY pretreatment had lower levels of pro-inflammatory markers and significantly higher total antioxidant capacity, total superoxide dismutase (SOD) and total glutathione peroxidase (GSH-Px), compared to the PM<sub>2.5</sub>-exposed group without pretreatment (181). The ability of antioxidant therapy to thwart the

perpetuation of inflammatory signaling associated with cardiac remodeling highlights the essential role of oxidative stress in the development of cardiac pathology following ambient air exposure. Understanding the proteins involved in the regulation of reactive oxygen species (ROS) may provide insight into long-term remodeling of the heart. While most population-derived analyses assess cardiovascular impact in blood samples, a study of the effects of UFP urban air pollution utilized post-mortem ventricular autopsies of 30 children and young adults to substantiate that early and prolonged cardiac stress can result in irreversible consequences (161). Compared to clean air controls, long-term UFP exposure results in significant upregulation of proteins involved in oxidative (prion protein (PRNP)) and endoplasmic reticulum (ER) (glucose regulated protein 78 (GRP78)) stress. These response markers of stress were disproportionately upregulated in the left, compared to right, ventricle. Along with abnormal left-ventricular histopathology, increased oxidative and ER stress markers suggest a compensation by the heart to attenuate the inflammatory effects of air pollution in response to UFP exposure (161). GRP78 elevation in cardiomyocytes is sufficient to promote myocyte growth, potentially through stimulation of cardiac-specific transcriptional factor GATA sequence binding protein 4 (GATA4) (182). Similar to UFP, nano-TiO<sub>2</sub> exposure in outbred mice can lead to an increase in cardiac lesions and a significant change in inflammation markers, including changes in transcription factors (signal transducer and activator of transcription (STAT) 1/3/6 and GATA 3/4) in the heart (71). The ability for oxidative and inflammatory proteins to activate transcription factors such as GATA4 is therefore notable, particularly following UFP/ENM exposure, as they appear to have strong correlations with cardiac hypertrophy. Fine PM exposures can also lead to sustained detrimental effects in the heart by altering the transcription factor profile. One example of this has been shown previously in a cohort of PM<sub>2.5</sub>-exposed mice (93). Cardiac remodeling through hypertrophy, QT interval prolongation, and fibrosis were correlated with elevated cAMP response element binding protein (CREB), as well as SOS Ras/Rac Guanine Nucleotide Exchange Factor 1 (SOS1), and glycogen synthase kinase 3 beta (GSK3 $\beta$ ) expression. Measuring biomarkers associated with myocardial infarction can also provide information on the extent of cardiac tissue dysfunction and death. An examination of the cardiovascular effects of a co-exposure model using silica nanoparticles (SiNP) and methylmercury (MeHg) has shown increases in myocardial edema, myocardial gap expansion, and myofibril disorder, as well as increases in activities of myocardial enzymes including cardiac troponin T (cTnT), atrial natriuretic peptide (ANP) and brain natriuretic peptide (BNP) compared

to the serum of single exposure and sham-exposed rats (176). The authors also report increased sarco/endoplasmic reticulum  $\text{Ca}^{2+}$ -ATPase (SERCA2), a potential marker of endoplasmic reticulum stress (69), in the co-exposure cohort along with oxidative stress. Similar to the preceding studies mentioned, co-exposures can induce cardiac remodeling by increasing oxidative and ER stress, and elevating prominent markers of heart failure. PM exposures, including UFP, ENM, and multi-component exposure, all have the ability to alter the transcription factor profile in the heart and lead to sustained detrimental effects on cardiac structure. The molecular adaptations to particle exposures that result in cardiac remodeling center around a theme of inflammation and oxidative stress, which may ultimately be regulated by a greater transcriptional and epigenetic adaptation following toxicant inhalation exposure.

### *Cardiac Hemodynamics*

The performance of the heart can highlight both the acute and chronic effects of toxicant inhalation exposure. Although cardiac remodeling provides an informative diagnostic standard for assessing the impacts of PM exposure, more immediate changes are captured in measures of heart function. Whether there is a sustained or transient perturbation to the heart is likely determined by the molecular cascades involved, such as transcriptional or epigenetic reprogramming.

Controlled studies on human exposure to PM allow for the most relevant simulation of pollutant exposure, while also limiting interference of confounding factors. Measurements of blood methylation levels in 15 healthy participants revealed that both fine and coarse concentrated ambient particle (CAP) exposures induce hypomethylation of the Alu repetitive transposable element and toll-like receptor 4 (TLR4) (6). Decreased methylation of the short interspersed nucleotide element, Alu, and TLR4 was also associated with higher systolic blood pressure post-exposure, which is similar to previous findings that have shown a role for hypomethylation in atherosclerosis (23). Other studies have reported similar findings with specific components of  $\text{PM}_{2.5}$ , including with black carbon (BC). Over a 90-day period, increased BC levels correlated with decreased methylation of Alu, while both carbon black and sulfate ( $\text{SO}_4$ ) were associated with decreased methylation of long interspersed nuclear element-1 (LINE-1) (102). Interestingly, in a study examining occupational exposure to  $\text{PM}_{2.5}$ , methylation of LINE-1 was significantly increased in peripheral blood leukocytes of participants, but was not directly associated with



declining heart rate variability (HRV) (44). When DNA methylation is altered, it has the potential to activate pro-inflammatory factors or repress anti-inflammatory factors, and can therefore activate pathways that are prevalent in the development of cardiovascular diseases. The discrepancy of whether toxicant exposure results in hypo- or hypermethylation can likely be attributed to different exposure environments (controlled or ambient), duration and concentration. The concentration of PM<sub>2.5</sub> during exposure was positively associated with toll-like receptor 2 (TLR2) methylation in older adults, further suggesting potentiation of the inflammatory response (188). Flavonoid supplementation can potentially limit TLR2 methylation, as correlations indicate, and ameliorate PM<sub>2.5</sub>-induced low frequency HRV. Another study that aimed to address the epigenetic regulation of inflammatory markers by PM exposure utilized young, healthy subjects who inhaled an array of PM compositions (PM<sub>10</sub>, PM<sub>2.5</sub>, PM<sub>1.0</sub> and PM<sub>0.5</sub>) over two sessions (158). These subjects presented with decreased HRV indicating a stress response, which is consistent with previous studies of PM exposure. Furthermore, PM<sub>2.5</sub> as well as quasi-ultrafine particles <0.50 µm were significantly associated with increased pro-inflammatory cytokine (interferon gamma (IFN- γ)) methylation, correlating with alterations in the parasympathetic nervous system as an adaptive response (158). Bind and colleagues however, reported that both PM<sub>2.5</sub> BC and PM<sub>2.5</sub> mass concentrations were associated with significantly lower methylation of immunoregulatory genes, IFN-γ and intercellular adhesion molecule 1 (ICAM-1) in individuals with low methylation levels prior to exposure (9). The main contributing factor that is likely responsible for these contradictory findings is the population that was studied. While Tobaldini et al. conducted a more controlled experiment with healthy, young males (n = 12), Bind et al. utilized a large cohort (n = 777) of elderly men with varying health conditions (9, 158). Other studies address epigenetic alterations of the cardiovascular system following PM inhalation exposure as well (99, 110), though without direct functional associations. Although the studies outlined provide a link between epigenetic mechanisms and cardiac function, specifically HRV, it remains unclear if epigenetic reprogramming is a primary mechanism for sustaining adaptations to PM exposures or if it is transiently changed with exposure. MicroRNA-378A, as well as other microRNAs, are potential molecular mediators of metabolic and cardiac dysfunction that ensue following ENM exposure (65). Nano-TiO<sub>2</sub> inhalation exposure induced diastolic dysfunction, E/A ratio elevation, and decreased myocardial performance indices, which were preserved in a microRNA knockout transgenic mouse model (microRNA-378A). The authors pointed to regulation of mitofusin 1

(Mfn1) expression through microRNA-378A as a mechanism for controlling mitochondrial dynamics following exposure (65). While the preceding studies examined epigenetic changes, the mechanisms of action were not elucidated. Multi-faceted assessments of how pollutants impact the epigenome and inflammation-associated genes are critical as both are implicated in processes mediating cardiovascular function impairment.

Inflammation plays a key role in pollutant exposure response in both individual particulate exposures and multi-component exposures. Co-exposure of sulfur dioxide (SO<sub>2</sub>), nitrogen dioxide (NO<sub>2</sub>), and PM<sub>2.5</sub>, typical air pollutants produced as a result of coal combustion, results in an enhanced inflammatory response with upregulation of COX-2, inducible nitric oxide synthase (iNOS), TNF- $\alpha$ , and IL-6 (184). The co-exposure contributed to decreased blood pressure and increased heart rate when compared to PM<sub>2.5</sub> alone. Similarly, IL-6, IL-8, and endothelin-1 (ET-1) were significantly associated with rises in carbon monoxide (CO), UFP and SO<sub>2</sub> concentrations in healthy individuals near a steel mill (86). The precursor for ET-1 (BET-1) was positively correlated with systolic blood pressure, while C-reactive protein (CRP) was correlated with increased heart rate. Protein ontology revealed a significant elevation of inflammation specific pathways (86). Combined high-dose PM<sub>2.5</sub> and ozone exposure also promotes cardiovascular functional injuries that are presented as abnormal electrocardiogram (ECG) results (extended QRS complex and depression of ST-segment) (163). The addition of ozone to the exposure paradigm propagated inflammatory and oxidative stress responses with elevated CRP, IL-6, creatine kinase (CK), lactate dehydrogenase (LDH), and malondialdehyde (MDA). These studies highlight the importance of controlled co-exposure studies for delineating the risk of ambient pollutants and combustion materials on cardiovascular hemodynamics and the associated inflammatory and oxidative stress mechanisms.

Co-exposure to CAPs and acrolein causes myocardial dyssynchrony, though through a less understood mechanism involving the activation of transient receptor potential cation channel A1 (TRPA1), which the authors report may act to increase cardiac risk, specifically in exposures with heterogeneous compositions (157). Along with channel proteins affecting cardiac conduction, modifications in the uptake and clearance of calcium can alter contractility within cardiomyocytes, further dysregulating the cardiac cycle. One of the more studied pathways is through SERCA2a. PM<sub>2.5</sub> exposure increased intracellular free calcium (Ca<sup>2+</sup>) that was associated with increased

ryanodine receptor 2 (RYR2) and decreased SERCA2a, which are responsible for shuttling  $\text{Ca}^{2+}$  from the sarcoplasmic reticulum to the cytoplasm and back, respectively (38). The changes in calcium handling may be a direct result of  $\text{PM}_{2.5}$ -induced oxidative stress, thereby contributing to contractile dysfunction in cardiomyocytes. In response to long-term exposure to  $\text{PM}_{2.5}$ , others have reported decreased fractional shortening, impaired mitral inflow patterns, depressed contractile reserve, along with decreased peak shortening and relengthening of isolated cardiomyocytes in C57BL/6 mice (170). Downregulation of SERCA2a in  $\text{PM}_{2.5}$ -exposed mice revealed abnormal  $\text{Ca}^{2+}$  cycling, as previously seen, but also elevation of  $\beta$ -myosin heavy chain ( $\beta$ -MHC) indicative of heart failure. Apart from contractility, tone of the vasculature within the heart can alter cardiac hemodynamics. A study of acute and sub-chronic inhalation exposure of Sprague Dawley rats to  $\text{PM}_{2.5}$  and  $\text{PM}_{0.1}$  separately elevated angiotensin II type 1 receptor ( $\text{AT}_1\text{R}$ ) mRNA (4). The sub-chronic exposure to both sizes of PM further increased  $\text{AT}_1\text{R}$  protein levels, expression of markers for myocardial adaptive response to damage (actin alpha 1 (Acta1) and Col3a) and IL-6, while decreasing antioxidant heme-oxygenase 1 (HO-1). The authors suggest that angiotensin overexpression can promote coronary artery wall thickness, which is likely to influence blood pressure in exposure models (4). Another study aimed to elucidate the effects of toxicant exposure on the regulation of blood pressure using 12-13 month-old spontaneously hypertensive rats (SHRs), which were exposed to ultrafine carbon particles (UFCP) (159). UFCP inhalation exposure resulted in increased blood pressure and heart rate, which was correlated with increased levels of serum CRP, plasma fibrinogen, and levels of ET-1 in the heart. UFCP exposure-induced hypertension in SHRs is also associated with elevated angiotensin II (AngII) in the blood, with increasing doses of UFCP diminishing the effectiveness of captopril, an angiotensin converting enzyme inhibitor (183). The diminished effectiveness of captopril suggests that increasing doses of UFP, may activate a variety of pathways outside of angiotensin to induce changes in blood pressure. These data suggest that regulation of blood pressure, like other cardiovascular responses, is a multifactorial pathway that is influenced by other circumstances, including genetic makeup and various environmental influences.

One of these environmental influences, high-fat diet feeding, is often used to model hyperlipidemia. Hyperlipidemic rats exposed to  $\text{PM}_{2.5}$  are susceptible to higher blood pressure, lower HRV, and higher levels of cardiomyocyte apoptosis, accompanied by decreased expression of antioxidant proteins, including SOD (167). Markedly, high-fat diet exposed mice, compared to

high fat diet alone, also revealed increased myocardial death through increased levels of cardiac troponin I (cTnI), LDH and CK. Animal models with a high propensity for metabolic dysfunction, such as AMP-activated protein kinase  $\alpha 2$  knockout (AMPK $\alpha 2^{-/-}$ ) mice that lack this crucial gene for fatty acid oxidation, are critical for understanding how PM<sub>2.5</sub> inhalation exposure impairs cardiovascular function in vulnerable populations (165). PM<sub>2.5</sub> exposure diminished left ventricular ejection fraction in AMPK $\alpha 2^{-/-}$  mice and promoted an oxidative and inflammatory environment through decreased expression of peroxiredoxin 5 (PRDX5), and increased expression of NF- $\kappa$ B and TNF- $\alpha$ . These studies highlight the importance of understanding the molecular changes that occur and the downstream effects on oxidative stress regulation in susceptible populations exposed to PM. UFP inhalation exposure in human subjects with metabolic syndrome can be specifically detrimental to cardiac repolarization, as demonstrated by the QRS complexity in those without the glutathione s-transferase mu 1 (GTSM1) protein, a pivotal antioxidant gene (36). In the complete cohort (participants with and without the GTSM1 mutation), UFP exposure elevated CRP and serum amyloid A (SAA) with subsequent decreases in plasminogen and thrombomodulin within blood, indicating an upregulation of inflammatory pathways and the critical role of antioxidant genes. On the contrary, sub-acute exposure to PM<sub>2.5</sub> in healthy adults was not correlated with increased inflammatory markers or altered vascular function (17). However, a 10  $\mu\text{g}/\text{m}^3$  increase in exposure was associated with decreased HRV, correlating to increased homeostatic model assessment of insulin resistance (HOMA-IR). This suggests the possibility that chronic periods of exposure to PM<sub>2.5</sub> could reduce insulin sensitivity and thus potentiate susceptibility to diabetes mellitus, though inflammation may not be the etiology implicated by this study (17). Particularly concerning is the notion that in obese mice, chronic exposure to PM<sub>2.5</sub> can prevent the beneficial effects of exercise on cardiac function and anti-inflammatory pathways (59). Sedentary mice that were exposed to PM<sub>2.5</sub> presented with increased left ventricular diameter (systolic and diastolic) that was not ameliorated in the exercised group. Moreover, PM<sub>2.5</sub> exposure enhanced CRP, ICAM-1, and vascular cell adhesion protein 1 (VCAM-1), which were elevated in the PM<sub>2.5</sub> exercised group as well (59). These results are similar to those seen in a previous study that reported the inability of moderate aerobic exercise to provide anti-inflammatory protection in mice exposed to PM<sub>2.5</sub> (103), which may be linked to expression of heat-shock protein 70 kilodalton (HSP70) (103, 140). The advantages of moderate exercise on cardiovascular function in obese mice (111, 126, 149), but not in obese mice exposed to PM<sub>2.5</sub>

(59), emphasizes the consequential results of PM<sub>2.5</sub> exposure in vulnerable populations. However, the use of a high-fat diet induced obesity model may be more relevant in substantiating whether fine particulate exposure hinders the ability of exercise to mitigate the detrimental cardiovascular effects in diabetic models, as the ob/ob model may have impaired exercise capacity (59).

### *Coagulation*

Within the lungs, the circulatory system provides a necessary pathway for mediation of the inflammatory response. Due to this close association of the pulmonary and circulatory systems, changes arising in blood have the potential to alter homeostasis within blood vessels. Alterations in the coagulation pathway, specifically through fibrinogen, have been reported following PM exposure.

Levels of a pollutant from wood smoke, Delta-C, are positively correlated with fibrinogen and negatively correlated with myeloperoxidase (MPO), an enzyme involved in the inflammatory pathway and platelet activation (32). The study also demonstrated that PM<sub>2.5</sub> and UFP retain a positive correlation with fibrinogen as well as CRP, sharing a similarity in the effects on blood coagulation with effects of Delta-C. In a co-exposure model of SiNPs and lead acetate (Pb), Feng et al. reported alterations to the blood clotting cascade evidenced by decreased tissue-type plasminogen activator (t-PA), tissue factor pathway inhibitor (TFPI), and antithrombin III (AT III), as well as elevated fibrinogen and D-dimer (D2D) (48). Following co-exposure, serum analyses revealed leukocytosis and thrombocytopenia, concomitant with increased expression of inflammatory markers (CRP, IL-6, and TNF- $\alpha$ ) and markers of heart failure (ANP and BNP). Overlap found between studies of varying particle sizes can help identify critical biomarkers of increased blood clotting that are a product of multi-component exposure in both human and animal models. Furthermore, others have shown that levels of fibrinogen can be increased by other ambient air pollution constituents (8). Specific associations between PM<sub>2.5</sub> BC and altered epigenetic modification status of tissue factor III (F3) were later reported by this group, indicating alterations to extrinsic blood coagulation (10). Decreased methylation of F3, which likely leads to increased transcription of the gene, can provide the initial stimulus for altering the response of thrombin and fibrinogen thereby increasing coagulation (29). Similarly, in a meta-population study, including 3275 participants, long-term rises in PM<sub>2.5</sub>, but not PM<sub>0.1</sub>, were matched with

significantly increased CRP and platelet count (160), suggesting an increased propensity for blood clotting.

Interestingly, annual average UFP exposure levels and fibrinogen were negatively associated, though not significantly, in human blood samples (90), which may have been a result of micro-environment compared to ambient concentrations. To better elucidate the dynamic relationship between ambient exposure and the time/concentration of the exposure in terms of their effects on the cardiovascular system, Lane et al. examined biomarkers in patients with varying levels of microenvironment exposures (time-activity adjusted) in addition to the annual average particle number concentration of UFPs. There were significant positive associations between time/concentration of exposure and inflammatory pathway genes in blood, including CRP and tumor necrosis factor receptor 2 (TNFR2) (90). These findings illustrate the significance of monitoring personal exposure levels, which may account for the differences seen in fibrinogen expression between studies that solely use annual outdoor particle concentrations and those that consider varying levels of individual microenvironment exposure. Modifying the coagulation pathway in individuals who are continuously exposed to high levels of pollutants through ambient air may provide a potential prophylactic strategy to prevent the inevitable high risk of CVD. Nootkatone, a sesquiterpenoid in grapefruit has potential as a pretreatment strategy for PM<sub>2.5</sub> diesel exhaust exposure through its ability to reduce blood clotting by decreasing plasminogen activator inhibitor-1 (PAI-1) and fibrinogen, and restoring thrombotic occlusion time in arterioles (114). The authors suggest that the pretreatment strategy activated nuclear factor erythroid-derived 2-like 2 (NRF2), which plays a key role in initiating HO-1, to provide protection from oxidative injury (114). While the studies discussed thus far have primarily utilized healthy cohorts, it is important to understand how the coagulation pathway is altered in at-risk populations as well. Elemental carbon UFP inhalation exposure modifies platelet activation in type 2 diabetic patients by increasing CD40 ligand (CD40L) expression in platelets, with a resulting decrease in soluble CD40 (sCD40) in blood (147). Higher CD40L levels, as a result of UFP exposure, exerted a stimulatory role on von Willebrand factor (vWF) and elevated its expression. Though this study revealed the adaptations of those with diabetes mellitus, it did not provide a control cohort to elucidate whether these effects of PM on coagulation are exaggerated in the at-risk population. Nonetheless, genes involved in the activation of pathways involving fibrinogen and platelet

activation are potential early biomarkers of increased CVD risk in healthy and vulnerable populations and require further clarification.

### *Vascular Dysfunction*

Along with mediating the blood clotting cascade, particulate exposure has the capacity to modify the integrity of vascular tissue, thus interfering with blood flow and cellular metabolism directly within the vasculature. Through direct damage to the vasculature, or mediation of the inflammatory response, particulate matter can cause blood vessels to become predisposed to ultrastructural changes. Atherosclerosis, which involves the build-up of fatty acids and cholesterol within the intima layer of arteries, is linked to PM exposure.

In an atherosclerotic transgenic mouse model (ApoE<sup>-/-</sup>), PM<sub>2.5</sub> exposure causes cardiac autonomic nervous system dysfunction concomitant with oxidative stress (123). Of note, the high-fat diet fed, atherosclerotic mice displayed a greater proclivity for oxidative damage, suggesting, once again, the impairment of cellular protective mechanisms in those who already have an altered metabolic profile. Similarly, concentrated PM<sub>2.5</sub> exposure significantly altered high-density lipoprotein (HDL) anti-oxidant and anti-inflammatory capacity (HDL oxidative index (HOI)), along with increased systolic blood pressure (132). However, ozone exposure in addition to the PM<sub>2.5</sub> exposure in this study did not exacerbate these effects, suggesting that short-term CAP and ozone co-exposure may not induce overt changes that are suggestive of atherosclerosis progression. On the other hand, long-term CAP exposure does contribute to the progression of atherosclerosis. Rao, et al. discovered that PM<sub>2.5</sub> exposure increased abnormal accumulation of an oxidized variant of cholesterol, 7-ketocholesterol (7-KCh), in macrophages and the aortic wall (133). PM<sub>2.5</sub>-exposed mice also presented with increased CD36 expression in plaque-macrophages, implicating CD36 in the accumulation of oxidized lipids, promoting atherogenesis. By reducing the number of CD36-positive macrophages, internalization of 7-KCh can be limited and therefore the oxidized lipids can be efficiently cleared from the vasculature (133). Along with altered macrophage clearance, other immune responses have been implicated in vascular maladaptation following particle exposure including changes to the innate immune response. ENM inhalation exposure resulted in translocation of nanomaterials to the heart, which initiated the complement cascade, setting off a local immune response, indicated by global complement factor

3 (C3) upregulation in the blood (77). This study demonstrates that alterations to the innate immune response may be a direct effect of translocated particles, but both studies (77, 133) highlight the importance of the inflammatory response and part of its role in altering vascular function. PM<sub>2.5</sub> exposure can impact vascular endothelial cell permeability pathways by causing an inflammatory response, which is a hallmark of increased vascular permeability. A recent study has demonstrated that long-term changes in vascular permeability are promoted specifically by IL-6 and sustained in-part by STAT3 phosphorylation (1). In rats, PM<sub>2.5</sub> exposure induced phosphorylation and subsequently expression of STAT3, which upregulated microRNA-21 expression (33). Increased microRNA-21 expression reduced tissue inhibitor of metalloproteinase 3 (TIMP3) expression and enhanced matrix metalloproteinase 9 (MMP9) expression. Ultimately, vascular endothelial dysfunction was linked to extracellular matrix remodeling propagated by STAT3 (33), which was likely promoted by the PM-induced inflammatory response. Changes in the composition of the vascular matrix could result in alterations to immune cell binding and further changes to diapedesis leading to vascular dysfunction.

In a 3820 non-current smoking patient population that was part of the Framingham Heart Study, acute PM<sub>2.5</sub> and BC exposure concentrations were inversely correlated with expression of P-selectin, suggesting decreased endothelial-surface cell adhesion (97). Along with changes to vascular structure, the ability for the endothelium to regenerate and adapt to pollutant exposure can be compromised. Typically, this occurs through the production of endothelial progenitor cells (EPCs) in response to vascular injury (50). However, PM<sub>2.5</sub> exposure diminishes circulating EPC levels, which may occur as a result of vascular endothelial growth factor (VEGF)-induced Akt and endothelial nitric oxide synthase (eNOS) phosphorylation (50, 62). Short-term CAP exposure in mice fed a control diet remarkably induced vascular insulin resistance, indicated by decreased Akt phosphorylation, and suppressed circulating levels of EPCs through activation of the NF- $\kappa$ B inflammatory pathway (63). Increasing insulin sensitivity prevented activation of these pathways, substantiating that PM<sub>2.5</sub> exposure can lead to insulin resistance and therefore type 2 diabetes in healthy populations (50). Furthermore, CAP-induced vascular insulin resistance was accompanied by increased vascular oxidative stress marked by mitochondrial SOD2 and glutathione s-transferase-P (GST-P) mRNA levels, and expression of protein-HNE adducts (63). Interestingly, 9-day CAP-exposure did not exacerbate high-fat diet induced changes in vascular insulin resistance (63), but a 30-day CAP exposure significantly aggravated systemic insulin resistance,



elevating glucose intolerance and HOMA-IR in high-fat diet-fed mice (64). In aortic tissue, both 9-day and 30-day CAP exposures resulted in decreased insulin-stimulated phosphorylation of Akt and eNOS, subsequently suppressing inhibition of the transcription factor NF- $\kappa$ B ( $I\kappa$ B $\alpha$ ) and promoting an inflammatory response (64). By treating with an antioxidant, 4-hydroxy-2,2,6,6-tetramethylpiperidine-1-oxyl (TEMPOL), CAP-induced inflammation and the associated vascular insulin resistance were alleviated in high-fat diet fed mice leading to the conclusion that short-term exposure to PM<sub>2.5</sub> triggers a pulmonary oxidative stress response that is able to elicit downstream vascular insulin resistance and inflammation (64).

Compounding environmental factors can further propagate the effects of particulate exposure. A study in type 2 diabetic Boston residents provided evidence that both PM<sub>2.5</sub> and BC are significantly associated with increased VCAM-1 and vWF in participants who have smoked in the past (118). These data indicate that prior exposure to smoking-related particulates, may exacerbate the inflammatory response seen with ambient PM<sub>2.5</sub> exposure, creating a greater risk for endothelial dysfunction and cardiovascular damage in type 2 diabetic patients. In an attempt to directly assess the physiological impact of PM<sub>2.5</sub> exposure on vasculature in a CVD at-risk population, Riggs et al. assessed individuals' reactive hyperemia index as a measure of endothelial function (135). Increasing concentrations of PM<sub>2.5</sub> significantly reduced the reactive hyperemia index and were associated with angiogenic signaling and inflammation markers, angiopoietin 1, placental growth factor (PIGF), VEGF, ICAM-1, and MMP9 and negatively associated with VCAM-1 and urinary F2-isoprostane (Isop), a measure of oxidative stress (135). Interestingly, incremental increases of PM<sub>2.5</sub> by 10  $\mu\text{g}/\text{m}^3$ , were also associated with increased pro-inflammatory cytokines including, monocyte chemoattractant protein 1 (MCP-1), macrophage inflammatory protein 1 $\alpha/\beta$  (MIP-1 $\alpha/\beta$ ) and IFN $\gamma$ -induced protein 10 (IP-10) in a cohort of young, healthy individuals with low CVD risk (127). Together, these studies indicate that PM<sub>2.5</sub> initiates changes in cytokines and growth factors, which lead to endothelial injury and an immune response that may result in acute cardiovascular events in both high-risk and low-risk CVD populations (127, 135). Furthermore, PM<sub>2.5</sub> exposure, in a subset of the same cohort, revealed an inverse association with ET-1, but a positive association with platelet factor 4 (PF-4) (51). Additionally, ET-1 was negatively associated with PF-4 following PM<sub>2.5</sub> exposure, which the authors conclude may be the result of an anti-angiogenic effect of the exposure that could also suppress endothelial repair (51, 127). Though this is contrary to previous studies reporting positive correlations between PM and

ET-1 (48, 86, 184), another acute exposure reported similar findings (56). Conversely, chronic exposure paradigms appear to cause elevated ET-1 levels (48, 86, 184). Current literature provides convincing evidence that particulate matter exposure causes a remarkable maladaptive vascular response that can lead to increased risk of CVD. However, understanding the genome-wide effects of exposure may provide a better understanding of the molecular mechanisms that are responsible for these alterations.

### *Cellular Stress and Death*

PM inhalation exposure-induced changes to the cardiovascular system can eventually trigger cell death pathways through varying mechanisms including oxidative stress (94). These pathways include apoptosis and necrosis, leading to programmed or uncontrolled cell death and subsequently cardiovascular hypertrophy.

One of the mechanisms that initiates the cell death pathways is damage to nuclear DNA. Assessment of blood from trucking industry participants revealed that 48 (elemental carbon (EC)), 260 (organic carbon (OC)), and 49 (PM<sub>2.5</sub>) differentially regulated genes were associated with each of the exposure; these expression profiles implicate genes regulating apoptosis, DNA and metal binding, and chronic heart and lung disease pathways (30). Consistent with these findings, exposure to PM<sub>2.5</sub> containing polycyclic aromatic hydrocarbons (PAHs), increased DNA damage and DNA damage response genes in a rodent model (186). These genes included 8-oxoguanine DNA glycosylase (OGG1) and growth arrest and DNA damage 153 (GADD153). PM exposure also altered genes involved in ROS regulation (glutathione S-transferase (GST) and SOD) (186). An increased expression of GST and decreased expression of SOD may promote a high oxidative environment with reduced ability to scavenge ROS, which may help propagate the effects of DNA damage. NOX4 is a prominent contributor of oxidative stress in the failing heart, and is associated with initiating increased DNA damage through this mechanism (89). PM<sub>2.5</sub> exposure in mice enhances not only inflammatory markers as previously reported (TNF- $\alpha$  and IL-1 $\beta$ ), but also myocardial apoptosis, NOX4, and NOX4 associated subunits, suggesting that the progression of cardiovascular disease may be dictated by ROS generation and the modification of antioxidant protein-levels, which are initially regulated by PM<sub>2.5</sub> exposure (173). While unregulated levels of ROS may function through multiple pathways to cause cell death, programmed cell death through

apoptosis has been linked to PM inhalation exposure through other channels. Hyperlipidemic rats exposed to PM<sub>2.5</sub> are more prone to cardiac apoptosis (167) that is mediated through c-Jun NH<sub>2</sub>-terminal kinase (JNK), P53 phosphorylation and downstream activation of (Bcl-2-associated X) Bax and Caspase-3 (167). The expression of both GST and JNK are modified following PM exposure, which implies the presence of an overlap among these pathways that mediate apoptosis as previously suggested (55). Similar results are seen in other vulnerable models such as mice that were challenged with myocardial infarction (98). PM inhalation exposure exacerbated left ventricular dysfunction and increased infarct size, with increased myocardial apoptosis through Caspase-3, Bax and B-cell lymphoma 2 (Bcl-2). Moreover, PM exposure may not immediately stimulate cell death, but rather result in reprogramming of the cell, making it susceptible to future insult. One way reprogramming may be occurring is through changes in microRNAs, which are associated with PM<sub>2.5</sub>, but not UFP, in the blood of individuals residing in multiple urban regions (43). Specifically, PM<sub>2.5</sub> is correlated with increased hsa-miR-197-3p and hsa-miR-99a-5p, which play roles in cell death and cancer (43, 180). PM<sub>2.5</sub> inhalation exposure was also linked to microRNAs involved in cardiovascular function, including decreased expression of microRNA-133a, 145-5p, and 499a-5p in plasma (84). Overall, these studies outline some of the potential mechanisms that initiate myocardial apoptosis and eventually lead to cardiovascular abnormalities due to particulate exposure.

### *Mitochondrial Bioenergetics and Ultrastructure*

In the cardiovascular system, slight perturbations to mitochondrial health could result in significant detriments and sustained pathology. The energy needed for the heart to contract is derived primarily through oxidative phosphorylation of mitochondrion (~95%) (189). Alterations to mitochondrial function are therefore implicated as a primary pathway for cardiovascular dysfunction and disease (117).

The integrity of mitochondrial DNA defines its respiratory potential, allowing for separation of individuals into a variety of haplogroups (138). Ambient air pollution has the potential to differentially effect individuals with diverse haplotype backgrounds (169). Haplogroup H (high ROS production) compared to haplogroup U (low ROS production) is more susceptible to quasi-ultrafine particle <0.25 μm exposure. Quasi-ultrafine particle exposure

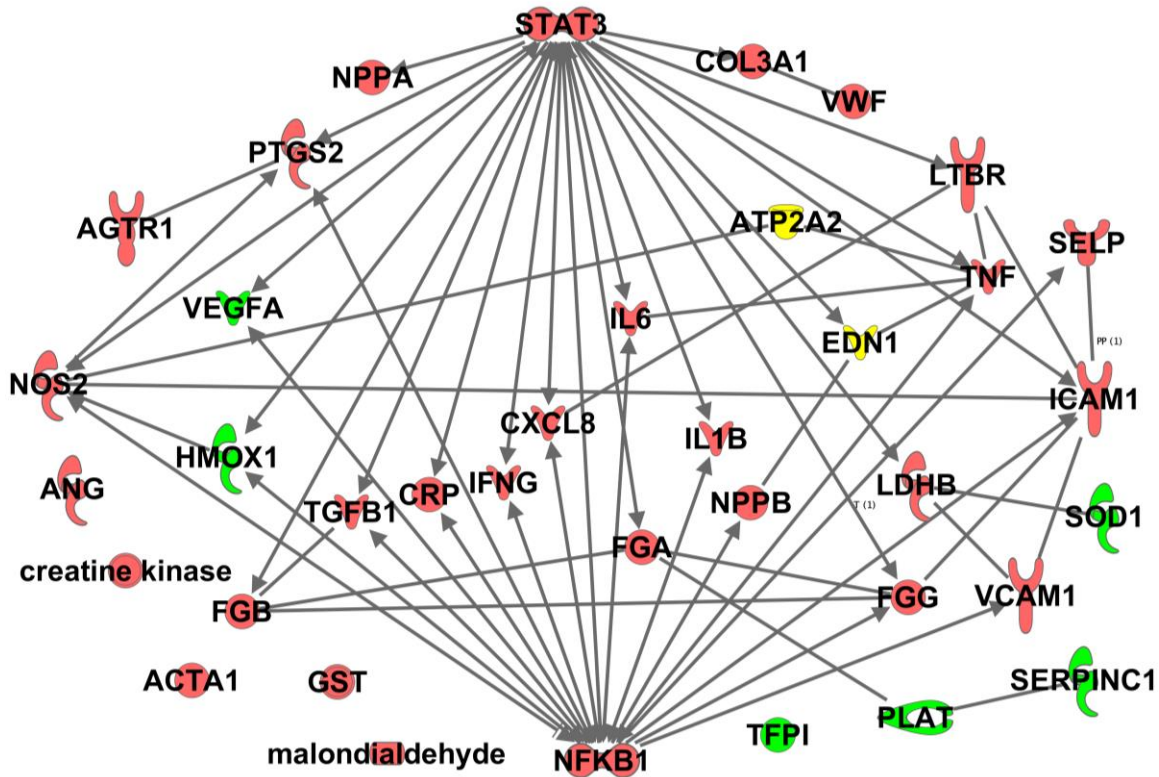
induced inflammation to a greater extent in haplogroup H than U, demonstrated by increased IL-6 and TNF- $\alpha$  (169). Furthermore, high doses of PM<sub>2.5</sub> result in cardiac mitochondrial ultrastructure (size and cristae formation) changes in addition to increased inflammation (95). These ultrastructural changes are supported by increases in mitochondrial fission 1 (FIS1), MFN1, MFN2, dynamin-related protein 1 (DRP1), and mitochondrial dynamin like GTPase (OPA1), which suggest alterations to the fission/fusion pathway (95). UFP exposure has also been linked to mitochondrial dysfunction (70). Exposure to UFP exacerbated ischemia/reperfusion damage in the isolated hearts of rats. Isolated cardiac mitochondria of UFP-exposed rats displayed decreased Ca<sup>2+</sup> buffering prior to the mitochondrial permeability transition pore (mPTP) opening, which indicates that exposure can increase mPTP Ca<sup>2+</sup> sensitization and therefore mitochondrial permeability (70). The alterations to fission/fusion proteins (95) and mitochondrial permeability (70) showcase changes to the composition and functionality of mitochondrion following exposure, which can propagate oxidative damage and initiate mPTP-associated cell death pathways to instigate cardiac damage. A single dose of ENM through inhalation exposure in mice, has the ability to trigger cardiac functional changes and mitochondrial dysregulation (116). However a transgenic mouse model for mitochondrial phospholipid hydroperoxide glutathione peroxidase (mPHGPx) was used to restore cardiac function, mitochondrial respiratory function, and abrogate ROS levels following nano-TiO<sub>2</sub> exposure. By increasing antioxidant defense through mPHGPx overexpression, proteomics revealed that changes in mitochondrial composition, including individual electron transport chain complex constituents, were protected from the detrimental effects of exposure (116). This study further validates the importance of antioxidant protection in preservation of mitochondrial structure and function, and should therefore be investigated as a potential protective approach.

PM exposure can modify the transcriptional capacity of the mitochondrion and likewise incite dysfunction through this approach. Boilermakers exposed to PM<sub>2.5</sub> were utilized in a study that aimed to elucidate the exposure-induced changes in methylation of mitochondrial DNA (19). Methylation of specific mitochondrially transcribed genes involved in ATP synthesis, including mitochondrially encoded tRNA phenylalanine (MT-TF) and mitochondrial 12s RNA (MT-RNR1), were not associated with PM<sub>2.5</sub> exposure. However, methylation of the mitochondrial promoter D-Loop was associated with PM<sub>2.5</sub> exposure. Participants with mitochondrial DNA hypermethylation were more vulnerable to the effects of PM<sub>2.5</sub> exposure on HRV (19). Inhalation of toxicant particles

may exert its effects on overall mitochondrial structure and function, and thus cardiovascular function, through ROS regulated and inflammatory pathways as the preceding studies indicate. Both increased inflammation and ROS have the ability to recruit methyltransferases, such as DNA methyltransferase 1 (DNMT1), and alter the methylome of various genes implicated in CVD, causing repression of the associated genes (83).

Though the molecular mechanisms behind cardiovascular impairment associated with particulate matter exposure vary based on the particle size, constituents, and physiochemical properties, there are common overlapping genes that appear to be modulated by multiple toxicants present in air pollution. **Figure 1.2**, created using Ingenuity Pathway Analysis (IPA), provides an interaction network of genes that are dysregulated following particulate inhalation exposure. IPA included genes that were upregulated, downregulated, or had diverse expression following more than one type of particulate exposure mentioned throughout this review. These genes can serve as potential early biomarkers of cardiovascular damage as a result of inhaled toxicant exposure.

**Figure 1.2: Ingenuity Pathway Analysis (IPA).**



**Figure 1.2:** Ingenuity pathway depicting the interaction network of genes that are dysregulated following particulate inhalation exposure. The genes included in the interaction network were associated with more than one type of particulate exposure. The interactions represent direct, validated experimental associations between genes that were increased (red), decreased (green), or found to have a diverse expression profile (yellow) following exposures. All abbreviations are defined in the Abbreviations section provided.

### Gestational Exposures

There has been an increasing volume of literature investigating how particulate exposure can affect vulnerable populations, including women during pregnancy. Due to the coinciding metabolic changes prompted by both diabetes/obesity and air pollution, particularly related to oxidative stress and inflammation, understanding the dynamics of both pathologies is critical in determining how pollutant exposure can alter the metabolome (117). Particulate exposure during gestation is a major risk-factor for gestational diabetes (105, 179). However, the effects of pollutant insult *in utero* on the offspring remain a critical gap in knowledge (11, 78, 100). This is particularly

concerning for fine and ultrafine particles that have the ability to enter circulation and reach the fetal side of the human placenta (12). Recent studies indicate that maternal toxicant inhalation exposure during gestation is a predisposing factor for CVD in offspring.

### *Oxidative Stress and Inflammation*

PM<sub>2</sub> exposure results in activation of oxidative and inflammatory pathways, as has been described in the previous sections. Preconception toxicant exposure, predisposes future offspring to the development of cardiac dysfunction (153). PM<sub>2.5</sub> preconception exposure in both parents decreases ejection fraction, fractional shortening, and cardiomyocyte contractility in 3-month old progeny (153). Inflammatory and oxidative pathways are thereby activated, resulting in increased IL-6, IL-15, NFκB, and CRP along with elevated fibrosis (Col3a1), similar to the results found in many direct exposure studies. Notably, calcium handling proteins, SERCA2a and phosphorylated phospholamban (p-PLN) are elevated in preconception PM<sub>2.5</sub> exposed offspring, as increased p-PLN loses its ability to inhibit SERCA2a. While PM-induced inflammation and oxidative stress are common in both direct and preconception exposures, SERCA2a is contrarily decreased in direct exposures (38, 170). One potential reason for this discrepancy may be that preconception exposure results in an adaptive response. Similar to direct and preconception exposure, PM<sub>2.5</sub> exposure during gestation also results in cardiac remodeling with associated inflammation (increased IL-6 and IL-1β) (155). Furthermore, extracellular matrix remodeling, marked by increased collagen-1, MMP9, and MMP13 expression, is also present in neonates following gestational exposure, but was not assessed into adulthood. Nevertheless, long-term maternal exposure to PM<sub>2.5</sub>, throughout gestation and lactation, enhanced activation of the inflammatory markers and myocardial apoptosis in both neonatal and weanling Sprague Dawley rats (27). UFP exposure to pregnant C57BL/6J dams led to fetal reabsorption and increased blood pressure in adult progeny (109). Increases in maternal serum inflammation during gestation, along with AT<sub>1</sub>R and angiotensin I-converting enzyme (ACE) activation in the lungs are suggested to contribute to progeny cardiovascular dysfunction both short and long-term. The notion that maternal and paternal exposure activates an inflammatory response in progeny from early life into adulthood is therefore well established, but whether the changing maternal environment (109), particle

translocation, or a combination of such factors are culpable in altering progeny development and metabolic function remains elusive.

In addition to inflammatory pathways, immune responses and oxidative stress pathways are changed in progeny who are exposed during gestation. Challenging progeny immune systems with house dust mite (HDM) allergen revealed a decreased immune response through lower IL-13 and IL-17, with higher serum levels of IL-10 following UFP exposure (139). This has also been demonstrated with UFP containing persistent free radicals (MCP230), which suppressed the T helper and T regulatory cells found within the lungs of offspring (166). Maternal ENM exposure during gestation may however, modulate a regulatory axis involving enhanced hypoxia inducible factor (HIF)-1 $\alpha$  activity and decreased mPHGPx expression, which are critical in the regulation of ROS in fetal and young adult cardiac development (87). Understanding how gestational exposure, as opposed to direct exposure, effects individuals will contribute in the development of preventative measures for vulnerable populations, including pregnant women and children, and promote safer limits of exposure thereby mitigating susceptibility to metabolic diseases and CVD in offspring.

### *Cellular Function*

Calcium regulated contraction is significantly affected throughout development in progeny exposed to particulate matter during gestation. Assessment of fourteen-day old progeny whose dams were exposed to PM<sub>2.5</sub> during gestation, revealed decreased cardiomyocyte contractility through calcium dynamics, with changes to proteins involved in calcium flux in the heart, SERCA-2a, p-PLN, Na<sup>+</sup>/Ca<sup>2+</sup> exchanger (NCX), calcium channel, voltage-dependent, L type, and alpha 1C subunit (CaV1.2) (154, 155). Offspring whose dams were exposed during gestation also present with major cardiac anomalies present into adulthood as a result of ENM-induced mitochondrial dysfunction. Nano-TiO<sub>2</sub> gestational exposure decreased diastolic cardiac function, marked by a 15% increase in E/A ratio, and diminished mitochondrial respiration in young adult progeny (66). These results were simultaneous with mitochondrial proton leak and increased uncoupling protein 2 (UCP2), as well as upregulation of mitochondrial metabolism proteins, carnitine palmitoyltransferase 1A (CPT1A) and pyruvate dehydrogenase (PDH) phosphorylation. ENM exposure during gestation also affects mitochondrial bioenergetics by limiting state 3 respiration



in the left ventricle of young adult progeny, coinciding with impaired endothelium dependent dilation in coronary and uterine arterioles (145). PM<sub>2.5</sub> gestational exposure can trigger myocardial apoptosis in a dose-dependent manner, as has been revealed in one day-old neonatal offspring from Wistar rats (164). Myocardial cell death likely occurred due to alterations in mitochondrial fission/fusion through OPA1, MFN1, DRP1, and FIS1 following PM<sub>2.5</sub> exposure during gestation (164). Utilizing functional genomics in addition to mitochondrial structural and bioenergetic assessment, may provide insight into the mechanisms driving the deficits observed in progeny whose dams were exposed to particulate matter during gestation.

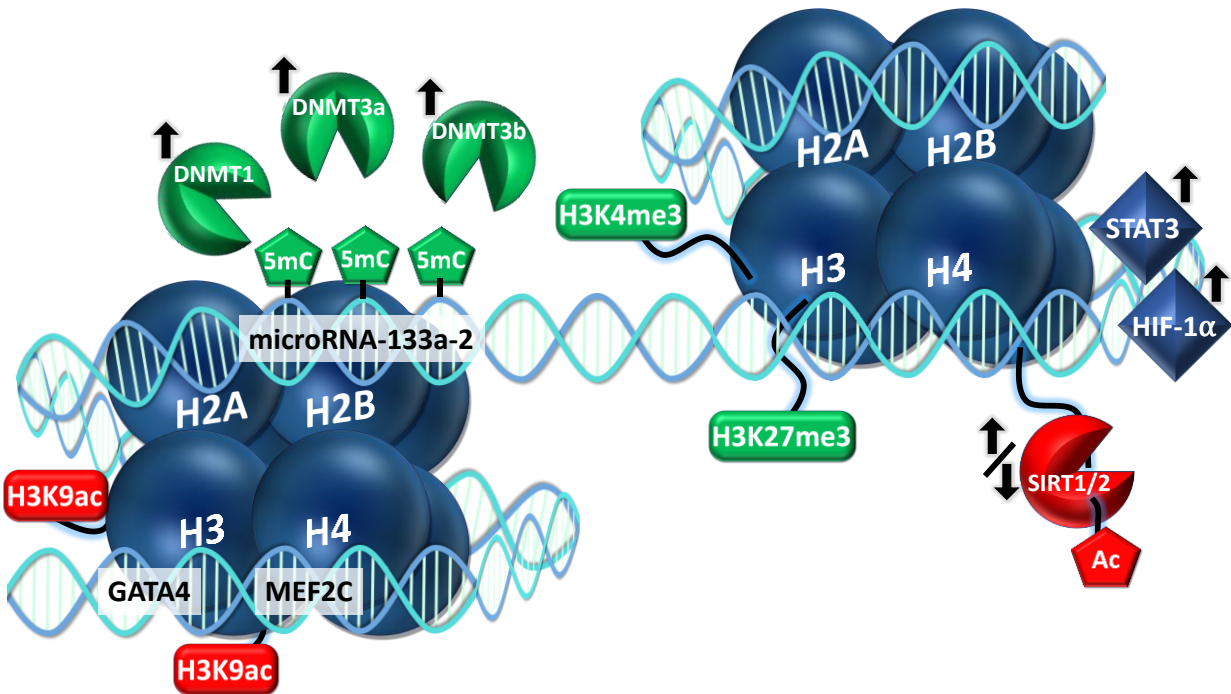
### *Epigenetics and Transcriptional Regulation*

Studies in progeny exposed to particulate exposure during a critical point in development such as gestation, reveal that cellular regulatory networks are substantially altered, likely contributing to sustained detrimental effects into adulthood. These regulatory systems include epigenetic remodeling as well as non-coding RNA networks, which can act to reprogram the basal cellular function in progeny and cause predisposition to metabolic disorders that modulate analogous pathways. Maternal PM<sub>2.5</sub> exposure during gestation can promote long-term cardiac remodeling and causes cardiac hypertrophy in young adult progeny, with an increase in both total histone acetylation and promoter acetylation of hypertrophy genes, GATA4 and myocyte enhancer factor 2C (Mef2c) (174). This further suggests the ability of gestational PM exposure to induce global epigenetic remodeling through transcriptional activation of acetylated regions in offspring. Supporting these findings, multiple additional studies have reported a cardiac hypertrophic/fibrotic phenotype, cardiac functional changes, and epigenetic reprogramming in early development due to gestational PM exposure (153, 155, 174). Preconception exposure in both parents to PM<sub>2.5</sub> resulted in progeny with decreased ejection fraction, fractional shortening, and cardiomyocyte contractility at twelve weeks of age (153). Epigenetic assessments suggested changes that were indicative of reprogramming induced by the particulate exposure, with decreased expression of the maintenance methyltransferase DNMT1, but increased histone deacetylase sirtuin (SIRT) 1/2. This pattern of expression may be explained by the ability of SIRT to regulate DNMTs and alter their activity. Similar to preconception exposure, PM<sub>2.5</sub> exposure during gestation also impaired cardiac function of progeny at twelve weeks of age, revealed by decreased fractional shortening and left

ventricular posterior wall thickness, and increased left ventricular systolic/diastolic diameters and collagen deposition in cardiac tissue (155). Epigenetic regulation likely contributed substantially to persistent cardiac detriments as seen in the preceding study. In contrast with preconception PM exposure (153), gestational exposure decreased SIRT1/2 and increased DNMT1, DNMT3a, and DNMT3b expression (155). Although there are differences in expression profiles of these epigenetic regulators that likely stem from the time of exposure (preconception vs. gestation), both are representative of profiles that can cause sustained biological detriments and/or susceptibility to pathologic insult. ENM inhalation exposure during gestation causes similar changes to DNA methylation machinery (87). Maternal exposure to nano-TiO<sub>2</sub> during gestation decreases cardiac output and increases left ventricular mass with a subsequent decrease in fractional shortening in progeny. These functional alterations were linked to elevated levels of 5-methylcytosine (5-mC), a marker of global DNA methylation, DNMT1 protein expression, and HIF-1 $\alpha$  activity (87). Along with DNA methylation, changes in the histone composition of DNA can contribute to modified gene expression profiles. Chromatin immunoprecipitation sequencing for histone 3 lysine 4/27 trimethylation (H3K4me3 and H3K27me3), coupled with the transcriptomic profiling of fetal cardiac tissue from dams exposed to ENM during gestation, has revealed significant changes to major pathways including immune adaptation and organismal growth (143). The authors suggest that cardiovascular outcomes at the young adult stage may actually be linked to liver and fetal development, evidenced through IPA protein ontology. MicroRNAs have also been implicated in metabolic changes in offspring as a result of gestational particulate exposure (57). Diesel exhaust exposure *in utero* decreased methylation of microRNA133a-2 at the promoter region in isolated neonatal cardiomyocytes (57). As the progeny aged, introducing stress, such as transverse aortic constriction, enhanced microRNA-133a-2 and decreased protein tyrosine phosphatase receptor type F (PTPRF) and peptidase domain containing associated with muscle regeneration 1 (PAMR1) expression, which mediate adult sensitivity to heart failure by inducing pathologic hypertrophic signaling or preventing antihypertrophic signaling (57). Currently longitudinal studies on the effects of maternal exposure to various pollutants on offspring cardiovascular function are limited. **Figure 1.3** provides a summary of the factors involved in epigenetic regulation that have been discussed in this review, in the context of preconception/gestational particulate inhalation exposure. Functional genomics studies that combine transcriptomic, proteomic, and metabolomic data in cohorts presenting with particulate-induced cardiovascular alterations will provide a more

thorough understanding of early epigenetic remodeling and its involvement in contributing to CVD predisposition later in life.

**Figure 1.3: Epigenetic Alterations.**



**Figure 1.3:** Epigenetic alterations observed following gestational and/or preconception particulate inhalation exposures. Gene expression of GATA4 and MEF2C are increased through promoter acetylation at H3K9. MicroRNA-133a-2 expression is repressed through elevated 5mC. DNA methyl transferases (DNMT1, DNMT3a, and DNMT3b) are all increased following exposure, along with increased expression of transcription factors (STAT3 and HIF-1 $\alpha$ ). H3K4me3 and H3K27me3 alterations are observed at promoter regions throughout the genome. The histone deacetylases, SIRT1/2, reveal a dysregulated expression profile in progeny exposed during gestation. All abbreviations are defined in the Abbreviations section provided.

## Future Directions

From a morning commute, to an occupational setting, to our very homes, exposure to particulates remains a central issue for debate and therapeutic/lifestyle interventions.

Industrialization and increased urbanization will continue to exacerbate issues concerning air quality and human health, unless better defined guidelines and limits are introduced. Although we provide a summary of the molecular mechanisms propagating cardiovascular decline following exposure in human and animal models, areas of research that are crucial in driving the field of molecular inhalation cardiovascular toxicology forward, still remain uncharted. Future investigations should aim to address understudied populations.

There are limited studies investigating whether increased particulate matter exposure is associated with higher rates of cardiac arrest. One study that aimed to assess this association in New York City reported that a  $10 \mu\text{g}/\text{m}^3$  increase in  $\text{PM}_{2.5}$  one day before and day of the event significantly increased the relative risk for a cardiac arrest in the warm season (141). Similar results were seen in Melbourne (35), Copenhagen (168), Indianapolis (137), and Houston (42). Contrarily, a study done in Stockholm (134) and several studies by a group in Washington (25, 92, 151), report no association between PM exposure and out-of-hospital cardiac arrests. Nonetheless, due to the high mortality rate associated with cardiac arrests, future studies should attempt to further clarify these associations through assessment of molecular markers.

There has been a growing body of literature exploring the adverse outcomes of PM exposure during gestation, including associations with metabolic dysregulation and cardiovascular deficits. In addition to a necessity for a better understanding of how particles induce specific changes during embryonic and fetal development, evaluation of the long-term effects is essential. This is particularly important for determining whether particulate exposure during gestation elicits alterations to the epigenome of offspring that can cause increased susceptibility to prevalent metabolic disorders, including diabetes mellitus (100). Notably, recent research has revealed the ability for prenatal and perinatal PM exposure to alter glucose metabolism (108) and elevate low-density lipoprotein cholesterol (LDL-C) (104), suggesting an increased risk of diabetes and atherosclerosis. However, the molecular mechanisms were not evaluated. In order to address these gaps in knowledge, focus must turn to the epigenetic effects following particle exposure during intrauterine and early childhood development concomitantly with metabolic assessments, which are currently meager (49, 78).

As we continue to shift the paradigm of cardiovascular research in inhalation toxicology, much of the cellular and molecular mechanisms are yet to be discerned. Cell culture models of

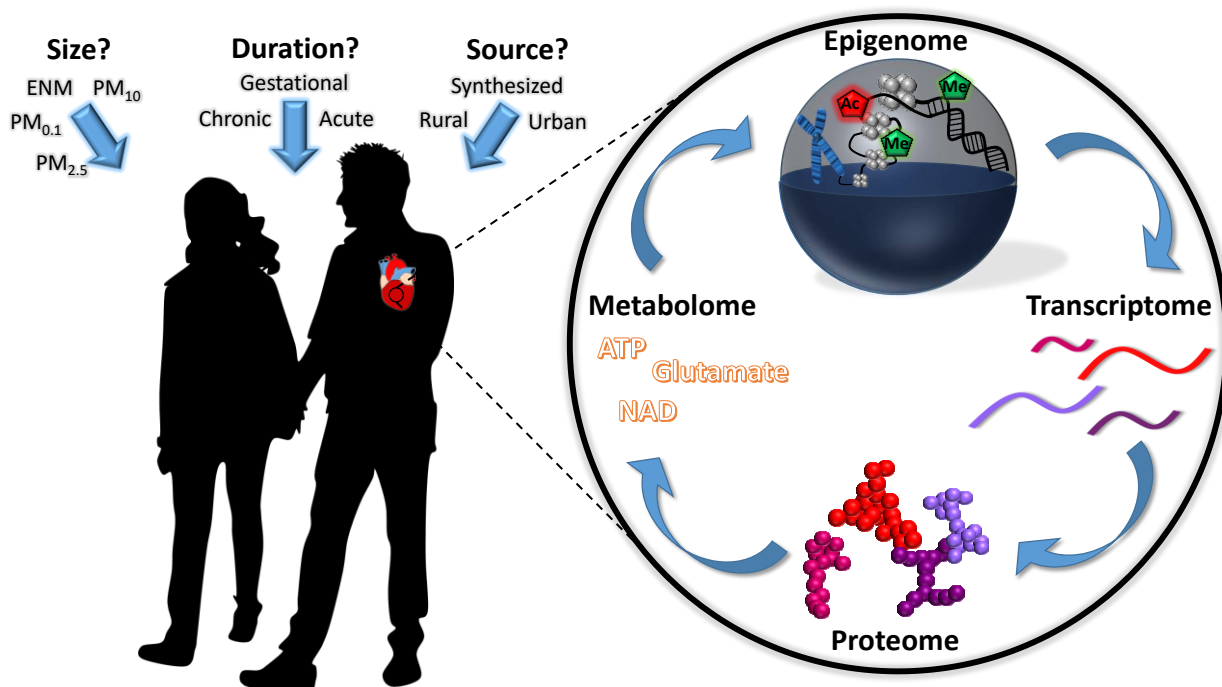
exposure interactions can help provide a foundational understanding of cell and organelle function that cannot be fully captured through *in vivo* inhalation studies. While it remains outside the scope of this review, *in vitro* models can provide a very granular, and controlled approach to mechanistic evaluations. Of note, authors have recently investigated the effects of PM<sub>2.5</sub> exposure (20, 34, 46, 73, 177, 178, 184), as well as the toxicology of nanomaterials and advanced materials (47, 75, 76, 176) in cells. Additionally, *in vitro* studies can provide preliminary data for determining how complex and dynamic mixtures of particulate and gaseous substances affect cardiomyocytes, establishing potential molecular mechanisms and thus setting a path for future *in vivo* experiments (3, 67, 120).

Most of the current research is focused on ambient PM<sub>2.5</sub> exposure, but with standards being set based on mass, UFP concentration is not accounted for thoroughly due to their low mass. However, the high surface area of UFP and ENM makes them considerably detrimental to health, potentially even more than fine and coarse PM (148). As most ambient PM exposures are performed by collection and monitoring of PM in different regions, the problem of variable PM composition in these regions also arises. Integration of ENM exposure with UFP and PM multi-component studies on both humans and mice, will allow for a more thorough interpretation of the direct molecular mechanisms by which pollutants induce toxicity, while also allowing the most relevant elucidation of overall health effects (148). Though co-exposure studies are becoming more common in exploring the effects of present-day air pollution constituents on cardiac function in healthy and metabolically-challenged systems (21, 45, 88, 119, 162), there is limited research assessing both cardiac function and the associated molecular mechanisms, leaving a critical gap in knowledge (3). This is one of the main limitations in many studies that could be addressed with the identification of altered candidate genes via functional genomic approaches.

A clear necessity exists for more encompassing “omics” based approaches. While investigators have begun to examine molecular modulators of the responses to inhalation exposure in the heart, including protein and gene markers for inflammation, few studies have examined the complete cellular protein, gene, or metabolic regulatory networks that coincide with the functional and structural changes. The integration of transcriptomics, epigenomics, proteomics, and other holistic approaches will provide a comprehensive understanding of cellular reprogramming, which can be impacted by the size, source and duration of particle inhalation exposure (**Figure 1.4**). The

implementation of these approaches will outline early biomarkers induced by particulate exposure, ultimately encouraging exposure limits and standards that more precisely prevent the adverse effects of inhaled toxicants.

**Figure 1.4: Overview of Factors Contributing to Cardiovascular Response to Toxicant Inhalation Exposure.**



**Figure 1.4:** An overview of various contributing factors that can differentially alter the cardiovascular responses to toxicant inhalation exposure is provided. Current gaps in knowledge are outlined, including the lack of systemic integration of omics data across varying inhalation exposure paradigms.

**Funding**

This work was supported by: The National Heart Lung Blood Institute (NHLBI) [R01 HL-128485] (JMH), American Heart Association [AHA-20PRE35080170] (AK), American Heart Association [AHA-17PRE33660333] (QAH), and the Community Foundation for the Ohio Valley Whipkey Trust.

**Disclosure Statement**

No potential conflict of interest was reported by the authors.

## References:

1. **Alsaffar H, Martino N, Garrett JP, and Adam AP.** Interleukin-6 promotes a sustained loss of endothelial barrier function via Janus kinase-mediated STAT3 phosphorylation and de novo protein synthesis. *Am J Physiol Cell Physiol* 314: C589-C602, 2018.
2. **Apte JSB, M Cohen, A.J. Ezzati, M., and Pope CA, 3rd.** Ambient PM2.5 Reduces Global and Regional Life Expectancy. *Environ Sci Technol Lett* 5: 546-551, 2018.
3. **Aragon MJ, Chrobak I, Brower J, Roldan L, Fredenburgh LE, McDonald JD, and Campen MJ.** Inflammatory and Vasoactive Effects of Serum Following Inhalation of Varied Complex Mixtures. *Cardiovasc Toxicol* 16: 163-171, 2016.
4. **Aztatzi-Aguilar OG, Uribe-Ramirez M, Arias-Montano JA, Barbier O, and De Vizcaya-Ruiz A.** Acute and subchronic exposure to air particulate matter induces expression of angiotensin and bradykinin-related genes in the lungs and heart: Angiotensin-II type-I receptor as a molecular target of particulate matter exposure. *Part Fibre Toxicol* 12: 17, 2015.
5. **Basner M, Riggs DW, and Conklin DJ.** Environmental Determinants of Hypertension and Diabetes Mellitus: Sounding Off About the Effects of Noise. *J Am Heart Assoc* 9: e016048, 2020.
6. **Bellavia A, Urch B, Speck M, Brook RD, Scott JA, Albeti B, Behbod B, North M, Valeri L, Bertazzi PA, Silverman F, Gold D, and Baccarelli AA.** DNA hypomethylation, ambient particulate matter, and increased blood pressure: findings from controlled human exposure experiments. *J Am Heart Assoc* 2: e000212, 2013.
7. **Bierkandt FS, Leibrock L, Wagener S, Laux P, and Luch A.** The impact of nanomaterial characteristics on inhalation toxicity. *Toxicol Res (Camb)* 7: 321-346, 2018.
8. **Bind MA, Baccarelli A, Zanobetti A, Tarantini L, Suh H, Vokonas P, and Schwartz J.** Air pollution and markers of coagulation, inflammation, and endothelial function: associations and epigenome-environment interactions in an elderly cohort. *Epidemiology* 23: 332-340, 2012.
9. **Bind MA, Coull BA, Peters A, Baccarelli AA, Tarantini L, Cantone L, Vokonas PS, Koutrakis P, and Schwartz JD.** Beyond the Mean: Quantile Regression to Explore the Association of Air Pollution with Gene-Specific Methylation in the Normative Aging Study. *Environ Health Perspect* 123: 759-765, 2015.
10. **Bind MA, Lepeule J, Zanobetti A, Gasparini A, Baccarelli A, Coull BA, Tarantini L, Vokonas PS, Koutrakis P, and Schwartz J.** Air pollution and gene-specific methylation in the Normative Aging Study: association, effect modification, and mediation analysis. *Epigenetics* 9: 448-458, 2014.
11. **Bommarito PA, Martin E, and Fry RC.** Effects of prenatal exposure to endocrine disruptors and toxic metals on the fetal epigenome. *Epigenomics* 9: 333-350, 2017.
12. **Bove H, Bongaerts E, Slenders E, Bijmens EM, Saenen ND, Gyselaers W, Van Eyken P, Plusquin M, Roeffaers MJB, Ameloot M, and Nawrot TS.** Ambient black carbon particles reach the fetal side of human placenta. *Nat Commun* 10: 3866, 2019.
13. **Bowdrige EC, Abukabda AB, Engles KJ, McBride CR, Batchelor TP, Goldsmith WT, Garner KL, Friend S, and Nurkiewicz TR.** Maternal Engineered Nanomaterial Inhalation During Gestation Disrupts Vascular Kisspeptin Reactivity. *Toxicol Sci* 169: 524-533, 2019.
14. **Braakhuis HM, Park MV, Gosens I, De Jong WH, and Cassee FR.** Physicochemical characteristics of nanomaterials that affect pulmonary inflammation. *Part Fibre Toxicol* 11: 18, 2014.



15. **Brook RD, Cakmak S, Turner MC, Brook JR, Crouse DL, Peters PA, van Donkelaar A, Villeneuve PJ, Brion O, Jerrett M, Martin RV, Rajagopalan S, Goldberg MS, Pope CA, 3rd, and Burnett RT.** Long-term fine particulate matter exposure and mortality from diabetes in Canada. *Diabetes Care* 36: 3313-3320, 2013.
16. **Brook RD, Rajagopalan S, Pope CA, 3rd, Brook JR, Bhatnagar A, Diez-Roux AV, Holguin F, Hong Y, Luepker RV, Mittleman MA, Peters A, Siscovick D, Smith SC, Jr., Whitsel L, Kaufman JD, American Heart Association Council on E, Prevention CotKiCD, Council on Nutrition PA, and Metabolism.** Particulate matter air pollution and cardiovascular disease: An update to the scientific statement from the American Heart Association. *Circulation* 121: 2331-2378, 2010.
17. **Brook RD, Xu X, Bard RL, Dvonch JT, Morishita M, Kaciroti N, Sun Q, Harkema J, and Rajagopalan S.** Reduced metabolic insulin sensitivity following sub-acute exposures to low levels of ambient fine particulate matter air pollution. *Sci Total Environ* 448: 66-71, 2013.
18. **Burnett R, Chen H, Szyszkowicz M, Fann N, Hubbell B, Pope CA, 3rd, Apte JS, Brauer M, Cohen A, Weichenthal S, Coggins J, Di Q, Brunekreef B, Frostad J, Lim SS, Kan H, Walker KD, Thurston GD, Hayes RB, Lim CC, Turner MC, Jerrett M, Krewski D, Gapstur SM, Diver WR, Ostro B, Goldberg D, Crouse DL, Martin RV, Peters P, Pinault L, Tjepkema M, van Donkelaar A, Villeneuve PJ, Miller AB, Yin P, Zhou M, Wang L, Janssen NAH, Marra M, Atkinson RW, Tsang H, Quoc Thach T, Cannon JB, Allen RT, Hart JE, Laden F, Cesaroni G, Forastiere F, Weinmayr G, Jaensch A, Nagel G, Concin H, and Spadaro JV.** Global estimates of mortality associated with long-term exposure to outdoor fine particulate matter. *Proc Natl Acad Sci U S A* 115: 9592-9597, 2018.
19. **Byun HM, Colicino E, Trevisi L, Fan T, Christiani DC, and Baccarelli AA.** Effects of Air Pollution and Blood Mitochondrial DNA Methylation on Markers of Heart Rate Variability. *J Am Heart Assoc* 5: 2016.
20. **Cai C, Huang J, Lin Y, Miao W, Chen P, Chen X, Wang J, and Chen M.** Particulate matter 2.5 induced arrhythmogenesis mediated by TRPC3 in human induced pluripotent stem cell-derived cardiomyocytes. *Arch Toxicol* 2019.
21. **Carll AP, Crespo SM, Filho MS, Zati DH, Coull BA, Diaz EA, Raimundo RD, Jaeger TNG, Ricci-Vitor AL, Papapostolou V, Lawrence JE, Garner DM, Perry BS, Harkema JR, and Godleski JJ.** Inhaled ambient-level traffic-derived particulates decrease cardiac vagal influence and baroreflexes and increase arrhythmia in a rat model of metabolic syndrome. *Part Fibre Toxicol* 14: 16, 2017.
22. **Cassee FR, Heroux ME, Gerlofs-Nijland ME, and Kelly FJ.** Particulate matter beyond mass: recent health evidence on the role of fractions, chemical constituents and sources of emission. *Inhal Toxicol* 25: 802-812, 2013.
23. **Castro R, Rivera I, Struys EA, Jansen EE, Ravasco P, Camilo ME, Blom HJ, Jakobs C, and Tavares de Almeida I.** Increased homocysteine and S-adenosylhomocysteine concentrations and DNA hypomethylation in vascular disease. *Clin Chem* 49: 1292-1296, 2003.
24. **Center\_for\_Disease\_Control\_and\_Prevention.** National Diabetes Statistics Report, 2020. Atlanta,GA: Centers for Disease Control and Prevention, U.S. Dept of Health and Human Services, 2020.
25. **Checkoway H, Levy D, Sheppard L, Kaufman J, Koenig J, and Siscovick D.** A case-crossover analysis of fine particulate matter air pollution and out-of-hospital sudden cardiac arrest. *Res Rep Health Eff Inst* 5-28; discussion 29-32, 2000.

26. **Chen H, Burnett RT, Kwong JC, Villeneuve PJ, Goldberg MS, Brook RD, van Donkelaar A, Jerrett M, Martin RV, Brook JR, and Copes R.** Risk of incident diabetes in relation to long-term exposure to fine particulate matter in Ontario, Canada. *Environ Health Perspect* 121: 804-810, 2013.
27. **Chen H, Chen X, Hong X, Liu C, Huang H, Wang Q, Chen S, Chen H, Yang K, and Sun Q.** Maternal exposure to ambient PM<sub>2.5</sub> exaggerates fetal cardiovascular maldevelopment induced by homocysteine in rats. *Environ Toxicol* 32: 877-889, 2017.
28. **Chin MT.** Basic mechanisms for adverse cardiovascular events associated with air pollution. *Heart* 101: 253-256, 2015.
29. **Chu AJ.** Tissue factor, blood coagulation, and beyond: an overview. *Int J Inflamm* 2011: 367284, 2011.
30. **Chu JH, Hart JE, Chhabra D, Garshick E, Raby BA, and Laden F.** Gene expression network analyses in response to air pollution exposures in the trucking industry. *Environ Health* 15: 101, 2016.
31. **Cohen AJ, Brauer M, Burnett R, Anderson HR, Frostad J, Estep K, Balakrishnan K, Brunekreef B, Dandona L, Dandona R, Feigin V, Freedman G, Hubbell B, Jobling A, Kan H, Knibbs L, Liu Y, Martin R, Morawska L, Pope CA, 3rd, Shin H, Straif K, Shaddick G, Thomas M, van Dingenen R, van Donkelaar A, Vos T, Murray CJL, and Forouzanfar MH.** Estimates and 25-year trends of the global burden of disease attributable to ambient air pollution: an analysis of data from the Global Burden of Diseases Study 2015. *Lancet* 389: 1907-1918, 2017.
32. **Croft DP, Cameron SJ, Morrell CN, Lowenstein CJ, Ling F, Zareba W, Hopke PK, Utell MJ, Thurston SW, Thevenet-Morrison K, Evans KA, Chalupa D, and Rich DQ.** Associations between ambient wood smoke and other particulate pollutants and biomarkers of systemic inflammation, coagulation and thrombosis in cardiac patients. *Environ Res* 154: 352-361, 2017.
33. **Dai J, Chen W, Lin Y, Wang S, Guo X, and Zhang QQ.** Exposure to Concentrated Ambient Fine Particulate Matter Induces Vascular Endothelial Dysfunction via miR-21. *Int J Biol Sci* 13: 868-877, 2017.
34. **Dai J, Sun C, Yao Z, Chen W, Yu L, and Long M.** Exposure to concentrated ambient fine particulate matter disrupts vascular endothelial cell barrier function via the IL-6/HIF-1 $\alpha$  signaling pathway. *FEBS Open Bio* 6: 720-728, 2016.
35. **Dennekamp M, Akram M, Abramson MJ, Tonkin A, Sim MR, Fridman M, and Erbas B.** Outdoor air pollution as a trigger for out-of-hospital cardiac arrests. *Epidemiology* 21: 494-500, 2010.
36. **Devlin RB, Smith CB, Schmitt MT, Rappold AG, Hinderliter A, Graff D, and Carraway MS.** Controlled exposure of humans with metabolic syndrome to concentrated ultrafine ambient particulate matter causes cardiovascular effects. *Toxicol Sci* 140: 61-72, 2014.
37. **Donaldson K, Tran L, Jimenez LA, Duffin R, Newby DE, Mills N, MacNee W, and Stone V.** Combustion-derived nanoparticles: a review of their toxicology following inhalation exposure. *Part Fibre Toxicol* 2: 10, 2005.
38. **Dong L, Sun W, Li F, Shi M, Meng X, Wang C, Meng M, Tang W, Liu H, Wang L, and Song L.** The harmful effects of acute PM<sub>2.5</sub> exposure to the heart and a novel preventive and therapeutic function of CEOs. *Sci Rep* 9: 3495, 2019.
39. **Du X, Jiang S, Bo L, Liu J, Zeng X, Xie Y, He Q, Ye X, Song W, and Zhao J.** Combined effects of vitamin E and omega-3 fatty acids on protecting ambient PM<sub>2.5</sub>-induced cardiovascular injury in rats. *Chemosphere* 173: 14-21, 2017.

40. **Du Y, Xu X, Chu M, Guo Y, and Wang J.** Air particulate matter and cardiovascular disease: the epidemiological, biomedical and clinical evidence. *J Thorac Dis* 8: E8-E19, 2016.
41. **Dugershaw BB, Aengenheister L, Hansen SSK, Hougaard KS, and Buerki-Thurnherr T.** Recent insights on indirect mechanisms in developmental toxicity of nanomaterials. *Part Fibre Toxicol* 17: 31, 2020.
42. **Ensor KB, Raun LH, and Persse D.** A case-crossover analysis of out-of-hospital cardiac arrest and air pollution. *Circulation* 127: 1192-1199, 2013.
43. **Espin-Perez A, Krauskopf J, Chadeau-Hyam M, van Veldhoven K, Chung F, Cullinan P, Piepers J, van Herwijnen M, Kubesch N, Carrasco-Turigas G, Nieuwenhuijsen M, Vineis P, Kleinjans JCS, and de Kok T.** Short-term transcriptome and microRNAs responses to exposure to different air pollutants in two population studies. *Environ Pollut* 242: 182-190, 2018.
44. **Fan T, Fang SC, Cavallari JM, Barnett IJ, Wang Z, Su L, Byun HM, Lin X, Baccarelli AA, and Christiani DC.** Heart rate variability and DNA methylation levels are altered after short-term metal fume exposure among occupational welders: a repeated-measures panel study. *BMC Public Health* 14: 1279, 2014.
45. **Farraj AK, Walsh L, Haykal-Coates N, Malik F, McGee J, Winsett D, Duvall R, Kovalcik K, Cascio WE, Higuchi M, and Hazari MS.** Cardiac effects of seasonal ambient particulate matter and ozone co-exposure in rats. *Part Fibre Toxicol* 12: 12, 2015.
46. **Feng L, Yang X, Asweto CO, Wu J, Zhang Y, Hu H, Shi Y, Duan J, and Sun Z.** Genome-wide transcriptional analysis of cardiovascular-related genes and pathways induced by PM2.5 in human myocardial cells. *Environ Sci Pollut Res Int* 24: 11683-11693, 2017.
47. **Feng L, Yang X, Asweto CO, Wu J, Zhang Y, Hu H, Shi Y, Duan J, and Sun Z.** Low-dose combined exposure of nanoparticles and heavy metal compared with PM2.5 in human myocardial AC16 cells. *Environ Sci Pollut Res Int* 24: 27767-27777, 2017.
48. **Feng L, Yang X, Shi Y, Liang S, Zhao T, Duan J, and Sun Z.** Co-exposure subacute toxicity of silica nanoparticles and lead acetate on cardiovascular system. *Int J Nanomedicine* 13: 7819-7834, 2018.
49. **Ferrari L, Carugno M, and Bollati V.** Particulate matter exposure shapes DNA methylation through the lifespan. *Clin Epigenetics* 11: 129, 2019.
50. **Finch J, and Conklin DJ.** Air Pollution-Induced Vascular Dysfunction: Potential Role of Endothelin-1 (ET-1) System. *Cardiovasc Toxicol* 16: 260-275, 2016.
51. **Finch J, Riggs DW, O'Toole TE, Pope CA, 3rd, Bhatnagar A, and Conklin DJ.** Acute exposure to air pollution is associated with novel changes in blood levels of endothelin-1 and circulating angiogenic cells in young, healthy adults. *AIMS Environ Sci* 6: 265-276, 2019.
52. **Fong KC, Di Q, Kloog I, Laden F, Coull BA, Koutrakis P, and Schwartz JD.** Relative toxicities of major particulate matter constituents on birthweight in Massachusetts. *Environ Epidemiol* 3: e047, 2019.
53. **Franck U, Odeh S, Wiedensohler A, Wehner B, and Herbarth O.** The effect of particle size on cardiovascular disorders--the smaller the worse. *Sci Total Environ* 409: 4217-4221, 2011.
54. **Ganguly K, Ettehadih D, Upadhyay S, Takenaka S, Adler T, Karg E, Krombach F, Kreyling WG, Schulz H, Schmid O, and Stoeger T.** Early pulmonary response is critical for extra-pulmonary carbon nanoparticle mediated effects: comparison of inhalation versus intra-arterial infusion exposures in mice. *Part Fibre Toxicol* 14: 19, 2017.
55. **Ghosh Dastidar S, Jagatheesan G, Haberzettl P, Shah J, Hill BG, Bhatnagar A, and Conklin DJ.** Glutathione S-transferase P deficiency induces glucose intolerance via JNK-

dependent enhancement of hepatic gluconeogenesis. *Am J Physiol Endocrinol Metab* 315: E1005-E1018, 2018.

56. **Giles LV, Tebbutt SJ, Carlsten C, and Koehle MS.** The effect of low and high-intensity cycling in diesel exhaust on flow-mediated dilation, circulating NOx, endothelin-1 and blood pressure. *PLoS One* 13: e0192419, 2018.

57. **Goodson JM, Weldy CS, MacDonald JW, Liu Y, Bammler TK, Chien WM, and Chin MT.** In utero exposure to diesel exhaust particulates is associated with an altered cardiac transcriptional response to transverse aortic constriction and altered DNA methylation. *FASEB J* 31: 4935-4945, 2017.

58. **Gordon T, and Reibman J.** Cardiovascular toxicity of inhaled ambient particulate matter. *Toxicol Sci* 56: 2-4, 2000.

59. **Grimmer JA, Tanwar V, Youtz DJ, Adelstein JM, Baine SH, Carnes CA, Baer LA, Stanford KI, and Wold LE.** Exercise does not ameliorate cardiac dysfunction in obese mice exposed to fine particulate matter. *Life Sci* 239: 116885, 2019.

60. **Gubala V, Johnston LJ, Krug HF, Moore CJ, Ober CK, Schwenk M, and Vert M.** Engineered nanomaterials and human health: Part 2. Applications and nanotoxicology (IUPAC Technical Report). *Pure and Applied Chemistry* 90: 1325-1356, 2018.

61. **Gubala V, Johnston LJ, Liu Z, Krug H, Moore CJ, Ober CK, Schwenk M, and Vert M.** Engineered nanomaterials and human health: Part 1. Preparation, functionalization and characterization (IUPAC Technical Report). *Pure and Applied Chemistry* 90: 1283-1324, 2018.

62. **Haberzettl P, Lee J, Duggineni D, McCracken J, Bolanowski D, O'Toole TE, Bhatnagar A, and Conklin DJ.** Exposure to ambient air fine particulate matter prevents VEGF-induced mobilization of endothelial progenitor cells from the bone marrow. *Environ Health Perspect* 120: 848-856, 2012.

63. **Haberzettl P, McCracken JP, Bhatnagar A, and Conklin DJ.** Insulin sensitizers prevent fine particulate matter-induced vascular insulin resistance and changes in endothelial progenitor cell homeostasis. *Am J Physiol Heart Circ Physiol* 310: H1423-1438, 2016.

64. **Haberzettl P, O'Toole TE, Bhatnagar A, and Conklin DJ.** Exposure to Fine Particulate Air Pollution Causes Vascular Insulin Resistance by Inducing Pulmonary Oxidative Stress. *Environ Health Perspect* 124: 1830-1839, 2016.

65. **Hathaway QA, Durr AJ, Shepherd DL, Pinti MV, Brandebura AN, Nichols CE, Kunovac A, Goldsmith WT, Friend SA, Abukabda AB, Fink GK, Nurkiewicz TR, and Hollander JM.** miRNA-378a as a key regulator of cardiovascular health following engineered nanomaterial inhalation exposure. *Nanotoxicology* 1-20, 2019.

66. **Hathaway QA, Nichols CE, Shepherd DL, Stapleton PA, McLaughlin SL, Stricker JC, Rellick SL, Pinti MV, Abukabda AB, McBride CR, Yi J, Stine SM, Nurkiewicz TR, and Hollander JM.** Maternal-engineered nanomaterial exposure disrupts progeny cardiac function and bioenergetics. *Am J Physiol Heart Circ Physiol* 312: H446-H458, 2017.

67. **Helfenstein M, Miragoli M, Rohr S, Muller L, Wick P, Mohr M, Gehr P, and Rothen-Rutishauser B.** Effects of combustion-derived ultrafine particles and manufactured nanoparticles on heart cells in vitro. *Toxicology* 253: 70-78, 2008.

68. **Hendren CO, Mesnard X, Droge J, and Wiesner MR.** Estimating production data for five engineered nanomaterials as a basis for exposure assessment. *Environ Sci Technol* 45: 2562-2569, 2011.

69. **Hojmann Larsen A, Frandsen A, and Treiman M.** Upregulation of the SERCA-type Ca<sup>2+</sup> pump activity in response to endoplasmic reticulum stress in PC12 cells. *BMC Biochem* 2: 4, 2001.
70. **Holland NA, Fraiser CR, Sloan RC, 3rd, Devlin RB, Brown DA, and Wingard CJ.** Ultrafine Particulate Matter Increases Cardiac Ischemia/Reperfusion Injury via Mitochondrial Permeability Transition Pore. *Cardiovasc Toxicol* 17: 441-450, 2017.
71. **Hong F, Wang L, Yu X, Zhou Y, Hong J, and Sheng L.** Toxicological effect of TiO<sub>2</sub> nanoparticle-induced myocarditis in mice. *Nanoscale Res Lett* 10: 1029, 2015.
72. **Hougaard KS, Campagnolo L, Chavatte-Palmer P, Tarrade A, Rousseau-Ralliard D, Valentino S, Park MV, de Jong WH, Wolterink G, Piersma AH, Ross BL, Hutchison GR, Hansen JS, Vogel U, Jackson P, Slama R, Pietroiusti A, and Cassee FR.** A perspective on the developmental toxicity of inhaled nanoparticles. *Reprod Toxicol* 56: 118-140, 2015.
73. **Hu H, Wu J, Li Q, Asweto C, Feng L, Yang X, Duan F, Duan J, and Sun Z.** Fine particulate matter induces vascular endothelial activation via IL-6 dependent JAK1/STAT3 signaling pathway. *Toxicol Res (Camb)* 5: 946-953, 2016.
74. **Huang W, Zhu T, Pan X, Hu M, Lu SE, Lin Y, Wang T, Zhang Y, and Tang X.** Air pollution and autonomic and vascular dysfunction in patients with cardiovascular disease: interactions of systemic inflammation, overweight, and gender. *Am J Epidemiol* 176: 117-126, 2012.
75. **Huerta-Garcia E, Ramos-Godinez MDP, Lopez-Saavedra A, Alfaro-Moreno E, Gomez-Crisostomo NP, Colin-Val Z, Sanchez-Barrera H, and Lopez-Marure R.** Internalization of Titanium Dioxide Nanoparticles Is Mediated by Actin-Dependent Reorganization and Clathrin- and Dynamin-Mediated Endocytosis in H9c2 Rat Cardiomyoblasts. *Chem Res Toxicol* 2019.
76. **Huerta-Garcia E, Zepeda-Quiroz I, Sanchez-Barrera H, Colin-Val Z, Alfaro-Moreno E, Ramos-Godinez MDP, and Lopez-Marure R.** Internalization of Titanium Dioxide Nanoparticles Is Cytotoxic for H9c2 Rat Cardiomyoblasts. *Molecules* 23: 2018.
77. **Husain M, Wu D, Saber AT, Decan N, Jacobsen NR, Williams A, Yauk CL, Wallin H, Vogel U, and Halappanavar S.** Intratracheally instilled titanium dioxide nanoparticles translocate to heart and liver and activate complement cascade in the heart of C57BL/6 mice. *Nanotoxicology* 9: 1013-1022, 2015.
78. **Janssen BG, Madhloum N, Gyselaers W, Bijmens E, Clemente DB, Cox B, Hogervorst J, Luyten L, Martens DS, Peusens M, Plusquin M, Provost EB, Roels HA, Saenen ND, Tsamou M, Vriens A, Winckelmans E, Vrijens K, and Nawrot TS.** Cohort Profile: The ENVIRONmental influence ON early AGEing (ENVIRONAGE): a birth cohort study. *Int J Epidemiol* 46: 1386-1387m, 2017.
79. **Jin Y, Wu Z, Wang N, Duan S, Wu Y, Wang J, Wu W, and Feng F.** Association of EGF Receptor and NLRs signaling with Cardiac Inflammation and Fibrosis in Mice Exposed to Fine Particulate Matter. *J Biochem Mol Toxicol* 30: 429-437, 2016.
80. **Jorgensen RB, Buhagen M, and Foreland S.** Personal exposure to ultrafine particles from PVC welding and concrete work during tunnel rehabilitation. *Occup Environ Med* 73: 467-473, 2016.
81. **Katsouyanni K.** Ambient air pollution and health. *Br Med Bull* 68: 143-156, 2003.
82. **Kessler R.** Engineered nanoparticles in consumer products: understanding a new ingredient. *Environ Health Perspect* 119: a120-125, 2011.

83. **Kietzmann T, Petry A, Shvetsova A, Gerhold JM, and Gorlach A.** The epigenetic landscape related to reactive oxygen species formation in the cardiovascular system. *Br J Pharmacol* 174: 1533-1554, 2017.
84. **Krauskopf J, Caiment F, van Veldhoven K, Chadeau-Hyam M, Sinharay R, Chung KF, Cullinan P, Collins P, Barratt B, Kelly FJ, Vermeulen R, Vineis P, de Kok TM, and Kleinjans JC.** The human circulating miRNome reflects multiple organ disease risks in association with short-term exposure to traffic-related air pollution. *Environ Int* 113: 26-34, 2018.
85. **Kuhlbusch TAJ, Wijnhoven SWP, and Haase A.** Nanomaterial exposures for worker, consumer and the general public. *Nanoimpact* 10: 11-25, 2018.
86. **Kumarathasan P, Vincent R, Blais E, Bielecki A, Guenette J, Filiatreault A, Brion O, Cakmak S, Thomson EM, Shutt R, Kauri LM, Mahmud M, Liu L, and Dales R.** Cardiovascular and inflammatory mechanisms in healthy humans exposed to air pollution in the vicinity of a steel mill. *Part Fibre Toxicol* 15: 34, 2018.
87. **Kunovac A, Hathaway QA, Pinti MV, Goldsmith WT, Durr AJ, Fink GK, Nurkiewicz TR, and Hollander JM.** ROS promote epigenetic remodeling and cardiac dysfunction in offspring following maternal engineered nanomaterial (ENM) exposure. *Part Fibre Toxicol* 16: 24, 2019.
88. **Kurhanewicz N, McIntosh-Kastrinsky R, Tong H, Walsh L, Farraj AK, and Hazari MS.** Ozone co-exposure modifies cardiac responses to fine and ultrafine ambient particulate matter in mice: concordance of electrocardiogram and mechanical responses. *Part Fibre Toxicol* 11: 54, 2014.
89. **Kuroda J, Ago T, Matsushima S, Zhai P, Schneider MD, and Sadoshima J.** NADPH oxidase 4 (Nox4) is a major source of oxidative stress in the failing heart. *Proc Natl Acad Sci U S A* 107: 15565-15570, 2010.
90. **Lane KJ, Levy JI, Scammell MK, Peters JL, Patton AP, Reisner E, Lowe L, Zamore W, Durant JL, and Brugge D.** Association of modeled long-term personal exposure to ultrafine particles with inflammatory and coagulation biomarkers. *Environ Int* 92-93: 173-182, 2016.
91. **Lelieveld J, Klingmuller K, Pozzer A, Poschl U, Fnais M, Daiber A, and Munzel T.** Cardiovascular disease burden from ambient air pollution in Europe reassessed using novel hazard ratio functions. *Eur Heart J* 40: 1590-1596, 2019.
92. **Levy D, Sheppard L, Checkoway H, Kaufman J, Lumley T, Koenig J, and Siscovick D.** A case-crossover analysis of particulate matter air pollution and out-of-hospital primary cardiac arrest. *Epidemiology* 12: 193-199, 2001.
93. **Li KL, and Lin YC.** PM2.5 induced cardiac hypertrophy via CREB/GSK3b/SOS1 pathway and metabolomics alterations. *Oncotarget* 9: 30748-30760, 2018.
94. **Li N, Sioutas C, Cho A, Schmitz D, Misra C, Sempf J, Wang M, Oberley T, Froines J, and Nel A.** Ultrafine particulate pollutants induce oxidative stress and mitochondrial damage. *Environ Health Perspect* 111: 455-460, 2003.
95. **Li R, Kou X, Geng H, Xie J, Tian J, Cai Z, and Dong C.** Mitochondrial damage: an important mechanism of ambient PM2.5 exposure-induced acute heart injury in rats. *J Hazard Mater* 287: 392-401, 2015.
96. **Li W, Dorans KS, Wilker EH, Rice MB, Ljungman PL, Schwartz JD, Coull BA, Koutrakis P, Gold DR, Keaney JF, Jr., Vasan RS, Benjamin EJ, and Mittleman MA.** Short-Term Exposure to Ambient Air Pollution and Biomarkers of Systemic Inflammation: The Framingham Heart Study. *Arterioscler Thromb Vasc Biol* 37: 1793-1800, 2017.
97. **Li W, Dorans KS, Wilker EH, Rice MB, Ljungman PL, Schwartz JD, Coull BA, Koutrakis P, Gold DR, Keaney JF, Jr., Vasan RS, Benjamin EJ, and Mittleman MA.** Short-

term exposure to ambient air pollution and circulating biomarkers of endothelial cell activation: The Framingham Heart Study. *Environ Res* 171: 36-43, 2019.

98. **Li X, Geng J, Chen Y, Chen F, Liu C, Xu Q, Zhao J, Hu J, Xie J, and Xu B.** Exposure to particulate matter induces cardiomyocytes apoptosis after myocardial infarction through NFkappaB activation. *Biochem Biophys Res Commun* 488: 224-231, 2017.

99. **Li Z, Li N, Guo C, Li X, Qian Y, Wu J, Yang Y, and Wei Y.** Genomic DNA methylation signatures in different tissues after ambient air particulate matter exposure. *Ecotoxicol Environ Saf* 179: 175-181, 2019.

100. **Lim CC, and Thurston GD.** Air Pollution, Oxidative Stress, and Diabetes: a Life Course Epidemiologic Perspective. *Curr Diab Rep* 19: 58, 2019.

101. **Liu L, Urch B, Szyszkowicz M, Evans G, Speck M, Van Huang A, Leingartner K, Shutt RH, Pelletier G, Gold DR, Brook JR, Godri Pollitt K, and Silverman FS.** Metals and oxidative potential in urban particulate matter influence systemic inflammatory and neural biomarkers: A controlled exposure study. *Environ Int* 121: 1331-1340, 2018.

102. **Madrigano J, Baccarelli A, Mittleman MA, Wright RO, Sparrow D, Vokonas PS, Tarantini L, and Schwartz J.** Prolonged exposure to particulate pollution, genes associated with glutathione pathways, and DNA methylation in a cohort of older men. *Environ Health Perspect* 119: 977-982, 2011.

103. **Mai AS, Dos Santos AB, Beber LCC, Basso RDB, Sulzbacher LM, Goettems-Fiorin PB, Frizzo MN, Rhoden CR, Ludwig MS, and Heck TG.** Exercise Training under Exposure to Low Levels of Fine Particulate Matter: Effects on Heart Oxidative Stress and Extra-to-Intracellular HSP70 Ratio. *Oxid Med Cell Longev* 2017: 9067875, 2017.

104. **McGuinn LA, Coull BA, Kloog I, Just AC, Tamayo-Ortiz M, Osorio-Yanez C, Baccarelli AA, Wright RJ, Tellez-Rojo MM, and Wright RO.** Fine particulate matter exposure and lipid levels among children in Mexico city. *Environ Epidemiol* 4: e088, 2020.

105. **Melody SM, Ford JB, Wills K, Venn A, and Johnston FH.** Maternal exposure to fine particulate matter from a large coal mine fire is associated with gestational diabetes mellitus: A prospective cohort study. *Environ Res* 183: 108956, 2020.

106. **Miller MR, and Newby DE.** Air pollution and cardiovascular disease: car sick. *Cardiovasc Res* 116: 279-294, 2020.

107. **Miller MR, Shaw CA, and Langrish JP.** From particles to patients: oxidative stress and the cardiovascular effects of air pollution. *Future Cardiol* 8: 577-602, 2012.

108. **Moody EC, Cantoral A, Tamayo-Ortiz M, Pizano-Zarate ML, Schnaas L, Kloog I, Oken E, Coull B, Baccarelli A, Tellez-Rojo MM, Wright RO, and Just AC.** Association of Prenatal and Perinatal Exposures to Particulate Matter With Changes in Hemoglobin A1c Levels in Children Aged 4 to 6 Years. *JAMA Netw Open* 2: e1917643, 2019.

109. **Morales-Rubio RA, Alvarado-Cruz I, Manzano-Leon N, Andrade-Oliva MD, Uribe-Ramirez M, Quintanilla-Vega B, Osornio-Vargas A, and De Vizcaya-Ruiz A.** In utero exposure to ultrafine particles promotes placental stress-induced programming of renin-angiotensin system-related elements in the offspring results in altered blood pressure in adult mice. *Part Fibre Toxicol* 16: 7, 2019.

110. **Mostafavi N, Vermeulen R, Ghantous A, Hoek G, Probst-Hensch N, Herceg Z, Tarallo S, Naccarati A, Kleinjans JCS, Imboden M, Jeong A, Morley D, Amaral AFS, van Nunen E, Gulliver J, Chadeau-Hyam M, Vineis P, and Vlaanderen J.** Acute changes in DNA methylation in relation to 24h personal air pollution exposure measurements: A panel study in four European countries. *Environ Int* 120: 11-21, 2018.

111. **Musman J, Pons S, Barau C, Caccia C, Leoni V, Berdeaux A, Ghaleh B, and Morin D.** Regular treadmill exercise inhibits mitochondrial accumulation of cholesterol and oxysterols during myocardial ischemia-reperfusion in wild-type and ob/ob mice. *Free Radic Biol Med* 101: 317-324, 2016.
112. **Nature\_Nanotechnology.** Nanoplastic should be better understood. *Nat Nanotechnol* 14: 299, 2019.
113. **Nazarenko Y, Zhen H, Han T, Lioy PJ, and Mainelis G.** Nanomaterial inhalation exposure from nanotechnology-based cosmetic powders: a quantitative assessment. *J Nanopart Res* 14: 2012.
114. **Nemmar A, Al-Salam S, Beegam S, Yuvaraju P, and Ali BH.** Thrombosis and systemic and cardiac oxidative stress and DNA damage induced by pulmonary exposure to diesel exhaust particles and the effect of nootkatone thereon. *Am J Physiol Heart Circ Physiol* 314: H917-H927, 2018.
115. **Nemmar A, Holme JA, Rosas I, Schwarze PE, and Alfaro-Moreno E.** Recent advances in particulate matter and nanoparticle toxicology: a review of the in vivo and in vitro studies. *Biomed Res Int* 2013: 279371, 2013.
116. **Nichols CE, Shepherd DL, Hathaway QA, Durr AJ, Thapa D, Abukabda A, Yi J, Nurkiewicz TR, and Hollander JM.** Reactive oxygen species damage drives cardiac and mitochondrial dysfunction following acute nano-titanium dioxide inhalation exposure. *Nanotoxicology* 12: 32-48, 2018.
117. **Niemann B, Rohrbach S, Miller MR, Newby DE, Fuster V, and Kovacic JC.** Oxidative Stress and Cardiovascular Risk: Obesity, Diabetes, Smoking, and Pollution: Part 3 of a 3-Part Series. *J Am Coll Cardiol* 70: 230-251, 2017.
118. **O'Neill MS, Veves A, Sarnat JA, Zanobetti A, Gold DR, Economides PA, Horton ES, and Schwartz J.** Air pollution and inflammation in type 2 diabetes: a mechanism for susceptibility. *Occup Environ Med* 64: 373-379, 2007.
119. **Ocelli F, Lanier C, Cuny D, Deram A, Dumont J, Amouyel P, Montaye M, Dauchet L, Dallongeville J, and Genin M.** Exposure to multiple air pollutants and the incidence of coronary heart disease: A fine-scale geographic analysis. *Sci Total Environ* 714: 136608, 2020.
120. **Okayama Y, Kuwahara M, Suzuki AK, and Tsubone H.** Role of reactive oxygen species on diesel exhaust particle-induced cytotoxicity in rat cardiac myocytes. *J Toxicol Environ Health A* 69: 1699-1710, 2006.
121. **Organisation for Economic Co-operation and Development.** The Economic Consequences of Outdoor Air Pollution Paris: OECD Publishing, 2016.
122. **Pearson JF, Bachireddy C, Shyamprasad S, Goldfine AB, and Brownstein JS.** Association between fine particulate matter and diabetes prevalence in the U.S. *Diabetes Care* 33: 2196-2201, 2010.
123. **Pei Y, Jiang R, Zou Y, Wang Y, Zhang S, Wang G, Zhao J, and Song W.** Effects of Fine Particulate Matter (PM<sub>2.5</sub>) on Systemic Oxidative Stress and Cardiac Function in ApoE(-/-) Mice. *Int J Environ Res Public Health* 13: 2016.
124. **Peters A, Hampel R, Cyrus J, Breitner S, Geruschkat U, Kraus U, Zareba W, and Schneider A.** Elevated particle number concentrations induce immediate changes in heart rate variability: a panel study in individuals with impaired glucose metabolism or diabetes. *Part Fibre Toxicol* 12: 7, 2015.



125. **Pietroiusti A, Stockmann-Juvala H, Lucaroni F, and Savolainen K.** Nanomaterial exposure, toxicity, and impact on human health. *Wiley Interdiscip Rev Nanomed Nanobiotechnol* 2018.
126. **Pons S, Martin V, Portal L, Zini R, Morin D, Berdeaux A, and Ghaleh B.** Regular treadmill exercise restores cardioprotective signaling pathways in obese mice independently from improvement in associated co-morbidities. *J Mol Cell Cardiol* 54: 82-89, 2013.
127. **Pope CA, 3rd, Bhatnagar A, McCracken JP, Abplanalp W, Conklin DJ, and O'Toole T.** Exposure to Fine Particulate Air Pollution Is Associated With Endothelial Injury and Systemic Inflammation. *Circ Res* 119: 1204-1214, 2016.
128. **Pope CA, 3rd, Burnett RT, Thurston GD, Thun MJ, Calle EE, Krewski D, and Godleski JJ.** Cardiovascular mortality and long-term exposure to particulate air pollution: epidemiological evidence of general pathophysiological pathways of disease. *Circulation* 109: 71-77, 2004.
129. **Pope CA, 3rd, Muhlestein JB, May HT, Renlund DG, Anderson JL, and Horne BD.** Ischemic heart disease events triggered by short-term exposure to fine particulate air pollution. *Circulation* 114: 2443-2448, 2006.
130. **Pope CA, 3rd, Turner MC, Burnett RT, Jerrett M, Gapstur SM, Diver WR, Krewski D, and Brook RD.** Relationships between fine particulate air pollution, cardiometabolic disorders, and cardiovascular mortality. *Circ Res* 116: 108-115, 2015.
131. **Qin G, Xia J, Zhang Y, Guo L, Chen R, and Sang N.** Ambient fine particulate matter exposure induces reversible cardiac dysfunction and fibrosis in juvenile and older female mice. *Part Fibre Toxicol* 15: 27, 2018.
132. **Ramanathan G, Yin F, Speck M, Tseng CH, Brook JR, Silverman F, Urch B, Brook RD, and Araujo JA.** Effects of urban fine particulate matter and ozone on HDL functionality. *Part Fibre Toxicol* 13: 26, 2016.
133. **Rao X, Zhong J, Maiseyeu A, Gopalakrishnan B, Villamena FA, Chen LC, Harkema JR, Sun Q, and Rajagopalan S.** CD36-dependent 7-ketocholesterol accumulation in macrophages mediates progression of atherosclerosis in response to chronic air pollution exposure. *Circ Res* 115: 770-780, 2014.
134. **Raza A, Bellander T, Bero-Bedada G, Dahlquist M, Hollenberg J, Jonsson M, Lind T, Rosenqvist M, Svensson L, and Ljungman PL.** Short-term effects of air pollution on out-of-hospital cardiac arrest in Stockholm. *Eur Heart J* 35: 861-868, 2014.
135. **Riggs DW, Zafar N, Krishnasamy S, Yeager R, Rai SN, Bhatnagar A, and O'Toole TE.** Exposure to airborne fine particulate matter is associated with impaired endothelial function and biomarkers of oxidative stress and inflammation. *Environ Res* 180: 108890, 2020.
136. **Robichaud CO, Uyar AE, Darby MR, Zucker LG, and Wiesner MR.** Estimates of upper bounds and trends in nano-TiO<sub>2</sub> production as a basis for exposure assessment. *Environ Sci Technol* 43: 4227-4233, 2009.
137. **Rosenthal FS, Carney JP, and Olinger ML.** Out-of-hospital cardiac arrest and airborne fine particulate matter: a case-crossover analysis of emergency medical services data in Indianapolis, Indiana. *Environ Health Perspect* 116: 631-636, 2008.
138. **Ruiz-Pesini E, Mishmar D, Brandon M, Procaccio V, and Wallace DC.** Effects of purifying and adaptive selection on regional variation in human mtDNA. *Science* 303: 223-226, 2004.
139. **Rychlik KA, Secrest JR, Lau C, Pulczynski J, Zamora ML, Leal J, Langley R, Myatt LG, Raju M, Chang RC, Li Y, Golding MC, Rodrigues-Hoffmann A, Molina MJ, Zhang R,**

- and Johnson NM.** In utero ultrafine particulate matter exposure causes offspring pulmonary immunosuppression. *Proc Natl Acad Sci U S A* 116: 3443-3448, 2019.
140. **Sancini G, Farina F, Battaglia C, Cifola I, Mangano E, Mantecca P, Camatini M, and Palestini P.** Health risk assessment for air pollutants: alterations in lung and cardiac gene expression in mice exposed to Milano winter fine particulate matter (PM2.5). *PLoS One* 9: e109685, 2014.
141. **Silverman RA, Ito K, Freese J, Kaufman BJ, De Claro D, Braun J, and Prezant DJ.** Association of ambient fine particles with out-of-hospital cardiac arrests in New York City. *Am J Epidemiol* 172: 917-923, 2010.
142. **Simkhovich BZ, Kleinman MT, and Kloner RA.** Air pollution and cardiovascular injury epidemiology, toxicology, and mechanisms. *J Am Coll Cardiol* 52: 719-726, 2008.
143. **Stapleton PA, Hathaway QA, Nichols CE, Abukabda AB, Pinti MV, Shepherd DL, McBride CR, Yi J, Castranova VC, Hollander JM, and Nurkiewicz TR.** Maternal engineered nanomaterial inhalation during gestation alters the fetal transcriptome. *Part Fibre Toxicol* 15: 3, 2018.
144. **Stapleton PA, Minarchick VC, McCawley M, Knuckles TL, and Nurkiewicz TR.** Xenobiotic particle exposure and microvascular endpoints: a call to arms. *Microcirculation* 19: 126-142, 2012.
145. **Stapleton PA, Nichols CE, Yi J, McBride CR, Minarchick VC, Shepherd DL, Hollander JM, and Nurkiewicz TR.** Microvascular and mitochondrial dysfunction in the female F1 generation after gestational TiO<sub>2</sub> nanoparticle exposure. *Nanotoxicology* 9: 941-951, 2015.
146. **Stebounova LV, Morgan H, Grassian VH, and Brenner S.** Health and safety implications of occupational exposure to engineered nanomaterials. *Wiley Interdiscip Rev Nanomed Nanobiotechnol* 4: 310-321, 2012.
147. **Stewart JC, Chalupa DC, Devlin RB, Frasier LM, Huang LS, Little EL, Lee SM, Phipps RP, Pietropaoli AP, Taubman MB, Utell MJ, and Frampton MW.** Vascular effects of ultrafine particles in persons with type 2 diabetes. *Environ Health Perspect* 118: 1692-1698, 2010.
148. **Stone V, Miller MR, Clift MJD, Elder A, Mills NL, Moller P, Schins RPF, Vogel U, Kreyling WG, Alstrup Jensen K, Kuhlbusch TAJ, Schwarze PE, Hoet P, Pietroiusti A, De Vizcaya-Ruiz A, Baeza-Squiban A, Teixeira JP, Tran CL, and Cassee FR.** Nanomaterials Versus Ambient Ultrafine Particles: An Opportunity to Exchange Toxicology Knowledge. *Environ Health Perspect* 125: 106002, 2017.
149. **Stoyell-Conti FF, Irigoyen MC, Sartori M, Ribeiro AA, Dos Santos F, Machi JF, Figueroa DMT, Rodrigues B, and De Angelis K.** Aerobic Training Is Better Than Resistance Training on Cardiac Function and Autonomic Modulation in Female ob/ob Mice. *Front Physiol* 10: 1464, 2019.
150. **Sturm R.** Local lung deposition of ultrafine particles in healthy adults: experimental results and theoretical predictions. *Ann Transl Med* 4: 420, 2016.
151. **Sullivan J, Ishikawa N, Sheppard L, Siscovick D, Checkoway H, and Kaufman J.** Exposure to ambient fine particulate matter and primary cardiac arrest among persons with and without clinically recognized heart disease. *Am J Epidemiol* 157: 501-509, 2003.
152. **Sun Q, Hong X, and Wold LE.** Cardiovascular effects of ambient particulate air pollution exposure. *Circulation* 121: 2755-2765, 2010.
153. **Tanwar V, Adelstein JM, Grimmer JA, Youtz DJ, Katapadi A, Sugar BP, Falvo MJ, Baer LA, Stanford KI, and Wold LE.** Preconception Exposure to Fine Particulate Matter Leads to Cardiac Dysfunction in Adult Male Offspring. *J Am Heart Assoc* 7: e010797, 2018.

154. **Tanwar V, Adelstein JM, Grimmer JA, Youtz DJ, Sugar BP, and Wold LE.** PM2.5 exposure in utero contributes to neonatal cardiac dysfunction in mice. *Environ Pollut* 230: 116-124, 2017.
155. **Tanwar V, Gorr MW, Velten M, Eichenseer CM, Long VP, 3rd, Bonilla IM, Shettigar V, Ziolo MT, Davis JP, Baine SH, Carnes CA, and Wold LE.** In Utero Particulate Matter Exposure Produces Heart Failure, Electrical Remodeling, and Epigenetic Changes at Adulthood. *J Am Heart Assoc* 6: 2017.
156. **Tanwar V, Katapadi A, Adelstein JM, Grimmer JA, and Wold LE.** Cardiac pathophysiology in response to environmental stress: a current review. *Curr Opin Physiol* 1: 198-205, 2018.
157. **Thompson LC, Walsh L, Martin BL, McGee J, Wood C, Kovalcik K, Pancras JP, Haykal-Coates N, Ledbetter AD, Davies D, Cascio WE, Higuchi M, Hazari MS, and Farraj AK.** Ambient Particulate Matter and Acrolein Co-Exposure Increases Myocardial Dyssynchrony in Mice via TRPA1. *Toxicol Sci* 167: 559-572, 2019.
158. **Tobaldini E, Bollati V, Prado M, Fiorelli EM, Pecis M, Bissolotti G, Albetti B, Cantone L, Favero C, Cogliati C, Carrer P, Baccarelli A, Bertazzi PA, and Montano N.** Acute particulate matter affects cardiovascular autonomic modulation and IFN-gamma methylation in healthy volunteers. *Environ Res* 161: 97-103, 2018.
159. **Upadhyay S, Stoeger T, George L, Schladweiler MC, Kodavanti U, Ganguly K, and Schulz H.** Ultrafine carbon particle mediated cardiovascular impairment of aged spontaneously hypertensive rats. *Part Fibre Toxicol* 11: 36, 2014.
160. **Viehmann A, Hertel S, Fuks K, Eisele L, Moebus S, Mohlenkamp S, Nonnemacher M, Jakobs H, Erbel R, Jockel KH, Hoffmann B, and Heinz Nixdorf Recall Investigator G.** Long-term residential exposure to urban air pollution, and repeated measures of systemic blood markers of inflammation and coagulation. *Occup Environ Med* 72: 656-663, 2015.
161. **Villarreal-Calderon R, Franco-Lira M, Gonzalez-Maciel A, Reynoso-Robles R, Harritt L, Perez-Guille B, Ferreira-Azevedo L, Drecktrah D, Zhu H, Sun Q, Torres-Jardon R, Aragon-Flores M, Calderon-Garciduenas A, Diaz P, and Calderon-Garciduenas L.** Up-regulation of mRNA ventricular PRNP prion protein gene expression in air pollution highly exposed young urbanites: endoplasmic reticulum stress, glucose regulated protein 78, and nanosized particles. *Int J Mol Sci* 14: 23471-23491, 2013.
162. **Wagner JG, Allen K, Yang HY, Nan B, Morishita M, Mukherjee B, Dvonch JT, Spino C, Fink GD, Rajagopalan S, Sun Q, Brook RD, and Harkema JR.** Cardiovascular depression in rats exposed to inhaled particulate matter and ozone: effects of diet-induced metabolic syndrome. *Environ Health Perspect* 122: 27-33, 2014.
163. **Wang G, Zhen L, Lu P, Jiang R, and Song W.** [Effects of ozone and fine particulate matter (PM2.5) on rat cardiac autonomic nervous system and systemic inflammation]. *Wei Sheng Yan Jiu* 42: 554-560, 2013.
164. **Wang H, Peng X, Cao F, Wang Y, Shi H, Lin S, Zhong W, and Sun J.** Cardiotoxicity and Mechanism of Particulate Matter 2.5 (PM2.5) Exposure in Offspring Rats During Pregnancy. *Med Sci Monit* 23: 3890-3896, 2017.
165. **Wang H, Shen X, Tian G, Shi X, Huang W, Wu Y, Sun L, Peng C, Liu S, Huang Y, Chen X, Zhang F, Chen Y, Ding W, and Lu Z.** AMPKalpha2 deficiency exacerbates long-term PM2.5 exposure-induced lung injury and cardiac dysfunction. *Free Radic Biol Med* 121: 202-214, 2018.

166. **Wang P, You D, Saravia J, Shen H, and Cormier SA.** Maternal exposure to combustion generated PM inhibits pulmonary Th1 maturation and concomitantly enhances postnatal asthma development in offspring. *Part Fibre Toxicol* 10: 29, 2013.
167. **Wang Q, Gan X, Li F, Chen Y, Fu W, Zhu X, Xu D, Long M, and Xu D.** PM2.5 Exposure Induces More Serious Apoptosis of Cardiomyocytes Mediated by Caspase3 through JNK/ P53 Pathway in Hyperlipidemic Rats. *Int J Biol Sci* 15: 24-33, 2019.
168. **Wichmann J, Folke F, Torp-Pedersen C, Lippert F, Ketznel M, Ellermann T, and Loft S.** Out-of-hospital cardiac arrests and outdoor air pollution exposure in Copenhagen, Denmark. *PLoS One* 8: e53684, 2013.
169. **Wittkopp S, Staimer N, Tjoa T, Gillen D, Daher N, Shafer M, Schauer JJ, Sioutas C, and Delfino RJ.** Mitochondrial genetic background modifies the relationship between traffic-related air pollution exposure and systemic biomarkers of inflammation. *PLoS One* 8: e64444, 2013.
170. **Wold LE, Ying Z, Hutchinson KR, Velten M, Gorr MW, Velten C, Youtz DJ, Wang A, Lucchesi PA, Sun Q, and Rajagopalan S.** Cardiovascular remodeling in response to long-term exposure to fine particulate matter air pollution. *Circ Heart Fail* 5: 452-461, 2012.
171. **World Health Organization.** Ambient air pollution: a global assessment of exposure and burden of disease. World Health Organization, 2016.
172. **World Health Organization.** Exposure to ambient air pollution from particulate matter for 2016 World Health Organization, 2018.
173. **Wu F, and Zhang J.** The involvement of Nox4 in fine particulate matter exposure-induced cardiac injury in mice. *J Toxicol Sci* 43: 171-181, 2018.
174. **Wu X, Pan B, Liu L, Zhao W, Zhu J, Huang X, and Tian J.** In utero exposure to PM2.5 during gestation caused adult cardiac hypertrophy through histone acetylation modification. *J Cell Biochem* 120: 4375-4384, 2019.
175. **Xing YF, Xu YH, Shi MH, and Lian YX.** The impact of PM2.5 on the human respiratory system. *J Thorac Dis* 8: E69-74, 2016.
176. **Yang X, Feng L, Zhang Y, Hu H, Shi Y, Liang S, Zhao T, Cao L, Duan J, and Sun Z.** Co-exposure of silica nanoparticles and methylmercury induced cardiac toxicity in vitro and in vivo. *Sci Total Environ* 631-632: 811-821, 2018.
177. **Yang X, Feng L, Zhang Y, Hu H, Shi Y, Liang S, Zhao T, Fu Y, Duan J, and Sun Z.** Cytotoxicity induced by fine particulate matter (PM2.5) via mitochondria-mediated apoptosis pathway in human cardiomyocytes. *Ecotoxicol Environ Saf* 161: 198-207, 2018.
178. **Yang X, Feng L, Zhang Y, Shi Y, Liang S, Zhao T, Sun B, Duan J, and Sun Z.** Integrative analysis of methylome and transcriptome variation of identified cardiac disease-specific genes in human cardiomyocytes after PM2.5 exposure. *Chemosphere* 212: 915-926, 2018.
179. **Ye B, Zhong C, Li Q, Xu S, Zhang Y, Zhang X, Chen X, Huang L, Wang H, Zhang Z, Huang J, Sun G, Xiong G, Yang X, Hao L, Yang N, and Wei S.** The Association of Ambient Fine Particulate Matter Exposure During Pregnancy with Blood Glucose Levels and Gestational Diabetes Mellitus Risk: A Prospective Cohort Study in Wuhan, China. *Am J Epidemiol* 2020.
180. **Yoshimura A, Sawada K, Nakamura K, Kinose Y, Nakatsuka E, Kobayashi M, Miyamoto M, Ishida K, Matsumoto Y, Kodama M, Hashimoto K, Mabuchi S, and Kimura T.** Exosomal miR-99a-5p is elevated in sera of ovarian cancer patients and promotes cancer cell invasion by increasing fibronectin and vitronectin expression in neighboring peritoneal mesothelial cells. *BMC Cancer* 18: 1065, 2018.

181. **Zeng X, Liu J, Du X, Zhang J, Pan K, Shan W, Xie Y, Song W, and Zhao J.** The protective effects of selenium supplementation on ambient PM2.5-induced cardiovascular injury in rats. *Environ Sci Pollut Res Int* 25: 22153-22162, 2018.
182. **Zhang G, Wang X, Bi X, Li C, Deng Y, Al-Hashimi AA, Luo X, Gillette TG, Austin RC, Wang Y, and Wang ZV.** GRP78 (Glucose-Regulated Protein of 78 kDa) Promotes Cardiomyocyte Growth Through Activation of GATA4 (GATA-Binding Protein 4). *Hypertension* 73: 390-398, 2019.
183. **Zhang X, Chen Y, Wei H, Qin Y, Hao Y, Zhu Y, Deng F, and Guo X.** Ultrafine carbon black attenuates the antihypertensive effect of captopril in spontaneously hypertensive rats. *Inhal Toxicol* 26: 853-860, 2014.
184. **Zhang Y, Ji X, Ku T, and Sang N.** Inflammatory response and endothelial dysfunction in the hearts of mice co-exposed to SO<sub>2</sub>, NO<sub>2</sub>, and PM<sub>2.5</sub>. *Environ Toxicol* 31: 1996-2005, 2016.
185. **Zhao J, Liu C, Bai Y, Wang TY, Kan H, and Sun Q.** IKK inhibition prevents PM<sub>2.5</sub>-exacerbated cardiac injury in mice with type 2 diabetes. *J Environ Sci (China)* 31: 98-103, 2015.
186. **Zhao L, Zhang L, Chen M, Dong C, Li R, and Cai Z.** Effects of Ambient Atmospheric PM<sub>2.5</sub>, 1-Nitropyrene and 9-Nitroanthracene on DNA Damage and Oxidative Stress in Hearts of Rats. *Cardiovasc Toxicol* 2018.
187. **Zheng Q, Liu H, Zhang J, and Chen D.** The effect of ambient particle matters on hospital admissions for cardiac arrhythmia: a multi-city case-crossover study in China. *Environ Health* 17: 60, 2018.
188. **Zhong J, Colicino E, Lin X, Mehta A, Kloog I, Zanobetti A, Byun HM, Bind MA, Cantone L, Prada D, Tarantini L, Trevisi L, Sparrow D, Vokonas P, Schwartz J, and Baccarelli AA.** Cardiac autonomic dysfunction: particulate air pollution effects are modulated by epigenetic immunoregulation of Toll-like receptor 2 and dietary flavonoid intake. *J Am Heart Assoc* 4: e001423, 2015.
189. **Zhou B, and Tian R.** Mitochondrial dysfunction in pathophysiology of heart failure. *J Clin Invest* 128: 3716-3726, 2018.

# Chapter 2: Specific Aim 1

## ROS Promote Epigenetic Remodeling and Cardiac Dysfunction in Offspring Following Maternal Engineered Nanomaterial (ENM) Exposure

Amina Kunovac<sup>1,2,4</sup>, Quincy A. Hathaway<sup>1,2,4</sup>, Mark V. Pinti<sup>3</sup>, William T. Goldsmith<sup>4,5</sup>, Andrya J. Durr<sup>1,2</sup>, Garrett K. Fink,<sup>1</sup> Timothy R. Nurkiewicz<sup>4,5</sup>, and John M. Hollander<sup>1,2,4</sup>

As published in Part Fibre Toxicol. 2019 Jun 18;16(1):24. doi: 10.1186/s12989-019-0310-8.

<sup>1</sup>Division of Exercise Physiology, West Virginia University School of Medicine, Morgantown, WV, USA.

<sup>2</sup>Mitochondria, Metabolism & Bioenergetics Working Group, West Virginia University School of Medicine, Morgantown, WV, USA. <sup>3</sup>West Virginia University School of Pharmacy, Morgantown, WV, USA. <sup>4</sup>Center for Inhalation Toxicology (iTOX), West Virginia University School of Medicine, Morgantown, WV, USA. <sup>5</sup>Department of Physiology & Pharmacology, Morgantown, WV, USA.

Amina Kunovac; [ak0086@mix.wvu.edu](mailto:ak0086@mix.wvu.edu), Quincy A. Hathaway; [qahathaway@mix.wvu.edu](mailto:qahathaway@mix.wvu.edu), Mark V. Pinti; [mpinti@mix.wvu.edu](mailto:mpinti@mix.wvu.edu), William T. Goldsmith; [wgoldsmi@hsc.wvu.edu](mailto:wgoldsmi@hsc.wvu.edu), Andrya J. Durr; [ajdurr@mix.wvu.edu](mailto:ajdurr@mix.wvu.edu), Garrett K. Fink; [gkf0001@mix.wvu.edu](mailto:gkf0001@mix.wvu.edu), Timothy R. Nurkiewicz; [tnurkiewicz@hsc.wvu.edu](mailto:tnurkiewicz@hsc.wvu.edu), John M. Hollander; [jhollander@hsc.wvu.edu](mailto:jhollander@hsc.wvu.edu)

Corresponding Author:

John M. Hollander, Ph.D., F.A.H.A.

Division of Exercise Physiology

West Virginia University School of Medicine

PO Box 9227

1 Medical Center Drive

Morgantown, WV 26506

Tel: 1-(304) 293-3683

Fax: 1-(304) 293-7105

Email: [jhollander@hsc.wvu.edu](mailto:jhollander@hsc.wvu.edu)

## Abstract

**Background:** Nano-titanium dioxide (nano-TiO<sub>2</sub>) is amongst the most widely utilized engineered nanomaterials (ENMs). However, little is known regarding the consequences maternal ENM inhalation exposure has on growing progeny during gestation. ENM inhalation exposure has been reported to decrease mitochondrial bioenergetics and cardiac function, though the mechanisms responsible are poorly understood. Reactive oxygen species (ROS) are increased as a result of ENM inhalation exposure, but it is unclear whether they impact fetal reprogramming. The purpose of this study was to determine whether maternal ENM inhalation exposure influences progeny cardiac development and epigenomic remodeling.

**Results:** Pregnant FVB dams were exposed to nano-TiO<sub>2</sub> aerosols with a mass concentration of  $12.09 \pm 0.26$  mg/m<sup>3</sup> starting at gestational day five (GD 5), for 6 hours over 6 non-consecutive days. Aerosol size distribution measurements indicated an aerodynamic count median diameter (CMD) of 156 nm with a geometric standard deviation (GSD) of 1.70. Echocardiographic imaging was used to assess cardiac function in maternal, fetal (GD 15), and young adult (11 weeks) animals. Electron transport chain (ETC) complex activities, mitochondrial size, complexity, and respiration were evaluated, along with 5-methylcytosine, Dnmt1 protein expression, and Hif1 $\alpha$  activity. Cardiac functional analyses revealed a 43% increase in left ventricular mass and 25% decrease in cardiac output (fetal), with an 18% decrease in fractional shortening (young adult). In fetal pups, hydrogen peroxide (H<sub>2</sub>O<sub>2</sub>) levels were significantly increased (~10 fold) with a subsequent decrease in expression of the antioxidant enzyme, phospholipid hydroperoxide glutathione peroxidase (GPx4). ETC complex activity IV was decreased by 68% and 46% in fetal and young adult cardiac mitochondria, respectively. DNA methylation was significantly increased in fetal pups following exposure, along with increased Hif1 $\alpha$  activity and Dnmt1 protein expression. Mitochondrial ultrastructure, including increased size, was observed at both fetal and young adult stages following maternal exposure.

**Conclusions:** Maternal inhalation exposure to nano-TiO<sub>2</sub> results in adverse effects on cardiac function that are associated with increased H<sub>2</sub>O<sub>2</sub> levels and dysregulation of the Hif1 $\alpha$ /Dnmt1 regulatory axis in fetal offspring. Our findings suggest a distinct interplay between ROS and epigenetic remodeling that leads to sustained cardiac contractile dysfunction in growing and young adult offspring following maternal ENM inhalation exposure.

**Keywords:** Inhalation; Mitochondria; Bioenergetics; Methylation; GPx4; Hydrogen Peroxide



## Background

An elevated risk of postnatal cardiovascular disease has been imputed to a toxic gestational environment, when the fetus is at a critical point of development (9, 15). The adverse effects of maternal prenatal disease and environment on future progeny were proposed as early as the 1990's with Barker's contribution of the Developmental Origins of Health and Disease hypothesis (4, 29). Recent studies have focused on the consequences of a baleful gestational environment, which include endocrine disruptors, toxic metals, and the subsequent increase in progeny developing cardiovascular, cancer, reproductive, immunological, and neurological diseases (5, 21, 36, 41, 64). However, investigation into organ dysfunction and the molecular consequences of maternal inhalation exposure to engineered nanomaterial (ENM) on developing offspring is lacking.

Titanium dioxide (TiO<sub>2</sub>) is one of the most widely used ENM, being incorporated into toothpaste, cosmetic products, food, paint, and in clinical settings for drug delivery due to its photocatalytic capabilities (47). Although TiO<sub>2</sub> has provided a wealth of benefits in these applications, the potential for adverse effects on manufacturers, consumers, and the environment raise safety concerns that warrant elucidation. Nano-TiO<sub>2</sub> exposure has been shown to have detrimental effects on mitochondrial bioenergetics and cardiovascular function, which are associated with increased levels of reactive oxygen species (ROS) (26). Mitochondrial and cardiac dysfunction are often related due in part to the cardiomyocytes' dependence on mitochondrial ATP generation necessary for maintaining contractile function. Mitochondria are a primary target of oxidant stress due to ROS generation that arises from the electron transport chain (ETC), which can lead to peroxidation of biomembranes and impairment of ATP production (55). As a result, antioxidant defenses are critical for mitochondrial functional preservation.

Using transcriptomics, we had previously found that maternal nano-TiO<sub>2</sub> inhalation exposure induces epigenetic remodeling in offspring through histone modifications (56). Interestingly, an antioxidant defense protein, phospholipid hydroperoxide glutathione peroxidase (GPx4), was the most significantly downregulated transcript (~9 fold) following exposure, when evaluating proteins that are involved in mitochondrial functional processes (PRJNA513051). GPx4 is an antioxidant enzyme that is a primary defense mechanism against oxidation of mitochondrial biomembranes. We have previously reported that overexpression of a mitochondrially-targeted GPx4, also known as mPHGPX, in a transgenic mouse model, was capable of ameliorating H<sub>2</sub>O<sub>2</sub> levels and improving mitochondrial and cardiac function in an acute

nano-TiO<sub>2</sub> inhalation exposure model (39), suggesting that it may be of particular relevance during ENM exposure.

The adverse health effects of gestational ENM exposure on developing offspring have among others been attributed to epigenetic alterations (26, 56). DNA methylation of cytosine, forming 5-methylcytosine (5mC), was one of the first epigenetic modifications identified and it predominantly occurs at 5-C-phosphate-G-3' (CpG sites). The maintenance DNA methyltransferase, DNMT 1, is responsible for mediating epigenetic memory by propagating the initial signal, whereas DNMT 3A/3B are responsible for *de novo* methylation (32). An increase in 5mC at regulatory regions often results in gene repression and silencing (31). The cell alters CpG methylation in an attempt to respond to environmental factors (28). During maternal ENM exposure, toxic metals can interact with the uterine environment and cross the placental barrier causing direct fetal exposure or indirectly eliciting a maternal immune response (9, 24). Additionally, a direct effect on the fetus may be occurring as a result of changes in maternal-fetal hemodynamics following maternal ENM inhalation exposure (1). ENM exposure during gestation may affect fetal cardiac methylation transiently or permanently, resulting in epigenetic reprogramming.

Previous studies have reported cardiovascular changes and epigenetic alterations in fetal-stage offspring of rats exposed to inhaled nano-TiO<sub>2</sub> during gestation, though the mechanisms remain elusive (26, 56). We hypothesized that maternal nano-TiO<sub>2</sub> exposure during gestation may evoke epigenetic remodeling in the fetus initiated through oxidative stress, diminishing cardiac bioenergetics and contractile function. In the current study, we utilized a mouse model of maternal ENM inhalation exposure to explicate the interrelation between ROS (H<sub>2</sub>O<sub>2</sub>) and pathogenesis to cardiac bioenergetic and contractile dysfunction at the acute stage (fetal) and chronic stage (young adult) in progeny. Our study is the first to implement a mouse model in the molecular examination of cardiac alterations elicited by maternal ENM inhalation exposure and the findings suggests that the persistent deleterious consequences observed at the fetal stage may involve sustained epigenetic reprogramming in the heart.

## Methods

### Animal Model

The West Virginia University Animal Care and Use Committee approved all animal studies which conformed to the most current National Institutes of Health (NIH) Guidelines for the Care and Use of Laboratory Animals manual. Friend Virus B NIH Jackson (FVB/NJ) mice (32 females, 12 males at 7 weeks) were purchased from Jackson Laboratory (Bar Harbor, ME). Because FVB mice have prominent pronuclei and reliably large litter sizes, this strain is useful in creating artificial models that are capable of overexpressing or knocking out specific genes, which could be useful in future investigations (65). Male and female FVB mice were housed in the West Virginia University Health Sciences Center Animal Facility and given access to a rodent diet and water *ad libitum*. Before mating, mice were acclimated for a minimum of 48 hours. Identification of the vaginal plug was used to verify pregnancy (~5 days) before the pregnant dams were placed randomly into either the Sham (15 pregnant dams) or nano-TiO<sub>2</sub> exposure (11 pregnant dams) group at approximately gestational day 5 (Sham = GD 4.4, nano-TiO<sub>2</sub> = GD 4.7) (6 exposure times). Echocardiographic assessments were performed on Sham and nano-TiO<sub>2</sub> exposed pregnant dams, as well as in the fetal (Sham = GD 14.4, nano-TiO<sub>2</sub> = GD 13.8) and young adult (Sham = 10.6 weeks, nano-TiO<sub>2</sub> = 10.5 weeks) offspring. Pregnant dams were euthanized (8 Sham and 6 nano-TiO<sub>2</sub> exposed), and the pups were removed from the uterus of the Sham and nano-TiO<sub>2</sub> exposed mothers. On average, pups and maternal tissue, were harvested at gestational days 15.4 (average of 9 pups per mom) and 14.8 (average of 10 pups per mom) from Sham and nano-TiO<sub>2</sub> dams, respectively. The specific gestational days may vary by +1 due to plug checks being administered every 24 hours. Each fetal sample contained all of the pooled tissue from one individual mother separated by heart, lung, and liver. Mothers (7 Sham and 5 nano-TiO<sub>2</sub> exposed) belonging to the portion of the cohort to be used for the young adult study were placed back in their individual cages after echocardiographic assessment. The offspring were born with the singly-housed mothers. Lactation was allowed to occur without intervention and offspring were weaned at 23.9 (Sham) and 22 (nano-TiO<sub>2</sub>) days, housed with offspring from the same mother, and separated by male and female, with no more than 5 animals per cage. Young adult offspring were euthanized, on average, at 10.8 weeks (Sham) and 10.7 weeks (nano-TiO<sub>2</sub>), followed by tissue collection. One, randomly selected young adult was assessed from each mother (7 Sham and 5 nano-TiO<sub>2</sub> exposed) for both groups, with 4 females, 3 males in the Sham group and 2 females,

3 males in the nano-TiO<sub>2</sub> group. The number of samples used per study may vary due to limitations in variability of heart size between fetuses, resulting in lower amounts of protein content.

### **Engineered Nanomaterial Inhalation Exposure**

Nano-TiO<sub>2</sub> P25 powder containing anatase (80%) and rutile (20%) TiO<sub>2</sub> was purchased from Evonik (Aeroxide TiO<sub>2</sub>, Parsipanny, NJ) and prepared by drying, sieving, and storing as previously described (35, 42). The primary particle size (21 nm), the specific surface area (48.08 m<sup>2</sup>/g), and the Zeta potential (-56.6 mV) have been previously reported (39, 42, 48). The use of the nanoparticle aerosol generator for rodent inhalation exposure has been previously described (25). Aerosol characterization of nano-TiO<sub>2</sub> data are shown in **Figure 2.1**. To model the lung burden of nano-TiO<sub>2</sub> exposure during manufacturing, a target aerosol mass concentration of 12 mg/m<sup>3</sup> of engineered nano-TiO<sub>2</sub> for a period of 360 minutes per day for 6 non-consecutive days was chosen. **Figure 2.1A** shows the mass concentration measurements over a typical exposure day; final measurements indicated a daily 360-minute equivalent average mass concentration of 12.09 ± 0.26 mg/m<sup>3</sup>. A high-resolution electrical low-pressure impactor (ELPI+; Dekati, Tampere, Finland), a scanning particle mobility sizer (SMPS 3938; TSI Inc., St. Paul, MN), and an aerodynamic particle sizer (APS 3321; TSI Inc., St. Paul, MN) were used to measure the size of the nano-TiO<sub>2</sub> aerosols. A log-normal fit of the data from the ELPI+ indicated an aerodynamic aerosol size distribution with a CMD of 156 nm and GSD of 1.70 (**Figure 2.1B**). A log-normal fit of the combined data from the SMPS and APS indicated a sized distribution with a CMD of 184 nm and GSD of 2.01 (**Figure 2.1C**). Scanning and transmission electron micrographs (SEM and TEM) of nano-TiO<sub>2</sub> aerosolized particles, sampled from the exposure chamber, are shown in **Figure 2.1D**. The dose required to match the appropriate lung deposition was calculated based on previously described mouse methodology (39). The formula  $D = F \times V \times C \times T$ , where F is the deposition fraction (10%), V is the minute ventilation based on body weight (36.4 ml) (46), C is the mass concentration (12.09 mg/m<sup>3</sup>) and T is the exposure duration (360 minutes), was employed (42, 57). This resulted in a daily deposited nano-TiO<sub>2</sub> lung dose of 15.85 µg (total six exposure dose =95.10 µg). Bedding material soaked with water was used in the exposure chamber to maintain a comfortable humidity during the exposure. Control animals were exposed to HEPA filtered air only with similar chamber conditions in terms of temperature and humidity. The last

exposure was conducted 48 hours prior to sacrifice and tissue harvesting. A timeline for the study can be seen in **Figure 2.1E**.

### **Echocardiography**

Echocardiographic assessments were carried out as previously described (26, 39, 40, 52), in both nano-TiO<sub>2</sub> exposed (n = 11) and Sham filtered-air exposed pregnant dams (n = 15) as well as in the pups at both the fetal (GD 14) and young adult (11 weeks) time points. Echocardiography was analyzed for one fetal pup (first pup in either the right or left horn (n = 15 Sham, n = 11 nano-TiO<sub>2</sub>)) and one young adult (n = 7 Sham, n = 5 nano-TiO<sub>2</sub>) from each mother that was exposed during gestation. Each mouse was anesthetized with inhalant isoflurane, which was then maintained at or below 1% isoflurane to ensure a physiologically relevant heart rate throughout the experiment and reduce the anesthetic-induced effects on cardiac function. Motion mode (M-mode) echocardiographic and Pulse Wave Doppler images were obtained using the Vevo 2100 Imaging System (Visual Sonics, Toronto, Canada).

In maternal and young adult animals, grayscale M-mode parasternal short-axis images at the mid-papillary level of the left ventricle (LV) were used for conventional echocardiographic analysis. In M-mode, interventricular septal, inner, and posterior wall measurements were taken to determine LV thickness on adjacent end-systolic and diastolic peaks in relation to LV trace analysis. Mitral valve Doppler echocardiography was used to assess diastolic function by taking measurements of E- and A- wave velocity, deceleration time, intraventricular relaxation/contraction time, E-wave-to-A-wave ratio, mitral valve area, etc. In fetal pups, cardiac function was also assessed using M-mode and B-mode stress strain by visualizing individual pups in the uterine horn (53). Pulse Wave Doppler echocardiography (Vascular Package) was also used to assess umbilical and uterine flow in pregnant dams using measures of peak systolic velocity, end diastolic velocity, and velocity-time integral (30). These measurements were calculated over three cardiac cycles and averaged. All echocardiographic measurements were acquired by one analyst blinded to the animal exposure group.

### **Speckle-Tracking-Based Strain**

Speckle-tracking-based strain assessments were completed using short and long axis B-mode images as previously described by our laboratory (26, 40, 52). During each cardiac cycle,

measures of strain (total deformation length divided by the original length of a segment, strain rate, displacement length, and velocity) were obtained (8, 44). Endocardium walls were traced and analyzed for three cardiac cycles using a speckle-tracking algorithm in Visual Sonics VevoStrain software (Toronto, Canada). Time-to-peak analysis for curvilinear data, allowing strain and strain rate to be determined, were generated. For maternal and young adult cohorts, speckle-tracking was performed on both long and short axis B-mode images, while fetal groups were only assessed in the short axis. All speckle-tracking-based strain analyses were completed by the same blinded analyst.

### **Fetal Cardiomyocyte Isolation**

Pregnant dams were euthanized one day after echocardiographic assessment, and pups were removed at GD 15 from the nano-TiO<sub>2</sub> exposed and Sham mouse uteri. Maternal and fetal hearts were removed through a midsagittal cut in the thoracic cavity and fetal hearts were pooled (one fetal heart from each exposed mother; Sham = 6 dams, nano-TiO<sub>2</sub> = 5 dams) as previously described (26, 54). The hearts were chopped up and initially washed with 1X ADS buffer (0.1 M NaCl, 1.2 mM NaH<sub>2</sub>PO<sub>4</sub>, 0.8 mM MgSO<sub>4</sub>, 5.4 mM KCl, and 5 mM glucose at pH 7.4). Digestive solution, comprised of 2 mg pancreatin (Sigma Aldrich, St. Louis, MO) and 2 mg of collagen type II (Worthington Biochemical, Lakewood, NJ), mixed with 2 mL of physiological 1X ADS buffer per heart digested, was used to isolate cells. The supernatant was removed from the tissue debris and centrifuged at 180 x g for 7 minutes after each saved digestion. The supernatant was discarded, and 2 ml of newborn calf serum were added to the cell suspension and stored in a 37°C incubator.

A Percoll gradient was made in a 15 mL conical tube for separation of cardiomyocytes from other cells of the heart as previously described (26, 54). The Percoll gradient (density = 1.130 g/ml) was made of two layers: clear (top, density = 1.059 g/ml) and red (bottom, density = 1.082 g/ml). After all cell collection steps, cells were centrifuged at 180 x g and resuspended in 2 ml of 1X ADS buffer, per five hearts. The 2 milliliters of cells were added to the top of the Percoll gradient and centrifuged at 1,620 x g for 30 minutes, with 9-min acceleration and deceleration time. The non-myocardial mesenchymal cells were aspirated, and the cardiac cells were extracted from the middle layer, washed with newborn calf serum, and placed in plating media (with fetal

bovine serum). Two hours after placing in plating media, cells were changed to maintenance media (no fetal bovine serum). Cells were counted using a hemocytometer.

### **Mitochondrial Isolation**

Young adult mice (one from each exposed mother; Sham = 7, nano-TiO<sub>2</sub> = 5) were sacrificed, and hearts were excised through a midsagittal cut in the thoracic cavity. Using differential centrifugation, isolation of mitochondrial, cytosolic, and nuclear fractions was achieved. Subsarcolemmal and interfibrillar mitochondrial subpopulations were isolated as previously described (43) with modifications by our laboratory (6, 7, 18). Due to the limited amount of subpopulation-specific mitochondria, the two subpopulations were combined. The isolated mitochondria were then resuspended in KME buffer (100mM KCl, 50mM MOPS and 0.5mM EGTA pH 7.4). Protein concentrations were determined using the Bradford method with bovine serum albumin as a standard (10).

### **Mitochondrial Respiration**

Freshly isolated mitochondria (from young adults) were used to analyze state 3 and state 4 respiration as previously described (16, 60), with modifications by our laboratory (25). Once isolated, mitochondria were resuspended in KME buffer and protein concentrations were determined. Mitochondrial protein was added to respiration buffer (80 mM KCl, 50 mM MOPS, 1 mmol/l EGTA, 5 mmol/l KH<sub>2</sub>PO<sub>4</sub> and 1 mg/ml BSA) and placed into a respiration chamber connected to a multi-unit (8 channel) Oxytherm Peltier Electrode apparatus (Hansatech Instruments, Norfolk, England). Glutamate (5 mM) and malate (5 mM) were used to initiate maximal complex I-mediated respiration. State 3 (250 mM ADP) and state 4 (ADP-limited) respiration data were expressed as nmol of oxygen consumed/min/mg protein.

### **Cellular and Tissue Bioenergetics**

Fetal isolated cardiomyocytes were plated on F96 V3 cell culture microplates and the Seahorse XF96 was used for analysis (Agilent Technologies, Santa Clara, CA) (26, 51). The pooled samples of fetal cardiomyocytes from the pups of Sham (one pup from each of 6 dams, n=1) and nano-TiO<sub>2</sub>-exposed (one pup from each of 5 dams, n = 1) females were analyzed 5 hours

after plating and normalized to cell number. With the pooled samples, 5-6 replicates per animal group were plated. Isolated cardiac tissue from the young adult offspring were plated on F24 V7-PS cell culture microplates. Oxygen consumption rate, extracellular acidification rate, and proton production rate were measured using oligomycin, carbonyl cyanide-*p*-trifluoromethoxyphenylhydrazone, antimycin A, and rotenone as previously described (66). Mitochondrial respiration measurements included ATP production, proton leak, basal respiration, maximal respiration, and spare capacity.

### **Mitochondrial Size and Internal Complexity**

Size and internal complexity were analyzed in mitochondria isolated from young adult offspring hearts using flow cytometry, as previously described (16, 18, 19, 25, 63). Isolated mitochondria were loaded with the fluorescent probe Mitotracker Deep Red 633 (Invitrogen) for assessment of mitochondrial size and internal complexity, utilizing the forward scatter (FSC), side scatter (SSC), and Sphero AccuCount Blank Particles, 2.0  $\mu\text{m}$  (Spherotech Inc., Lake Forest, IL) sizing beads. Sizing beads allowed for absolute measurement of mitochondrial size through FSC. All flow cytometric measures were captured using the LSRFortessa (BD Biosciences, Franklin Lakes, NJ) at the West Virginia University Flow Cytometry & Single Cell Core Facility. To process data, FCS Express Flow Research Edition (De Novo Software, Glendale, CA) was implemented.

### **Electron Transport Chain (ETC) Complex Activities**

ETC Complex activities (I, III, IV, V) were measured in maternal, fetal, and young adult hearts, placenta, and fetal and young adult liver and lung as previously described (6, 16, 26, 51). For the maternal, fetal, and young adult analyses, whole tissue was homogenized using the Polytron PowerGen 500 S1 tissue homogenizer (Fisher Scientific, Hampton, NH) in RIPA buffer (Life Technologies, Grand Island, NY). The Bradford assay provided normalization of samples by protein content (10). Complex I (reduction of decylubiquinone), complex III (reduction of cytochrome *c*), complex IV (oxidation of reduced cytochrome C), and complex V (pyruvate kinase and phosphoenolpyruvate and ATP production) activities were measured. Final values were expressed as nanomoles consumed per minute per milligram of protein, which was equal to the nanomoles of NADH oxidized per minute per milligram of protein.



## **Hydrogen Peroxide (H<sub>2</sub>O<sub>2</sub>) Production**

Cardiac H<sub>2</sub>O<sub>2</sub> production was analyzed in maternal, fetal, and young adult hearts, placenta, and in fetal and young adult liver and lung using Amplex Red fluorescent dye in the presence of Horse Radish Peroxidase (HRP). The Amplex Red fluorescent dye reacts with H<sub>2</sub>O<sub>2</sub> producing resorufin, a red fluorescent oxidation product. Experiments were carried out using the manufacturer's protocol with minor modifications (39). Cardiac protein was incubated with HRP and Amplex Red dye was added, followed by initiation of mitochondrial H<sub>2</sub>O<sub>2</sub> production using glutamate and malate as substrates. The Flex Station 3 fluorescent plate reader (Molecular Devices, Sunnyvale, CA) was used to assess changes in fluorescence over time and allowed for quantification of H<sub>2</sub>O<sub>2</sub> production normalized per milligram of protein. Due to its electrical neutrality providing the ability to infiltrate out of the mitochondrial membrane, measuring H<sub>2</sub>O<sub>2</sub> as a method of assessing mitochondrial ROS production is a well-established method, along with being more quantitative than methods used to detect other ROS (58). Additionally, assessment of H<sub>2</sub>O<sub>2</sub> levels is particularly important due to its high reactivity towards imperative cellular targets, as compared to using other methods of determining ROS levels such as measuring superoxide, which is not as reactive (58).

## **Western Blot Analyses**

4-12% gradient Bis-Tris gels were used in SDS-PAGE as previously described (3, 6, 7, 18, 40, 60). Protein sample concentrations were standardized with bovine serum albumin using the Bradford method (10). The primary antibodies used included the following: GPx4 (product no.: 10005258, Cayman Chemical, Ann Arbor, MI), Hif1 $\alpha$  (product no.: sc53546, Santa Cruz Biotechnology INC., Dallas, TX), Dnmt1 (product no.: sc271729, Santa Cruz Biotechnology), and Dnmt3b (product no.: ab2851, Abcam, Cambridge, MA). The anti-GAPDH primary antibody (product no.: ab8245, Abcam) was used to normalize protein levels for each blot. Secondary antibodies used included the following: goat anti-mouse IgG HRP conjugate (product no.: 31430; Pierce Biotechnology, Rockford, IL) and goat anti-rabbit IgG HRP conjugate (product no.: 10004301; Cayman Chemical). Pierce enhanced chemiluminescence Western blotting substrate (Pierce Biotechnology) was used to detect signal per manufacturer's instructions. The G:Box Bioimaging system (Syngene, Frederick, MD) was used to detect signals, and data were captured

using GeneSnap/GeneTools software (Syngene). Image J Software (NIH, Bethesda, MD) was used to analyze densitometry. All values were expressed as optical density with arbitrary units.

### **5-mC DNA Analyses**

20 mg of fetal and young adult tissue was cut into  $\sim 2 \text{ mm}^3$  and the DNeasy Blood & Tissue Kit (Qiagen, Hilden, Germany) was used, per manufacturer's instructions, to isolate total DNA. DNA methylation (5-methylcytosine; 5-mC) levels were quantified in the fetal and young adult using a 5-mC DNA ELISA kit (Catalog no: D5326: Zymo Research Corp., Irvine, CA), per manufacturer's instructions. Briefly, 100 ng of DNA was run per well in duplicate on a 96-well plate. DNA was denatured and bound to the 96-well plates. An anti-5-Methylcytosine monoclonal antibody was used with a secondary antibody and HRP developer. Absorbance was measured using the Flex Station 3 fluorescent plate reader (Molecular Devices, Sunnyvale, CA) at 450nm. Using a logarithmic second-order regression equation, total percent (%) methylation was determined.

### **Hif1 $\alpha$ Transcription Factor Analyses**

Hif1 $\alpha$  transcription factor activity was assessed in maternal and fetal hearts, placenta, and fetal lung and liver tissue samples using the Hif1 $\alpha$  Transcription Factor Assay kit (Catalog no: 10006910: Cayman Chemical, Ann Arbor, MI), per manufacturer's instructions. Briefly, fetal nuclear extracts were run, 10  $\mu\text{L}$  per well, in duplicate on a 96-well plate, with the Hif1 $\alpha$  response element immobilized. Hif1 $\alpha$  binds to the response element forming an active HIF transcription factor, which was detected using a Hif1 $\alpha$  primary antibody and a secondary antibody conjugated to HRP. Colorimetric analysis was performed using the Flex Station 3 fluorescent plate reader (Molecular Devices, Sunnyvale, CA) at 450 nm. The Hif1 $\alpha$ transcription factor activity was normalized using the Bradford method and reported per microgram of protein (10).

### **DNMT Activity Analyses**

DNMT activity in fetal heart was measured using a colorimetric assay kit (Catalog no: P-3009: Epigentek Group Inc., Farmingdale, NY), per manufacturer's instructions. Nuclear extracts were loaded onto a 48-well microplate with Adomet, a universal DNMT substrate, and incubated allowing the DNMT enzymes in the protein sample to transfer methyl groups from Adomet to

cytosine, methylating DNA. The wells were washed, and the methylated DNA was captured using an anti-5-mC antibody, then detected using a secondary antibody and enhancer solution. Absorbance was measured using the Flex Station 3 fluorescent plate reader (Molecular Devices, Sunnyvale, CA) at a wavelength of 450 nm and DNMT activity was proportional to the optical density intensity measured. Samples were normalized using the Bradford method and reported per microgram of protein (10).

### ***Ex Vivo* Micro-CT**

Microcomputed tomography (micro-CT) was used to examine the anatomy of the fetal mouse circulatory system as previously described (67). Briefly, one fetus was dissected from a nano-TiO<sub>2</sub> exposed dam and fixed in 10% formalin for 24 hours before being stained with Lugol (product no.: L6146: Sigma Aldrich) solution containing iodine for one week. The fetus was then taken out of the Lugol solution and transferred to a 0.1 N iodine solution (product no.: SI861: Fisher Scientific, Hampton, NH) for one week. After staining, the sample was embedded in agar to be imaged on a high-resolution micro-CT scanner. Imaging, which took approximately six hours, was done with the scanner set to a voltage of 100kV and current at 100μA.

### **Transmission Electron Microscopy**

Mitochondrial ultrastructure was analyzed in four whole fetal hearts, two from each a Sham and nano-TiO<sub>2</sub> exposed mother, after being processed and imaged at the WVU Electron Microscopy Histopathology and Tissue Bank. Due to their small size, the whole fetal hearts were fixed in EM Primary Fixative (3% glutaraldehyde buffered with 0.1 M Cacodylate buffer) for 48 hours. After rinsing in 0.1 M Cacodylate buffer, the samples were fixed in 1% osmium tetroxide/0.8% potassium ferricyanide solution for 1.5 hours, followed by an additional series of 0.1 M Cacodylate buffer washes. Samples were dehydrated through graded alcohols (50%, 75%, 95%, 100%) and acetone, and tissue were infiltrated with a mixture of acetone/resin for one hour each at decreasing ratios (2:1, 1:1, 1:2) followed by 2 infiltrations with pure resin for an hour each under vacuum. The whole fetal hearts were embedded into flat embedding molds and cured at 70°C overnight. 15. Samples were then cut into 85nm sections on a LEICA UCT 9 Ultramicrotome (Leica Microsystems, Wetzlar, Germany) and mounted on copper-coated 200 mesh VELCO grids (2 per sample). The grids were stained with uranyl acetate and lead citrate solutions and imaged

using the JEOL 1010 TEM with side-mount AMT digital camera (JOEL, Akishima, Tokyo, Japan). Semi-quantitative analyses of mitochondrial size were processed through Fiji (NIH). Six to eight randomly selected TEM images of mitochondria per group were used to perform analyses. Mitochondria were quantified through black & white thresholding using the Shanbhag method (50), through individual tracings, color inversion, and quantification.

### **Statistics**

All statistical analyses were performed using GraphPad Prism Software Version 7 for Windows (GraphPad Software, La Jolla CA). To determine statistical significance between Sham and nano-TiO<sub>2</sub>-exposed groups, a two-tailed Student's t-test was used. Statistical difference was defined by  $P \leq 0.05 = *$ ,  $P \leq 0.01 = **$ ,  $P \leq 0.001 = ***$ . All data are presented as the mean  $\pm$  the standard error (SEM) of the mean.

## Results

### Cardiac Function in Maternal, Fetal, and Young Adult Animals

Although nano-TiO<sub>2</sub> inhalation exposure has been shown to negatively impact cardiac function in murine models (26, 56), it is not known if these effects are mimicked following maternal exposure in the fetus. In pregnant dams and fetal and young adult offspring, M-mode (**Table 2.1**) was used to assess cardiac function. Both diastolic diameter and volume were significantly decreased in the nano-TiO<sub>2</sub> exposed pregnant dams as well as stroke volume and cardiac output. Pulse Wave Doppler indices revealed a significant decrease in the Mitral Valve (MV)-A velocity and a significant increase in MV deceleration - acceleration, MV deceleration time, and E/A ratio in the nano-TiO<sub>2</sub> exposed mothers (**Figure 2.2A-D**). Pulse Wave Doppler revealed no significant changes in uterine flow (Supplemental Table 1), but a significant decrease in umbilical end-diastolic velocity (**Figure 2.2E**). This effect may be occurring as a result of increased vascular resistance in the *in utero* circulation, which has been shown to reduce placental perfusion (1) and could increase the rate of perinatal mortality (20).

To better understand how maternal exposure alters fetal circulation, a micro-CT was performed in a maternal nano-TiO<sub>2</sub> exposed progeny (**Figure 2.2F**). The umbilical vein, whose diameter can be measured as way of determining vascular resistance, is also illustrated (**Figure 2.2F**). **Figure 2.2G** shows a representative image of the uterine horn with two pups closest to the cervix, as well as an illustration of how fetal cardiac tissue was gated. In order to assess fetal cardiac function, each individual pup was visualized in the uterine horn and echocardiographic scans were performed *in utero* to determine the effects of maternal ENM inhalation exposure. In the fetal pups, M-mode measurements revealed a significant decrease in cardiac output and a decrease in LV mass, indicating a decrease in heart size (**Table 2.1**). Following maternal ENM inhalation exposure, young adult offspring showed a significant decrease in ejection fraction and fractional shortening compared to controls, indicating changes in LV pump (**Table 2.1**). Pulse Wave Doppler measurements were also taken at the young adult stage and indicated a significant decrease in MV deceleration - acceleration and deceleration time (**Figure 2.2H-I**).

Speckle-tracking stress strain assessments of the pregnant dams and fetal and young adult offspring are included (**Supplemental Table 2.2-2.5**). The maternal stress-strain measurements indicated diastolic dysfunction by an increase in long axis diastolic radial velocity and strain rate, with a significant decrease in long axis systolic radial displacement, radial velocity, and short axis

circumferential strain. Short axis systolic radial strain rate and circumferential displacement were both significantly decreased in the fetal offspring of ENM-exposed dams. Short axis diastolic radial displacement was significantly decreased in the young adult and diastolic longitudinal displacement was significantly increased.

### **Mitochondrial Bioenergetics**

In order to elucidate whether the cardiac dysfunction seen in the offspring of ENM-exposed dams was associated with dysregulation of mitochondrial bioenergetics, mitochondrial respiration was assessed in isolated cardiomyocytes of the fetal pups as well as in isolated mitochondria and whole tissue from young adult progeny. Basal and maximal respiration and ATP production were decreased in the fetal pups of nano-TiO<sub>2</sub> exposed dams as compared to those of Sham-exposed dams (**Figure 2.3A**). No changes in state 3 and state 4 respiration, using both glucose and fatty acid-mediated metabolism, were observed between the Sham- and nano-TiO<sub>2</sub> exposed young adult offspring (**Supplemental Figure 2.1A**), though in isolated cardiac tissue from the young adult, an overall decrease in oxygen consumption rate was observed (**Figure 2.3B**). ETC complex activities were evaluated in the fetal (**Figure 2.3C**) and young adult (**Figure 2.3D**) progeny heart with additional measurements made in the maternal heart, placenta, and fetal and young adult lung and liver (**Supplemental Figure 2.1B-E**). Interestingly, in the placenta, there was a significant decrease in complexes III, IV and V activities in the nano-TiO<sub>2</sub> exposed dams. ETC complex IV activity (**Figure 2.3C-D**) was significantly decreased in both the fetal and young adult offspring heart of ENM-exposed dams, further supporting alterations to mitochondrial bioenergetics (37).

### **H<sub>2</sub>O<sub>2</sub>-Mediated Pathways**

H<sub>2</sub>O<sub>2</sub> production was assessed in maternal, fetal, and young adult hearts, placenta, as well as in fetal and young adult liver and lung. There was a significant increase in H<sub>2</sub>O<sub>2</sub> content in the fetal hearts of pups whose dams were exposed to nano-TiO<sub>2</sub> (**Figure 2.4A**), with a decrease in H<sub>2</sub>O<sub>2</sub> content in the liver (**Supplemental Figure 2.2A**). There were no significant changes in H<sub>2</sub>O<sub>2</sub> content in the young adult offspring heart (**Figure 2.4A**) or other young adult tissues (**Supplemental Figure 2.2A**). Hif1 $\alpha$  activity was measured to assess how H<sub>2</sub>O<sub>2</sub> may influence the transcription factor activity and binding. Hif1 $\alpha$  activity was significantly increased in the hearts of fetal offspring whose dams were exposed to nano-TiO<sub>2</sub> (**Figure 2.4B**) as well as in the maternal

heart (**Supplemental Figure 2.2B**). Intriguingly, there was a decrease in activity in the fetal lung and liver tissues following nano-TiO<sub>2</sub> inhalation exposure (**Supplemental Figure 2.2B**).

Because Hif1 $\alpha$  is a regulator of Dnmt1 expression, we determined whether H<sub>2</sub>O<sub>2</sub>, induced through nano-TiO<sub>2</sub> inhalation exposure, was concomitant with increased transcription of Dnmt1 and, ultimately, DNA methylation patterns. Dnmt1 protein expression in the fetal heart revealed a significant increase in pups whose dams were exposed to nano-TiO<sub>2</sub> (**Figure 2.4C**). Although there was an increase in Dnmt1 protein expression following exposure, Dnmt activity was not significantly altered (**Supplemental Figure 2.2C**). Additionally, we found that Dnmt3b expression was not changed, following maternal inhalation exposure to ENM in fetal offspring (**Supplemental Figure 2.2D**). Global DNA methylation levels displayed a significant increase in the hearts of the pups whose dams were exposed to nano-TiO<sub>2</sub> (**Figure 2.4D**). While we observed an increase in 5-mC DNA methylation in fetal pups whose dams were exposed to nano-TiO<sub>2</sub>, development into adulthood revealed an inverse relationship, with a significant decrease in global DNA methylation (**Supplemental Figure 2.2E**). Augmented 5-mC DNA methylation levels at the fetal stage indicate that maternal nano-TiO<sub>2</sub> exposure during gestation potentially results in the repression of vital genes, which could lead to detrimental dysfunction. Furthermore, cardiac DNA methylation at the fetal and young adult stages reveal an aberrant DNA methylation pattern, which may be attributed to the Hif1 $\alpha$ /Dnmt1 regulatory axis.

#### **GPx4 Expression and Mitochondrial Structure**

We next determined whether enhanced H<sub>2</sub>O<sub>2</sub> levels are associated with the repression of GPx4 protein expression. A significant diminution of GPx4 protein expression was revealed in the fetal hearts of pups whose dams were exposed to nano-TiO<sub>2</sub> during gestation (**Figure 2.4E**), while GPx4 protein levels were unchanged in the young adult offspring (**Figure 2.4F**).

To determine if exposure to nano-TiO<sub>2</sub> affected fetal mitochondrial ultrastructure, TEM was implemented to assess mitochondrial size and complexity (**Figure 2.5A**). Using a semi-quantitative approach, mitochondrial area and internal complexity were shown to be similar between the Sham and nano-TiO<sub>2</sub> groups, while mitochondrial roundness revealed a decrease in the hearts of the maternal nano-TiO<sub>2</sub> exposed fetal offspring (**Figure 2.5B**). To gain insight into the impact of gestational nano-TiO<sub>2</sub> exposure on mitochondrial ultrastructure at the young adult stage, mitochondrial size (**Figure 2.5C**) and complexity (**Figure 2.5D**) were evaluated through

flow cytometry. FSC (size) and SSC (internal complexity) were significantly increased in young adult offspring whose dams were exposed to nano-TiO<sub>2</sub> during gestation. These data are suggestive of an alteration to mitochondrial ultrastructure as a result of gestational nano-TiO<sub>2</sub> exposure; the altered shape of fetal mitochondria could potentially influence the chronic changes to mitochondrial size and internal complexity in the young adults, precipitating sustained bioenergetic and cardiac dysfunction into adulthood.



## Discussion

The use of nanotechnology continues to increase in both the variety of applicable fields, as well as the prevalence within those fields. Nano-TiO<sub>2</sub>'s high refractive index offers high opacity and resistance to corrosion making it beneficial in the industries of paints, inks, papers, and plastics (47). Unfortunately, the repercussions of the rampant use of ENMs remain unclear, along with the mechanisms and solutions to the potential negative consequences. In order to determine how the current exposure paradigm, which achieved a lung burden of 95.10 µg over 6 days, reflects ENM occupational exposure in humans in a manufacturing setting, alveolar surface area was used as previously described (2, 26, 56, 59). The mouse alveolar surface area is 0.05 m<sup>2</sup> (59). Therefore, the mouse lung burden of 95.10 µg would result in 1,902 µg/m<sup>2</sup>. Since the human alveolar surface area is 102 m<sup>2</sup>, the human lung burden with this exposure paradigm would be 194.0 mg. Furthermore, the number of working days it would take to achieve this lung burden in humans was calculated:

$$\text{nano - TiO}_2 \text{ aerosol concentration} \cdot \text{minute ventilation} \\ \cdot \text{exposure duration} \cdot \text{deposition fraction},$$

with the following values:

$$194.0 \text{ mg} = \text{nano - TiO}_2 \text{ aerosol concentration} \\ \cdot 7600 \text{ ml/min} \cdot (8 \text{ hrs/day} \cdot 60 \text{ min/hr}) \cdot 14\%,$$

therefore:

$$194.0 \text{ mg} = \text{nano - TiO}_2 \text{ aerosol concentration} \\ \cdot 0.51 \text{ m}^3/\text{day} \\ 76 \text{ days} = 194.0 \text{ mg} / ((5 \text{ mg/m}^3) \cdot 0.51 \text{ m}^3) \text{ nano-TiO}_2.$$

The National Institute for Occupational Safety and Health (NIOSH) Recommended Exposure Limit for nano-TiO<sub>2</sub> aerosol concentration is 0.3 mg/m<sup>3</sup>, while the Permissible Exposure Limit set by the Occupational Safety and Health Administration is 5 mg/m<sup>3</sup> (56). Consequently, it would require 76 days for a human to achieve analogous lung burdens with the exposure paradigm used in this study. Thus, the findings are of practical relevance for those exposed in an occupational context. Importantly, our results demonstrate that H<sub>2</sub>O<sub>2</sub>-induced stress from maternal nano-TiO<sub>2</sub> inhalation exposure impacts global DNA methylation remodeling, and is associated with sustained mitochondrial bioenergetic and cardiac contractile dysfunction.

Functioning mitochondria are necessary for providing the immense energy requirement that drives cardiac contraction and relaxation. Thus, mitochondrial dysfunction has been widely implicated as a precipitator of cardiac contractile dysfunction. ROS, such as H<sub>2</sub>O<sub>2</sub>, are a by-product of oxidative phosphorylation, and as a result, the mitochondrion is an initial site of generation and damage. Pathological conditions, such as those presented by ENM exposure, have been associated with enhanced ROS production and mitochondrial dysfunction in cardiac tissue that may precede contractile dysfunction (39). H<sub>2</sub>O<sub>2</sub> accumulation in the heart following maternal inhalation exposure to ENMs was significantly associated with negative consequences in the growing fetus, but the direct link between maternal exposure and increased progeny cardiac H<sub>2</sub>O<sub>2</sub> is unknown. One theory suggests that changes in the placental environment, through changes in circulatory flow or inflammation, can trigger tissue specific alterations in the progeny (17).

In the current study we have shown that umbilical blood flow, through a reduction in end-diastolic velocity, was significantly altered (**Figure 2.2E**). Following an ENM exposure paradigm similar to the paradigm used for the current study, an increase in placental vascular resistance was reported, substantiating the antagonistic effects of nano-TiO<sub>2</sub> exposure during gestation (1). Valentino et al. further validate placental circulatory remodeling through a significant decline in placental flow in rabbits, which was observed following gestational exposure to diesel exhaust (61). Additionally, they report decreased vascularization of the placental bed contributing to the effect. Along with diminished maternal-to-fetal blood flow following inhaled gases and particulates, an inflammatory response promoted through the vasculature could also be a contributing factor in untoward cardiovascular events in the growing progeny. Interleukin 1 beta (IL-1 $\beta$ ), IL-6, and monocyte chemoattractant protein-1 (MCP-1) were shown to be significantly elevated in maternal serum following inhalation exposure to ultrafine particulate matter (38). While the direct link between cardiac ROS production/accumulation and alterations to the placental environment are currently unknown, a strong link between placental mitochondrial health (**Supplemental Figures 2.1C-E**) and fetal cardiovascular outcomes is undoubtedly present. Following maternal ENM inhalation exposure, direct interaction of the ENM with the fetus, maternal immune responses, or other responses involving alterations in blood supply or content could all contribute to increased ROS in the cardiac tissue of the growing fetus. This increased fetal ROS, which is returned to baseline in the young adult, likely contributes to sustained cellular

consequences, such as abnormal mitochondrial bioenergetics and ultrastructure which have been observed following ENM exposure, as well as disruption to the epigenome (25, 56).

Under normal conditions, oxygen-dependent prolyl hydroxylases target Hif1 $\alpha$  for proteasomal degradation; however, during hypoxic conditions, such as when ROS levels are elevated, prolyl hydroxylase activity is limited by the lack of oxygen and therefore results in the stabilization of Hif1 $\alpha$  permitting dimerization with Hif1 $\beta$ , which is constitutively expressed (13, 22, 34, 49). This promotes the formation of an active HIF transcription factor complex (14). The Dnmt1 and Dnmt3b promoter regions contain the hypoxia response element (HRE), a consensus sequence for a Hif1 $\alpha$  binding site (62). We found a significant increase in Dnmt1 protein expression, but not activity, further substantiating our hypothesis that in a high ROS environment, elevated Hif1 $\alpha$  activity leads to hypermethylation by causing an increase in Dnmt1 protein expression through promoter binding. DNA hypermethylation can cause enhanced profibrotic gene expression and the hypermethylation of CpG islands of vital genes, causing loss of gene expression (62). This could in turn propagate mitochondrial dysfunction and increased size associated with ENM exposure and increased ROS.

While the direct effects of ROS, such as disruption of protein structure and function, pose a significant threat to cellular health, indirect effects, such as ROS-mediated epigenetic remodeling, can have equal, if not more pronounced, ramifications. In melanoma cells, detachment from the plating surface revealed an increase in ROS, including H<sub>2</sub>O<sub>2</sub>, as well as an increase in global DNA methylation and Dnmt1 expression (11). When introducing an antioxidant, global DNA hypermethylation and Dnmt1 increased expression was shown to be prevented. Outside of global methylation, ROS can induce site-specific methylation profiles. H<sub>2</sub>O<sub>2</sub> has been shown to increase DNMT1 expression, resulting in hypermethylation and decreased expression of runt domain transcription factor 3 (RUNX3) (33). Additionally, increased H<sub>2</sub>O<sub>2</sub> has been linked to DNA hypermethylation and silencing of miRNAs, which regulate the expression of multiple genes and gene pathways in the cell (27). ROS have been linked to epigenetic modification of the promoter region of other glutathione peroxide family members (GPX3) (45).

The schema provided in **Figure 2.6** encompasses the overall mechanism hypothesized based on the data in the current study. At the fetal stage, cardiac function is negatively impacted through increased H<sub>2</sub>O<sub>2</sub> levels, which can have negative consequences on mitochondrial function and bioenergetics. The increased H<sub>2</sub>O<sub>2</sub> can also lead to an activation of Hif1 $\alpha$  activity, which is

then able to transcriptionally activate the promoter region of a variety of genes, including Dnmt1 and other epigenetic machinery. Augmenting Dnmt1 expression would lead to a global or site-specific increase in methylation, and in turn repress pivotal genes such as GPx4. By decreasing antioxidant defenses (GPx4), a futile cycle would be propagated through a decreased ability to scavenge ROS such as H<sub>2</sub>O<sub>2</sub>, resulting in a further increase in ROS. Cardiac and mitochondrial dysfunction are therefore sustained into adulthood due to epigenomic remodeling that occurred at the fetal stage.

The role of epigenetic remodeling has been investigated in terms of the intrauterine environment and external stressors may have negative implications on the growing fetus (23, 64). The offspring of mothers who had diabetes mellitus or were obese during gestation showed increased incidence of epigenetic changes and an increased risk of type 2 diabetes mellitus and other metabolic disorders that can lead to cardiovascular dysfunction (12). Alterations in the epigenome of young adult offspring were also shown as a potential result of ENM exposure in pregnant rats, which could enhance susceptibility to future insult (56). The demonstration of such changes in a mouse model, as detailed in this study, opens up the possibility of examining the fetal and young adult offspring epigenome using genetic manipulations (25, 39).

This study suggests potential mechanisms such as ROS, that can contribute to epigenomic remodeling of the fetus, *in utero*, but the study is limited in unveiling larger pathways associated with increased genome methylation. We provide a mechanism whereby ROS scavenging is decreased, leading to the accumulation of ROS and ultimately methylation of the genome, but it is likely that this pathway is more dynamic with other epigenetic machinery and transcription factors that are altered. Future experimentation into the specific genes and regulatory pathways that are hypermethylated may provide better insight into the mechanisms contributing to the sustained mitochondrial and cardiac dysfunction observed.

## **Conclusions**

This study highlights disruptions in cardiac and mitochondrial function in offspring of nano-TiO<sub>2</sub> exposed mice during gestation. These dysfunctions are sustained into adulthood and are most likely due to epigenetic reprogramming, mediated through enhanced H<sub>2</sub>O<sub>2</sub> which occurs during gestation in the growing fetus. Increased methylation and decreased GPx4 levels suggest repression of important antioxidant proteins, thus perpetuating the inability to control elevated ROS levels and leading to mitochondrial and cardiac dysfunction.

## **Declarations**

### *Ethics approval and consent to participate*

The West Virginia University Animal Care and Use Committee approved all animal studies, which conformed to the most current National Institutes of Health (NIH) Guidelines for the Care and Use of Laboratory Animals manual.

### *Consent for publication*

Not applicable

### *Availability of data and material*

All data generated or analyzed during this study are included in this published article [and its supplementary information files].

### *Competing interests*

The authors declare that they have no competing interests

### *Funding*

R01 HL-128485 (JMH), R01 ES-015022 (TRN), AHA-17PRE33660333 (QAH), DGE-1144676 (QAH, TRN), WV-INBRE support by NIH Grant P20GM103434, WVU Flow Cytometry & Single Cell Core supported by MBRCC CoBRE Grant GM103488 and Fortessa S10 Grant OD016165, and the Community Foundation for the Ohio Valley Whipkey Trust (JMH).

### *Authors' contributions*

AK, QAH, TRN, and JMH conceptualized the project and experimental measures. WTG managed the nano-TiO<sub>2</sub> exposure paradigm. AK, QAH, and AJD handled animals, including management and tissue dissection. AK, QAH, MVP, AJD, and GKF performed experimentation. AK and QAH analyzed and processed results. AK, QAH, MVP, WTG, TRN, and JMH contributed to the writing and editing of the manuscript.

### *Acknowledgements*

We would like to thank Sherri A. Friend and the National Institute for Occupational Safety and Health, Morgantown, WV, USA for providing scanning and transmission electron micrographs of nano-TiO<sub>2</sub> aerosolized particles.

## References:

1. **Abukabda AB, Bowdridge EC, McBride CR, Batchelor TP, Goldsmith WT, Garner KL, Friend S, and Nurkiewicz TR.** Maternal titanium dioxide nanomaterial inhalation exposure compromises placental hemodynamics. *Toxicol Appl Pharmacol* 367: 51-61, 2019.
2. **Abukabda AB, McBride CR, Batchelor TP, Goldsmith WT, Bowdridge EC, Garner KL, Friend S, and Nurkiewicz TR.** Group II innate lymphoid cells and microvascular dysfunction from pulmonary titanium dioxide nanoparticle exposure. *Part Fibre Toxicol* 15: 43, 2018.
3. **Adiotomre PN, Johnstone FD, and Laing IA.** Effect of absent end diastolic flow velocity in the fetal umbilical artery on subsequent outcome. *Arch Dis Child Fetal Neonatal Ed* 76: F35-38, 1997.
4. **Almond D, and Currie J.** Killing Me Softly: The Fetal Origins Hypothesis. *J Econ Perspect* 25: 153-172, 2011.
5. **Bakshi MV, Azimzadeh O, Merl-Pham J, Verreet T, Hauck SM, Benotmane MA, Atkinson MJ, and Tapio S.** In-Utero Low-Dose Irradiation Leads to Persistent Alterations in the Mouse Heart Proteome. *PLoS One* 11: e0156952, 2016.
6. **Baseler WA, Dabkowski ER, Jagannathan R, Thapa D, Nichols CE, Shepherd DL, Croston TL, Powell M, Razunguzwa TT, Lewis SE, Schnell DM, and Hollander JM.** Reversal of mitochondrial proteomic loss in Type 1 diabetic heart with overexpression of phospholipid hydroperoxide glutathione peroxidase. *Am J Physiol Regul Integr Comp Physiol* 304: R553-565, 2013.
7. **Baseler WA, Dabkowski ER, Williamson CL, Croston TL, Thapa D, Powell MJ, Razunguzwa TT, and Hollander JM.** Proteomic alterations of distinct mitochondrial subpopulations in the type 1 diabetic heart: contribution of protein import dysfunction. *Am J Physiol Regul Integr Comp Physiol* 300: R186-200, 2011.
8. **Blessberger H, and Binder T.** Two dimensional speckle tracking echocardiography: clinical applications. *Heart* 96: 2032-2040, 2010.
9. **Bommarito PA, Martin E, and Fry RC.** Effects of prenatal exposure to endocrine disruptors and toxic metals on the fetal epigenome. *Epigenomics* 9: 333-350, 2017.
10. **Bradford MM.** A rapid and sensitive method for the quantitation of microgram quantities of protein utilizing the principle of protein-dye binding. *Anal Biochem* 72: 248-254, 1976.
11. **Campos AC, Molognoni F, Melo FH, Galdieri LC, Carneiro CR, D'Almeida V, Correa M, and Jasiulionis MG.** Oxidative stress modulates DNA methylation during melanocyte anchorage blockade associated with malignant transformation. *Neoplasia* 9: 1111-1121, 2007.
12. **Cerychova R, Bohuslavova R, Papousek F, Sedmera D, Abaffy P, Benes V, Kolar F, and Pavlinkova G.** Adverse effects of Hif1a mutation and maternal diabetes on the offspring heart. *Cardiovasc Diabetol* 17: 68, 2018.
13. **Chandel NS, McClintock DS, Feliciano CE, Wood TM, Melendez JA, Rodriguez AM, and Schumacker PT.** Reactive oxygen species generated at mitochondrial complex III stabilize hypoxia-inducible factor-1 $\alpha$  during hypoxia: a mechanism of O<sub>2</sub> sensing. *J Biol Chem* 275: 25130-25138, 2000.
14. **Chang TC, Huang CJ, Tam K, Chen SF, Tan KT, Tsai MS, Lin TN, and Shyue SK.** Stabilization of hypoxia-inducible factor-1 $\alpha$  by prostacyclin under prolonged hypoxia via reducing reactive oxygen species level in endothelial cells. *J Biol Chem* 280: 36567-36574, 2005.



15. **Crispi F, Miranda J, and Gratacos E.** Long-term cardiovascular consequences of fetal growth restriction: biology, clinical implications, and opportunities for prevention of adult disease. *Am J Obstet Gynecol* 218: S869-S879, 2018.
16. **Croston TL, Thapa D, Holden AA, Tveter KJ, Lewis SE, Shepherd DL, Nichols CE, Long DM, Olfert IM, Jagannathan R, and Hollander JM.** Functional deficiencies of subsarcolemmal mitochondria in the type 2 diabetic human heart. *Am J Physiol Heart Circ Physiol* 307: H54-65, 2014.
17. **D'Errico JN, and Stapleton PA.** Developmental onset of cardiovascular disease-Could the proof be in the placenta? *Microcirculation* e12526, 2018.
18. **Dabkowski ER, Baseler WA, Williamson CL, Powell M, Razunguzwa TT, Frisbee JC, and Hollander JM.** Mitochondrial dysfunction in the type 2 diabetic heart is associated with alterations in spatially distinct mitochondrial proteomes. *Am J Physiol Heart Circ Physiol* 299: H529-540, 2010.
19. **Dabkowski ER, Williamson CL, Bukowski VC, Chapman RS, Leonard SS, Peer CJ, Callery PS, and Hollander JM.** Diabetic cardiomyopathy-associated dysfunction in spatially distinct mitochondrial subpopulations. *Am J Physiol Heart Circ Physiol* 296: H359-369, 2009.
20. **Gagnon R, Van den Hof M, Diagnostic Imaging Committee E, Council of the Society of O, and Gynaecologists of C.** The use of fetal Doppler in obstetrics. *J Obstet Gynaecol Can* 25: 601-614; quiz 615-606, 2003.
21. **Gauthier TW, Ping XD, Gabelaia L, and Brown LA.** Delayed neonatal lung macrophage differentiation in a mouse model of in utero ethanol exposure. *Am J Physiol Lung Cell Mol Physiol* 299: L8-16, 2010.
22. **Gerald D, Berra E, Frapart YM, Chan DA, Giaccia AJ, Mansuy D, Pouyssegur J, Yaniv M, and Mehta-Grigoriou F.** JunD reduces tumor angiogenesis by protecting cells from oxidative stress. *Cell* 118: 781-794, 2004.
23. **Gluckman PD, Hanson MA, Buklijas T, Low FM, and Beedle AS.** Epigenetic mechanisms that underpin metabolic and cardiovascular diseases. *Nat Rev Endocrinol* 5: 401-408, 2009.
24. **Grafmueller S, Manser P, Diener L, Diener PA, Maeder-Althaus X, Maurizi L, Jochum W, Krug HF, Buerki-Thurnherr T, von Mandach U, and Wick P.** Bidirectional Transfer Study of Polystyrene Nanoparticles across the Placental Barrier in an ex Vivo Human Placental Perfusion Model. *Environ Health Perspect* 123: 1280-1286, 2015.
25. **Hathaway QA, Durr AJ, Shepherd DL, Pinti MV, Brandebura AN, Nichols CE, Kunovac A, Goldsmith WT, Friend SA, Abukabda AB, Fink GK, Nurkiewicz TR, and JM aH.** miRNA-378a as a key regulator of cardiovascular health following engineered nanomaterial inhalation exposure. *Nanotoxicology* 1-20, 2019.
26. **Hathaway QA, Nichols CE, Shepherd DL, Stapleton PA, McLaughlin SL, Stricker JC, Rellick SL, Pinti MV, Abukabda AB, McBride CR, Yi J, Stine SM, Nurkiewicz TR, and Hollander JM.** Maternal-engineered nanomaterial exposure disrupts progeny cardiac function and bioenergetics. *Am J Physiol Heart Circ Physiol* 312: H446-H458, 2017.
27. **He J, Xu Q, Jing Y, Agani F, Qian X, Carpenter R, Li Q, Wang XR, Peiper SS, Lu Z, Liu LZ, and Jiang BH.** Reactive oxygen species regulate ERBB2 and ERBB3 expression via miR-199a/125b and DNA methylation. *EMBO Rep* 13: 1116-1122, 2012.
28. **He Z, Zhang R, Jiang F, Hou W, and Hu C.** Role of genetic and environmental factors in DNA methylation of lipid metabolism. *Genes Dis* 5: 9-15, 2018.

29. **Heindel JJ, and Vandenberg LN.** Developmental origins of health and disease: a paradigm for understanding disease cause and prevention. *Curr Opin Pediatr* 27: 248-253, 2015.
30. **Hernandez-Andrade E, Ahn H, Szalai G, Korzeniewski SJ, Wang B, King M, Chaiworapongsa T, Than NG, and Romero R.** Evaluation of utero-placental and fetal hemodynamic parameters throughout gestation in pregnant mice using high-frequency ultrasound. *Ultrasound Med Biol* 40: 351-360, 2014.
31. **Jang HS, Shin WJ, Lee JE, and Do JT.** CpG and Non-CpG Methylation in Epigenetic Gene Regulation and Brain Function. *Genes (Basel)* 8: 2017.
32. **Jin B, and Robertson KD.** DNA methyltransferases, DNA damage repair, and cancer. *Adv Exp Med Biol* 754: 3-29, 2013.
33. **Kang KA, Zhang R, Kim GY, Bae SC, and Hyun JW.** Epigenetic changes induced by oxidative stress in colorectal cancer cells: methylation of tumor suppressor RUNX3. *Tumour Biol* 33: 403-412, 2012.
34. **Kim GH, Ryan JJ, and Archer SL.** The role of redox signaling in epigenetics and cardiovascular disease. *Antioxid Redox Signal* 18: 1920-1936, 2013.
35. **Knuckles TL, Yi J, Frazer DG, Leonard HD, Chen BT, Castranova V, and Nurkiewicz TR.** Nanoparticle inhalation alters systemic arteriolar vasoreactivity through sympathetic and cyclooxygenase-mediated pathways. *Nanotoxicology* 6: 724-735, 2012.
36. **Leung YK, Govindarajah V, Cheong A, Veevers J, Song D, Gear R, Zhu X, Ying J, Kendler A, Medvedovic M, Belcher S, and Ho SM.** Gestational high-fat diet and bisphenol A exposure heightens mammary cancer risk. *Endocr Relat Cancer* 24: 365-378, 2017.
37. **Li Y, Park JS, Deng JH, and Bai Y.** Cytochrome c oxidase subunit IV is essential for assembly and respiratory function of the enzyme complex. *J Bioenerg Biomembr* 38: 283-291, 2006.
38. **Morales-Rubio RA, Alvarado-Cruz I, Manzano-Leon N, Andrade-Oliva MD, Uribe-Ramirez M, Quintanilla-Vega B, Osornio-Vargas A, and De Vizcaya-Ruiz A.** In utero exposure to ultrafine particles promotes placental stress-induced programming of renin-angiotensin system-related elements in the offspring results in altered blood pressure in adult mice. *Part Fibre Toxicol* 16: 7, 2019.
39. **Nichols CE, Shepherd DL, Hathaway QA, Durr AJ, Thapa D, Abukabda A, Yi J, Nurkiewicz TR, and Hollander JM.** Reactive oxygen species damage drives cardiac and mitochondrial dysfunction following acute nano-titanium dioxide inhalation exposure. *Nanotoxicology* 12: 32-48, 2018.
40. **Nichols CE, Shepherd DL, Knuckles TL, Thapa D, Stricker JC, Stapleton PA, Minarchick VC, Erdely A, Zeidler-Erdely PC, Alway SE, Nurkiewicz TR, and Hollander JM.** Cardiac and mitochondrial dysfunction following acute pulmonary exposure to mountaintop removal mining particulate matter. *Am J Physiol Heart Circ Physiol* 309: H2017-2030, 2015.
41. **Nilsson E, Larsen G, Manikkam M, Guerrero-Bosagna C, Savenkova MI, and Skinner MK.** Environmentally induced epigenetic transgenerational inheritance of ovarian disease. *PLoS One* 7: e36129, 2012.
42. **Nurkiewicz TR, Porter DW, Hubbs AF, Cumpston JL, Chen BT, Frazer DG, and Castranova V.** Nanoparticle inhalation augments particle-dependent systemic microvascular dysfunction. *Part Fibre Toxicol* 5: 1, 2008.
43. **Palmer JW, Tandler B, and Hoppel CL.** Biochemical properties of subsarcolemmal and interfibrillar mitochondria isolated from rat cardiac muscle. *J Biol Chem* 252: 8731-8739, 1977.

44. **Pavlopoulos H, and Nihoyannopoulos P.** Strain and strain rate deformation parameters: from tissue Doppler to 2D speckle tracking. *Int J Cardiovasc Imaging* 24: 479-491, 2008.
45. **Peng DF, Hu TL, Schneider BG, Chen Z, Xu ZK, and El-Rifai W.** Silencing of glutathione peroxidase 3 through DNA hypermethylation is associated with lymph node metastasis in gastric carcinomas. *PLoS One* 7: e46214, 2012.
46. **R. W. Bide SJA, E. Yee.** Estimation of Human Toxicity from Animal Inhalation Toxicity Data: 1. Minute Volume - Body Weight Relationships Between Animals and Man. edited by Suffield DRE. Alberta, Canada: National Defence, 1997.
47. **Robichaud CO, Uyar AE, Darby MR, Zucker LG, and Wiesner MR.** Estimates of upper bounds and trends in nano-TiO<sub>2</sub> production as a basis for exposure assessment. *Environ Sci Technol* 43: 4227-4233, 2009.
48. **Sager TM, Kommineni C, and Castranova V.** Pulmonary response to intratracheal instillation of ultrafine versus fine titanium dioxide: role of particle surface area. *Part Fibre Toxicol* 5: 17, 2008.
49. **Salceda S, and Caro J.** Hypoxia-inducible factor 1alpha (HIF-1alpha) protein is rapidly degraded by the ubiquitin-proteasome system under normoxic conditions. Its stabilization by hypoxia depends on redox-induced changes. *J Biol Chem* 272: 22642-22647, 1997.
50. **Shanbhag AG.** Utilization of Information Measure as a Means of Image Thresholding. *Cvgip-Graph Model Im* 56: 414-419, 1994.
51. **Shepherd DL, Hathaway QA, Pinti MV, Nichols CE, Durr AJ, Sreekumar S, Hughes KM, Stine SM, Martinez I, and Hollander JM.** Exploring the mitochondrial microRNA import pathway through Polynucleotide Phosphorylase (PNPase). *J Mol Cell Cardiol* 110: 15-25, 2017.
52. **Shepherd DL, Nichols CE, Croston TL, McLaughlin SL, Petrone AB, Lewis SE, Thapa D, Long DM, Dick GM, and Hollander JM.** Early detection of cardiac dysfunction in the type 1 diabetic heart using speckle-tracking based strain imaging. *J Mol Cell Cardiol* 90: 74-83, 2016.
53. **Spurney CF, Lo CW, and Leatherbury L.** Fetal mouse imaging using echocardiography: a review of current technology. *Echocardiography* 23: 891-899, 2006.
54. **Sreejit P, Kumar S, and Verma RS.** An improved protocol for primary culture of cardiomyocyte from neonatal mice. *In Vitro Cell Dev Biol Anim* 44: 45-50, 2008.
55. **Srinivasan S, and Avadhani NG.** Cytochrome c oxidase dysfunction in oxidative stress. *Free Radic Biol Med* 53: 1252-1263, 2012.
56. **Stapleton PA, Hathaway QA, Nichols CE, Abukabda AB, Pinti MV, Shepherd DL, McBride CR, Yi J, Castranova VC, Hollander JM, and Nurkiewicz TR.** Maternal engineered nanomaterial inhalation during gestation alters the fetal transcriptome. *Part Fibre Toxicol* 15: 3, 2018.
57. **Stapleton PA, Minarchick VC, Cumpston AM, McKinney W, Chen BT, Sager TM, Frazer DG, Mercer RR, Scabilloni J, Andrew ME, Castranova V, and Nurkiewicz TR.** Impairment of coronary arteriolar endothelium-dependent dilation after multi-walled carbon nanotube inhalation: a time-course study. *Int J Mol Sci* 13: 13781-13803, 2012.
58. **Starkov AA.** Measurement of mitochondrial ROS production. *Methods Mol Biol* 648: 245-255, 2010.
59. **Stone KC, Mercer RR, Gehr P, Stockstill B, and Crapo JD.** Allometric relationships of cell numbers and size in the mammalian lung. *Am J Respir Cell Mol Biol* 6: 235-243, 1992.
60. **Thapa D, Nichols CE, Lewis SE, Shepherd DL, Jagannathan R, Croston TL, Tveter KJ, Holden AA, Baseler WA, and Hollander JM.** Transgenic overexpression of mitofilin

attenuates diabetes mellitus-associated cardiac and mitochondria dysfunction. *J Mol Cell Cardiol* 79: 212-223, 2015.

61. **Valentino SA, Tarrade A, Aioun J, Mourier E, Richard C, Dahirel M, Rousseau-Ralliard D, Fournier N, Aubriere MC, Lallemand MS, Camous S, Guinot M, Charlier M, Aujean E, Al Adhami H, Fokkens PH, Agier L, Boere JA, Cassee FR, Slama R, and Chavatte-Palmer P.** Maternal exposure to diluted diesel engine exhaust alters placental function and induces intergenerational effects in rabbits. *Part Fibre Toxicol* 13: 39, 2016.

62. **Watson CJ, Collier P, Tea I, Neary R, Watson JA, Robinson C, Phelan D, Ledwidge MT, McDonald KM, McCann A, Sharaf O, and Baugh JA.** Hypoxia-induced epigenetic modifications are associated with cardiac tissue fibrosis and the development of a myofibroblast-like phenotype. *Hum Mol Genet* 23: 2176-2188, 2014.

63. **Williamson CL, Dabkowski ER, Baseler WA, Croston TL, Alway SE, and Hollander JM.** Enhanced apoptotic propensity in diabetic cardiac mitochondria: influence of subcellular spatial location. *Am J Physiol Heart Circ Physiol* 298: H633-642, 2010.

64. **Wolstenholme JT, Edwards M, Shetty SR, Gatewood JD, Taylor JA, Rissman EF, and Connelly JJ.** Gestational exposure to bisphenol a produces transgenerational changes in behaviors and gene expression. *Endocrinology* 153: 3828-3838, 2012.

65. **Wong K, Bumpstead S, Van Der Weyden L, Reinholdt LG, Wilming LG, Adams DJ, and Keane TM.** Sequencing and characterization of the FVB/NJ mouse genome. *Genome Biol* 13: R72, 2012.

66. **Yoshida S, Tsutsumi S, Muhlebach G, Sourbier C, Lee MJ, Lee S, Vartholomaïou E, Tatokoro M, Beebe K, Miyajima N, Mohny RP, Chen Y, Hasumi H, Xu W, Fukushima H, Nakamura K, Koga F, Kihara K, Trepel J, Picard D, and Neckers L.** Molecular chaperone TRAP1 regulates a metabolic switch between mitochondrial respiration and aerobic glycolysis. *Proc Natl Acad Sci U S A* 110: E1604-1612, 2013.

67. **Zhou YQ, Cahill LS, Wong MD, Seed M, Macgowan CK, and Sled JG.** Assessment of flow distribution in the mouse fetal circulation at late gestation by high-frequency Doppler ultrasound. *Physiol Genomics* 46: 602-614, 2014.

**Table 2.1: M-Mode Echocardiography**

Parameter	Maternal		Fetal		Young Adult	
	Sham	Ex	Sham	Ex	Sham	Ex
<b>Heart Rate (BPM)</b>	672.05 ± 8.30	685.39 ± 7.01	134.28 ± 8.72	118.94 ± 3.40	649.49 ± 23.72	601.87 ± 65.46
<b>Diameter;s (mm)</b>	0.58 ± 0.05	0.59 ± 0.08	0.25 ± 0.02	0.24 ± 0.02	<b>0.38 ± 0.05</b>	<b>0.73 ± 0.13*</b>
<b>Diameter;d (mm)</b>	<b>2.70 ± 0.08</b>	<b>2.43 ± 0.05*</b>	0.71 ± 0.02	0.69 ± 0.03	1.95 ± 0.13	2.25 ± 0.15
<b>Volume;s (uL)</b>	0.64 ± 0.16	0.53 ± 0.16	0.05 ± 0.01	0.04 ± 0.01	<b>0.14 ± 0.06</b>	<b>0.58 ± 0.13**</b>
<b>Volume;d (uL)</b>	<b>27.60 ± 1.92</b>	<b>21.15 ± 1.13**</b>	0.85 ± 0.08	0.79 ± 0.08	12.64 ± 2.21	14.50 ± 0.58
<b>Stroke Volume (uL)</b>	<b>26.96 ± 1.83</b>	<b>20.43 ± 1.08*</b>	0.80 ± 0.07	0.74 ± 0.07	12.46 ± 2.17	13.92 ± 0.48
<b>Ejection Fraction (%)</b>	97.84 ± 0.43	96.72 ± 0.99	95.16 ± 0.84	94.79 ± 0.67	<b>98.84 ± 0.33</b>	<b>94.65 ± 1.53*</b>
<b>Fractional Shortening (%)</b>	78.56 ± 1.67	75.89 ± 2.95	65.68 ± 2.31	65.62 ± 1.56	<b>80.80 ± 1.89</b>	<b>68.38 ± 3.14**</b>
<b>Cardiac Output (mL/min)</b>	<b>18.17 ± 1.31</b>	<b>13.79 ± 0.67*</b>	<b>0.10 ± 0.01</b>	<b>0.08 ± 0.01*</b>	8.30 ± 1.68	9.35 ± 0.34
<b>LV Mass (mg)</b>	88.03 ± 4.89	75.53 ± 8.13	<b>0.42 ± 0.04</b>	<b>0.74 ± 0.13*</b>	83.42 ± 7.13	79.05 ± 5.59

**Table 2.1: M-mode echocardiography imaging following maternal nano-TiO<sub>2</sub> inhalation exposure.** Measurements were taken for a minimum of 3 consecutive systolic and diastolic peaks and troughs for maternal (n = 15 Sham, n = 11 Ex), fetal (n = 15 Sham, n = 11 Ex), and young adult (n = 7 Sham, n = 5 Ex). Sham = control filtered air exposed, Ex = nano-TiO<sub>2</sub> exposed, Maternal (M) = 12 week old pregnant dams, Fetal (F) = GD (15), Young Adult (YA) = 11 weeks, Diameter;d = diastolic diameter, Diameter;s = systolic diameter, LV Mass = left ventricular mass, V;d = volume during diastole, V;s = volume during systole. All data are presented as the mean ± standard error of the mean (SEM). \* =  $P \leq 0.05$ , \*\* =  $P \leq 0.01$ , \*\*\* =  $P \leq 0.001$  for Ex vs. Sham.

Figure 2.1: Exposure Paradigm

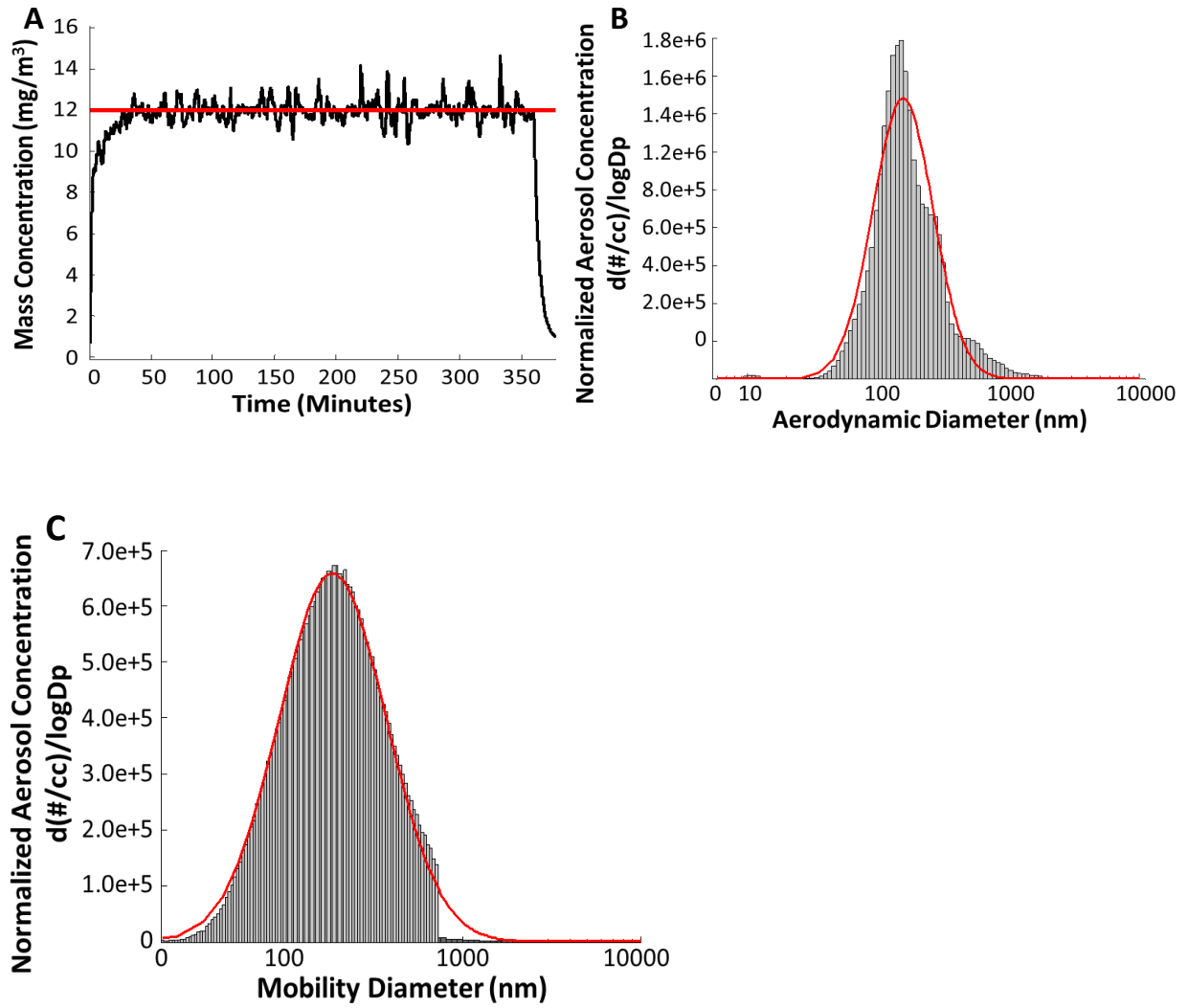
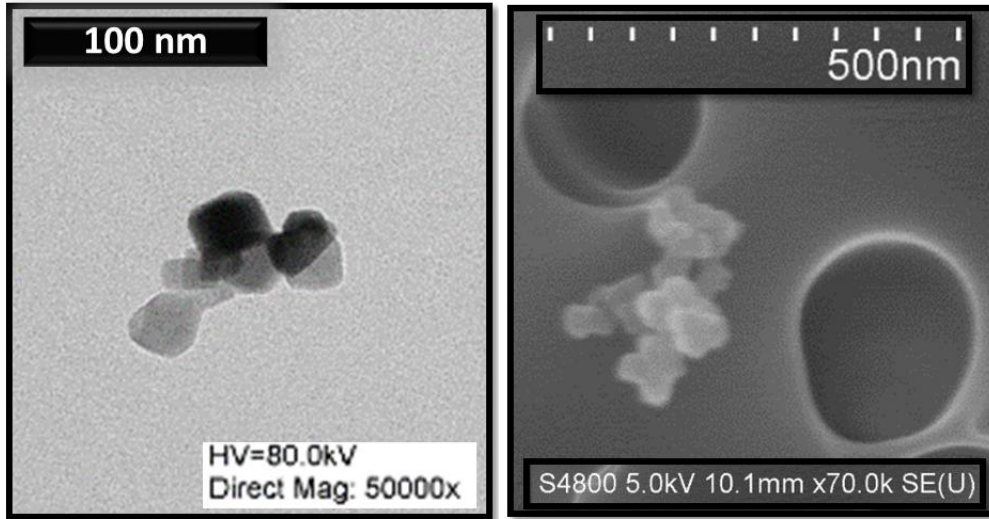
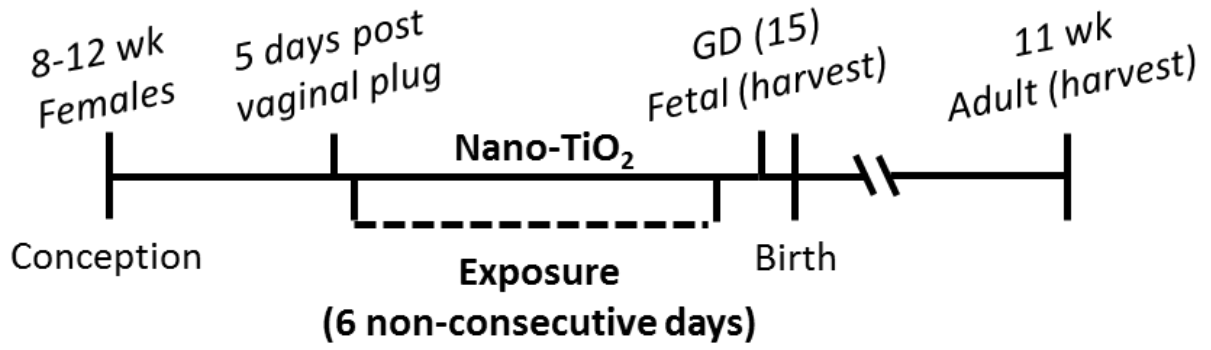


Figure 2.1:

D



E





**Figure 2.1: Maternal nano-TiO<sub>2</sub> inhalation exposure paradigm.** (A) Real-time aerosol mass concentration measurements of engineered nano-TiO<sub>2</sub> during a typical maternal exposure with the target concentration indicated by the red line (12mg/m<sup>3</sup>). (B) Aerodynamic diameter of nano-TiO<sub>2</sub> (CMD = 156 nm) measured by high resolution electric low-pressure impactor (ELPI+). (C) Diameter of nano-TiO<sub>2</sub> (CMD = 184 nm) measured by combining scanning mobility particle sizer (SMPS) and aerodynamic particle sizer (APS) measurements. Red line indicates log-normal fit. (D) Transmission and scanning electron micrographs of nano-TiO<sub>2</sub> aerosolized particles. (E) A timeline of the study. CMD = Count Median Diameter. All data are presented as the mean ± standard error of the mean (SEM).

Figure 2.2: Pulse Wave Doppler and the Fetal Environment

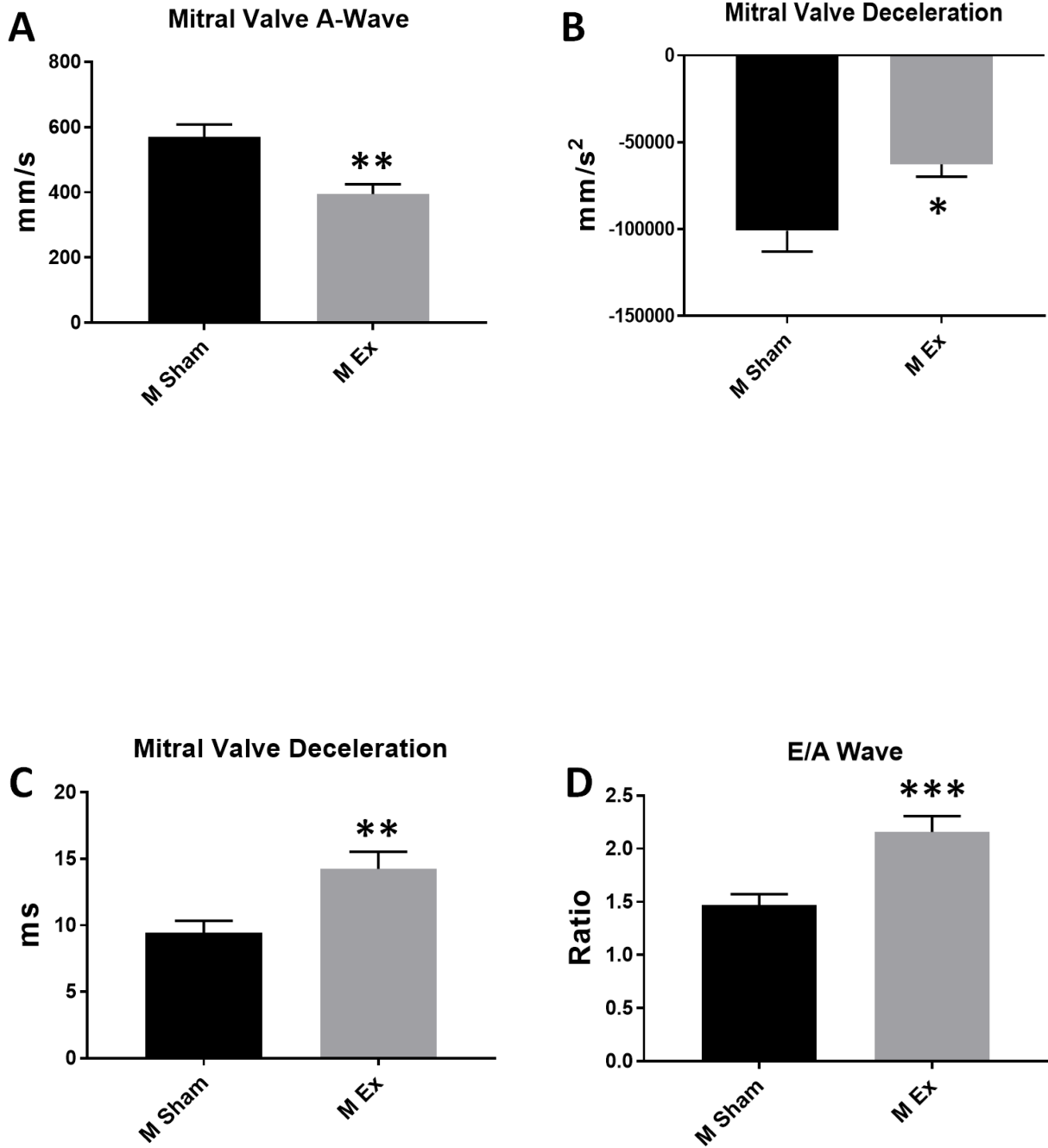


Figure 2.2:

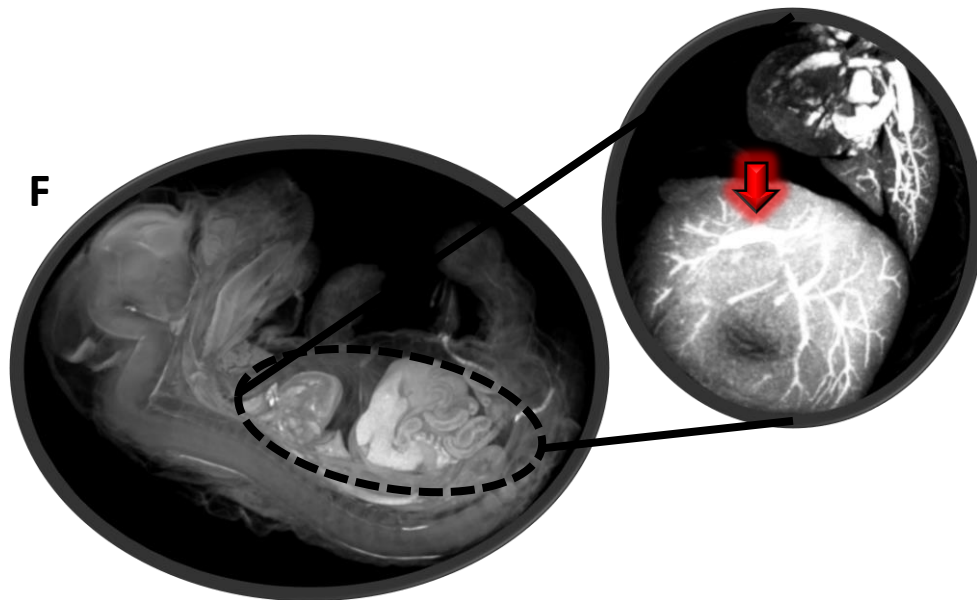
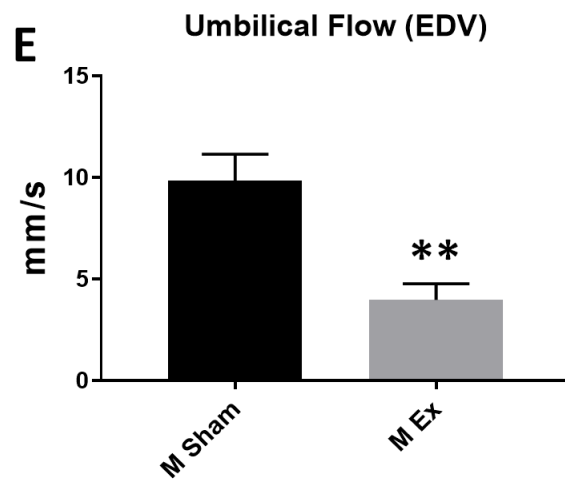
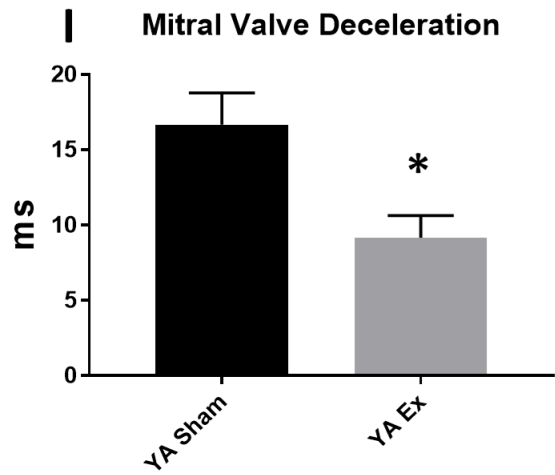
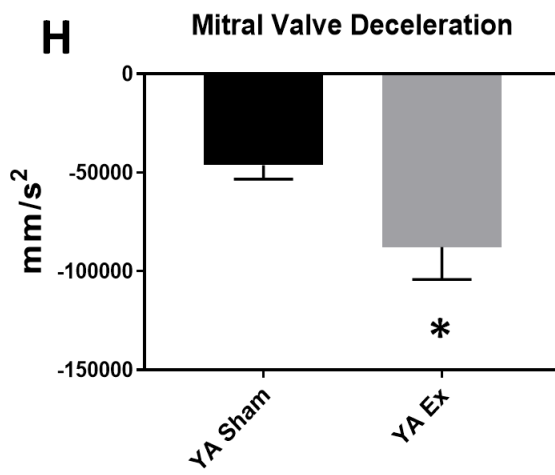
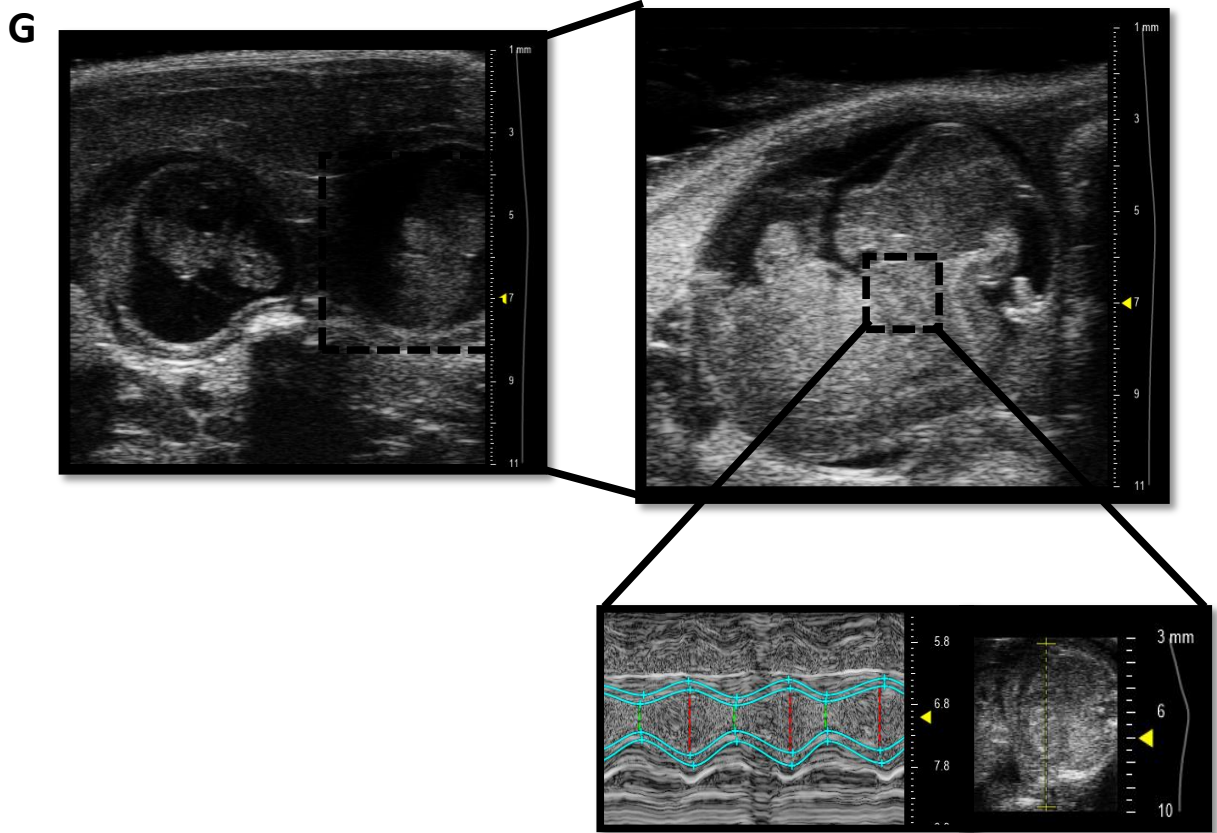


Figure 2.2:



**Figure 2.2: Pulse Wave Doppler assessment of Sham vs. nano-TiO<sub>2</sub> exposed dams and their offspring.** (A) Maternal (n = 15 Sham, n = 11 Ex) Pulse Wave Doppler-Mitral Valve imaging illustrating changes in MV-A velocity. (B) Maternal (n = 15 Sham, n = 11 Ex) Pulse Wave Doppler-Mitral Valve imaging illustrating changes in MV Deceleration speed. (C) Maternal (n = 15 Sham, n = 11 Ex) Pulse Wave Doppler-Mitral Valve imaging illustrating changes in MV Deceleration time. (D) Maternal (n = 15 Sham, n = 11 Ex) Pulse Wave Doppler-Mitral Valve imaging illustrating changes in E/A ratio. (E) Pulse Wave Doppler-Flow indices revealed a change in umbilical EDV. (F) Representative micro-CT image illustrating fetal organ complexity at GD 15 and the umbilical vein (circled in red). (G) Ultrasound image showing uterine horn containing two fetal pups, a single fetal pup, and echocardiographic gating of the fetal with a representative M-mode measurement. (H) Pulse Wave Doppler-Mitral Valve of young adult (n = 7 Sham, n = 5 Ex) following maternal exposure indicating changes in MV Deceleration speed. (I) Pulse Wave Doppler-Mitral Valve of young adult (n = 7 Sham, n = 5 Ex) following maternal exposure indicating changes in MV Deceleration time. Sham = control filtered air exposed, Ex = nano-TiO<sub>2</sub> exposed, Maternal (M) = 12-week-old pregnant dams, Fetal (F) = GD (15), Young Adult (YA) = 11 weeks, MV = Mitral Valve, EDV = End Diastolic Velocity, micro-CT = micro computed tomography. All data are presented as the mean  $\pm$  standard error of the mean (SEM). \* =  $P \leq 0.05$ , \*\* =  $P \leq 0.01$ , \*\*\* =  $P \leq 0.001$  for Ex vs. Sham.

Figure 2.3: Fetal and Young Adult Bioenergetics

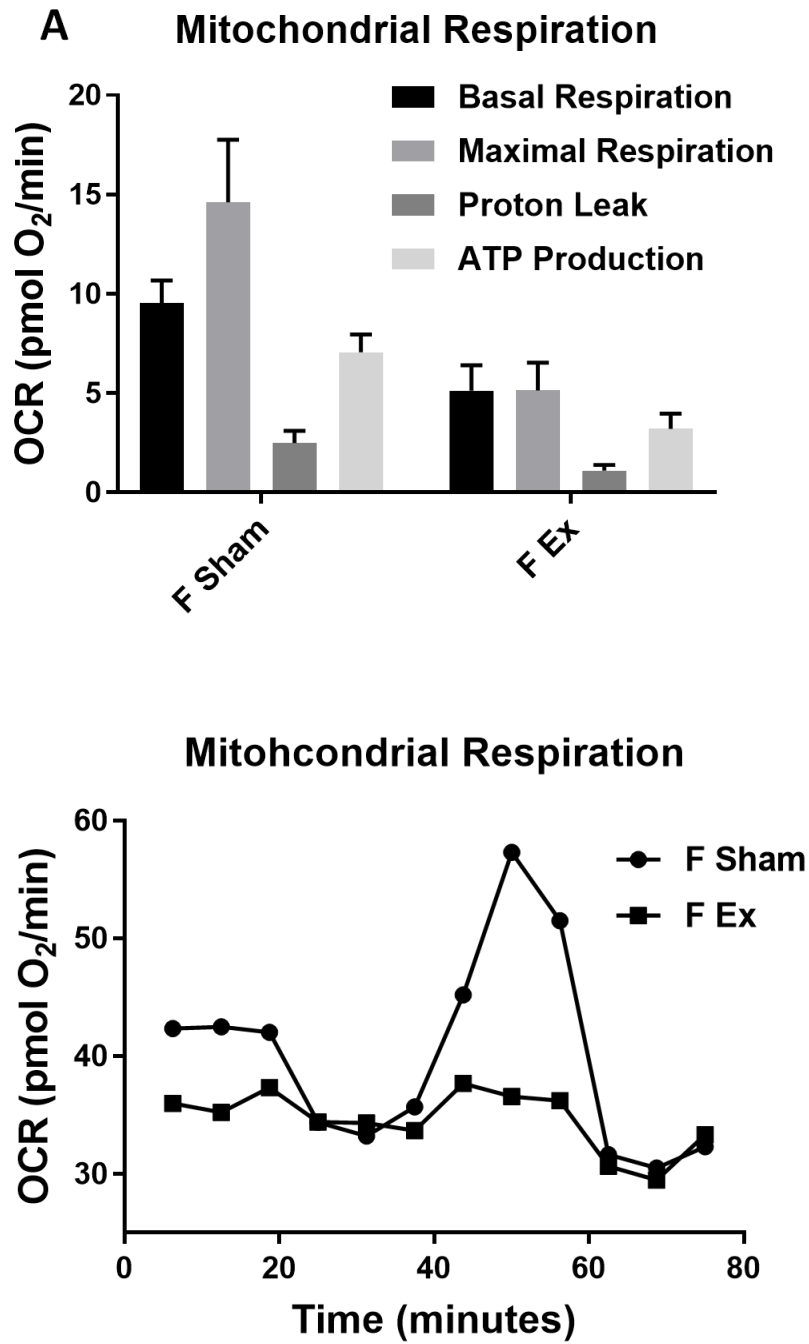
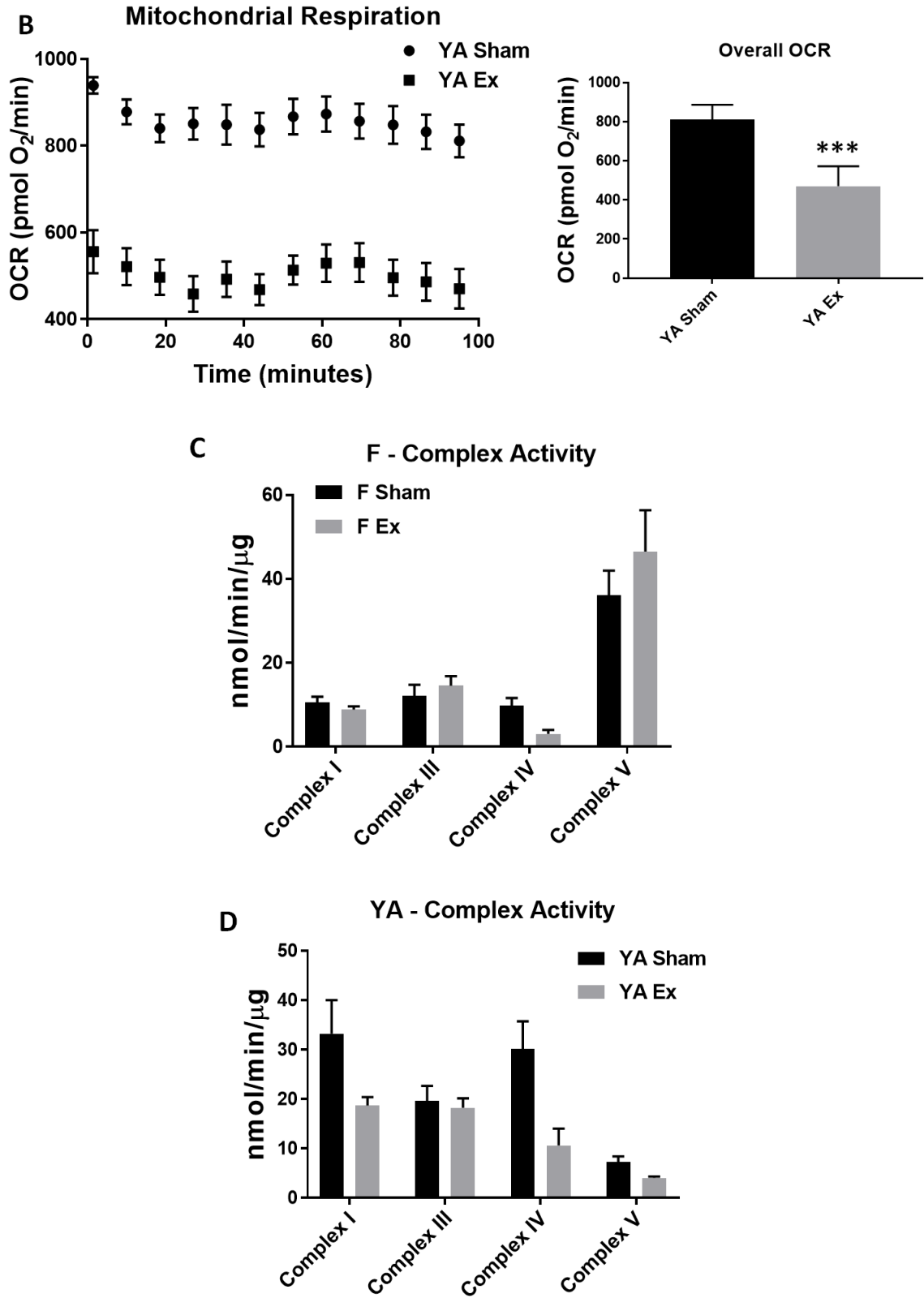


Figure 2.3:



**Figure 2.3: Mitochondrial bioenergetics from fetal and young adult offspring following maternal nano-TiO<sub>2</sub> inhalation exposure.** (A) Seahorse analyses of cardiomyocytes at the fetal stage (n = 1 Sham (one fetal heart from each of 6 dams pooled), n = 1 Ex (one fetal heart from each of 5 dams pooled) plated as 5-6 replicates) indicating changes in ATP production and basal and maximal respiration. (B) Seahorse analysis of young adult (n = 7 Sham, n = 5 Ex) animals demonstrating a significant change in overall OCR. (C) ETC Complex Activities for complexes I, III, IV, V (ATP synthase) in fetal offspring (n = 6 Sham, n = 5 Ex). (D) ETC Complex Activities for complexes I, III, IV, V (ATP synthase) in young adult offspring (n = 7 Sham, n = 5 Ex). Sham = control filtered air exposed, Ex = nano-TiO<sub>2</sub> exposed, Maternal (M) = 12-week-old pregnant dams, Fetal (F) = GD (15), Young Adult (YA) = 11 weeks, OCR=Oxygen Consumption Rate, ETC = Electron Transport Chain. Complex V is measured as nmol/min/mg of tissue. All data are presented as the mean ± standard error of the mean (SEM). \* = P ≤ 0.05, \*\* = P ≤ 0.01, \*\*\* = P ≤ 0.001 for Ex vs. Sham.



Figure 2.4: Fetal and Young Adult ROS and Methylation

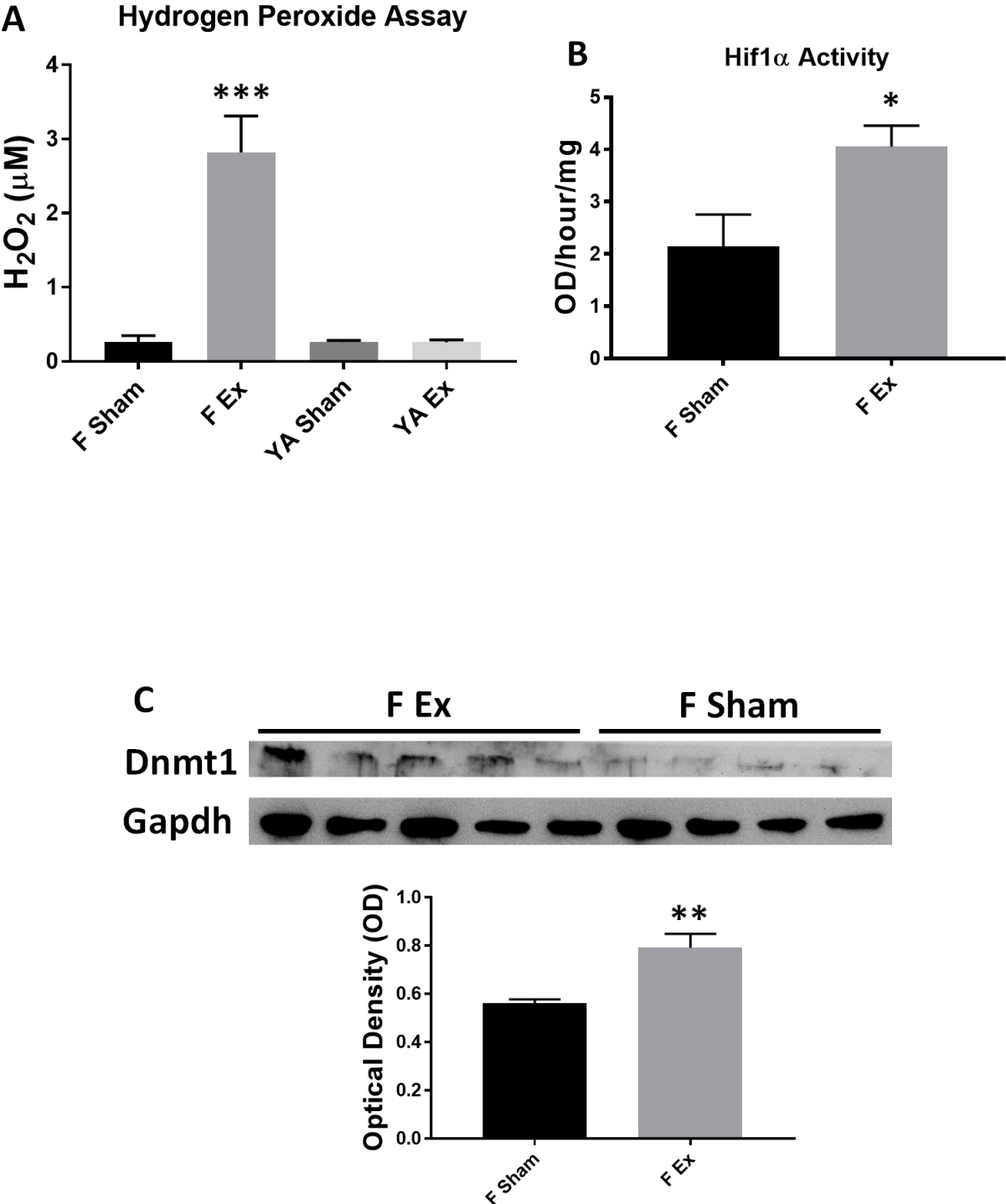


Figure 2.4:

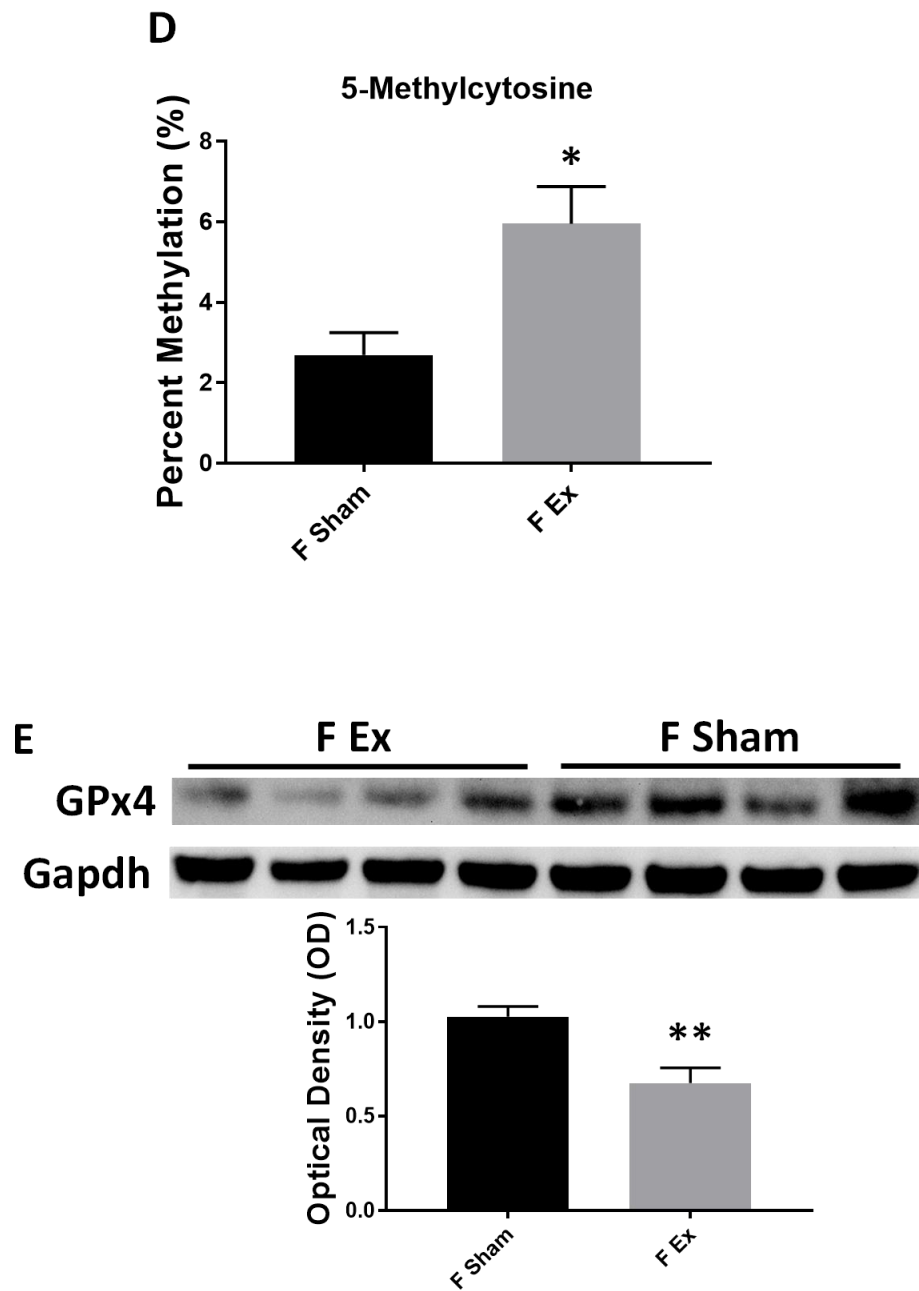
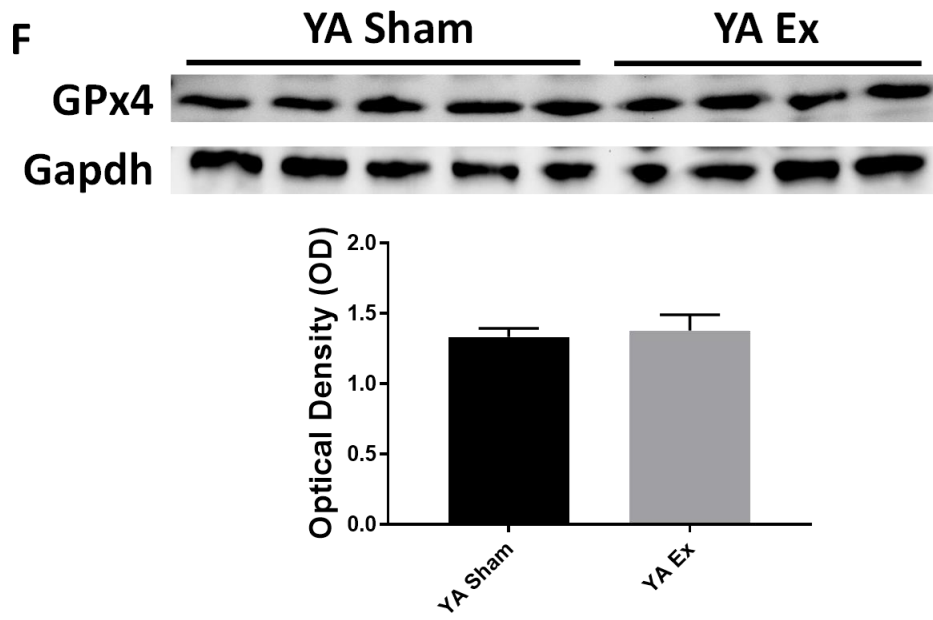


Figure 2.4:



**Figure 2.4: Mechanisms governing cardiac and mitochondrial dysfunction following maternal nano-TiO<sub>2</sub> inhalation exposure.** (A) Hydrogen peroxide (H<sub>2</sub>O<sub>2</sub>) concentration in fetal (n = 6 Sham, n = 5 Ex) and young adult (n = 7 Sham, n = 5 Ex) animals, normalized to protein content. (B) Hif1 $\alpha$  activity was measured in fetal (n = 4 Sham, n = 5 Ex) heart and normalized to protein content. (C) Dnmt1 protein expression was assessed in fetal (n = 4 Sham, n = 5 Ex) heart and normalized using anti-Gapdh primary antibody. (D) Global 5-methylcytosine (5-mC) DNA methylation levels were evaluated in fetal (n = 6 Sham, n = 5 Ex) hearts, normalized to DNA concentration. (E) GPx4 levels were assessed in fetal (n = 4 Sham, n = 4 Ex) and (F) young adult (n = 4 Sham, n = 5 Ex) animals and normalized using anti-Gapdh primary antibody. Sham = control filtered air exposed, Ex = nano-TiO<sub>2</sub> exposed, Maternal (M) = 12-week old pregnant dams, Fetal (F) = GD (15), Young Adult (YA) = 11 weeks, Hif1 $\alpha$  = Hypoxia-inducible factor 1-alpha, Dnmt1 = DNA (cytosine-5)-methyltransferase 1, GPx4 = Glutathione peroxidase 4. All data are presented as the mean  $\pm$  standard error of the mean (SEM). \* = P  $\leq$  0.05, \*\* = P  $\leq$  0.01, \*\*\* = P  $\leq$  0.001 for Ex vs. Sham.

Figure 2.5: Mitochondrial Ultrastructure

A

F Sham

F Ex

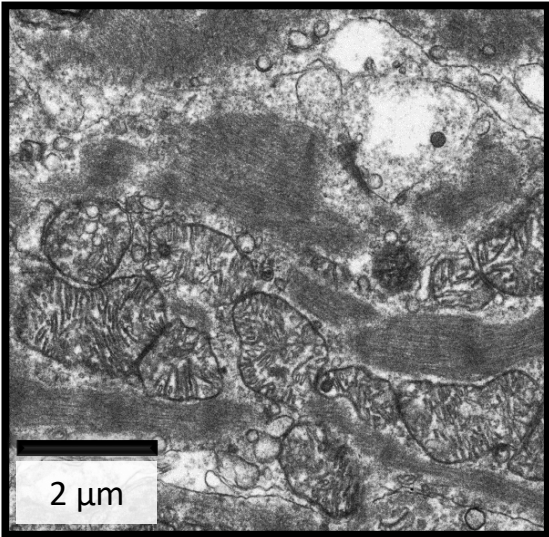
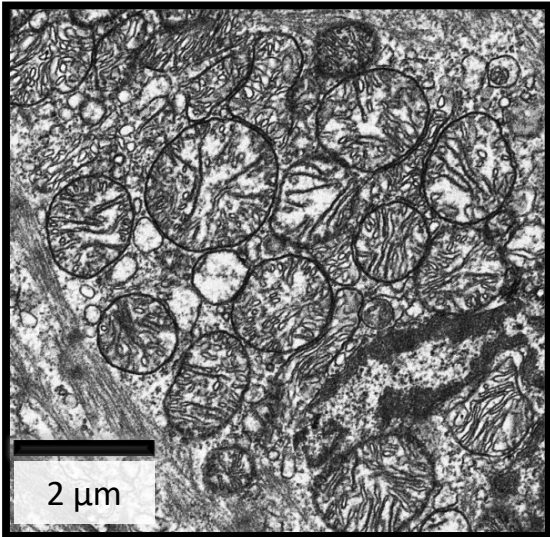
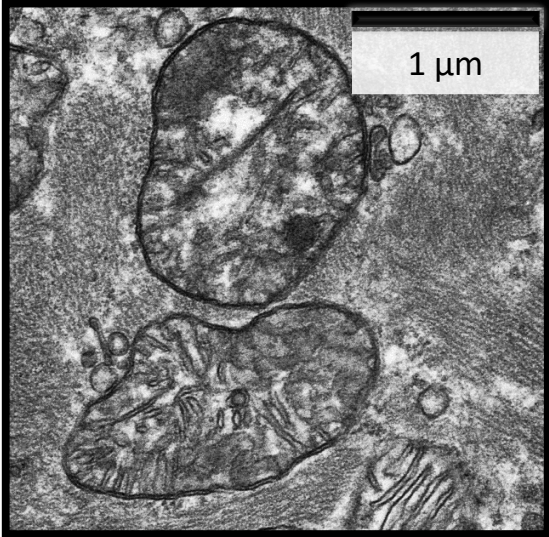
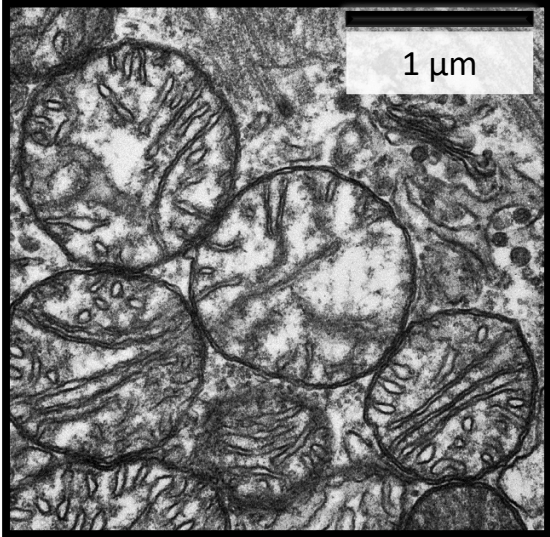


Figure 2.5:

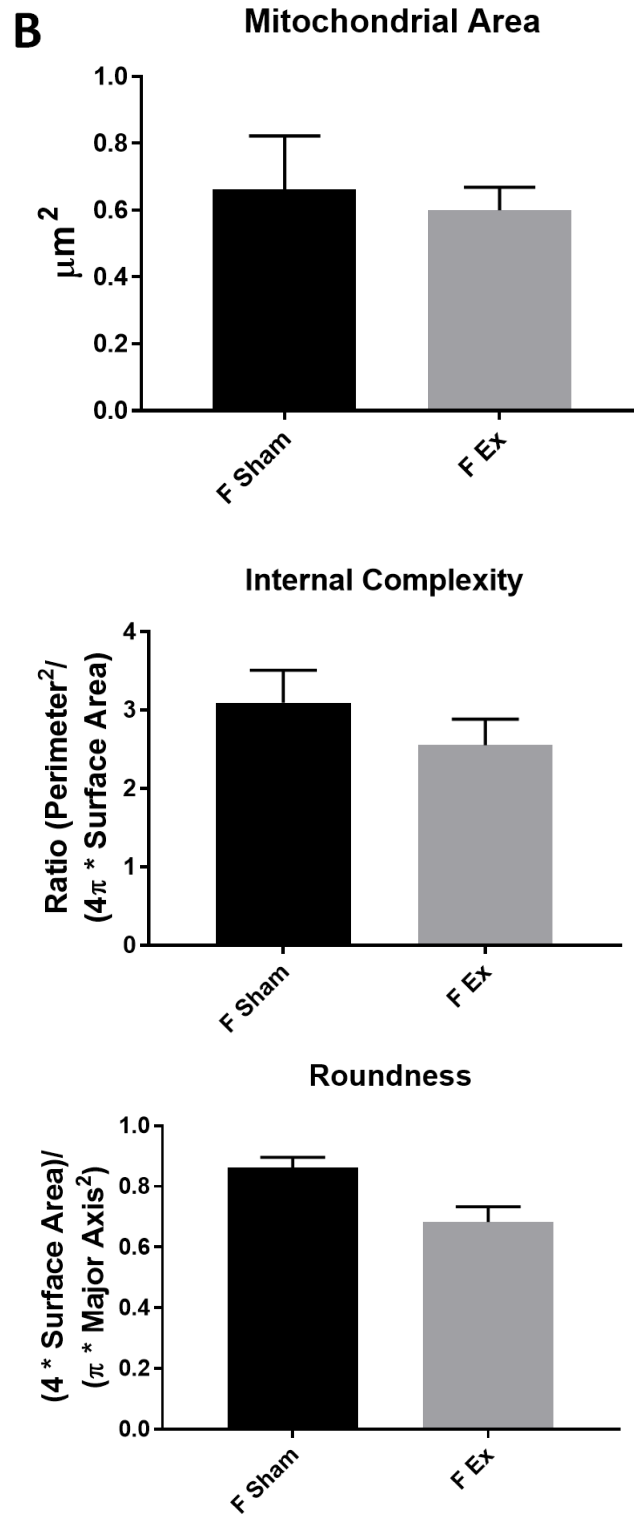
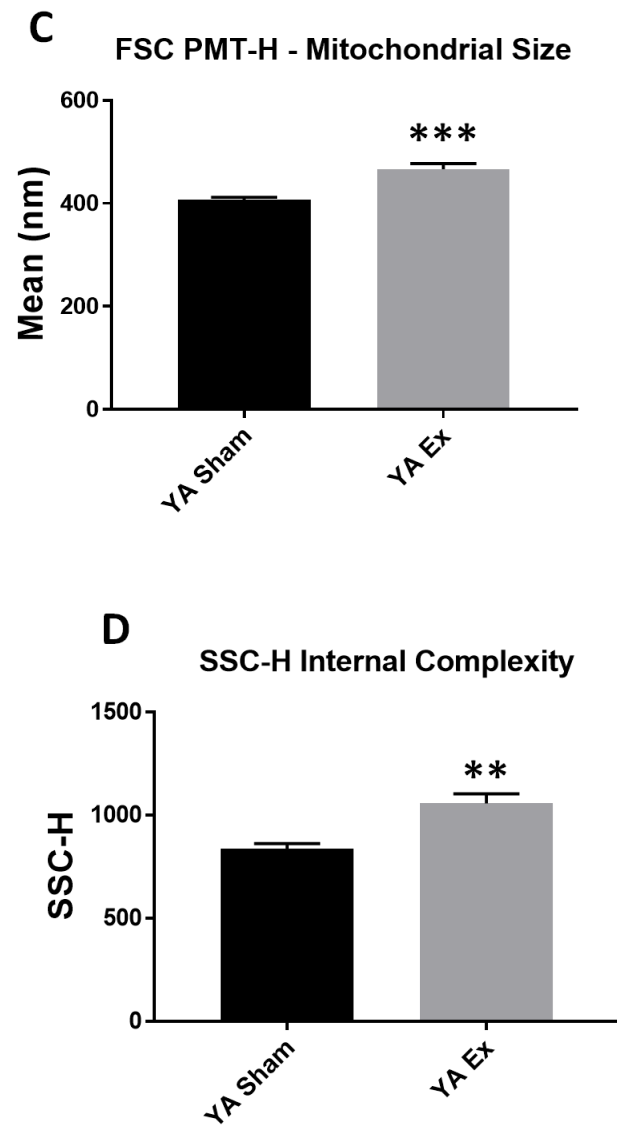


Figure 2.5:

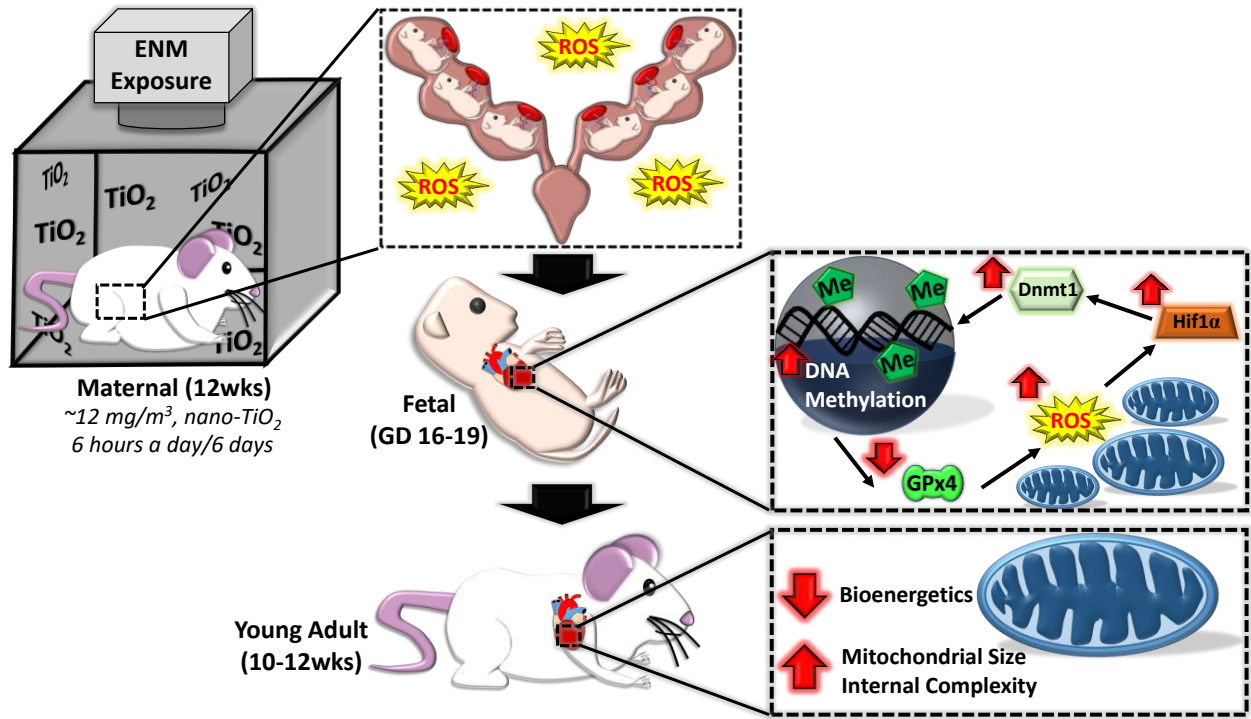


**Figure 2.5: Mitochondrial ultrastructure following maternal nano-TiO<sub>2</sub> inhalation exposure.**

(A) Transmission electron micrographs (TEM) of fetal cardiac tissue following Sham and nano-TiO<sub>2</sub> maternal inhalation exposure. (B) Mitochondrial area, internal complexity (form factor), and roundness (0-1, where 1 = perfect spheroid) were assessed through TEM (n = 2 Sham, n = 2 Ex). (C) Mitochondrial size and (D) internal complexity were determined in young adult (n = 7 Sham, n = 5 Ex) animals through FSC and SSC gating, staining mitochondria with MitoTracker™ Deep Red FM/633. Sham = control filtered air exposed, Ex = nano-TiO<sub>2</sub> exposed, Maternal (M) = 12-week old pregnant dams, Fetal (F) = GD (15), Young Adult (YA) = 11 weeks, FSC = Forward Scatter, SSC = Side Scatter. All data are presented as the mean ± standard error of the mean (SEM). \* = P ≤ 0.05, \*\* = P ≤ 0.01, \*\*\* = P ≤ 0.001 for Ex vs. Sham.



Figure 2.6: Overview



**Figure 2.6: Illustration of molecular pathways altered during maternal nano-TiO<sub>2</sub> inhalation exposure and physiological ramifications.** Following maternal exposure, increased ROS in fetal cardiac tissue and decreased mitochondrial ROS scavenging through GPx4 perpetuates a positive feedback-loop where increased Hif1 $\alpha$  activity acts to transcriptionally activate Dnmt1 and ultimately increase global 5-methylcytosine levels. While ROS returns to control levels in the young adult animals, fetal insult negatively influences mitochondrial and cardiac function in maternal nano-TiO<sub>2</sub> inhalation exposed progeny into adulthood. Maternal (M) = 12-week-old pregnant dams, Fetal (F) = GD (15), Young Adult (YA) = 11 weeks, ROS = reactive oxygen species, GPx4 = Glutathione peroxidase 4, Hif1 $\alpha$  = Hypoxia-inducible factor 1-alpha, Dnmt1 = DNA (cytosine-5)-methyltransferase 1, Me = 5-methylcytosine.

**Supplemental Table 2.1: Pulse-Wave Doppler Maternal Flow**

<b>Parameters</b>	<b>Units</b>	<b>M Sham Uterine</b>	<b>M Ex Uterine</b>	<b>M Sham Umbilical</b>	<b>M Ex Umbilical</b>
<b>End-Diastolic Velocity</b>	mm/s	46.66 ± 4.203	45.31 ± 6.686	<b>9.864 ± 1.287</b>	<b>3.994 ± 0.792**</b>
<b>Peak-Systolic Velocity</b>	mm/s	129.3 ± 14.26	112.6 ± 11.57	84.04 ± 10.20	78.03 ± 7.367
<b>Velocity Time Integral</b>	(VTI) mm	8.252 ± 0.786	8.296 ± 1.192	9.433 ± 0.907	8.012 ± 0.924
<b>Velocity Time Integral</b>	(Mean Vel) mm/s	81.54 ± 8.967	74.12 ± 8.954	36.83 ± 4.997	33.81 ± 3.237
<b>Velocity Time Integral</b>	(Mean Grad) mmHg	0.025 ± 0.004	0.024 ± 0.005	0.007 ± 0.002	0.005 ± 0.001
<b>Velocity Time Integral</b>	(Peak Vel) mm/s	124.8 ± 12.46	118.79 ± 12.88	84.43 ± 10.15	78.14 ± 7.381
<b>Velocity Time Integral</b>	(Peak Grad) mmHg	0.077 ± 0.017	0.061 ± 0.012	0.033 ± 0.008	0.026 ± 0.004

**Supplemental Table 2.1: Pulse Wave Doppler-Flow echocardiography for umbilical and uterine flow following maternal nano-TiO<sub>2</sub> exposure.** Maternal (n = 12 Sham, n = 8 Ex).

Sham = control filtered air exposed, Ex = nano-TiO<sub>2</sub> exposed, Maternal (M) = 12-week old pregnant dams. All data are presented as the mean  $\pm$  standard error of the mean (SEM). \* =  $P \leq 0.05$ , \*\* =  $P \leq 0.01$ , \*\*\* =  $P \leq 0.001$  for Ex vs. Sham.

**Supplemental Table 2.2: Stress-Strain Analysis – Short Axis – Diastole**

<b>Parameters</b>	<b>Units</b>	<b>M Sham</b>	<b>M Ex</b>	<b>F Sham</b>	<b>F Ex</b>	<b>YA Sham</b>	<b>YA Ex</b>
<b>Heart Rate</b>	beats/ min	670.1 ± 9.4	684.2 ± 9.1	123.6 ± 8.186	123.9 ± 9.679	632.1 ± 24.78	689.3 ± 8.156
<b>Radial Velocity (Endo)</b>	Pk cm/s	-3.913 ± 0.13	-3.336 ± 0.324	-0.227 ± 0.033	-0.163 ± 0.011	-2.210 ± 0.262	-2.481 ± 0.366
<b>Radial Displacement (Endo)</b>	Pk mm	-0.004 ± 0.001	-0.008 ± 0.002	-0.005 ± 0.005	-0.011 ± 0.004	<b>-0.0002 ± 0.0001</b>	<b>-0.020 ± 0.009*</b>
<b>Radial Strain (Endo)</b>	Pk %	-4.192 ± 1.288	-2.497 ± 0.536	-29.80 ± 7.744	-13.28 ± 3.711	-2.687 ± 1.264	-8.834 ± 4.281
<b>Radial Strain Rate (Endo)</b>	Pk 1/s	-29.26 ± 4.182	-22.28 ± 1.672	-54.07 ± 4.292	-60.89 ± 4.576	-16.58 ± 2.631	-30.13 ± 10.87
<b>Circumferential Velocity (Endo)</b>	Pk deg/s	-698.1 ± 94.69	-811.1 ± 155.1	-444.17 ± 83.60	-398.8 ± 51.49	-608.8 ± 67.48	-473.5 ± 1215.5
<b>Circumferential Displacement (Endo)</b>	Pk deg	-2.101 ± 0.603	-3.930 ± 1.974	<b>-6.367 ± 1.440</b>	<b>-16.62 ± 3.183**</b>	-6.108 ± 2.036	-6.623 ± 4.394
<b>Circumferential Strain (Endo)</b>	Pk %	5.644 ± 1.792	2.076 ± 0.646	9.881 ± 4.341	7.888 ± 2.411	22.89 ± 21.61	15.58 ± 8.565
<b>Circumferential Strain Rate (Endo)</b>	Pk 1/s	47.67 ± 2.911	51.29 ± 3.699	12.660 ± 1.975	10.58 ± 1.394	38.43 ± 2.817	47.02 ± 11.50

**Supplemental Table 2.2: Diastole cardiac stress-strain in the short axis.** B-Mode images were used to examine radial and circumferential stress-strain parameters in the short axis during diastole in maternal (n = 11 Sham, n = 15 Ex), fetal (n = 9 Sham, n = 9 Ex), and young adult (n = 7 Sham, n = 5 Ex) animals. Sham = control filtered air exposed, Ex = nano-TiO<sub>2</sub> exposed, Maternal (M) = 12-weekold pregnant dams, Fetal (F) = GD (15), Young Adult (YA) = 11 weeks. All data are presented as the mean ± standard error of the mean (SEM). \* =  $P \leq 0.05$ , \*\* =  $P \leq 0.01$ , \*\*\* =  $P \leq 0.001$  for Ex vs. Sham.

**Supplemental Table 2.3: Stress-Strain Analysis – Short Axis – Systole**

<b>Parameters</b>	<b>Units</b>	<b>M Sham</b>	<b>M Ex</b>	<b>F Sham</b>	<b>F Ex</b>	<b>YA Sham</b>	<b>YA Ex</b>
<b>Heart Rate</b>	beats/min	670.1 ± 9.4	684.2 ± 9.1	123.6 ± 8.186	123.9 ± 9.679	632.1 ± 24.78	689.3 ± 8.156
<b>Radial Velocity (Endo)</b>	Pk cm/s	2.951 ± 0.133	2.854 ± 0.170	0.194 ± 0.035	0.173 ± 0.014	2.404 ± 0.258	2.754 ± 0.317
<b>Radial Displacement (Endo)</b>	Pk mm	0.769 ± 0.022	0.700 ± 0.049	0.143 ± 0.012	0.128 ± 0.009	0.549 ± 0.060	0.629 ± 0.057
<b>Radial Strain (Endo)</b>	Pk %	<b>39.26 ± 3.328</b>	<b>52.37 ± 4.428*</b>	10.76 ± 0.960	11.82 ± 2.382	35.49 ± 2.510	39.28 ± 19.79
<b>Radial Strain Rate (Endo)</b>	Pk 1/s	19.35 ± 2.023	19.47 ± 1.664	<b>54.07 ± 9.664</b>	<b>8.464 ± 1.889**</b>	27.10 ± 6.571	25.22 ± 8.153
<b>Circumferential Velocity (Endo)</b>	Pk deg/s	695.5 ± 104.4	810.9 ± 113.9	404.25 ± 68.07	356.7 ± 37.99	724.9 ± 143.5	440.85 ± 46.91
<b>Circumferential Displacement (Endo)</b>	Pk deg	6.384 ± 0.652	4.883 ± 0.817	<b>11.62 ± 2.265</b>	<b>2.954 ± 0.724**</b>	3.190 ± 0.899	4.512 ± 1.424
<b>Circumferential Strain (Endo)</b>	Pk %	<b>-38.54 ± 4.448</b>	<b>-54.51 ± 2.811*</b>	-27.86 ± 2.405	-25.12 ± 3.225	-39.90 ± 7.110	-39.94 ± 8.000
<b>Circumferential Strain Rate (Endo)</b>	Pk 1/s	-44.57 ± 4.357	-46.94 ± 4.056	-12.63 ± 1.676	-8.919 ± 0.432	-45.53 ± 4.426	-45.22 ± 12.34

**Supplemental Table 2.3: Systolic cardiac stress-strain in the short axis.** B-Mode images were used to examine radial and circumferential stress-strain parameters in the short axis during systole in maternal (n = 11 Sham, n = 15 Ex), fetal (n = 9 Sham, n = 9 Ex), and young adult (n = 7 Sham, n = 5 Ex) animals. Sham = control filtered air exposed, Ex = nano-TiO<sub>2</sub> exposed, Maternal (M) = 12-week old pregnant dams, Fetal (F) = GD (15), Young Adult (YA) = 11 weeks. All data are presented as the mean ± standard error of the mean (SEM). \* =  $P \leq 0.05$ , \*\* =  $P \leq 0.01$ , \*\*\* =  $P \leq 0.001$  for Ex vs. Sham.



**Supplemental Table 2.4: Stress-Strain Analysis – Long Axis – Diastole**

<b>Parameters</b>	<b>Units</b>	<b>M Sham</b>	<b>M Ex</b>	<b>YA Sham</b>	<b>YA Ex</b>
<b>Heart Rate</b>	beats/min	681.3 ± 11.66	708.0 ± 11.75	581.9 ± 54.00	679.1 ± 4.952
<b>Radial Velocity (Endo)</b>	Pk cm/s	<b>-2.640 ± 0.146</b>	<b>-2.152 ± 0.128*</b>	-1.691 ± 0.043	-1.736 ± 0.121
<b>Radial Displacement (Endo)</b>	Pk mm	-0.006 ± 0.002	-0.002 ± 0.001	-0.003 ± 0.001	-0.007 ± 0.003
<b>Radial Strain (Endo)</b>	Pk %	-1.047 ± 0.234	-0.782 ± 0.213	-1.413 ± 0.280	-0.725 ± 0.282
<b>Radial Strain Rate (Endo)</b>	Pk 1/s	<b>-14.25 ± 0.980</b>	<b>-10.94 ± 0.933*</b>	-9.768 ± 0.949	-9.205 ± 1.083
<b>Longitudinal Velocity (Endo)</b>	Pk deg/s	-1.579 ± 0.246	-1.690 ± 0.152	-1.105 ± 0.119	-0.873 ± 0.169
<b>Longitudinal Displacement (Endo)</b>	Pk deg	-0.021 ± 0.006	-0.034 ± 0.010	<b>-0.140 ± 0.034</b>	<b>-0.036 ± 0.016*</b>
<b>Longitudinal Strain (Endo)</b>	Pk %	<b>4.654 ± 1.262</b>	<b>0.933 ± 0.352*</b>	2.209 ± 0.737	1.841 ± 0.528
<b>Longitudinal Strain Rate (Endo)</b>	Pk 1/s	9.834 ± 1.207	11.89 ± 1.223	9.890 ± 1.586	9.867 ± 2.347

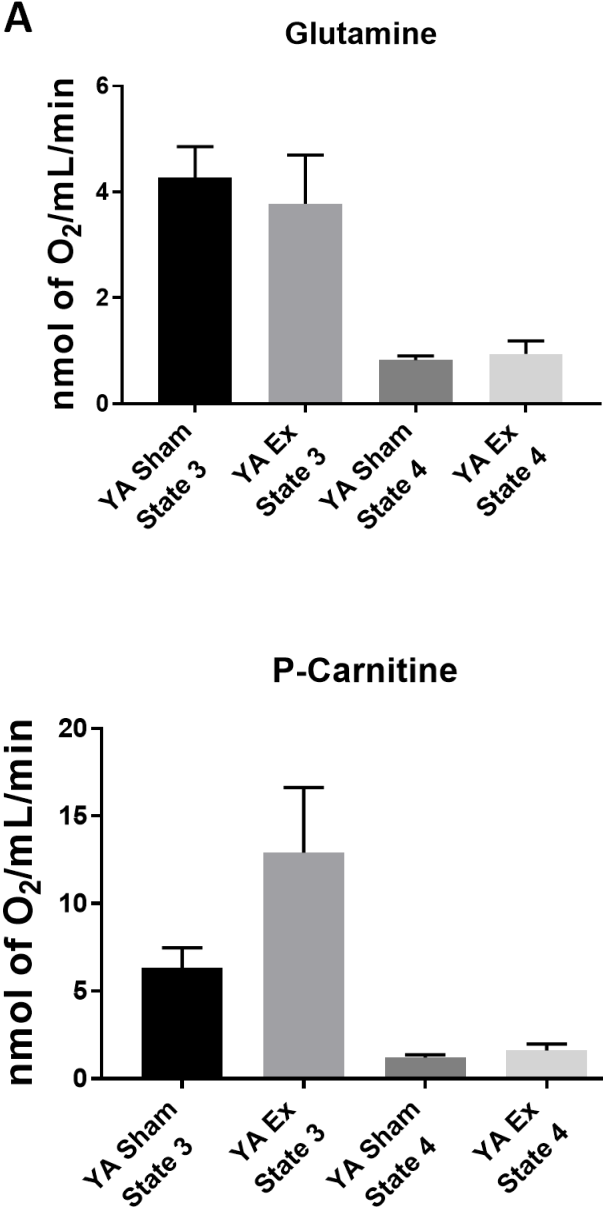
**Supplemental Table 2.4: Diastolic cardiac stress-strain in the long axis.** B-Mode images were used to examine longitudinal and circumferential stress-strain parameters in the long axis during diastole in maternal (n = 11 Sham, n = 15 Ex), fetal (n = 9 Sham, n = 9 Ex), and young adult (n = 7 Sham, n = 5 Ex) animals. Sham = control filtered air exposed, Ex = nano-TiO<sub>2</sub> exposed, Maternal (M) = 12-week old pregnant dams, Fetal (F) = GD (15), Young Adult (YA) = 11 weeks. All data are presented as the mean ± standard error of the mean (SEM). \* =  $P \leq 0.05$ , \*\* =  $P \leq 0.01$ , \*\*\* =  $P \leq 0.001$  for Ex vs. Sham.

**Supplemental Table 2.5: Stress-Strain Analysis – Long Axis – Systole**

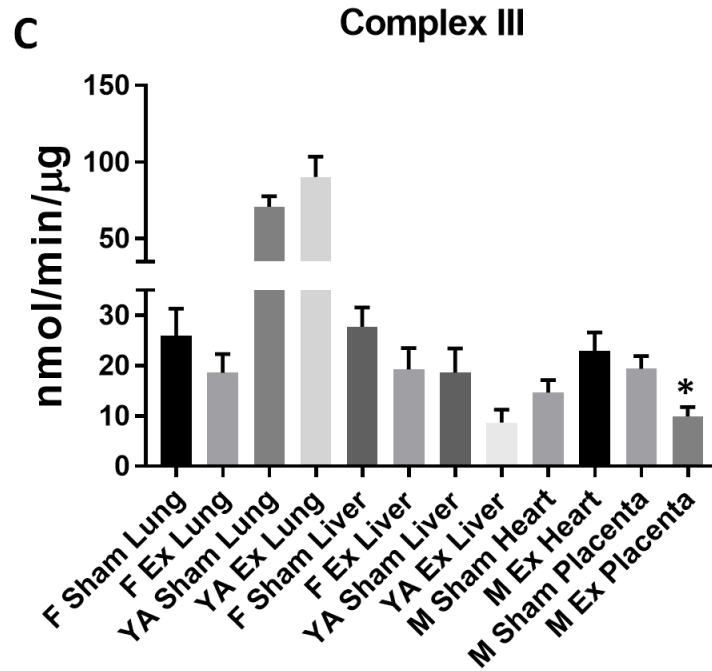
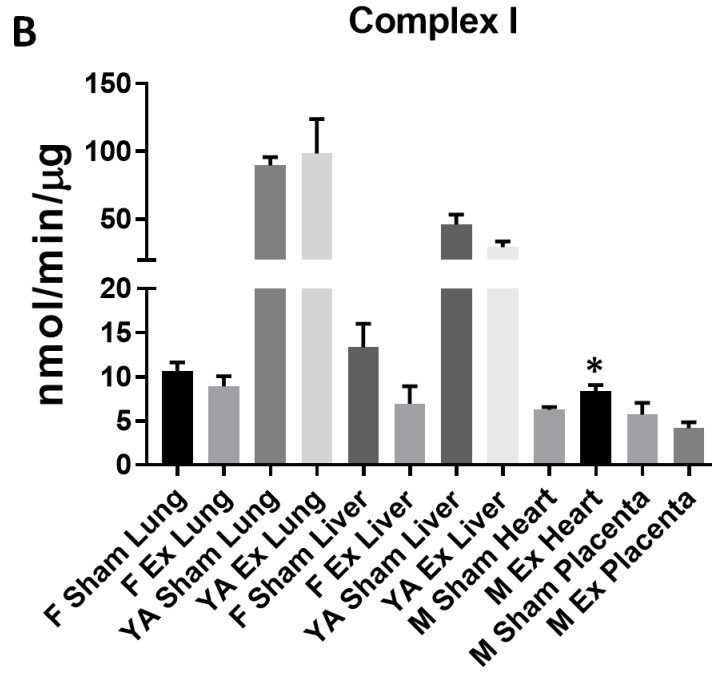
<b>Parameters</b>	<b>Units</b>	<b>M Sham</b>	<b>M Ex</b>	<b>YA Sham</b>	<b>YA Ex</b>
<b>Heart Rate</b>	beats/min	681.3 ± 11.66	708.0 ± 11.75	581.9 ± 54.00	679.1 ± 4.952
<b>Radial Velocity (Endo)</b>	Pk cm/s	<b>2.054 ± 0.091</b>	<b>1.787 ± 0.060*</b>	2.003 ± 0.142	1.954 ± 0.070
<b>Radial Displacement (Endo)</b>	Pk mm	<b>0.574 ± 0.023</b>	<b>0.469 ± 0.022**</b>	0.468 ± 0.037	0.479 ± 0.038
<b>Radial Strain (Endo)</b>	Pk %	33.33 ± 2.797	27.53 ± 2.388	27.39 ± 3.189	27.33 ± 0.595
<b>Radial Strain Rate (Endo)</b>	Pk 1/s	12.07 ± 1.203	10.94 ± 1.357	9.365 ± 0.809	10.49 ± 0.621
<b>Longitudinal Velocity (Endo)</b>	Pk deg/s	1.245 ± 0.131	1.466 ± 0.092	0.997 ± 0.215	0.923 ± 0.248
<b>Longitudinal Displacement (Endo)</b>	Pk deg	0.237 ± 0.040	0.247 ± 0.035	0.065 ± 0.011	0.100 ± 0.022
<b>Longitudinal Strain (Endo)</b>	Pk %	-7.070 ± 1.597	-10.40 ± 1.741	-12.15 ± 2.510	-16.87 ± 2.052
<b>Longitudinal Strain Rate (Endo)</b>	Pk 1/s	<b>-7.309 ± 2.845</b>	<b>-11.80 ± 1.789*</b>	-10.40 ± 1.282	-8.526 ± 1.306

**Supplemental Table 2.5: Systolic cardiac stress-strain in the long axis.** B-Mode images were used to examine longitudinal and circumferential stress-strain parameters in the long axis during systole in maternal (n = 11 Sham, n = 15 Ex), fetal (n = 9 Sham, n = 9 Ex), and young adult (n = 7 Sham, n = 5 Ex) animals. Sham = control filtered air exposed, Ex = nano-TiO<sub>2</sub> exposed, Maternal (M) = 12-week old pregnant dams, Fetal (F) = GD (15), Young Adult (YA) = 11 weeks. All data are presented as the mean ± standard error of the mean (SEM). \* =  $P \leq 0.05$ , \*\* =  $P \leq 0.01$ , \*\*\* =  $P \leq 0.001$  for Ex vs. Sham.

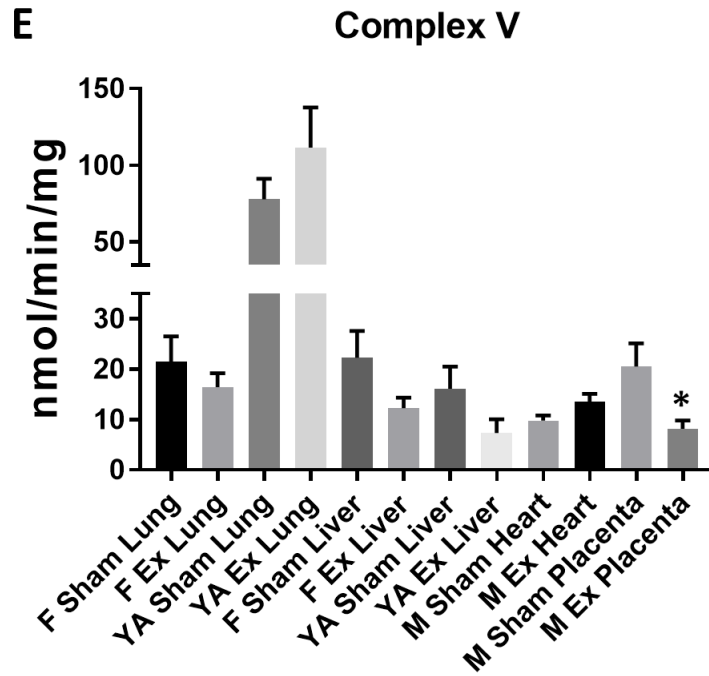
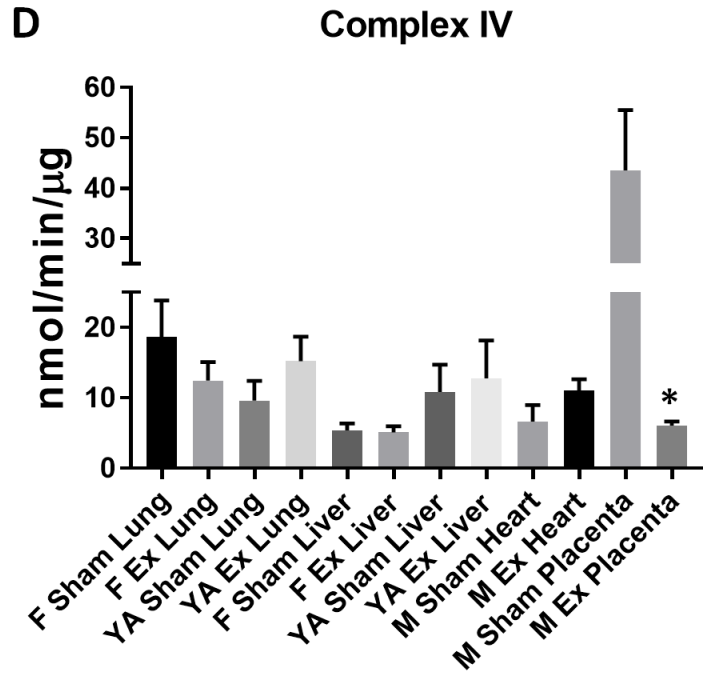
Supplemental Figure 2.1: Bioenergetics



Supplemental Figure 2.1:



Supplemental Figure 2.1:

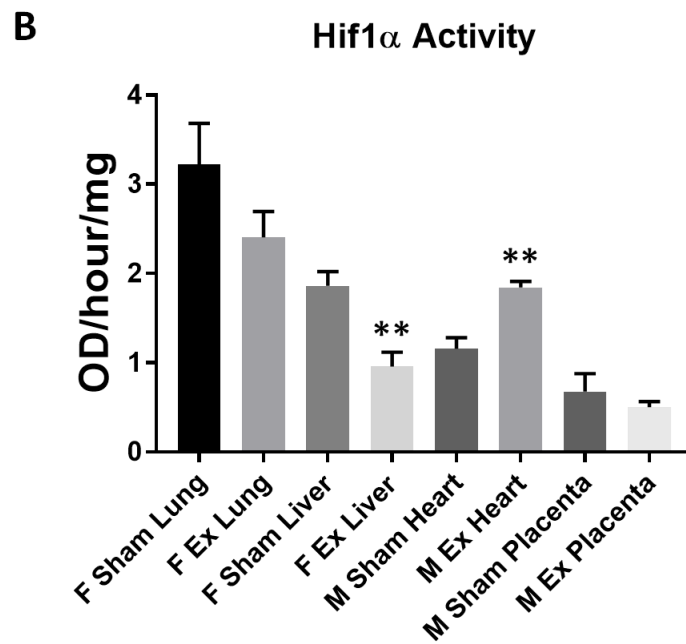
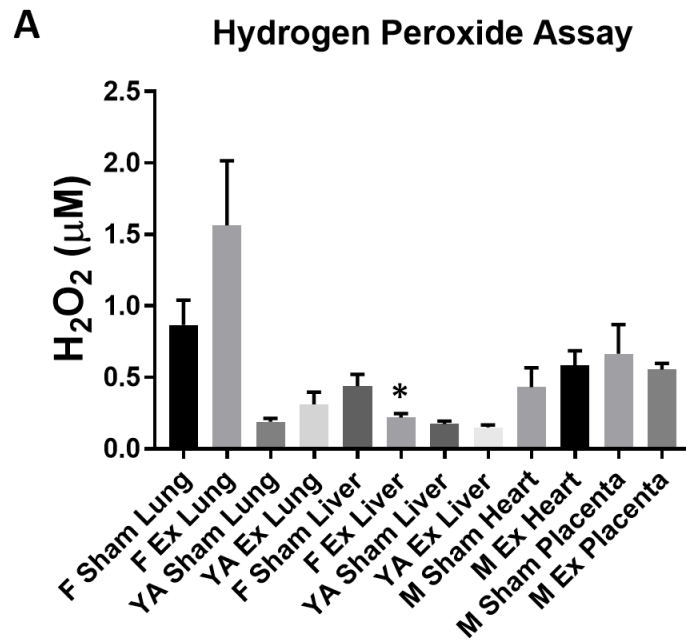


**Supplemental Figure 2.1: Mitochondrial bioenergetics of other tissues and organ systems.**

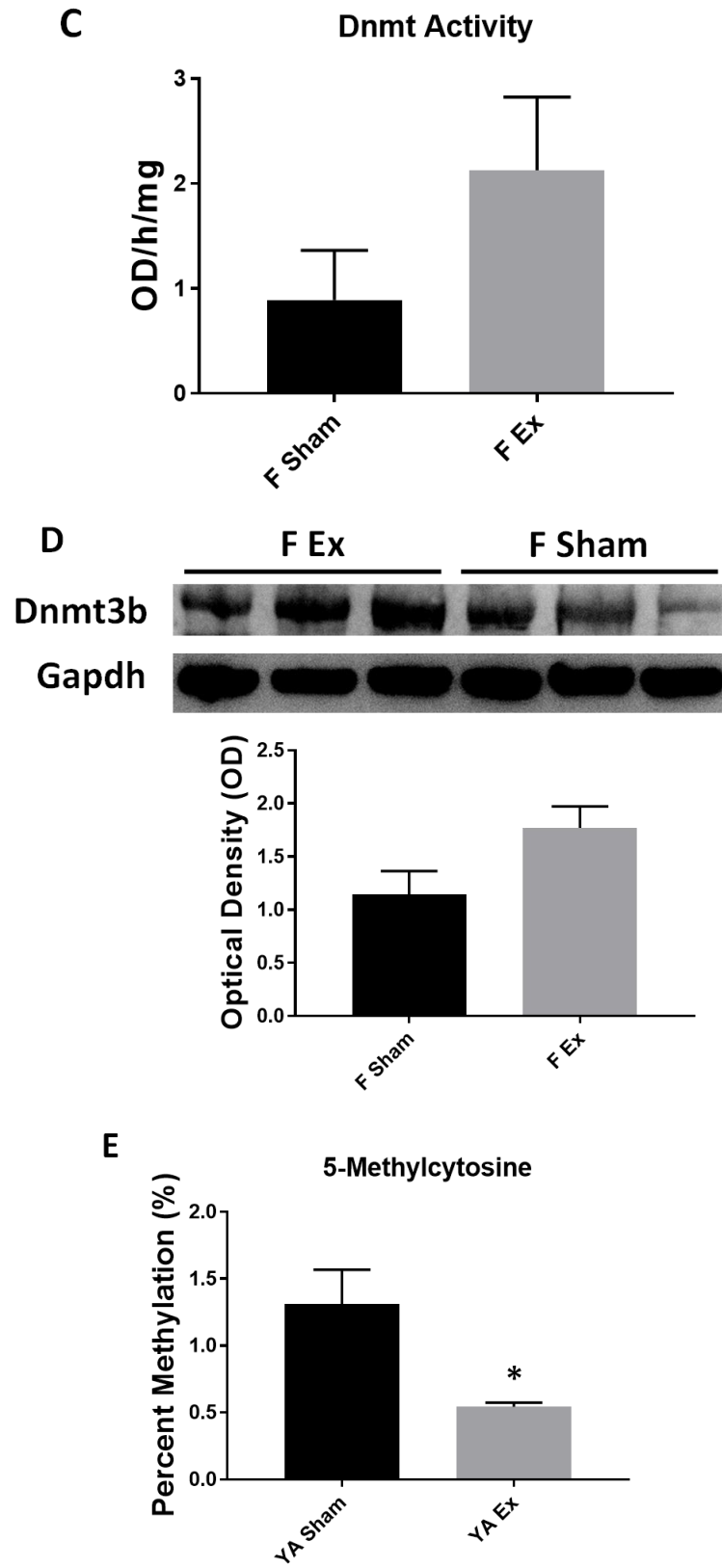
(A) In young adult (n = 7 Sham, n = 5 Ex) animals state 3 and state 4 respiration was assessed using glucose (glutamine) and fatty-acid-mediated pathways (palmitoyl carnitine), normalized to number of mitochondria. (B) ETC complex activities for complex I in fetal, young adult, and maternal tissues. (C) ETC complex activities for complex III in fetal, young adult, and maternal tissues. (D) ETC complex activities for complex IV in fetal, young adult, and maternal tissues. (E) ETC complex activities for complex V (ATP synthase) in fetal, young adult, and maternal tissues. Sham = control filtered air exposed, Ex = nano-TiO<sub>2</sub> exposed, Maternal (M) = 12-week old pregnant dams, Fetal (F) = GD (15), Young Adult (YA) = 11 weeks, P-Carnitine = palmitoyl carnitine. All data are presented as the mean ± standard error of the mean (SEM). \* =  $P \leq 0.05$ , \*\* =  $P \leq 0.01$ , \*\*\* =  $P \leq 0.001$  for Ex vs. Sham.



Supplemental Figure 2.2: ROS-Mediated Effects



Supplemental Figure 2.2:



**Supplemental Figure 2.2: ROS-mediated pathways in other tissues and organ systems. (A)** Hydrogen peroxide ( $H_2O_2$ ) concentration in fetal, young adult, and maternal tissues normalized to protein content. **(B)** Hif1 $\alpha$  activity was measured in fetal and maternal tissues and normalized to protein content. **(C)** Activity of DNA methyltransferases (Dnmts) in fetal (n = 4 Sham, n = 5 Ex) heart tissue, normalized to protein content. **(D)** Dnmt3b expression levels were assessed in young adult (n = 3 Sham, n = 3 Ex) animals and normalized using anti-Gapdh primary antibody. **(E)** Global 5-mC DNA methylation levels were evaluated in young adult (n = 7 Sham, n = 5 Ex) hearts, normalized to DNA concentration. Sham = control filtered air exposed, Ex = nano-TiO<sub>2</sub> exposed, Maternal (M) = 12-week old pregnant dams, Fetal (F) = GD (15), Young Adult (YA) = 11 weeks, Hif1 $\alpha$  = Hypoxia-inducible factor 1-alpha. Dnmt3b = DNA (cytosine-5)-methyltransferase 3b. All data are presented as the mean  $\pm$  standard error of the mean (SEM). \* =  $P \leq 0.05$ , \*\* =  $P \leq 0.01$ , \*\*\* =  $P \leq 0.001$  for Ex vs. Sham.

# Chapter 3: Specific Aim 2

## Enhanced Antioxidant Capacity Prevents Epitranscriptomic and Cardiac Alterations in Adult Offspring Gestationally-Exposed to ENM

Amina Kunovac<sup>1,2,3</sup>, Quincy A. Hathaway<sup>1,2,3</sup>, Mark V. Pinti<sup>2,4</sup>, Andrya J. Durr<sup>1,2</sup>, Andrew D. Taylor<sup>1,2</sup>, William T. Goldsmith<sup>3,5</sup>, Krista L. Garner<sup>3,5</sup>, Timothy R. Nurkiewicz<sup>3,5</sup>, and John M. Hollander<sup>1,2,3</sup>

As published in *Nanotoxicology*. 2021 May 8:1-20. doi: 10.1080/17435390.2021.1921299. Online ahead of print.

<sup>1</sup>Division of Exercise Physiology, West Virginia University School of Medicine, Morgantown, WV, USA.

<sup>2</sup>Mitochondria, Metabolism & Bioenergetics Working Group, West Virginia University School of Medicine, Morgantown, WV, USA. <sup>3</sup>Center for Inhalation Toxicology (iTOX), West Virginia University School of Medicine, Morgantown, WV, USA. <sup>4</sup>West Virginia University School of Pharmacy, Morgantown, WV, USA. <sup>5</sup>Department of Physiology & Pharmacology, West Virginia University School of Medicine, Morgantown, WV, USA.

Amina Kunovac; [ak0086@mix.wvu.edu](mailto:ak0086@mix.wvu.edu), Quincy A. Hathaway; [qahathaway@mix.wvu.edu](mailto:qahathaway@mix.wvu.edu), Mark V. Pinti; [mpinti@mix.wvu.edu](mailto:mpinti@mix.wvu.edu), Andrya J. Durr; [ajdurr@mix.wvu.edu](mailto:ajdurr@mix.wvu.edu), Andrew D. Taylor; [adt0023@mix.wvu.edu](mailto:adt0023@mix.wvu.edu), Krista L. Garner; [kg0048@mix.wvu.edu](mailto:kg0048@mix.wvu.edu), William T. Goldsmith; [wgoldsmi@hsc.wvu.edu](mailto:wgoldsmi@hsc.wvu.edu), Timothy R. Nurkiewicz; [tnurkiewicz@hsc.wvu.edu](mailto:tnurkiewicz@hsc.wvu.edu), and John M. Hollander; [jhollander@hsc.wvu.edu](mailto:jhollander@hsc.wvu.edu)

Corresponding Author:

John M. Hollander, Ph.D., F.A.H.A.

Division of Exercise Physiology

West Virginia University School of Medicine

PO Box 9227

1 Medical Center Drive

Morgantown, WV 26506

Tel: 1-(304) 293-3683

Fax: 1-(304) 293-7105

Email: [jhollander@hsc.wvu.edu](mailto:jhollander@hsc.wvu.edu)

## Abstract

Maternal engineered nanomaterial (ENM) exposure during gestation has been associated with negative long-term effects on cardiovascular health in progeny. Here we evaluate an epitranscriptomic mechanism that contributes to these chronic ramifications and whether overexpression of mitochondrial phospholipid hydroperoxide glutathione peroxidase (mPHGPx) can preserve cardiovascular function and bioenergetics in offspring following gestational nano-titanium dioxide (TiO<sub>2</sub>) inhalation exposure. Wild-type (WT) and mPHGPx (Tg) dams were exposed to nano-TiO<sub>2</sub> aerosols with a mass concentration of  $12.01 \pm 0.50$  mg/m<sup>3</sup> starting from gestational day (GD) 5 for a period of 360 mins/day for 6 non-consecutive days over an 8-day period. Echocardiography was performed in pregnant dams, adult (11-week old) and fetal (GD 14) progeny. Mitochondrial function and global N<sup>6</sup>-methyladenosine (m<sup>6</sup>A) content were assessed in adult progeny. MPHGPx enzymatic function was further evaluated in adult progeny and m<sup>6</sup>A-RNA immunoprecipitation (RIP) was combined with RT-qPCR to evaluate m<sup>6</sup>A content in the 3'-UTR. Following gestational ENM exposure, global longitudinal strain (GLS) was 32% lower in WT adult offspring of WT dams, with preservation in WT offspring of Tg dams. MPHGPx activity was significantly reduced in WT offspring (29%) of WT ENM-exposed dams, but preserved in progeny of Tg dams. M<sup>6</sup>A-RIP-qPCR for the SEC insertion sequence region of mPHGPx revealed hypermethylation in WT offspring from ENM-exposed WT dams, which was thwarted in the presence of the maternal transgene. Our findings implicate that m<sup>6</sup>A hypermethylation of mPHGPx may be culpable for diminished antioxidant capacity and resultant mitochondrial and cardiac deficits that persist into adulthood following gestational ENM inhalation exposure.

**Keywords:** Environmental exposure, GPx4, Mitochondria, N<sup>6</sup>-methyladenosine, M<sup>6</sup>A

## Introduction

While engineered nanomaterials (ENMs) and advance materials, have enabled important innovations in biomedical engineering, the increased potential for their interactions with biological tissues warrants assessment of their ability to elicit undesirable toxicological effects (11, 15, 52). The application of nano-titanium dioxide (nano-TiO<sub>2</sub>), a commonly utilized ENM, escalated by 300% from 2011-2013 in consumer products (72). The primary route of exposure is inhalation, which allows particles to enter the bloodstream and systemically impact the body (66). The size of these particles ( $\geq 1$  dimension that is  $\leq 100$  nm in diameter), plays a critical role in their ability to access systemic circulation and promote cardiovascular damage (32, 36, 52, 55, 66). Nano-TiO<sub>2</sub> has been implicated in alterations to cardiovascular hemodynamics and mitochondrial dysregulation (23, 24, 45). Exposure to ENMs are of particular concern for vulnerable populations such as the developing fetus (11, 21). Although research relating to particulate matter exposure during gestational development and the associated detriments are receiving more attention, therapeutic interventions are limited and the identification of mechanisms responsible for long term effects remain undefined.

Initial studies from our laboratory have determined that maternal ENM inhalation exposure during gestation elicits cardiac contractile dysfunction and bioenergetic disruption in the developing fetus (35), which are sustained into adulthood (24, 35). At the fetal stage, the functional deficits were attributed to an increased production of reactive oxygen species (ROS) (marked by hydrogen peroxide (H<sub>2</sub>O<sub>2</sub>) levels) and downregulation of mitochondria phospholipid hydroperoxide glutathione peroxidase (mPHGPx) (35), an antioxidant enzyme that protects cells from oxidative stress. Because mPHGPx scavenges hydroperoxides, limiting diffusion of H<sub>2</sub>O<sub>2</sub> from the mitochondrion into other cellular regions, its expression is critical for decreasing ROS influence on nuclear genome regulation. MPHGPx has the ability to mitigate cardiac dysfunction and bioenergetic dysregulation in several contexts (6, 16, 26) , including acute nano-TiO<sub>2</sub> exposure (45). However, whether enhanced antioxidant capacity can provide a protective role to fetal and adult offspring following maternal ENM inhalation exposure during gestation remains unexplored.

In a previous study from our laboratory, we reported mitochondrial and cardiac contractile decrements in the fetal stage that were sustained into adulthood following maternal ENM inhalation exposure (35). Though the mechanism by which these detriments are sustained is

unclear, epitranscriptomic modifications resulting from maternal ENM exposure may be contributing to the persistent cardiac mitochondrial dysfunction observed. Of interest was our observation of increased ROS and concomitant diminution of mPHGPx protein expression at the fetal stage which may have been associated with epigenetic reprogramming that occurs following particulate exposure (11, 21, 29, 33, 35, 63, 71). Specifically, epitranscriptomic mechanisms may be responsible for degradation of mRNA and/or functional deficits in proteins (19, 37, 44). N<sup>6</sup>-methyladenosine (m<sup>6</sup>A) is the most prevalent post-transcriptional mRNA modification in eukaryotes and has been associated with various pathologies (13, 14, 19, 39, 56, 77). Elevated stress levels have the ability to alter m<sup>6</sup>A machinery and therefore modulate transcript stability by adding and removing methylation marks (9, 19, 37, 61, 77). M<sup>6</sup>A sites are known to be enriched near stop codons and in 3'-untranslated regions (UTR) of mRNA (73), thereby influencing translation (43). Investigation of m<sup>6</sup>A sites in crucial coding regions of nuclear genome-encoded mitochondrial mRNAs that are pivotal for antioxidant defense maintenance is of particular interest, as it may provide insight into mechanisms that result in the longitudinal outcomes of maternal ENM exposure during gestation.

We hypothesize that altered m<sup>6</sup>A status of the 3'-UTR of mPHGPx in the hearts of adult offspring contributes to mitochondrial and cardiac functional deficits and that overexpression of mPHGPx (in the mother or pup) can preserve these functional alterations following maternal ENM inhalation exposure. Through the use of differential breeding strategies, we were able to determine that the maternal transgene is protective for the fetus and the benefit is sustained in adult offspring, regardless of whether the progeny also possessed the transgene. Following gestational ENM inhalation exposure, mPHGPx enzymatic activity was entirely preserved only in offspring whose dams were mPHGPx transgenic. M<sup>6</sup>A methylation was highly enriched in the 3'-UTR of mPHGPx in wild-type (WT) offspring exposed *in utero* to nano-TiO<sub>2</sub>, but maternal mPHGPx overexpression prevented this modification. Our findings suggest that enhancing antioxidant defense in the pregnant dam may provide offspring with the most protection from epitranscriptomic remodeling and subsequent long-term cardiovascular repercussions that arise following gestational nano-TiO<sub>2</sub> inhalation exposure.

## Materials and Methods

### *Animal Model*

The West Virginia University Animal Care and Use Committee approved all animal studies which conform to the most current National Institutes of Health (NIH) Guidelines for the Care and Use of Laboratory Animals (8<sup>th</sup> edition) manual. Male and female transgenic (mPHGPx (+/+)) and wild-type (mPHGPx (-/-)) mice with a FVB/NJ genetic background were housed in the West Virginia University Health Sciences Center Animal Facility. All animals were given access to a rodent diet and water *ad libitum*. The mPHGPx transgenic mouse model has been previously described by our laboratory (6, 16). Briefly, to achieve overexpression of mPHGPx, the gene was placed under the control of the cytomegalovirus promoter, which provides robust transgene expression. Transgene screening was performed on tail clip DNA of 3-week old mice using a qPCR approach in which we probed for mPHGPx using a fluorometric probe (Product no. Mm00515041\_m1, Applied Biosystems, Foster City, CA). Increased mPHGPx protein content and improved scavenging ability for phosphatidylcholine hydroperoxide (PCOOH) and hydrogen peroxide (H<sub>2</sub>O<sub>2</sub>) in the mPHGPx transgenic mice indicated a functionally active enzyme (16). MPHGPx overexpression as an antioxidant protective strategy was tested in multiple contexts utilizing complementary breeding strategies (**Figure 3.1A-B**). Because mPHGPx mice are heterozygous transgenic, the transgene status of the donor parent (paternal vs. maternal) impacts the nature of the protective strategy provided to the offspring. Presence of the paternal mPHGPx transgene (Paternal mPHGPx Maternal Exposure (PPME)) enabled a portion of the litter (~50%) to be mPHGPx transgenic positive (**Figure 3.1A, right panel**) and thus presented the opportunity to determine whether fetal mPHGPx transgene presence is protective in utero and adult offspring. Presence of the maternal mPHGPx transgene (Maternal mPHGPx Maternal Exposure (MPME)) enabled a portion of the litter (~50%) to be mPHGPx transgenic (Tg) as well, but with the added benefit of the maternal mPHGPx transgene (**Figure 3.1A, left panel**). This breeding strategy allowed us to delineate whether mPHGPx transgene presence in the environment provided by the dam is beneficial to non-transgenic progeny or additional benefit to transgenic progeny. Pregnancy was verified by identifying the vaginal plug. Approximately 5 days after identification of the vaginal plug (gestational day 5 (GD 5)), the pregnant dams were designated into either sham or nano-TiO<sub>2</sub> exposure groups. Echocardiographic assessments were performed on adult offspring



(11 weeks old), as well as pregnant dams (12 weeks old) and fetal-stage progeny (GD 14). For the adult offspring study, pups remained with the singly-housed dams until weaning age (19 days) at which point they were housed with littermates and separated by sex, with no more than 5 animals per cage. Adult progeny were euthanized at ~11 weeks of age and hearts were excised for further analyses. From each adult litter, one animal of each genotype (WT/Tg) was randomly selected and designated N = 1, alternating selection of male and female offspring to control for sex as a biological variable. All offspring were genotyped using the qPCR method described above. Pregnant dams were euthanized one day following echocardiographic imaging (GD 15), the pups were removed and tail clips were collected for genotyping. Adult offspring and pregnant dams were euthanized through sedation with 5% isoflurane and subsequent cervical dislocation. A timeline of the study is provided in **Figure 3.1C**.

### ***Engineered Nanomaterial Inhalation Exposure***

The ENM inhalation exposure paradigm utilized in the current study has been previously described (23). Nano-TiO<sub>2</sub> P25 powder containing anatase (80%) and rutile (20%) TiO<sub>2</sub> was purchased from Evonik (Aeroxide TiO<sub>2</sub>, Parsipanny, NJ) and prepared by drying, sieving, and storing (23, 34, 47). The primary particle characteristics have been previously reported including the size (21 nm), the specific surface area (48.08 m<sup>2</sup>/g), and the Zeta potential (-56.6 mV) (45, 47, 58). Nano-TiO<sub>2</sub> was aerosolized with a high-pressure acoustical generator (HPAG; IES techno, Morgantown, WV), and has been detailed in previous studies (23) involving rodent inhalation exposure. **Figure 3.2** provides data outlining the aerosol characterization of nano-TiO<sub>2</sub>. In order to recapitulate a lung burden typically seen in a manufacturing setting exposure (35), a target aerosol mass concentration of 12 mg/m<sup>3</sup> of engineered nano-TiO<sub>2</sub> was chosen, for a period of 360 minutes per day for 6 non-consecutive days over an 8-day period, with a whole-body exposure chamber. This level was based on human equivalent alveolar doses during pregnancy and is explained in more detail later in the manuscript. The real-time TiO<sub>2</sub> aerosol mass concentration readings (pDR-1500; Thermo Environmental Instruments Inc., Franklin, MA) over a typical exposure day were sampled from an exposure chamber (**Figure 3.2A**) and verified by gravimetric measurements during each exposure. Final gravimetric measurements indicated a daily 360-minute equivalent average mass concentration of 12.01 ± 0.50 mg/m<sup>3</sup>. A high-resolution electrical

low-pressure impactor (ELPI+; Dekati, Tampere, Finland), a scanning particle mobility sizer (SMPS 3938; TSI Inc., St. Paul, MN), and a Nano Micro-Orifice Uniform Deposit Impactor (MOUDI 115R; MSP Corp, Shoreview, MN) were used to measure the size of the nano-TiO<sub>2</sub> aerosols. A log-normal fit of the data from the ELPI+ indicated a geometric count median diameter (CMD) of 0.163 μm with a geometric standard deviation (GSD) of 1.77 (**Figure 3.2B**). A log-normal fit of the data from the SMPS indicated a CMD of 0.190 μm with a GSD of 1.97 (**Figure 3.2C**). A log normal fit of the data from the MOUDI indicated a mass median aerodynamic diameter (MMAD) of 0.968 μm with a GSD of 2.56 (**Figure 3.2D**). Transmission and scanning electron micrographs (TEM and SEM) of nano-TiO<sub>2</sub> aerosolized particles, sampled from the exposure chamber have been previously published (35). The dose required to match the appropriate lung deposition was calculated based on previously described mouse methodology modified to reflect alveolar deposition only (45). The formula  $D = F \times V \times C \times T$ , where F is the alveolar deposition fraction (4.40%) ((Multiple Path Particle Dosimetry Model (MPPD v3.04)) (2), V is the minute ventilation based on body weight (36.4 ml) (10), C is the mass concentration (12.01 mg/m<sup>3</sup>) and T is the exposure duration (6 hours), was employed (47, 64). This resulted in a daily deposited nano-TiO<sub>2</sub> alveolar dose of 6.92 μg (total six exposure dose = 41.55 μg). When this alveolar burden is normalized with respect to alveolar surface area (mouse<sub>sa</sub> = 0.05m<sup>3</sup>, human<sub>sa</sub> = 102 m<sup>3</sup>) and matched to a human breathing the same aerosol, it corresponds to a human alveolar deposition of 84.76 mg. This is equivalent to an approximately 79 day exposure at the NIOSH recommended exposure limit (REL) of 2.4 mg/m<sup>3</sup> for fine TiO<sub>2</sub> established in 2011 (17) (F = 12.24% (MMPD), V = 7.6 L). Since factory workers are exposed to airborneTiO<sub>2</sub> levels of ~ 0.65 mg/m<sup>3</sup> (51) and the human gestational period is 9 months, we feel that our exposure concentration levels are highly relevant to the female worker population. To maintain a comfortable humidity during the exposure, bedding material was soaked in water and placed in the exposure chamber. Control animals (sham) were exposed to HEPA filtered air, rather than nano-TiO<sub>2</sub>, in a designated chamber with similar chamber conditions. The final exposure was administered 48 hours prior to sacrifice and tissue harvesting.

### ***Echocardiography***

Cardiac contractile function was assessed in adult offspring (11 weeks old) using the Vevo2100 High Frequency Ultrasound system (Visual Sonics, Toronto, Canada) to obtain Motion mode (M-mode) images as previously described (35). Anesthesia was induced using inhalant isoflurane, which was then maintained at ~1.5% in order to achieve a physiologically relevant heart rate. Images were acquired with a linear array transducer at 32–40 MHz, with a frame rate of 233–401 frames/second. M-mode images were also obtained for pregnant dams (12 weeks old) and their fetal progeny (GD 14). For fetal echocardiographic imaging, pups in the right and left uterine horns were imaged sequentially, which allowed us to correlate the assessed cardiac function with the genotype of that specific pup. For adult offspring analyses, one animal of each genotype (WT/Tg) from each exposed (sham/nano-TiO<sub>2</sub>) dam (PPME (WT mom) or MPME (Tg mom)) was selected at random. Measurements were calculated over three cardiac cycles and averaged.

Speckle-tracking-based strain evaluations were performed using parasternal long and short axis B-mode images as previously described by our laboratory (24, 35, 46, 59). A speckle-tracking algorithm in Visual Sonics VevoStrain software (Toronto, Canada) was employed to trace the endocardium and epicardium walls. Data were analyzed for three cardiac cycles using time-to-peak analysis for curvilinear data. Measures of systolic strain including deformation, strain rate, displacement, and velocity were obtained. For adult progeny, speckle-tracking was performed on both long- and short-axis images. For fetal progeny, speckle-tracking was performed on short-axis images. All echocardiographic measurements were acquired by one analyst blinded to the animal exposure group and genotype.

### ***Electron Transport Chain (ETC) Complex Activities***

ETC Complex activities (I, III, IV, and V) were measured in hearts of adult offspring as previously described (4, 6, 24). Whole tissue was homogenized using the Polytron PowerGen 500 S1 tissue homogenizer (Fisher Scientific, Hampton, NH) in NP-40 buffer (20mM Tris, 137mM NaCl, 10% Glycerol, 1% Triton x100, 2mM EDTA) (25). Samples were centrifuged for 10 minutes at 10,000 xg (4°C) and the supernatant was used for the activity assays. The protein homogenates were used to measure activities of ETC complexes I, III, IV, and V (ATP synthase). ETC complex I and III activities were determined by measuring the reduction of decylubiquinone (I) and

cytochrome c (III) in cardiac protein lysate of adult offspring. ETC complex IV activity was determined by measuring the oxidation of reduced cytochrome c, while complex V activity was determined by measuring oligomycin-sensitive ATPase activity through pyruvate kinase and phosphoenolpyruvate in cardiac protein lysate of adult offspring. The Molecular Devices Flex Station 3 Multi-Mode microplate reader (Sunnyvale, CA) was used to measure all assays spectrophotometrically. Protein content was normalized using the Bradford method, with bovine serum albumin protein assay standards. Final values were expressed as Unit/nanogram (I-IV) or milligram (V) of protein, where Unit = nanomoles of substrate oxidized  $\cdot$  minute<sup>-1</sup>.

### ***Total Glutathione Peroxidase (GPx) Activity***

Total GPx activity was measured using a GPx Activity Kit from Cayman Chemical (item no. 703102, Ann Arbor, MI). The Cayman Chemical GPx Activity Kit determines all glutathione-dependent peroxidase activity indirectly through a coupled reaction with glutathione reductase (GR). The cumene hydroperoxide in this assay is reduced by GPx producing oxidized glutathione (GSSG), which can then be recycled to its reduced state by GR and NADPH. The oxidation of NADPH results in a decrease in absorbance at 340nm that is proportional to the GPx activity, when it is the rate limiting factor. The experiment was carried out using the manufacturer's protocol, with minor modifications: Heart lysate (in NP-40) samples were diluted with sample buffer and 20  $\mu$ l of the diluted heart lysate was used for the assay. Absorbance was read once every minute for 6 minutes at 340 nm using the Molecular Devices Flex Station 3 Multi-Mode microplate reader. Absorbance values were retrospectively normalized to protein content with the Bradford assay (12).

### ***MPHGPx Activity***

To determine mitochondrial phospholipid hydroperoxide glutathione peroxidase (GPx4) activity, phosphatidylcholine hydroperoxide (PCOOH), a specific substrate of MPHGPx, was synthesized as previously described (67). L- $\alpha$ -Phosphatidylcholine Type III/S (PC) (item no. P3782; Sigma-Aldrich, St. Louis, MO) was slowly added to a Tris/Base buffer (0.2 M, pH 8.8, 3mM sodium deoxycholate (item no. D6750, Sigma-Aldrich)) while stirring at medium-high

speed. Once a cloudy emulsion of small droplets was visible, additional Tris/Base buffer was introduced with continuous stirring until the solution was clear. A volume of soybean lipoxidase Type V (item no. L6632, Sigma-Aldrich) was added that equaled 250,000 U to initiate the synthesis reaction followed with continuous stirring for 1 hour. A Sep-Pak C-18 cartridge (item no. 020515, Waters, Milford, MA) was activated with methanol and equilibrated with ddH<sub>2</sub>O, then used to purify the PCOOH with a 30 ml glass syringe (item no. Z314374, Sigma-Aldrich). The cartridge was washed with water to remove water-soluble substances and the PCOOH was eluted from the C18 resin with methanol. The concentration of PCOOH was determined at A<sub>234</sub> using the NanoDrop ND-100 (Thermo Fisher Scientific, Waltham, MA) and diluted to a desired concentration with methanol. The PCOOH was immediately used as the substrate (in place of cumene hydroperoxide) with the Glutathione Peroxidase Assay Kit (Cayman) as described above, with absorbance readings every 30 seconds for 6 minutes at 340nm with the Molecular Devices Flex Station 3 Multi-Mode microplate reader. All samples were blanked with background wells (no sample) and normalized to protein content.

### ***Mitochondrial Isolation***

Adult progeny were sacrificed at 11 weeks of age, and hearts were excised through a midsagittal cut in the thoracic cavity. Isolation of mitochondrial subpopulations was achieved through differential centrifugation as previously described (6, 48). The two subpopulations were combined and utilized as a total mitochondrial fraction for subsequent analyses. KME buffer (100mM KCl, 50mM MOPS and 0.5mM EGTA pH 7.4) was used to resuspend isolated mitochondria. Protein concentrations were determined using the Bradford method with bovine serum albumin as a standard (12).

### ***Hydrogen Peroxide (H<sub>2</sub>O<sub>2</sub>) Production***

Hydrogen peroxide (H<sub>2</sub>O<sub>2</sub>) production was evaluated in total tissue lysate and isolated mitochondria from adult offspring in order to determine mitochondrial ROS production (35, 45, 65). The Invitrogen™ Amplex™ Red Hydrogen Peroxide Assay Kit (product no. A2218; Thermo Fisher) was utilized per manufacturer's instructions and assays performed spectrophotometrically.

In the presence of horseradish peroxidase (HRP), the Amplex™ Red reagent produces a red fluorescent oxidation product when the reagent reacts with H<sub>2</sub>O<sub>2</sub>. The oxidation product, resorufin, was detected spectrophotometrically at 560 nm and data were normalized to protein content.

### ***Global m<sup>6</sup>A Methylation***

Total RNA was purified from heart samples that were digested with QIAzol lysis reagent (item no. 79306, Qiagen, Hilden, Germany) from one adult offspring of each genotype (WT/Tg) from each dam (PPME/MPME) from each exposure group (sham/nano-TiO<sub>2</sub>) using the miRNeasy Mini Kit (item no. 217004, Qiagen). Global m<sup>6</sup>A methylation was quantified in total RNA using the EpiQuik™ m<sup>6</sup>A RNA Methylation Quantification Kit (item no. P-9005; EpiGentek, Farmingdale, NY) per manufacturer's instructions. Briefly, total RNA samples were diluted to a standard concentration of 200 ng with IDTE buffer. Dilution of the provided positive control allowed for the generation of a standard curve. RNA was bound to the assay wells through incubation with the binding solution. An optimized m<sup>6</sup>A capture antibody was added to the wells, incubated, and washed, followed by addition of the detection antibody and enhancer solution. The color developing solution was then introduced and incubated for 2 minutes, until the color changed to blue, at which point the stop solution was added. Absorbance was read at 450 nm using the Molecular Devices Flex Station 3 Multi-Mode microplate reader. A standard curve was used to determine global m<sup>6</sup>A levels in each sample.

### ***Immunoprecipitation (m<sup>6</sup>A-RIP)***

Total RNA was purified from whole heart samples from PPME and MPME WT adult offspring from each exposure group (sham/nano-TiO<sub>2</sub>) using the miRNeasy Kit (Qiagen) described above.

### ***RNA Fragmentation***

Before the immunoprecipitation was carried out, the RNA samples were fragmented using the NEBNext Magnesium RNA Fragmentation kit (item no. E6150s; New England Biolabs) (5,

76). To determine the necessary length of incubation to achieve desired fragmentation (~130 nt), samples were incubated for 1-10 minutes at 94°C. The 10 samples were analyzed with the Bioanalyzer 2100 (Agilent Technologies, Santa Clara, CA) to determine the size distribution of the fragments.

### *m<sup>6</sup>A-RIP*

The EpiMark N6-Methyladenosine Enrichment Kit (item no. E1610S; New England Biolabs, Ipswich, MA) was used to enrich m<sup>6</sup>A modified RNA per manufacturer's instructions, with minor modifications. RNA samples were fragmented at 94°C for 3 minutes (5). Dynabeads™ Protein G magnetic beads from Thermo Fisher Scientific (product no. 10003D) were washed and resuspended in Reaction Buffer. An anti-N6-Methyladenosine (m<sup>6</sup>A) rabbit monoclonal antibody (product no. 56593, Cell Signaling Technology, Danvers, MA) was bound to the beads, followed by the addition of the fragmented total RNA (100ng) and RNasin® Plus RNase Inhibitor (product no. N2611; Promega, Madison, WI). The normal Rabbit IgG control (product no. 2729, Cell Signaling Technology), an unconjugated rabbit polyclonal antibody, was used as a non-specific IgG control for the immunoprecipitation. After the immunoprecipitation, RNA was eluted with Buffer RLT (product no. 79216; Qiagen) then cleaned and concentrated using Dynabeads™ MyOne™ Silane (product no. 37002D; Life Technologies, Carlsbad, CA). The RNA samples from both input and immunoprecipitated samples were examined by RT-qPCR to quantify m<sup>6</sup>A enrichment.

### *RT-qPCR*

WT adult offspring heart samples (from WT/Tg and sham/nano-TiO<sub>2</sub> exposed dams) were prepared for downstream analysis by reverse-transcribing the input and immunoprecipitated RNA using the Applied Biosystems High Capacity cDNA Reverse Transcription Kit (product no. 4368814; Thermo Fisher Scientific) per manufacturer's protocol. RT-qPCR was utilized to evaluate m<sup>6</sup>A enrichment of the mPHGPx 3'-UTR, specifically the region containing the crucial selenocysteine (Sec) insertion sequence (SECIS) (13, 28). Primers for mPHGPx and a control, GAPDH, were designed using Primer3Plus (7) and the sequences are listed in **Supplemental**

**Table 3.1** (Additional file 3.1). Quantification was achieved with SYBR<sup>®</sup> Green master mix (product no. A25742, Thermo Fisher Scientific) using the Applied Biosystems 7500 Fast Real-Time PCR system. Samples were run in triplicate. Enrichment fold was calculated using the  $\Delta Ct$  value of the IP normalized to the  $\Delta Ct$  of the input, relative to the dilution factor (20% input; dilution factor = 5), and normalized to GAPDH, as illustrated below (42).

$$\Delta Ct[\text{Normalized IP}] = Ct [IP] - (Ct[\text{Input}] - \text{Log}_2(\text{Dilution Factor}))$$

$$\Delta \Delta Ct = \Delta Ct [\text{Normalized IP}_{(mPHGPx)}] - \Delta Ct [\text{Normalized IP}_{(GAPDH)}]$$

$$\text{Fold enrichment} = 2^{(-\Delta \Delta Ct)}$$

### *Statistics*

All statistical analyses were performed using GraphPad Prism Software Version 8 for Windows (GraphPad Software, La Jolla CA). For adult offspring analyses, from each MPME or PPME cohort, one animal of each genotype (WT/Tg) from a given exposure (sham and nano-TiO<sub>2</sub>) was randomly selected and designated N = 1. For fetal analyses, each pregnant dam that was exposed (sham/nano-TiO<sub>2</sub>) was considered one observation, with each genetic group (WT/Tg) considered as N = 1. Data were analyzed using a two-way analysis of variance (ANOVA) method to evaluate mPHGPx presence and nano-TiO<sub>2</sub> maternal exposure. Normality was determined using the D'Agostino-Pearson test. Tukey's multiple comparison method was performed following the two-way ANOVA to evaluate effects within the PPME and MPME groups. Statistical difference was defined by  $P \leq 0.05$ . The presence of a letter above a specific group denotes statistical significance between those two groups as determined by Tukey's multiple comparisons test. For functional assays performed using adult hearts, a two-tailed Student's t-test was also employed to evaluate whether maternal nano-TiO<sub>2</sub> inhalation exposure during gestation elicited a change between offspring of the same genotype. The presence of a dagger (†) above a given group indicates statistical significance between WT Sham and WT TiO<sub>2</sub> or Tg Sham and Tg TiO<sub>2</sub> of the same maternal genetic group (MPME or PPME). For qPCR data, a one-way ANOVA was employed followed by a Tukey's multiple comparisons test to determine significant differences in



m<sup>6</sup>A fold enrichment across WT offspring groups. All data are presented as the mean  $\pm$  the standard error of the mean (SEM).

## Results

### *Cardiac Function*

Deleterious changes in cardiac structure and function have previously been identified in offspring following maternal nano-TiO<sub>2</sub> inhalation exposure during gestation (24, 35). Conventional M-mode evaluations determined that adult offspring of WT dams (PPME) who were gestationally-exposed to nano-TiO<sub>2</sub> presented with higher systolic diameter and volume, as well as lower ejection fraction and fractional shortening than those whose dams were sham-exposed (**Table 3.1**). Additionally, adult offspring whose dams were mPHGPx Tg (MPME) overall had significantly lower diastolic diameter and volume, stroke volume, and cardiac outputs than PPME offspring regardless of exposure (**Table 3.1**). Adult offspring heart rates were unchanged regardless of exposure or genotype (**Additional file 3.1: Supplemental Table 3.2**).

When examining the dams, WT nano-TiO<sub>2</sub>-exposed mice had significantly decreased diastolic diameter and volume when compared to WT sham-exposed dams, as well as reduced pump function indicated by stroke volume and cardiac output reductions (**Additional file 3.1: Supplemental Table 3.3**). Furthermore, relative wall thickness was significantly increased following ENM exposure in WT dams, but not in the mPHGPx Tg dams (**Additional file 3.1: Supplemental Table 3.3**). Maternal heart rate remained unchanged between all exposure groups (**Additional file 3.1: Supplemental Table 3.4**). At the fetal stage, in order to correlate the assessed cardiac function with the genotype of that specific pup, pups in the right and left uterine horns were sequentially imaged (**Figure 3.3A**). A representative trace of the fetal pup's left ventricle (LV) in M-mode is shown in **Figure 3.3B**. A group-dependent effect was found, with the MPME fetal offspring demonstrating higher diastolic diameter and volume, as well as higher stroke volume and cardiac output than the PPME offspring (**Additional file 3.1: Supplemental Table 3.5**). MPME fetal offspring also had significantly higher heart rates (**Additional file 3.1: Supplemental Table 3.2**). Decreased function in the PPME WT offspring following gestational ENM exposure confirms previous findings (35) and substantiate the susceptibility of WT offspring to cardiovascular changes due to maternal nano-TiO<sub>2</sub> exposure, which may be a result of limited antioxidant capacity.

Speckle-tracking based stress strain assessments were performed during systole in fetal and adult offspring groups of all dams (**Table 3.2 and Additional file 3.1: Supplemental Table 3.6-**

7). Long-axis measurements in adult offspring demonstrated that endocardial global longitudinal strain (GLS) was significantly lower in PPME WT offspring whose dams were exposed to nano-TiO<sub>2</sub> compared to sham-exposed (**Table 3.2**). The PPME WT pups also had a significantly lower GLS than PPME Tg adults, who were both progeny of nano-TiO<sub>2</sub> exposed dams. (**Table 3.2**). A group dependent effect was seen with MPME progeny having higher radial and longitudinal strain rates, and diminished longitudinal displacement compared to PPME progeny. Group dependent effects were also observed in the parasternal short axis between the MPME (**Additional file 3.1: Supplemental Table 3.6**). **Figures 3.3 C and D** provide representative B-mode images of a fetal pup *in utero* during end diastole and end systole, respectively, as well as speckle-tracking traces correlating to each of these frames (**Figure 3.3 E-F**). At the fetal stage, short-axis radial and circumferential strain rates were significantly lower in both the PPME WT and Tg groups whose dams were exposed to nano-TiO<sub>2</sub> than the pups of the same respective genotype whose dams were sham-exposed (**Additional file 1: Supplemental Table 3.7**). Further, these data also revealed a group dependent effect based on maternal genotype (MPME vs PPME). Overall, these changes appear to suggest that enhanced maternal antioxidant protection may provide sufficient protection to thwart cardiac maladaptation that is precipitated by ENM exposure.

### ***ETC Complex Activities***

ETC complex activity assays were performed on protein lysate samples of adult offspring (**Figure 3.4**). Two-way ANOVA analysis revealed no significant difference between PPME and MPME offspring for complex I (**Figure 3.4A**) and complex III activities (**Figure 3.4B**), but MPME offspring had significantly higher activities for both complex IV (**Figure 3.4C**) and V (**Figure 3.4D**). Individual t-tests were implemented to better delineate exposure specific differences between offspring of the same genotype (WT or Tg) and same cohort (PPME or MPME). The PPME WT offspring of ENM-exposed dams had significantly diminished complex I (**Figure 3.4A**) and IV (**Figure 3.4C**) activities than PPME WT offspring whose dams were sham-exposed. These findings are consistent with previously published data from our laboratory (35).

### ***GPx Activity and H<sub>2</sub>O<sub>2</sub> Production***

Total GPx enzymatic activity (including all isoforms) was measured in adult offspring. MPME offspring had a significantly higher level of total GPx activity than the PPME offspring (**Figure 3.5A**). Within the PPME group, Tg offspring of sham-exposed dams had elevated enzymatic activity compared to their WT littermates (**Figure 3.5A**). To assess specific mPHGPx activity, phosphatidylcholine (PCOOH) was used as a substrate. Within the PPME group, the Tg sham adult offspring had the highest level of mPHGPx activity and was significantly higher than the other three PPME groups, including the PPME Tg offspring whose dams were nano-TiO<sub>2</sub> exposed (**Figure 3.5B**). In the MPME group, the Tg sham and Tg nano-TiO<sub>2</sub> groups were both significantly higher than their littermate controls (**Figure 3.5B**). Student's t-tests were used to delineate exposure specific differences between offspring with the same genotype from the same cohort (PPME or MPME). These analyses revealed that in the PPME group, gestational exposure to ENM resulted in lower mPHGPx activity regardless of the offspring's genotype (**Figure 3.5B**).

Previously published data from our laboratory have indicated that maternal ENM exposure during gestation resulted in increased H<sub>2</sub>O<sub>2</sub> levels at the fetal stage, which was not sustained into adulthood (35). In the current study, H<sub>2</sub>O<sub>2</sub> levels were unchanged in adult offspring (**Figure 3.5C**), which was consistent with our previous findings. H<sub>2</sub>O<sub>2</sub> levels were also evaluated in isolated mitochondria. H<sub>2</sub>O<sub>2</sub> levels were elevated in PPME WT adult offspring whose dams were gestationally-exposed to ENM when compared to PPME WT adult offspring whose dams were gestationally-sham-exposed (**Figure 3.5D**). These data overall indicate that maternal exposure to nano-TiO<sub>2</sub> during gestation results in decreased hydroperoxide scavenging and increased ROS, while maternal antioxidant protection has the potential to prevent these detriments.

### ***Global and mPHGPx M<sup>6</sup>A Methylation***

Alterations in the relative abundance of m<sup>6</sup>A modifications can affect RNA metabolism and are associated with various diseases, including metabolic diseases affecting the heart (38). The SEC insertion sequence (SECIS), which is present in the 3'-UTR of mPHGPx and allows for the insertion of the crucial selenocysteine, contains potential m<sup>6</sup>A sites (40, 75). To investigate whether altered total m<sup>6</sup>A methylation plays a role in the diminished mPHGPx activity in offspring whose dams were exposed to nano-TiO<sub>2</sub>, we quantified global m<sup>6</sup>A in RNA isolated from the hearts of adult offspring (**Figure 3.6A**). Initial analyses indicated that global m<sup>6</sup>A status was

statistically unchanged between the groups, but individual t-tests revealed that MPME Tg offspring whose dams were exposed to nano-TiO<sub>2</sub> had significantly lower levels of m<sup>6</sup>A methylation than MPME Tg offspring whose dams were sham-exposed (**Figure 3.6A**).

In order to evaluate the SEC region of mPHGPx in WT offspring, RNA was fragmented and used to perform an m<sup>6</sup>A RNA immunoprecipitation, followed by qPCR for a specific region of the mPHGPx 3'-UTR. RNA fragmentation incubation time was determined using the Bioanalyzer 2100. A 3-minute incubation was deemed the most appropriate in order to achieve ~130 nt fragments (**Figure 3.6B**) (5). RMBase v2.0 software predicted the presence of m<sup>6</sup>A sites at the 3'-UTR of mPHGPx mRNA specifically within the SECIS region (**Figure 3.6C**). RT-qPCR revealed that PPME WT adult offspring whose dams were exposed to nano-TiO<sub>2</sub> had significantly higher m<sup>6</sup>A levels in the 3'-UTR region of mPHGPx than the control group (PPME WT sham) (**Figure 3.6D**), as well as both the sham and nano-TiO<sub>2</sub> MPME WT groups. These data indicate that gestational exposure in WT dams, has the ability to modulate epitranscriptome reprogramming that is present in offspring at adulthood. The increase in m<sup>6</sup>A enrichment in the PPME WT offspring of ENM-exposed dams may be responsible for the persistent mitochondrial bioenergetic and cardiac functional detriments. Additionally enhanced maternal antioxidant capacity may provide protection from the initial stimuli responsible for the altered m<sup>6</sup>A status of mPHGPx.

## Discussion

With the inevitable increase in production and application of ENM-enabled products in manufacturing, biomedicine, and general consumer use, a thorough understanding of the longitudinal repercussions is necessary for the development of preventative and protective strategies for workers and consumers. This is of particular importance during fetal growth, where a toxicological insult may elicit immediate and long-term deleterious effects. In this study, we have demonstrated that increased antioxidant defense in the maternal environment is capable of providing preservation to cardiac contractile function potentially through the maintenance of mitochondrial bioenergetics. Furthermore, the presence of the maternal transgene preserved m<sup>6</sup>A status at the 3'-UTR of mPHGPx in offspring despite gestational ENM inhalation exposure. Our data point to a maladaptation in the epitranscriptomic signature as the mechanism responsible for diminished bioenergetics and cardiac contractile deficits in adult offspring following maternal exposure.

Left ventricular ejection fraction (LVEF) has been widely used as a key measure of cardiac contractile function and as a prognostic tool for heart failure (53). The dependence of this parameter on load, can limit reproducibility, necessitating a more reliable marker of cardiac function (1, 30). Global longitudinal strain (GLS), a measure of myocardial deformation, is the most commonly utilized clinical application of strain imaging (20, 41). GLS appears to be a better predictor of cardiovascular outcomes than LVEF, with better reproducibility (3, 31). Decreases in GLS, as seen in the PPME WT offspring following exposure, highlight the susceptibility of this group to future cardiovascular events (**Table 3.2**). The preservation of GLS in the MPME group is therefore noteworthy as the antioxidant protective strategy provided by the mother was able to sufficiently protect her offspring from long-term adverse cardiovascular complications.

Maternal ENM exposure during gestation interferes with fetal development and has long-term consequences for offspring that persist into adulthood (11, 15, 27, 69). The importance of the maternal environment are outlined by the developmental origins of health and disease (DOHaD) hypothesis and supported by an increasing number of studies (70). The current study highlights how amplifying antioxidant capacity in the maternal environment can deter the maladaptive cardiovascular changes that persist into adulthood, regardless of the progeny's genotype. Although transgenic expression provides a limitation to clinical uses of maternal antioxidant protection, we

establish a basis for investigating other potential antioxidant protective strategies. One example is mitoquinone mesylate (MitoQ), a mitochondrial-targeted antioxidant that has showed promise in improving mitochondrial dysfunction, reducing hydrogen peroxide production, and antioxidant enzyme activity (50, 54). MitoQ also has the ability to prevent the long-term impacts of maternal cigarette smoke exposure on progeny by mitigating renal total ROS in the mothers and offspring at adulthood (68). Future investigations should aim to determine whether supplementation with antioxidant-boosting therapeutics during pregnancy can provide the same protective effect to progeny as maternal mPHGPx overexpression.

As a relatively new area of research in ENM inhalation exposure toxicology, there are few studies that investigate the detailed epitranscriptomic mechanisms associated with the exposures. However, a recent study demonstrated that in A549 cells, global m<sup>6</sup>A was decreased following particulate matter exposure as a result of altered m<sup>6</sup>A modulator genes (14). Although this study was performed using lung epithelial cells, it is one of the first studies to highlight the concept that exposure to environmental toxicants has the ability to alter m<sup>6</sup>A RNA methylation profiles. M<sup>6</sup>A has previously been established to preferentially occur around stop codons, with high enrichment in 3'-UTRs of human and mouse transcriptomes (18, 43). Further, the 3'-UTR of mPHGPx is a critical region as it is the location of the Sec incorporation machinery, which enables the catalytic activity of this peroxide scavenging protein (28). To ensure proper function of mPHGPx as a peroxide scavenger, proper selenocysteine (Sec) incorporation is required, which involves the recoding of a UGA codon from “Stop” to “Sec” via a complex that is assembled at a specific region of the 3'-UTR known as the SECIS (28, 60). Recoding occurs through an eEFSec/Sec-tRNA<sup>Sec</sup> complex binding to Sec binding protein 2 (SBP2), which is anchored to the SECIS in the 3'-UTR. Alterations to the SECIS region, may affect the efficiency of Sec incorporation and thus alter the catalytic activity and/or expression of mPHGPx by retaining the premature termination codon, potentially resulting in decay (60, 62). Modulation of this critical region may be the mechanism that results in the persistent adverse outcomes of maternal ENM inhalation exposure into adulthood.

Early studies of m<sup>6</sup>A modifications determined that m<sup>6</sup>A primarily occurs in two possible sequences, Gm<sup>6</sup>AC or Am<sup>6</sup>AC (74), but have further been specified as RRACH (R = A/G and H = A/C/U) (8, 18, 75). Interestingly, RMBase v2.0 software, which was utilized as a way of

scanning for RRACH motifs, predicted m<sup>6</sup>A sites at the 3'-UTR of mPHGPx mRNA specifically within the SECIS region (75), as demonstrated in **Figure 3.6C**. The presence of m<sup>6</sup>A sites in this region was also confirmed in a recent study that aimed to assess the methylome of human and mouse tissue (40). Papp et al. reported that inefficient selenoprotein synthesis can increase sensitivity to oxidative stress, which is one potential explanation for the alterations seen at the fetal stage following gestational ENM inhalation exposure (49). Moreover, increased methylation, shown in **Figure 3.6**, may alter Sec incorporation by changing the secondary structure of the SECIS hairpin (57) and preventing SBP2 from anchoring the incorporation complex to the RNA (22). This in turn may be leading to inefficient mPHGPx hydroperoxide scavenging (28) at the adult stage. The decrease in mPHGPx protein expression at the fetal stage compared to the maintenance of expression, but diminution of mPHGPx activity at the adult stage, will require further investigation. A possible explanation is that the epitranscriptomic remodeling occurring at the adult stage may differ from the initial reprogramming that occurred *in utero* following maternal nano-TiO<sub>2</sub> inhalation exposure.

**Figure 3.7** provides an overview of the mechanisms involved in the long-term ramifications of maternal ENM inhalation exposure during gestation on offspring. Overexpression of mPHGPx in the pregnant dam limits H<sub>2</sub>O<sub>2</sub> (ROS) production, thereby mitigating changes to mitochondrial bioenergetics and cardiac contractile function in adult progeny. However, without the overexpression of mPHGPx in the maternal environment, ROS production is not controlled following nano-TiO<sub>2</sub> exposure during gestation, resulting in downstream effects on cardiac function and mitochondrial bioenergetics. This occurs, in part, as a result of elevated m<sup>6</sup>A methylation at the SECIS region of mPHGPx, which disrupts Sec incorporation and diminishes mPHGPx catalytic activity. The current study highlights the therapeutic potential of enhanced antioxidant protection in the maternal environment during gestation (**Figure 3.7**). Increased hydroperoxide scavenging through this approach can provide protection for offspring into adulthood from the deleterious effects of maternal particulate exposure during gestation, without the need for supplementation by the progeny. Overexpression of mPHGPx in the pregnant dam likely circumvents the initial surge of oxidative stress that is elicited by the xenobiotic exposure, through a mechanism that involves epitranscriptomic reprogramming.



At the adult stage, maternal ENM exposure during gestation was associated with altered m<sup>6</sup>A methylation of mPHGPx that contributes to diminished enzymatic activity and persistent cardiac contractile alterations. These findings highlight a specific targeted alteration to the epitranscriptome that may be mechanistically linked to sustained bioenergetic and cardiac dysfunction associated with gestational ENM exposure. Alterations to the epitranscriptome presented in this study provide a new perspective on the role of m<sup>6</sup>A methylation changes in the fields of cardiovascular ENM inhalation exposure toxicology. Our study introduces a protective strategy that can be implemented to safeguard developing progeny against long-term cardiovascular ramifications.

## **Acknowledgements**

We would like to thank Sherri A. Friend and the National Institute for Occupational Safety and Health, Morgantown, WV, USA for contributing in the physicochemical characterization of the nano-TiO<sub>2</sub> aerosolized particles.

## **Disclosure of Interest**

The authors report no conflict of interest.

## **Funding**

This work was supported by: The National Heart Lung Blood Institute (NHLBI) under Grant [R01 HL-128485] (JMH), the National Institute of Environmental Health Sciences (NIEHS) under Grant [R01 ES-015022] (TRN), American Heart Association under Grant [AHA-20PRE35080170] (AK), American Heart Association under Grant [AHA-17PRE33660333] (QAH), National Institute on Aging (NIA) under Grant [5 T32 AG 52375-3] (KLG), WVU Genomics Core Facility support by CTSI Grant [U54GM104942], WVU Animal Models & Imaging Facility supported by the WVU Cancer Institute and NIH grants [P20 RR016440] and [P30 RR032138/GM103488], and the Community Foundation for the Ohio Valley Whipkey Trust (JMH).

## References:

1. **Amzulescu MS, De Craene M, Langet H, Pasquet A, Vancraeynest D, Pouleur AC, Vanoverschelde JL, and Gerber BL.** Myocardial strain imaging: review of general principles, validation, and sources of discrepancies. *Eur Heart J Cardiovasc Imaging* 20: 605-619, 2019.
2. **Anjilvel S, and Asgharian B.** A multiple-path model of particle deposition in the rat lung. *Fundam Appl Toxicol* 28: 41-50, 1995.
3. **Ashish K, Faisaluddin M, Bandyopadhyay D, Hajra A, and Herzog E.** Prognostic value of global longitudinal strain in heart failure subjects: A recent prototype. *Int J Cardiol Heart Vasc* 22: 48-49, 2019.
4. **Barrientos A, Fontanesi F, and Diaz F.** Evaluation of the mitochondrial respiratory chain and oxidative phosphorylation system using polarography and spectrophotometric enzyme assays. *Curr Protoc Hum Genet* Chapter 19: Unit19 13, 2009.
5. **Barros-Silva D, Lobo J, Guimaraes-Teixeira C, Carneiro I, Oliveira J, Martens-Uzunova ES, Henrique R, and Jeronimo C.** VIRMA-Dependent N6-Methyladenosine Modifications Regulate the Expression of Long Non-Coding RNAs CCAT1 and CCAT2 in Prostate Cancer. *Cancers (Basel)* 12: 2020.
6. **Baseler WA, Dabkowski ER, Jagannathan R, Thapa D, Nichols CE, Shepherd DL, Croston TL, Powell M, Razunguzwa TT, Lewis SE, Schnell DM, and Hollander JM.** Reversal of mitochondrial proteomic loss in Type 1 diabetic heart with overexpression of phospholipid hydroperoxide glutathione peroxidase. *Am J Physiol Regul Integr Comp Physiol* 304: R553-565, 2013.
7. **Baseler WA, Dabkowski ER, Williamson CL, Croston TL, Thapa D, Powell MJ, Razunguzwa TT, and Hollander JM.** Proteomic alterations of distinct mitochondrial subpopulations in the type 1 diabetic heart: contribution of protein import dysfunction. *Am J Physiol Regul Integr Comp Physiol* 300: R186-200, 2011.
8. **Batista PJ.** The RNA Modification N(6)-methyladenosine and Its Implications in Human Disease. *Genomics Proteomics Bioinformatics* 15: 154-163, 2017.
9. **Berulava T, Buchholz E, Elerdashvili V, Pena T, Islam MR, Lbik D, Mohamed BA, Renner A, von Lewinski D, Sacherer M, Bohnsack KE, Bohnsack MT, Jain G, Capece V, Cleve N, Burkhardt S, Hasenfuss G, Fischer A, and Toischer K.** Changes in m6A RNA methylation contribute to heart failure progression by modulating translation. *Eur J Heart Fail* 22: 54-66, 2020.
10. **Bide RW, Armour SJ, and Yee E.** Estimation of Human Toxicity From Animal Inhalation Toxicity Data:1. Minute Volume-Body Weight Relationships Between Animals And Man Defence Research Establishment Suffield, 1997.
11. **Bommarito PA, Martin E, and Fry RC.** Effects of prenatal exposure to endocrine disruptors and toxic metals on the fetal epigenome. *Epigenomics* 9: 333-350, 2017.
12. **Bradford MM.** A rapid and sensitive method for the quantitation of microgram quantities of protein utilizing the principle of protein-dye binding. *Anal Biochem* 72: 248-254, 1976.
13. **Castellanos-Rubio A, Santin I, Olazagoitia-Garmendia A, Romero-Garmendia I, Jauregi-Miguel A, Legarda M, and Bilbao JR.** A novel RT-QPCR-based assay for the relative quantification of residue specific m6A RNA methylation. *Sci Rep* 9: 4220, 2019.
14. **Cayir A, Barrow TM, Guo L, and Byun HM.** Exposure to environmental toxicants reduces global N6-methyladenosine RNA methylation and alters expression of RNA methylation modulator genes. *Environ Res* 175: 228-234, 2019.

15. **Crispi F, Miranda J, and Gratacos E.** Long-term cardiovascular consequences of fetal growth restriction: biology, clinical implications, and opportunities for prevention of adult disease. *Am J Obstet Gynecol* 218: S869-S879, 2018.
16. **Dabkowski ER, Williamson CL, and Hollander JM.** Mitochondria-specific transgenic overexpression of phospholipid hydroperoxide glutathione peroxidase (GPx4) attenuates ischemia/reperfusion-associated cardiac dysfunction. *Free Radic Biol Med* 45: 855-865, 2008.
17. **Department of Health and Human Services CfDCaP, National Institute for Occupational Safety and Health.** Occupational Exposure to Titanium Dioxide. 2011.
18. **Dominissini D, Moshitch-Moshkovitz S, Schwartz S, Salmon-Divon M, Ungar L, Osenberg S, Cesarkas K, Jacob-Hirsch J, Amariglio N, Kupiec M, Sorek R, and Rechavi G.** Topology of the human and mouse m6A RNA methylomes revealed by m6A-seq. *Nature* 485: 201-206, 2012.
19. **Engel M, Eggert C, Kaplick PM, Eder M, Roh S, Tietze L, Namendorf C, Arloth J, Weber P, Rex-Haffner M, Geula S, Jakovcevski M, Hanna JH, Leshkowitz D, Uhr M, Wotjak CT, Schmidt MV, Deussing JM, Binder EB, and Chen A.** The Role of m(6)A/m-RNA Methylation in Stress Response Regulation. *Neuron* 99: 389-403 e389, 2018.
20. **Ersboll M, Valeur N, Mogensen UM, Andersen MJ, Moller JE, Velazquez EJ, Hassager C, Sogaard P, and Kober L.** Prediction of all-cause mortality and heart failure admissions from global left ventricular longitudinal strain in patients with acute myocardial infarction and preserved left ventricular ejection fraction. *J Am Coll Cardiol* 61: 2365-2373, 2013.
21. **Ferrari L, Carugno M, and Bollati V.** Particulate matter exposure shapes DNA methylation through the lifespan. *Clin Epigenetics* 11: 129, 2019.
22. **Fletcher JE, Copeland PR, Driscoll DM, and Krol A.** The selenocysteine incorporation machinery: interactions between the SECIS RNA and the SECIS-binding protein SBP2. *RNA* 7: 1442-1453, 2001.
23. **Hathaway QA, Durr AJ, Shepherd DL, Pinti MV, Brandebura AN, Nichols CE, Kunovac A, Goldsmith WT, Friend SA, Abukabda AB, Fink GK, Nurkiewicz TR, and Hollander JM.** miRNA-378a as a key regulator of cardiovascular health following engineered nanomaterial inhalation exposure. *Nanotoxicology* 13: 644-663, 2019.
24. **Hathaway QA, Nichols CE, Shepherd DL, Stapleton PA, McLaughlin SL, Stricker JC, Rellick SL, Pinti MV, Abukabda AB, McBride CR, Yi J, Stine SM, Nurkiewicz TR, and Hollander JM.** Maternal-engineered nanomaterial exposure disrupts progeny cardiac function and bioenergetics. *Am J Physiol Heart Circ Physiol* 312: H446-H458, 2017.
25. **Hathaway QA, Roth SM, Pinti MV, Sprando DC, Kunovac A, Durr AJ, Cook CC, Fink GK, Chevront TB, Grossman JH, Aljahli GA, Taylor AD, Giromini AP, Allen JL, and Hollander JM.** Machine-learning to stratify diabetic patients using novel cardiac biomarkers and integrative genomics. *Cardiovasc Diabetol* 18: 78, 2019.
26. **Hollander JM, Lin KM, Scott BT, and Dillmann WH.** Overexpression of PHGPx and HSP60/10 protects against ischemia/reoxygenation injury. *Free Radic Biol Med* 35: 742-751, 2003.
27. **Hougaard KS, Campagnolo L, Chavatte-Palmer P, Tarrade A, Rousseau-Ralliard D, Valentino S, Park MV, de Jong WH, Wolterink G, Piersma AH, Ross BL, Hutchison GR, Hansen JS, Vogel U, Jackson P, Slama R, Pietroiusti A, and Cassee FR.** A perspective on the developmental toxicity of inhaled nanoparticles. *Reprod Toxicol* 56: 118-140, 2015.
28. **Ingold I, Berndt C, Schmitt S, Doll S, Poschmann G, Buday K, Roveri A, Peng X, Porto Freitas F, Seibt T, Mehr L, Aichler M, Walch A, Lamp D, Jastroch M, Miyamoto S,**

- Wurst W, Ursini F, Arner ESJ, Fradejas-Villar N, Schweizer U, Zischka H, Friedmann Angeli JP, and Conrad M. Selenium Utilization by GPX4 Is Required to Prevent Hydroperoxide-Induced Ferroptosis. *Cell* 172: 409-422 e421, 2018.
29. Janssen BG, Madhloum N, Gyselaers W, Bijmens E, Clemente DB, Cox B, Hogervorst J, Luyten L, Martens DS, Peusens M, Plusquin M, Provost EB, Roels HA, Saenen ND, Tsamou M, Vriens A, Winckelmans E, Vrijens K, and Nawrot TS. Cohort Profile: The ENVIRONmental influence ON early AGEing (ENVIRONAGE): a birth cohort study. *Int J Epidemiol* 46: 1386-1387m, 2017.
30. Kalam K, Otahal P, and Marwick TH. Prognostic implications of global LV dysfunction: a systematic review and meta-analysis of global longitudinal strain and ejection fraction. *Heart* 100: 1673-1680, 2014.
31. Karlsen S, Dahlslett T, Grenne B, Sjoli B, Smiseth O, Edvardsen T, and Brunvand H. Global longitudinal strain is a more reproducible measure of left ventricular function than ejection fraction regardless of echocardiographic training. *Cardiovasc Ultrasound* 17: 18, 2019.
32. Kessler R. Engineered nanoparticles in consumer products: understanding a new ingredient. *Environ Health Perspect* 119: a120-125, 2011.
33. Kietzmann T, Petry A, Shvetsova A, Gerhold JM, and Gorkach A. The epigenetic landscape related to reactive oxygen species formation in the cardiovascular system. *Br J Pharmacol* 174: 1533-1554, 2017.
34. Knuckles TL, Yi J, Frazer DG, Leonard HD, Chen BT, Castranova V, and Nurkiewicz TR. Nanoparticle inhalation alters systemic arteriolar vasoreactivity through sympathetic and cyclooxygenase-mediated pathways. *Nanotoxicology* 6: 724-735, 2012.
35. Kunovac A, Hathaway QA, Pinti MV, Goldsmith WT, Durr AJ, Fink GK, Nurkiewicz TR, and Hollander JM. ROS promote epigenetic remodeling and cardiac dysfunction in offspring following maternal engineered nanomaterial (ENM) exposure. *Part Fibre Toxicol* 16: 24, 2019.
36. Kunovac A, Hathaway QA, Pinti MV, Taylor AD, and Hollander JM. Cardiovascular adaptations to particle inhalation exposure: molecular mechanisms of the toxicology. *Am J Physiol Heart Circ Physiol* 319: H282-H305, 2020.
37. Leonardi A, Evke S, Lee M, Melendez JA, and Begley TJ. Epitranscriptomic systems regulate the translation of reactive oxygen species detoxifying and disease linked selenoproteins. *Free Radic Biol Med* 143: 573-593, 2019.
38. Li Y, Wang J, Huang C, Shen M, Zhan H, and Xu K. RNA N6-methyladenosine: a promising molecular target in metabolic diseases. *Cell Biosci* 10: 19, 2020.
39. Linder B, and Jaffrey SR. Discovering and Mapping the Modified Nucleotides That Comprise the Epitranscriptome of mRNA. *Cold Spring Harb Perspect Biol* 11: 2019.
40. Liu J, Li K, Cai J, Zhang M, Zhang X, Xiong X, Meng H, Xu X, Huang Z, Peng J, Fan J, and Yi C. Landscape and Regulation of m(6)A and m(6)Am Methylome across Human and Mouse Tissues. *Mol Cell* 77: 426-440 e426, 2020.
41. Mani A. Global longitudinal strain imaging and its utility in assessing risk in early stages of hypertension. *J Clin Hypertens (Greenwich)* 21: 1711-1712, 2019.
42. Marmisolle FE, Garcia ML, and Reyes CA. RNA-binding protein immunoprecipitation as a tool to investigate plant miRNA processing interference by regulatory proteins of diverse origin. *Plant Methods* 14: 9, 2018.
43. Meyer KD. m(6)A-mediated translation regulation. *Biochim Biophys Acta Gene Regul Mech* 1862: 301-309, 2019.

44. **Min KW, Zealy RW, Davila S, Fomin M, Cummings JC, Makowsky D, McDowell CH, Thigpen H, Hafner M, Kwon SH, Georgescu C, Wren JD, and Yoon JH.** Profiling of m6A RNA modifications identified an age-associated regulation of AGO2 mRNA stability. *Aging Cell* 17: e12753, 2018.
45. **Nichols CE, Shepherd DL, Hathaway QA, Durr AJ, Thapa D, Abukabda A, Yi J, Nurkiewicz TR, and Hollander JM.** Reactive oxygen species damage drives cardiac and mitochondrial dysfunction following acute nano-titanium dioxide inhalation exposure. *Nanotoxicology* 12: 32-48, 2018.
46. **Nichols CE, Shepherd DL, Knuckles TL, Thapa D, Stricker JC, Stapleton PA, Minarchick VC, Erdely A, Zeidler-Erdely PC, Alway SE, Nurkiewicz TR, and Hollander JM.** Cardiac and mitochondrial dysfunction following acute pulmonary exposure to mountaintop removal mining particulate matter. *Am J Physiol Heart Circ Physiol* 309: H2017-2030, 2015.
47. **Nurkiewicz TR, Porter DW, Hubbs AF, Cumpston JL, Chen BT, Frazer DG, and Castranova V.** Nanoparticle inhalation augments particle-dependent systemic microvascular dysfunction. *Part Fibre Toxicol* 5: 1, 2008.
48. **Palmer JW, Tandler B, and Hoppel CL.** Biochemical properties of subsarcolemmal and interfibrillar mitochondria isolated from rat cardiac muscle. *J Biol Chem* 252: 8731-8739, 1977.
49. **Papp LV, Lu J, Striebel F, Kennedy D, Holmgren A, and Khanna KK.** The redox state of SECIS binding protein 2 controls its localization and selenocysteine incorporation function. *Mol Cell Biol* 26: 4895-4910, 2006.
50. **Park SY, Pekas EJ, Headid RJ, 3rd, Son WM, Wooden TK, Song J, Layec G, Yadav SK, Mishra PK, and Pipinos, II.** Acute mitochondrial antioxidant intake improves endothelial function, antioxidant enzyme activity, and exercise tolerance in patients with peripheral artery disease. *Am J Physiol Heart Circ Physiol* 319: H456-H467, 2020.
51. **Pelcova D, Barosova H, Kukutschova J, Zdimal V, Navratil T, Fenclova Z, Vlckova S, Schwarz J, Zikova N, Kacer P, Komarc M, Belacek J, and Zakharov S.** Raman microspectroscopy of exhaled breath condensate and urine in workers exposed to fine and nano TiO<sub>2</sub> particles: a cross-sectional study. *J Breath Res* 9: 036008, 2015.
52. **Pietroiusti A, Stockmann-Juvala H, Lucaroni F, and Savolainen K.** Nanomaterial exposure, toxicity, and impact on human health. *Wiley Interdiscip Rev Nanomed Nanobiotechnol* 2018.
53. **Ponikowski P, Voors AA, Anker SD, Bueno H, Cleland JGF, Coats AJS, Falk V, Gonzalez-Juanatey JR, Harjola VP, Jankowska EA, Jessup M, Linde C, Nihoyannopoulos P, Parissis JT, Pieske B, Riley JP, Rosano GMC, Ruilope LM, Ruschitzka F, Rutten FH, van der Meer P, and Group ESCSD.** 2016 ESC Guidelines for the diagnosis and treatment of acute and chronic heart failure: The Task Force for the diagnosis and treatment of acute and chronic heart failure of the European Society of Cardiology (ESC) Developed with the special contribution of the Heart Failure Association (HFA) of the ESC. *Eur Heart J* 37: 2129-2200, 2016.
54. **Ribeiro Junior RF, Dabkowski ER, Shekar KC, KA OC, Hecker PA, and Murphy MP.** MitoQ improves mitochondrial dysfunction in heart failure induced by pressure overload. *Free Radic Biol Med* 117: 18-29, 2018.
55. **Robichaud CO, Uyar AE, Darby MR, Zucker LG, and Wiesner MR.** Estimates of upper bounds and trends in nano-TiO<sub>2</sub> production as a basis for exposure assessment. *Environ Sci Technol* 43: 4227-4233, 2009.
56. **Ross-Innes CS, Stark R, Teschendorff AE, Holmes KA, Ali HR, Dunning MJ, Brown GD, Gojis O, Ellis IO, Green AR, Ali S, Chin SF, Palmieri C, Caldas C, and Carroll JS.**

Differential oestrogen receptor binding is associated with clinical outcome in breast cancer. *Nature* 481: 389-393, 2012.

57. **Roundtree IA, Evans ME, Pan T, and He C.** Dynamic RNA Modifications in Gene Expression Regulation. *Cell* 169: 1187-1200, 2017.

58. **Sager TM, Kommineni C, and Castranova V.** Pulmonary response to intratracheal instillation of ultrafine versus fine titanium dioxide: role of particle surface area. *Part Fibre Toxicol* 5: 17, 2008.

59. **Shepherd DL, Nichols CE, Croston TL, McLaughlin SL, Petrone AB, Lewis SE, Thapa D, Long DM, Dick GM, and Hollander JM.** Early detection of cardiac dysfunction in the type 1 diabetic heart using speckle-tracking based strain imaging. *J Mol Cell Cardiol* 90: 74-83, 2016.

60. **Shetty SP, and Copeland PR.** Selenocysteine incorporation: A trump card in the game of mRNA decay. *Biochimie* 114: 97-101, 2015.

61. **Shi H, Wang X, Lu Z, Zhao BS, Ma H, Hsu PJ, Liu C, and He C.** YTHDF3 facilitates translation and decay of N(6)-methyladenosine-modified RNA. *Cell Res* 27: 315-328, 2017.

62. **Squires JE, Stoytchev I, Forry EP, and Berry MJ.** SBP2 binding affinity is a major determinant in differential selenoprotein mRNA translation and sensitivity to nonsense-mediated decay. *Mol Cell Biol* 27: 7848-7855, 2007.

63. **Stapleton PA, Hathaway QA, Nichols CE, Abukabda AB, Pinti MV, Shepherd DL, McBride CR, Yi J, Castranova VC, Hollander JM, and Nurkiewicz TR.** Maternal engineered nanomaterial inhalation during gestation alters the fetal transcriptome. *Part Fibre Toxicol* 15: 3, 2018.

64. **Stapleton PA, Minarchick VC, Cumpston AM, McKinney W, Chen BT, Sager TM, Frazer DG, Mercer RR, Scabilloni J, Andrew ME, Castranova V, and Nurkiewicz TR.** Impairment of coronary arteriolar endothelium-dependent dilation after multi-walled carbon nanotube inhalation: a time-course study. *Int J Mol Sci* 13: 13781-13803, 2012.

65. **Starkov AA.** Measurement of mitochondrial ROS production. *Methods Mol Biol* 648: 245-255, 2010.

66. **Stebounova LV, Morgan H, Grassian VH, and Brenner S.** Health and safety implications of occupational exposure to engineered nanomaterials. *Wiley Interdiscip Rev Nanomed Nanobiotechnol* 4: 310-321, 2012.

67. **Stolwijk JM, Falls-Hubert KC, Searby CC, Wagner BA, and Buettner GR.** Simultaneous detection of the enzyme activities of GPx1 and GPx4 guide optimization of selenium in cell biological experiments. *Redox Biol* 32: 101518, 2020.

68. **Sukjammong S, Chan YL, Zakarya R, Nguyen LT, Anwer AG, Zaky AA, Santianont R, Oliver BG, Goldys E, Pollock CA, Chen H, and Saad S.** MitoQ supplementation prevent long-term impact of maternal smoking on renal development, oxidative stress and mitochondrial density in male mice offspring. *Sci Rep* 8: 6631, 2018.

69. **Sun J, Zhang Q, Wang Z, and Yan B.** Effects of nanotoxicity on female reproductivity and fetal development in animal models. *Int J Mol Sci* 14: 9319-9337, 2013.

70. **Swanson JM, Entringer S, Buss C, and Wadhwa PD.** Developmental origins of health and disease: environmental exposures. *Semin Reprod Med* 27: 391-402, 2009.

71. **Tanwar V, Gorr MW, Velten M, Eichenseer CM, Long VP, 3rd, Bonilla IM, Shettigar V, Ziolo MT, Davis JP, Baine SH, Carnes CA, and Wold LE.** In Utero Particulate Matter Exposure Produces Heart Failure, Electrical Remodeling, and Epigenetic Changes at Adulthood. *J Am Heart Assoc* 6: 2017.

72. **Vance ME, Kuiken T, Vejerano EP, McGinnis SP, Hochella MF, Jr., Rejeski D, and Hull MS.** Nanotechnology in the real world: Redeveloping the nanomaterial consumer products inventory. *Beilstein J Nanotechnol* 6: 1769-1780, 2015.
73. **Wan Y, Tang K, Zhang D, Xie S, Zhu X, Wang Z, and Lang Z.** Transcriptome-wide high-throughput deep m(6)A-seq reveals unique differential m(6)A methylation patterns between three organs in *Arabidopsis thaliana*. *Genome Biol* 16: 272, 2015.
74. **Wei CM, and Moss B.** Nucleotide sequences at the N6-methyladenosine sites of HeLa cell messenger ribonucleic acid. *Biochemistry* 16: 1672-1676, 1977.
75. **Xuan JJ, Sun WJ, Lin PH, Zhou KR, Liu S, Zheng LL, Qu LH, and Yang JH.** RMBase v2.0: deciphering the map of RNA modifications from epitranscriptome sequencing data. *Nucleic Acids Res* 46: D327-D334, 2018.
76. **Zeng Y, Wang S, Gao S, Soares F, Ahmed M, Guo H, Wang M, Hua JT, Guan J, Moran MF, Tsao MS, and He HH.** Refined RIP-seq protocol for epitranscriptome analysis with low input materials. *PLoS Biol* 16: e2006092, 2018.
77. **Zhong X, Yu J, Frazier K, Weng X, Li Y, Cham CM, Dolan K, Zhu X, Hubert N, Tao Y, Lin F, Martinez-Guryn K, Huang Y, Wang T, Liu J, He C, Chang EB, and Leone V.** Circadian Clock Regulation of Hepatic Lipid Metabolism by Modulation of m(6)A mRNA Methylation. *Cell Rep* 25: 1816-1828 e1814, 2018.



Table 3.1: M-mode echocardiography for adult progeny

Parameter	PPME	PPME	PPME	PPME	MPME	MPME	MPME	MPME
	WT Sham <sub>a</sub>	WT TiO <sub>2</sub> <sub>b</sub>	Tg Sham <sub>c</sub>	Tg TiO <sub>2</sub> <sub>d</sub>	WT Sham <sub>e</sub>	WT TiO <sub>2</sub> <sub>f</sub>	Tg Sham <sub>g</sub>	Tg TiO <sub>2</sub> <sub>h</sub>
Diameter;s (mm)	0.61 ± 0.05	<b>0.85 ± 0.08<sub>a,d</sub></b>	0.66 ± 0.07	0.51 ± 0.06	0.63 ± 0.05	0.60 ± 0.02	0.57 ± 0.02	0.72 ± 0.06
Diameter;d (mm)	2.12 ± 0.04	2.27 ± 0.08	2.15 ± 0.09	2.07 ± 0.07	<b><u>1.98 ± 0.08</u></b>	<b><u>1.98 ± 0.07</u></b>	<b><u>1.88 ± 0.06</u></b>	<b><u>2.07 ± 0.07</u></b>
Volume;s (uL)	0.58 ± 0.13	<b>1.47 ± 0.35<sub>a,c,d</sub></b>	0.73 ± 0.19	0.38 ± 0.11	0.60 ± 0.11	0.56 ± 0.02	0.46 ± 0.05	0.94 ± 0.24
Volume;d (uL)	14.78 ± 0.61	17.85 ± 1.66	15.63 ± 1.56	14.09 ± 1.25	<b><u>12.61 ± 1.31</u></b>	<b><u>12.65 ± 1.11</u></b>	<b><u>11.00 ± 0.92</u></b>	<b><u>14.21 ± 1.31</u></b>
Stroke Volume (uL)	14.19 ± 0.63	16.38 ± 1.34	14.90 ± 1.43	13.71 ± 1.16	<b><u>12.01 ± 1.21</u></b>	<b><u>12.08 ± 1.12</u></b>	<b><u>10.54 ± 0.87</u></b>	<b><u>13.27 ± 1.50</u></b>
Ejection Fraction (%)	96.02 ± 0.94	<b>92.22 ± 1.29<sub>a,d</sub></b>	95.55 ± 0.91	97.48 ± 0.59	95.34 ± 0.41	95.43 ± 0.53	95.82 ± 0.13	93.35 ± 2.30
Fractional Shortening (%)	71.25 ± 2.37	<b>62.99 ± 2.24<sub>a,d</sub></b>	69.84 ± 2.37	75.72 ± 2.37	68.64 ± 1.24	69.64 ± 1.92	69.52 ± 0.35	65.40 ± 4.27
Cardiac Output (mL/min)	10.08 ± 0.56	10.32 ± 0.77	9.67 ± 1.07	9.06 ± 0.81	<b><u>7.60 ± 1.44</u></b>	<b><u>8.00 ± 0.71</u></b>	<b><u>6.80 ± 0.78</u></b>	<b><u>9.19 ± 1.20</u></b>
Relative Wall Thickness	1.23 ± 0.06	1.20 ± 0.06	1.17 ± 0.12	1.36 ± 0.06	1.18 ± 0.06	1.27 ± 0.06	1.35 ± 0.05	1.15 ± 0.10

**Table 3.1:** M-mode echocardiography was performed in adult offspring (11 weeks of age) following maternal inhalation exposure. Bold text indicates significant data defined by  $P \leq 0.05$ . A two-way ANOVA determined statistical difference between PPME and MPME denoted with underlined values for that parameter. A letter next to a given group denotes statistical significance between the marked group and the group represented by each letter based on a Tukey's multiple-comparisons test. All data are presented as the mean  $\pm$  the standard error of the mean (SEM). PPME WT Sham, n = 7; PPME WT TiO<sub>2</sub>, n = 6; PPME Tg Sham, n = 6; PPME Tg TiO<sub>2</sub>, n = 5; MPME WT Sham, n = 4; MPME WT TiO<sub>2</sub>, n = 5; MPME Tg Sham, n = 5; MPME Tg TiO<sub>2</sub>, n = 4. PPME = Paternal mPHGPx maternal exposure, MPME = Maternal mPHGPx maternal exposure, WT Sham = wild-type offspring whose dam was exposed to control air, Tg Sham = mPHGPx transgenic offspring whose dam was exposed to control air, WT TiO<sub>2</sub> = wild-type offspring whose dam was exposed to nano-TiO<sub>2</sub>, Tg TiO<sub>2</sub> = mPHGPx transgenic offspring whose dam was exposed to nano-TiO<sub>2</sub>, s = systolic, d = diastolic.

**Table 3.2: Adult progeny systolic stress-strain in the long-axis**

Parameter	Units	PPME	PPME	PPME	PPME	MPME	MPME	MPME	MPME
		WT Sham <sub>a</sub>	WT TiO <sub>2</sub> <sub>b</sub>	Tg Sham <sub>c</sub>	Tg TiO <sub>2</sub> <sub>d</sub>	WT Sham <sub>e</sub>	WT TiO <sub>2</sub> <sub>f</sub>	Tg Sham <sub>g</sub>	Tg TiO <sub>2</sub> <sub>h</sub>
<b>Radial Velocity</b>	Pk cm/s	2.01 ± 0.17	1.89 ± 0.12	1.82 ± 0.10	<b>2.52 ± 0.16<sub>c</sub></b>	2.03 ± 0.21	2.46 ± 0.23	2.23 ± 0.15	2.08 ± 0.26
<b>Radial Displacement</b>	Pk mm	0.47 ± 0.03	0.43 ± 0.03	0.44 ± 0.04	<b>0.61 ± 0.02<sub>a,b,c</sub></b>	0.40 ± 0.00	0.55 ± 0.04	0.47 ± 0.05	0.52 ± 0.03
<b>Radial Strain</b>	Pk %	27.82 ± 1.84	25.95 ± 2.85	25.54 ± 3.37	31.55 ± 2.74	26.48 ± 2.58	32.90 ± 2.72	30.69 ± 3.08	23.67 ± 1.49
<b>Radial Strain Rate</b>	Pk 1/s	9.10 ± 0.83	8.20 ± 0.67	8.62 ± 1.13	11.12 ± 1.16	<u><b>11.34 ± 1.55</b></u>	<u><b>11.80 ± 1.02</b></u>	<u><b>11.31 ± 0.34</b></u>	<u><b>8.50 ± 0.97</b></u>
<b>Longitudinal Velocity</b>	Pk deg/s	1.14 ± 0.16	1.19 ± 0.18	1.00 ± 0.18	1.07 ± 0.20	1.16 ± 0.36	1.09 ± 0.28	1.28 ± 0.60	0.95 ± 0.15
<b>Longitudinal Displacement</b>	Pk deg	0.18 ± 0.01	0.12 ± 0.04	0.15 ± 0.06	0.11 ± 0.02	<u><b>0.04 ± 0.01</b></u>	<u><b>0.06 ± 0.01</b></u>	<u><b>0.06 ± 0.01</b></u>	<u><b>0.12 ± 0.04</b></u>
<b>Longitudinal Strain</b>	Pk %	-10.99 ± 2.13	-9.51 ± 2.00	-9.16 ± 0.90	-15.81 ± 3.41	-5.38 ± 2.61	-7.98 ± 1.52	-12.99 ± 2.78	-10.68 ± 4.73
<b>Longitudinal Strain Rate</b>	Pk 1/s	-7.63 ± 0.58	-6.86 ± 0.76	-7.06 ± 1.01	-9.34 ± 0.76	<u><b>-7.45 ± 0.85</b></u>	<u><b>-8.93 ± 1.35</b></u>	<u><b>-14.26 ± 1.35<sub>e,f,h</sub></b></u>	<u><b>-7.49 ± 1.18</b></u>
<b>Global Longitudinal Strain (GLS)</b>	AU	24.26 ± 1.54	<b>16.49 ± 1.97<sub>a,d</sub></b>	19.85 ± 2.20	<b>28.51 ± 1.88<sub>c</sub></b>	20.07 ± 2.25	23.58 ± 3.52	22.67 ± 1.86	22.29 ± 2.44

**Table 3.2:** Peak strain and strain-rate values acquired from B-mode images for longitudinal and radial dimensions in adult progeny (11 weeks of age) following maternal inhalation exposure. Bold text indicates significant data defined by  $P \leq 0.05$ . A two-way ANOVA determined statistical difference between PPME and MPME denoted with underlined values for that parameter. A letter next to a given group denotes statistical significance between the marked group and the group represented by each letter based on a Tukey's multiple-comparisons test. All data are presented as the mean  $\pm$  the standard error of the mean (SEM). PPME WT Sham, n = 7; PPME WT TiO<sub>2</sub>, n = 6; PPME Tg Sham, n = 6; PPME Tg TiO<sub>2</sub>, n = 5; MPME WT Sham, n = 4; MPME WT TiO<sub>2</sub>, n = 5; MPME Tg Sham, n = 5; MPME Tg TiO<sub>2</sub>, n = 4. PPME = Paternal mPHGPx maternal exposure, MPME = Maternal mPHGPx maternal exposure, WT Sham = wild-type offspring whose dam was exposed to control air, Tg Sham = mPHGPx transgenic offspring whose dam was exposed to control air, WT TiO<sub>2</sub> = wild-type offspring whose dam was exposed to nano-TiO<sub>2</sub>, Tg TiO<sub>2</sub> = mPHGPx transgenic offspring whose dam was exposed to nano-TiO<sub>2</sub>, GLS = global longitudinal strain, Pk = peak.

Figure 3.1:

A

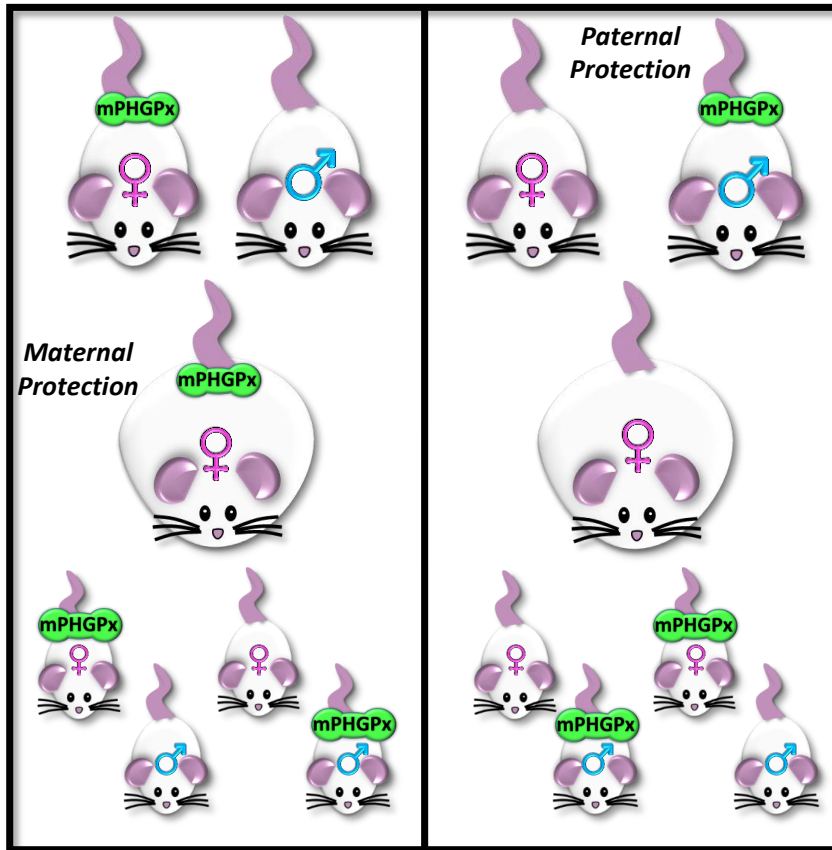
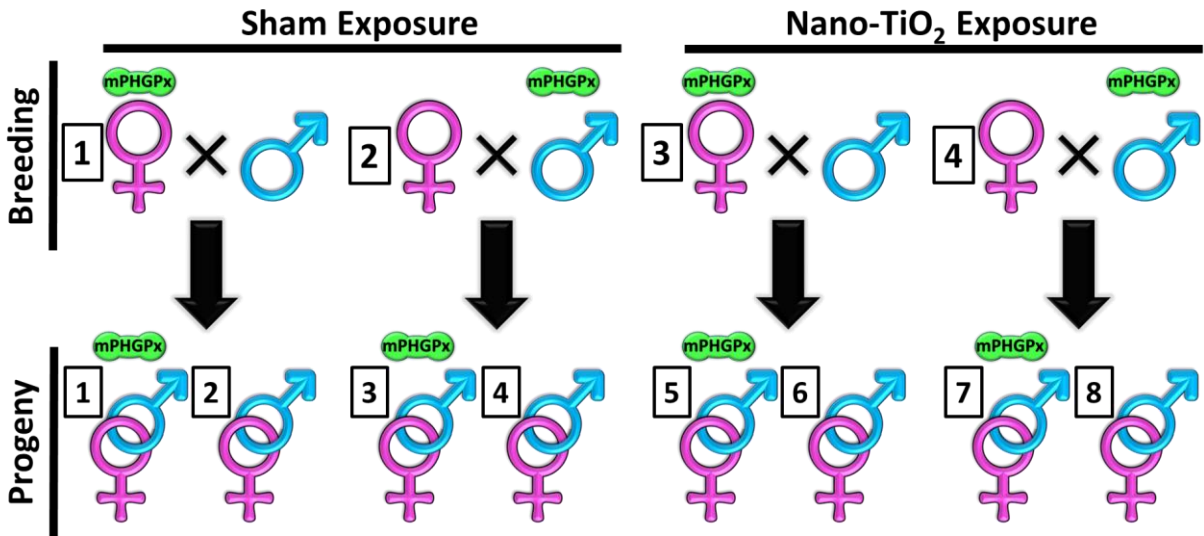
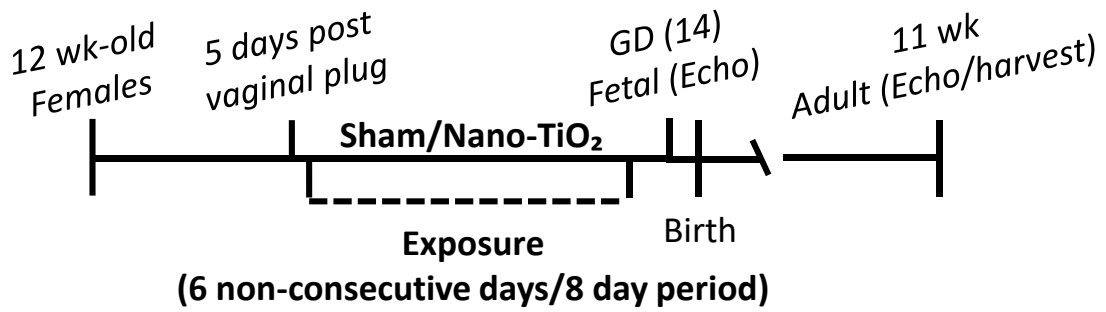


Figure 3.1:

B

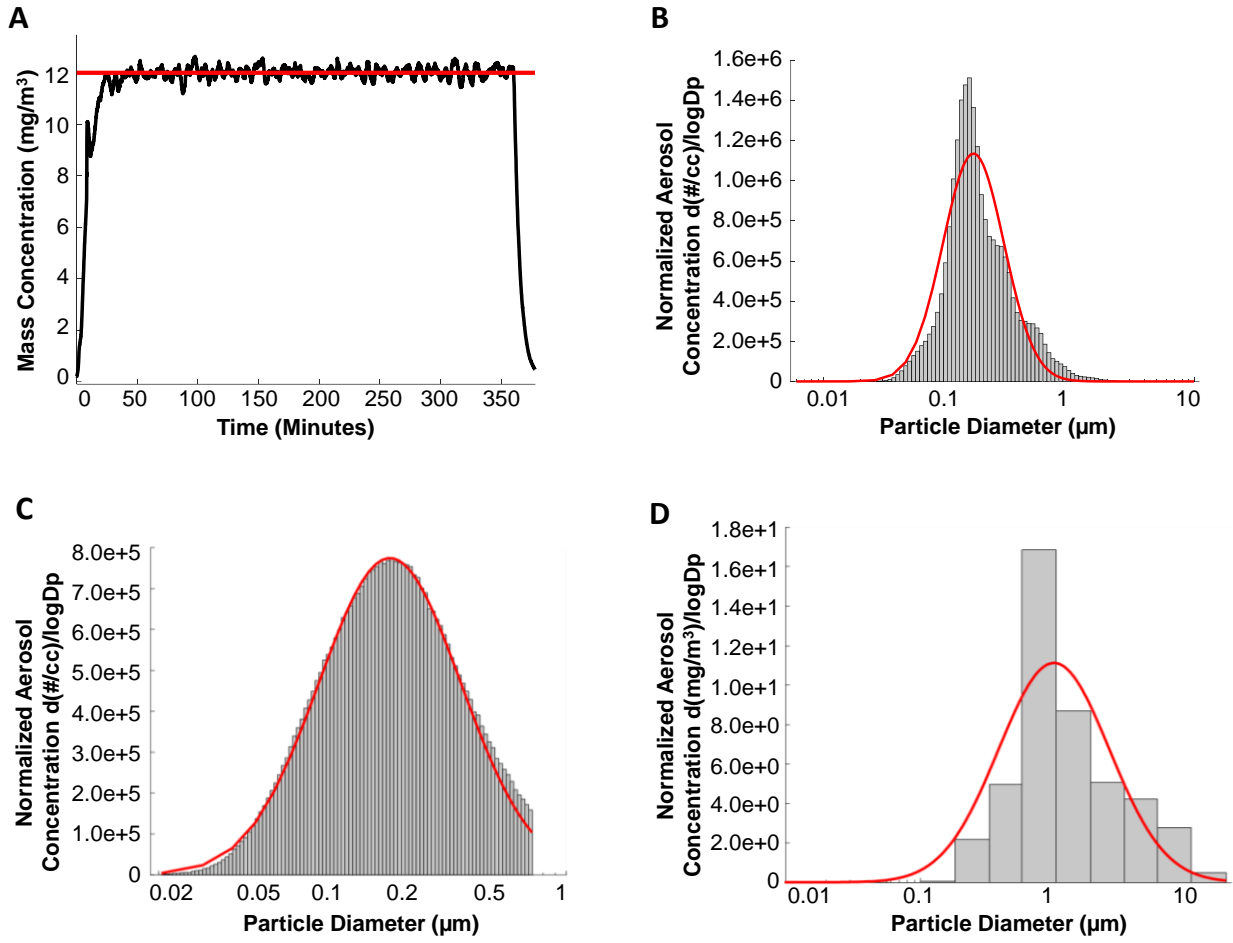


C



**Figure 3.1: MPHGPx mouse breeding strategy.** (A) Schematic of mPHGPx breeding strategies with transgene effect on offspring from maternal (left) or paternal (right) transgene. (B) Schematic of exposure paradigm that was implemented for each group, representing all groups that were utilized in the study. (C) A timeline of the study. MPHGPx = mitochondrial phospholipid hydroperoxide glutathione peroxidase.

Figure 3.2:





**Figure 3.2: Maternal nano-TiO<sub>2</sub> inhalation exposure characteristics.** (A) Real-time (black line) aerosol mass concentration measurements with the red line indicating the target concentration (12 mg/m<sup>3</sup>) of a typical 360 min maternal nano-TiO<sub>2</sub> inhalation exposure. (B) Count size distribution of the nano-TiO<sub>2</sub> aerosols measured with a high resolution electric low-pressure impactor (ELPI+). The red line designates the log normal distribution obtained with the log probability plot method (CMD = 0.163 μm, with a GSD = 1.77). (C) Count size distribution of nano-TiO<sub>2</sub> aerosols measured with a scanning mobility particle sizer (SMPS) with the red line representing a log normal fit of the data (CMD = 0.190 μm, GSD = 1.97). (D) Mass size distribution of nano-TiO<sub>2</sub> aerosols measured with a Nano Micro-Orifice Uniform Deposit Impactor (MOUDI). The red line represents a log normal fit of the data indicating a mass median aerodynamic diameter (MMAD) of 0.968 μm and a GSD of 2.56. CMD = Count Median Diameter, GSD = Geometric Standard Deviation.

Figure 3.3

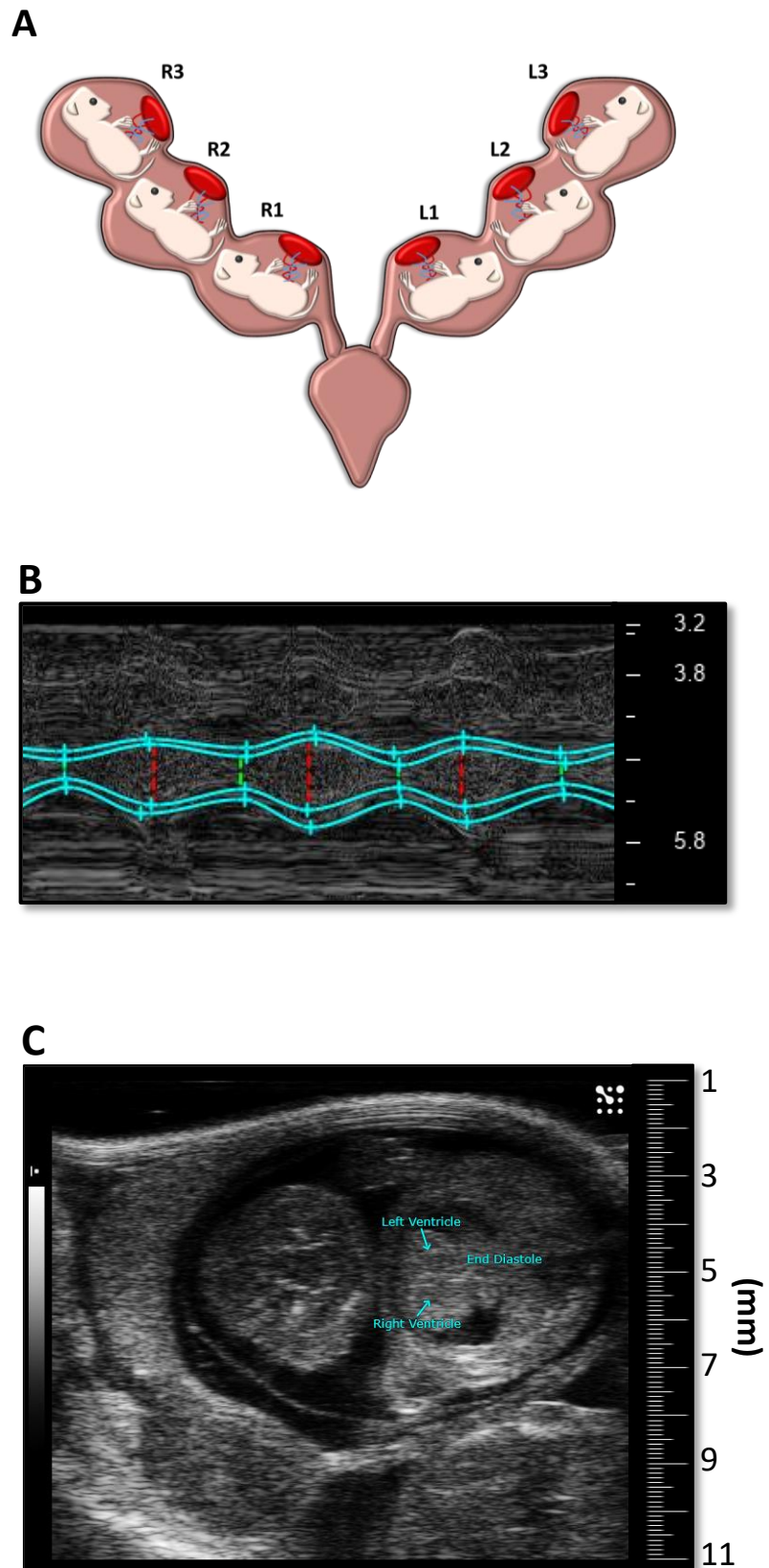
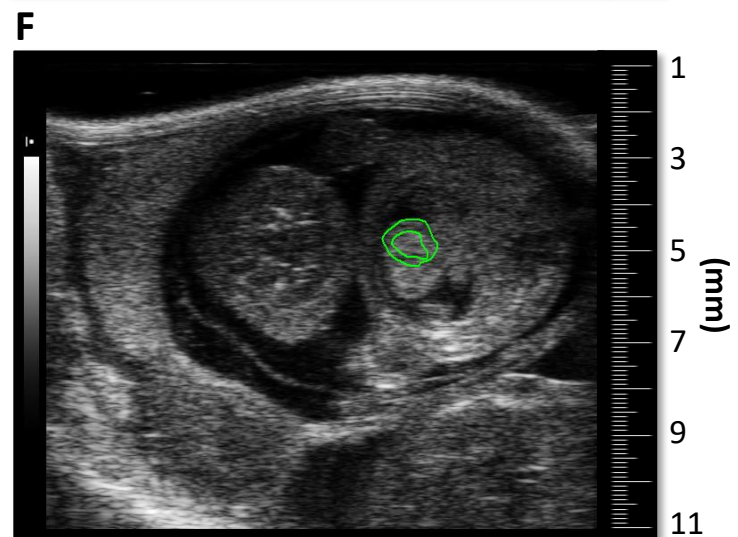
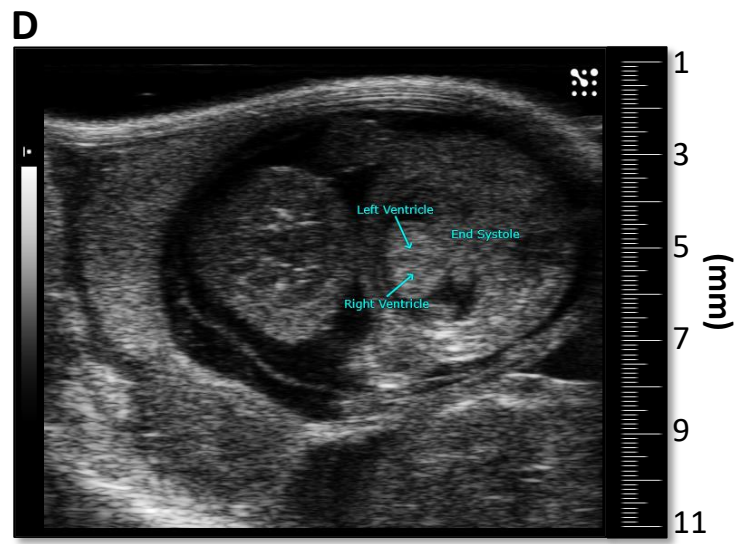


Figure 3.3:



**Figure 3.3: Assessment of fetal pup cardiac function *in utero*.** (A) Graphical depiction of the uterine horn and the pup identification system. (B) Representative M-mode echocardiographic scan of a fetal pup with the short-axis left ventricular trace (blue). (C-D) Representative B-mode scan of a fetal pup with the left and right ventricles identified by blue arrows at end diastole (C) and end systole (D). (E-F) Representative B-mode scan in the short-axis of a fetal pup at with green outlines indicating tracking of the epicardium and endocardium borders through (E) end diastole and (F) end systole. R = right, L = left.

Figure 3.4

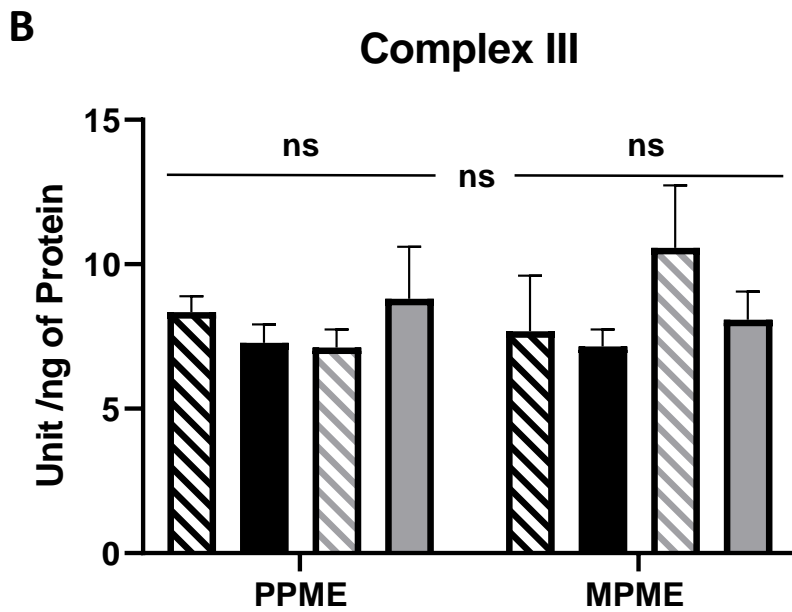
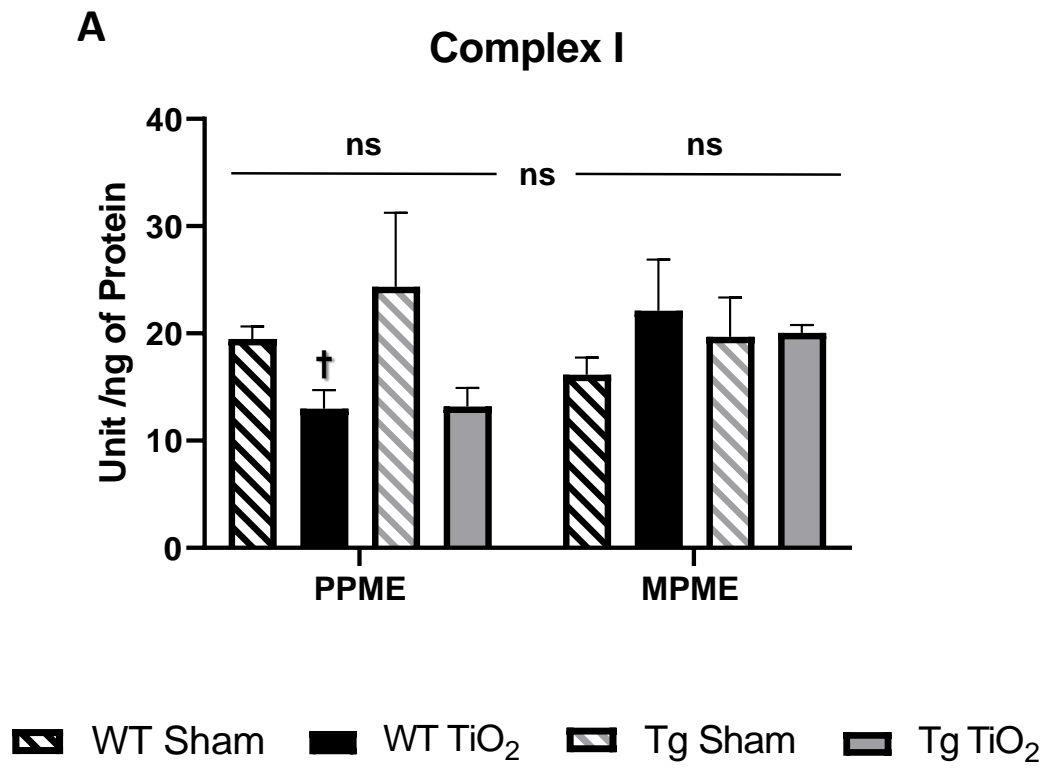
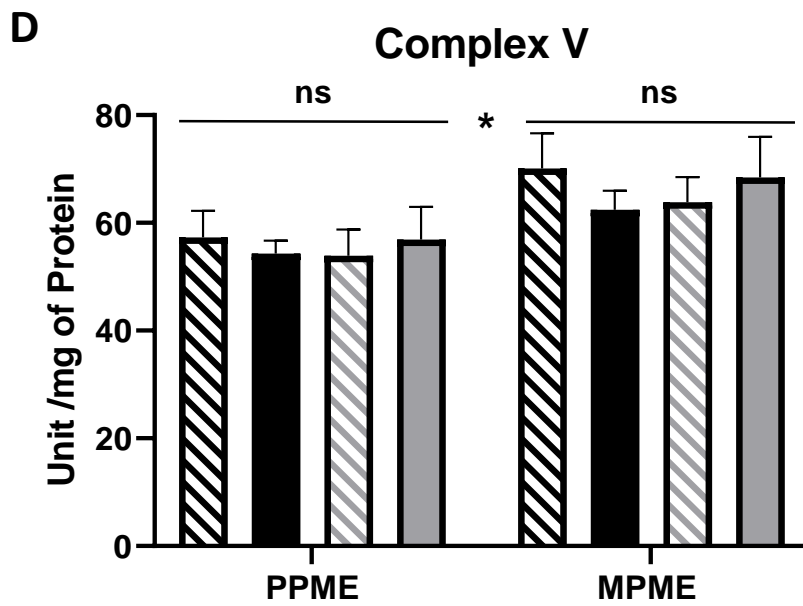
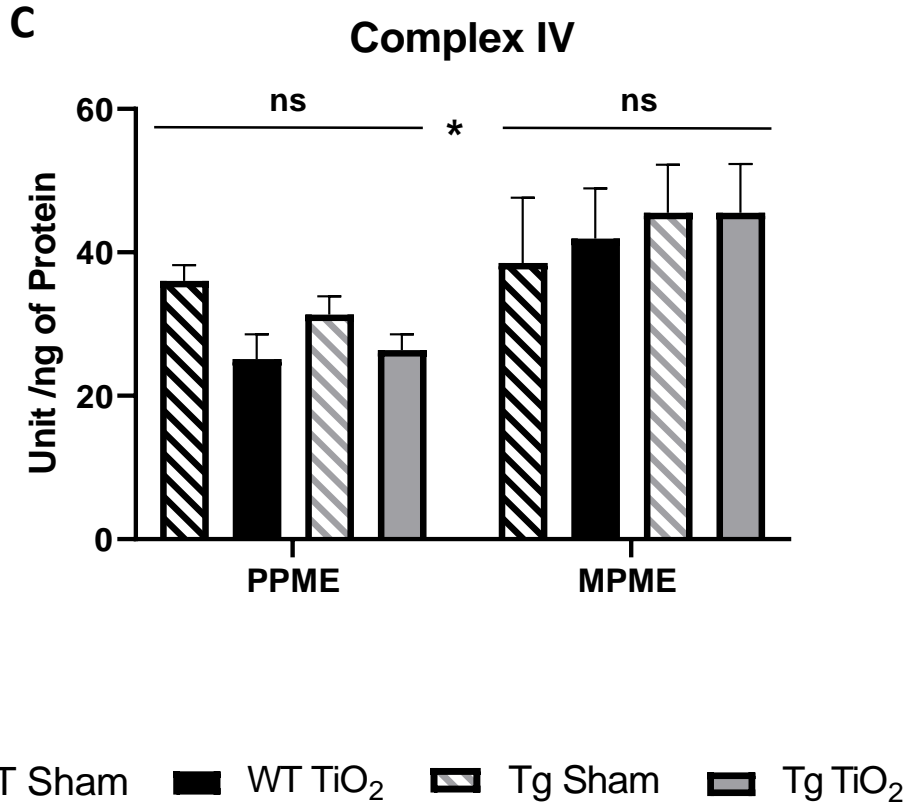


Figure 3.4



**Figure 3.4: Electron transport chain (ETC) complex activities of adult PPME and MPME offspring. (A-D)** Electron transport chain (ETC) activities assessed in cardiac protein lysate of adult offspring for (A) complex I, (B) complex III, (C) complex IV, and (D) complex V (ATP Synthase). PPME WT Sham, n = 7; PPME WT TiO<sub>2</sub>, n = 6; PPME Tg Sham, n = 6; PPME Tg TiO<sub>2</sub>, n = 5; MPME WT Sham, n = 4; MPME WT TiO<sub>2</sub>, n = 5; MPME Tg Sham, n = 7; MPME Tg TiO<sub>2</sub>, n = 4. Adult = 11 weeks old. Statistical difference was defined by  $P \leq 0.05$ . \* = group difference determined by a two-way ANOVA and ns = no statistical difference. A letter above a group denotes statistical significance between those groups based on a Tukey's multiple-comparisons test. A dagger (†) above a group indicates statistical significance between WT Sham and WT TiO<sub>2</sub> or Tg Sham and Tg TiO<sub>2</sub> of the same maternal genetic group (MPME or PPME) based on a Student's t-test. All data are presented as the mean  $\pm$  the standard error of the mean (SEM). Adult = 11 weeks of age, mPHGPx = mitochondrial phospholipid hydroperoxide glutathione peroxidase, PPME = Paternal mPHGPx maternal exposure, MPME = Maternal mPHGPx maternal exposure, WT Sham = wild-type offspring whose dam was exposed to control air, Tg Sham = mPHGPx transgenic offspring whose dam was exposed to control air, WT TiO<sub>2</sub> = wild-type offspring whose dam was exposed to nano-TiO<sub>2</sub>, Tg TiO<sub>2</sub> = mPHGPx transgenic offspring whose dam was exposed to nano-TiO<sub>2</sub>, Unit = nanomoles of substrate oxidized  $\cdot$  minute<sup>-1</sup>.

1.

Figure 3.5

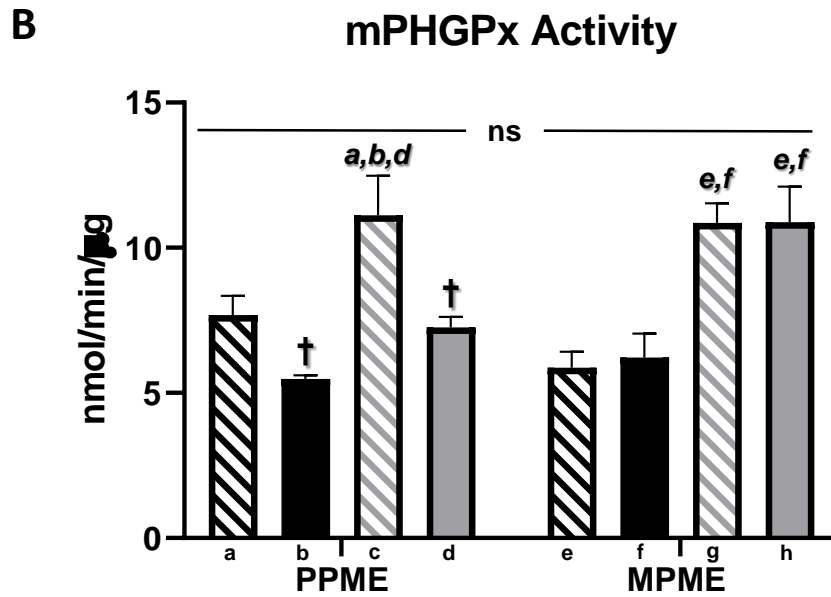
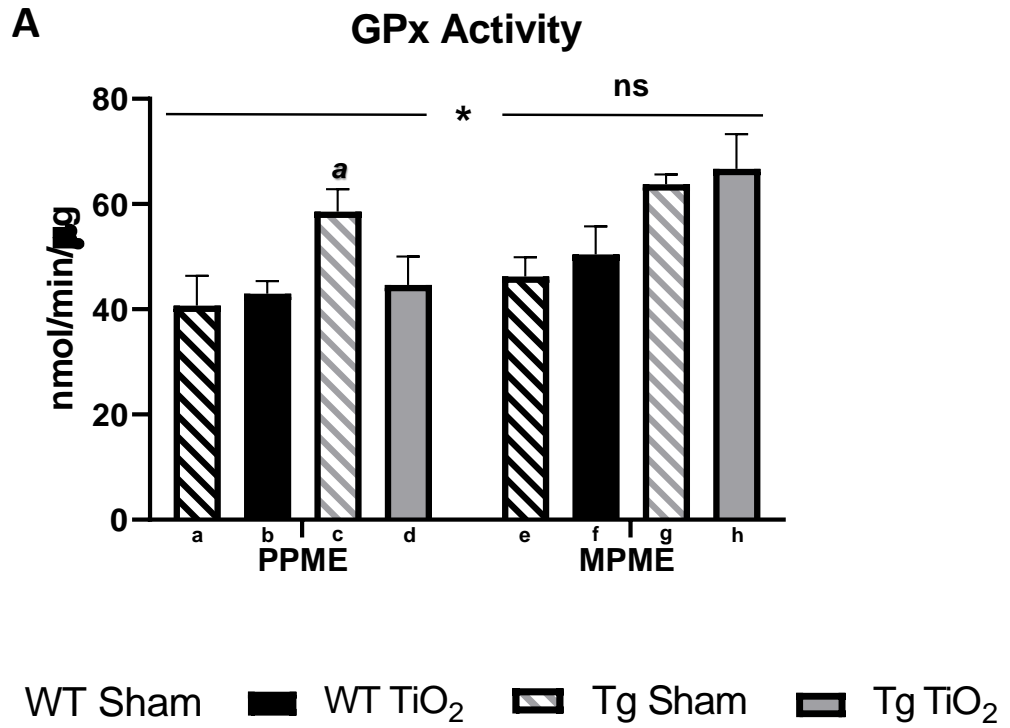
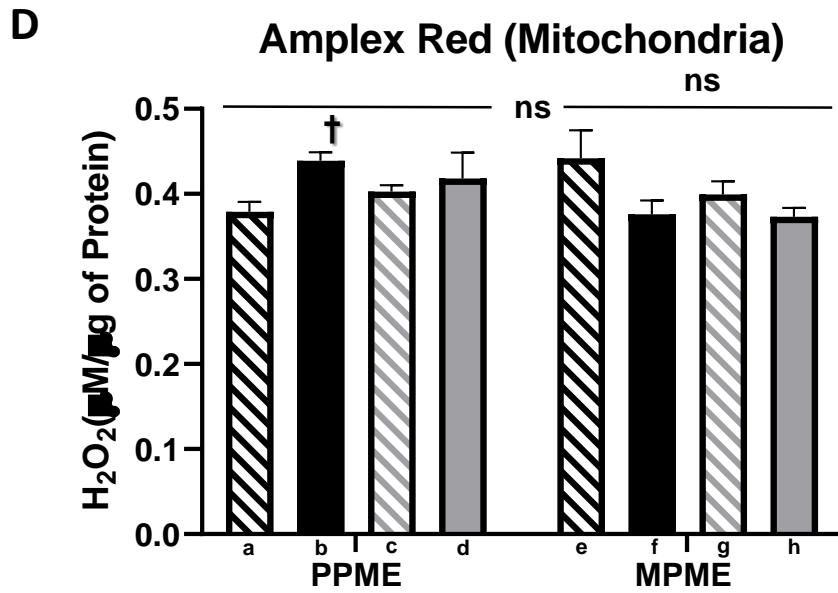
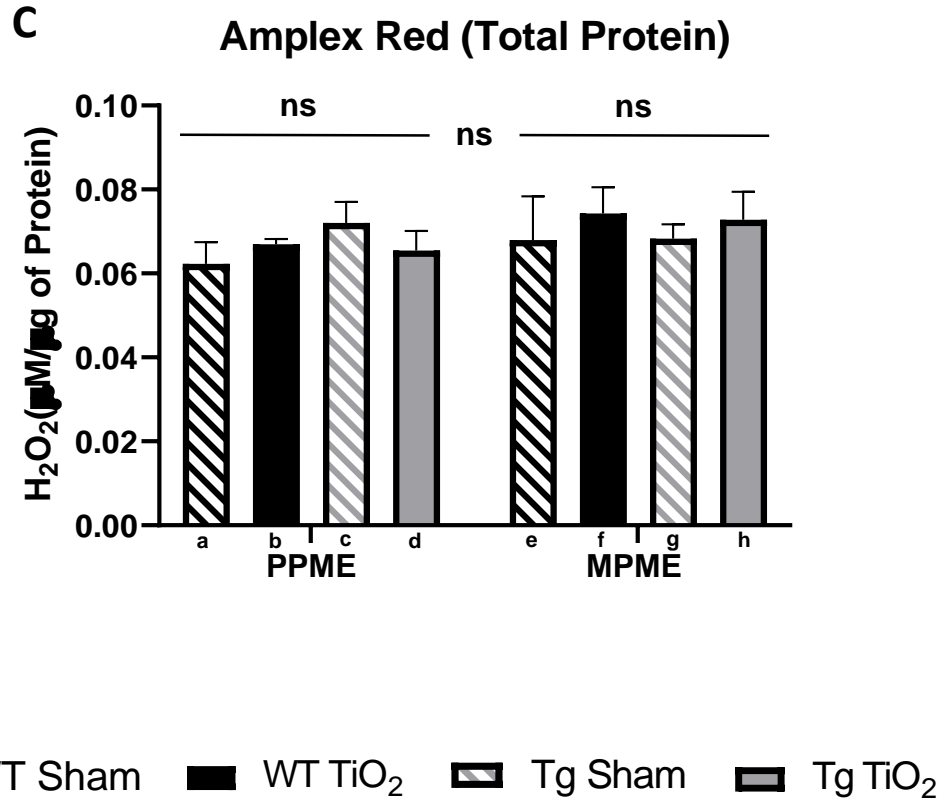




Figure 3.5:



**Figure 3.5: Antioxidant activity and H<sub>2</sub>O<sub>2</sub> production in adult offspring following gestational inhalation exposure.** (A) Total GPx activity in cardiac protein lysate determined by cumene hydroperoxide as substrate and normalized to protein content. (B) Mitochondrial GPx (mPHGPx) activity in cardiac protein lysate determined by phosphatidylcholine hydroperoxide (PCOOH) as substrate and normalized to protein content. (C) Total hydrogen peroxide (H<sub>2</sub>O<sub>2</sub>) concentration in cardiac protein lysate normalized to protein content. (D) Hydrogen peroxide (H<sub>2</sub>O<sub>2</sub>) concentration in cardiac isolated mitochondria of adult offspring normalized to protein content. PPME WT Sham, n = 7 (protein) and n = 6 (mitochondria); PPME WT TiO<sub>2</sub>, n = 6; PPME Tg Sham, n = 6 (protein) and n = 5 (mitochondria); PPME Tg TiO<sub>2</sub>, n = 5; MPME WT Sham, n = 4; MPME WT TiO<sub>2</sub>, n = 5; MPME Tg Sham, n = 7; MPME Tg TiO<sub>2</sub>, n = 4. Statistical difference was defined by  $P \leq 0.05$ . \* = group difference determined by a two-way ANOVA and ns = no statistical difference. A letter above a group denotes statistical significance between those groups based on a Tukey's multiple-comparisons test. A dagger (†) above a group indicates statistical significance between WT Sham and WT TiO<sub>2</sub> or Tg Sham and Tg TiO<sub>2</sub> of the same maternal genetic group (MPME or PPME) based on a Student's t-test. All data are presented as the mean  $\pm$  the standard error of the mean (SEM). Adult = 11 weeks of age, mPHGPx = Mitochondrial phospholipid hydroperoxide glutathione peroxidase, PPME = Paternal mPHGPx maternal exposure, MPME = Maternal mPHGPx maternal exposure, WT Sham = wild-type offspring whose dam was exposed to control air, Tg Sham = mPHGPx transgenic offspring whose dam was exposed to control air, WT TiO<sub>2</sub> = wild-type offspring whose dam was exposed to nano-TiO<sub>2</sub>, Tg TiO<sub>2</sub> = mPHGPx transgenic offspring whose dam was exposed to nano-TiO<sub>2</sub>.

Figure 3.6:

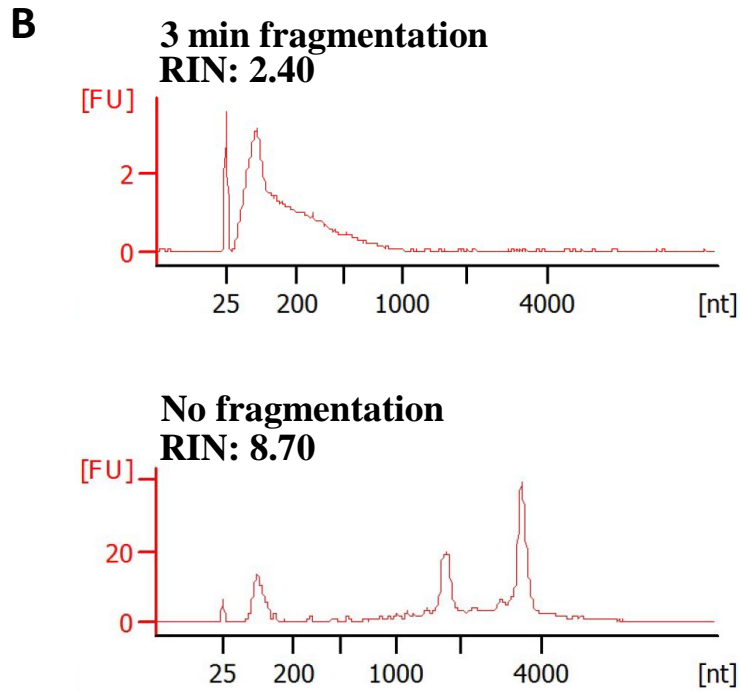
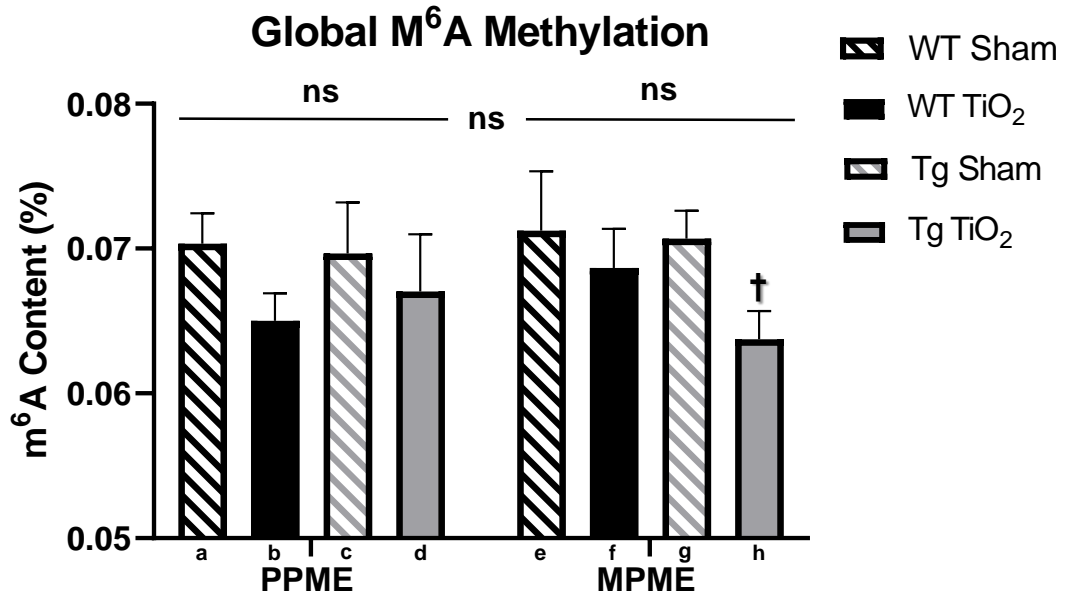
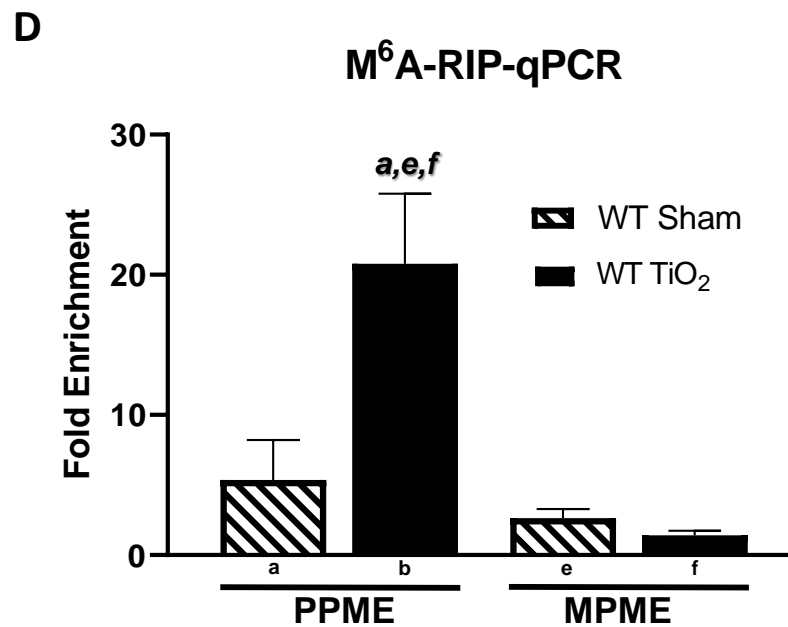
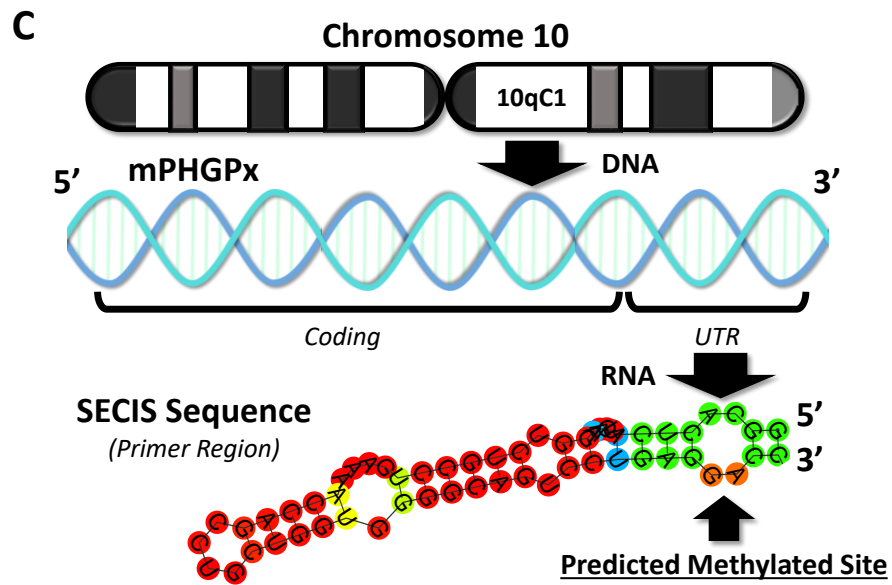
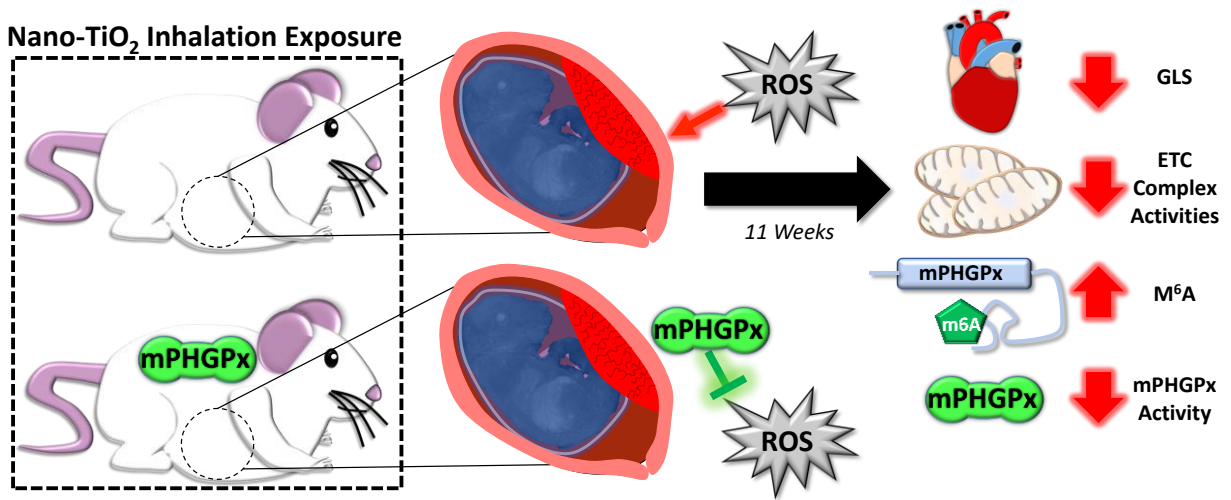


Figure 3.6:



**Figure 3.6: Epitranscriptomic mechanism contributing to diminished antioxidant scavenging ability following maternal nano-TiO<sub>2</sub> inhalation exposure.** (A) Global m<sup>6</sup>A content was determined as a percentage (%) of total RNA isolated from adult offspring cardiac tissue. PPME WT Sham, n = 6; PPME WT TiO<sub>2</sub>, n = 5; PPME Tg Sham, n = 6; PPME Tg TiO<sub>2</sub>, n = 5; MPME WT Sham, n = 4; MPME WT TiO<sub>2</sub>, n = 5; MPME Tg Sham, n = 6; MPME Tg TiO<sub>2</sub>, n = 4. (B) Isolated RNA with 3 min fragmentation utilized to achieve ~130 nt fragments (top) compared to no fragmentation (bottom). (C) Schematic of the predicted m<sup>6</sup>A site in the 3'-UTR of the mouse mPHGPx mRNA, specifically within the SECIS region. (D) M<sup>6</sup>A-RIP-qPCR for mPHGPx (3'-UTR region including potential m<sup>6</sup>A site). N= 4 per group (ran in triplicate). Statistical difference was defined by  $P \leq 0.05$  (ns = no significance) based on a one or two-way ANOVA, where appropriate. A letter above a group denotes statistical significance between those groups based on a Tukey's multiple-comparisons test. A dagger (†) above a group indicates statistical significance between WT Sham and WT TiO<sub>2</sub> or Tg Sham and Tg TiO<sub>2</sub> of the same maternal genetic group (MPME or PPME) based on a Student's t-test. All data are presented as the mean  $\pm$  the standard error of the mean (SEM). Adult = 11 weeks old, mPHGPx = mitochondrial phospholipid hydroperoxide glutathione peroxidase, M<sup>6</sup>A = N<sup>6</sup>-Methyladenosine, PPME = Paternal mPHGPx maternal exposure, MPME = Maternal mPHGPx maternal exposure, WT Sham = wild-type offspring whose dam was exposed to control air, Tg Sham = mPHGPx transgenic offspring whose dam was exposed to control air, WT TiO<sub>2</sub> = wild-type offspring whose dam was exposed to nano-TiO<sub>2</sub>, Tg TiO<sub>2</sub> = mPHGPx transgenic offspring whose dam was exposed to nano-TiO<sub>2</sub>, RIN = RNA integrity number, SECIS = selenocysteine insertion sequence.

Figure 3.7:



**Figure 3.7: Physiological and molecular consequences of gestational nano-TiO<sub>2</sub> inhalation exposure in adult offspring.** Following gestational exposure, elevated ROS levels in the progeny are concomitant with cardiac functional alterations that can be mitigated by overexpression of maternal mPHGPx. Augmented mitochondrial ROS plays a key role in the persistence of deficits into adulthood (11 weeks of age) characterized by diminished GLS and ETC complex activities. A mechanism that could promote the sustained consequences is initiated by high oxidative stress, which increases m<sup>6</sup>A methylation at the SECIS in the 3'-UTR of mPHGPx. Ultimately, this may tamper with the SECIS binding region for the SBP2 that is vital for the incorporation of selenocysteine and the catalytic activity of mPHGPx. Decreased mPHGPx activity then propagates mitochondrial bioenergetic deficits, limiting overall cardiac performance in the adult offspring. MPHGPx = mitochondrial phospholipid hydroperoxide glutathione peroxidase, ROS = reactive oxygen species, GLS = global longitudinal strain, ETC = electron transport chain, m<sup>6</sup>A = N<sup>6</sup>-methyladenosine, SECIS = Selenocysteine insertion sequence, SBP2 = SECIS binding protein 2.

**Supplemental Table 3.1: Primer sequences**

<b>Gene Name</b>	<b>Forward (5' – 3')</b>	<b>Reverse (5' – 3')</b>
GPx4	CCUACAAGUGUGUGCCCUA	AGGCCUCUGGACCUUCCUC
GAPDH	AACTTTGGCATTGTGGAAGG	ACACATTGGGGGTAGGAACA



**Supplemental Table 3.1:** Primers were designed for m<sup>6</sup>A-RIP-qPCR using Primer-BLAST through NCBI and Primer3. Sequence information was obtained from the University of Santa Cruz (UCSC) genome browser from the mouse GRCm38/mm10 assembly.

**Supplemental Table 3.2: Adult and fetal progeny heart rates following maternal inhalation exposure**

<b>Heart Rate (BPM)</b>	<b>PPME WT Sham<sub>a</sub></b>	<b>PPME WT TiO<sub>2</sub><sub>b</sub></b>	<b>PPME Tg Sham<sub>c</sub></b>	<b>PPME Tg TiO<sub>2</sub><sub>d</sub></b>	<b>MPME WT Sham<sub>e</sub></b>	<b>MPME WT TiO<sub>2</sub><sub>f</sub></b>	<b>MPME Tg Sham<sub>g</sub></b>	<b>MPME Tg TiO<sub>2</sub><sub>h</sub></b>
<b>Fetal</b>	85.67 ± 5.98	127.92 ± 5.85	107.07 ± 17.75	155.22 ± 6.87	<b><u>140.26 ± 13.73</u></b>	<b><u>163.17 ± 41.65</u></b>	<b><u>145.040 ± 12.40</u></b>	<b><u>160.60 ± 26.36</u></b>
<b>Adult</b>	716.68 ± 13.74	666.99 ± 14.29	666.37 ± 17.91	661.19 ± 21.95	676.38 ± 50.98	676.14 ± 8.66	641.98 ± 39.60	691.58 ± 18.90

**Supplemental Table 3.2:** Heart rates were obtained for adult (11 weeks) and fetal (GD 14) offspring during echocardiographic assessment. Bold and underlined values indicate a statistically significant difference between fetal PPME and MPME offspring heart rates as determined by a two-way ANOVA and defined by  $P \leq 0.05$ . All data are presented as the mean  $\pm$  the standard error of the mean (SEM). Adult offspring: PPME WT Sham, n = 7; PPME WT TiO<sub>2</sub>, n = 6; PPME Tg Sham, n = 6; PPME Tg TiO<sub>2</sub>, n = 5; MPME WT Sham, n = 4; MPME WT TiO<sub>2</sub>, n = 5; MPME Tg Sham, n = 5; MPME Tg TiO<sub>2</sub>, n = 4. Fetal offspring: PPME WT Sham, n = 3; PPME WT TiO<sub>2</sub>, n = 7; PPME Tg Sham, n = 3; PPME Tg TiO<sub>2</sub>, n = 7; MPME WT Sham, n = 7; MPME WT TiO<sub>2</sub>, n = 4; MPME Tg Sham, n = 6; MPME Tg TiO<sub>2</sub>, n = 6. PPME = Paternal mPHGPx maternal exposure, MPME = Maternal mPHGPx maternal exposure, WT Sham = wild-type offspring whose dam was exposed to control air, Tg Sham = mPHGPx transgenic offspring whose dam was exposed to control air, WT TiO<sub>2</sub> = wild-type offspring whose dam was exposed to nano-TiO<sub>2</sub>, Tg TiO<sub>2</sub> = mPHGPx transgenic offspring whose dam was exposed to nano-TiO<sub>2</sub>, GD = gestational day.

**Supplemental Table 3.3: M-mode echocardiography for pregnant dams**

Parameter	WT Sham <sub>a</sub>	WT TiO <sub>2</sub> <sub>b</sub>	Tg Sham <sub>c</sub>	Tg TiO <sub>2</sub> <sub>d</sub>
<b>Diameter;s (mm)</b>	0.89 ± 0.05	0.82 ± 0.07	0.70 ± 0.04	0.80 ± 0.09
<b>Diameter;d (mm)</b>	2.62 ± 0.08	<b>2.30 ± 0.08<sub>a</sub></b>	2.51 ± 0.02	2.46 ± 0.06
<b>Volume;s (uL)</b>	1.58 ± 0.20	1.41 ± 0.30	0.86 ± 0.16	1.41 ± 0.30
<b>Volume;d (uL)</b>	25.60 ± 1.93	<b>18.70 ± 1.57<sub>a</sub></b>	22.8 ± 0.54	21.70 ± 1.32
<b>Stroke Volume (uL)</b>	23.30 ± 1.60	<b>17.30 ± 1.36<sub>a</sub></b>	21.9 ± 0.41	20.40 ± 1.21
<b>Ejection Fraction (%)</b>	93.00 ± 0.76	92.90 ± 1.15	96.3 ± 0.61	93.60 ± 1.25
<b>Fractional Shortening (%)</b>	64.60 ± 1.58	64.90 ± 2.18	72.40 ± 1.53	67.50 ± 3.55
<b>Cardiac Output (mL/min)</b>	15.50 ± 1.04	<b>11.40 ± 0.98<sub>a</sub></b>	14.00 ± 0.37	13.50 ± 0.72
<b>Relative Wall Thickness</b>	0.81 ± 0.03	<b>1.12 ± 0.09<sub>a</sub></b>	0.930 ± 0.03	0.97 ± 0.06

**Supplemental Table 3.3:** M-mode echocardiography was performed in pregnant dams (GD 14) following gestational inhalation exposure to control air or ENM aerosols. Bold text indicates a statistically significant difference between the highlighted group and the group referenced by the letter next to it, as determined by a one-way ANOVA with a Tukey's multiple comparisons test and defined by  $P \leq 0.05$ . WT Sham, n = 11; WT TiO<sub>2</sub>, n = 12; Tg Sham, n = 11; Tg TiO<sub>2</sub>, n = 10. WT = wild-type, Tg = mPHGPx transgenic, s = systolic, d = diastolic, GD = gestational day.

**Supplemental Table 3.4: Maternal heart rates following gestational inhalation exposure**

<b>Heart Rate (BPM)</b>	<b>WT Sham<sub>a</sub></b>	<b>WT TiO<sub>2</sub><sub>b</sub></b>	<b>Tg Sham<sub>c</sub></b>	<b>Tg TiO<sub>2</sub><sub>d</sub></b>
<b>Maternal</b>	667.90 ± 10.50	655.56 ± 13.40	638.44 ± 17.20	667.39 ± 17.80

**Supplemental Table 3.4:** Heart rates were obtained for pregnant dams (GD 14) during echocardiographic assessment, following gestational inhalation exposure. WT Sham, n = 11; WT TiO<sub>2</sub>, n = 12; Tg Sham, n = 11; Tg TiO<sub>2</sub>, n = 10. WT = wild-type, Tg = mPHGPx transgenic. GD = gestational day.

Supplemental Table 3.5: M-mode echocardiography for fetal progeny

Parameter	PPME WT Sham <sub>a</sub>	PPME WT TiO <sub>2</sub> <sub>b</sub>	PPME Tg Sham <sub>c</sub>	PPME Tg TiO <sub>2</sub> <sub>d</sub>	MPME WT Sham <sub>e</sub>	MPME WT TiO <sub>2</sub> <sub>f</sub>	MPME Tg Sham <sub>g</sub>	MPME Tg TiO <sub>2</sub> <sub>h</sub>
Diameter;s (mm)	0.31 ± 0.02	0.27 ± 0.02	0.33 ± 0.07	0.34 ± 0.03	0.29 ± 0.02	0.43 ± 0.08	0.30 ± 0.01	0.35 ± 0.03
Diameter;d (mm)	0.76 ± 0.04	0.70 ± 0.05	0.78 ± 0.07	0.78 ± 0.04	<b><u>0.80 ±</u></b> <b><u>0.05</u></b>	<b><u>0.87 ±</u></b> <b><u>0.08</u></b>	<b><u>0.82 ±</u></b> <b><u>0.06</u></b>	<b><u>0.92 ±</u></b> <b><u>0.04</u></b>
Volume;s (uL)	0.08 ± 0.01	0.06 ± 0.01	0.11 ± 0.06	0.12 ± 0.03	0.07 ± 0.02	<b>0.22 ±</b> <b>0.08<sub>e</sub></b>	0.08 ± 0.01	0.13 ± 0.03
Volume;d (uL)	0.98 ± 0.12	0.83 ± 0.15	1.09 ± 0.26	1.10 ± 0.19	<b><u>1.18 ±</u></b> <b><u>0.22</u></b>	<b><u>1.48 ±</u></b> <b><u>0.32</u></b>	<b><u>1.30 ±</u></b> <b><u>0.23</u></b>	<b><u>1.72 ±</u></b> <b><u>0.24</u></b>
Stroke Volume (uL)	0.89 ± 0.11	0.77 ± 0.14	0.98 ± 0.20	0.98 ± 0.16	<b><u>1.11 ±</u></b> <b><u>0.20</u></b>	<b><u>1.26 ±</u></b> <b><u>0.24</u></b>	<b><u>1.22 ±</u></b> <b><u>0.22</u></b>	<b><u>1.60 ±</u></b> <b><u>0.21</u></b>
Ejection Fraction (%)	91.45± 0.32	92.68 ± 1.22	90.97 ± 3.02	89.85 ± 1.41	94.07 ± 0.70	<b>86.66 ±</b> <b>3.67<sub>e,g,h</sub></b>	93.56 ± 0.44	93.13 ± 1.12
Fractional Shortening (%)	58.86 ± .58	61.36 ± 2.20	58.46 ± 5.58	56.70 ± 2.35	63.60 ± 1.34	<b>52.30 ±</b> <b>5.30<sub>e</sub></b>	63.09 ± 1.56	62.040 ± 2.21
Cardiac Output (mL/min)	0.05 ± 0.00	0.05 ± 0.01	0.06 ± 0.01	0.06 ± 0.01	<b><u>0.09 ±</u></b> <b><u>0.02</u></b>	<b><u>0.11 ±</u></b> <b><u>0.02</u></b>	<b><u>0.09 ±</u></b> <b><u>0.02</u></b>	<b><u>0.10 ±</u></b> <b><u>0.01</u></b>
Relative Wall Thickness	0.59 ± 0.11	0.46 ± 0.07	0.35 ± 0.01	0.57 ± 0.09	0.42 ± 0.08	0.40 ± 0.06	0.40 ± 0.08	0.48 ± 0.03



**Supplemental Table 3.5:** M-mode echocardiography was performed in fetal offspring (GD 14) following maternal inhalation exposure. Bold text indicates significant data defined by  $P \leq 0.05$ . A two-way ANOVA determined statistical difference between PPME and MPME denoted with underlined values for that parameter. A letter next to a given group denotes statistical significance between the marked group and the group represented by each letter based on a Tukey's multiple-comparisons test. All data are presented as the mean  $\pm$  the standard error of the mean (SEM). PPME WT Sham, n = 3; PPME WT TiO<sub>2</sub>, n = 7; PPME Tg Sham, n = 3; PPME Tg TiO<sub>2</sub>, n = 7; MPME WT Sham, n = 7; MPME WT TiO<sub>2</sub>, n = 4; MPME Tg Sham, n = 6; MPME Tg TiO<sub>2</sub>, n = 6. PPME = Paternal mPHGPx maternal exposure, MPME = Maternal mPHGPx maternal exposure, WT Sham = wild-type offspring whose dam was exposed to control air, Tg Sham = mPHGPx transgenic offspring whose dam was exposed to control air, WT TiO<sub>2</sub> = wild-type offspring whose dam was exposed to nano-TiO<sub>2</sub>, Tg TiO<sub>2</sub> = mPHGPx transgenic offspring whose dam was exposed to nano-TiO<sub>2</sub>, s = systolic, d = diastolic.

**Supplemental Table 3.6: Adult progeny systolic stress-strain in the short-axis**

Parameter	Units	PPME WT Sham <sub>a</sub>	PPME WT TiO <sub>2</sub> <sub>b</sub>	PPME Tg Sham <sub>c</sub>	PPME Tg TiO <sub>2</sub> <sub>d</sub>	MPM E WT Sham <sub>e</sub>	MPM E WT TiO <sub>2</sub> <sub>f</sub>	MPM E Tg Sham <sub>g</sub>	MPM E Tg TiO <sub>2</sub> <sub>h</sub>
<b>Radial Velocity</b>	Pk cm/s	2.69 ±	2.82 ±	2.58 ±	2.74 ±	2.35 ±	2.34 ±	2.60 ±	2.62 ±
		0.22	0.33	0.14	0.12	0.21	0.27	0.30	0.30
<b>Radial Displacement</b>	Pk mm	0.61 ±	0.65 ±	0.57 ±	0.67 ±	<b><u>0.47 ±</u></b>	<b><u>0.47 ±</u></b>	<b><u>0.50 ±</u></b>	<b><u>0.57 ±</u></b>
		0.04	0.06	0.06	0.05	<b><u>0.07</u></b>	<b><u>0.03</u></b>	<b><u>0.08</u></b>	<b><u>0.03</u></b>
<b>Radial Strain</b>	Pk %	43.42	45.16	38.74	45.45	<b><u>37.72</u></b>	<b><u>30.35</u></b>	<b><u>32.33</u></b>	<b><u>35.54</u></b>
		± 3.68	± 3.27	± 4.65	± 2.66	<b><u>± 2.52</u></b>	<b><u>± 3.13</u></b>	<b><u>± 5.05</u></b>	<b><u>± 5.31</u></b>
<b>Radial Strain Rate</b>	Pk 1/s	15.24 ± 1.08	17.48 ± 1.10	14.21 ± 0.79	15.08 ± 0.70	15.48 ± 0.54	12.35 ± 1.86	14.01 ± 0.90	14.21 ± 2.58
<b>Circumferentia l Velocity</b>	Pk deg/s	736.92	506.27	596.50	611.58	867.56	724.07	583.47	612.95
		± 150.19	± 32.36	± 121.12	± 41.31	± 154.99	± 132.03	± 86.97	± 43.03
<b>Circumferentia l Displacement</b>	Pk deg	7.37 ±	7.24 ±	7.08 ±	7.05 ±	9.43 ±	8.37 ±	4.88 ±	6.30 ±
		1.67	2.92	2.87	1.89	4.52	2.07	1.12	1.56
<b>Circumferentia l Strain</b>	Pk %	-46.81	-55.29	-43.68	-52.79	<b><u>-38.49</u></b>	<b><u>-42.26</u></b>	<b><u>-35.29</u></b>	<b><u>-42.69</u></b>
		± 3.53	± 2.82	± 1.50	± 2.88	<b><u>± 8.83</u></b>	<b><u>± 6.94</u></b>	<b><u>± 4.32</u></b>	<b><u>± 6.94</u></b>
<b>Circumferentia l Strain Rate</b>	Pk 1/s	-42.28 ± 3.95	-52.41 ± 7.85	-37.53 ± 5.26	-49.63 ± 8.50	-38.61 ± 1.97	-42.40 ± 9.65	-45.37 ± 6.64	-51.42 ± 3.43

**Supplemental Table 3.6:** Peak strain and strain-rate values acquired from B-mode images for circumferential and radial dimensions in adult progeny (11 weeks of age) following maternal inhalation exposure. Bold and underlined values indicate a statistically significant difference between fetal PPME and MPME offspring values for that parameter as determined by a two-way ANOVA and defined by  $P \leq 0.05$ . All data are presented as the mean  $\pm$  the standard error of the mean (SEM). PPME WT Sham, n = 7; PPME WT TiO<sub>2</sub>, n = 6; PPME Tg Sham, n = 6; PPME Tg TiO<sub>2</sub>, n = 5; MPME WT Sham, n = 4; MPME WT TiO<sub>2</sub>, n = 5; MPME Tg Sham, n = 5; MPME Tg TiO<sub>2</sub>, n = 4. PPME = Paternal mPHGPx maternal exposure, MPME = Maternal mPHGPx maternal exposure, WT Sham = wild-type offspring whose dam was exposed to control air, Tg Sham = mPHGPx transgenic offspring whose dam was exposed to control air, WT TiO<sub>2</sub> = wild-type offspring whose dam was exposed to nano-TiO<sub>2</sub>, Tg TiO<sub>2</sub> = mPHGPx transgenic offspring whose dam was exposed to nano-TiO<sub>2</sub>, Pk = peak.

**Supplemental Table 3.7: Fetal progeny systolic stress-strain in the short-axis**

Parameter	Units	PPME WT Sham <sub>a</sub>	PPME WT TiO <sub>2</sub> <sub>b</sub>	PPME Tg Sham <sub>c</sub>	PPME Tg TiO <sub>2</sub> <sub>d</sub>	MPM E WT Sham <sub>e</sub>	MPM E WT TiO <sub>2</sub> <sub>f</sub>	MPM E Tg Sham <sub>g</sub>	MPM E Tg TiO <sub>2</sub> <sub>h</sub>
Radial Velocity	Pk cm/s	0.23 ± 0.02	<b>0.12 ±</b> <b>0.02</b> <sub>a,c</sub>	0.22 ± 0.05	<b>0.12 ±</b> <b>0.02</b> <sub>a,c</sub>	0.19 ± 0.02	0.16 ± 0.02	0.16 ± 0.02	0.17 ± 0.01
Radial Displacement	Pk mm	0.13 ± 0.01	<b>0.06 ±</b> <b>0.01</b> <sub>a,c</sub>	0.12 ± 0.04	<b>0.05 ±</b> <b>0.01</b> <sub>a,c</sub>	<b>0.06 ±</b> <b>0.01</b>	<b>0.05 ±</b> <b>0.01</b>	<b>0.04 ±</b> <b>0.01</b>	<b>0.04 ±</b> <b>0.01</b>
Radial Strain	Pk %	18.95 ± 3.65	9.92 ± 2.22	19.96 ± 6.92	8.72 ± 1.33	21.03 ± 5.08	16.21 ± 2.49	14.07 ± 3.10	22.38 ± 6.19
Radial Strain Rate	Pk 1/s	13.16 ± 3.10	<b>3.75 ±</b> <b>0.65</b> <sub>a</sub>	7.58 ± 3.13	<b>3.37 ±</b> <b>0.34</b> <sub>a</sub>	<b>9.30 ±</b> <b>0.67</b>	<b>11.75</b> <b>± 3.45</b>	<b>11.07</b> <b>± 1.61</b>	<b>10.55</b> <b>± 3.12</b>
Circumferentia l Velocity	Pk deg/s	389.31 ± 62.28	213.06 ± 29.75	425.89 ± 170.71	298.10 ± 67.32	<b>466.39</b> <b>±</b> <b>42.24</b>	<b>442.01</b> <b>±</b> <b>79.04</b>	<b>401.68</b> <b>±</b> <b>65.57</b>	<b>507.34</b> <b>±</b> <b>56.69</b>
Circumferentia l Displacement	Pk deg	13.47 ± 1.97	<b>5.36 ±</b> <b>1.35</b> <sub>a</sub>	11.74 ± 2.11	7.91 ± 0.84	<b>15.34</b> <b>± 1.83</b>	<b>11.66</b> <b>± 1.00</b>	<b>13.86</b> <b>± 0.91</b>	<b>11.38</b> <b>± 1.72</b>
Circumferentia l Strain	Pk %	-36.36 ± 3.16	<b>-21.07</b> <b>±</b> <b>3.09</b> <sub>a,c</sub>	-37.92 ± 6.78	<b>-20.79</b> <b>±</b> <b>0.88</b> <sub>a,c</sub>	-29.53 ± 2.68	-26.04 ± 3.70	-23.51 ± 0.81	-24.53 ± 4.69
Circumferentia l Strain Rate	Pk 1/s	-16.47 ± 1.82	-10.23 ± 2.81	-13.68 ± 3.19	-9.50 ± 1.77	<b>-18.25</b> <b>± 1.71</b>	<b>-17.42</b> <b>± 1.08</b>	<b>-14.70</b> <b>± 1.54</b>	<b>-18.48</b> <b>± 2.85</b>

**Supplemental Table 3.7:** Peak strain and strain-rate values acquired from B-mode images for circumferential and radial dimensions in fetal progeny (GD 14) following maternal inhalation exposure. Bold text indicates significant data defined by  $P \leq 0.05$ . A two-way ANOVA determined statistical difference between PPME and MPME denoted with underlined values for that parameter. A letter next to a given group denotes statistical significance between the marked group and the group represented by each letter based on a Tukey's multiple-comparisons test. All data are presented as the mean  $\pm$  the standard error of the mean (SEM). PPME WT Sham, n = 3; PPME WT TiO<sub>2</sub>, n = 7; PPME Tg Sham, n = 3; PPME Tg TiO<sub>2</sub>, n = 7; MPME WT Sham, n = 7; MPME WT TiO<sub>2</sub>, n = 4; MPME Tg Sham, n = 6; MPME Tg TiO<sub>2</sub>, n = 6. PPME = Paternal mPHGPx maternal exposure, MPME = Maternal mPHGPx maternal exposure, WT Sham = wild-type offspring whose dam was exposed to control air, Tg Sham = mPHGPx transgenic offspring whose dam was exposed to control air, WT TiO<sub>2</sub> = wild-type offspring whose dam was exposed to nano-TiO<sub>2</sub>, Tg TiO<sub>2</sub> = mPHGPx transgenic offspring whose dam was exposed to nano-TiO<sub>2</sub>, GD = gestational day, Pk = peak.

# Chapter 4: Specific Aim 3

## Increased N<sup>6</sup>-Methyladenosine in Fetal Offspring following Gestational Nano-TiO<sub>2</sub> Inhalation Exposure Decreases Mitochondrial Transcript and Protein Expression

Amina Kunovac, PhD<sup>1,2,3</sup>, Quincy A. Hathaway, PhD<sup>4</sup>, Dharendra Thapa, PhD<sup>1,2</sup>, Andrya J. Durr, BS<sup>1,2</sup>, Andrew D. Taylor, BS<sup>1,2</sup>, Saira Rizwan, BS<sup>1,2</sup>, Daud Sharif, BS<sup>5</sup>, Stephen J. Valentine, PhD<sup>5</sup>, Timothy R. Nurkiewicz, PhD<sup>3,6</sup>, and John M. Hollander, PhD<sup>1,2,3</sup>

<sup>1</sup>Division of Exercise Physiology, West Virginia University School of Medicine, Morgantown, WV, USA. <sup>2</sup>Mitochondria, Metabolism & Bioenergetics Working Group, West Virginia University School of Medicine, Morgantown, WV, USA. <sup>3</sup>Center for Inhalation Toxicology (iTOX), West Virginia University School of Medicine, Morgantown, WV, USA. <sup>4</sup>Heart and Vascular Institute, West Virginia University School of Medicine, Morgantown, WV, USA. <sup>5</sup>Department of Chemistry, West Virginia University, Morgantown, WV, USA. <sup>6</sup>Department of Physiology & Pharmacology, Morgantown, WV, USA.

### Corresponding Author:

John M. Hollander, Ph.D., F.A.H.A.

Division of Exercise Physiology

West Virginia University School of Medicine

1 Medical Center Drive, PO Box 9227

Morgantown, WV 26506

Tel: 1-(304) 293-3683; Fax: 1-(304) 293-7105

Email: [jhollander@hsc.wvu.edu](mailto:jhollander@hsc.wvu.edu)

**Word Count:** 8873

## Abstract

**Background:** N<sup>6</sup>-methyladenosine (m<sup>6</sup>A) is the most prominent epitranscriptomic modification in eukaryotes, but its implications on adaptive changes within the gestational environment are poorly understood. We propose that cardiac m<sup>6</sup>A methylation in fetal offspring exposed gestationally to nano-TiO<sub>2</sub> alters mitochondrial bioenergetics through changes in mRNA and protein stability.

**Methods:** 10-week-old female FVB/NJ wild type mice (n=14) were purchased. Mice were mated and on gestational day (GD) 5 underwent 6 non-consecutive days of whole-body inhalation exposure. Mice were exposed to filtered room air or nano-TiO<sub>2</sub> with a target aerosol mass concentration of 12 mg/m<sup>3</sup>. At GD 15 mice were sacrificed and cardiac RNA and mitochondrial proteins extracted. Immunoprecipitation with m<sup>6</sup>A antibodies was performed followed by sequencing of immunoprecipitant (m<sup>6</sup>A) and input (mRNA) on the Illumina NextSeq 2000. Protein extraction, preparation, and LC-MS/MS was used for mitochondrial protein quantification.

**Results:** There were no differences in maternal or fetal pup weights, number of pups, or pup heart weight between exposure groups. Transcriptomic sequencing revealed 3,648 differentially expressed genes in nano-TiO<sub>2</sub> exposed mice (*P*<sub>adj</sub>≤0.05). Genes involved in mitochondrial bioenergetics were significantly downregulated (83 or 85 genes). 921 genes revealed significant m<sup>6</sup>A methylation sites (*P*<sub>adj</sub>≤0.10). 311 genes were identified to have significantly altered gene expression (mRNA) as well as differentially methylated sites. Pathway analysis of these genes revealed that mRNA degradation and ubiquitin-mediated proteolysis were common pathways. Mitochondrial proteomics showed decreased ATP Synthase expression in the exposed group.

**Conclusions:** M<sup>6</sup>A methylation likely affects the longevity of transcripts and translated proteins in fetal progeny following nano-TiO<sub>2</sub> exposure, ultimately affecting mitochondrial function.

**Keywords:** Epitranscriptomics; Bioenergetics; Heart, 3' UTR; m<sup>6</sup>A; Bioinformatics

## Introduction

Epigenetic reprogramming is one of the main mechanisms responsible for adverse effects on long-term health outcomes following environmental exposure to toxicants (1, 43). While studies of transient DNA and histone modifications have provided significant insight into the field of toxicology, the advent of chemical modifications at the level of mRNA has introduced a new layer of complexity. The study of mRNA chemical modifications, otherwise known as epitranscriptomics, provides a new perspective for understanding how alterations in the stability of mRNA transcripts can impact the maternal environment, shaping the health of the offspring. N<sup>6</sup>-methyladenosine (m<sup>6</sup>A) is the most abundant mRNA modification in eukaryotes (52) and has the capacity to alter the translational capacity of transcripts. There is currently very little understanding if/how m<sup>6</sup>A modifications impact fetal development following gestational particulate or ENM exposure.

The epigenetic modifications that were implicated in the long-term effects of environmental exposure thus far have centered primarily around oxidative stress, DNA methylation, and histone post-translational modifications (37, 39). However post-transcriptional modifications and their role in regulating RNA function have recently gained traction. Methylation of bases can alter RNA structure, folding, stability, degradation, localization, and thereby its interactions with other RNAs or proteins (21, 52). Recently, N<sup>6</sup>-methyladenosine (m<sup>6</sup>A) has been suggested to play a prominent role in epitranscriptomic reprogramming following particle inhalation exposure (7, 8, 23). M<sup>6</sup>A, which is the most prevalent internal, post-transcriptional RNA modification, occurs in ~30% of transcripts, and plays a pivotal role in numerous physiological systems (51). In addition to being highly abundant in mammalian mRNA, it is also vastly conserved across eukaryotic species including, yeast, plants, and mammals (10, 13).

To understand the effects of m<sup>6</sup>A in disease, one must first understand the regulators involved in writing, erasing, and reading these prevalent modifications. The writers are responsible for the co-transcriptional addition of a methyl group at the N6 position of the adenosine in the consensus sequence DRACH (D=A/G/U; R=A/G, H=A/C/U) (21, 22, 52). Methyltransferase-like protein 3 (METTL3) is the main player in the writer complex which also includes adaptor proteins. The two predominant demethylases in mammals that are responsible for removing the m<sup>6</sup>A marks are fat mass and obesity-associated protein (FTO) and  $\alpha$ -ketoglutarate-dependent dioxygenase



homolog 5 (ALKBH5) (52). However, m<sup>6</sup>A is not the primary target for FTO as has been recently discovered, rather the primary target of FTO is N<sup>6</sup>,2'-O-dimethyladenosine (m<sup>6</sup>A<sub>m</sub>) (28). Lastly, the m<sup>6</sup>A reader proteins include YTH domain (YT521-B homology) containing proteins, YTHDC1 and YTHDF1/2/3, which appear to each play their own individual role in mRNA processing based on the presence or absence of m<sup>6</sup>A marks. When YTHDC1 binds to the m<sup>6</sup>A mark (mainly in the nucleus), it can affect splicing and/or mRNA export, whereas YTHDF1 promotes mRNA translation (22). On the other hand, the reader protein YTHDF2 favors mRNA decay. YTHDF3 works with both YTHDF1 and YTHDF2 to enhance each respective activity (40). Dysregulation of m<sup>6</sup>A can thereby alter gene expression that can lead to changes in cellular function and the onset of cancer, psychiatric disorders, metabolic diseases, and cardiovascular disease (51, 52).

The overall landscape of m<sup>6</sup>A remains to be elucidated in offspring hearts following maternal ENM inhalation exposure during gestation. In this study we implement transcriptome-wide mapping of m<sup>6</sup>A by combining RNA immunoprecipitation and RNA sequencing (m<sup>6</sup>A-RIP-seq) to elucidate the role of m<sup>6</sup>A methylation on diminished cardiac and mitochondrial function in fetal offspring following gestational exposure to nano-TiO<sub>2</sub> (23, 24). MRNA and m<sup>6</sup>A analyses revealed genes with overlapping pathways, such as regulation of RNA degradation and ubiquitin-mediated proteolysis. Both transcriptomic and mitochondrial proteomic data highlighted how significant decreases in mitochondrial genes were found following exposure. Our data emphasize how gestational exposure to ENMs can alter m<sup>6</sup>A methylation and indirectly regulate critical cellular processes, such as mitochondrial bioenergetics.

## Materials and Methods

### *Animal Model*

Friend Virus B NIH Jackson (FVB/NJ) wild type mice (14 females, 7 males at 10 weeks) were purchased from Jackson Laboratory (Bar Harbor, ME). Animals were housed in the West Virginia University Health Sciences Center Animal Facility with access to a standard chow diet and water *ad libitum*. All animals were allowed a 48-hour acclimation period before being handled. Females were housed in groups of 4 per cage and introduced to male bedding three days prior to being introduced to the males for breeding. This was implemented to take advantage of the Whitten effect, which states that females are most receptive to mating on the third night after exposure to male pheromones that are found in urine (47). This allows us to synchronize the females' estrous cycles prior to mating and therefore increases the number of females becoming pregnant at similar time points and leading to well age-matched cohorts.

A harem breeding strategy was utilized with two females and one male per cage set up on the third night following exposure to male bedding. Females were checked for vaginal plugs in the early morning after they were set-up with the males. Pregnancy was verified with identification of a vaginal plug at which point females were randomly separated into sham (7 pregnant dams) and nano-TiO<sub>2</sub> (7 pregnant dams) groups. On approximately gestational day (GD) 5, maternal inhalation exposure was initiated for each respective exposure group (sham or nano-TiO<sub>2</sub>) that occurred for 6 hours/day, for 6 days over an 8-day period. Pregnant dams (7 Sham, 7 nano-TiO<sub>2</sub>) were euthanized on GD 15 and the pups were removed from the uteri. The dams, pups, and pup hearts were weighed and weights recorded (**Table 4.1**). The hearts of fetal offspring were pooled per each litter which was considered n=1. The hearts of offspring of 3 sham and 3 nano-TiO<sub>2</sub>-exposed dams were saved in RNAprotect Tissue Reagent (Item no. 76105; Qiagen, Hilden, Germany) in cryotubes, flash frozen, and stored in -80°C for future analysis. The hearts of offspring of the other 4 sham and 4 nano-TiO<sub>2</sub>-exposed dams were immediately processed for mitochondrial isolation as described below. The West Virginia University Animal Care and Use Committee approved all animal studies which conform to the most current National Institutes of Health (NIH) Guidelines for the Care and Use of Laboratory Animals (8<sup>th</sup> edition) manual.

### *Engineered Nanomaterial (ENM) Inhalation Exposure*

Our laboratory has previously detailed the engineered nanomaterial (ENM) inhalation exposure paradigm implemented in this study (14, 23, 24). Nano-TiO<sub>2</sub> P25 powder was purchased from Evonik (Aeroxide TiO<sub>2</sub>, Parsipanny, NJ) which was composed of anatase (80%) and rutile (20%) TiO<sub>2</sub>. Prior to aerosolization, the nano-TiO<sub>2</sub> powder was prepared by drying, sieving, and storing (14, 18, 23, 24, 31). Previous studies from our laboratory and colleagues have outlined the primary particle characteristics including the size (21 nm), Zeta potential (−56.6 mV), and the specific surface area (48.08 m<sup>2</sup>/g) (30, 31, 38).

A high-pressure acoustical generator (HPAG; IES techno, Morgantown, WV) was utilized for nano-TiO<sub>2</sub> aerosolization as has been previously done for rodent inhalation exposure studies (14, 23, 24). **Figure 4.1** outlines the details of nano-TiO<sub>2</sub> aerosol characterization. Using a whole-body exposure chamber, a target aerosol mass concentration of 12 mg/m<sup>3</sup> of engineered nano-TiO<sub>2</sub> was implemented for a period of 360 minutes per day for 6 non-consecutive days, over an 8-day period (23). The relevance of this concentration lies in its ability to recapitulate the lung burden of a person who works in a manufacturing setting, based on the human equivalent alveolar doses during pregnancy and has been previously detailed by our laboratory (23). Alveolar deposition fraction (F), minute ventilation based on body weight (V), the mass concentration (C), and exposure duration (T) were used with the equation  $D = F \times V \times C \times T$ . This allowed us to determine that the daily deposited nano-TiO<sub>2</sub> alveolar dose was 6.92 μg (total six exposure dose = 41.55 μg).

The real-time TiO<sub>2</sub> aerosol mass concentration readings were sampled from the exposure chamber during a typical exposure day (**Figure 4.1A**). These concentrations were verified by gravimetric measurements during each exposure, which resulted in an average mass concentration of 12 mg/m<sup>3</sup> during the 360-minute period. To determine the size distribution of the nano-TiO<sub>2</sub> aerosols, a high-resolution electrical low-pressure impactor (ELPI+; Dekati, Tampere, Finland), and a scanning particle mobility sizer (SMPS 3938; TSI Inc., St. Paul, MN) were employed. The ELPI+ data indicated a geometric count median diameter (CMD) of 172 nm with a geometric standard deviation (GSD) of 1.96 (**Figure 4.1B**). The SMPS data indicated a CMD of 112 nm with a GSD of 2.14 (**Figure 4.1C**). The exposure chamber contained bedding material that was soaked in water to maintain a comfortable humidity level during exposure. Control animals (sham) were

exposed to HEPA filtered air with similar chamber conditions in a designated control chamber. The final exposure was administered 48 hours prior to sacrifice and tissue harvesting.

### *RNA Isolation and Fragmentation*

Total RNA was extracted from pooled fetal heart samples (sham, n =3; nano-TiO<sub>2</sub>, n=3) using QIAzol lysis reagent (item no. 79306, Qiagen). Samples were homogenized in QIAzol using a rotor-stator homogenizer and further processed using the miRNeasy Mini Kit (item no. 217004, Qiagen) per manufacturer's protocol. Concentrations were determined for each sample using the NanoDrop ND-100 (Thermo Fisher Scientific, Waltham, MA). Spike-in controls obtained from the EpiMark N6-Methyladenosine Enrichment Kit (item no. E1610S; NEB) were prepared following the manufacturer's protocol. Briefly, the m<sup>6</sup>A control RNA contains m<sup>6</sup>A modified RNA (*Gaussia* luciferase), which was transcribed in the presence of 20% m<sup>6</sup>ATP and 80% ATP and the unmodified control RNA (*Cypridina* luciferase) contains no modifications. 1 μL of the m<sup>6</sup>A control RNA and 1 μL of the unmodified control RNA were added to each sample prior to fragmentation. The fetal cardiac total RNA samples (3 μg) were fragmented into ~250-350-nucleotide fragments using the NEBNext Magnesium RNA Fragmentation kit (item no. E6150S; New England Biolabs (NEB), Ipswich, MA) at 65°C for 5 minutes, followed by addition of the stop solution (26, 53), previously shown (23). The Monarch RNA Cleanup Kit (item no T2030L; NEB) was performed per manufacturer's protocol. Samples were eluted with 20 μL of nuclease-free water and concentrations were determined using the NanoDrop ND-100 (Thermo Fisher Scientific). 2 μL of fragmented total RNA was saved from each sample to be used as input and the rest was used for m<sup>6</sup>A RNA immunoprecipitation followed by sequencing (m<sup>6</sup>A-RIP-seq).

### *Immunoprecipitation (m<sup>6</sup>A-RIP) with Low Input Samples*

The protocol used in our study was adapted from m<sup>6</sup>A-RIP protocols described in “Refined RIP-seq protocol for epitranscriptome analysis with low input materials” (53) and “Landscape and Regulation of m<sup>6</sup>A and m<sup>6</sup>Am Methylome across Human and Mouse Tissues” (26), with modifications. In a 1.5 mL microcentrifuge tube (per sample), 30 μL of protein-A magnetic beads (item no. 10002D; Thermo Fisher Scientific) and 30 μL of protein-G magnetic beads (item no.

10004D; Thermo Fisher Scientific) were mixed, magnetic field applied, and supernatant removed. The mixture of beads was washed twice with 400  $\mu$ L of IPP buffer (10 mM Tris-HCl, 150 mM NaCl, pH 7.5; 0.1% IGEPAL CA-630) and resuspended in 500  $\mu$ L of IPP buffer. 5  $\mu$ g of affinity purified anti-m<sup>6</sup>A polyclonal antibody (item no. ABE572-I; MilliporeSigma, Burlington, MA) was added to the beads and incubated overnight at 4°C. An additional tube with the mixture of beads received 5  $\mu$ g of the normal rabbit IgG control antibody (item no. 2729; Cell Signaling Technology (CST), Danvers, MA) and was also incubated overnight at 4°C. The magnetic field was applied and supernatant removed, followed by washing the antibody-bead mixture twice with IPP buffer. In a 1.5 mL microcentrifuge tube, a 500  $\mu$ L mixture was prepared containing 100  $\mu$ L of 5X IPP buffer, fragmented total RNA (diluted with nuclease-free water to a volume of 395  $\mu$ L), and 5  $\mu$ L of RNasin Plus RNase Inhibitor (item no. N2611; Promega, Madison, WI).

The antibody-bead mixture was resuspended in the 500  $\mu$ L mixture containing the fragmented RNA and incubated with orbital rotation at 4°C for 2 hours, followed by application of the magnetic field, removal of the supernatant, and two washes with 1,000  $\mu$ L of IPP buffer. The bead-antibody-RNA mixture was then washed twice with 1,000  $\mu$ L of low-salt IPP buffer (10 mM Tris-HCl, 50 mM NaCl, pH 7.5; 0.1% IGEPAL CA-630) and twice with 1,000  $\mu$ L of high-salt IPP buffer (10 mM Tris-HCl, 500 mM NaCl, pH 7.5; 0.1% IGEPAL CA-630). A competitive elution buffer was then prepared containing 6.7 mM N<sup>6</sup>-methyladenosine 5'-monophosphate sodium salt (item no. M2780, Sigma-Aldrich) in IPP buffer. Each immunoprecipitation (IP) sample was resuspended in 100  $\mu$ L of the m<sup>6</sup>A competitive elution buffer with continuous shaking at 4°C for 1 hour. The magnetic field was applied, which allowed us to collect the supernatant (eluted m<sup>6</sup>A RNA) into a new tube. The eluted RNA was further purified using the RNeasy MinElute Cleanup Kit (item no. 74204; Qiagen) following manufacturer's protocol. The m<sup>6</sup>A enriched RNA was eluted by adding 14  $\mu$ L of ultrapure H<sub>2</sub>O directly to the center of the membrane and centrifuging for 1.5 mins at full speed. Samples were stored at -80°C until initiation of the library preparation procedure.

### *Library Prep and Sequencing*

Library preparation was performed on immunoprecipitated (IP) and total (input) RNA samples from sham (n = 3) and nano-TiO<sub>2</sub> (n = 3) gestationally-exposed fetal offspring hearts

using the NEB<sup>®</sup> Single Cell/Low Input RNA Library Prep kit for Illumina<sup>®</sup> (item no. E6420S, NEB) and Illumina<sup>®</sup> compatible NEB<sup>®</sup> UDIs (item no. E6440S, NEB), which mitigate sample misassignment due to index-hopped reads. The Agilent 2100 BioAnalyzer (Agilent Technologies, Santa Clara, CA) was employed to determine the size distribution of RNA. Libraries were PCR amplified for 10 cycles and NEB UDIs were used for indexing by amplifying for 8 cycles. The RNA sample concentrations were quantified using a Qubit Fluorometer (Thermo Fisher Scientific). The samples were sequenced using the Illumina NextSeq 2000 (Illumina Inc., San Diego, CA) at Marshall University as paired end (PE) 2x50 bp reads.

### *Analysis of RNA-Seq Data*

Adapters were trimmed from Fastq files through Flexbar v3.5 (36). The trimmed Fastq files were processed using paired-end alignment with HISAT2 v2.2.1 and the resulting BAM files were aligned to the mouse reference genome (*Mus musculus*, GRCm39, Ensemble version 104) for input and IP samples. Peaks showing significant enrichment in the IP samples vs. corresponding input samples for all submitted replicates were detected using RADAR v0.2.1 (56), with a fragment length of 297 base pairs and bin size of 25 base pairs. Peak reads coverage for transcripts were visualized with RADAR and the Integrative Genome Browser (IGV) browser (5, 12, 25, 35).

Input mRNA samples were further processed for full decoy-aware transcriptomic analyses using Salmon v1.5.2 (33) on the mouse reference genome (*Mus musculus*, GRCm39, Ensemble version 104) and processed in R using tximport v1.22.0 (41). Differential gene expression was performed through DESeq2 v1.34.0 (27). Visualization of data was accomplished through ggplot2 v3.3.5 (48) and pheatmap v1.0.12. Pathway analysis was performed through PathFindR v1.6.3 (44).

### *Mitochondrial Isolation*

Fetal pups were sacrificed at GD 15 and their hearts were excised through a midsagittal cut in the thoracic cavity. Mitochondria were isolated as previously described (32), with modifications by our laboratory (2, 3, 9). The two subpopulations of mitochondria (subsarcolemmal and

interfibrillar) were combined at the end of the protocol to achieve a total mitochondrial population. Samples were resuspended in KME buffer (100mM KCl, 50mM MOPS and 0.5mM EGTA pH 7.4) with protease inhibitor cocktail (PIC).

### *Sample Preparation for Mitochondrial Proteomics*

Label-free proteomics sample preparation was performed on fetal cardiac isolate mitochondria (sham, n=4; nano-TiO<sub>2</sub>, n=4) based off the “Plasma protein digestion” protocol described by Valentine et. al. with several modifications (45). 37 µL, containing about 24 µg of protein, as measured by the Bradford assay, of isolated fetal cardiac mitochondria (in KME+PIC) was placed in a SpeedVac for 3.5 hours to dry out the sample. Samples were resuspended in 20 µL of Dissolution buffer (8 M Urea, 50 mM Tris-HCl - pH 8.2)) and their protein concentrations were determined using the NanoDrop™ One Microvolume UV-Vis Spectrophotometer (Thermo Fisher Scientific). 12 µg of protein per sample was used for the rest of the sample preparation procedure. 1.2 µL of DTT reducing agent (100 mM DTT (item no. V3151, Promega) in 8 M urea and 100 mM ammonium bicarbonate – pH 8.2) was added to each sample followed by a 2-hour incubation at 37°C, with gentle agitation. After reducing the disulfide bonds, samples were placed on ice. Protein alkylation was then achieved using 1.2 µL of iodoacetamide (225 mM iodoacetamide (item no. I6125, Sigma-Aldrich) in 8 M urea and 100 mM ammonium bicarbonate – pH 8.2), which was made fresh.

The reaction was allowed to proceed in darkness, on ice for 2 hours. Next, 1.2 µL of cysteine blocking reagent (100 mM L-cysteine (item no. 168149, Sigma-Aldrich) in 8 M urea and 100 mM ammonium bicarbonate – pH 8.2) was added to the mixture to remove any remaining reagent, followed by a 30-minute incubation at room temperature with gentle agitation. Following this reaction, enough Dilution solution (100 mM ammonium bicarbonate – pH 8.2) was added to each sample to bring the urea to a 2 M concentration. Protein digestion was initiated by the addition of Trypsin solution (appropriate amount of trypsin in 2 M urea, 100 mM ammonium bicarbonate – pH 8.2) to a final concentration of 50:1 protein:trypsin and incubated for 24 hours at 37°C, with gentle agitation. Peptide cleanup was performed using Thermo Scientific Pierce™ C18 Spin Columns (item no. 89873) per manufacturer’s instructions and samples were eluted using acetonitrile. Samples were dried using a centrifugal concentrator (Labconco) and stored at -20°C

for LC-MS/MS analysis. Prior to LC-MS/MS analysis, each sample was resuspended in 100  $\mu$ L of formic acid buffer. Due to limited quantities of protein, the four samples in each group were pooled to produce sham (n=2) and nano-TiO<sub>2</sub> (n=2).

### *LC Separation*

20  $\mu$ L of digest solution was injected onto a reversed phase liquid chromatography (column (10 cm  $\times$  2.1 mm ID, 5  $\mu$ m particle dia). A flow rate of 300  $\mu$ L/min was employed for the reversed-phase separation. Gradient elution was performed using two buffers. Buffer A consisted of HPLC-grade water with 1% formic acid and Buffer B was acetonitrile with 1% formic acid. During LC separations the solvent contribution from Buffer B was 0.1%, 0.1%, 25%, 80%, 90%, 90%, and 0.1% at 0, 2, 27, 37, 42, 52, and 57 minutes, respectively.

### *Mass Spectrometer*

Data were collected on an orbitrap mass spectrometer (Q-Exactive, Thermo Scientific). Experiments were conducted in positive ion mode and data dependent analysis was employed. Throughout the LC separation, a full MS scan was collected followed by 5 MS<sub>2</sub> scans. Resolving power settings of 70,000 and 17,500 were utilized for the precursor and MS<sub>2</sub> scans, respectively. The respective AGC settings were 1E6 and 1E5. A normalized collision energy of 30 was employed for MS<sub>2</sub> analyses. Finally, a dynamic exclusion time of 10 s was employed for the separations.

### *Data Processing*

Raw data files from the Q-Exactive mass spectrometer were imported into the Proteome Discoverer software suite (Thermo Scientific). The SEQUEST search engine was employed for peptide identification. The SwissProt (v2017-10-25) database for *Mus musculus* was employed for peptide ion identification. The search employed a minimum peptide length of 5 residues and allowed for 3 missed cleavages using Trypsin as the enzyme used for digestion. A precursor mass tolerance of 12 ppm and a fragment ion mass tolerance of 0.03 Da was employed. A static



modification of 57.021 Da (C, carbamidomethyl)) was employed in the searches. A value of 0.1 was used for protein and peptide validation settings.

### *Proteomic Analysis*

After the results were obtained, analysis was performed using an exponentially modified protein abundance index (emPAI) to estimate absolute protein amounts based on the number of sequenced peptides per protein (16). Briefly, only high quality peptides were selected based on the Score Sequest HT: A Sequest HT and mitochondrial proteins were identified using MitoCarta3.0 (34). The protein abundance index (PAI) was calculated with **Equation 1** using the “total peptides” count per protein for  $N_{\text{observed}}$  and the  $N_{\text{observable}}$  was determined using ExPASy server (49). The emPAI was then calculated as shown in **Equation 2**. The emPAI values for the two samples per group was averaged for each respective group (sham and nano-TiO<sub>2</sub>) and compared.

**Equation 1** 
$$PAI = \frac{N_{\text{observed}}}{N_{\text{observable}}}$$

**Equation 2** 
$$emPAI = 10^{PAI} - 1$$

### *Data Code Availability*

All code used in the bioinformatic processing of samples is provided <https://github.com/qahathaway/mRNA-m6A-Proteomics>. Additionally, supplementary data files are included as XLSX files included in the manuscript, as well as provided on the GitHub account. Raw sequencing files have been uploaded to Gene Expression Omnibus (GEO) under accession:

### *Statistics*

Statistical analyses were conducted in the R v4.1.1 environment. DESeq2 implements the Wald Test, using the Benjamini-Hochberg procedure. The FDR for this study was set to 0.05 for the transcriptomic analyses and 0.10 for m<sup>6</sup>A peak calling. All measures of significance are

reported as adjusted  $P$ -values ( $P_{adj}$ ). The RADAR package used for peak calling implements a Gamma-Poisson Distribution Model, which is a type of random effect model.

## Results

### *Study Design*

The study design (**Figure 4.1D**) highlights the use of mRNA and m<sup>6</sup>A sequencing on whole heart tissue and proteomics on isolated mitochondria. Maternal dams were euthanized at gestational day (GD) 15. Each dam was considered an n=1. No significant differences were observed between maternal and fetal pup weights, pup number, or pup heart weights (**Table 4.1**).

### *Transcriptomics*

In performing the m<sup>6</sup>A-RIP-Seq, the input controls provided overall transcript abundance, which showcases the changes to mRNA seen following gestational nano-TiO<sub>2</sub> exposure in fetal offspring. Sample distances were projected both using multidimensional scaling (MDS) (**Figure 4.2A**) as well as distribution with variance stabilizing transformation (VST) (**Supplemental Figure 4.1A**). Both techniques illustrate distinct stratification between the two groups. An illustration of the VST, as well as Log<sub>2</sub> normalized counts and regularized-logarithm (rlog) transformations, are provided (**Supplemental Figure 4.1B**). Differential expression analysis was performed and revealed a total of 3,648 genes that were significantly changed following exposure (**Figure 4.2B**). Examining the top 1,000 genes, sorted by *P*<sub>adj</sub> value, we see that two-thirds are upregulated, while 1/3 is downregulated between groups (**Figure 4.2C**). Additionally, Figure 2C shows that the sham and nano-TiO<sub>2</sub> groups hierarchically cluster separately.

Our previous investigations have shown that mitochondrial dysfunction, specifically alterations to bioenergetics, have correlated with cardiovascular functional impairments, such as reduced ejection fraction, changes to left ventricular size, and alterations of strain of the heart (15, 23, 24). Electron transport chain proteins were significantly decreased for all mitochondrial complexes (**Figure 4.2D**). When examining all mitochondrial genes, decreased expression was seen across most categories of mitochondrial genes (**Supplemental Figure 4.2**). Interestingly, mitochondrial electron transport chain genes (**Figure 4.2D**) and mitochondrial ribosomal metabolism (**Supplemental Figure 4.2**) were the two pathways most significantly impacted following nano-TiO<sub>2</sub> exposure. Also of interest, mitochondrial glutathione peroxidase 4 (Gpx4)

(**Supplemental Figure 4.1C**) was significantly decreased, which we have previously shown to be an important mediator of ROS levels in gestationally and directly exposed mice (23, 30).

#### *Epitranscriptomics through N<sup>6</sup>-methyladenosine (m<sup>6</sup>A)*

Using both the input (unmodified mRNA) and immunoprecipitated RNA with our m<sup>6</sup>A antibodies, we wanted to examine if specific sites were being methylated, or demethylated, following nano-TiO<sub>2</sub> exposure (**Figure 4.3**). Principal Component Analysis (PCA) revealed distinct separation of the sham and nano-TiO<sub>2</sub> groups (**Figure 4.4A**). Through differential peak analyses, we were further able to determine that the majority of m<sup>6</sup>A sites were occurring in the 3' untranslated regions (UTRs) (**Figure 4.4B**), which is supported by previous literature (29). We then plotted all the differentially methylated sites, revealing significant upregulating of m<sup>6</sup>A methylation following exposure (**Figure 4.4C**).

Our next step was to assess if the mRNA identified in the input samples and the differentially methylated sites overlapped. Of the 3,648 differentially expressed genes and 921 unique genes containing significant m<sup>6</sup>A modifications, 311 overlapped (**Figure 4.4D**). The mRNA expression was primarily increased in these genes, suggesting a predominately activating effect of m<sup>6</sup>A on gene expression/transcript longevity.

#### *mRNA/m<sup>6</sup>A Shared Features*

We next wanted to understand how the 311 genes identified in both mRNA and m<sup>6</sup>A were related to cellular and molecular pathways. Using gene ontology through KEGG, we hierarchically clustered the pathways and represented the top genes within the pathways for the 3,648 differentially expressed genes (**Figure 4.5A**) as well as the 311 shared genes (**Figure 4.5B**). The shared pathway revealed significant overlap with the pathway containing all genes in a few notable ways, including ubiquitin-mediated proteolysis, RNA degradation, spliceosome, and HIF-1 signaling. Interestingly, we see that in the all-gene ontology pathway (**Figure 4.5A**), oxidative phosphorylation is one of the top pathways, though not represented in the shared analysis (**Figure 4.5B**).

The common pathways between the two groups are mainly larger regulator pathways, controlling the transcription, translation, and turnover of proteins. We include the detailed molecular pathway for RNA degradation in the all-gene (**Supplemental Figure 4.3A**) and shared (**Supplemental Figure 4.3B**) analyses that highlight genes, such as CCR4-NOT transcription complex subunit 1 (Cnot1) and 5'-3' exoribonuclease 2 (Xrn2), likely upregulated through m<sup>6</sup>A modification. We also provide an illustration of the entire gene (**Supplemental Figure 4.4A-B**) and specific region (**Supplemental Figure 4.4C-D**) that are differentially methylated.

### *Mitochondrial Proteomics*

Our last objective was to analyze the mitochondrial proteome to define if transcriptional alterations directly aligned with protein level expression. Our workflow included isolating mitochondrion from fetal heart tissue, isolating the protein, and processing the peptides through LC-MS/MS (**Figure 4.6A**). The protein abundance index (emPAI) was calculated only for mitochondrial proteins identified with a high confidence in both the sham and nano-TiO<sub>2</sub> groups. Of the mitochondrial proteins, those belonging to ATP Synthase, including Atp5a1, Atp5b, Atp5c1, Atp5pb, and complex I, Nudufs1 and Nudufv2, showed the most consistent downregulation in the nano-TiO<sub>2</sub> exposure group (**Figure 4.6B**). Additionally, peroxiredoxin 3 (Prdx3), a critical mitochondrial antioxidant, revealed the largest decrease between the sham and exposed groups (**Figure 4.6B**).

## Discussion

Fetal development is an intricate process that requires a significant number of regulatory processes. A baleful gestational environment can result in disease predisposition, in addition to immediate consequences of fetal development. M<sup>6</sup>A methylation can transiently alter cellular function and may play a significant role in the response to toxicants during gestation. The results of our study emphasize the impact of m<sup>6</sup>A methylation on regulatory pathways within the heart, largely involved with the transcription, translation, and longevity of proteins within the cell. Along with changes to oxidative phosphorylation, acute changes to the m<sup>6</sup>A methylome may predispose offspring to future adverse outcomes.

Exposure to environmental toxicants is associated with developmental reprogramming that alters normal physiological responses and thereby leads to disease susceptibility including metabolic diseases (43, 46). Specifically, prenatal maternal exposure to benzene, diesel exhaust, and fine particulate matter lead to glucose intolerance and elevated insulin resistance (20), weight gain (6), and metabolic syndrome (50), respectively, in adulthood. As cardiovascular disease remains the leading cause of death worldwide, researchers have begun investigating whether m<sup>6</sup>A mRNA modifications can serve as diagnostic or therapeutic targets (19, 42). Transcriptome-wide assessments of cardiac samples from human and murine models of dilated cardiomyopathy were assessed by Kmietczyk et. al (17). They found that hypermethylation was prominent in failing human hearts and confirmed the dynamic and regulatory capabilities of m<sup>6</sup>A in this diseased state.

Furthermore, research has also shown that m<sup>6</sup>A is a novel stress-response mechanism in the heart that attempts to maintain normal cardiac function (11). Specifically, Dorn and colleagues implemented genetic tools to modulate m<sup>6</sup>A levels via METTL3 levels, thereby generating cardiac-restricted gain- and loss-of-function mouse models that allowed them to identify m<sup>6</sup>A methylation by METTL3 as a dynamic response that is enhanced with cardiac hypertrophy. Contrarily, they determined that m<sup>6</sup>A hypomethylation drives eccentric cardiomyocyte remodeling and dysfunction (11). Another group examined the m<sup>6</sup>A landscape in heart hypertrophy and heart failure as well (4). In addition to confirming that cardiac hypertrophy and failure are accompanying by m<sup>6</sup>A methylation changes, the authors found that hypomethylated transcripts played a role in mitochondrial function and metabolic processes, while hypermethylated transcripts were also associated with metabolic processes as well as response to growth factor and muscle stretch (4).

Similarly, in patients with heart failure with preserved ejection fraction, the m<sup>6</sup>A landscape and its regulators were altered such that the several methyltransferase complex constituents, including METTL3, were up-regulated, in addition to demethylase FTO, and reader YTHDF2 (54). Despite an increased interest in the role of m<sup>6</sup>A methylation in cardiovascular disease, studies have mainly focused on heart failure specifically and have yet to elucidate in depth the contribution from ALKBH5 (22).

Although recent studies have determined that m<sup>6</sup>A is easily altered by stress and other external stimuli (11), its status particularly in the heart, following exposure to environmental toxicants remains to be elucidated. Following exposure to fine particulate matter (PM<sub>2.5</sub>), there was a global decrease in m<sup>6</sup>A methylation, concomitant with elevated expression of methyltransferase complex components (METTL3 and WTAP), demethylases (FTO and ALKBH5), and the reader protein HNRNPC (7). However, this study involved a short-term exposure on A549 cells, which still leaves the question of how different tissue types respond to environmental exposures and how long-term exposure may alter this response. Recent work from our laboratory has demonstrated that maternal inhalation exposure to ENM during a critical point in fetal development results in cardiac dysfunction, mitochondrial bioenergetic disruption, and an increase in global m<sup>6</sup>A content (23).

Notably, m<sup>6</sup>A levels were ameliorated in the presence of enhanced antioxidant capacity that was mitochondrially targeted in the pregnant mother. It has become clear that a specific and balanced m<sup>6</sup>A RNA distribution is crucial to maintain homeostasis and evade disease, though the precise mechanisms underpinning the process remain unknown. Zhang et. al. similarly investigated the effects of carbon black nanoparticle exposure during pregnancy on m<sup>6</sup>A status in offspring, but specifically in the case of neurobehavior deficits (55). The authors determined that the exposure decreased m<sup>6</sup>A modification in the cortex, along with neurobehavioral deficits and cortex injuries in the offspring. These studies substantiate the idea that m<sup>6</sup>A methylation status is likely disease and tissue specific.

Our current study forwards the concept that differential m<sup>6</sup>A methylation of genes can have untoward effects of cardiac function. While our model uses transcriptomics, epitranscriptomics, and proteomics to provide a multi-omics approach toward mechanistically detailing fetal cardiac changes, the approach was limited by the amount of tissue available. In our proteomics approach,

we needed to pool our groups to further condense the protein for adequate analyses, losing the ability to make true statistical inferences on the data. Additionally, the proteins found to be decreased in both the ATP Synthase complex and complex I do not consist of the same transcripts shown to be decreased in the transcriptomic analyses. Though, there is evidence to support that m<sup>6</sup>A methylation is acting at an indirect, rather than direct, level to modify transcript and protein expression.

The analyses indicate that m<sup>6</sup>A methylation is predominately occurring in pathways altering transcription of mRNA (spliceosome pathway), stability of transcripts (RNA degradation pathway), and protein longevity (ubiquitin-mediated proteolysis pathway). While the same mRNA and protein changes may not completely align, this could be explained through these different indirect mechanisms decreasing abundance. Further, of the differentially expressed mRNA genes, *Mettl14*, a key regulatory writer of m<sup>6</sup>A methylation marks, is shown to be increased and supports the findings of significantly increased m<sup>6</sup>A methylation overall in the nano-TiO<sub>2</sub> group.

We provide for the first time a comprehensive, multi-omics approach that includes epitranscriptomics in the investigation of fetal progeny following toxicant exposure. This framework helped to identify how m<sup>6</sup>A methylation can be globally increased in the heart following exposure, and how the pathways, such as RNA degradation and ubiquitin-mediated proteolysis, play a role in regulating mitochondrial bioenergetics. These data substantiate the need to further investigate RNA modifications as a mechanism for adaptive fetal responses. Future work should seek to identify the persistence of these marks, and whether other RNA modifications also contribute to modifying the fetal transcriptome and proteome.



## **Acknowledgments**

We would like to acknowledge the WVU Genomics Core Facility, Morgantown WV for support provided to help make this publication possible and CTSI Grant #U54 GM104942 which in turn provides financial support to the Core Facility. We would like to thank Sherri A. Friend and the National Institute for Occupational Safety and Health, Morgantown, WV, USA for contributing to the physicochemical characterization of the nano-TiO<sub>2</sub> aerosolized particles.

## **Funding**

This work was supported by The National Heart, Lung, and Blood Institute (NHLBI) under Grant [R01 HL-128485] (JMH), the National Institute of Environmental Health Sciences (NIEHS) under Grant [R01 ES-015022] (TRN), American Heart Association under Grant [AHA-20PRE35080170] (AK), American Heart Association under Grant [AHA-17PRE33660333] (QAH), and the Community Foundation for the Ohio Valley Whipkey Trust (JMH)

## **Conflict of Interest**

Quincy A. Hathaway is the Chief Science Officer for Aspirations LLC. No other potential conflicts of interest are reported by the author(s).

## **Author Contributions**

AK, QAH, DT, SJV, and JMH conceived and planned the experiments. AK, QAH, DT, AJD, ADT, SR, and DS carried out the experiments. AK, QAH, AJD, ADT, and SR contributed to sample preparation. DS and SJV processed samples for proteomic analyses. AK, QAH, DT, and JMH contributed to the interpretation of the results. AK took the lead in writing the manuscript. All authors provided critical feedback and helped shape the research, analysis, and manuscript.

## **Contribution to the Field**

The current study helps to expand our understanding of how environmental exposures impact our health. Importantly, this study uses a gestational model where we want to understand how exposure to toxicants during pregnancy can impact the developing fetus. We know that changes to the fetus can occur at the level of DNA, through temporary modifications known as “epigenetics”. What is unknown, is whether other changes, outside of DNA modifications, can also cause the growing fetus to have adverse outcomes. One of the major adverse outcomes of environmental exposure is cardiovascular complications. We have previously shown that these cardiovascular complications can be linked to changes at the level of mitochondria, with decreased ability to produce energy. “Epitranscriptomics” is a term used to describe temporary changes at the level of mRNA. Our goal in the current study was to fully detail the impact of these RNA modifications on shaping fetal health following exposure. Our novel approach inspected both mRNA abundance as well as the amount of mRNA modifications present. We then coupled this information with protein level changes in the mitochondrion. Our result suggests that RNA modifications can influence expression of RNA and protein of mitochondrial genes.

## References

1. **Barouki R, Melen E, Herceg Z, Beckers J, Chen J, Karagas M, Puga A, Xia Y, Chadwick L, Yan W, Audouze K, Slama R, Heindel J, Grandjean P, Kawamoto T, and Nohara K.** Epigenetics as a mechanism linking developmental exposures to long-term toxicity. *Environ Int* 114: 77-86, 2018.
2. **Baseler WA, Dabkowski ER, Jagannathan R, Thapa D, Nichols CE, Shepherd DL, Croston TL, Powell M, Razunguzwa TT, Lewis SE, Schnell DM, and Hollander JM.** Reversal of mitochondrial proteomic loss in Type 1 diabetic heart with overexpression of phospholipid hydroperoxide glutathione peroxidase. *Am J Physiol Regul Integr Comp Physiol* 304: R553-565, 2013.
3. **Baseler WA, Dabkowski ER, Williamson CL, Croston TL, Thapa D, Powell MJ, Razunguzwa TT, and Hollander JM.** Proteomic alterations of distinct mitochondrial subpopulations in the type 1 diabetic heart: contribution of protein import dysfunction. *Am J Physiol Regul Integr Comp Physiol* 300: R186-200, 2011.
4. **Berulava T, Buchholz E, Elerdashvili V, Pena T, Islam MR, Lbik D, Mohamed BA, Renner A, von Lewinski D, Sacherer M, Bohnsack KE, Bohnsack MT, Jain G, Capece V, Cleve N, Burkhardt S, Hasenfuss G, Fischer A, and Toischer K.** Changes in m6A RNA methylation contribute to heart failure progression by modulating translation. *Eur J Heart Fail* 22: 54-66, 2020.
5. **Berulava T, Buchholz E, Elerdashvili V, Pena T, Islam MR, Lbik D, Mohamed BA, Renner A, von Lewinski D, Sacherer M, Bohnsack KE, Bohnsack MT, Jain G, Capece V, Cleve N, Burkhardt S, Hasenfuss G, Fischer A, and Toischer K.** Changes in m6A RNA methylation contribute to heart failure progression by modulating translation. *Eur J Heart Fail* 2019.
6. **Bolton JL, Smith SH, Huff NC, Gilmour MI, Foster WM, Auten RL, and Bilbo SD.** Prenatal air pollution exposure induces neuroinflammation and predisposes offspring to weight gain in adulthood in a sex-specific manner. *FASEB J* 26: 4743-4754, 2012.
7. **Cayir A, Barrow TM, Guo L, and Byun HM.** Exposure to environmental toxicants reduces global N6-methyladenosine RNA methylation and alters expression of RNA methylation modulator genes. *Environ Res* 175: 228-234, 2019.
8. **Cui YH, Yang S, Wei J, Shea CR, Zhong W, Wang F, Shah P, Kibriya MG, Cui X, Ahsan H, He C, and He YY.** Autophagy of the m(6)A mRNA demethylase FTO is impaired by low-level arsenic exposure to promote tumorigenesis. *Nat Commun* 12: 2183, 2021.
9. **Dabkowski ER, Baseler WA, Williamson CL, Powell M, Razunguzwa TT, Frisbee JC, and Hollander JM.** Mitochondrial dysfunction in the type 2 diabetic heart is associated with alterations in spatially distinct mitochondrial proteomes. *Am J Physiol Heart Circ Physiol* 299: H529-540, 2010.
10. **Dominissini D, Moshitch-Moshkovitz S, Schwartz S, Salmon-Divon M, Ungar L, Osenberg S, Cesarkas K, Jacob-Hirsch J, Amariglio N, Kupiec M, Sorek R, and Rechavi G.** Topology of the human and mouse m6A RNA methylomes revealed by m6A-seq. *Nature* 485: 201-206, 2012.
11. **Dorn LE, Lasman L, Chen J, Xu X, Hund TJ, Medvedovic M, Hanna JH, van Berlo JH, and Accornero F.** The N(6)-Methyladenosine mRNA Methylase METTL3 Controls Cardiac Homeostasis and Hypertrophy. *Circulation* 139: 533-545, 2019.
12. **Engel M, Eggert C, Kaplick PM, Eder M, Roh S, Tietze L, Namendorf C, Arloth J, Weber P, Rex-Haffner M, Geula S, Jakovcevski M, Hanna JH, Leshkowitz D, Uhr M,**

- Wotjak CT, Schmidt MV, Deussing JM, Binder EB, and Chen A.** The Role of m(6)A/m-RNA Methylation in Stress Response Regulation. *Neuron* 99: 389-403 e389, 2018.
13. **Fu Y, Dominissini D, Rechavi G, and He C.** Gene expression regulation mediated through reversible m(6)A RNA methylation. *Nat Rev Genet* 15: 293-306, 2014.
  14. **Hathaway QA, Durr AJ, Shepherd DL, Pinti MV, Brandebura AN, Nichols CE, Kunovac A, Goldsmith WT, Friend SA, Abukabda AB, Fink GK, Nurkiewicz TR, and Hollander JM.** miRNA-378a as a key regulator of cardiovascular health following engineered nanomaterial inhalation exposure. *Nanotoxicology* 13: 644-663, 2019.
  15. **Hathaway QA, Nichols CE, Shepherd DL, Stapleton PA, McLaughlin SL, Stricker JC, Rellick SL, Pinti MV, Abukabda AB, McBride CR, Yi J, Stine SM, Nurkiewicz TR, and Hollander JM.** Maternal-engineered nanomaterial exposure disrupts progeny cardiac function and bioenergetics. *Am J Physiol Heart Circ Physiol* 312: H446-H458, 2017.
  16. **Ishihama Y, Oda Y, Tabata T, Sato T, Nagasu T, Rappsilber J, and Mann M.** Exponentially modified protein abundance index (emPAI) for estimation of absolute protein amount in proteomics by the number of sequenced peptides per protein. *Mol Cell Proteomics* 4: 1265-1272, 2005.
  17. **Kmietczyk V, Riechert E, Kalinski L, Boileau E, Malovrh E, Malone B, Gorska A, Hofmann C, Varma E, Jurgensen L, Kamuf-Schenk V, Altmuller J, Tappu R, Busch M, Most P, Katus HA, Dieterich C, and Volkers M.** m(6)A-mRNA methylation regulates cardiac gene expression and cellular growth. *Life Sci Alliance* 2: 2019.
  18. **Knuckles TL, Yi J, Frazer DG, Leonard HD, Chen BT, Castranova V, and Nurkiewicz TR.** Nanoparticle inhalation alters systemic arteriolar vasoreactivity through sympathetic and cyclooxygenase-mediated pathways. *Nanotoxicology* 6: 724-735, 2012.
  19. **Komal S, Zhang LR, and Han SN.** Potential regulatory role of epigenetic RNA methylation in cardiovascular diseases. *Biomed Pharmacother* 137: 111376, 2021.
  20. **Koshko L, Debarba LK, Sacla M, de Lima JBM, Didyuk O, Fakhoury P, and Sadagurski M.** In Utero Maternal Benzene Exposure Predisposes to the Metabolic Imbalance in the Offspring. *Toxicol Sci* 180: 252-261, 2021.
  21. **Kumar S, and Mohapatra T.** Deciphering Epitranscriptome: Modification of mRNA Bases Provides a New Perspective for Post-transcriptional Regulation of Gene Expression. *Front Cell Dev Biol* 9: 628415, 2021.
  22. **Kumari R, Ranjan P, Suleiman ZG, Goswami SK, Li J, Prasad R, and Verma SK.** mRNA modifications in cardiovascular biology and disease: with a focus on m6A modification. *Cardiovasc Res* 2021.
  23. **Kunovac A, Hathaway QA, Pinti MV, Durr AJ, Taylor AD, Goldsmith WT, Garner KL, Nurkiewicz TR, and Hollander JM.** Enhanced antioxidant capacity prevents epitranscriptomic and cardiac alterations in adult offspring gestationally-exposed to ENM. *Nanotoxicology* 1-20, 2021.
  24. **Kunovac A, Hathaway QA, Pinti MV, Goldsmith WT, Durr AJ, Fink GK, Nurkiewicz TR, and Hollander JM.** ROS promote epigenetic remodeling and cardiac dysfunction in offspring following maternal engineered nanomaterial (ENM) exposure. *Part Fibre Toxicol* 16: 24, 2019.
  25. **Liu J, Li K, Cai J, Zhang M, Zhang X, Xiong X, Meng H, Xu X, Huang Z, Peng J, Fan J, and Yi C.** Landscape and Regulation of m(6)A and m(6)Am Methylome across Human and Mouse Tissues. *Mol Cell* 2019.

26. **Liu J, Li K, Cai J, Zhang M, Zhang X, Xiong X, Meng H, Xu X, Huang Z, Peng J, Fan J, and Yi C.** Landscape and Regulation of m(6)A and m(6)Am Methylome across Human and Mouse Tissues. *Mol Cell* 77: 426-440 e426, 2020.
27. **Love MI, Huber W, and Anders S.** Moderated estimation of fold change and dispersion for RNA-seq data with DESeq2. *Genome Biol* 15: 550, 2014.
28. **Mauer J, Luo X, Blanjoie A, Jiao X, Grozhik AV, Patil DP, Linder B, Pickering BF, Vasseur JJ, Chen Q, Gross SS, Elemento O, Debart F, Kiledjian M, and Jaffrey SR.** Reversible methylation of m(6)Am in the 5' cap controls mRNA stability. *Nature* 541: 371-375, 2017.
29. **Meyer KD, Saletore Y, Zumbo P, Elemento O, Mason CE, and Jaffrey SR.** Comprehensive analysis of mRNA methylation reveals enrichment in 3' UTRs and near stop codons. *Cell* 149: 1635-1646, 2012.
30. **Nichols CE, Shepherd DL, Hathaway QA, Durr AJ, Thapa D, Abukabda A, Yi J, Nurkiewicz TR, and Hollander JM.** Reactive oxygen species damage drives cardiac and mitochondrial dysfunction following acute nano-titanium dioxide inhalation exposure. *Nanotoxicology* 12: 32-48, 2018.
31. **Nurkiewicz TR, Porter DW, Hubbs AF, Cumpston JL, Chen BT, Frazer DG, and Castranova V.** Nanoparticle inhalation augments particle-dependent systemic microvascular dysfunction. *Part Fibre Toxicol* 5: 1, 2008.
32. **Palmer JW, Tandler B, and Hoppel CL.** Biochemical properties of subsarcolemmal and interfibrillar mitochondria isolated from rat cardiac muscle. *J Biol Chem* 252: 8731-8739, 1977.
33. **Patro R, Duggal G, Love MI, Irizarry RA, and Kingsford C.** Salmon provides fast and bias-aware quantification of transcript expression. *Nat Methods* 14: 417-419, 2017.
34. **Rath S, Sharma R, Gupta R, Ast T, Chan C, Durham TJ, Goodman RP, Grabarek Z, Haas ME, Hung WHW, Joshi PR, Jourdain AA, Kim SH, Kotrys AV, Lam SS, McCoy JG, Meisel JD, Miranda M, Panda A, Patgiri A, Rogers R, Sadre S, Shah H, Skinner OS, To TL, Walker MA, Wang H, Ward PS, Wengrod J, Yuan CC, Calvo SE, and Mootha VK.** MitoCarta3.0: an updated mitochondrial proteome now with sub-organelle localization and pathway annotations. *Nucleic Acids Res* 49: D1541-D1547, 2021.
35. **Robinson JT, Thorvaldsdottir H, Winckler W, Guttman M, Lander ES, Getz G, and Mesirov JP.** Integrative genomics viewer. *Nat Biotechnol* 29: 24-26, 2011.
36. **Roehr JT, Dieterich C, and Reinert K.** Flexbar 3.0 - SIMD and multicore parallelization. *Bioinformatics* 33: 2941-2942, 2017.
37. **Ruiz-Hernandez A, Kuo CC, Rentero-Garrido P, Tang WY, Redon J, Ordovas JM, Navas-Acien A, and Tellez-Plaza M.** Environmental chemicals and DNA methylation in adults: a systematic review of the epidemiologic evidence. *Clin Epigenetics* 7: 55, 2015.
38. **Sager TM, Kommineni C, and Castranova V.** Pulmonary response to intratracheal instillation of ultrafine versus fine titanium dioxide: role of particle surface area. *Part Fibre Toxicol* 5: 17, 2008.
39. **Seo MY, Kim SH, and Park MJ.** Air pollution and childhood obesity. *Clin Exp Pediatr* 63: 382-388, 2020.
40. **Shi H, Wang X, Lu Z, Zhao BS, Ma H, Hsu PJ, Liu C, and He C.** YTHDF3 facilitates translation and decay of N(6)-methyladenosine-modified RNA. *Cell Res* 27: 315-328, 2017.
41. **Soneson C, Love MI, and Robinson MD.** Differential analyses for RNA-seq: transcript-level estimates improve gene-level inferences. *F1000Res* 4: 1521, 2015.

42. Sweaad WK, Stefanizzi FM, Chamorro-Jorganes A, Devaux Y, Emanuelli C, and CA EU-CCA. Relevance of N6-methyladenosine regulators for transcriptome: Implications for development and the cardiovascular system. *J Mol Cell Cardiol* 160: 56-70, 2021.
43. Trevino LS, Dong J, Kaushal A, Katz TA, Jangid RK, Robertson MJ, Grimm SL, Ambati CSR, Putluri V, Cox AR, Kim KH, May TD, Gallo MR, Moore DD, Hartig SM, Foulds CE, Putluri N, Coarfa C, and Walker CL. Epigenome environment interactions accelerate epigenomic aging and unlock metabolically restricted epigenetic reprogramming in adulthood. *Nat Commun* 11: 2316, 2020.
44. Ulgen E, Ozisik O, and Sezerman OU. pathfindR: An R Package for Comprehensive Identification of Enriched Pathways in Omics Data Through Active Subnetworks. *Front Genet* 10: 858, 2019.
45. Valentine SJ, Kurulugama RT, Bohrer BC, Merenbloom SI, Sowell RA, Mechref Y, and Clemmer DE. Developing IMS-IMS-MS for rapid characterization of abundant proteins in human plasma. *International Journal of Mass Spectrometry* 283: 149-160, 2009.
46. Walker CL. Epigenomic reprogramming of the developing reproductive tract and disease susceptibility in adulthood. *Birth Defects Res A Clin Mol Teratol* 91: 666-671, 2011.
47. Whitten WK. Modification of the oestrous cycle of the mouse by external stimuli associated with the male. *J Endocrinol* 13: 399-404, 1956.
48. Wickham H. *ggplot2: Elegant Graphics for Data Analysis*. New York: Springer-Verlag New York, 2016.
49. Wilkins MR, Gasteiger E, Bairoch A, Sanchez JC, Williams KL, Appel RD, and Hochstrasser DF. Protein identification and analysis tools in the ExpASY server. *Methods Mol Biol* 112: 531-552, 1999.
50. Wu G, Brown J, Zamora ML, Miller A, Satterfield MC, Meininger CJ, Steinhauser CB, Johnson GA, Burghardt RC, Bazer FW, Li Y, Johnson NM, Molina MJ, and Zhang R. Adverse organogenesis and predisposed long-term metabolic syndrome from prenatal exposure to fine particulate matter. *Proc Natl Acad Sci U S A* 116: 11590-11595, 2019.
51. Yang C, Hu Y, Zhou B, Bao Y, Li Z, Gong C, Yang H, Wang S, and Xiao Y. The role of m(6)A modification in physiology and disease. *Cell Death Dis* 11: 960, 2020.
52. Zaccara S, Ries RJ, and Jaffrey SR. Reading, writing and erasing mRNA methylation. *Nat Rev Mol Cell Biol* 20: 608-624, 2019.
53. Zeng Y, Wang S, Gao S, Soares F, Ahmed M, Guo H, Wang M, Hua JT, Guan J, Moran MF, Tsao MS, and He HH. Refined RIP-seq protocol for epitranscriptome analysis with low input materials. *PLoS Biol* 16: e2006092, 2018.
54. Zhang B, Xu Y, Cui X, Jiang H, Luo W, Weng X, Wang Y, Zhao Y, Sun A, and Ge J. Alteration of m6A RNA Methylation in Heart Failure With Preserved Ejection Fraction. *Front Cardiovasc Med* 8: 647806, 2021.
55. Zhang S, Meng P, Cheng S, Jiang X, Zhang J, Qin X, Tang Q, Bai L, Zou Z, and Chen C. Pregnancy exposure to carbon black nanoparticles induced neurobehavioral deficits that are associated with altered m(6)A modification in offspring. *Neurotoxicology* 81: 40-50, 2020.
56. Zhang Z, Zhan Q, Eckert M, Zhu A, Chryplewicz A, De Jesus DF, Ren D, Kulkarni RN, Lengyel E, He C, and Chen M. RADAR: differential analysis of MeRIP-seq data with a random effect model. *Genome Biol* 20: 294, 2019.

**Table 4.1: Maternal and Fetal Pup Characteristics**

<b>Sample</b>	<b>Maternal Weight (g)</b>	<b>Number of Pups in Litter</b>	<b>Average Pup Weight (g)</b>	<b>Average Pup Heart Weight (g)</b>
Sham Exposure				
1	31.9	8	0.61	0.0038
2	34.1	10	0.56	0.0030
3	34.1	10	0.56	0.0026
4	33.8	10	0.60	0.0036
5	32.0	9	0.39	0.0023
<b>Average</b>	$33.2 \pm 0.51$	$9.4 \pm 0.40$	$0.54 \pm 0.04$	$0.0031 \pm 0.0003$
Nano-TiO <sub>2</sub> Exposure				
1	34.7	10	0.61	0.0038
2	36.0	10	0.66	0.0043
3	35.6	9	0.66	0.0039
4	31.7	10	0.34	0.0026
5	35.7	9	0.61	0.0037
<b>Average</b>	$33.7 \pm 0.79$	$9.6 \pm 0.24$	$0.58 \pm 0.06$	$0.0037 \pm 0.0003$

**Table 4.1: Maternal and fetal pup characteristics.** Dams from sham (n=5) and nano-TiO<sub>2</sub> (n=5) inhalation exposure were assessed. All weights given are wet weights.



**Graphical Abstract:**

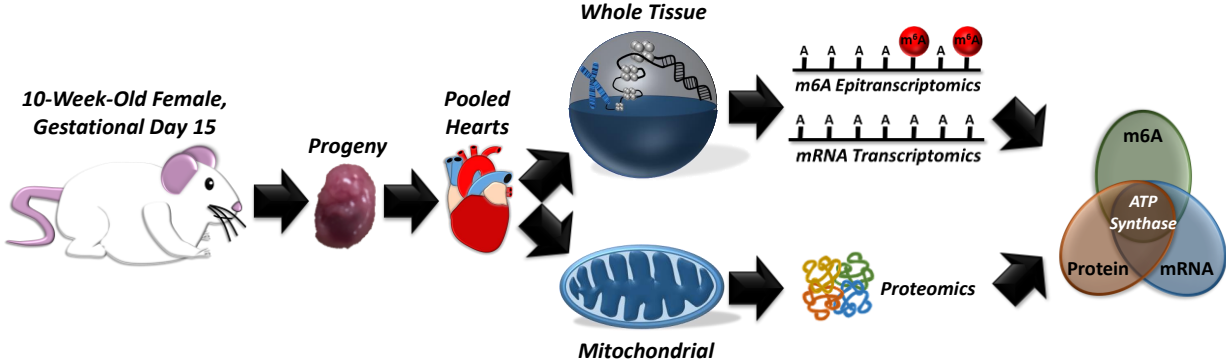


Figure 4.1:

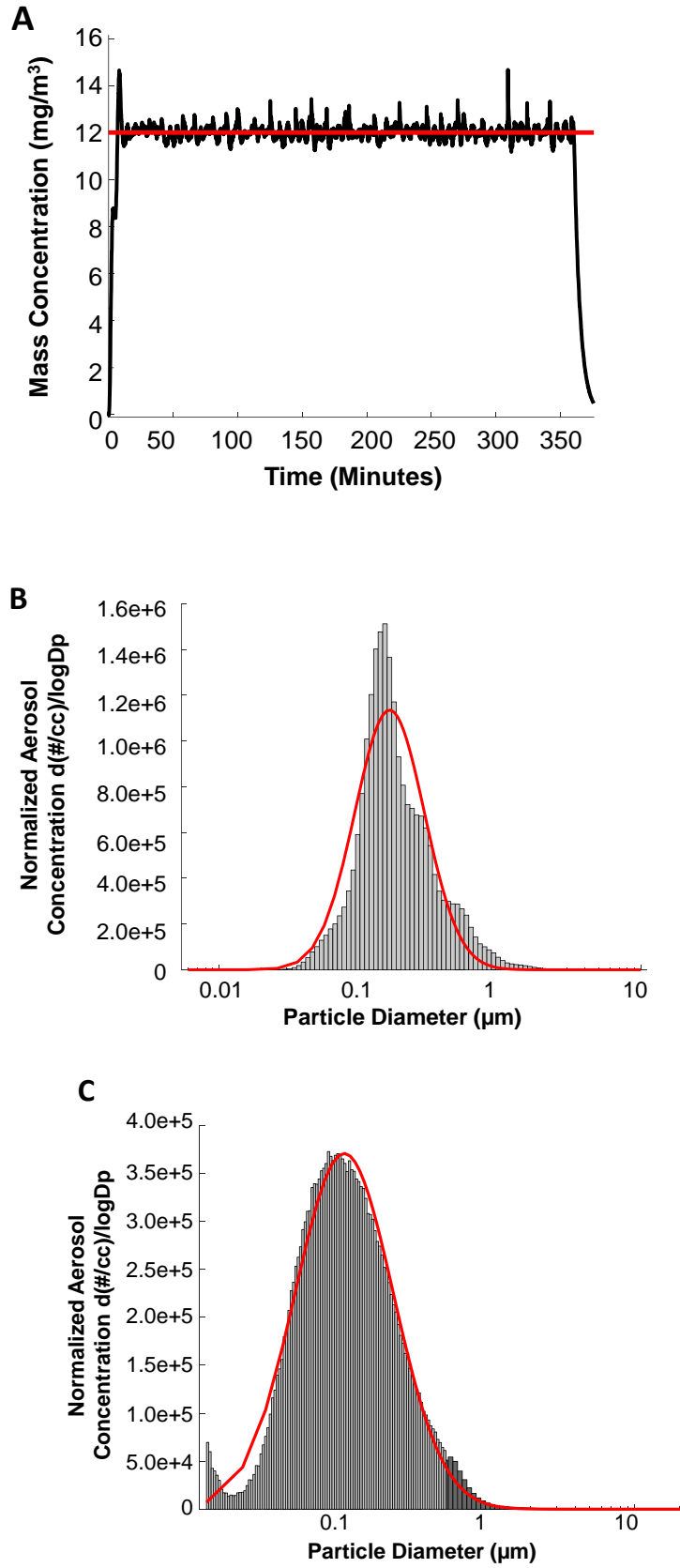
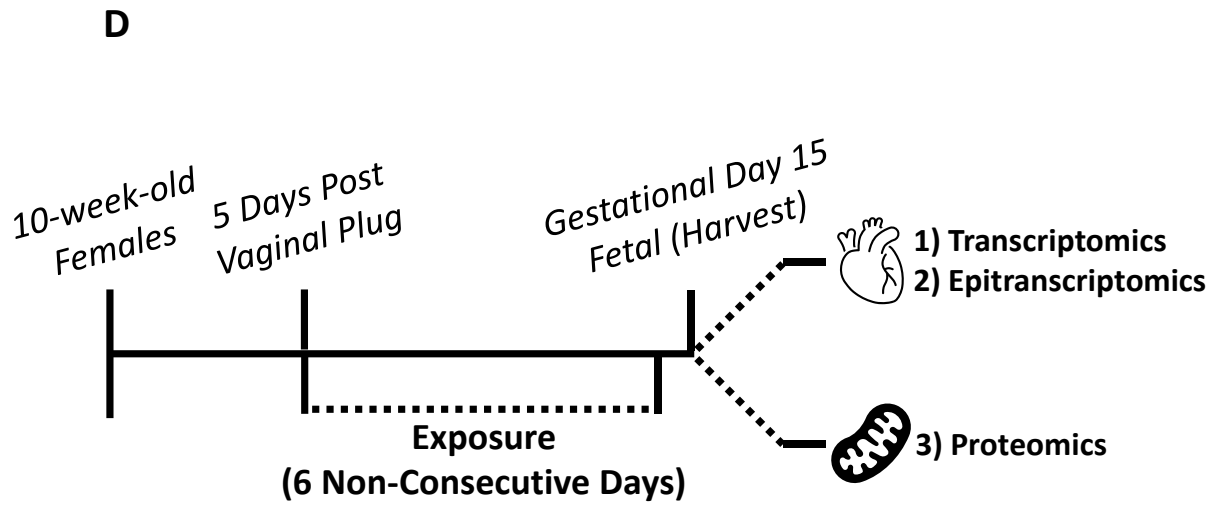


Figure 4.1:



**Figure 4.1: Characteristics of maternal whole-body inhalation exposure.** (A) A target aerosol mass concentration of  $12 \text{ mg/m}^3$  of engineered nano-TiO<sub>2</sub> was implemented for a period of 360 minutes per day for 6 non-consecutive days, over an 8-day period. These concentrations were verified by gravimetric measurements during each exposure, which resulted in an average mass concentration of  $12 \text{ mg/m}^3$  during the 360-minute period. (B) High-resolution electrical low-pressure impactor (ELPI+) indicated a geometric count median diameter (CMD) of 172 nm with a geometric standard deviation (GSD) of 1.96. (C) Scanning particle mobility sizer (SMPS) indicated a CMD of 112 nm with a GSD of 2.14. (D) Exposure model paradigm including the allocation of tissue on gestational day (GD) 15.

Figure 4:2:

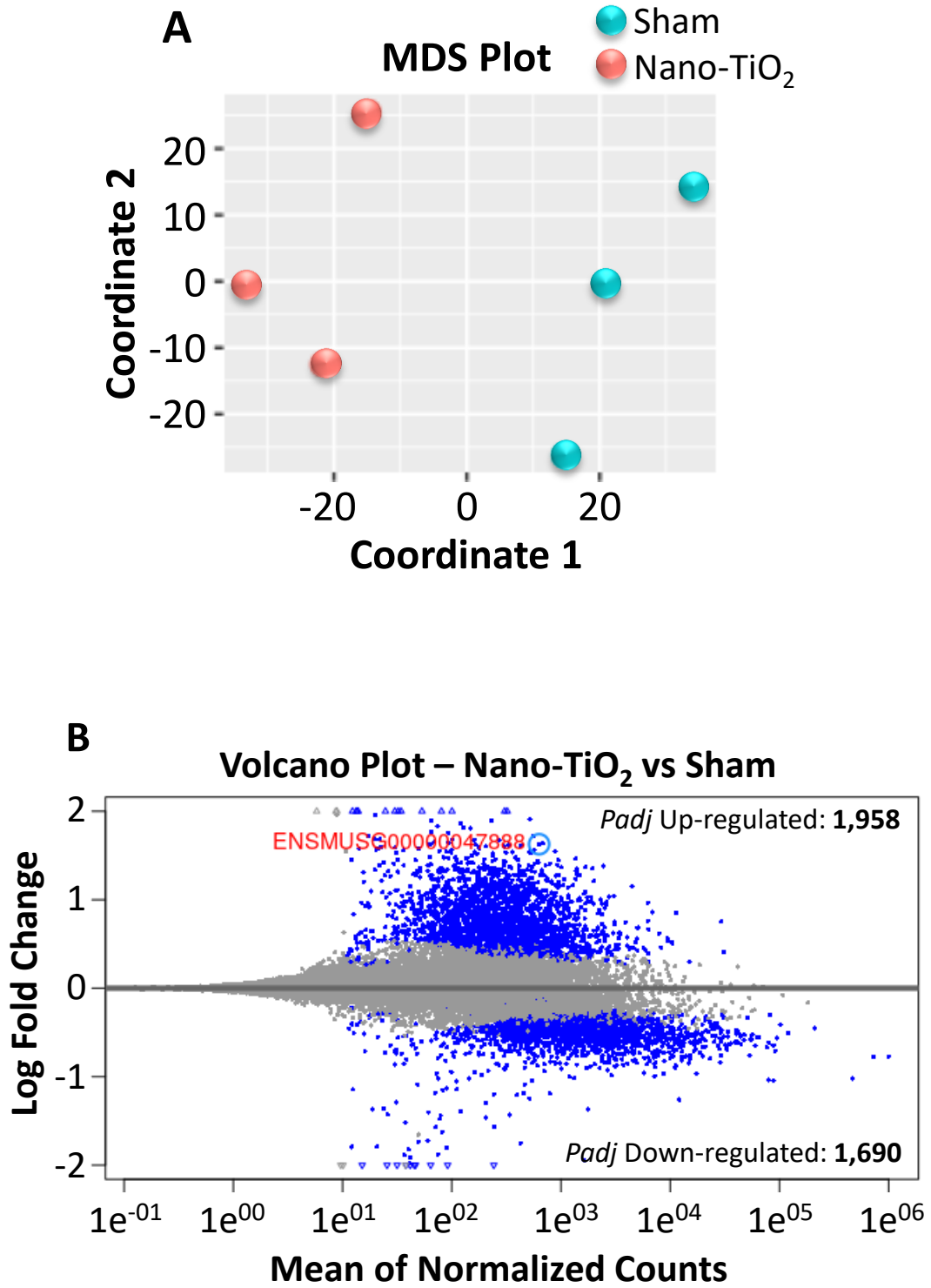


Figure 4.2:

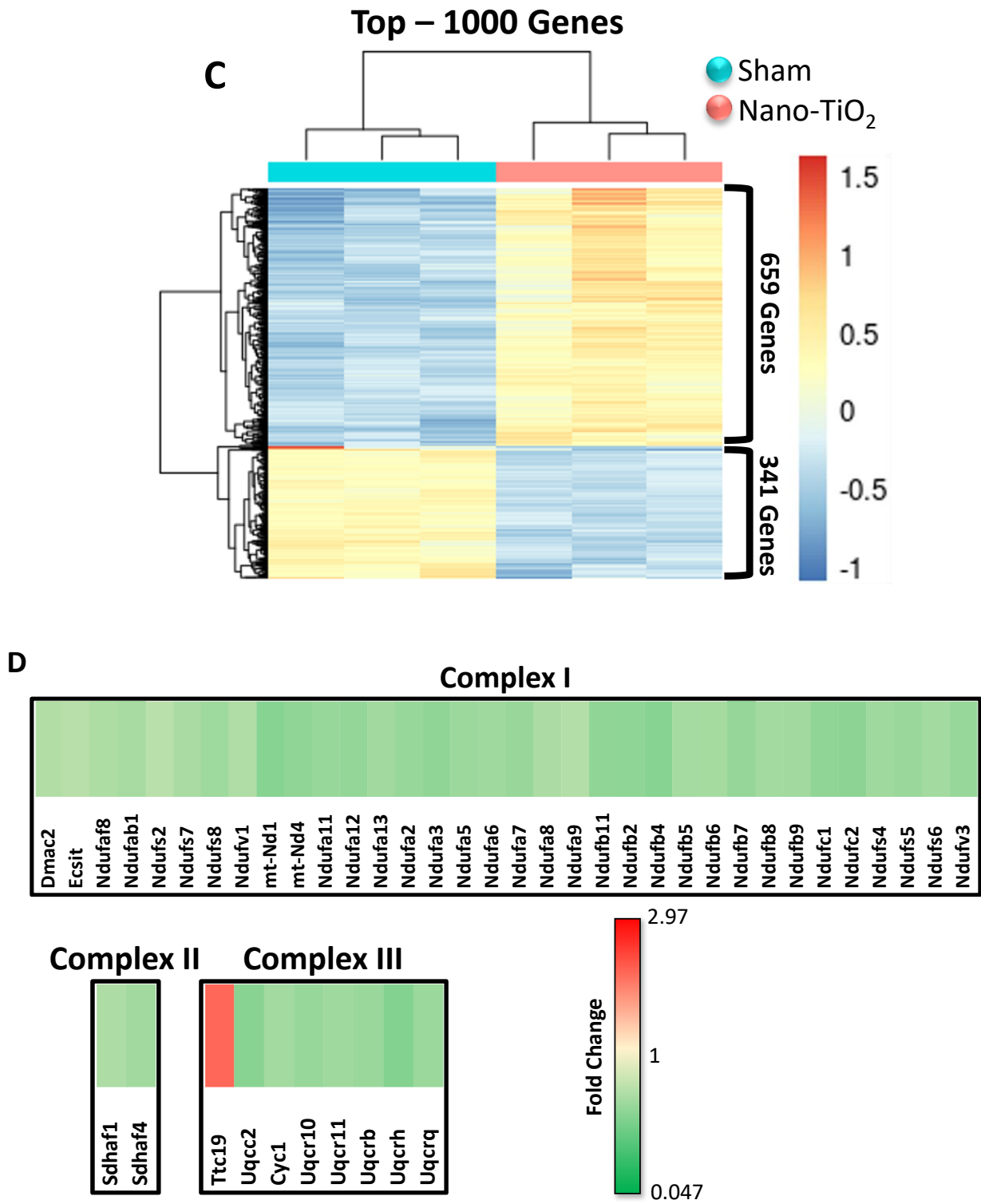
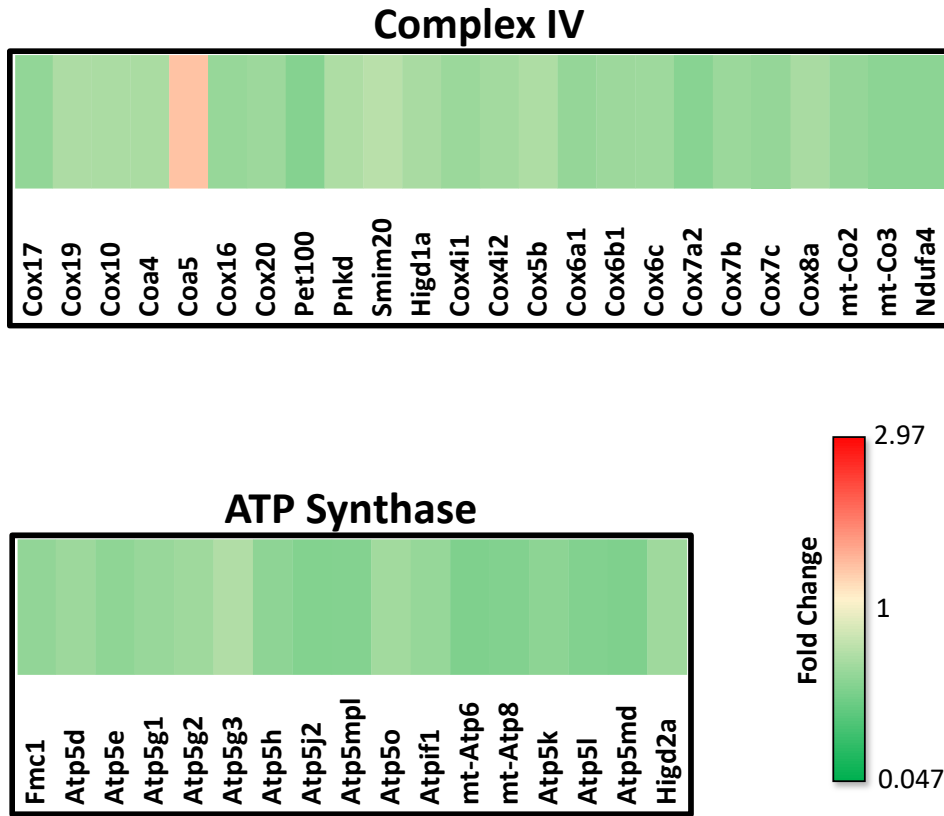


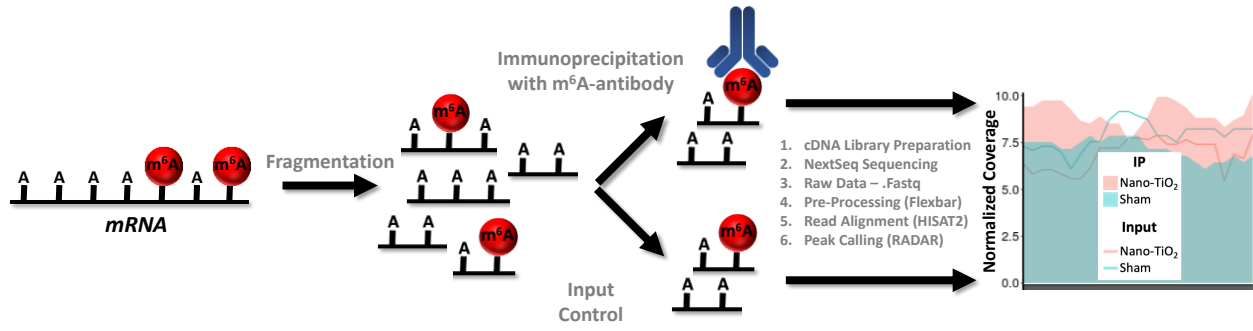
Figure 4.2D:



**Figure 4.2: Transcriptomic analysis of fetal cardiac tissue.** (A) Multidimensional Scaling (MDS) plot of sham (n=3) and nano-TiO<sub>2</sub> (n=3) gestationally exposed fetal progeny. (B) Volcano plot depicting the Log<sub>2</sub> fold change observed following differential expression analysis. The top gene (lowest *Padj* value) is listed. (C) Heatmap depicting the top 1,000 genes, as sorted in ascending order by *Padj* value. The provided scale is in Log<sub>2</sub> fold change. (D) Heatmap of differentially expressed mitochondrial genes within the electron transport chain oxidative phosphorylation pathway. Genes were classified based on MitoCarta3.0 (34). The provided scale is in fold change. Genes were differentially expressed if *Padj* ≤ 0.05, FDR = 0.05. Differences are illustrated as nano-TiO<sub>2</sub> (n=3) compared to sham (n=3). Sham = fetal progeny of maternal dams exposed to filtered air, Nano-TiO<sub>2</sub> = fetal progeny of maternal dams exposed to 12 mg/m<sup>3</sup> of nano-TiO<sub>2</sub> for 360-minute periods for 6 days, Complex I = NADH:ubiquinone oxidoreductase, Complex II = succinate dehydrogenase, Complex III = coenzyme Q – cytochrome c reductase, Complex IV = cytochrome c oxidase, ATP Synthase = mitochondrial electron transport chain complex V.



Figure 4.3:



**Figure 4.3: Schematic overview of N<sup>6</sup>-methyladenosine (m<sup>6</sup>A) analyses.** First, RNA was isolated from fetal pup hearts. Next, RNA was fragmented, with an average fragment size of 297 base pairs. 10% of each sample was saved as an input control while 90% of the sample was immunoprecipitated with m<sup>6</sup>A antibodies. RNA was barcoded and reverse transcribed into cDNA. Sequencing was performed on the Illumina NextSeq with paired-end (PE) 2x50 reads. Adapters were trimmed from Fastq files, files were aligned to the mouse genome, and differential peak calling was performed. Sham = fetal progeny of maternal dams exposed to filtered air, Nano-TiO<sub>2</sub> = fetal progeny of maternal dams exposed to 12 mg/m<sup>3</sup> of nano-TiO<sub>2</sub> for 360-minute periods for 6 days, Input = unprocessed mRNA, IP = mRNA derived from immunoprecipitation with m<sup>6</sup>A antibodies.

Figure 4.4:

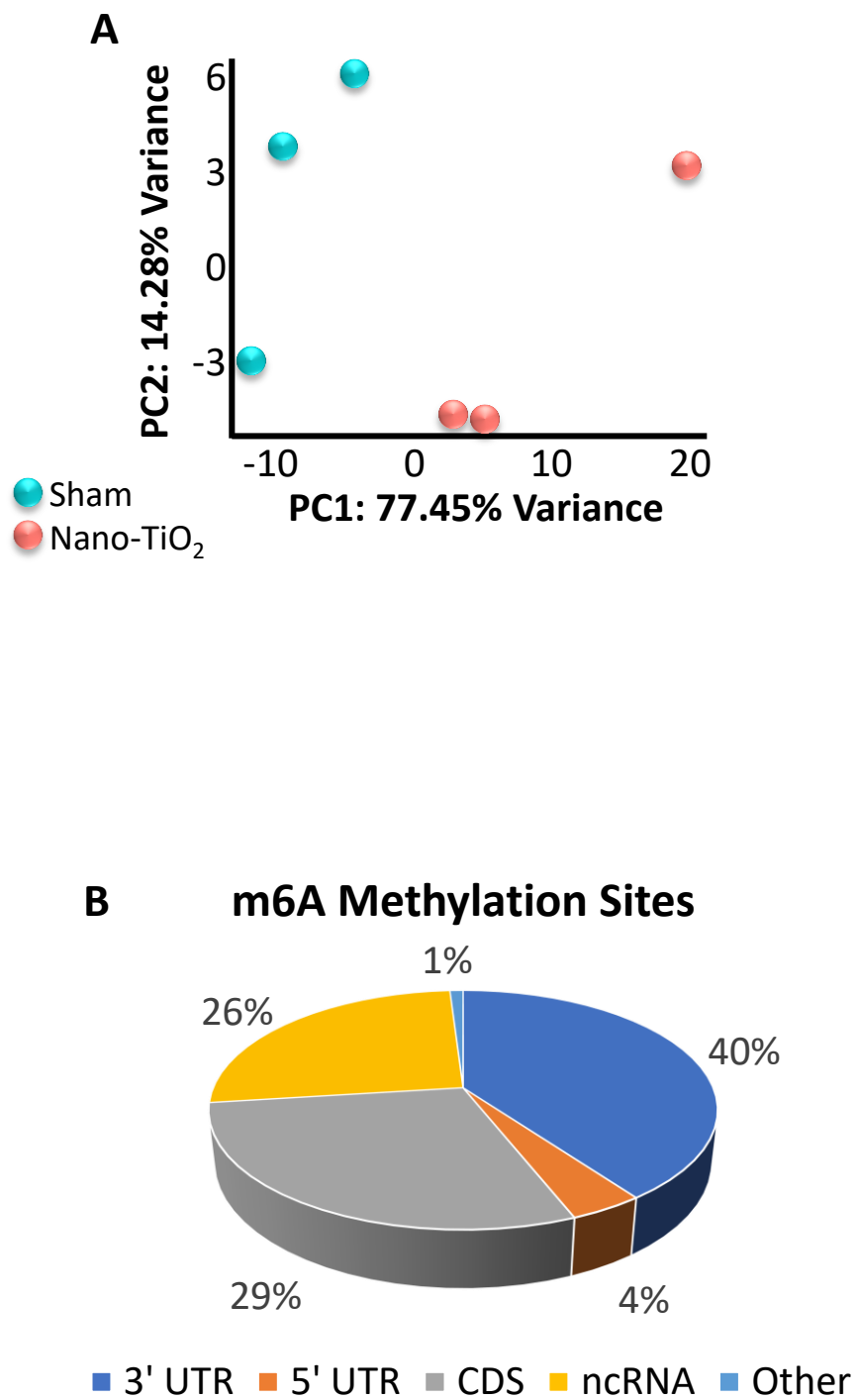


Figure 4.4:

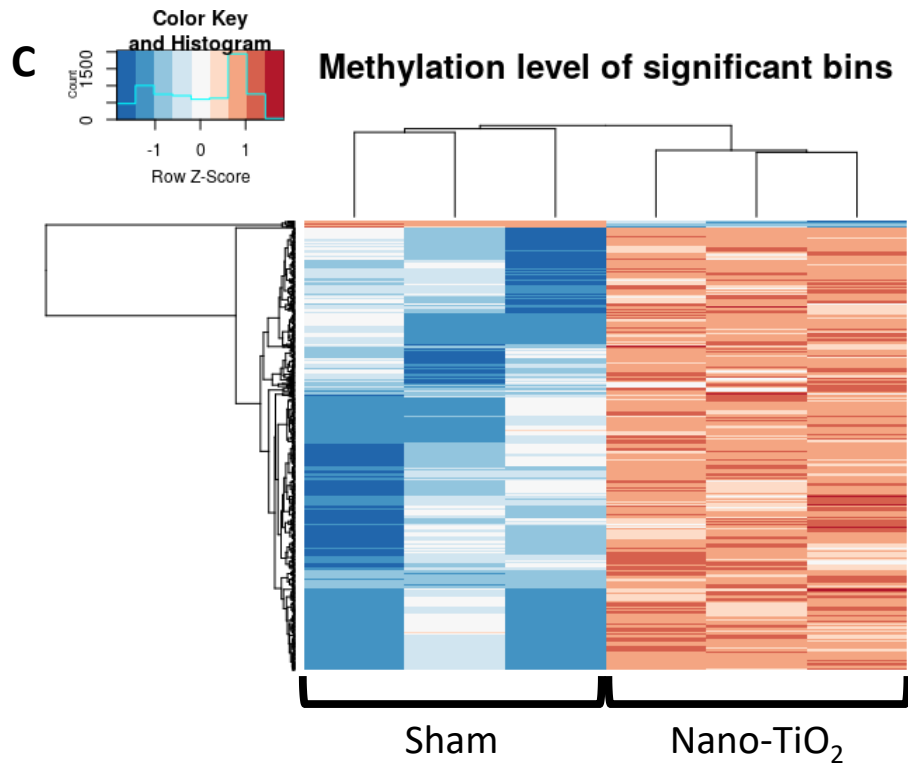
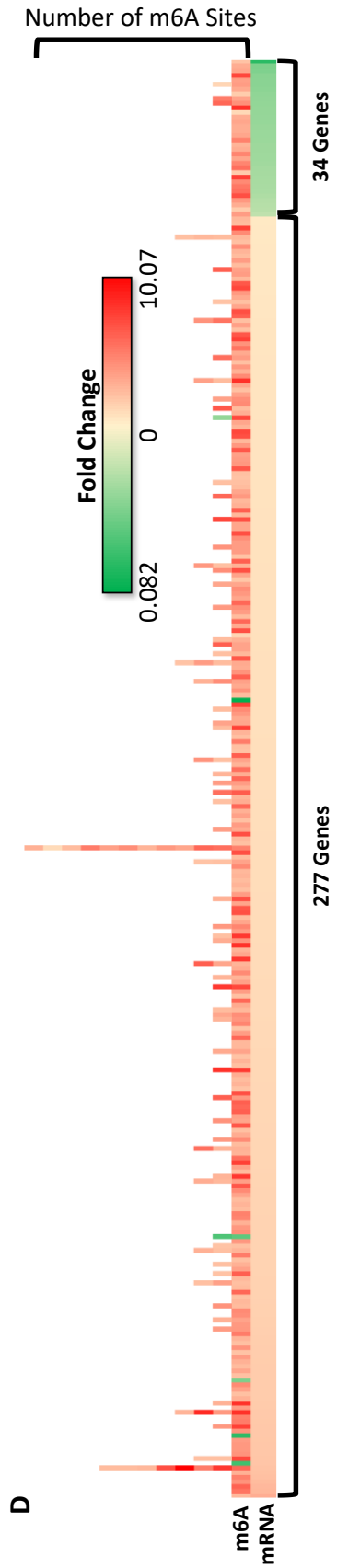


Figure 4.4D:



**Figure 4.4: Epitranscriptomic analysis of fetal cardiac tissue.** (A) Principal Component Analysis (PCA) plot of sham (n=3) and nano-TiO<sub>2</sub> (n=3) gestationally exposed fetal progeny. (B) Pie chart depicting the distribution of m<sup>6</sup>A sites identified by location across genomic space. (C) Heatmap of the 1,135 differentially m<sup>6</sup>A methylated sites across 921 genes. Z-Score is defined as (gene expression value in sample of interest) – (mean expression across all samples)/standard deviation. Bins were defined as 25 base-pair regions. (D) Heatmap of the shared 331 genes that were both identified in the transcriptomic and epitranscriptomic analyses. The provided scale is in fold change. Genes were differentially expressed if  $P_{adj} \leq 0.10$ , FDR=0.10. Sham = fetal progeny of maternal dams exposed to filtered air, Nano-TiO<sub>2</sub> = fetal progeny of maternal dams exposed to 12 mg/m<sup>3</sup> of nano-TiO<sub>2</sub> for 360-minute periods for 6 days, 3' UTR = 3' untranslated region of a gene, 5' UTR = 5' untranslated region of a gene, CDS = coding DNA sequence, ncRNA = non-coding RNA, Other = other regions in genomic space not specified.

Figure 4.5:

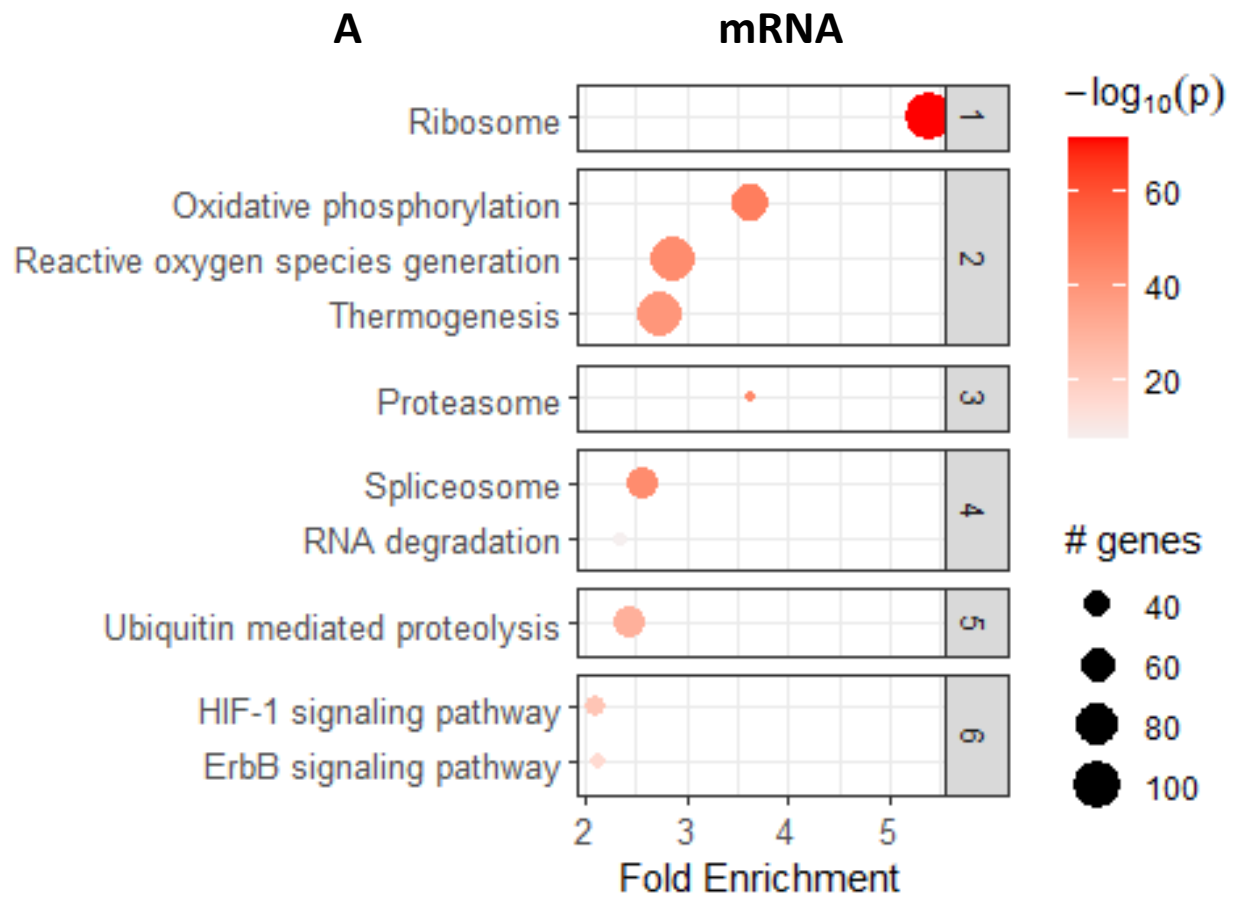
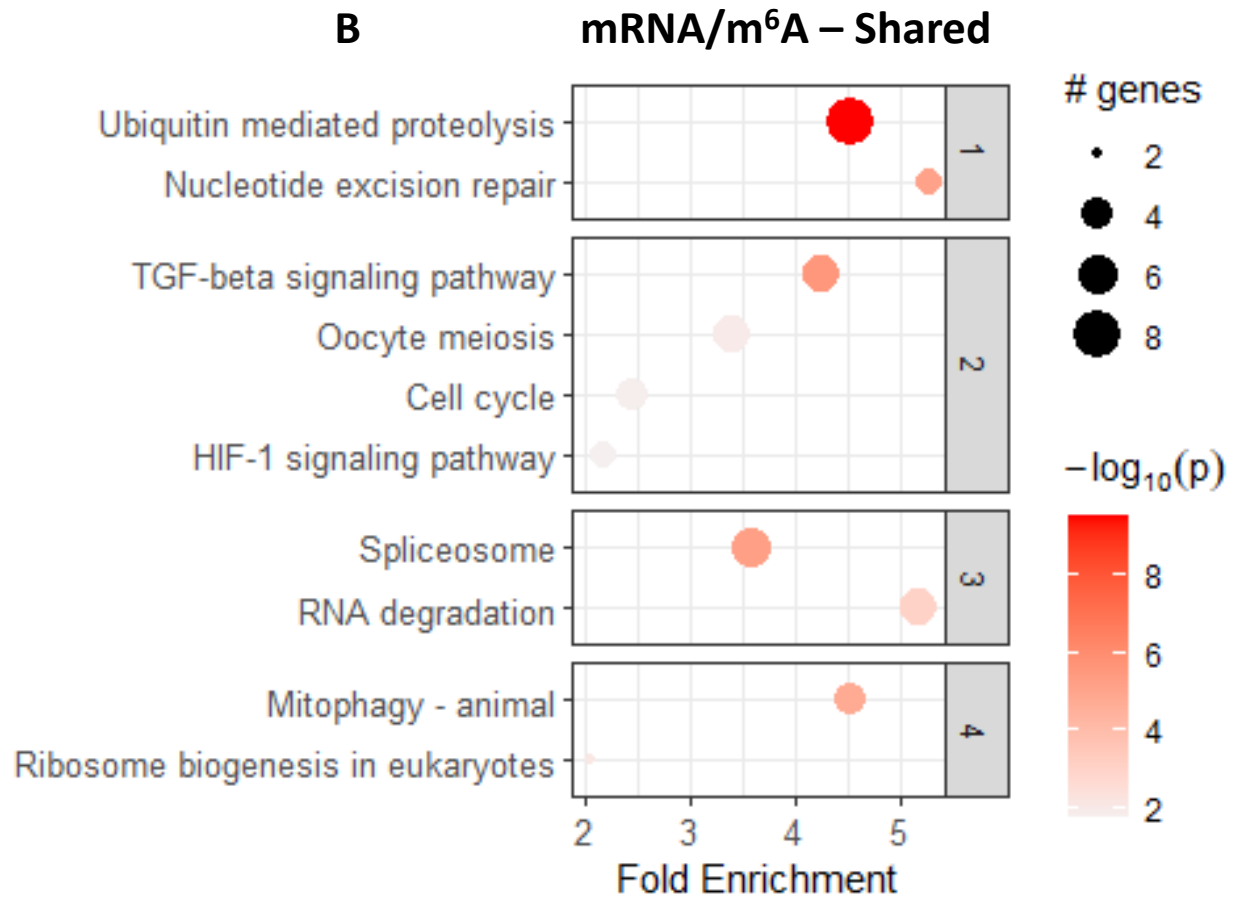


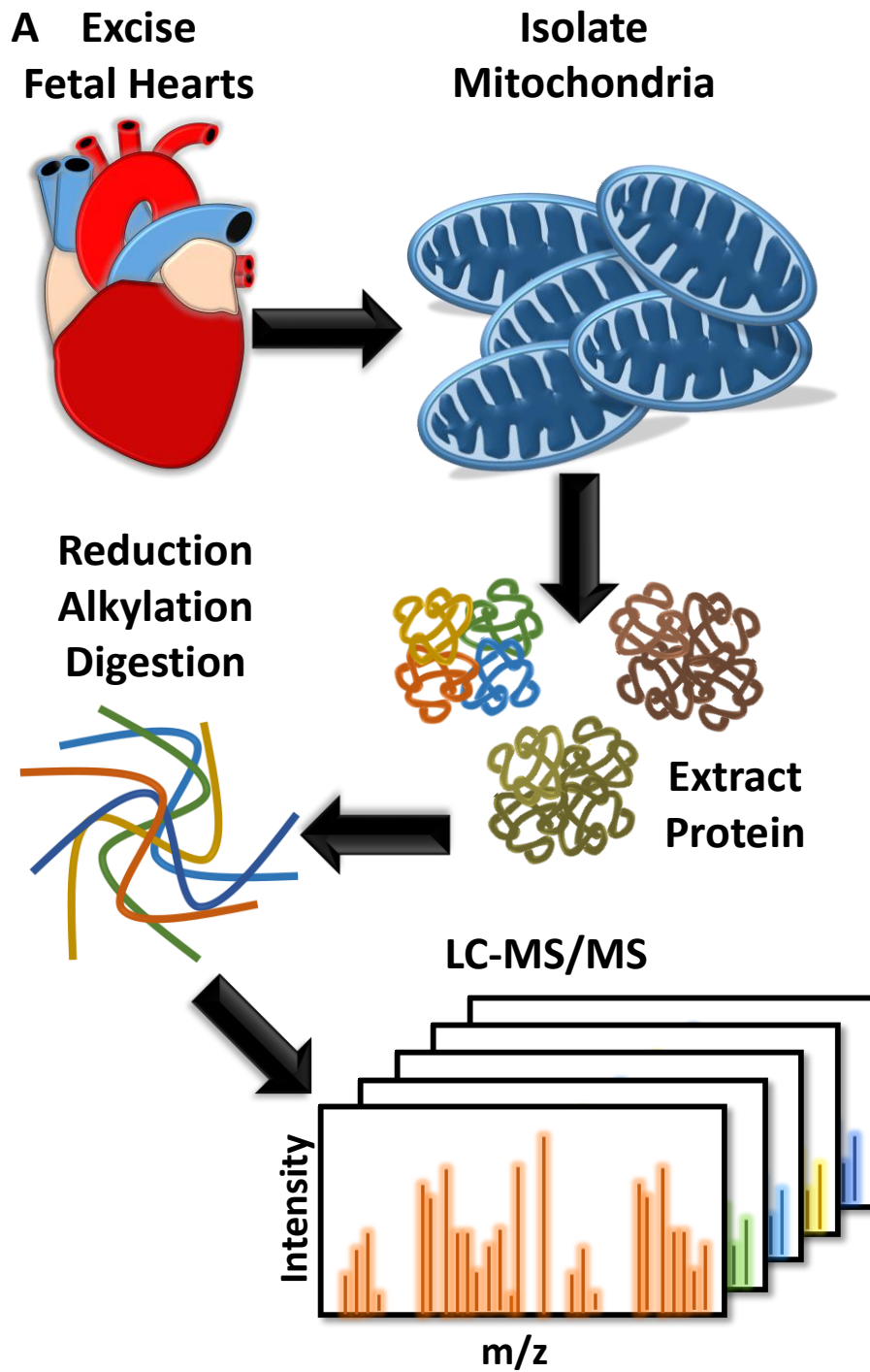
Figure 4.5:







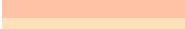
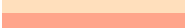
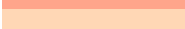

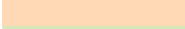

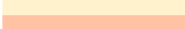
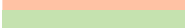
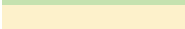

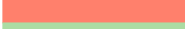














**Figure 4.5: Pathway analysis of differentially expressed genes.** (A) Pathway analysis of the 3,648 genes differentially expressed in the transcriptomic analysis. (B) Pathway analysis of those genes (311) that also coincided with differentially methylated sites. Both pathways are presented as hierarchically clustered pathways, with the top (A) six and (B) four pathways represented along with other similar pathways within each clustered group. Genes were differentially expressed if  $P_{adj} \leq 0.05$ , FDR=0.05

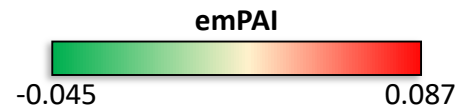
Figure 4.6:



**Figure 4.6:**

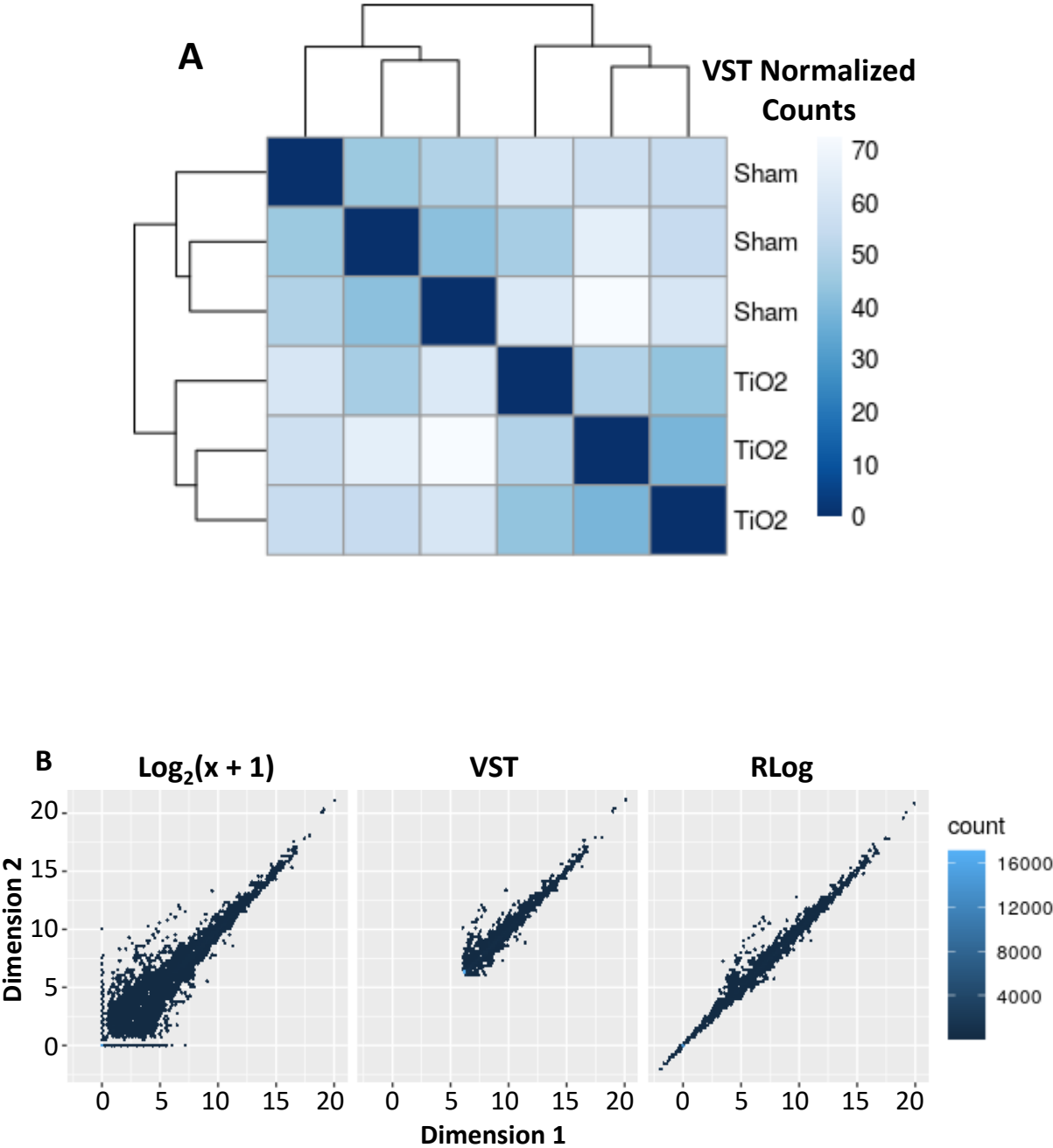
**B**

Protein	emPAI – Sham	emPAI – Exp	Exp vs. Sham	Pathway
Got2	0.0922	0.0684		Metabolism > Amino acid metabolism
Pdha1	0.0416	0.0576		Metabolism > Pyruvate metabolism
Pdhb	0.0795	0.0969		Metabolism > Pyruvate metabolism
Cs	0.1134	0.1202		Metabolism > TCA cycle
Fh1	0.0661	0.0938		Metabolism > TCA cycle
Ogdh	0.0373	0.0472		Metabolism > TCA cycle
Prdx3	0.0890	0.0437		Metabolism > ROS and glutathione metabolism
Hadha	0.0756	0.0852		Metabolism > Lipid metabolism
Slc25a4	0.2119	0.2047		Metabolism > Nucleotide metabolism
Slc25a5	0.2284	0.2284		Metabolism > Nucleotide metabolism
Tufm	0.0558	0.0732		Mitochondrial central dogma > Translation
Ndufs1	0.0862	0.0759		OXPHOS > Complex I
Ndufs7	0.0446	0.0444		OXPHOS > Complex I
Ndufv2	0.0840	0.0715		OXPHOS > Complex I
Ndufa13	0.1498	0.1906		OXPHOS > Complex I
Sdha	0.0730	0.0581		OXPHOS > Complex II
Cox6b1	0.1152	0.1152		OXPHOS > Complex IV
Atp5a1	0.2627	0.2440		OXPHOS > Complex V
Atp5b	0.3457	0.3169		OXPHOS > Complex V
Atp5c1	0.1112	0.0827		OXPHOS > Complex V
Atp5pb	0.0952	0.0841		OXPHOS > Complex V
Hspd1	0.1077	0.1082		Protein import, sorting and homeostasis
Hspe1	0.2702	0.3567		Protein import, sorting and homeostasis
Phb	0.0961	0.1073		Protein import, sorting and homeostasis
Phb2	0.1365	0.1277		Protein import, sorting and homeostasis
Vdac1	0.1309	0.1015		Mitochondrial permeability transition pore
Vdac3	0.0622	0.0703		Mitochondrial permeability transition pore

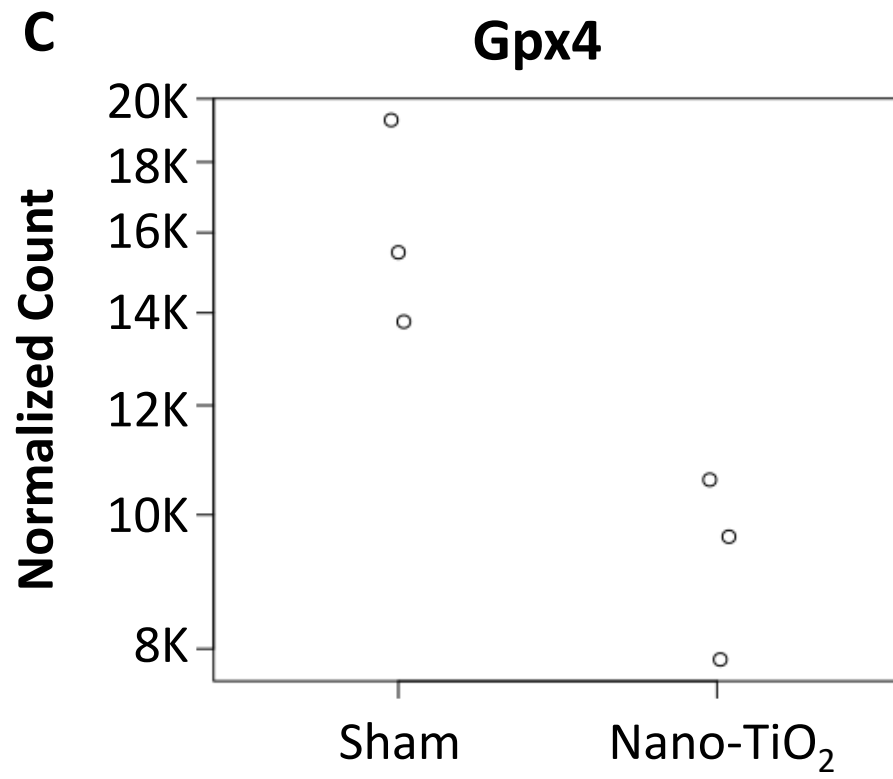


**Figure 4.6: Mitochondrial proteomics.** (A) Schematic depicting the processes of mitochondrial isolation, protein extraction, peptide preparation, and peak identification. (B) Mitochondrial proteins that were identified with high confidence in the analyses. The provided scale is the difference between emPAI values between the sham and nano-TiO<sub>2</sub> groups. Proteins are organized based on MitoCarta3.0 designations (34). Sham = fetal progeny of maternal dams exposed to filtered air, Exp = fetal progeny of maternal dams exposed to 12 mg/m<sup>3</sup> of nano-TiO<sub>2</sub> for 360-minute periods for 6 days, LC-MS/MS = liquid chromatography with tandem mass spectrometry.

Supplemental Figure 4.1:

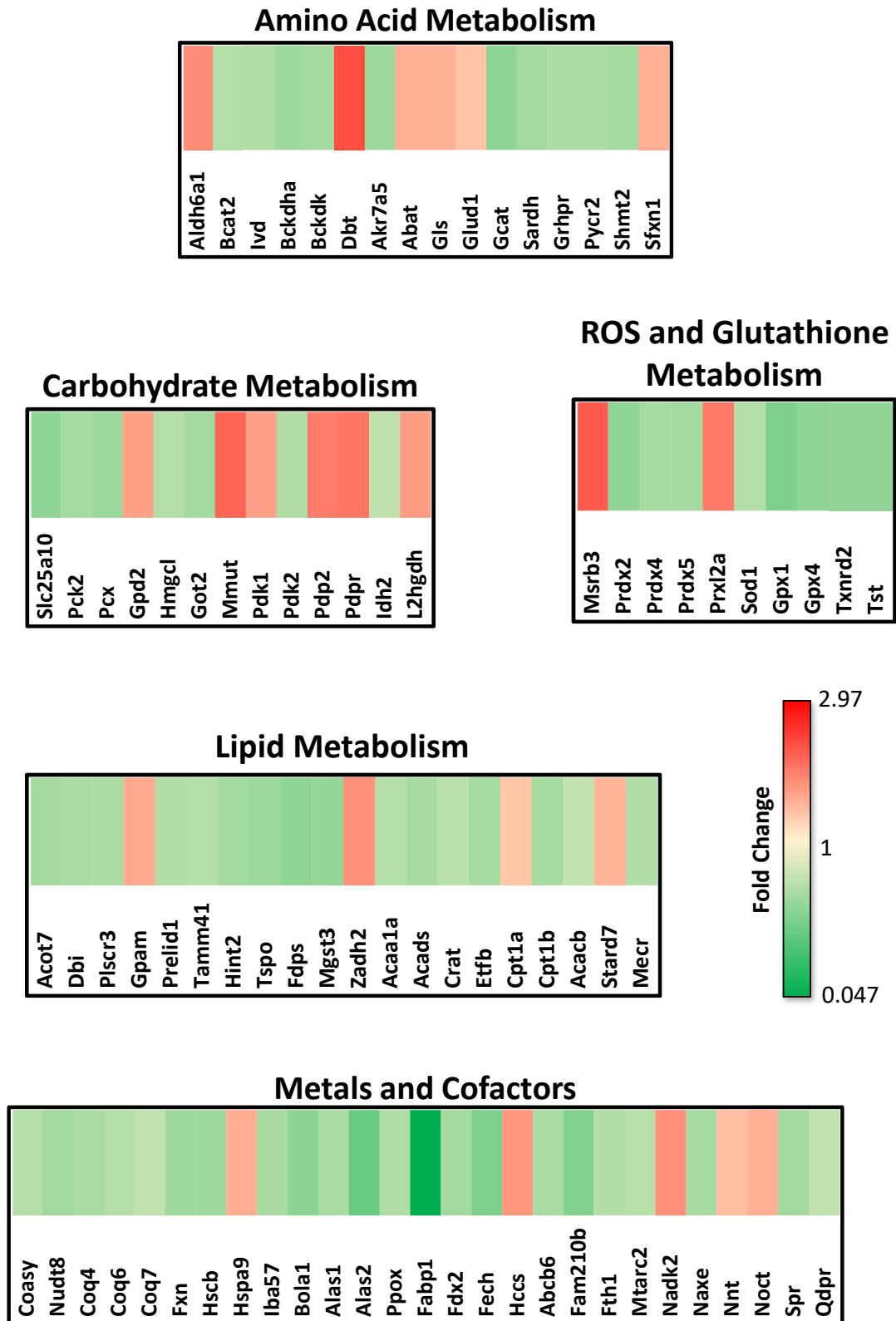


Supplemental Figure 4.1:



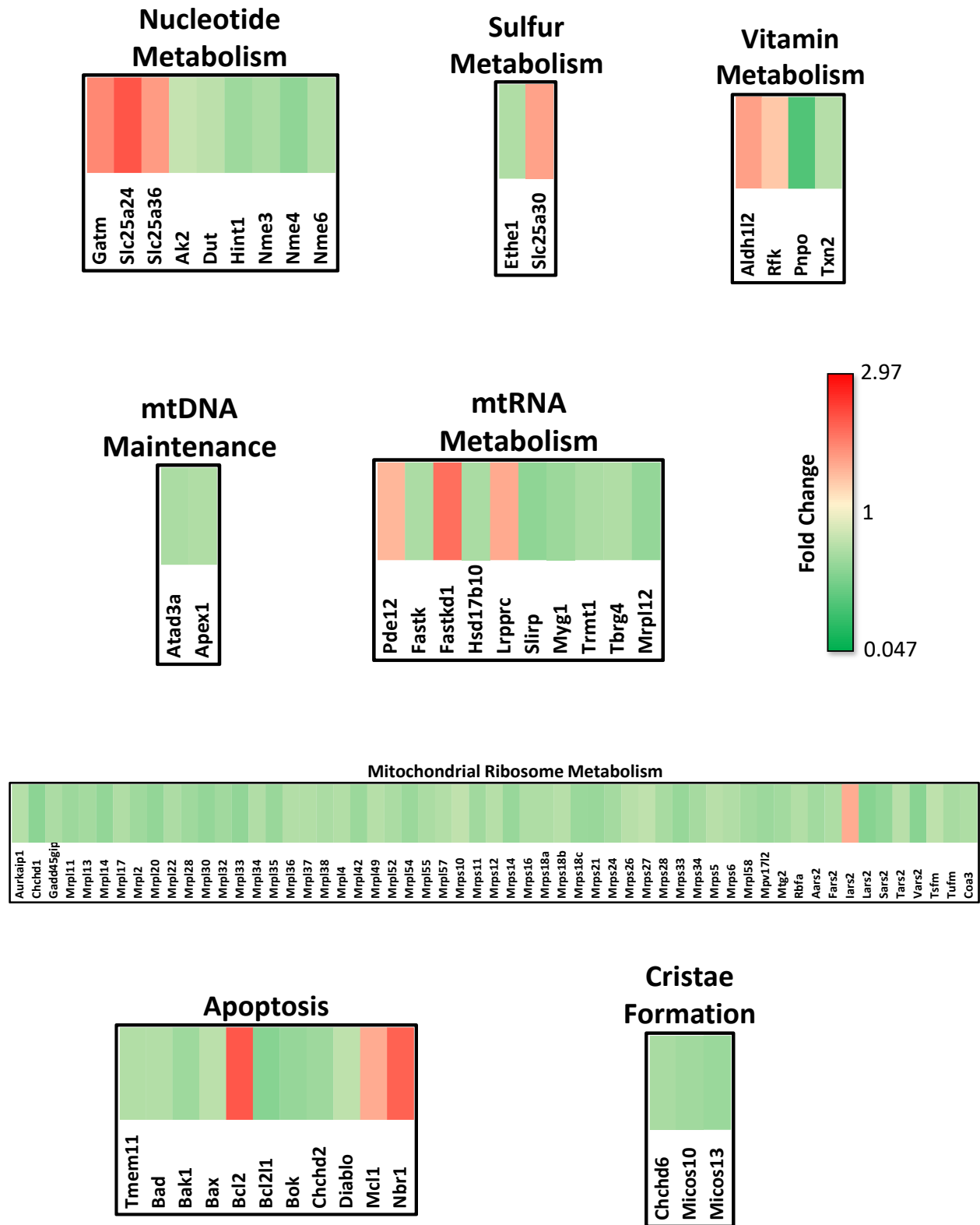
**Supplemental Figure 4.1: Transcriptomic processing and pre-processing.** (A) Sample distribution heatmap using variance stabilizing transformation (VSD) normalized counts. (B) Multidimensional Scaling (MDS) of counts that are  $\text{Log}_2$  transformations of normalized counts (left), VST (middle), and regularized-logarithm (rlog) transformations (right). (C) An example of normalized counts for Gpx4 in the sham (n=3) and nano-TiO<sub>2</sub> (n=3) groups. Genes were differentially expressed if  $P_{adj} \leq 0.05$ , FDR=0.05. Sham = fetal progeny of maternal dams exposed to filtered air, Nano-TiO<sub>2</sub> = fetal progeny of maternal dams exposed to 12 mg/m<sup>3</sup> of nano-TiO<sub>2</sub> for 360-minute periods for 6 days, Gpx4 = mitochondrial glutathione peroxidase 4.

Supplemental Figure 4.2:

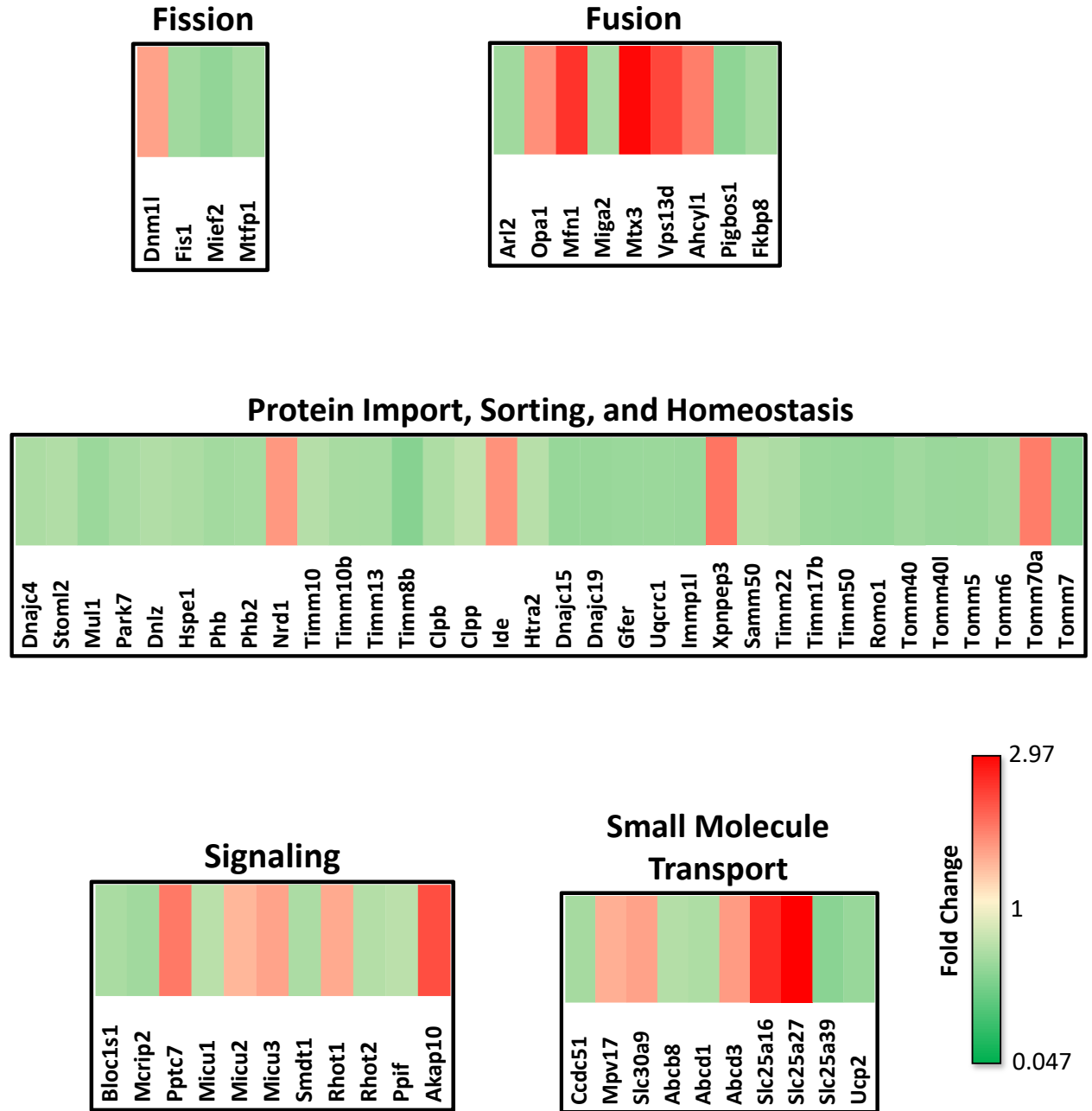




Supplemental Figure 4.2:



Supplemental Figure 4.2:

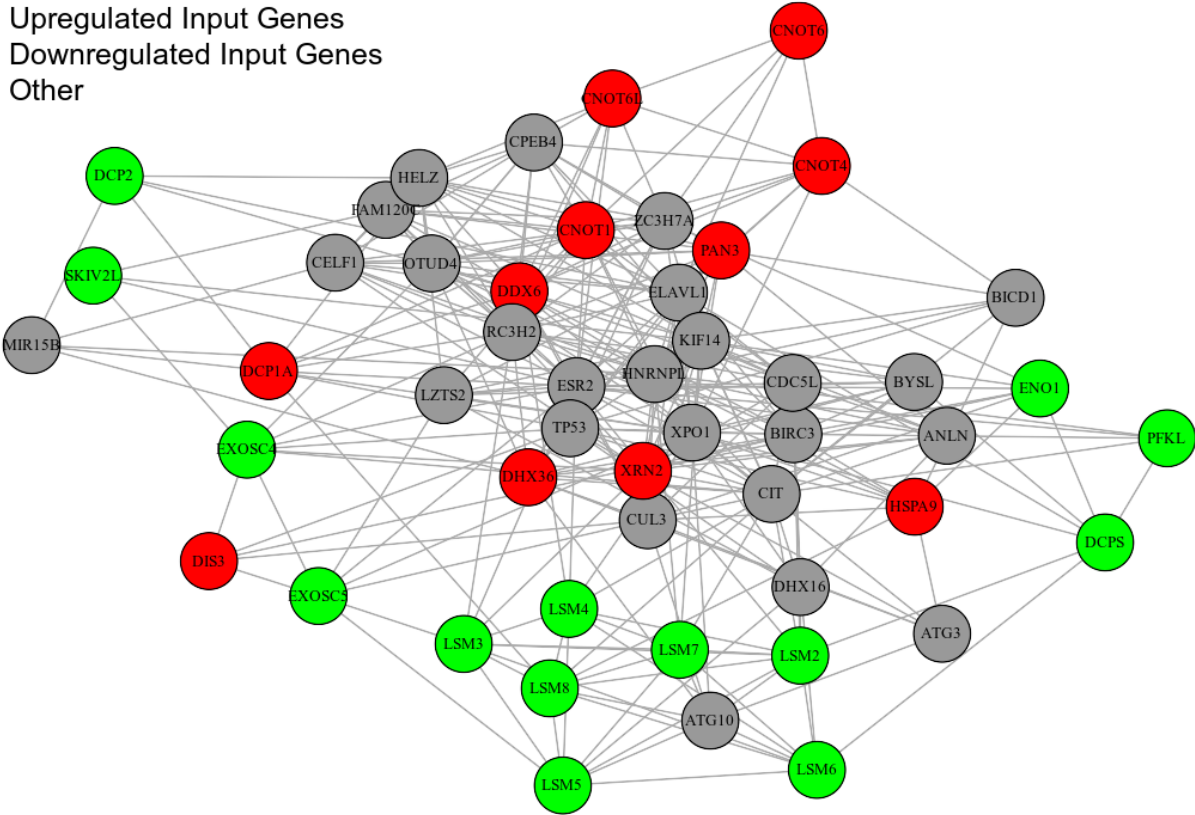


**Supplemental Figure 4.2: Differentially expressed mitochondrial genes not belonging to oxidative phosphorylation.** (A) Heatmap of differentially expressed mitochondrial genes. Genes were classified based on MitoCarta3.0. The provided scale is in fold change. Genes were differentially expressed if  $P_{adj} \leq 0.05$ , FDR=0.05. Differences are illustrated as nano-TiO<sub>2</sub> (n=3) compared to sham (n=3). Sham = fetal progeny of maternal dams exposed to filtered air, Nano-TiO<sub>2</sub> = fetal progeny of maternal dams exposed to 12 mg/m<sup>3</sup> of nano-TiO<sub>2</sub> for 360-minute periods for 6 days.

Supplemental Figure 4.3:

### A RNA Degradation Pathway – mRNA

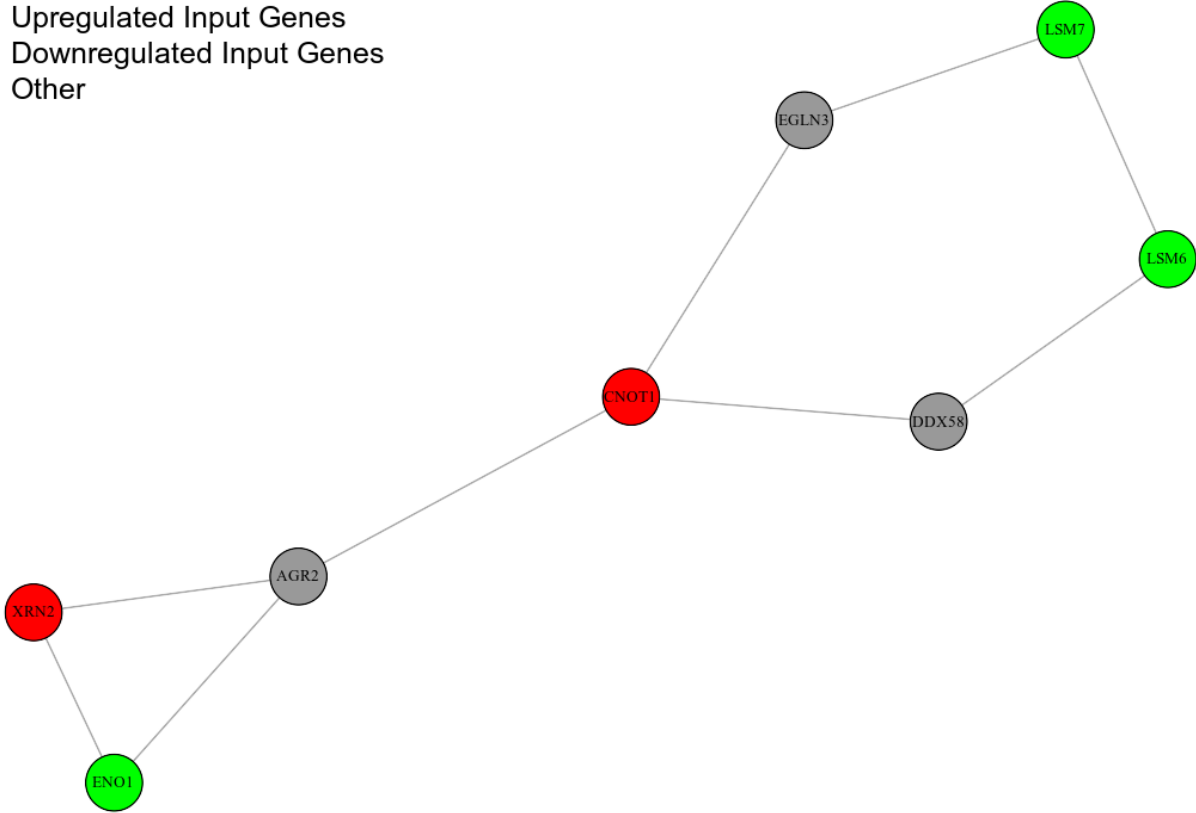
- Upregulated Input Genes
- Downregulated Input Genes
- Other



Supplemental Figure 4.3:

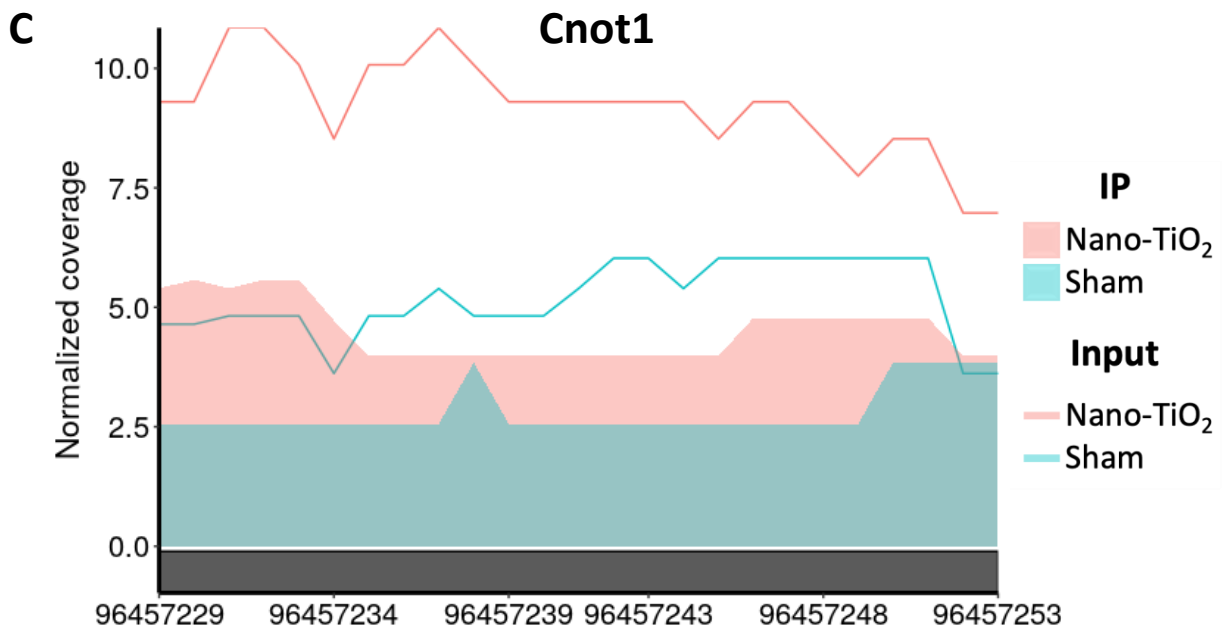
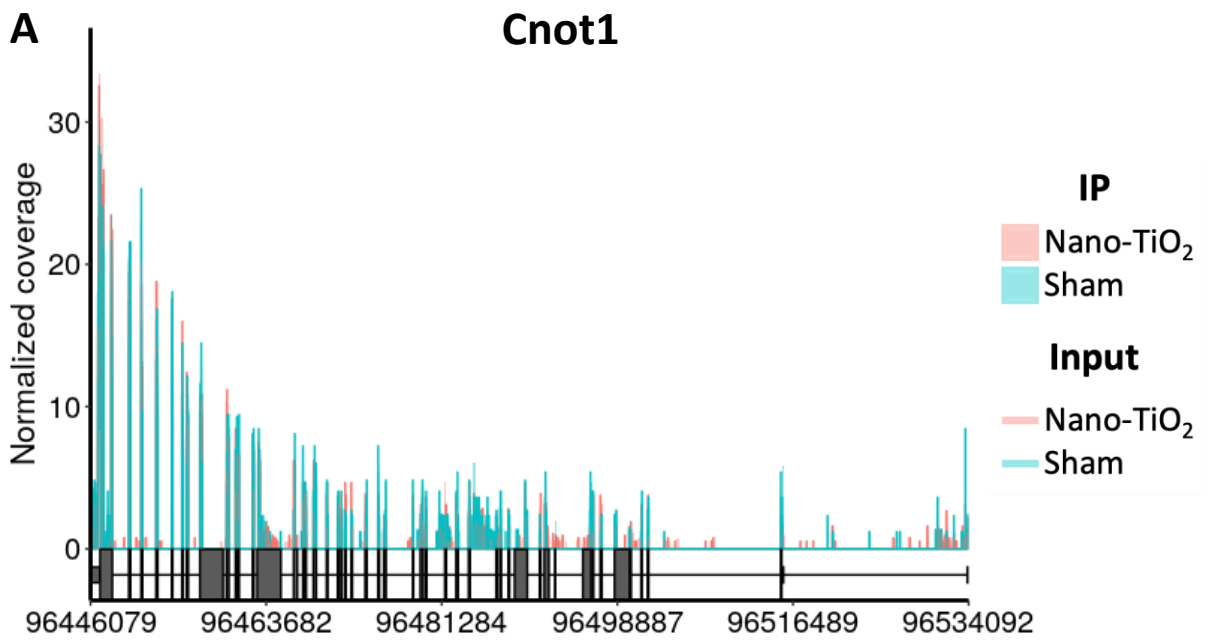
**B RNA Degradation Pathway – mRNA/m6A Shared**

- Upregulated Input Genes
- Downregulated Input Genes
- Other

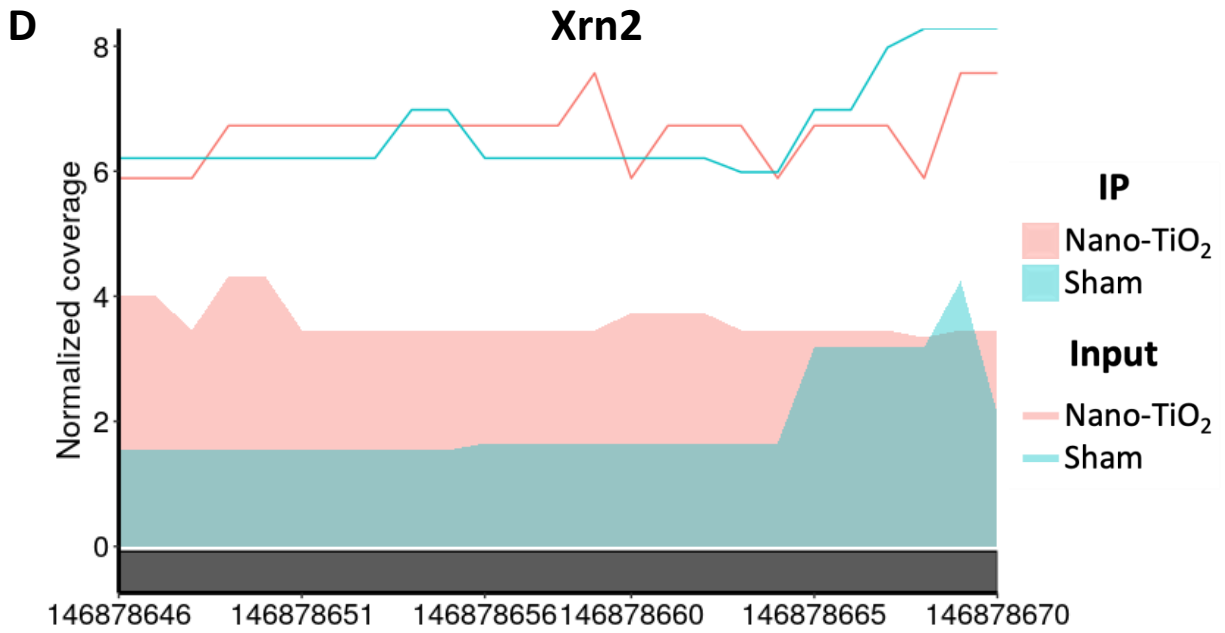
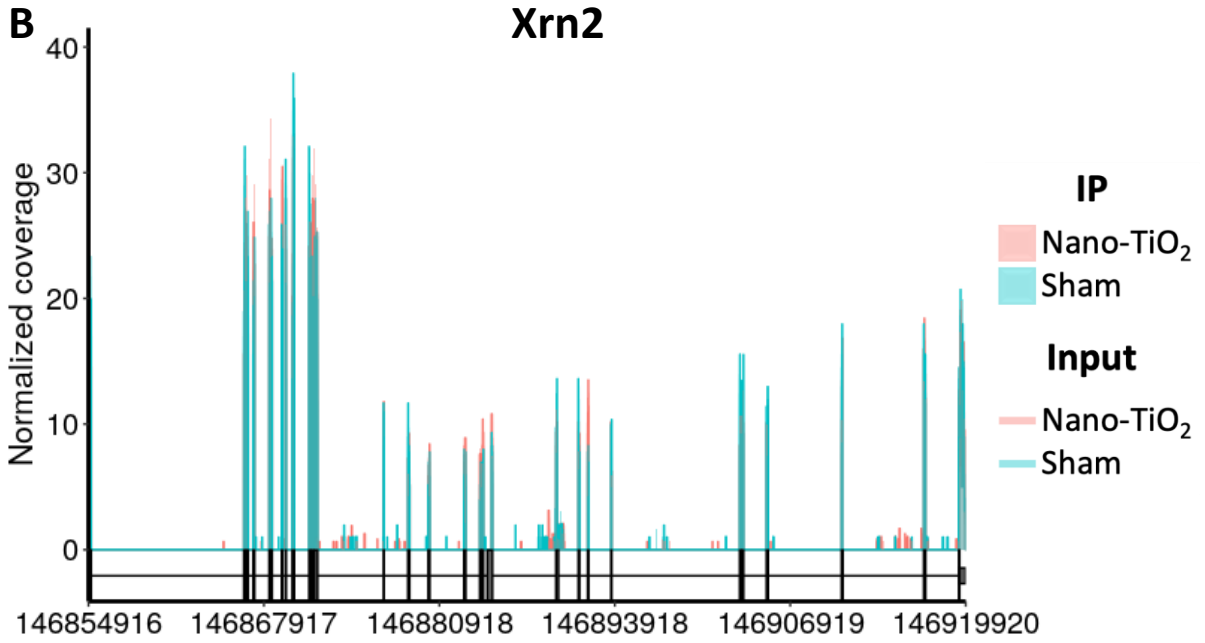


**Supplemental Figure 4.3: RNA Degradation pathway identified through PathFindR.** (A) Of the 3,648 genes differentially expressed in the transcriptomic data between sham (n=3) and nano-TiO<sub>2</sub> (n=3), the highlighted genes were identified in the RNA degradation pathway. (B) Of the shared 311 genes between the mRNA and m<sup>6</sup>A peak analysis, the highlighted genes were identified in the RNA degradation pathway. “Other” indicates genes not shown to be differentially expressed between sham and nano-TiO<sub>2</sub>. Genes were differentially expressed if  $P_{adj} \leq 0.05$ , FDR=0.05. Sham = fetal progeny of maternal dams exposed to filtered air, Nano-TiO<sub>2</sub> = fetal progeny of maternal dams exposed to 12 mg/m<sup>3</sup> of nano-TiO<sub>2</sub> for 360-minute periods for 6 days.

Supplemental Figure 4.4:



Supplemental Figure 4.4:





**Supplemental Figure 4.4: N<sup>6</sup>-methyladenosine (m<sup>6</sup>A) peak calling of RNA Degradation pathway genes.** The entire gene region of (A) Cnot1 and (B) Xrn2 reveals m<sup>6</sup>A methylation across the gene. Normalized coverage to input samples was gated across samples to display regions where m<sup>6</sup>A was significantly increased for (C) Cnot1 and (D) Xrn2. IP expression is designated by filled boxes while input samples are represented by lines. The x-axis represents the genomic location. Genes were differentially expressed if  $P_{adj} \leq 0.10$ , FDR=0.10. Sham = fetal progeny of maternal dams exposed to filtered air, Nano-TiO<sub>2</sub> = fetal progeny of maternal dams exposed to 12 mg/m<sup>3</sup> of nano-TiO<sub>2</sub> for 360-minute periods for 6 days, Input = unprocessed mRNA, IP = mRNA derived from immunoprecipitation with m<sup>6</sup>A antibodies.

## Chapter 5: General Discussion

The work within this dissertation aims to ascertain the repercussions of inhalation exposure to engineered nanomaterials (ENM), particularly nano-TiO<sub>2</sub>, during gestation on offspring cardiac function, the epigenetic and epitranscriptomic mechanism that contribute to these detriments, as well as the potential for therapeutic prevention with the implementation of an antioxidant defense strategy. With the proliferative increase in nanoparticle applicability in multiple industries, comes also the necessity for thorough evaluation and understanding of any adverse effects that such ubiquitous exposure can emanate. The research herein, attempts to ascertain these adverse effects through approaches that include examination of functional cardiac effects, down to the organelle that plays a pivotal role in heart contraction, the mitochondrion, and furthermore the chemical modifications that likely contribute to sustained dysfunction into later stages of life in a mouse model. The long-term goal of the research performed was to identify mechanisms contributing to the pathological effects of xenobiotic exposure as a prerequisite to developing strategies for reducing risks to public health.

The central hypothesis is that changes in the m<sup>6</sup>A methylome, concomitant with an altered mitochondrial proteome at the fetal stage, precipitate cardiac contractile dysfunction that is sustained into adulthood following maternal ENM inhalation exposure. Sustained dysfunction may be averted through limiting ROS via overexpression of mPHGPx. The particularly intriguing aspect of this central hypothesis is the idea of epitranscriptomic remodeling and the implications this holds. Within my research, the focus really does not stray from understanding the effects of maternal toxicant inhalation exposure during gestation on the offspring heart function and mitochondrial function. However, the concept of reprogramming may have even more detrimental outcomes that include inclining the system to be more susceptible to diseases that also alter similar pathways such as metabolism. To date, this possibility has not been explored, but may, in part, explain the simultaneous increasing rates of childhood obesity and applications of nanoparticles and increased air pollutants. The changes seen in mitochondrial function, specifically with decreased electron transport chain complex activities, in both fetal and adult progeny of dams exposed to nano-TiO<sub>2</sub> during gestation, is similar to what our laboratory has previously seen with a type 2 diabetic mouse model (6). It is therefore plausible that even if ETC complex activities are

only diminished as an immediate response (at the fetal stage) or minimally altered at the adult stage following gestational ENM exposure, the offspring's capacity to manage a secondary insult, such as high-fat diet-(HFD) induced obesity, is significantly limited. This may result in a more severe and rapidly progressing type 2 diabetic phenotype. Nevertheless, the research described within this dissertation lays the basic groundwork necessary for further research in the field of inhalation toxicology and both the short and long-term repercussions of it.

The objective of Specific Aim 1 was to elucidate the effects of maternal nano-TiO<sub>2</sub> inhalation exposure during gestation on cardiac contractile function and mitochondrial function in fetal offspring and whether these detriments persist into adulthood. The evidence provided in this study pointed towards a connection between elevated ROS, specifically hydrogen peroxide (H<sub>2</sub>O<sub>2</sub>), levels and cardiac bioenergetic and contractile dysfunctions at the acute (fetal) and chronic (adult) stages. Based off the data acquired during this project, we postulated that elevated ROS in the maternal gestational environment affected the fetal epigenome such that when combined with a decrease in mitochondrial ROS scavenging capacity via diminished GPX4 protein levels, results in a positive feed-back loop. The mitigation of antioxidant capacity thus perpetuates increased ROS levels in fetal mitochondria and is concomitant with an increase in Hif1 $\alpha$ , which can transcriptionally activate Dnmt1. Through augmented Dnmt1 levels, global 5mC methylation in the fetal offspring is increased and thereby may be further diminishing GPX4 levels, resulting in a sustained effect into adulthood. The chronic effect seen however cannot be explained by the same epigenetic modification nor diminished GPX4 protein levels that are seen at the fetal stage. Notably however, mitochondrial bioenergetics, size, and internal complexity were all affected negatively. This brings to light the potential of mitochondrial reprogramming as a result of enhanced ROS, which although not discussed or investigated in this work, is a plausible hypothesis. It is also unlikely that 5mC methylation of GPX4 is solely responsible for the changes in mitochondrial structure and function and ultimately cardiac dysfunction that persist long-term. Moreover, evaluating the role of selenium is also critical in explicating diminished GPX4 content at the fetal stage.

As a result of the maternal inhalation exposures occurring at a critical timepoint in fetal development, the consequential phenotype may therefore be pathological. During mouse embryonic cardiac development, the mitochondrial permeability transition pore (mPTP) closes

when the cardiomyocyte is maturing, which occurs between embryonic day 9.5 and 13.5 (45). The purpose of this closure is to increase mitochondrial membrane potential to promote aerobic respiration and to decrease ROS levels in the cardiomyocytes. It is possible that the increased ROS levels seen in the fetal progeny may be occurring as a consequence of a high-stress state in the maternal environment as the nano-TiO<sub>2</sub> inhalation exposure occurs during this specific time in gestation. This may alter the ability of the mPTP to close as is necessary, making it unable to lower the ROS levels which instead remain high for an extended period. In turn, the mitochondria may be reprogrammed in an attempt to overcompensate for the deficiency, which could alter heart development in the vulnerable population (22).

It is important to note that the mechanism by which the effects of gestational nano-TiO<sub>2</sub> exposure are being transferred to the fetus and sustained into adulthood remains relatively elusive. While our studies are able to establish the presence of mitochondrial and cardiac changes, concomitant with a high ROS environment in the cardiac tissue, there are a multitude of possibilities in terms of how this occurs. While the research presented in this dissertation mainly investigated H<sub>2</sub>O<sub>2</sub> and mitochondrial dysfunction as the key source of ROS, there are other cellular mechanisms that may play a role in the resultant oxidative stress seen following exposure. Some of those pathways include xanthine oxidase, NADPH oxidase, and uncoupling of NO synthase. Nano-sized particulate matter can exert its effects through both direct and indirect mechanisms. Recent studies have proposed the ability of certain particles including black carbon (28) and nanopolystyrene (2) to cross the placental barrier and potentially induce direct effects to the developing fetus. However, the prevailing theory suggests that the consequences of particle exposure generally arise from lung inflammation and an associated ROS increase, in conjunction with other indirect effects elicited by the maternal exposure (5, 31). On the other hand, if particles are indeed translocating across the placental barrier, the quantities are likely incredibly limited and practically inconsequential. It is therefore unlikely that such minimal amounts could be behind such a significant impact on the progeny at both the acute and chronic stages. Consequently, one of the main possibilities goes back to inflammation (17, 25, 27). A case could be made that there is an initial interaction between the particles and lung tissue that precipitates an inflammatory response that causes both free radical and inflammatory cytokine release, along with other mediators of inflammation into the circulation. Even though primary inflammation occurs in the lungs, there are immune cells and inflammatory mediators that regain access to the blood and

continue perpetuating an inflammatory reaction. Higher amounts of macrophages, neutrophils, and other immune cells may then increase ROS levels in the blood and furthermore result in a hostile gestational environment due to the maternal systemic distribution of ROS (17, 25). Previous studies have determined that nano-TiO<sub>2</sub> inhalation exposure during gestation results in impaired vascular reactivity of the umbilical vein, umbilical artery, as well as increases placental vascular resistance (1, 9, 10). This may be another consequence of the perpetuating inflammatory reaction that can occur when alveolar macrophages interact with particulate matter is a change in endothelial cells. Particularly, studies of ENM inhalation exposure during gestation have shown altered endothelium-dependent placental hemodynamics, while endothelium-independent placental hemodynamics were not impacted. It is possible that a kisspeptin-dependent mechanism is the culprit when it comes to disruption of the normal gestational endocrine vascular axis following gestational ENM exposure. Specifically, nano-TiO<sub>2</sub> exposure augmented the effects of kisspeptin on vasoconstriction (3). Kisspeptin is a neuropeptide that binds to its respective G-coupled receptor (Kiss1R) and triggers a cascade that results in release of intracellular calcium, leading to smooth muscle contraction. Therefore, a potential repercussion of these findings is an increase in reactivity to this vasoconstrictor, which may be responsible for insufficient placental perfusion and increased resistance, mitigating oxygen availability for the pups *in utero*. Notably, unpublished data from our laboratory showed a decrease in Prdx1 mRNA expression (*P*<sub>adj</sub> = 0.002), which has been established as a form of protection against excessive endothelial activation. Diminished Prdx1 levels in mice resulted in a model that is susceptible to chronic inflammation (18). These studies emphasize the real possibility that there are several pathways that work in a cooperative manner to ensue the damage that is seen in offspring following maternal ENM inhalation exposure. Nevertheless, it is clear that more work remains to fully elucidate the source of the ROS and the connection between the elevated levels and sustained cardiac and mitochondrial effects in mice gestationally exposed to nano-TiO<sub>2</sub>. As this field of research continues to grow, the truth will likely lie in the possibility that multiple pathways are simultaneously at play.

Regardless of the mechanism by which the fetus is impacted, we still recognize the importance of the sustained alterations that are carried into adulthood. Unlike at the fetal stage, young adult offspring whose dams were gestationally exposed to ENM presented with a decrease in 5mC methylation (21). This is an interesting finding such that it suggests that other epigenetic and/or epitranscriptomic mechanisms are involved. While the research presented in Specific Aim

1 of this dissertation investigated Dnmt levels and global 5mC methylation status, other investigators have looked at histone modifications associated with disease following environmental exposure as well as altered miRNA and other non-coding RNA levels (13). The first evidence that maternal ENM inhalation exposure contributes to modifications to the fetal epigenome identified changes in histone 3 lysine 4 tri-methylation (H3K4me3) and histone 3 lysine 27 tri-methylation (H3K27me3) in the fetal offspring hearts (37). Our laboratory has also published data that indicates changes to miRNA levels following inhalation exposure, specifically miRNA-378a that were associated with mitochondrial functional diminutions (11). The possibility of other non-coding RNAs however has not been investigated in this dissertation or otherwise. As mentioned earlier, it is highly unlikely that one specific DNA modification is responsible for both the fetal and adult mitochondrial and cardiac detriments that are associated with maternal inhalation exposure to particulate matter during gestation. Further research is required to determine whether long non-coding RNA (lncRNA) distribution, for example, is altered as lncRNA has multiple regulatory roles including regulating translation, miRNA sequestration, guiding chromatin remodeling, and inhibiting or promoting binding of transcription factors and cofactors to gene promoters and thus control the transcription of target genes (16). It is thereby possible that several of these mechanisms are working together to result in a globally altered and sustained mitochondrial profile and ultimately chronically diminished cardiac function.

Although the focus of our research and others in the field of inhalation toxicology has prominently been epigenetics, there is an increasing amount of interest surrounding the epitranscriptome (4, 24, 44). While both epigenetics and epitranscriptomics play a role in influencing gene expression, there is a distinct difference between the two. Epigenetics encompasses DNA modifications, histone modifications, and nucleosome occupancy, which can influence the structure of chromatin as well as the function of the genes that are affected (8). The most prevalently studied epigenetic modification is 5-methylcytosine (5mC), which was studied in Specific Aim 1 as mentioned previously. Epitranscriptomics, on the other hand, refers to post-transcriptional modifications in both coding and non-coding RNAs, with the most prominent modification being N<sup>6</sup>-methyladenosine(m<sup>6</sup>A) (7). The study of the epitranscriptome is gaining traction as discoveries have verified that post-transcriptional modifications such as m<sup>6</sup>A have their own set of writers (responsible for addition of the methylation mark(s)), erasers (responsible for removal of the methylation mark(s)), and readers (responsible for determining the fate of the

mRNA with the methylation mark(s)). This has initiated a burgeoning field of possibilities in terms of researching and elucidating the effects that modifications have on gene expression, regulation, and furthermore their roles in diseases. This provides a new opportunity to understand not only the role of DNA modifications or RNA modifications individually, but the combined role they may be playing in disease and how one may influence the other (15). Because recent discoveries have established the link between environmental toxicant exposure and the most abundant mRNA modification, m<sup>6</sup>A, in the second part of my dissertation we wanted to determine whether this modification played a role in the acute and chronic repercussions on progeny gestationally exposed to ENM.

The objective of Specific Aim 2 was to determine whether enhanced mPHGPx expression preserves cardiac contractile function and bioenergetics in adult offspring following maternal ENM inhalation exposure, and whether m<sup>6</sup>A methylation contributes to altered antioxidant capacity. Our study specifically focused on the mPHGPx mRNA and whether m<sup>6</sup>A modifications played a role in the diminished mPHGPx activity found in adult offspring hearts following maternal ENM inhalation exposure. The reasoning behind the focus on the 3'UTR of mPHGPx specifically is two-fold; (1) the 3'UTR of mPHGPx contains the selenocysteine (Sec) incorporation machinery, which is vital for the catalytic activity of this enzyme to promote H<sub>2</sub>O<sub>2</sub> scavenging and evade damage to the mitochondrial membrane, and (2) m<sup>6</sup>A is highly enriched in the 3'UTR and around stop codons. Notably, this is of interest as changes to the Sec incorporation sequence (SECIS), the critical region located in the 3'UTR of mPHGPx, can alter the binding ability for the complex that recodes a “Stop” codon to a “Sec” codon and allows for the catalytic activity to be viable (14, 35). M<sup>6</sup>A-RIP-qPCR for this particular region determined that there in fact was an increased amount of m<sup>6</sup>A methylation occurring in wild-type offspring gestationally exposed to nano-TiO<sub>2</sub>, concomitant with decreased mPHGPx activity. These findings, though limited in terms of sample size, highlight the value of understanding the role of m<sup>6</sup>A as it relates to epitranscriptomic reprogramming associated with sustained effects. However, a more broad scale approach would be beneficial in detailing other aspects of mPHGPx that may be altered through this prominent modification and whether these modifications are detrimental (as in the case presented in Specific Aim 2) or the possibility that the modification is actually necessary for proper function as is the case with the Sec tRNA. The epitranscriptomic writer, alkylation repair homolog 8 (ALKBH8), is a tRNA methyltransferase that adds methylation marks to the wobble

uridine of the Sec tRNA to allow for synthesis of selenoproteins. (40) Without this methylation mark, selenoprotein levels are diminished and mitochondrial reprogramming ensues. Not investigated in this study is the likelihood that modulator proteins (readers and writers) are altered, but other studies have shown that environmental exposure to toxicants alters expression of RNA methylation modulator genes including METTL3, WTAP, FTO and ALKBH5. It is also of utmost importance that other genes be investigated that are required for mitochondrial function and ROS regulation. This can provide new targets for the prevention or treatment of ROS-induced cardiac effects in fetal and adult offspring of mother exposed to nanoparticulate matter during pregnancy.

As the importance of antioxidant defense and limiting ROS levels became abundantly clear through our preliminary studies, the potential of alleviating the adverse effects on fetal and adult offspring gestationally exposed to nano-TiO<sub>2</sub> became of interest. Based off our laboratories previous work with the mPHGPx mouse models, this model was chosen as it increases H<sub>2</sub>O<sub>2</sub> scavenging and thereby decreases mitochondrial ROS levels. This endeavor required implementation of a novel breeding strategy that would allow us to test the benefits of increased antioxidant capacity from several points of origin; (1) fetal, (2) maternal, as well as (3) fetal and maternal. Interestingly, our original prediction that the combined maternal environment mPHGPx overexpression and fetal pup mPHGPx overexpression protection would be the most protective profile, as compared to wild type pups from wild type mothers that were gestationally exposed to ENM was not supported. We did not expect to see that there was a trivial difference between the protection provided by just the maternal environment providing increased antioxidant defense and the combined maternal and fetal mPHGPx overexpression. This was therefore the first study to show that enhancing antioxidant defense in the mother during pregnancy may suffice for limiting cardiac and mitochondrial deficits associated with gestational nano-TiO<sub>2</sub> inhalation exposure. Furthermore, the offspring of mPHGPx ENM-exposed mothers did not present with increased m<sup>6</sup>A methylation in the mPHGPx 3'UTR region, unlike the offspring of wild type ENM-exposed dams. Despite the limitations associated with using a transgenic mouse model, this study unlocks the possibility that supplementation with a mitochondrially-targeted antioxidant therapeutic during pregnancy may be able to provide the same beneficial protection in humans, in regards to avoiding the repercussions of acute and sustained cardiac detriments, in offspring gestationally exposed to ENM. Mitigating ROS in the mother and gestational environment using a supplement, such as mitoquinol (a mitochondrially targeted form of CoQ10), is the next step in protecting future



generations from the consequences of particulate matter exposure (30, 39). Furthermore, other antioxidant supplements may be of benefit, however, our study supports the beneficial role of targeting the mitochondrion specifically to protect from dysregulation and diminished bioenergetic function.

The objective of Specific Aim 3 was to determine whether disruption of mitochondrial bioenergetics and cardiovascular dysfunction elicited by maternal exposure can be attributed to epitranscriptomic remodeling that is associated with an altered mitochondrial proteome that is incapable of managing high levels of ROS. To gain a better understanding of the broad-scale m<sup>6</sup>A changes that may be occurring at the fetal stage that result in long-term dysfunction, we performed m<sup>6</sup>A-RIP-sequencing as well as label-free mitochondrial proteomics on fetal cardiac samples obtained following maternal inhalation exposure of sham air and nano-TiO<sub>2</sub> aerosolized particles. The novelty of this study lies in the application of multi-omics approaches including epitranscriptomics, transcriptomics, and proteomics. Such an approach is vital in moving the field forward, towards a more integrative approach that allows researchers to see the bigger picture while also understanding the detailed mechanisms involved with pathologies of not only the heart but all the organ systems. The connection between mitochondrial bioenergetic dysregulation and the mRNA expression levels presented in **Figure 4.2D** is apparent. All, but 2, mRNAs that are part of the electron transport chain complexes were significantly decreased in the nano-TiO<sub>2</sub> gestationally exposed offspring. The possibility that this was an experimental fluke is rejected by the data presented in **Supplemental Figure 4.2** which demonstrates the dynamic expression changes seen within other pathways. These data further substantiate the notion that there is a dysregulation of expression levels to pivotal genes, which then results in mitigation of mitochondrial activity previously reported by our laboratory (12, 20, 21, 26). Markedly, GPX4 mRNA expression was significantly decreased in fetal offspring gestationally exposed to ENM (**Supplemental Figure 4.1**). This is consistent with previously published data from our laboratory which determined that GPX4 activity (20) and GPX4 protein expression (21) were decreased in fetal and adult offspring, respectively, that were gestationally exposed to ENM.

As GPX proteins are selenoproteins, it is a reasonable assumption that the diminishment of GPX4 may be attributed to a decrease in selenium. Notably, unpublished data from our laboratory determined that following gestational ENM exposure, the only glutathione peroxidase

proteins that were altered were GPX1 ( $P_{adj} = 0.005$ ) and GPX8 ( $P_{adj} = 0.024$ ). Although this is interesting, it leads us to believe that a limitation in selenium is likely not responsible for diminished GPX4 levels. The reason for that lies in the discovery that selenium is prioritized for synthesis of GPX4, therefore if selenium concentrations were the issue in this situation, we would expect all of the other GPX proteins to be decreased significantly as well (33). However, based on our unpublished data mRNA expression of other selenoproteins were significantly decreased including selenoprotein M ( $P_{adj} = 0.001$ ), selenoprotein H ( $P_{adj} = 0.029$ ), and selenoprotein W ( $P_{adj} = 0.005$ ), but others were increased such as selenoprotein T ( $P_{adj} = 0.025$ ), suggesting dynamic changes that are likely unrelated to selenium availability. This further indicates that a potential limited availability of selenium was not responsible for decreased GPX4 mRNA and activity. Other constituents of the oxidative stress pathway that should be considered are glutathione (GSH), catalase (CAT), superoxide dismutase (SOD), and peroxiredoxins (PRDX). Environmental stress, such as exposure to particulate matter can derive free radicals that react with oxygen, thereby producing superoxide, which can then result in either production of peroxynitrite (superoxide interacting with nitric oxide) or  $H_2O_2$  via a dismutase reaction catalyzed by SOD (29). The antioxidant activities of CAT and GSH/GPX are then responsible for detoxifying the  $H_2O_2$  produced in the previous step, otherwise hydroxyl radicals are produced via the Fenton reaction. It is therefore necessary to understand whether expression of these antioxidant enzymes is diminished following gestational ENM exposure, or if this suppression is only limited to GPX4. Unpublished data from our laboratory indicated that mRNA expression of the catalase was not changed ( $P_{adj} = 0.060$ ), while glutathione synthetase expression ( $P_{adj} = 0.004$ ) and SOD1 expression were significantly decreased ( $P_{adj} = 0.017$ ). These data may therefore suggest that decreased GPX4 is not the only contributor to elevated ROS in offspring maternally exposed to ENM. However, protein expression levels of these members of the oxidative stress pathway were not examined due to the limitation that our proteomic assessments were performed on isolated mitochondria from cardiac tissue of fetal offspring. Nevertheless, protein expression data, presented in Chapter 4, highlights the apparent decrease in PRDX3 (**Figure 4.6**), which also scavenges  $H_2O_2$  in mitochondria, as well as lipid peroxides and peroxynitrites, and is required to maintain normal mitochondrial function (41, 43). It is necessary that this pathway be further examined in order to truly be able to delineate if there is one specific antioxidant enzyme that can

be supplemented in a mother during pregnancy to avoid the detriments to mitochondrial and contractile function seen in offspring.

Evaluation of the shared pathways seen between the genes with altered mRNA expression and m<sup>6</sup>A levels determined that ubiquitin mediated proteolysis was the top pathway. This unexpected finding is intriguing as a recent study reported that YTHDF3 is involved in ubiquitin mediated proteolysis (42). As mentioned earlier, YTHDF3 affects translation and decay of methylated mRNAs depending on whether it is interacting with YTHDF1 (translation) or YTHDF2 (decay) (36). Modulating expression of YTHDF3 can therefore affect the RNA binding activity of the other two proteins, changing the fate of the m<sup>6</sup>A methylated mRNA by altering stability. As part of the study done in Chapter 4, we found that YTHDF3 mRNA expression was significantly increased (*P*<sub>adj</sub> = 0.002) in offspring whose dams were exposed gestationally. Although this mechanism is far from elucidated, our research as well as research from other laboratories mentioned herein, suggest that explicating this connection may be valuable in better understanding how the fate of m<sup>6</sup>A methylated mRNAs is regulated.

### ***Limitations***

The work presented within this dissertation contributes to the understanding of the shortcomings associated with increased ENM utilization and the possibility of circumventing these shortcomings using an accessible supplement during pregnancy. Nevertheless, there are limitations that must be taken into consideration. The inhalation exposure protocol utilized in all three Specific Aims involve a whole-body exposure, which results in not only inhalation exposure, but also dermal exposure. Additionally, as the mice continue to groom themselves throughout the exposure, ingestion of nano-TiO<sub>2</sub> becomes a concern. Future studies should attempt to compare the difference in lung burden between a nose-only and whole-body exposure, as well as the presence of particles in the gastrointestinal tract. Furthermore, working with fetal samples presents the limitation of fetal tissue size. Tissue size resulted in restrictions in terms of the experiments we were able to run principally for understanding mitochondrial bioenergetics with the mPHGPx transgenic and wild type offspring.

In Specific Aims 2 and 3, m<sup>6</sup>A RNA immunoprecipitation (m<sup>6</sup>A(me)-RIP) was employed in order to capture m<sup>6</sup>A modified mRNAs. M<sup>6</sup>A-RIP is one of the most used methodologies for this purpose, but comes with limitations of its own. In general, this method does not have the ability to differentiate N<sup>6</sup>-methyladenosine (m<sup>6</sup>A) from 6,2'-O-dimethyladenosine (m<sup>6</sup>Am) (19). Although m<sup>6</sup>Am is very limited, it still introduces an aspect of uncertainty as to what we are actually capturing with the RNA immunoprecipitation procedure. Future studies would benefit from utilizing m<sup>6</sup>A individual-nucleotide resolution cross-linking and immunoprecipitation (miCLIP), which can accurately differentiate between the two modifications. This method still requires further development to accommodate for small sample sizes though. Lastly, m<sup>6</sup>A-RIP-qPCR, which was used in Specific Aim 2, is restricted by the fact that it has high variation among biological replicates and therefore requires a greater number of replicates for reliable data (19). Similarly, m<sup>6</sup>A-RIP-seq, which was used in Specific Aim 3, is limited by the high risk of false positive results. Further validation of the results with either a more reliable method such as miCLIP or with a greater sample size is needed in order to definitively be able to confirm the reprogramming phenotype seen in the fetal offspring.

The proteomics analysis performed in Specific Aim 3, though interesting, is limited by sample size and therefore statistical analyses were not possible. To achieve the protein concentrations necessary to perform label-free proteomics, fetal cardiac mitochondrial samples were pooled from 2 mother's litters per each exposure group (sham/nano-TiO<sub>2</sub>). In order to verify the findings presented in our study, it is of utmost importance that these studies be repeated with a greater sample size that will allow for more tangible answers.

### ***Future Directions***

In the US between 2011 and 2012, 5,300 children and adolescents (10-19 years old) were diagnosed with type 2 diabetes and ~90% of adults diagnosed with type 2 diabetes were overweight or obese (38). With the growing prevalence of obesity and metabolic syndromes such as type 2 diabetes, assessment of prominent environmental risk factors must be elucidated. Like the suggested effects of ENMs on m<sup>6</sup>A, recent studies have reported that in type 2 diabetic patients, m<sup>6</sup>A was significantly reduced in peripheral blood RNA, concomitant with an upregulation of the demethylase FTO (34). Based on the similarities in metabolic pathways that are altered by both

inhaled particle exposure and high-fat diet-induced obesity (27), future investigations should focus on understanding whether maternal exposure to inhaled particles during pregnancy predisposes offspring to type 2 diabetes in young adulthood. A potential starting point for such studies would likely include “omics” based approaches that include epitranscriptomics, proteomics, metabolomics, and epigenomics profiling which will allow for a better understanding of the mechanisms (i.e. inflammation and oxidative stress) that are activated due to inhaled particle exposure and play instrumental roles in eliciting cardiovascular deficits. Specifically, future studies should investigate the role of NF- $\kappa$ B in offspring whose dams were gestationally exposed. NF- $\kappa$ B is associated with insulin resistance, obesity, and atherosclerosis, which have overlapping pathways with what is seen following exposure (23). H<sub>2</sub>O<sub>2</sub> has the ability to result in translocation of NF- $\kappa$ B so understanding how ROS influences this pivotal mediatory of inflammatory responses and how the two work hand in hand, will allow for a better understanding of different mechanisms driving ROS accumulation and long term mitochondrial and cardiac health effects.

As previously discussed, blood flow to the placenta may play a critical role in initiation of the series of events that occur leading to long term cardiac contractile and mitochondrial dysfunction. Future studies should attempt to assess blood flow and the inflammatory pathways that likely contribute to elevated ROS levels as well as potential endothelial dysfunction. A thorough examination of other forms of ROS such as nitric oxide and xanthine oxidase may also provide more insight into the mechanisms involved. Understanding these key aspects will allow for a more complete picture of the mechanisms in place, thereby making a more clear path for treatment and prevention.

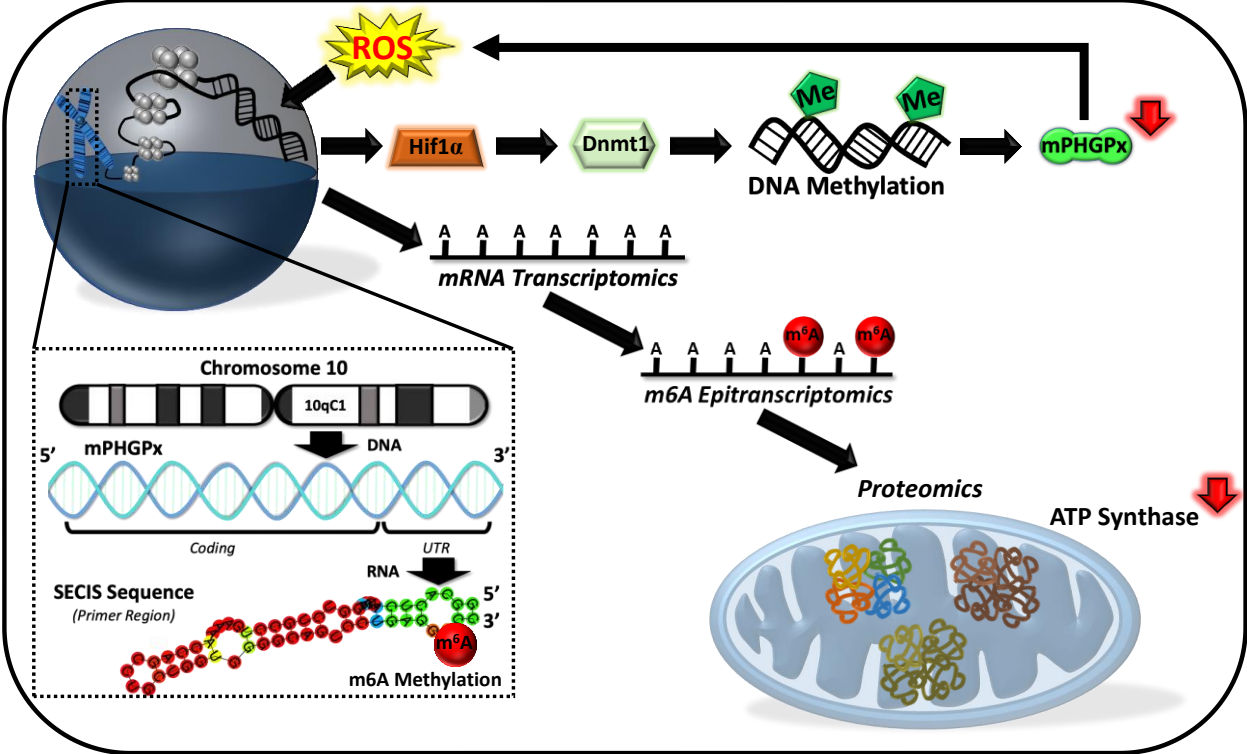
As indicated by the findings from our laboratory and others, enhancing antioxidant defense is a plausible route to investigate as a prophylactic and/or therapeutic strategy. Although our studies used genetic modification to overexpress the ROS scavenging antioxidant protein, mPHGPx, there are other forms of mitochondrially targeted antioxidants that should be evaluated in the context of inhaled particle exposure and its associated mechanisms. As indicated by our recent study (Chapter 3) (20), increasing maternal antioxidant defense was sufficient to protect the offspring from long-term adverse cardiac and mitochondrial functional alterations. The clinical relevance of this study is one that is highlighted by the suggestion that an antioxidant strategy that is delivered to the pregnant mother may allow for complete evasion of pollutant-associated long-

term cardiovascular defects in offspring. One example of a deliverable antioxidant strategy that has recently gained traction is mitoquinone mesylate (Mito-Q). A recent study that investigated the effects of vehicle exhausted exposure as a form of toxicological stress that leads to behavioral deficits utilized Mito-Q to ameliorate oxidative stress levels that were triggering mitochondrial impairment in the brain (32). Treating the mother during pregnancy with Mito-Q may serve a similar protective profile for the progeny as the mPHGPx overexpression, thereby limiting ROS upsurges during inhaled particle exposure and avoiding mitochondrial bioenergetic dysregulation. This would likely allow for the maintenance of normal cardiac function at both the fetal and adult stages in progeny.

### *Conclusions*

Overall, the data presented within this dissertation strongly support the idea that maternal inhalation exposure to ENM results in differentially altered epigenetic and epitranscriptomic methylation status in progeny cardiac tissue at both the fetal and adult stages of life. These changes culminate in a mitochondrial phenotype that is associated with a high ROS environment, bioenergetic dysregulation, and ultimately, cardiac dysfunction. These studies also demonstrate a potential supplemental preventative measure that can be administered to mitigate the effects of gestational toxicant inhalation exposure. Based on the data presented within this dissertation, we accept the hypothesis that changes in the m<sup>6</sup>A methylome, concomitant with an altered mitochondrial proteome at the fetal stage, precipitate cardiac contractile dysfunction that is sustained into adulthood following maternal ENM inhalation exposure. The novelty of epitranscriptomic and epigenetic modifications studied herein advances the field such that it provides a stepping stone for future studies to assess the interactions of these modifications and how they can be exploited for therapeutic strategies. A summary of the overall conclusions and findings within this dissertation is illustrated in **Figure 5.1**.

Figure 5.1: Specific Aims Overview



## References

1. **Abukabda AB, Bowdridge EC, McBride CR, Batchelor TP, Goldsmith WT, Garner KL, Friend S, and Nurkiewicz TR.** Maternal titanium dioxide nanomaterial inhalation exposure compromises placental hemodynamics. *Toxicol Appl Pharmacol* 367: 51-61, 2019.
2. **Bommarito PA, Martin E, and Fry RC.** Effects of prenatal exposure to endocrine disruptors and toxic metals on the fetal epigenome. *Epigenomics* 9: 333-350, 2017.
3. **Bowdridge EC, Abukabda AB, Engles KJ, McBride CR, Batchelor TP, Goldsmith WT, Garner KL, Friend S, and Nurkiewicz TR.** Maternal Engineered Nanomaterial Inhalation During Gestation Disrupts Vascular Kisspeptin Reactivity. *Toxicol Sci* 169: 524-533, 2019.
4. **Cayir A, Barrow TM, Guo L, and Byun HM.** Exposure to environmental toxicants reduces global N6-methyladenosine RNA methylation and alters expression of RNA methylation modulator genes. *Environ Res* 175: 228-234, 2019.
5. **Crispi F, Miranda J, and Gratacos E.** Long-term cardiovascular consequences of fetal growth restriction: biology, clinical implications, and opportunities for prevention of adult disease. *Am J Obstet Gynecol* 218: S869-S879, 2018.
6. **Dabkowski ER, Baseler WA, Williamson CL, Powell M, Razunguzwa TT, Frisbee JC, and Hollander JM.** Mitochondrial dysfunction in the type 2 diabetic heart is associated with alterations in spatially distinct mitochondrial proteomes. *Am J Physiol Heart Circ Physiol* 299: H529-540, 2010.
7. **Dominissini D, Moshitch-Moshkovitz S, Schwartz S, Salmon-Divon M, Ungar L, Osenberg S, Cesarkas K, Jacob-Hirsch J, Amariglio N, Kupiec M, Sorek R, and Rechavi G.** Topology of the human and mouse m6A RNA methylomes revealed by m6A-seq. *Nature* 485: 201-206, 2012.
8. **Fico A, Di Croce L, and Matarazzo MR.** Interplay between DNA and RNA Modifications: A Constantly Evolving Process. *Epigenomes* 4: 26, 2020.
9. **Fournier SB, D'Errico JN, and Stapleton PA.** Uterine Vascular Control Preconception and During Pregnancy. *Compr Physiol* 11: 1871-1893, 2021.
10. **Fournier SB, Kallontzi S, Fabris L, Love C, and Stapleton PA.** Effect of Gestational Age on Maternofetal Vascular Function Following Single Maternal Engineered Nanoparticle Exposure. *Cardiovasc Toxicol* 19: 321-333, 2019.
11. **Hathaway QA, Durr AJ, Shepherd DL, Pinti MV, Brandebura AN, Nichols CE, Kunovac A, Goldsmith WT, Friend SA, Abukabda AB, Fink GK, Nurkiewicz TR, and JM aH.** miRNA-378a as a key regulator of cardiovascular health following engineered nanomaterial inhalation exposure. *Nanotoxicology* 1-20, 2019.
12. **Hathaway QA, Durr AJ, Shepherd DL, Pinti MV, Brandebura AN, Nichols CE, Kunovac A, Goldsmith WT, Friend SA, Abukabda AB, Fink GK, Nurkiewicz TR, and Hollander JM.** miRNA-378a as a key regulator of cardiovascular health following engineered nanomaterial inhalation exposure. *Nanotoxicology* 1-20, 2019.
13. **Hou L, Zhang X, Wang D, and Baccarelli A.** Environmental chemical exposures and human epigenetics. *Int J Epidemiol* 41: 79-105, 2012.
14. **Ingold I, Berndt C, Schmitt S, Doll S, Poschmann G, Buday K, Roveri A, Peng X, Porto Freitas F, Seibt T, Mehr L, Aichler M, Walch A, Lamp D, Jastroch M, Miyamoto S, Wurst W, Ursini F, Arner ESJ, Fradejas-Villar N, Schweizer U, Zischka H, Friedmann Angeli JP, and Conrad M.** Selenium Utilization by GPX4 Is Required to Prevent Hydroperoxide-Induced Ferroptosis. *Cell* 172: 409-422 e421, 2018.



15. **Kan RL, Chen J, and Sallam T.** Crosstalk between epitranscriptomic and epigenetic mechanisms in gene regulation. *Trends Genet* 2021.
16. **Karlsson O, and Baccarelli AA.** Environmental Health and Long Non-coding RNAs. *Curr Environ Health Rep* 3: 178-187, 2016.
17. **Kelley AS, Banker M, Goodrich JM, Dolinoy DC, Burant C, Domino SE, Smith YR, Song P XK, and Padmanabhan V.** Early pregnancy exposure to endocrine disrupting chemical mixtures are associated with inflammatory changes in maternal and neonatal circulation. *Sci Rep* 9: 5422, 2019.
18. **Kisucka J, Chauhan AK, Patten IS, Yesilaltay A, Neumann C, Van Etten RA, Krieger M, and Wagner DD.** Peroxiredoxin1 prevents excessive endothelial activation and early atherosclerosis. *Circ Res* 103: 598-605, 2008.
19. **Kumari R, Ranjan P, Suleiman ZG, Goswami SK, Li J, Prasad R, and Verma SK.** mRNA modifications in cardiovascular biology and disease: with a focus on m6A modification. *Cardiovasc Res* 2021.
20. **Kunovac A, Hathaway QA, Pinti MV, Durr AJ, Taylor AD, Goldsmith WT, Garner KL, Nurkiewicz TR, and Hollander JM.** Enhanced antioxidant capacity prevents epitranscriptomic and cardiac alterations in adult offspring gestationally-exposed to ENM. *Nanotoxicology* 1-20, 2021.
21. **Kunovac A, Hathaway QA, Pinti MV, Goldsmith WT, Durr AJ, Fink GK, Nurkiewicz TR, and Hollander JM.** ROS promote epigenetic remodeling and cardiac dysfunction in offspring following maternal engineered nanomaterial (ENM) exposure. *Part Fibre Toxicol* 16: 24, 2019.
22. **Lee MY, Leonardi A, Begley TJ, and Melendez JA.** Loss of epitranscriptomic control of selenocysteine utilization engages senescence and mitochondrial reprogramming(). *Redox Biol* 28: 101375, 2020.
23. **Liu T, Zhang L, Joo D, and Sun SC.** NF-kappaB signaling in inflammation. *Signal Transduct Target Ther* 2: 2017.
24. **Malovic E, Ealy A, Kanthasamy A, and Kanthasamy AG.** Emerging Roles of N6-Methyladenosine (m6A) Epitranscriptomics in Toxicology. *Toxicol Sci* 181: 13-22, 2021.
25. **Miller MR, Shaw CA, and Langrish JP.** From particles to patients: oxidative stress and the cardiovascular effects of air pollution. *Future Cardiol* 8: 577-602, 2012.
26. **Nichols CE, Shepherd DL, Hathaway QA, Durr AJ, Thapa D, Abukabda A, Yi J, Nurkiewicz TR, and Hollander JM.** Reactive oxygen species damage drives cardiac and mitochondrial dysfunction following acute nano-titanium dioxide inhalation exposure. *Nanotoxicology* 12: 32-48, 2018.
27. **Niemann B, Rohrbach S, Miller MR, Newby DE, Fuster V, and Kovacic JC.** Oxidative Stress and Cardiovascular Risk: Obesity, Diabetes, Smoking, and Pollution: Part 3 of a 3-Part Series. *J Am Coll Cardiol* 70: 230-251, 2017.
28. **Pietrojusti A, Stockmann-Juvala H, Lucaroni F, and Savolainen K.** Nanomaterial exposure, toxicity, and impact on human health. *Wiley Interdiscip Rev Nanomed Nanobiotechnol* 2018.
29. **Redza-Dutordoir M, and Averill-Bates DA.** Activation of apoptosis signalling pathways by reactive oxygen species. *Biochim Biophys Acta* 1863: 2977-2992, 2016.
30. **Ribeiro Junior RF, Dabkowski ER, Shekar KC, KA OC, Hecker PA, and Murphy MP.** MitoQ improves mitochondrial dysfunction in heart failure induced by pressure overload. *Free Radic Biol Med* 117: 18-29, 2018.

31. **Robichaud CO, Uyar AE, Darby MR, Zucker LG, and Wiesner MR.** Estimates of upper bounds and trends in nano-TiO<sub>2</sub> production as a basis for exposure assessment. *Environ Sci Technol* 43: 4227-4233, 2009.
32. **Salvi A, Liu H, and Salim S.** Involvement of oxidative stress and mitochondrial mechanisms in air pollution-related neurobiological impairments. *Neurobiol Stress* 12: 100205, 2020.
33. **Schriever SC, Barnes KM, Evenson JK, Raines AM, and Sunde RA.** Selenium requirements are higher for glutathione peroxidase-1 mRNA than gpx1 activity in rat testis. *Exp Biol Med (Maywood)* 234: 513-521, 2009.
34. **Shen F, Huang W, Huang JT, Xiong J, Yang Y, Wu K, Jia GF, Chen J, Feng YQ, Yuan BF, and Liu SM.** Decreased N(6)-methyladenosine in peripheral blood RNA from diabetic patients is associated with FTO expression rather than ALKBH5. *J Clin Endocrinol Metab* 100: E148-154, 2015.
35. **Shetty SP, and Copeland PR.** Selenocysteine incorporation: A trump card in the game of mRNA decay. *Biochimie* 114: 97-101, 2015.
36. **Shi H, Wang X, Lu Z, Zhao BS, Ma H, Hsu PJ, Liu C, and He C.** YTHDF3 facilitates translation and decay of N(6)-methyladenosine-modified RNA. *Cell Res* 27: 315-328, 2017.
37. **Stapleton PA, Hathaway QA, Nichols CE, Abukabda AB, Pinti MV, Shepherd DL, McBride CR, Yi J, Castranova VC, Hollander JM, and Nurkiewicz TR.** Maternal engineered nanomaterial inhalation during gestation alters the fetal transcriptome. *Part Fibre Toxicol* 15: 3, 2018.
38. **Statistics NCFH.** 2011–2014 National Health and Nutrition Examination Survey (NHANES). edited by Prevention CfDca.
39. **Sukjamnong S, Chan YL, Zakarya R, Nguyen LT, Anwer AG, Zaky AA, Santiyanont R, Oliver BG, Goldys E, Pollock CA, Chen H, and Saad S.** MitoQ supplementation prevent long-term impact of maternal smoking on renal development, oxidative stress and mitochondrial density in male mice offspring. *Sci Rep* 8: 6631, 2018.
40. **Truitt ML, and Ruggero D.** New frontiers in translational control of the cancer genome. *Nat Rev Cancer* 17: 332, 2017.
41. **Wonsey DR, Zeller KI, and Dang CV.** The c-Myc target gene PRDX3 is required for mitochondrial homeostasis and neoplastic transformation. *Proc Natl Acad Sci U S A* 99: 6649-6654, 2002.
42. **Xu D, Shao J, Song H, and Wang J.** The YTH Domain Family of N6-Methyladenosine "Readers" in the Diagnosis and Prognosis of Colonic Adenocarcinoma. *Biomed Res Int* 2020: 9502560, 2020.
43. **Zhang H, Go YM, and Jones DP.** Mitochondrial thioredoxin-2/peroxiredoxin-3 system functions in parallel with mitochondrial GSH system in protection against oxidative stress. *Arch Biochem Biophys* 465: 119-126, 2007.
44. **Zhang S, Meng P, Cheng S, Jiang X, Zhang J, Qin X, Tang Q, Bai L, Zou Z, and Chen C.** Pregnancy exposure to carbon black nanoparticles induced neurobehavioral deficits that are associated with altered m(6)A modification in offspring. *Neurotoxicology* 81: 40-50, 2020.
45. **Zhao Q, Sun Q, Zhou L, Liu K, and Jiao K.** Complex Regulation of Mitochondrial Function During Cardiac Development. *J Am Heart Assoc* 8: e012731, 2019.

# Chapter 6: Supplemental

## Left Ventricular Segmental Stress-Strain Identifies Unique Myocardial Deformation Patterns Following Intrinsic and Extrinsic Stressors in Mice

Amina Kunovac, BS<sup>1,2</sup>, Quincy A. Hathaway, PhD<sup>3</sup>, Emily N. Burrage, BS<sup>4</sup>, Tyler Coblenz, BS<sup>1</sup>, Eric E. Kelley, PhD<sup>5</sup>, Partho P. Sengupta, MD, DM<sup>3,6</sup>, John M. Hollander, PhD<sup>1,2</sup>, Paul D. Chantler, PhD<sup>1,2,4</sup>

Manuscript Under Review at Ultrasound in Medicine and Biology (Manuscript Number: UMB-D-21-00654)

<sup>1</sup>Division of Exercise Physiology, West Virginia University, School of Medicine, Morgantown, WV, USA, <sup>2</sup>Mitochondria, Metabolism & Bioenergetics Working Group, West Virginia University, Morgantown, WV, USA, <sup>3</sup>Heart and Vascular Institute, West Virginia University, Morgantown, WV, USA, <sup>4</sup>Department of Neuroscience, West Virginia University, School of Medicine, Morgantown, WV, USA, <sup>5</sup>Department of Physiology and Pharmacology, West Virginia University, School of Medicine, Morgantown, WV, USA, <sup>6</sup>Rutgers Robert Wood Johnson University Hospital, New Brunswick, NJ, USA.

**Running Title:** Identifying Unique Patterns of Myocardial Deformation

### Corresponding Author

Quincy A. Hathaway, PhD

PO Box 9227

Room 3033-A HSC North

1 Medical Center Drive, Morgantown, WV 26506.

Phone: 724-255-4637

Email: [qahathaway@mix.wvu.edu](mailto:qahathaway@mix.wvu.edu)

## Abstract

We utilized segmental stress strain analysis to evaluate whether intrinsic (diet-induced obesity (DIO)) and extrinsic (unpredictable chronic mild stress (UCMS)) stressors can alter deformational patterns of the left ventricle and act as a unique “fingerprint” for characterization. 6-week-old, male C57BL/6J mice were randomized into lean or obese groups (N = 24/group). The obese group underwent 12 weeks of DIO with a high-fat diet (HFD). At 18 weeks, lean and obese mice were further randomized into UCMS and non-UCMS groups to elicit a chronically stressed phenotype (UCMS; 7 hrs/day, 5 days/week, for 8 weeks). M-Mode, Pulse-Wave Doppler, and speckle tracking echocardiography were assessed at baseline (6 weeks), post-HFD (18 weeks), and post-UCMS (26 weeks). Supervised machine learning with 10-fold cross validation was applied to the DIO and UCMS groups. Comparing obese to lean mice, the machine learning model provided robust prediction (AUC: 0.921), radial strain of the lateral wall and anterior free wall being most important. Changes in radial strain of the lateral wall (-64%,  $P \leq 0.001$ ) and anterior free wall (-53%,  $P < 0.001$ ) were more dramatically altered than ejection fraction (-9%,  $P < 0.001$ ) and global longitudinal strain (-16%,  $P = 0.08$ ). The ability to predict mice that underwent UCMS, irrespective of diet, was assessed (AUC: 0.886) revealing longitudinal strain rate of the anterior mid wall and radial strain of the posterior septal wall as the top features. The wall segments indicate a predilection for changes in deformation patterns to the free wall (DIO) and septal wall (UCMS), indicating disease-specific alterations to the myocardium.

## Introduction

Cardiovascular diseases contribute to nearly one-third of all deaths in the world, accounting for 17.9 million deaths in 2019 (2). Left ventricular (LV) dysfunction plays a major role in precipitating mortality in the context of cardiovascular diseases, which heightens the need for a better understanding of LV pathology. In general, overt functional and/or structural modifications of the LV begin as subclinical modifications at the molecular and cellular level that further culminate into adverse clinical outcomes (5). Being able to predict how stressors will modify the LV is important in both a basic understanding of the disease and how to model treatment options.

The initial clinical findings of pathological changes to the LV can be observed using stress-strain parameters. Speckle tracking stress-strain can identify deformation patterns across a variety of regions within the LV, including the longitudinal, circumferential, and radial axes. Global longitudinal strain (GLS) has been used as a marker for predicting outcomes, such as all-cause mortality (24) and morbidity (4), as well as cardiovascular disease (22). The measurement of stress-strain parameters, such as GLS, has also been shown to be more reproducible than left ventricular ejection fraction, regardless of the level of expertise of the technician (11). While GLS is a powerful measurement for modeling the early changes in deformation patterns of the LV, it does not address how varying insults could preferentially affect certain areas of the LV myocardium, and if these regions can act as a “fingerprint” in the identification of an insult retrospectively.

The current study investigates a novel concept that suggests a role for different forms of physiological stressors to cause unique deformational patterning of the LV. We investigate how diet-induced obesity (DIO) and unpredictable chronic mild stress (UCMS) alter stress-strain parameters in the murine LV and if they can be differentiated from one another. Our findings highlight how segmental stress-strain parameters, when compared to other common echocardiographic techniques, provide superior predictive power in correctly identifying DIO and UCMS animals. Additionally, segmental patterns of deformation are unique across these physiological insults, with changes in segmental stress-strain clearly identifiable even in animals that have already undergone LV remodeling (i.e., DIO).

## Methods

### *Murine Model and Diet-Induced Obesity (DIO) Protocol*

6-week-old male C57BL/6J mice (Stock No: 000664; The Jackson laboratory. ME, USA) were randomized into lean (N=24) or obese (N=24) groups. Mice in the obese group underwent 12 weeks of diet induced obesity (DIO) (Research Diet D12492; NJ, USA) with a caloric composition of 20 kcal% protein, 20 kcal% carbohydrate, and 60 kcal% fat. To elicit a chronically stressed phenotype at 18 weeks of age, mice in the lean and obese groups were further randomized into unpredictable chronic mild stress (UCMS) and non-UCMS groups. The final groups reflect lean non-UCMS (N=12), lean-UCMS (N=12), obese-non-UCMS (N=12), and obese-UCMS (N=12) at 26 weeks old. Body weight was measured in the morning at 6, 18 and 26 weeks of age. At 26 weeks of age, mice were euthanized. All experiments used only male mice. All animal studies, including animal housing, sedation, euthanasia, and experimentation were approved by The West Virginia University Animal Care and Use Committee and conformed to the most current National Institutes of Health (NIH) Guidelines for the Care and Use of Laboratory Animals manual.

### *Unpredictable Chronic Mild Stress (UCMS) Protocol*

The UCMS protocol is a well-defined model to induce a depressive state in rodents (29). Rodents undergoing UCMS manifest with clinically relevant depressive symptoms such as anhedonia and learned helplessness (29) with alterations in brain structure and function parallel to clinical depression (16). Mice were singly housed in UCMS groups, and exposed to the following mild environmental stressors in randomly chosen sequences for 8 hours each day, 5 days/week, over the course of 8 weeks:

1. *Damp bedding* – 10 oz. of water was added to each standard cage.
2. *Bath* – all bedding was removed and ~0.5 inches of water was added to empty cage. Water temperature was room temperature, ~24°C.
3. *Cage Tilt* – cage was tilted to 45 degrees without bedding.
4. *Social stress* – each rat was switched into a cage of a neighboring mouse.
5. *No bedding* – all bedding was removed from the cage.
6. *Alteration of light/dark cycles* –turning lights off/on in random increments for scheduled

period.

### *Echocardiography*

Mice were anesthetized with inhaled isoflurane at 2.5% in combination with 100% oxygen (25). Imaging was performed while mice were maintained under anesthesia using 1% isoflurane. Vital signs were measured using a rectal probe to monitor temperature and limb leads for electrocardiogram. A 32–55 MHz linear array transducer was used to acquire ultrasound images with the Vevo2100 Imaging System (Visual Sonics, Toronto, Canada) at a frame rate of 200–425 frames/second. A trained, ultrasound technician at the West Virginia University Animal Models and Imaging Facility performed all imaging. M-mode images were acquired at the mid-papillary level of the LV in the parasternal short axis, with LV volumes and masses calculated through the Vevo2100 system. Measurements in M-mode were calculated over four consecutive cardiac cycles and averaged. M-Mode and pulse-wave (PW) Doppler tracings were divided between two skilled technicians who were blinded to the assigned groups.

### *Speckle Tracking Echocardiography*

Strain analysis was applied to B-Mode videos captured in the parasternal short and long axes using the Visual Sonics VevoStrain software (Toronto, Canada) (25). Using speckle tracking software, points were designated along with endocardium and epicardium of the LV. The LV in parasternal short axis was segmented into six regions of interest: anterior free (AF), lateral (L), posterior (P), inferior free (IF), posterior septum (PS), and anterior septum (AS). Additionally, the LV in parasternal long axis was segmented into six regions of interest: anterior base (AB), anterior mid (AM), anterior apex (AA), posterior apex (PA), posterior mid (PM), and posterior base (PB). All of the individual segments were used in the proceeding analyses. Strain and strain rate were used for subsequent analyses. Doppler tracings were divided between two skilled technicians who were blinded to the assigned groups.

### *Machine Learning Pipeline*

Features from M-Mode (N=14), PW Doppler (N=13), strain analysis (N=57), as well as features including heart rate, root mean square of successive difference between heart beats (RMSSD), and dyssynchrony were used for analyses. Multicollinearity of features were assessed

using corrplot (v.0.90) (27) in R (v4.0.3). Machine learning was performed using BigML (<https://bigml.com>. BigML, Inc. Corvallis, Oregon, USA, 2011) using a mixed supervised/unsupervised platform (AutoML). A 75% training/testing and 25% holdout split was implemented to separate the data along with 10-fold cross validation. The top 3 most predictive models built on the 75% training/testing set were combined into a fusion model that was evaluated on the 25% holdout data. The evaluation data was extracted from BigML and used in the R environment to generate receiver operating characteristic (ROC) curves using pROC (v1.17.0.1) (21) and ggplot2 (v3.3.3) (28). Feature importance was assessed using packages randomForest (v.4.6-14) (12) and rfUtilities (v.2.1-5) (9) in R. All code can be found here: [https://github.com/qahathaway/DIO and UCMS](https://github.com/qahathaway/DIO_and_UCMS).

### *Statistics*

All statistical analyses were performed using GraphPad Prism v9.1.0 (GraphPad Software). Outliers were first removed using a ROUT test prior to analyses. On clean data, the D'Agostino-Pearson omnibus (K2) test was implemented to determine whether the data were normally distributed. Correlation tests were implemented to determine whether normalization of hemodynamic parameters using body weights or LV mass was necessary. For normally distributed data, the Pearson correlation coefficients were computed whereas the nonparametric Spearman correlation was applied to non-normally distributed data. Normally distributed data were then analyzed using either a one-way analysis of variance test (ANOVA) (Tukey's post hoc test) or a two-sided unpaired Student's t-test. Data that did not follow Gaussian distribution were analyzed using either a Kruskal-Wallis test (Dunn's post hoc test) or a Mann Whitney test, depending on the number of groups being compared. Significant differences between paired ROC curves were evaluated using DeLong's test (7, 21, 26). Results were considered statically significant if  $P \leq 0.05$ . All data are reported as the means  $\pm$  the standard error of the mean (SEM).



## Results

### *Study Paradigm*

An overview of the study design is provided to illustrate the three timepoints that were assessed in our analyses (**Figure 6.1A**). Briefly, echocardiography was performed at weeks 6, 18, and 26. High fat diet (HFD) was administered for 12 weeks followed by 8 weeks of unpredictable chronic mild stress (UCMS). Body weights were assessed at each time point (**Figure 6.1B**). As expected, in the presence of a 12-week HFD regime the obese group gained 18.72 grams while the lean group only gained 7.33 grams compared to their baseline assessments. In the presence of UCMS, the HFD mice failed to gain more weight, unlike their non-UCMS counterparts. Additionally, the weight lost by the lean group of mice was statistically significant in the UCMS group, but not the non-UCMS group (**Figure 6.1B**).

### *Traditional Echocardiographic Assessments*

First, we wanted to understand if functional and structural changes of the LV would be observed following HFD. Measures of systolic and diastolic function for the baseline (6-week-old) and post-diet (18-week-old) animals are provided for M-Mode (**Table 6.1**) and PW Doppler (**Table 6.2**). The lean group of animals (18-week-old) compared to their baseline assessments (6-week-old) revealed increased ejection fraction (EF) (88.33% vs. 81.80%) and fractional shortening (FS) (60.11% vs. 50.88%) and decreased systolic volumes (3.828  $\mu$ l vs. 7.997  $\mu$ l) (**Table 6.1**), but did not exhibit significant changes in left ventricle (LV) mass (120.5 mg vs 109.8 mg). The obese group of animals (18-week-old) presented with a significantly decreased EF (76.38% vs. 88.33%) and FS (45.32% vs. 60.11%) compared to the lean cohort (18-week-old) with a significantly elevated LV mass (150.7 mg vs. 120.5 mg) and stroke volume (38.35  $\mu$ l vs. 26.72  $\mu$ l) (**Table 6.1**). PW Doppler also revealed other poorly adaptive functional changes in the obese group (**Table 6.2**). This included decreases in the obese groups MV A (333.0 mm/s vs. 395.6 mm/s) and increased E/A ratio (1.869 vs. 1.583) compared to their baseline. These data suggest that the obese cohort (18-week-old) has both LV functional impairments, through decreased pump efficiency (lower EF and FS), as well as changes in atrial function (lower MV A and higher E/A ratio). The functional changes, along with increased LV mass and stroke volume, indicate the burden of the

HFD on cardiovascular function in the obese animals. Comparisons not discussed (**Table 6.1** and **Table 6.2**) as well as the individual data points (**Additional File 6.1**) are provided.

### *Speckle Tracking Echocardiography and Data Discovery Pathway*

Our next step was to apply the stress strain workflow to the B-Mode videos in the parasternal short and long axes (**Figure 6.2A**), which included segmental strain analysis. The LV segments are anatomically defined regions of the myocardium in both the short (**Figure 6.2A**) and long (**Figure 6.2B**) axes. The raw data obtained from these analyses are included (**Additional File 6.1**). Now, with data including M-Mode, PW Doppler, and segmental strain for the baseline (6-week-old) and the lean (18-week-old) and obese (18-week-old) cohorts, we applied our machine learning pipeline (**Figure 6.2C**). We first examined the data for the existence of strong collinearity within our feature sets (**Supplemental Figure 6.1**) and removed features with strong correlations ( $>0.85$ ) to decrease selection bias within the machine learning algorithms. Our machine learning pipeline included a mixed supervised/unsupervised platform that allowed for discovery of unique connections (unsupervised) and objective evaluations of the model (supervised).

### *Machine Learning – Obese versus Non-Obese*

Our objective was to compare non-obese animals (N=72, baseline + lean groups) with obese animals (N=24, obese group) to determine the predictive accuracy of our features for correctly identifying each animal into its respective group. Compiling all features together from M-Mode, PW Doppler, and strain analysis, there was a strong predictive accuracy (AUC: 0.969) for correctly delineating between obese and non-obese animals (**Figure 6.3A, line 1**). We then wanted to elucidate whether specific echocardiographic assessments (i.e. M-Mode, PW Doppler, or strain analysis) provided additional insights. There were no differences when comparing the compiled dataset to M-Mode (AUC: 0.969 vs. 0.968,  $P=0.99$ ) (**Figure 6.3A, line 2**) and strain analysis (AUC: 0.969 vs. 0.938,  $P=0.25$ ), (**Figure 6.3A, line 4**) but a significant difference when only PW Doppler was used (AUC: 0.969 vs. 0.746,  $P=0.05$ ) (**Figure 6.3A, line 3**). We further wanted to understand what features were most important in the construction of the machine learning model.

Using feature importance through randomForest, we show that the top two most important features in predicting obese vs. non-obese animals were radial strain of the anterior free wall and LV mass (**Figure 6.3B**). We also include the statistics for the top five most important features, as defined by randomForest (**Figure 6.3C**). Of note, four of the five top features were strain-based parameters, with only one parameter from M-Mode. Also, strain features offer a greater percent difference between groups (radial strain of the anterior free wall, -54%, radial strain of all segments, -45%, radial strain of the lateral wall, -64%, and radial strain rate of the anterior free wall, -35%) compared to M-Mode (LV mass, +33%). To better understand which features were important in the prediction of obese vs. non-obese mice, we further investigated the top five most important features in M-Mode (**Supplemental Figure 6.2A**), PW Doppler (**Supplemental Figure 6.3A**), and strain analysis (**Supplemental Figure 6.4A**) individually. This also included the traditional statistical analyses for M-Mode (**Supplemental Figure 6.2B**), PW Doppler (**Supplemental Figure 6.3B**), and strain analysis (**Supplemental Figure 6.4B**). These analyses suggest that a clear distinction is present between obese and non-obese animals when assessments derived from M-Mode and/or strain analysis are implemented. Additionally, the anterior free wall and lateral wall are disproportionately impacted by the obese phenotype.

#### *Machine Learning – Post-Unpredictable Chronic Mild Stress (UCMS)*

With an interest in understanding how a unique patterning may present following different insults, we further followed these animals throughout an 8-week UCMS protocol. We assessed if, irrespective of diet, we would be able to determine which animals received the UCMS protocol (N=22), compared to those that did not (N=22). Again, we first examined the data for the existence of strong collinearity within our feature sets (**Supplemental Figure 6.2**) and removed features with strong correlations ( $>0.85$ ) to decrease selection bias within the machine learning algorithms. The prediction of stressed (UCMS) versus non-stressed (non-UCMS) animals was robust (AUC: 0.868) (**Figure 6.4A**). RandomForest was used to select the top five most important features (**Figure 6.4B**) and the statistical representation of the features are also provided (**Figure 6.4C**). As expected, heart rate variability (HRV) was also significantly reduced post-UCMS (-49%) (**Figure 6.4D**). The averages of velocity, displacement, strain, and strain rate calculated in the parasternal short axis for the radial and circumferential dimensions (**Supplemental Table 6.1**) and in the long

axis for the longitudinal and circumferential dimensions (**Supplemental Table 6.2**) are included, along with all data used in the machine learning pipeline (**Additional File 6.1**).

Using the information gained from the post-diet and post-stress cohorts, we provide an illustration of the myocardial regions most significantly impacted by the stressors (**Figure 6.5**). We illustrate how the normal (**Figure 6.5A**) parasternal short and long axis segments compare to the post-diet (**Figure 6.5B**) and post-stress (**Figure 6.5C**) groups. While the anterior free and lateral wall are consistently altered between groups, the induction of stress (UCMS) appears to cause a more global impact on the myocardium. Conversely, high-fat diet feeding appeared to specifically affect the anterior free and lateral walls.

## Discussion

Recognizing the early markers of myocardial deformation is critical in alleviating the morbidity and mortality rates associated with cardiovascular disease. In recent years, the applications of speckle-tracking echocardiography have expanded significantly (10, 15, 19, 23). The sensitivity and specificity associated with strain imaging plays a crucial role in its increasingly prevalent use. Numerous studies have demonstrated the predictive value of strain echocardiography in terms of morbidity and mortality in the context of various cardiovascular diseases, particularly when compared to the prognostic information provided by ejection fraction alone (13). Although the ability of speckle-tracking to identify subclinical left ventricular dysfunction in many disease states is becoming more recognized, there is a scarcity of information on its potential to distinguish multiple insults via regional alterations. This study highlights the abilities of segmental stress-strain to identify specific regions of the LV that undergo wall motion abnormalities. Further, independent of diet, segmental stress-strain acts as a sensitive diagnostic marker for mapping additional insults, such as chronic stress (UCMS).

In 2018, 34.2 million Americans over the age of 18, were diagnosed with type 2 diabetes mellitus (T2DM). This number continues to grow and affect younger populations as the rate of individuals with high-fat diet induced obesity continuously increases (1). Cardiovascular disease, is a major cause of mortality in patients with T2DM around the world, affecting about 32% of those individuals (8). Detection of myocardial changes prior to overt dysfunction is therefore critical in reducing the number of cardiovascular related deaths. Notably, wall motion abnormalities can be detected prior to complications or changes in ejection fraction as previously demonstrated on a cohort of T2DM patients, with normal ejection fractions (6). The study revealed that conventional parameters could not detect LV dysfunction as early as global longitudinal strain (GLS) could, which was calculated using speckle-tracking echocardiography. Similarly, a study on obese children and adolescents without other comorbidities revealed that, although there were no difference between the ejection fractions of the obese and non-obese groups, GLS correlated negatively with body mass index (BMI) (3).

Furthermore, speckle-tracking echocardiography has been utilized to look at characteristic changes that occur in type 1 diabetes mellitus (T1DM) as compared to the changes seen in T2DM (14). The authors demonstrated that strain and strain rate parameters are valuable in describing the

dynamic changes in contractility, active relaxation, and LV stiffness between T1DM and T2DM animal models. Subclinical myocardial dysfunction can also be detected by speckle-tracking echocardiography in T1DM patients as evidenced by several previous studies (18, 20, 25). A previous study from our laboratory, performed on a T1DM animal model, assessed speckle tracking stress-strain, particularly using segmental analysis in both the short and long axes. Changes in myocardial strain were detected after only 1-week post diabetic onset, while conventional measures and diastolic dysfunction were not seen until 6 weeks post diabetic-onset. Segmental stress-strain analyses highlighted region-specific changes, specifically in the posterior and free wall regions throughout T1DM progression (25), while our data suggest that the anterior free and lateral walls are most significantly impacted with diet-induced obesity.

Although there has been a recent increase in literature relating to the usefulness of speckle-tracking echocardiography, there is a limited number of studies that investigate region specific changes as they correlate to specific insults. Nevertheless, a recent study that investigated the progression of T1DM in an animal model attempted to elucidate region specific changes after discovering decreases in both GLS and GLS rate (18). This study is of great importance as it verified segmental changes with MALDI-Imaging mass spectrometry. However, this study does not demonstrate how this information is applicable in a clinical setting for promoting early detection and intervention of cardiovascular diseases. Further, traditional statistical approaches are limited in their ability to provide information regarding generalizability and predictive accuracy. Zhang et. al., applied machine learning to speckle-tracking echocardiography features to create a predictive model for coronary heart disease (30). This is one example of how stress-strain imaging can play a pivotal role in the development of early detection screening tools using artificial intelligence approaches, which continues to hold promising future clinical applications.

Our study explores the implications of multiple insults on cardiovascular health, though we did not follow the animals for cardiovascular outcomes (i.e. stroke, heart failure, etc.). While we acknowledge the importance of tangible, outcome-based assessments, both the protocols involving diet-induced obesity (validated with body weight, LV mass, and ejection fraction) and unpredictable chronic mild stress (UCMS) (validated previously, (16, 29)) included objective standards. Additionally, the machine learning pipeline did not identify any regions within the parasternal long axis as significantly contributing to the differentiation of obese from non-obese

as well as UCMS from non-UCMS mice. The parasternal long axis view of the LV is perpendicular to the transducer, making it the best angle for reflection of the ultrasound beam (17). This suggests that the collection of longitudinal strain data should result in less noise and signal disturbance, further heightening our conclusions that no substantial alterations are occurring within that axis.

## **Conclusion**

This is the first study to present speckle-tracking echocardiography as a tool for uniquely “fingerprinting” multiple cardiovascular insults through segmental strain analysis. These insults included intrinsic (diet-induced obesity) and extrinsic (chronic stress) stressors to cardiovascular function that were correctly stratified using a combination of strain-based analyses with machine learning algorithms. The data presented highlight how clinical applications should consider evaluating if known contributors of cardiovascular dysfunction, such as diabetes, obesity, stress, and others, have distinctive, regional patterns that can be identified using segmental strain-based analyses. In this way, the multifaceted contribution leading to cardiovascular disease can be better understood, and targeted interventions applied.



## **Declarations**

### *Consent for publication*

Not applicable

### *Availability of Data and Materials*

The datasets and computer code produced in this study are available in the following databases

- Source Code: Github: [https://github.com/qahathaway/DIO and UCMS](https://github.com/qahathaway/DIO_and_UCMS)
- Datasets: Supplemental Data: Additional File 1

### *Competing Interests*

Partho P. Sengupta is a consultant to Heart Sciences, Ultromics, and Kencor Health. The other authors have nothing to disclose.

### *Funding*

This work was supported by: 20PRE35080170/AK/2020 (AK), NSF: #1920920 (PPS), R01 HL-128485 (JMH), 17PRE33660333/QAH/2017 (QAH), NIH, BINP R56 NS117754-01 (PDC), and the Community Foundation for the Ohio Valley Whipkey Trust (JMH).

### *Authors' contributions*

Designing research studies (AK, QAH, ENB, EEK, PPS, JMH, PDC), conducting experiments (AK, QAH, ENB, TC), acquiring data (AK, QAH, ENB, TC), analyzing data (AK, QAH, EEK, PPS, JMH, PDC), writing the manuscript (AK, QAH, PPS, JMH, PDC). The author Quincy A. Hathaway had full access to all the data in the study and takes responsibility for the integrity of the data and the accuracy of the data analysis. All authors read and approved the final manuscript.

### *Acknowledgements*

We would like to acknowledge and thank Sarah L. McLaughlin (Biological Technician – Animal Models and Imaging Facility) who performed echocardiography.

## References

1. (CDC) CfDCaP. Diabetes Fast Facts <https://www.cdc.gov/diabetes/basics/quick-facts.html>. [July 12 2021].
2. (WHO) WHO. Cardiovascular diseases (CVDs) WHO. [https://www.who.int/en/news-room/fact-sheets/detail/cardiovascular-diseases-\(cvds\)](https://www.who.int/en/news-room/fact-sheets/detail/cardiovascular-diseases-(cvds)). [10 July 2021].
3. **Barbosa JA, Mota CC, Simoes ESAC, Nunes Mdo C, and Barbosa MM.** Assessing pre-clinical ventricular dysfunction in obese children and adolescents: the value of speckle tracking imaging. *Eur Heart J Cardiovasc Imaging* 14: 882-889, 2013.
4. **Biering-Sorensen T, Biering-Sorensen SR, Olsen FJ, Sengelov M, Jorgensen PG, Mogelvang R, Shah AM, and Jensen JS.** Global Longitudinal Strain by Echocardiography Predicts Long-Term Risk of Cardiovascular Morbidity and Mortality in a Low-Risk General Population: The Copenhagen City Heart Study. *Circ Cardiovasc Imaging* 10: 2017.
5. **Burchfield JS, Xie M, and Hill JA.** Pathological ventricular remodeling: mechanisms: part 1 of 2. *Circulation* 128: 388-400, 2013.
6. **Conte L, Fabiani I, Barletta V, Bianchi C, Maria CA, Cucco C, De Filippi M, Miccoli R, Prato SD, Palombo C, and Di Bello V.** Early Detection of Left Ventricular Dysfunction in Diabetes Mellitus Patients with Normal Ejection Fraction, Stratified by BMI: A Preliminary Speckle Tracking Echocardiography Study. *J Cardiovasc Echogr* 23: 73-80, 2013.
7. **DeLong ER, DeLong DM, and Clarke-Pearson DL.** Comparing the areas under two or more correlated receiver operating characteristic curves: a nonparametric approach. *Biometrics* 44: 837-845, 1988.
8. **Einarson TR, Acs A, Ludwig C, and Panton UH.** Prevalence of cardiovascular disease in type 2 diabetes: a systematic literature review of scientific evidence from across the world in 2007-2017. *Cardiovasc Diabetol* 17: 83, 2018.
9. **Evans JS, Murphy MA, Holden ZA, and Cushman SA.** *Modeling species distribution and change using Random Forests*. New York: Springer, 2011.
10. **Gupta K, Kakar TS, Gupta A, Singh A, Gharpure N, Aryal S, Hawi R, Lloyd SG, Booker J, Hage FG, Prabhu SD, Nanda NC, and Bajaj NS.** Role of left ventricle deformation analysis in stress echocardiography for significant coronary artery disease detection: A diagnostic study meta-analysis. *Echocardiography* 36: 1084-1094, 2019.
11. **Karlsen S, Dahlslett T, Grenne B, Sjoli B, Smiseth O, Edvardsen T, and Brunvand H.** Global longitudinal strain is a more reproducible measure of left ventricular function than ejection fraction regardless of echocardiographic training. *Cardiovasc Ultrasound* 17: 18, 2019.
12. **Liaw A, and Wiener M.** Classification and Regression by randomForest. *R News* 2: 18-22, 2002.
13. **Luis SA, Chan J, and Pellikka PA.** Echocardiographic Assessment of Left Ventricular Systolic Function: An Overview of Contemporary Techniques, Including Speckle-Tracking Echocardiography. *Mayo Clin Proc* 94: 125-138, 2019.
14. **Matyas C, Kovacs A, Nemeth BT, Olah A, Braun S, Tokodi M, Barta BA, Benke K, Ruppert M, Lakatos BK, Merkely B, and Radovits T.** Comparison of speckle-tracking echocardiography with invasive hemodynamics for the detection of characteristic cardiac dysfunction in type-1 and type-2 diabetic rat models. *Cardiovasc Diabetol* 17: 13, 2018.
15. **Meng S, Guo L, and Li G.** Early changes in right ventricular longitudinal function in chronic asymptomatic alcoholics revealed by two-dimensional speckle tracking echocardiography. *Cardiovasc Ultrasound* 14: 16, 2016.

16. **Mineur YS, Belzung C, and Crusio WE.** Functional implications of decreases in neurogenesis following chronic mild stress in mice. *Neuroscience* 150: 251-259, 2007.
17. **Mitchell C, Rahko PS, Blauwet LA, Canaday B, Finstuen JA, Foster MC, Horton K, Ogunyankin KO, Palma RA, and Velazquez EJ.** Guidelines for Performing a Comprehensive Transthoracic Echocardiographic Examination in Adults: Recommendations from the American Society of Echocardiography. *J Am Soc Echocardiogr* 32: 1-64, 2019.
18. **Pappritz K, Grune J, Klein O, Hegemann N, Dong F, El-Shafeey M, Lin J, Kuebler WM, Kintscher U, Tschope C, and Van Linthout S.** Speckle-tracking echocardiography combined with imaging mass spectrometry assesses region-dependent alterations. *Sci Rep* 10: 3629, 2020.
19. **Parsaee M, Saedi S, Joghataei P, Azarkeivan A, and Alizadeh Sani Z.** Value of speckle tracking echocardiography for detection of clinically silent left ventricular dysfunction in patients with beta-thalassemia. *Hematology* 22: 554-558, 2017.
20. **Ringle A, Dornhorst A, Rehman MB, Ruisanchez C, and Nihoyannopoulos P.** Evolution of subclinical myocardial dysfunction detected by two-dimensional and three-dimensional speckle tracking in asymptomatic type 1 diabetic patients: a longterm follow-up study. *Echo Res Pract* 4: 73-81, 2017.
21. **Robin X, Turck N, Hainard A, Tiberti N, Lisacek F, Sanchez JC, and Muller M.** pROC: an open-source package for R and S+ to analyze and compare ROC curves. *BMC Bioinformatics* 12: 77, 2011.
22. **Romano S, Mansour IN, Kansal M, Gheith H, Dowdy Z, Dickens CA, Buto-Colletti C, Chae JM, Saleh HH, and Stamos TD.** Left Ventricular global longitudinal strain predicts heart failure readmission in acute decompensated heart failure. *Cardiovasc Ultrasound* 15: 6, 2017.
23. **Saccheri MC, Cianciulli TF, Morita LA, Mendez RJ, Beck MA, Guerra JE, Cozzarin A, Puente LJ, Balletti LR, and Lax JA.** Speckle tracking echocardiography to assess regional ventricular function in patients with apical hypertrophic cardiomyopathy. *World J Cardiol* 9: 363-370, 2017.
24. **Sengelov M, Jorgensen PG, Jensen JS, Bruun NE, Olsen FJ, Fritz-Hansen T, Nochioka K, and Biering-Sorensen T.** Global Longitudinal Strain Is a Superior Predictor of All-Cause Mortality in Heart Failure With Reduced Ejection Fraction. *JACC Cardiovasc Imaging* 8: 1351-1359, 2015.
25. **Shepherd DL, Nichols CE, Croston TL, McLaughlin SL, Petrone AB, Lewis SE, Thapa D, Long DM, Dick GM, and Hollander JM.** Early detection of cardiac dysfunction in the type 1 diabetic heart using speckle-tracking based strain imaging. *J Mol Cell Cardiol* 90: 74-83, 2016.
26. **Sun X, and Xu W.** Fast Implementation of DeLong's Algorithm for Comparing the Areas Under Correlated Receiver Operating Characteristic Curves. *IEEE Signal Processing Letters* 21: 1389-1393, 2014.
27. **T. W, and V. S.** R package 'corrplot': Visualization of a Correlation Matrix. 2021.
28. **Wickham H.** *ggplot2: Elegant Graphics for Data Analysis.* New York: Springer-Verlag New York, 2016.
29. **Willner P.** Validity, reliability and utility of the chronic mild stress model of depression: a 10-year review and evaluation. *Psychopharmacology (Berl)* 134: 319-329, 1997.

30. **Zhang J, Zhu H, Chen Y, Yang C, Cheng H, Li Y, Zhong W, and Wang F.** Ensemble machine learning approach for screening of coronary heart disease based on echocardiography and risk factors. *BMC Med Inform Decis Mak* 21: 187, 2021.

## Tables

**Table 6.1 – M-Mode Parameters**

<b>Parameter</b>	<b>Baseline <sup>a</sup></b>	<b>Lean <sup>b</sup></b>	<b>Obese <sup>c</sup></b>
<b>Heart Rate (BPM)</b>	475.2 ± 16.57	581.1 ± 25.83 <sup>a</sup>	474.3 ± 21.43 <sup>b</sup>
<b>Diameter; s (mm)</b>	1.547 ± 0.073	1.166 ± 0.103 <sup>a</sup>	1.948 ± 0.101 <sup>a,b</sup>
<b>Diameter; d (mm)</b>	3.079 ± 0.067	2.823 ± 0.075	3.468 ± 0.098 <sup>a,b</sup>
<b>Volume; s (µL)</b>	7.997 ± 0.864	3.828 ± 0.727 <sup>a</sup>	13.41 ± 1.430 <sup>a,b</sup>
<b>Volume; d (µL)</b>	38.71 ± 1.960	31.06 ± 2.125	51.76 ± 3.156 <sup>a,b</sup>
<b>Stroke Volume (µL)</b>	30.71 ± 1.240	26.72 ± 1.316	38.35 ± 1.892 <sup>a,b</sup>
<b>Ejection Fraction (%)</b>	81.80 ± 1.323	88.33 ± 1.667 <sup>a</sup>	76.38 ± 1.743 <sup>a,b</sup>
<b>Fractional Shortening (%)</b>	50.88 ± 1.510	60.11 ± 2.708 <sup>a</sup>	45.32 ± 1.770 <sup>b</sup>
<b>Cardiac Output (mL/min)</b>	14.00 ± 0.497	15.12 ± 0.730	17.29 ± 0.853 <sup>a</sup>
<b>LV Mass (mg)</b>	109.8 ± 3.198	120.5 ± 4.632	150.7 ± 5.765 <sup>a,b</sup>
<b>LVAW; s (mm)</b>	1.717 ± 0.031	1.938 ± 0.046 <sup>a</sup>	1.858 ± 0.044 <sup>a</sup>
<b>LVAW; d (mm)</b>	1.051 ± 0.025	1.213 ± 0.031 <sup>a</sup>	1.186 ± 0.048 <sup>a</sup>
<b>LVPW; s (mm)</b>	1.378 ± 0.409	1.635 ± 0.058 <sup>a</sup>	1.401 ± 0.051 <sup>b</sup>
<b>LVPW; d (mm)</b>	0.969 ± 0.037	1.112 ± 0.054	1.051 ± 0.044

**Table 6.1:** M-Mode assessments for the baseline (6-week-old) (N=48), lean (18-week-old) (N=24), and obese (18-week-old) (N=24). Outliers were removed using a ROUT test, the D'Agostino-Pearson omnibus (K2) test was implemented to determine normal distribution, and an ANOVA/Tukey's post hoc test (normally distributed) or Kruskal-Wallis test/Dunn's post hoc test (non-normally distributed) were used to determine significance. Results were considered statically significant if  $P \leq 0.05$ . All data are reported as the means  $\pm$  the standard error of the mean (SEM). <sup>a</sup> = statistically different than the baseline group, <sup>b</sup> = statistically different than the lean group, s = systolic, d = diastolic, LV = left ventricle, AW = anterior wall, PW = posterior wall.

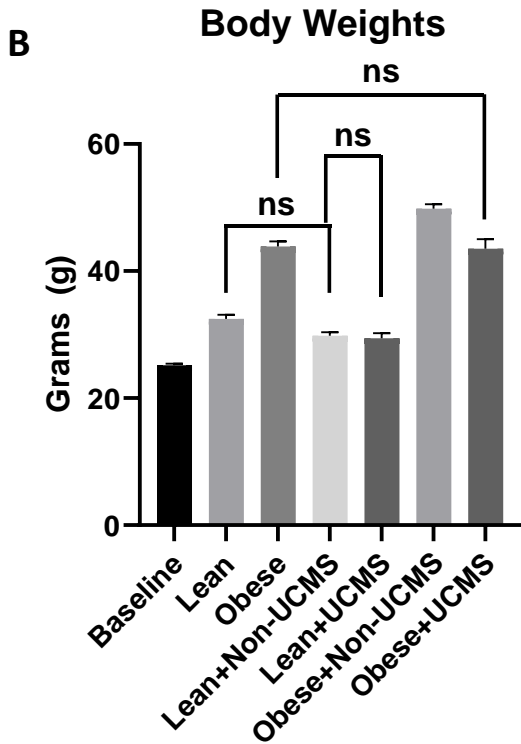
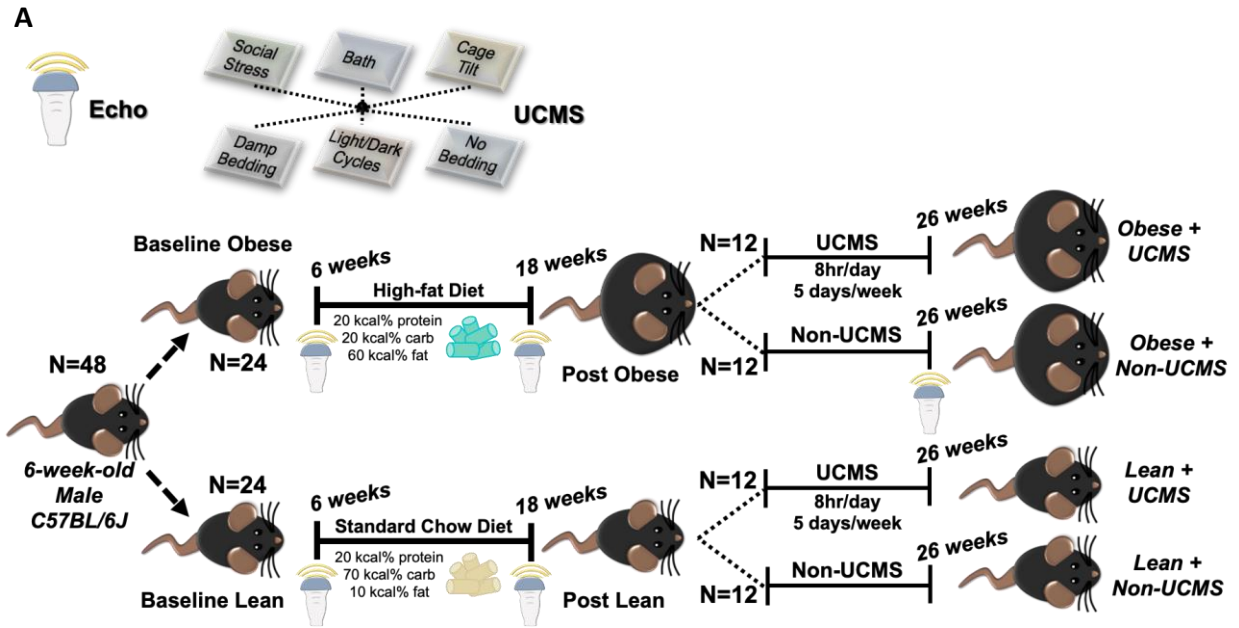
**Table 6.2 – Pulse Wave (PW) Doppler**

<b>Parameter</b>	<b>Baseline <sup>a</sup></b>	<b>Lean <sup>b</sup></b>	<b>Obese <sup>c</sup></b>
<b>AET (ms)</b>	41.09 ± 0.948	31.30 ± 1.559 <sup>a</sup>	39.98 ± 1.444 <sup>b</sup>
<b>IVCT (ms)</b>	17.10 ± 1.096	11.28 ± 0.775 <sup>a</sup>	18.19 ± 0.691 <sup>b</sup>
<b>IVRT (ms)</b>	19.21 ± 0.509	20.31 ± 1.194	19.09 ± 0.641
<b>MV A (mm/s)</b>	395.6 ± 13.48	380.9 ± 16.22	333.0 ± 11.97 <sup>a</sup>
<b>MV Decel (mm/s<sup>2</sup>)</b>	-26523 ± 1067	-35276 ± 2315 <sup>a</sup>	-24536 ± 1190 <sup>b</sup>
<b>MV Decel (ms)</b>	22.93 ± 0.747	18.53 ± 0.769 <sup>a</sup>	24.78 ± 1.220 <sup>b</sup>
<b>MV E (mm/s)</b>	614.9 ± 18.43	659.5 ± 27.85	606.9 ± 19.71
<b>NFT (ms)</b>	77.77 ± 1.767	63.22 ± 1.525 <sup>a</sup>	76.60 ± 1.813 <sup>b</sup>
<b>LV MPI IV</b>	0.898 ± 0.030	1.094 ± 0.090	0.965 ± 0.053
<b>LV MPI NFT</b>	0.908 ± 0.032	1.107 ± 0.090	0.954 ± 0.055
<b>MV Area (mm<sup>2</sup>)</b>	35.12 ± 1.383	41.80 ± 2.110 <sup>a</sup>	32.41 ± 1.645 <sup>b</sup>
<b>MV E/A</b>	1.583 ± 0.037	1.768 ± 0.078	1.869 ± 0.088 <sup>a</sup>
<b>MV PHT (ms)</b>	6.649 ± 0.216	5.373 ± 0.223 <sup>a</sup>	7.186 ± 0.354 <sup>b</sup>



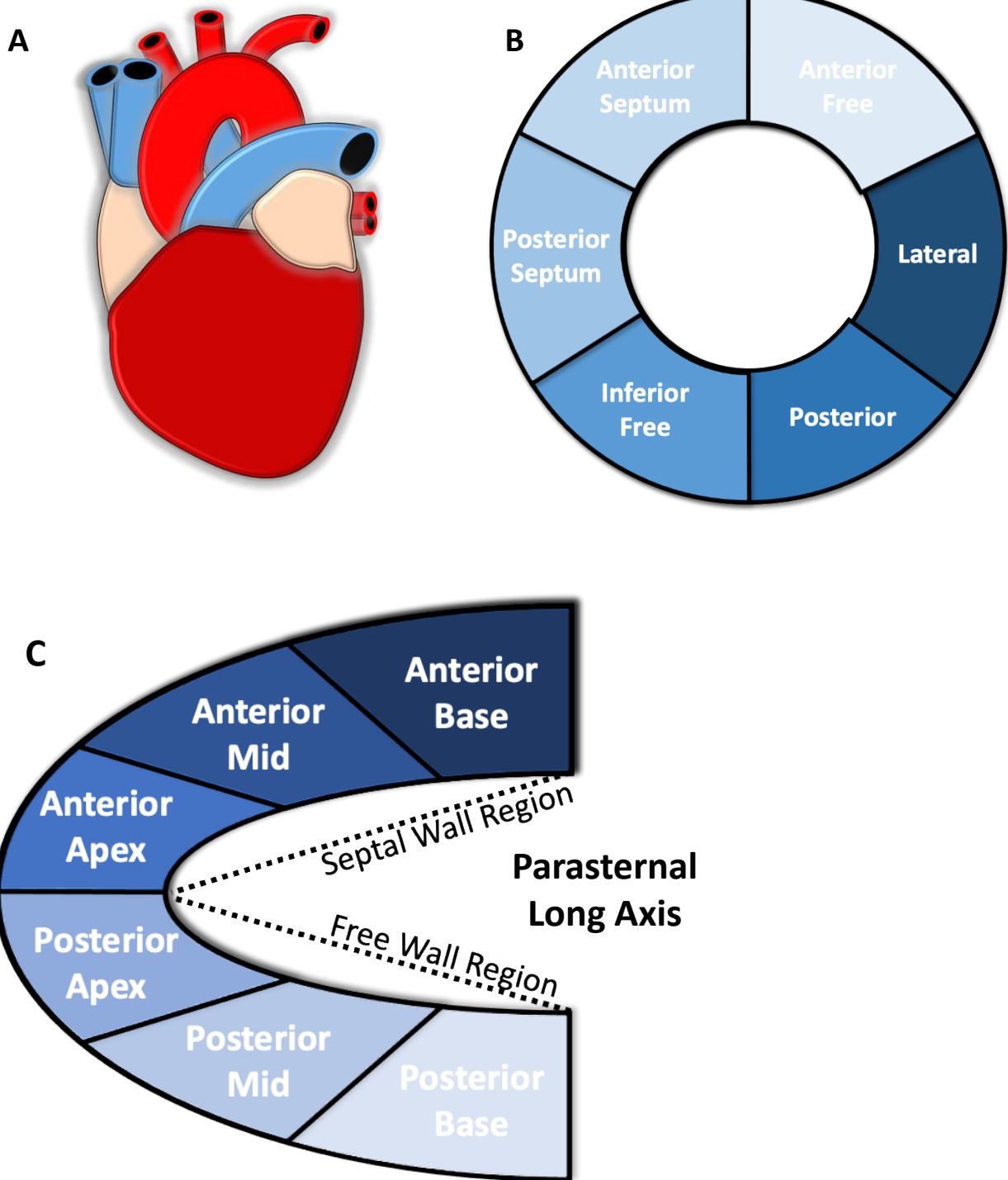
**Table 6.2:** PW Doppler assessments for the baseline (6-week-old) (N=48), lean (18-week-old) (N=24), and obese (18-week-old) (N=24). Outliers were removed using a ROUT test, the D'Agostino-Pearson omnibus (K2) test was implemented to determine normal distribution, and an ANOVA/Tukey's post hoc test (normally distributed) or Kruskal-Wallis test/Dunn's post hoc test (non-normally distributed) were used to determine significance. Results were considered statically significant if  $P \leq 0.05$ . All data are reported as the means  $\pm$  the standard error of the mean (SEM). <sup>a</sup> = statistically different than the baseline group, <sup>b</sup> = statistically different than the lean group, LV = left ventricle, AET = aortic ejection time, MV = mitral valve, IVCT = isovolumetric contraction time, IVRT, isovolumetric relaxation time, Decel = deceleration, MPI = myocardial performance index, NFT = no flow time, PHT = pressure half-time.

Figure 6.1



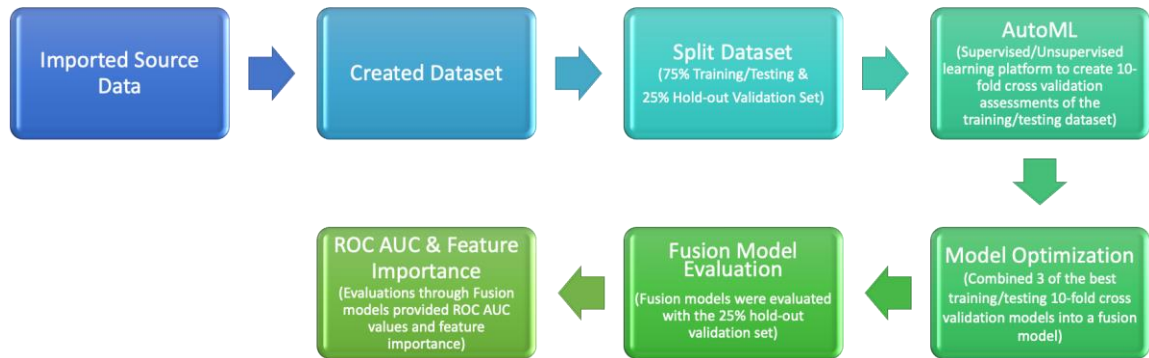
**Figure 6.1: Experimental paradigm and body weights.** (A) High-fat diet (HFD) feeding and stress protocol: 6-weekold, male C57BL/6J mice were randomized into lean (N=24) and obese (N=24) groups. Mice in the obese group underwent 12 weeks of diet induced obesity (DIO), while the lean group consumed standard chow. At 18 weeks of age, mice in the lean and obese groups were further randomized into unpredictable chronic mild stress (UCMS) (N=22) and non-UCMS (N=22) groups to elicit a chronically stressed phenotype over an 8-week period. Echocardiography was performed at baseline (6 weeks, N=48), post-diet (18 weeks, N=48), and post-stress (26 weeks, N=44) time points. (B) Body weights in grams for each cohort. All comparisons are statistically significant except for those labeled “ns”. The D’Agostino-Pearson omnibus (K2) test was implemented to determine normal distribution, and an ANOVA/Tukey’s post hoc test (normally distributed) was used to determine significance. Results were considered statically significant if  $P \leq 0.05$ . All data are reported as the means  $\pm$  the standard error of the mean (SEM). Ns = not significantly different.

Figure 6.2:



**Figure 6.2:**

**D**



**Figure 6.2: Segmental strain and machine learning pipeline.** (A) The LV in parasternal short axis was segmented into six regions of interest: anterior free (AF), lateral (L), posterior (P), inferior free (IF), posterior septum (PS), and anterior septum (AS). Additionally, (B) the LV in parasternal long axis was segmented into six regions of interest: anterior base (AB), anterior mid (AM), anterior apex (AA), posterior apex (PA), posterior mid (PM), and posterior base (PB). (C) Data were imported and used to create a dataset containing segmental speckle tracking stress-strain, M-Mode, and Pulse Wave Doppler, that were then split (75% Training/Testing and 25% Hold-out validation sets). A mixed supervised/unsupervised machine learning model was used through the BigML platform that provided 10-cross validation models of the Training/Testing dataset. The top 3 models for each analysis were then fused to create a more holistic model. The data were evaluated using the AUC generated from the hold-out dataset, as an indication of the accuracy of the model for predicting the desired outcome (HFD or UCMS).

Figure 6.3:

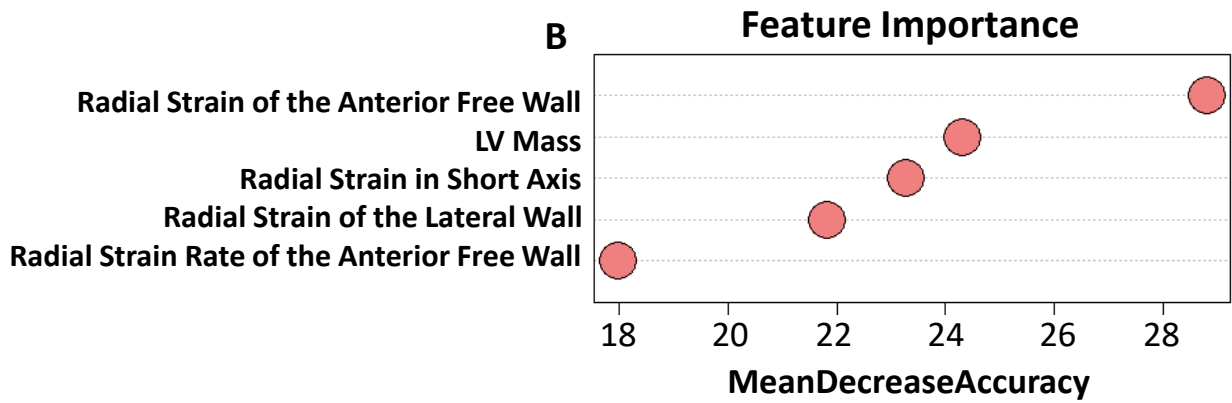
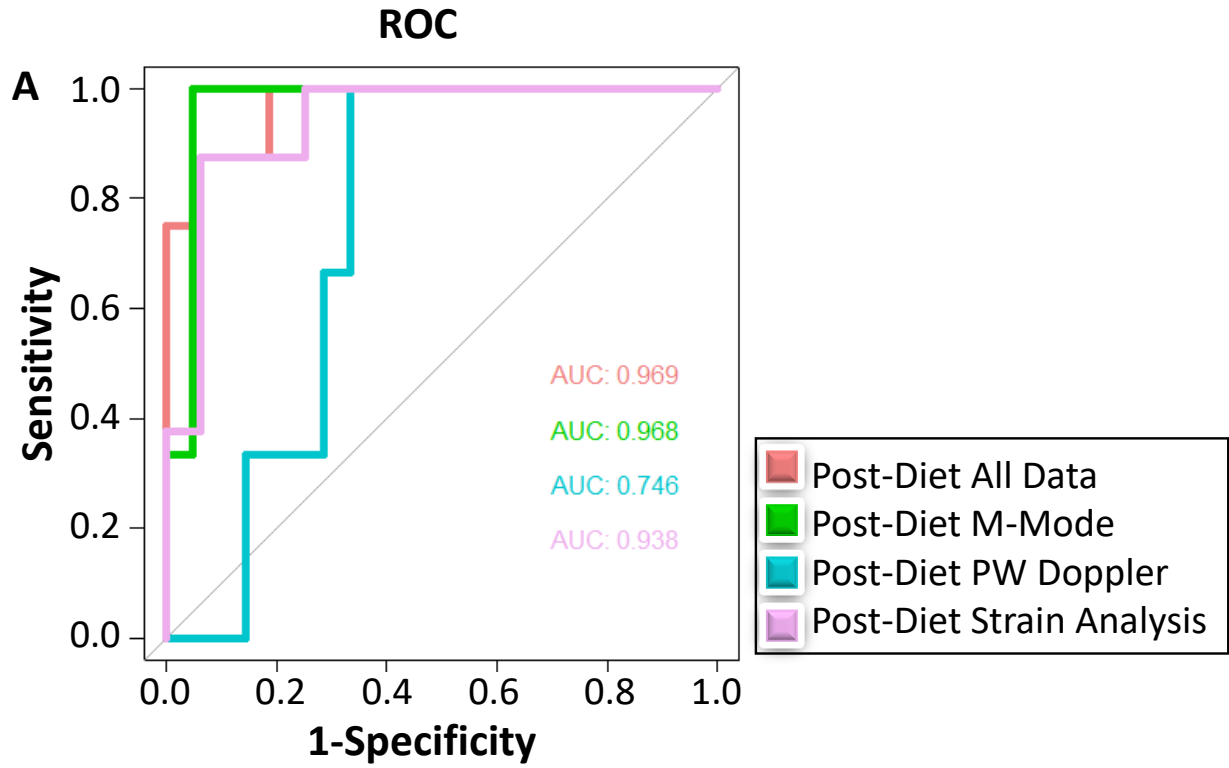
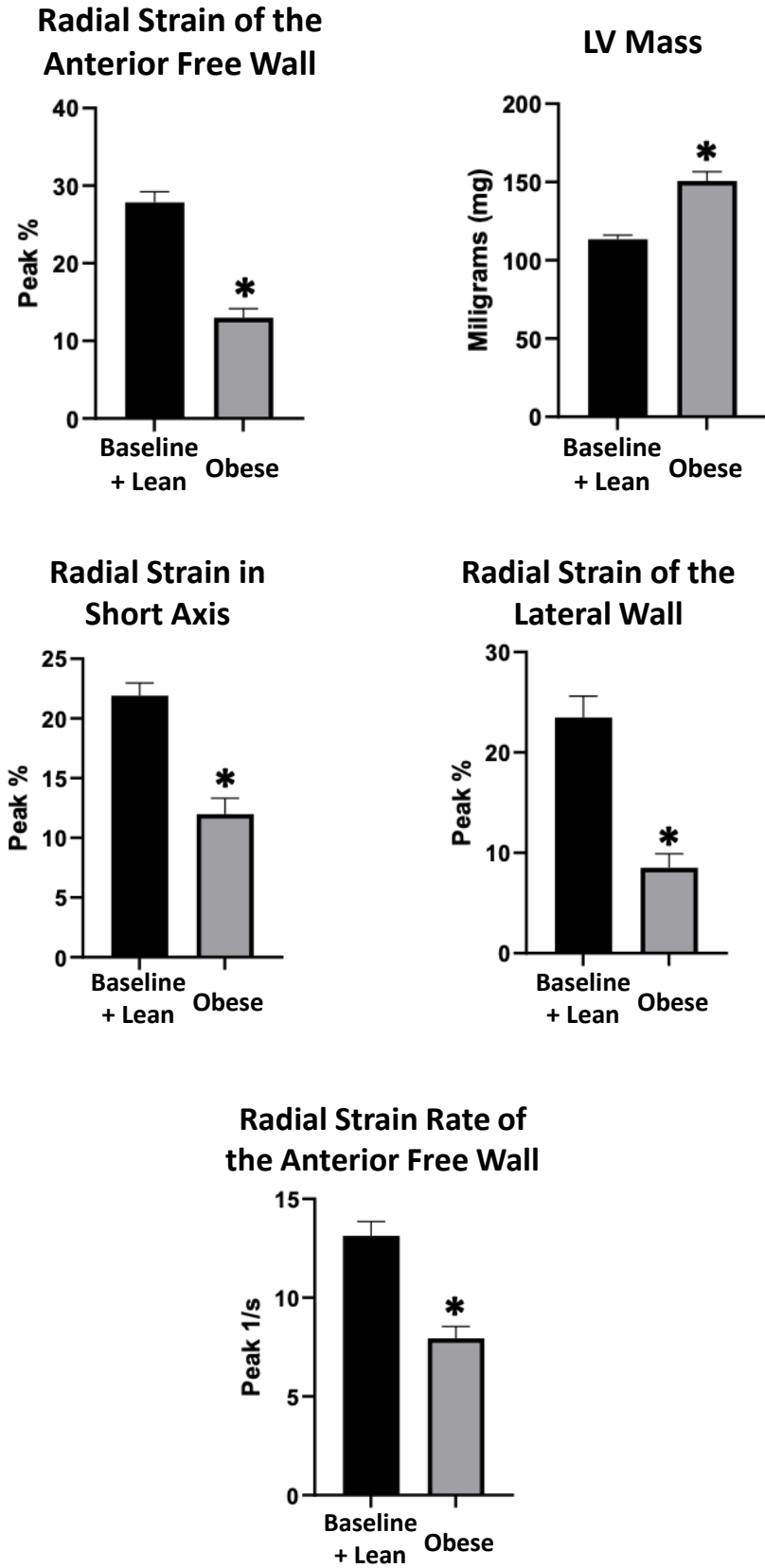


Figure 6.3:

C





**Figure 6.3: Obese versus non-obese analyses.** Features derived from M-mode, Pulse Wave (PW) Doppler, and strain analyses were used in machine learning applications for non-obese (baseline and lean, N=72) and obese (N=24) mice. Implementation of AutoML, model optimization, and fusion model evaluation were performed. (A) ROC curves were graphed, and AUC scores calculated. (B) Feature importance was determined using randomForest and evaluated based on MeanDecreaseAccuracy. (C) The top five most important features are provided with their values. Outliers were removed using a ROUT test, the D'Agostino-Pearson omnibus (K2) test was implemented to determine normal distribution, and a two-sided unpaired Student's t-test (normally distributed) or Mann Whitney test (non-normally distributed) were used to determine significance. Results were considered statically significant if  $P \leq 0.05$  and indicated by “\*”. All data are reported as the means  $\pm$  the standard error of the mean (SEM). Post-Diet = post high-fat diet induced obesity.

Figure 6.4:

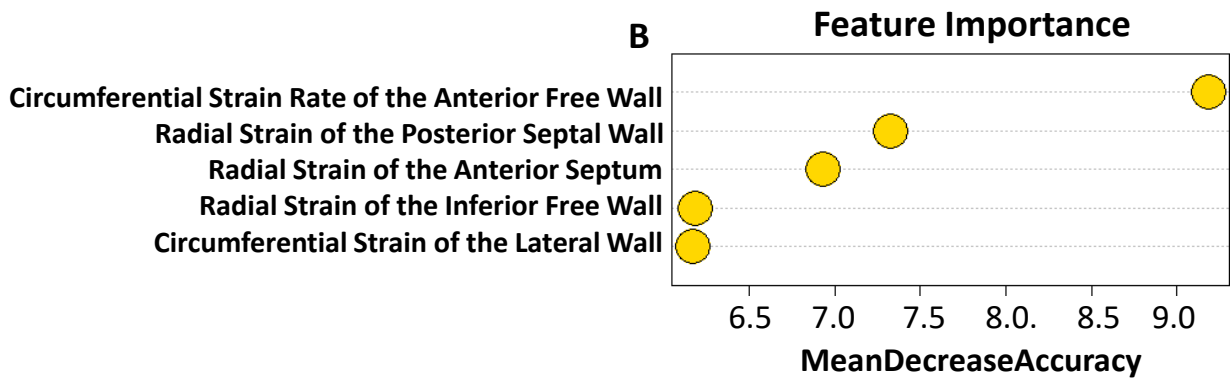
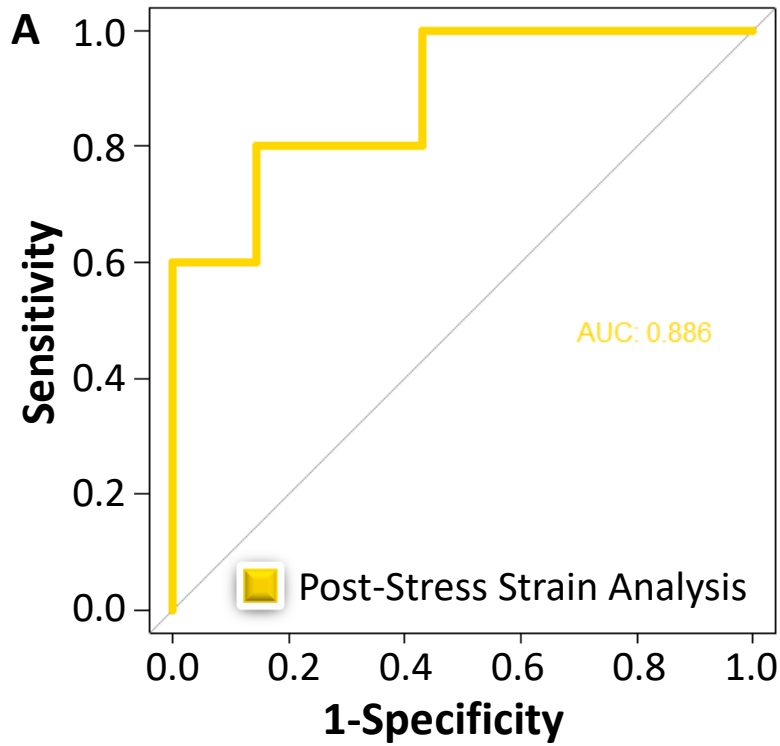


Figure 6.4:

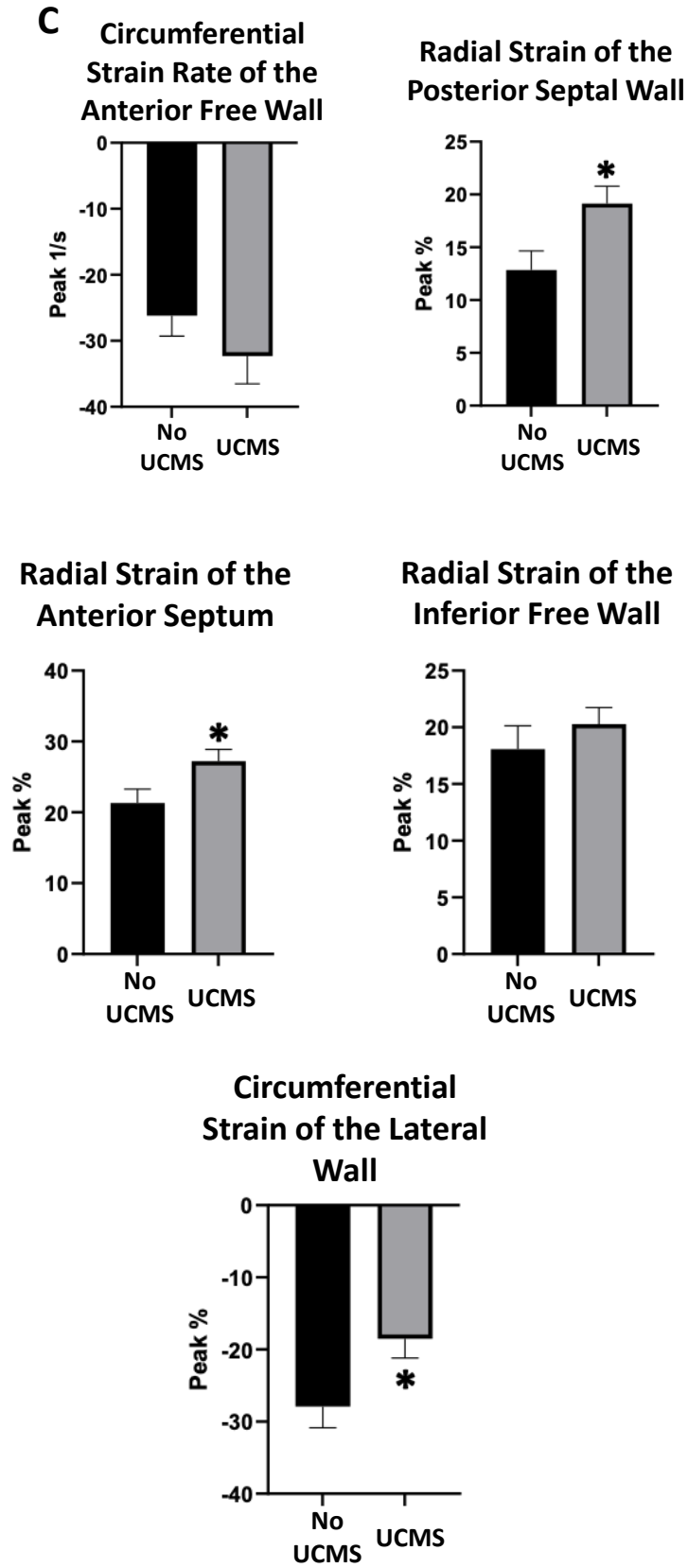
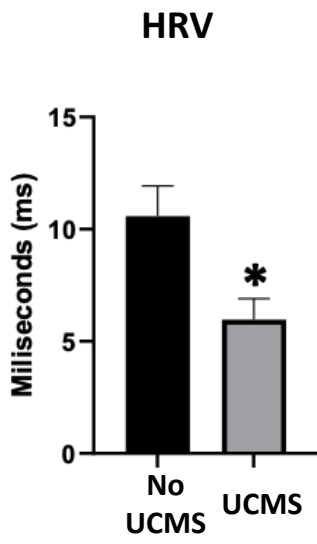


Figure 6.4:

D



**Figure 6.4: UCMS versus non-UCMS analyses, irrespective of diet.** Features derived from strain analyses were used in machine learning applications for non-UCMS (N=22) and UCMS (N=22) mice at 26 weeks. Implementation of AutoML, model optimization, and fusion model evaluation were performed. (A) The ROC curve was graphed, and AUC score calculated. (B) Feature importance was determined using randomForest and evaluated based on MeanDecreaseAccuracy. (C) The top five most important features are provided with their values. (D) Heart rate variability (HRV) is also shown for comparison. Outliers were removed using a ROUT test, the D’Agostino-Pearson omnibus (K2) test was implemented to determine normal distribution, and a two-sided unpaired Student’s t-test (normally distributed) or Mann Whitney test (non-normally distributed) were used to determine significance. Results were considered statically significant if  $P \leq 0.05$  and indicated by “\*”. All data are reported as the means  $\pm$  the standard error of the mean (SEM).

Figure 6.5:

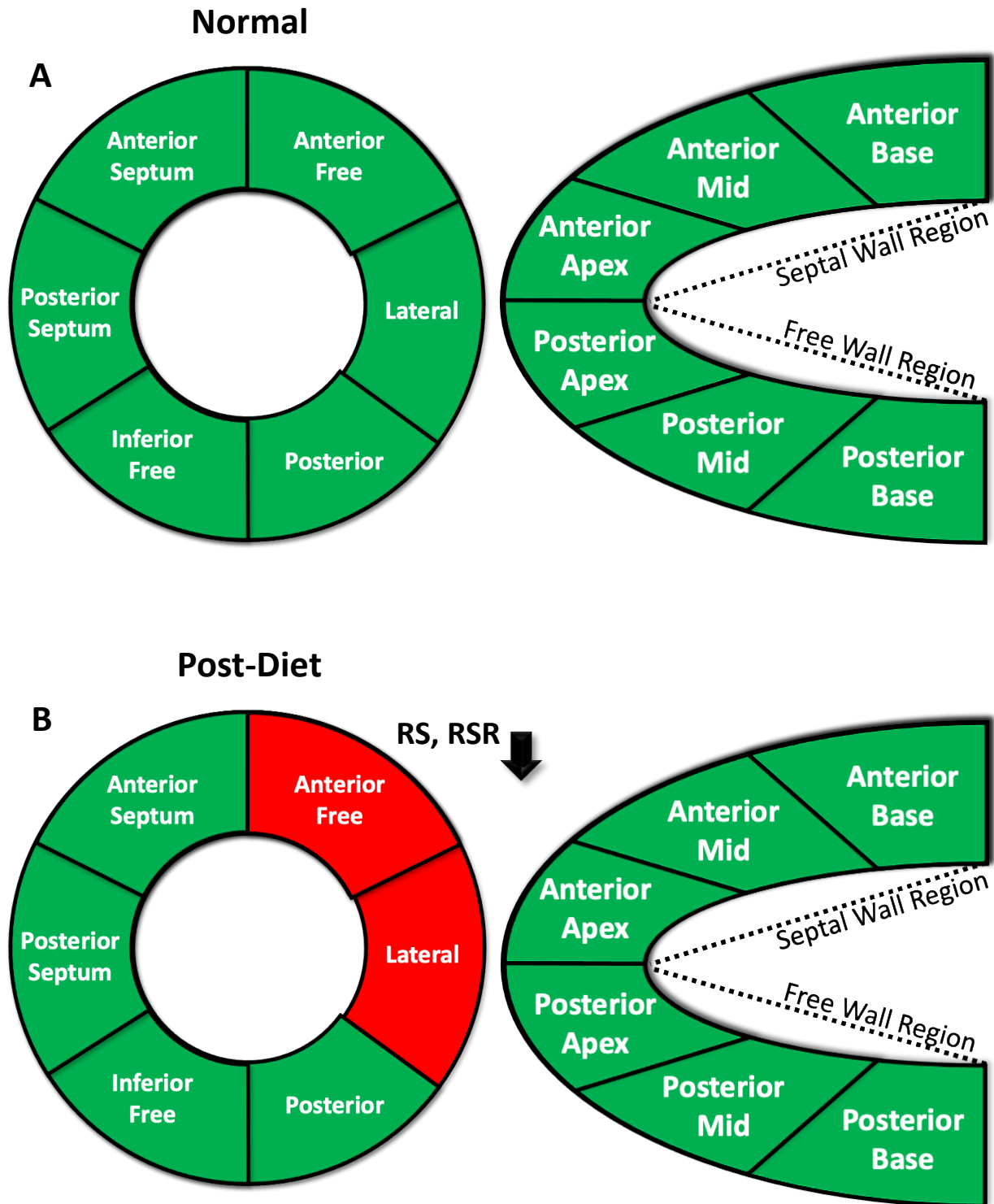
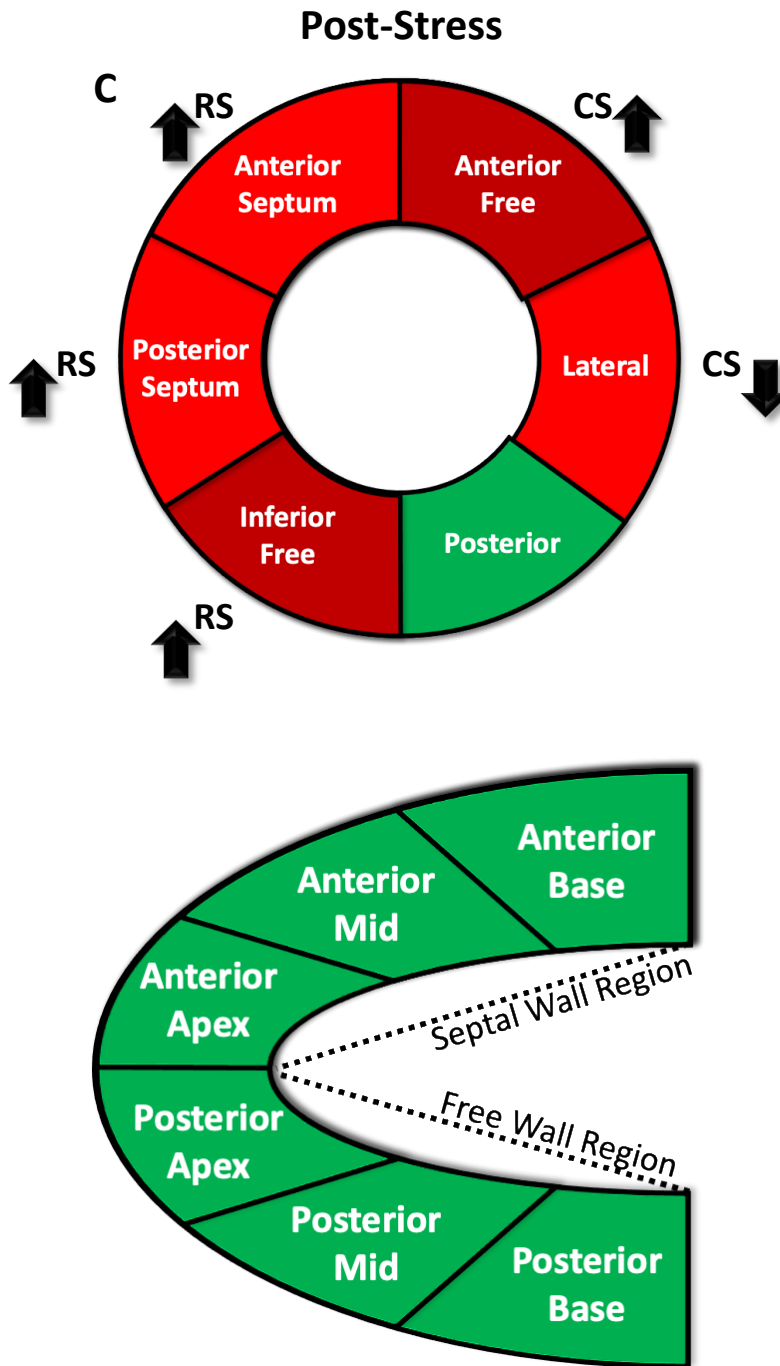


Figure 6.5:



**Figure 6.5: Overview of regional impacts of diet-induced obesity (DIO) and unpredictable chronic mild stress (UCMS).** The (A) normal, (B) post-diet, and (C) post-stress segmental strain profiles are shown. Green indicates baseline strain function for the indicated left ventricular (LV) region. Bright red indicates a region identified as important by one or more of the top predictive features that is also statistically significantly different. Dark red indicates a region identified as important by one or more of the top predictive features, but that is not statistically significantly different. RS = radial strain, RSR = radial strain rate, CS = circumferential strain. Post-Diet = post high-fat diet induced obesity.



## Supplemental Tables

### Supplemental Table 6.1 – Short-Axis Systolic Stress-Strain

Parameter	Units	Baseline <sup>a</sup>	Lean <sup>b</sup>	Obese <sup>c</sup>	Non-UCMS <sup>d</sup>	UCMS
Radial Velocity	Pk cm/s	1.663 ± 0.067	2.200 ± 0.094 <sup>a</sup>	1.680 ± 0.060 <sup>b</sup>	2.159 ± 0.120 <sup>a,c</sup>	2.285 ± 0.110 <sup>a,c</sup>
Radial Displacement	Pk mm	0.398 ± 0.016	0.474 ± 0.014 <sup>a</sup>	0.313 ± 0.023 <sup>a,b</sup>	0.353 ± 0.029 <sup>b</sup>	0.395 ± 0.017
Radial Strain	Pk %	20.33 ± 1.279	25.55 ± 1.039 <sup>a</sup>	11.99 ± 1.334 <sup>a,b</sup>	17.29 ± 1.875 <sup>b,c</sup>	19.30 ± 1.043 <sup>c</sup>
Radial Strain Rate	Pk 1/s	8.561 ± 0.401	12.96 ± 0.491 <sup>a</sup>	8.019 ± 0.624 <sup>b</sup>	17.25 ± 3.183 <sup>a,c</sup>	17.86 ± 3.485 <sup>a,c</sup>
Circumferential Velocity	Pk deg/s	324.6 ± 20.31	607.2 ± 79.89 <sup>a</sup>	292.7 ± 24.17 <sup>b</sup>	489.0 ± 38.41 <sup>a,c</sup>	600.3 ± 71.32 <sup>a,c</sup>
Circumferential Displacement	Pk deg	3.584 ± 0.363	6.055 ± 0.635 <sup>a</sup>	2.238 ± 0.419 <sup>b</sup>	6.263 ± 0.789 <sup>a,c</sup>	5.570 ± 0.840 <sup>c</sup>
Circumferential Strain	Pk %	-22.78 ± 1.255	-23.64 ± 1.151	-16.79 ± 0.956 <sup>a,b</sup>	-20.49 ± 1.982	-22.20 ± 1.788
Circumferential Strain Rate	Pk 1/s	-13.83 ± 1.010	-17.24 ± 1.526	-12.16 ± 1.276	-20.29 ± 1.850 <sup>a,c</sup>	-21.12 ± 1.912 <sup>a,c</sup>

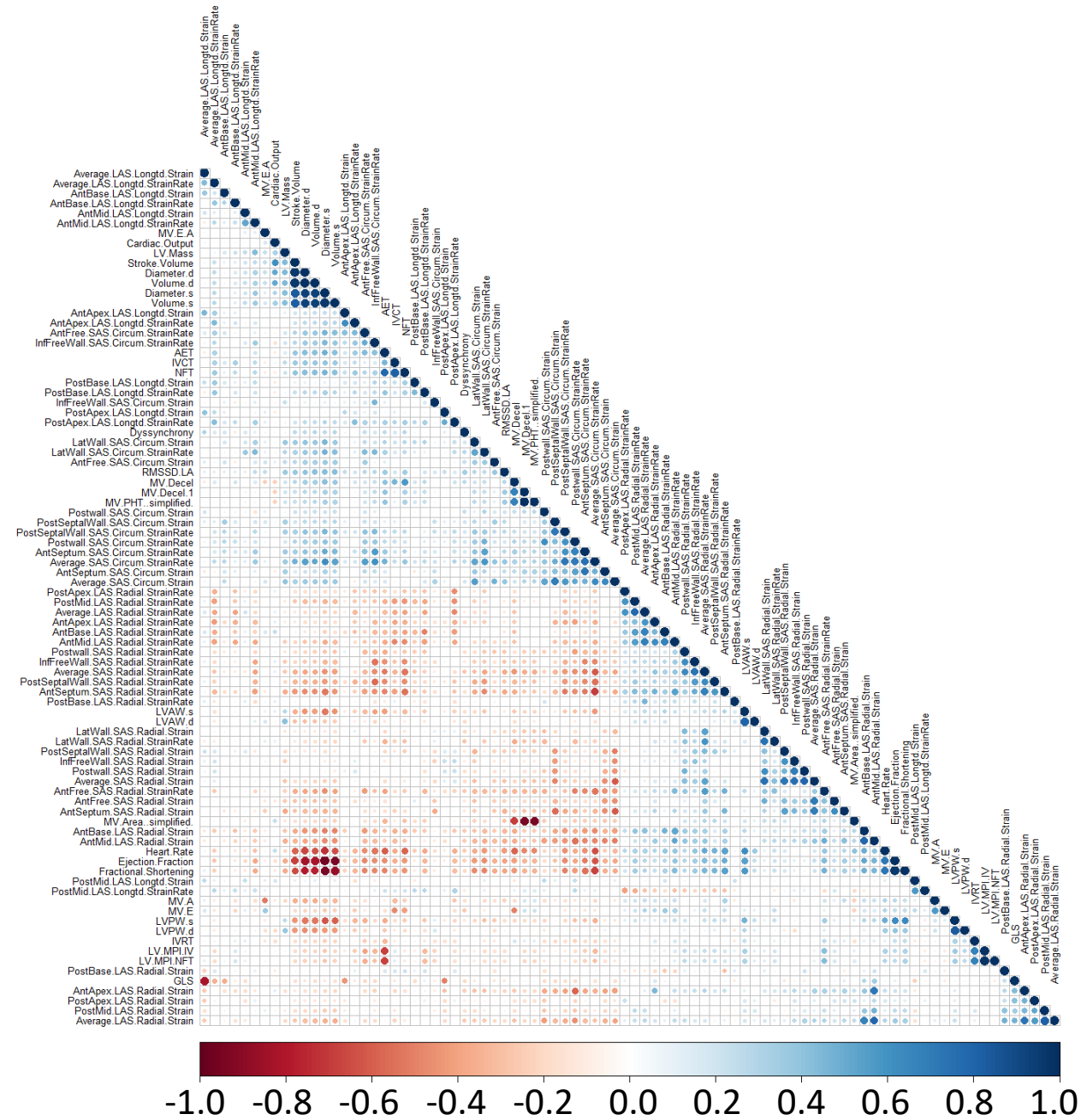
**Supplemental Table 6.1:** Short-axis systolic stress-strain assessments for the baseline (6-week-old) (N=48), lean (18-week-old) (N=24), obese (18-week-old) (N=24), non-UCMS (26-week-old) (N=24), UCMS (26-week-old) (N=24). Outliers were removed using a ROUT test, the D'Agostino-Pearson omnibus (K2) test was implemented to determine normal distribution, and an ANOVA/Tukey's post hoc test (normally distributed) or Kruskal-Wallis test/Dunn's post hoc test (non-normally distributed) were used to determine significance. Results were considered statically significant if  $P \leq 0.05$ . All data are reported as the means  $\pm$  the standard error of the mean (SEM). <sup>a</sup> = statistically different than the baseline group, <sup>b</sup> = statistically different than the lean group, <sup>c</sup> = statistically different than the obese group, <sup>d</sup> = statistically different than the non-UCMS group. Pk = peak, UCMS = unpredictable chronic mild stress.

**Supplemental Table 6.2 – Long-Axis Systolic Stress-Strain**

<b>Parameter</b>	<b>Units</b>	<b>Baseline <sup>a</sup></b>	<b>Lean <sup>b</sup></b>	<b>Obese <sup>c</sup></b>	<b>Non-UCMS <sub>d</sub></b>	<b>UCMS</b>
<b>Radial Velocity</b>	<b>Pk cm/s</b>	<b>1.348 ± 0.064</b>	<b>1.952 ± 0.112 <sup>a</sup></b>	<b>1.557 ± 0.080</b>	<b>1.957 ± 0.129 <sup>a</sup></b>	<b>1.965 ± 0.102 <sup>a</sup></b>
<b>Radial Displacement</b>	<b>Pk mm</b>	<b>0.297 ± 0.015</b>	<b>0.354 ± 0.022</b>	<b>0.255 ± 0.022 <sup>b</sup></b>	<b>0.296 ± 0.026</b>	<b>0.336 ± 0.020</b>
<b>Radial Strain</b>	<b>Pk %</b>	<b>13.72 ± 0.938</b>	<b>15.06 ± 1.454</b>	<b>8.300 ± 1.161 <sup>a,b</sup></b>	<b>11.31 ± 1.412</b>	<b>13.04 ± 1.140</b>
<b>Radial Strain Rate</b>	<b>Pk 1/s</b>	<b>7.184 ± 0.409</b>	<b>9.932 ± 0.6481 <sup>a</sup></b>	<b>7.343 ± 0.507</b>	<b>12.34 ± 2.513 <sup>a</sup></b>	<b>18.04 ± 6.371</b>
<b>Longitudinal Velocity</b>	<b>Pk deg/s</b>	<b>0.973 ± 0.063</b>	<b>0.851 ± 0.064</b>	<b>0.975 ± 0.082</b>	<b>1.327 ± 0.139 <sup>a,b</sup></b>	<b>1.146 ± 0.098</b>
<b>Longitudinal Displacement</b>	<b>Pk deg</b>	<b>0.120 ± 0.014</b>	<b>0.083 ± 0.013</b>	<b>0.091 ± 0.011</b>	<b>0.119 ± 0.015</b>	<b>0.120 ± 0.016</b>
<b>Longitudinal Strain</b>	<b>Pk %</b>	<b>-9.665 ± 0.714</b>	<b>-9.236 ± 1.040</b>	<b>-8.658 ± 0.870</b>	<b>-7.621 ± 1.229</b>	<b>-8.732 ± 1.063</b>
<b>Longitudinal Strain Rate</b>	<b>Pk 1/s</b>	<b>-6.602 ± 0.355</b>	<b>-8.329 ± 0.611</b>	<b>-6.934 ± 0.612</b>	<b>-12.74 ± 1.384 <sup>a,b,c</sup></b>	<b>-10.25 ± 1.207 <sup>a</sup></b>

**Supplemental Table 6.2:** Long-axis systolic stress-strain assessments for the baseline (6-week-old) (N=48), lean (18-week-old) (N=24), obese (18-week-old) (N=24), non-UCMS (26-week-old) (N=24), UCMS (26-week-old) (N=24). Outliers were removed using a ROUT test, the D'Agostino-Pearson omnibus (K2) test was implemented to determine normal distribution, and an ANOVA/Tukey's post hoc test (normally distributed) or Kruskal-Wallis test/Dunn's post hoc test (non-normally distributed) were used to determine significance. Results were considered statically significant if  $P \leq 0.05$ . All data are reported as the means  $\pm$  the standard error of the mean (SEM). <sup>a</sup> = statistically different than the baseline group, <sup>b</sup> = statistically different than the lean group, <sup>c</sup> = statistically different than the obese group, <sup>d</sup> = statistically different than the non-UCMS group. Pk = peak, UCMS = unpredictable chronic mild stress.

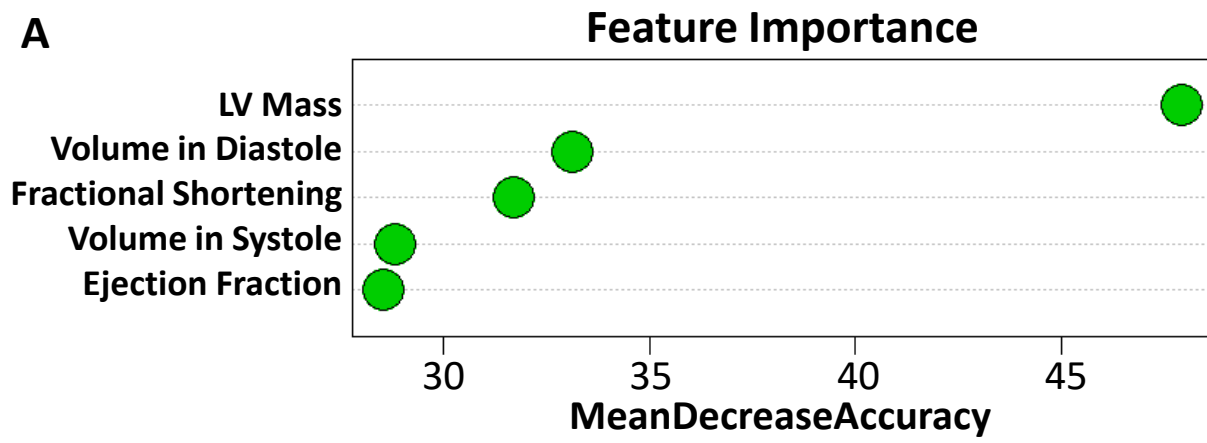
# Supplemental Figure 6.1:



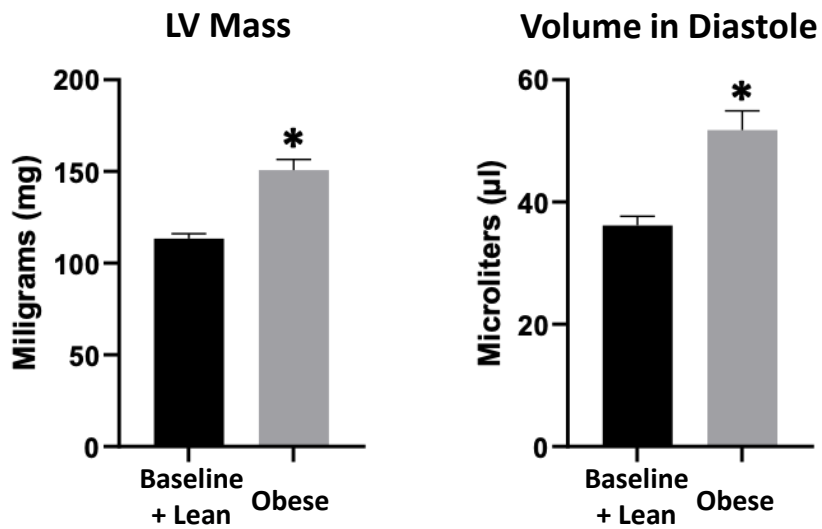
**Supplemental Figure 6.1: Multicollinearity – Post-Diet.** Features derived from M-mode, Pulse Wave (PW) Doppler, and strain analyses were used in machine learning applications for non-obese (baseline and lean, N=72) and obese (N=24) mice. Multicollinearity of features was assessed using corrplot (v.0.90) to prevent data bias. Highly correlated variables were removed to eliminate the possibility of impacting our machine learning algorithms.

Supplemental Figure 6.2:

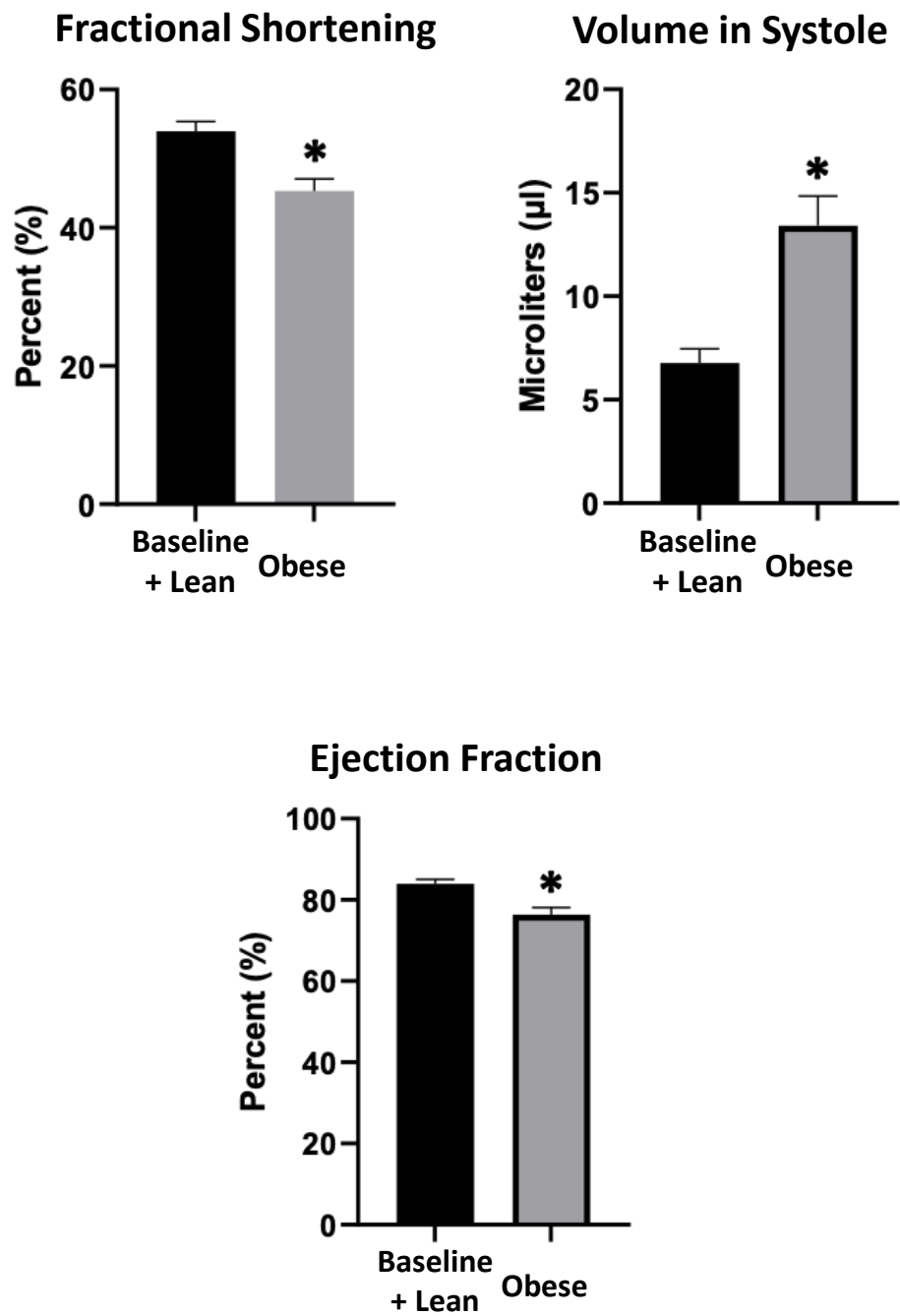
**A**



**B**



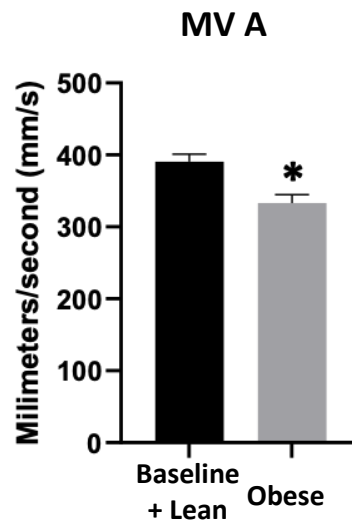
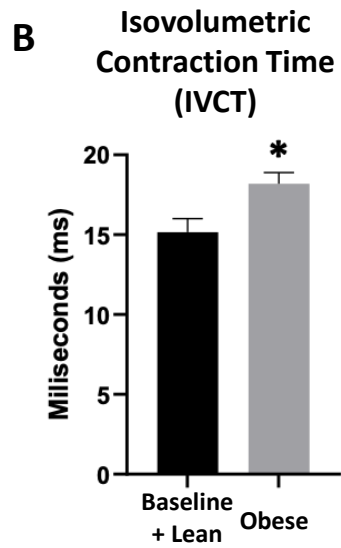
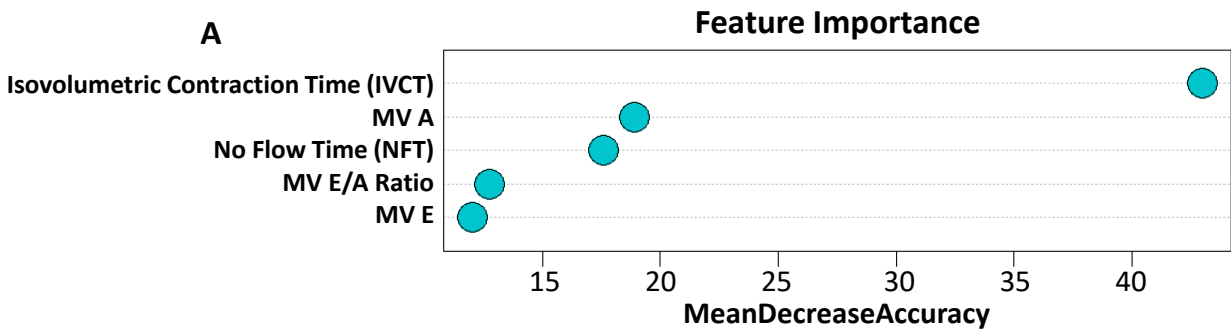
Supplemental Figure 6.2:



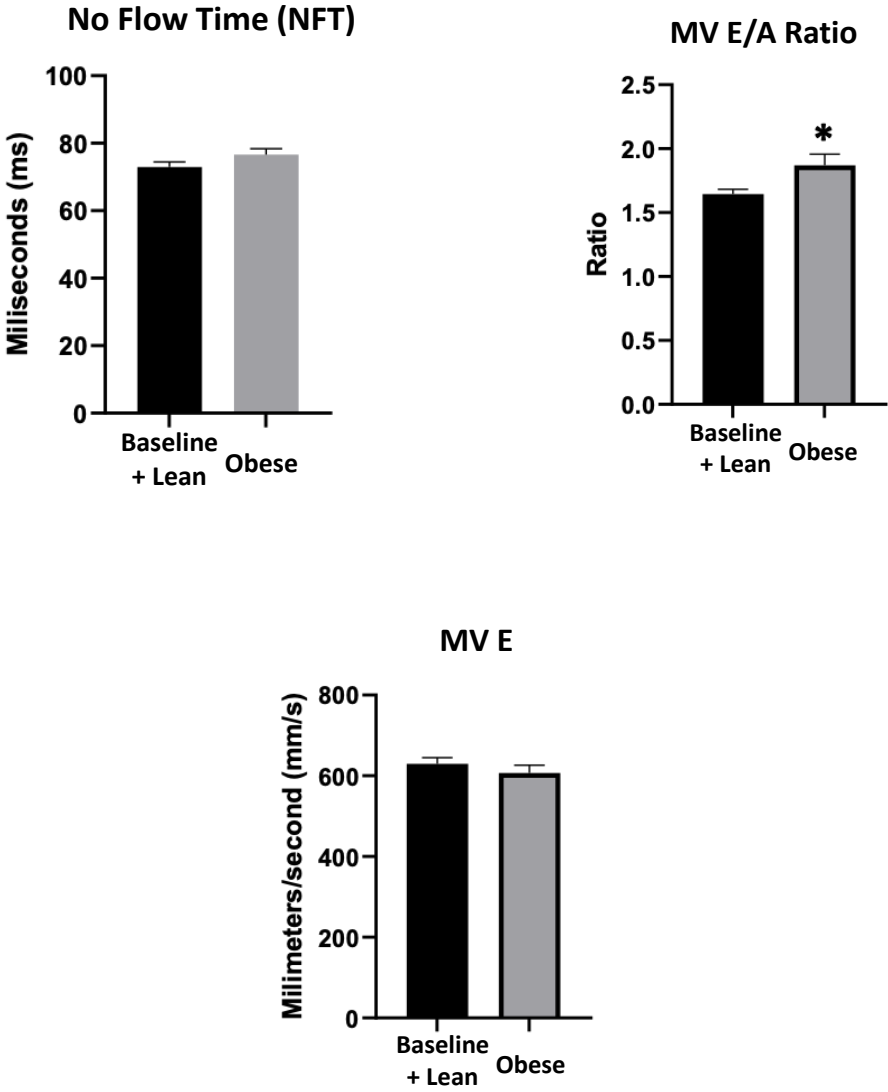


**Supplemental Figure 6.2: Feature Importance Post-Diet M-Mode.** Features derived from M-mode for non-obese (baseline and lean, N=72) and obese (N=24) mice. **(A)** Feature importance was determined using randomForest and evaluated based on MeanDecreaseAccuracy. **(B)** The top five most important features are provided with their values. Outliers were removed using a ROUT test, the D'Agostino-Pearson omnibus (K2) test was implemented to determine normal distribution, and a two-sided unpaired Student's t-test (normally distributed) or Mann Whitney test (non-normally distributed) were used to determine significance. Results were considered statically significant if  $P \leq 0.05$  and indicated by “\*”. All data are reported as the means  $\pm$  the standard error of the mean (SEM). Post-Diet = post high-fat diet induced obesity, LV = left ventricle.

Supplemental Figure 6.3:

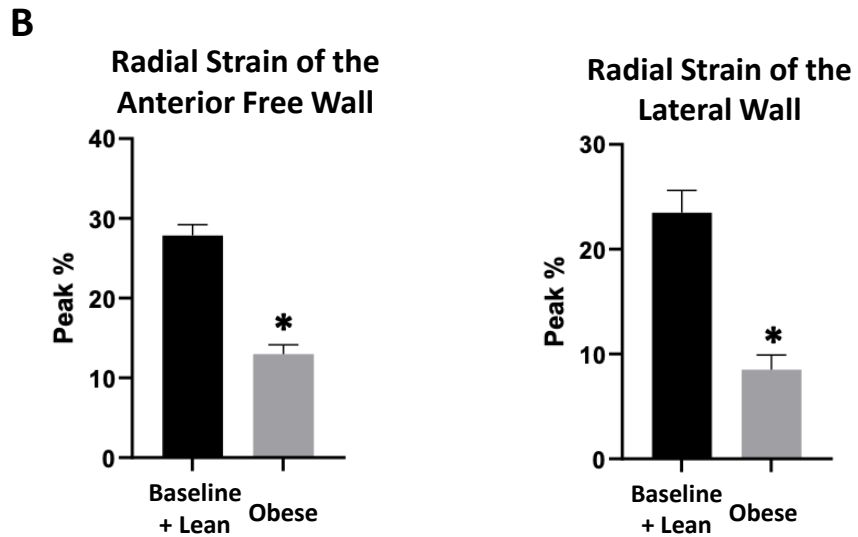
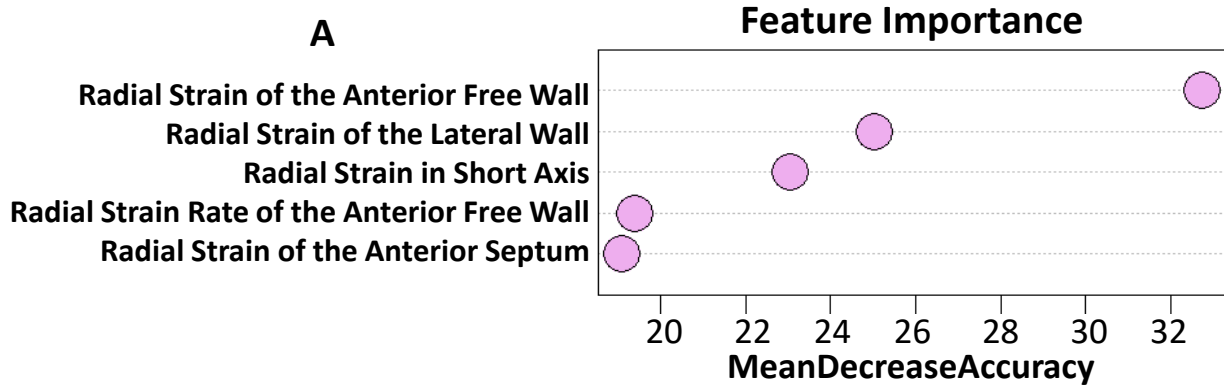


Supplemental Figure 6.3B

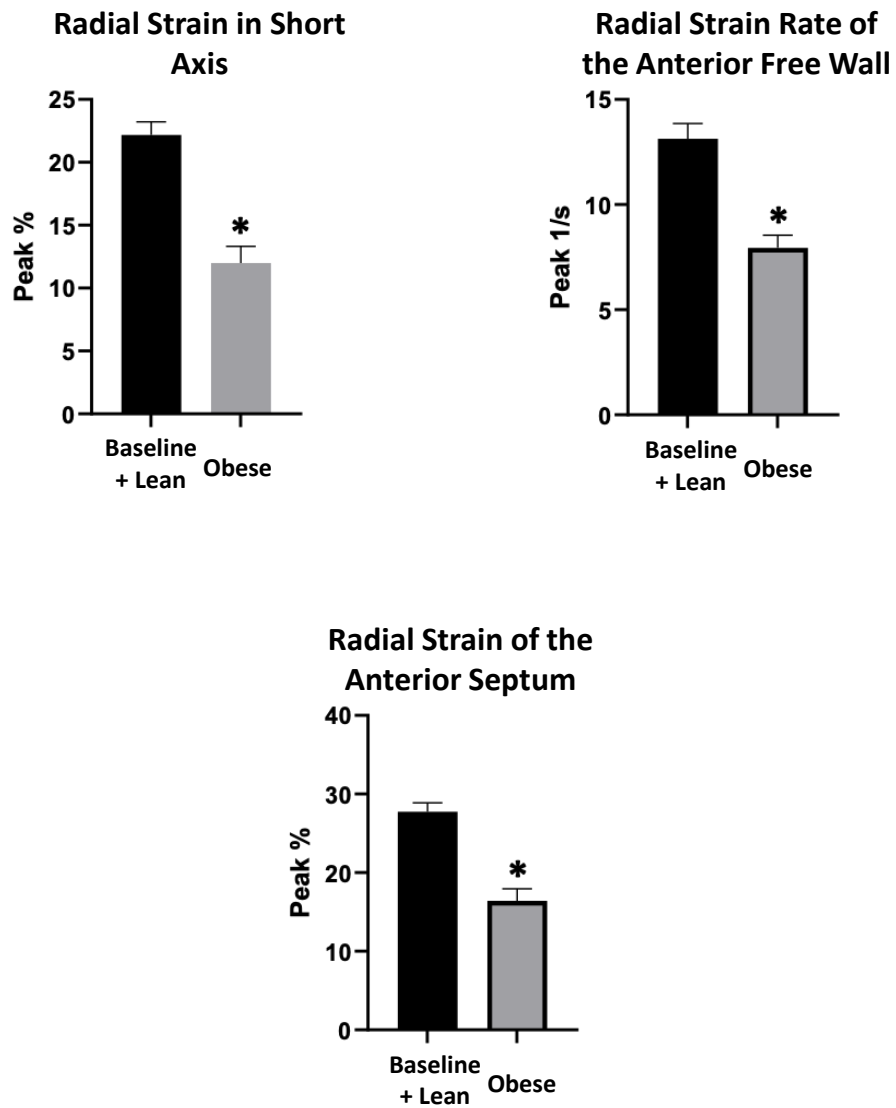


**Supplemental Figure 6.3: Feature Importance Post-Diet PW Doppler.** Features derived from Pulse Wave (PW) Doppler for non-obese (baseline and lean, N=72) and obese (N=24) mice. **(A)** Feature importance was determined using randomForest and evaluated based on MeanDecreaseAccuracy. **(B)** The top five most important features are provided with their values. Outliers were removed using a ROUT test, the D'Agostino-Pearson omnibus (K2) test was implemented to determine normal distribution, and a two-sided unpaired Student's t-test (normally distributed) or Mann Whitney test (non-normally distributed) were used to determine significance. Results were considered statically significant if  $P \leq 0.05$  and indicated by “\*”. All data are reported as the means  $\pm$  the standard error of the mean (SEM). Post-Diet = post high-fat diet induced obesity, MV = mitral valve.

Supplemental Figure 6.4:

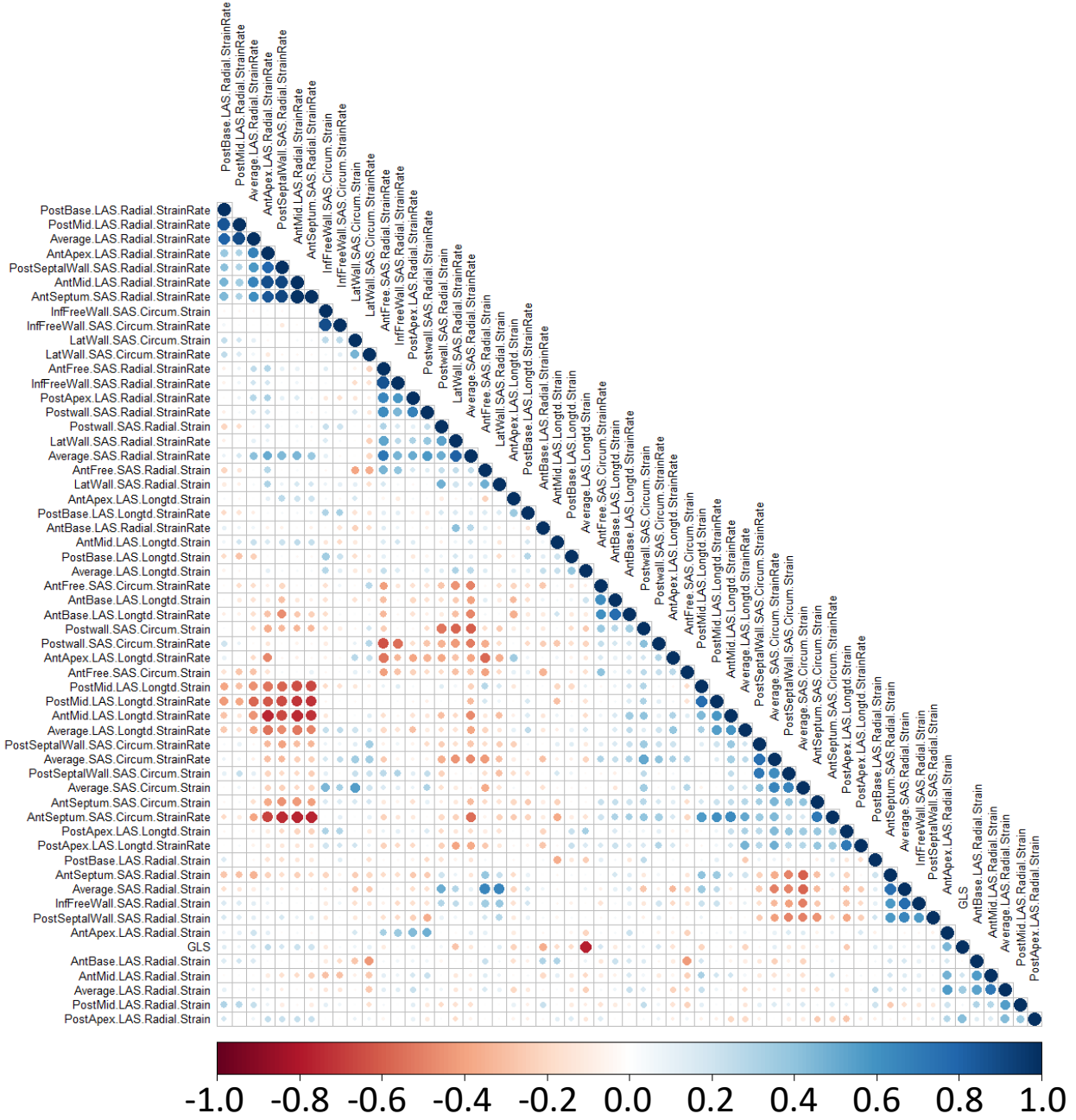


Supplemental Figure 6.4B:



**Supplemental Figure 6.4: Feature Importance Post-Diet Stress-Strain.** Features derived from stress-strain analyses for non-obese (baseline and lean, N=72) and obese (N=24) mice. **(A)** Feature importance was determined using randomForest and evaluated based on MeanDecreaseAccuracy. **(B)** The top five most important features are provided with their values. Outliers were removed using a ROUT test, the D'Agostino-Pearson omnibus (K2) test was implemented to determine normal distribution, and a two-sided unpaired Student's t-test (normally distributed) or Mann Whitney test (non-normally distributed) were used to determine significance. Results were considered statically significant if  $P \leq 0.05$  and indicated by “\*”. All data are reported as the means  $\pm$  the standard error of the mean (SEM). Post-Diet = post high-fat diet induced obesity.

Supplemental Figure 6.5:





**Supplemental Figure 6.5: Multicollinearity – Post-Stress.** Features derived from stress-strain analyses were used in machine learning applications for non-UCMS (N=22) and UCMS (N=22) mice at 26 weeks of age. Multicollinearity of features was assessed using corrplot (v.0.90) to prevent data bias. Highly correlated variables were removed to eliminate the possibility of impacting our machine learning algorithms.

# Curriculum Vitae

Amina Kunovac

---

ak0086@mix.wvu.edu

## Education

### DOCTOR OF PHILOSOPHY | AUGUST 2021 | WEST VIRGINIA UNIVERSITY

- *Applied and Molecular Pathophysiology (Division of Exercise Physiology)*
- Graduate Research Assistant: GPA – 3.87
- Graduate student member of the American Heart Association
- Member of the WVU Mitochondria, Metabolism & Bioenergetics Working Group
- Member of the WVU Center of Inhalation Toxicology
- Experiential Learning (1 Credit Hour): Online Review Course in Medical Genetics and Genetic Counseling
- Morgantown, WV

### BACHELOR OF SCIENCE | MAY 2016 | UNIVERSITY OF NEW HAVEN

- *B.S. Biology - Pre-Med* (Magna Cum Laude)
- *B.S. Forensic Science - Forensic Biology* (Magna Cum Laude); Minor: Chemistry
- Member of Alpha Lambda Delta National Honor Society
- Member of Honor Society for Experiential Education
- Resident Assistant
- West Haven, CT

## Manuscripts (In Preparation/Under Review)

### **Synergistic Transcriptomic and Mitochondrial Function Alterations after Single and Repeated Carbon Black and Ozone Inhalation Co-exposures.**

Hathaway QA\*, Majumder N\*, Goldsmith WT, **Kunovac A**, Pinti MV, Harkema JR, Castranova V, Hollander JM, Hussain S. Submitted to Particle and Fibre Toxicology: April 14, 2021.

### **Primary Sequence and Secondary Structure of Nuclear-Encoded Long Non-Coding RNAs Predict Binding to Mitochondrial PNPase.**

Hathaway QA, Taylor AD, **Kunovac A**, Pinti MV, Newman MS, Cook CC, Winters MT, Westemeier E, Fink GK, Durr AJ, Shepherd DL, Robart AR, Martinez I, Hollander JM. Submitted to Journal of Biological Chemistry: April 22, 2021.

**Genome-wide expression reveals potential biomarkers in breast cancer bone metastasis.**

Singh Y, Subbarao N, Jamini A, Hathaway QA, **Kunovac A**, Erickson B, Swarup V, and Narayan Singh H. *In preparation*.

**Left Ventricular Segmental Stress-Strain Identifies Unique Myocardial Deformation Patterns Following Intrinsic and Extrinsic Stressors in Mice.**

**Kunovac A**, Hathaway QA, Burrage EN, Coblenz T, Kelley EE, Sengupta PP, Hollander JM, Chantler PD  
Manuscript Under Review at Ultrasound in Medicine and Biology (Manuscript Number UMB-D-21-00654).  
Submitted September 1, 2021.

## Peer-Reviewed Publications

**Enhanced Antioxidant Capacity Prevents Epitranscriptomic and Cardiac Alterations in Adult Offspring Gestationally-Exposed to ENM.**

**Kunovac A**, Hathaway QA, Pinti MV, Durr AJ, Taylor AD, Goldsmith WT, Garner KL, Nurkiewicz TR, Hollander JM. *Nanotoxicology*. 2021 May 8:1-20. doi: 10.1080/17435390.2021.1921299. Online ahead of print. PMID: 33969789

**Cardiovascular Adaptations to Particle Inhalation Exposure: Molecular Mechanisms of the Toxicology.**

**Kunovac A**, Hathaway QA, Pinti MV, Taylor AD, Hollander JM. *Am J Physiol Heart Circ Physiol*. 2020 Jun 12; 1:319(2):H282-H305. doi: 10.1152/ajpheart.00026.2020. PMID: 32559138

**ROS Promote Epigenetic Remodeling and Cardiac Dysfunction in Offspring Following Maternal Engineered Nanomaterial (ENM) Exposure.**

**Kunovac A**, Hathaway QA, Pinti MV, Goldsmith WT, Durr AJ, Fink GK, Nurkiewicz TR, Hollander JM. *Part Fibre Toxicol*. 2019 Jun 18;16(1):24. doi: 10.1186/s12989-019-0310-8. PMID: 31215478

**Machine Learning, Diabetes Mellitus, and Cardiovascular Risk: A Personalized Medicine Approach to Disease Diagnosis.**

Hathaway QA, Roth SM, Pinti PV, Sprando DC, **Kunovac A**, Durr AJ, Cook CC, Fink GK, Cheuvront TB, Grossman JH, Aljahli GA, Taylor AD, Giromini AP, Allen JL, Hollander JM. *Cardiovascular Diabetology*. 2019 June 11; 18(1):78. doi: 10.1186/s12933-019-0879-0. PMID: 31185988

**miRNA-378a as a key regulator of cardiovascular health following engineered nanomaterial inhalation exposure.**

Hathaway QA, Durr AJ, Shepherd DL, Pinti MV, Brandebura AN, Nichols CE, **Kunovac A**, Goldsmith WT, Friend SA, Abukabda AB, Fink GK, Nurkiewicz TR, Hollander JM. *Nanotoxicology*. 2019 Feb 1:1-20. doi: 10.1080/17435390.2019.1570372. PMID: 30704319

**Mitochondrial Dysfunction in Type 2 Diabetes Mellitus: An Organ-Based Analysis.**

Pinti MV, Fink GK, Hathaway QA, Durr AJ, **Kunovac A**, Hollander JM. *Am J Physiol Endocrinol Metab*. 2019 Feb 1;316(2):E268-E285. doi: 10.1152/ajpendo.00314.2018. Epub 2019 Jan 2. PMID: 30601700

**Mitochondrial proteome disruption in the diabetic heart through targeted epigenetic regulation at the mitochondrial heat shock protein 70 (mtHsp70) nuclear locus.**

Shepherd DL\*, Hathaway QA\*, Nichols CE, Durr AJ, Pinti MV, Hughes KM, **Kunovac A**, Stine SM, Hollander JM. *J Mol Cell Cardiol.* 2018 Jun;119:104-115. doi: 10.1016/j.yjmcc.2018.04.016. Epub 2018 May 4. PMID: 29733819

*\*These authors contributed equally*

## Relevant Skills and Techniques

Four years of experience designing and executing experiments involving a wide variety of molecular biology techniques including, but not limited to: Microbiome-sequencing analysis, RNA-seq analysis, Statistics, Bioinformatics, Genotyping, RT-qPCR, Animal Colony Maintenance, Western Blotting, ELISAs, Gel Electrophoresis, Mitochondrial Isolations, Mitochondrial Bioenergetic Assays, Mitochondrial Respiration, and Clinical Specimen Handling (including right atrial appendage).

Other skills and experiences include training in the following:

- Echocardiographic analyses on fetal and adult mouse hearts
- Data Science
- Grant writing
- Manuscript writing, editing, and preparing for publication
- Coordinating and collaborating with other laboratories
- Presenting at various conferences
- Training and teaching other graduate students (laboratory techniques, writing, and how to collaborate with other laboratories)
- Didactic Teaching

## Research Presentations

### **Experimental Biology (EB), Virtual: 2021**

Poster Presentation, abstract entitled “Identifying Unique Patterns of Myocardial Deformation through Segmental Speckle Tracking Stress Strain Following High-Fat Diet” (April 27-30, 2021)

### **Cardiopulmonary Physiology (EXPH 787) – Guest Lecturer – West Virginia University, Morgantown, WV: 2020**

A 1-hour lecture how to perform speckle-tracking stress strain and conventional echocardiography and in human and mouse cohorts and the applications of each modality (September 11, 2020)

### **NHLBI Mitochondrial Biology Symposium, Bethesda, MD: 2019**

Poster presentation, abstract entitled “Antioxidant Protection Attenuates Cardiac and Mitochondrial Dysfunction in Offspring Following Maternal Engineered Nanomaterial Exposure” (September 27, 2019)

### **Experimental Biology (EB), Orlando, FL: 2019**

Poster presentation, abstract entitled “Elevated ROS and Epigenetic Remodeling Disrupt Cardiac Function in Offspring Following Maternal Engineered Nanomaterial (ENM) Exposure” (April 9, 2019)

**West Virginia University, Van Liere Research Day, Morgantown, WV: 2019**

Poster presentation entitled “Maternal Engineered Nanomaterial (ENM) Exposure Augments ROS Inciting Epigenetic Remodeling and Cardiac Dysfunction in Offspring” (March 22, 2019)

**West Virginia University Center for Inhalation Toxicology (iTOX), Morgantown, WV – WINTER MEETING.**

Oral Presentation talk entitled “Maternal Engineered Nanomaterial (ENM) Exposure Augments ROS and Epigenetic Remodeling Inciting Cardiac Dysfunction in Offspring” (November 28, 2018)

## Honors and Distinctions

### ***Outstanding Doctoral Student Award – Exercise Physiology***

Background: Award bestowed on individuals in the Exercise Physiology doctoral program who exhibit exemplary performance in academic and professional standards, such as publications, GPA, collaborations, teaching, etc.

Awarded: May 15, 2021

### ***American Heart Association Predoctoral Fellowship***

Background: Two-year predoctoral award received for project entitled “Cardiac Epitranscriptomic and Mitochondrial Remodeling in Progeny Following Maternal Engineered Nanomaterial Exposure”.

Awarded: January 31, 2020 – December 31, 2021

### ***Mitochondria, Metabolism & Bioenergetics Working Group Travel Award – EB 2020***

Background: Award designed to monetarily support conference registration costs for mitochondrial research. The work presented included a poster presentation entitled “Glutathione Peroxidase Influence on Cardiac Remodeling in Progeny of Dams Exposed to Engineered Nanomaterials During Gestation”

Awarded: February 3, 2020

### ***WVU Center for Inhalation Toxicology (iTOX) Travel Award – SOT 2020***

Background: Award designed to monetarily support toxicology research. The work presented included a poster entitled “Transient and Sustained Antioxidant Protection in Progeny Following Gestational Engineered Nanomaterial Inhalation Exposure”.

Awarded: February 11, 2020

## Peer-Reviewed Accepted Abstracts

**IDENTIFYING UNIQUE PATTERNS OF MYOCARDIAL DEFORMATION THROUGH SEGMENTAL SPECKLE TRACKING STRESS STRAIN FOLLOWING HIGH-FAT DIET**

**Kunovac A**, Burrage EN, Coblenz T, Kelley EE, Sengupta PP, Hollander JM, Hathaway QA, Chantler PD. – *Experimental Biology (EB), Virtual: 2021*

**MODELLING THE PULMONARY TRANSCRIPTOME IN A DOSE AND SUBSTRATE-DEPENDENT MANNER: CARBON BLACK AND OZONE CO-EXPOSURE**

Hathaway QA, Majumder N, **Kunovac A**, Xie Z, Pinti MV, Harkema JR, Nurkiewicz TR, Hollander JM, and Hussain S. – *Society of Toxicology (SOT), Virtual: 2021*

**GLUTATHIONE PEROXIDASE INFLUENCE ON CARDIAC REMODELING IN PROGENY OF DAMS EXPOSED TO ENGINEERED NANOMATERIALS DURING GESTATION**

**Kunovac A**, Hathaway QA, Taylor AD, Durr AJ, Goldsmith WT, Pinti MV, Fink GK, Nurkiewicz TR, and Hollander JM. – *Experimental Biology (EB), San Diego, CA: 2020*

**MICRORNA-378A LOSS ENHANCES MITOCHONDRIAL BIOENERGETICS AND LESSENS CARDIAC CONTRACTILE DYSFUNCTION IN THE TYPE 2 DIABETIC HEART**

Durr AJ, Hathaway QA, **Kunovac A**, Taylor AD, Pinti MV, McLaughlin SL, Shepherd DL, Singh AK, and Hollander JM. – *Experimental Biology (EB), San Diego, CA: 2020*

**LOSS OF FUNCTIONAL NON-CODING RNA DIVERSITY IN DIABETIC CARDIAC MITOCHONDRIA**

Taylor AD, Hathaway QA, **Kunovac A**, Pinti MV, Cook CC, Fink GK, Durr AJ, and Hollander JM. – *Experimental Biology (EB), San Diego, CA: 2020*

**TRANSIENT AND SUSTAINED ANTIOXIDANT PROTECTION IN PROGENY FOLLOWING GESTATIONAL ENGINEERED NANOMATERIAL INHALATION EXPOSURE**

**Kunovac A**, Hathaway QA, Taylor AD, Pinti MV, Goldsmith WT, Fink GK, Durr AJ, Nurkiewicz TR, and Hollander JM. – *Society of Toxicology (SOT), Anaheim, CA: 2020*

**ANTIOXIDANT PROTECTION ATTENUATES CARDIAC AND MITOCHONDRIAL DYSFUNCTION IN OFFSPRING FOLLOWING MATERIAL ENGINEERED NANOMATERIAL EXPOSURE**

**Kunovac A**, Hathaway QA, Durr AJ, Goldsmith WT, Taylor AD, Pinti MV, Fink GK, Nurkiewicz TR, and Hollander JM. – *NHLBI Mitochondrial Biology Symposium, Bethesda, MD: 2019*

**APPLYING MACHINE-LEARNING TO DISEASE DIAGNOSIS THROUGH PATIENT-MATCHED OMICS PROFILES**

Hathaway QA, Roth SM, Pinti, MV, Sprando DC, **Kunovac A**, Durr AJ, Cook CC, Fink GK, Chevront TB, Grossman JH, Aljahli GA, Taylor AD, Giromini AP, Allen JL, and Hollander JM. – *NHLBI Mitochondrial Biology Symposium, Bethesda, MD: 2019*

**LOSS OF MICRORNA-378A FUNCTION RESTORES MITOCHONDRIAL BIOENERGETICS IN A TYPE 2 DIABETIC MOUSE MODEL**

Durr AJ, Hathaway QA, Taylor AD, **Kunovac A**, Pinti MV, Shepherd DL, Fink GK, and Hollander JM. – *NHLBI Mitochondrial Biology Symposium, Bethesda, MD: 2019*

**IMPACT OF DIABETES MELLITUS ON MITOCHONDRIAL MIRNA DIVERSITY AND RELATED CELLULAR PATHWAYS**

Taylor AD, Hathaway QA, **Kunovac A**, Pinti MV, Cook CC, Fink GK, Durr AJ, Shepherd DL, Robart AR, and Hollander JM. – *NHLBI Mitochondrial Biology Symposium, Bethesda, MD: 2019*

**ELEVATED ROS AND EPIGENETIC REMODELING DISRUPT CARDIAC FUNCTION IN OFFSPRING FOLLOWING MATERNAL ENGINEERED NANOMATERIAL (ENM) EXPOSURE**

**Kunovac A**, Hathaway QA, Pinti MV, Durr AJ, Fink GK, Goldsmith WT, Nurkiewicz TR, and Hollander JM. – *Experimental Biology (EB), Orlando, FL: 2019*

**USING MACHINE LEARNING TO PREDICT THE DEVELOPMENT OF DIABETES AND POTENTIAL BIOMARKERS LINKED TO CARDIAC RISK**

Hathaway QA, Pinti MV, Roth SM, Sprando DC, **Kunovac A**, Durr AJ, Cook CC, Fink GK, Chevront TB, Grossman JH, Aljahli GA, Roberts HG, Salman M, Giromini AP, and Hollander JM. – *Experimental Biology (EB), Orlando, FL: 2019*

**MICRORNA CHANGES IN DIABETIC CARDIAC MITOCHONDRIA: WHAT ARE THEY DOING THERE?**

Pinti MV, Hathaway QA, **Kunovac A**, Durr AJ, Cook CC, Roberts HG, Salman M, and Hollander JM. – *Experimental Biology (EB), Orlando, FL: 2019*

**STRESS STRAIN SPECKLE-TACKING SEGMENTAL ANALYSIS REVEALS EARLY INDICATIONS OF DIASTOLIC DYSFUNCTION IN A TYPE 2 MOUSE MODEL OF DIABETES MELLITUS**

Durr AJ, Hathaway QA, Pinti MV, Shepherd DL, **Kunovac A**, and Hollander JM. – *Experimental Biology (EB), Orlando, FL: 2019*

**MATERNAL ENGINEERED NANOMATERIAL (ENM) EXPOSURE AUGMENTS ROS INCITING EPIGENETIC REMODELING AND CARDIAC DYSFUNCTION IN OFFSPRING**

**Kunovac A**, Hathaway QA, Pinti MV, Fink GK, Goldsmith WT, Durr AJ, Nurkiewicz TR, and Hollander JM. – *West Virginia University Van Liere, Morgantown, WV: 2019*

## **Mentorship**

**West Virginia University | Graduate Research Assistant | January 2017 – Current**

- **Summer Students**
  - Dylan Holland (2019) – Medical school summer research rotation
    - Currently: Medical student class of 2022 at West Virginia University
- **Undergraduate Students**
  - Matt Knauff (Fall 2019 – Present) – Undergraduate part-time research
    - Currently: Undergraduate student in Exercise Physiology
  - Garrett Fink (Spring 2018 – Present) – Undergraduate part-time research
    - Currently: Undergraduate student in Exercise Physiology
- **Research Rotations**
  - Joseph Agba (Fall 2019) – Graduate research rotations
    - Currently: Undifferentiated graduate student in the Biomedical Sciences program
  - Andrew Giromini (Fall 2018) – Graduate research rotations
    - Currently: Undifferentiated graduate student in the Biomedical Sciences program
- **Graduate Students**

Saira Rizwan (Fall 2020-Present)-Graduate research rotations

- Currently: Graduate Research Assistant for Dr. John Hollander, West Virginian University, Department of Exercise Physiology

Andrew Taylor (Fall 2018-Present) – Graduate research rotations

- Currently: Graduate Research Assistant for Dr. John Hollander, West Virginian University, Department of Exercise Physiology

## Community Outreach and Volunteer Work

**Smokey Mountain Home for Children – Severville, TN | Greene Valley Church of God | July 2018**

- 7-day trip to volunteer at a home for foster children and neglected youth. Approximately 50-80 children living at the facility, with a widow's center housing 30-40 women.
- Work included painting, sanding, cleaning, drywall work, remodeling, moving furniture and equipment, etc.
- Outreach activities included talking and interacting with the youth through sports and while working within the living quarters.

**Volunteer, Yale New Haven Hospital -Children's Surgical Unit– New Haven, CT | 2013-2015**

Provided help and human connection necessary to ease the stress of the patients going through difficult times.

## Undergraduate Work Experience

Forensic Science Study Abroad Program-Chaperone - July 2016

- Assisted in coordinating a trip to Sydney, Australia and the University of Technology, Sydney-Bodies Farm.

Resident Assistant - Office of Residential Life, University of New Haven - 2013-2016

- Develop community between 70 residents through creative programming while implementing University policies

Resident Assistant - Forensic Science Living Learning Community-Office of Residential Life, University of New Haven

2014-2015

- Developed community between 40 residents by creating programs involving Forensic Science topics to introduce first-year Forensic Science students to possible career paths, while also implementing University policies.

## Undergraduate Honors and Distinctions

Inductee of the Honor Society for Experiential Education-Gold Level

April 2016



Summer Undergraduate Research Fellow  
Summer 2015

Inductee of Alpha Lambda Delta Honor Society  
Spring 2013

Dean's List, University of New Haven  
2012-2016

Distinguished Scholar Award (\$12,000 per academic year)  
2012-2016

SAT Writing Award (\$1,000 per academic year)  
2012-2016

## **Language**

### **Fluent**

#### **English**

*Written and Spoken*

#### **Bosnian**

*Written and Spoken*

#### **Croatian**

*Written and Spoken*